

UNCLASSIFIED

AD NUMBER
AD801005
NEW LIMITATION CHANGE
TO Approved for public release, distribution unlimited
FROM Distribution authorized to U.S. Gov't. agencies and their contractors; Administrative/Operational Use; 24 Jun 1966. Other requests shall be referred to Commander, U.S. Army Tank Automotive Center, Warren, MI 48090.
AUTHORITY
USATAC ltr, 6 Dec 1966

THIS PAGE IS UNCLASSIFIED

AD-11

Engineering Methods for the Design and Selection of Materials Against Fracture

E. T. Wessel, W. G. Clark and W. K. Wilson
Westinghouse Research Laboratories

TECHNICAL LIBRARY
REFERENCE COPY



Final Technical Report
Contract No. DA-30-069-AMC-602(T)
June 24, 1966

ATAC

20020726150

COMPONENTS RESEARCH & DEVELOPMENT LABORATORIES

U.S. ARMY TANK AUTOMOTIVE CENTER WARREN, MICHIGAN

AN 28548

The findings in this report are not to be construed as an official Department of the Army position, unless so designated by other authorized documents.

Copy No. 2

ENGINEERING METHODS FOR THE DESIGN AND
SELECTION OF MATERIALS AGAINST FRACTURE

Final Technical Report

by

E. T. Wessel, W. G. Clark, W. K. Wilson

June 24, 1966

Contract No. DA-30-069-AMC-602(T)
Department of the Army Project No. 1 - DO-24401-A-105
Ordnance Management Structure (OMS) Code No. 5025.11.26800.01.01
U.S. Army Tank-Automotive Center
Warren, Michigan 48090

Westinghouse Research Laboratories
Pittsburgh, Pennsylvania 15235

Reproduced From
Best Available Copy

AM 28548

ABSTRACT

Various approaches to the brittle fracture problem were reviewed and evaluated in terms of their applicability for satisfying ATAC's need for engineering procedures to be applied to materials selection and design criteria for the prevention of fracture in the future use of high-strength materials. Linear elastic fracture mechanics technology was selected as the most applicable approach.

A comprehensive review of the state of the art in fracture mechanics technology is presented. The fracture mechanics data available in the literature for high-strength steels, aluminum and titanium alloys were reviewed and evaluated with respect to their validity as fracture toughness parameters. All applicable fracture toughness data are tabulated. Additional fracture toughness (K_{Ic}) data were generated in the program for HP 9-4-25 steel, 7079-T6 aluminum and 6Al-4V titanium. Crack growth rates as a function of the stress intensity (K_I) were also determined for the steel and aluminum alloys.

Engineering procedures and criteria for utilizing fracture mechanics technology were developed. Their application is illustrated by solutions to realistic hypothetical problems in the areas of design; evaluation and selection of materials; evaluations of nondestructive inspection capabilities; establishment of specifications, acceptance standards, and quality control procedures; and evaluating overall performance and life expectancy characteristics of the finished product. Detailed considerations in all of these areas are exemplified by solutions of problems associated with the design and production of a hypothetical pressure vessels.

FOREWORD

For the convenience of the reader, this report has been divided into 12 major divisions, each of which is separated by an index tab. The material within any division deals with a given subject and essentially is a self-contained unit. A table of contents and a list of tables and illustrations is provided at the beginning of each division. Similarly the references for each division are provided at the end of each division and the figures and tables are integrated within the text. Thus, the reader can readily focus attention to divisions of particular interest to his activity.

The 12 major divisions are as follows:

Division	Section Numbers	Contents
1.	1. through 5.	General description of program
2.	6.1	Review and selection of an approach
3.	6.2	State-of-the-art for linear elastic fracture mechanics
4.	7.1	Fracture toughness (K_{Ic}) data from literature
5.	7.2	Generation of fracture toughness data
6.	7.3	Generation of crack growth rate data
7.	8.1	Introduction to the application of fracture mechanics technology
8.	8.2	Information required in utilizing fracture mechanics technology

9.	8.3	Application of the technology
10.	8.4	Example problems for a hypothetical pressure vessel
11.	Appendex I	Tabulation of K_{Ic} fracture toughness data
12.	Appendex II	Ultrasonic method for detecting fracture initiation and crack extension

A more detailed description of the material contained within each section of each division may be derived from the Table of Contents which follows.

TABLE OF CONTENTS

	<u>Page</u>
1. INTRODUCTION	2
1.1 General Background and Problem	2
1.2 Phases of the Program	3
1.3 Authorization for the Program	3
2. OBJECT	4
3. SUMMARY	5
4. CONCLUSIONS	7
5. RECOMMENDATIONS	9
6. PHASE I - GENERAL REVIEW AND SELECTION OF AN APPROACH	11
6.1 Review of General Approaches to Brittle Fracture	11
6.1.1 Introduction and ATAC Philosophy	15
6.1.2 Transition Temperature Approach	16
6.1.2.1 Tests for Determining Transition Temperatures	17
6.1.2.2 Significance and Application of the Transition Temperature Approach	26
a. Considerations in the Selection of a Transition Temperature Criterion	27
b. Applicability for Comparison Purposes	29
c. Applicability to Design Situations	30
d. Applications Where the Use of the Transition Temperature Approach is Uncertain	35
e. Transition Temperature Based Fracture Analysis Diagram	36
f. General Summary of Applicability of Transition Temperature Approach	40
6.1.2.3 Applicability of Transition Temperature Approach to ATAC's Interest and Project Goals	40

TABLE OF CONTENTS (Cont.)

	<u>Page</u>
6.1.3 Stress Analysis Approach	41
6.1.3.1 Stress Criteria	42
a. Use of Fracture Curve	42
b. Maximum Stress	45
c. Stress Concentration Factor Approach	45
d. Use of Stress Gradient as a Parameter	50
e. Applicability of Stress Criteria	50
6.1.3.2 Strain Criteria	51
a. Exhaustion of Ductility	51
b. Critically Strained Volume Criteria	53
c. Use of Strain Hardening Exponent	53
d. Crack Opening Displacement Criteria	54
e. Applicability of Strain Criteria	54
6.1.3.3 Linear Elastic Fracture Mechanics	55
a. Energy Criteria	55
b. Stress Intensity Criteria	59
c. Applicability of Linear Elastic Fracture Mechanics	63
6.1.3.4 Elastic-Plastic Analysis	63
6.1.3.5 Statistical Considerations	64
6.1.4 Selection of the Most Applicable Approach	65
6.2 Summary of the State of the Art of Fracture Mechanics	82
6.2.1 Description of the Evolution of the Approach	82
6.2.2 Description of Basic Terminology	83
6.2.2.1 Fracture Appearance	83
6.2.2.2 Brittle Fracture and Ductile Fracture	85
6.2.2.3 Frangible and Tough	86
6.2.2.4 Modes of Fracture	86
6.2.2.5 Energy Release Rate	88
6.2.2.6 Stress Intensity Factor	88
6.2.2.7 Plane Stress and Plane Strain	91
6.2.2.8 Plastic Zone Size	92
6.2.2.9 Fracture Mode Transition with Variation in Plate Thickness	95
6.2.2.10 Effect of Plate Width	96
6.2.2.11 Plastic Zone Size Correction Factor	97
6.2.2.12 Slow Crack Growth	98

TABLE OF CONTENTS (Cont.)

	<u>Page</u>
6.2.3 Influence of Mechanical and Metallurgical Variables	101
6.2.3.1 Mechanical Variables	101
6.2.3.2 Metallurgical Variables	105
6.2.4 Summary of Tests for Plane Strain Fracture Toughness (K_{Ic} or G_{Ic})	111
6.2.4.1 Types of Specimens	111
6.2.4.2 Calibration of Specimens	113
6.2.4.3 Fatigue Cracking of Test Specimens	113
6.2.4.4 Instrumentation for K_{Ic} Testing	130
6.2.4.5 Summary and Comparison of Specimens	131
6.2.4.6 Summary	132
6.2.5 General Experience in Applying Fracture Mechanics	132
6.2.6 Limitations of Fracture Mechanics	133
 7. PHASE II - DATA COLLECTION	 144
7.1 Literature Survey	144
7.1.1 Introduction	144
7.1.2 Evaluation Criteria	144
7.1.3 Compilation of Data	146
7.1.4 Discussion	148
7.1.5 Summary	152
7.2 Generation of K_{Ic} Data	157
7.2.1 Material	157
7.2.2 Specimen Preparation	160
7.2.3 Test Procedure	163
7.2.4 Results and Discussion	170
7.2.5 Summary	189
7.3 Generation of Slow Crack Growth Data	206
7.3.1 Introduction	206
7.3.2 Material and Specimen Preparation	207
7.3.3 Test Procedure	207
7.3.4 Results and Discussion	209
7.3.5 Summary	217

TABLE OF CONTENTS (Cont.)

	<u>Page</u>
8. PHASE III - APPLICATION OF FRACTURE MECHANICS TECHNOLOGY221
8.1 Introduction221
8.1.1 Generalized Description of the Use of Fracture Mechanics Technology221
8.1.1.1 Brittle Fracture During Static Loading222
8.1.1.2 Slow Crack Growth During Cyclic Loading224
8.1.1.3 Summary226
8.2 Information Required in Utilizing Fracture Mechanics Technology231
8.2.1 Material Properties231
8.2.2 Stress Information234
8.2.3 Defect Characterization235
8.2.4 Expressions Appropriate to Geometry and Loading Conditions . .	.237
8.2.5 Type of Loading248
8.3 Application of Information, Procedures and Data256
8.3.1 Design Considerations256
8.3.2 Evaluation and Selection of Materials257
8.3.2.1 Evaluating Resistance to Catastrophic Failure for Static Loading257
a. Acquiring Basic Design Information and Material Requirements257
b. Selection of Basic Type of Fracture Toughness Specimen258
c. Selection of Size of Test Specimen and Testing for K_{Ic}258
d. Evaluation of Materials Based on K_{Ic} Data and Design Requirements259
e. Summary263
8.3.2.2 Evaluation and Selection of Materials for Resistance to Fracture Under Cyclic or Sustained Loading Conditions264
a. Obtaining Crack Growth Rate Data265
b. Evaluation of Crack Growth Rate Data265
c. Summary of Possible Crack Growth Behaviors273
8.3.3 Quality Control Inspection and Specifications280
8.3.3.1 Inspection and Quality Control281
8.3.3.2 Quality Control Specifications283
8.3.3.3 Summary284

TABLE OF CONTENTS (Cont.)

	<u>Page</u>
8.3.4 Performance and Life Expectancy Evaluation	285
8.3.4.1 Information Needed to Make Life Evaluation	286
8.3.4.2 Procedure for Estimating Life Under Cyclic Loading Condition	288
8.3.4.3 Limitations of Procedure	290
8.3.4.4 Simplified Method of Predicting Cyclic Life	292
8.3.4.5 Life Predictions When Slow Crack Growth Occurs Under Sustained Loading	295
8.3.5 Summary	297
8.4 Application of Fracture Mechanics Technology in a Hypothetical Pressure Vessel	301
8.4.1 Operational Requirements and Initial Design Considerations . .	301
8.4.2 Evaluation and Selection of a Material	304
8.4.2.1 Consideration of Fabrication Techniques	304
8.4.2.2 Initial Evaluation of Materials	305
a. Critical Defect Sizes for Failure During Proof Testing	306
b. Nondestructive Inspection Capabilities	308
c. Considerations of Cyclic Life and Initial Flaw Sizes	311
8.4.2.3 Reconsideration of Material Selection	313
a. Reduction in Design Stresses	314
8.4.2.4 Using a Lower-Strength, Higher-Toughness Steel	316
a. Critical Defect Sizes for Failure	316
b. Cyclic Crack Growth Considerations	318
c. Reducing the Weight of the Vessel	319
8.4.2.5 Summary of Final Selection of a Material	322
8.4.3 Establishing Specifications, Inspection and Acceptance Criteria	324
8.4.4 Proof Testing and Life Expectancy Evaluation	327
8.4.4.1 Proof Testing	327
a. Crack Growth Under Sustained Loading	330
b. Leak or Failure During Proof Testing	332
8.4.4.2 Evaluation of Life Expectancy	333
a. Minimum Life Resulting from Undetected Flaws	333
b. Maximum Life for No Detectable Flaws	334
c. Realistic Life Expectancy Based on Maximum Allowable Size Flaws	335
8.4.5 Summary	337

TABLE OF CONTENTS (Cont.)

	<u>Page</u>
APPENDIX I Tabulation of Plane Strain Fracture Toughness Data	339
APPENDIX II Ultrasonic Detection of Fracture Initiation and Extension in the W.O.L. Type Fracture Toughness Specimen	379
ACKNOWLEDGMENTS	396
DISTRIBUTION LIST	397
DD FORM 1473	401

LIST OF FIGURES

SECTION 6.1

<u>Figure</u>		<u>Page</u>
1	Schematic representation of the various transition temperatures obtainable from the results of Charpy V-notch impact tests . .	18
2	Schematic representation of the relative positions of the crack-starter transition temperatures on the Charpy V-notch energy curve.	21
3	The effect of temperature on the fracture stress and fracture appearance of sharply notched, high strength sheet specimens of a 12% Cr steel	22
4	The effect of temperature on the stress required for the propagation of a brittle crack.	24
5	Various transition temperatures obtained on a given plate of steel.	25
6	Schematic illustration of the Charpy V-notch impact behavior of two unlike materials.	30
7	The effect of temperature on the stress required for propagation of fracture (schematic).	33
8	Fracture analysis diagram.	38
9	Ludwik's fracture concept.	43
10	Effect of change in strain rate $\dot{\epsilon}$ or temperature T on fracture stress	43
11	True stress-strain curves; after Beeuwkes. . .	44

LIST OF FIGURES (Cont.)

<u>Figure</u>		<u>Page</u>
12	Elliptic crack in an infinite sheet subjected to normal uniaxial stress.	47
13	Influence of material and specimen geometry on notch strength behavior.	48
14	Effect of the equivalent particle size on the K_{tm} vs K curve of a brittle material. . .	49
15	Stress-strain curve for a small amount of strain hardening.	52
16	Effect of notch radius on apparent G_c . Schematic based on data for Aluminum 7075-T6 sheets 1/16 in. thick.	59
17	Coordinates measured from the leading edge of a crack and the stress components in the crack tip stress field.	61

SECTION 6.2

1	Modes of fracture.	84
2	(a) Brittle fracture at component level	86
	(b) Ductile fracture at component level	86
3	Basic modes of crack surface displacements . . .	87
4	Coordinates measured from the leading edge of a crack and the stress components in the crack tip stress field	90
5	Approximation of plastic zone sizes under plane strain and plane stress conditions	94
6	Three-dimensional schematic diagram of the crack surface, the crack front and the plastic zone	94
7	Dependence of K_C and fracture appearance on thickness of plate specimens	95

LIST OF FIGURES (Cont.)

<u>Figure</u>		<u>Page</u>
8	Effect of specimen width on K_c	97
9	Correlation of crack growth rates 7075-T6 aluminum alloy under sinusoidal loading with cyclic change in stress intensity, ΔK	99
10	Crack growth rate versus field parameter for 100 percent R.H. at 80°F. Data for H-11 steel at 230 ksi yield strength.	100
11	Summary plot: crack growth rates versus stress field parameter for several relative humidities at 80°F	100
12	The effect of strain rate on the K_{Ic} fracture toughness of an 18 Ni maraging steel-300 grade .	103
13	Fracture toughness as a function of strain rate for mild steel at several temperatures. . .	103
14	Expected general behavior of K_{Ic} as a function of strain rate	106
15	Temperature dependence of K_{Ic} fracture toughness of annealed A302B steel, WOL specimen . . .	106
16	Temperature dependence of the fracture toughness of a Ni MoV forging steel	107
17	Temperature dependence of fracture toughness for ship plate	107
18	The effect of tempering temperature on the yield strength and fracture toughness of SAE 4340 steel plate	109
19	Temperature dependence of K_{Ic} fracture toughness of various lots of A302B steel	110
20	Variability of room temperature fracture toughness with yield strength for 18 Ni maraging steel	112
21	K_{Ic} as a function of yield strength for 18 Ni maraging steel (various aging treatments). . . .	112

LIST OF FIGURES (Cont.)

<u>Figure</u>		<u>Page</u>
22	Symmetrical center - cracked plate	115
23	Symmetrical edge - cracked plate	116
24	Single-edge-notched plate (tension).	117
25	Notched bend specimen (three-point loaded) . . .	118
26	Notched bend specimen (four-point loaded). . . .	119
27	Surface cracked plate.	120
28	Circumferentially notched and fatigue - cracked round bar.	121
29	Symmetrical center notched disc (rotor or spin specimen)	122
30	Wedge-opening-loading (WOL) type center- line loaded specimen	123
31	K calibration for the center-cracked plate specimen	124
32	K calibration for the single-edge crack tension specimen	125
33	K calibrations for bend specimens.	126
34	K calibration for circumferentially cracked- notched round bar.	127
35	K calibrations for compact crack-line loaded specimens	128
36	Calibration - numeric constant " C_3 " as a function of the a_0/W ratio for the "T" type WOL specimen	129

SECTION 7.1

1	Variability of room temperature toughness with yield strength for 18% Ni Maraging steel. .	150
---	---	-----

LIST OF FIGURES (Cont.)

<u>Figure</u>		<u>Page</u>
2	K_{Ic} as a function of yield strength for 18% Ni maraging steel (various amounts of cold work) . . .	151
3	K_{Ic} as a function of yield strength for 18% Ni maraging steel (various aging treatments)	151
 <u>SECTION 7.2</u> 		
1	"As Received" Microstructure of each alloy system investigated	159
2	Tensile specimens used in this investigation. . .	161
3	Charpy V-notch impact test specimen	162
4	Wedge-opening-loading (WOL) "X" type fracture toughness specimens.	164
5	Wedge-opening-loading (WOL) "T" type fracture toughness specimens.	164
6	WOL fracture toughness specimen ("2X" Geometry)	165
7	WOL fracture toughness specimen ("1T" Geometry)	166
8	WOL fracture toughness specimen ("2T" Geometry)	166
9	25,000 lb. Westinghouse crank machine for fatigue cracking fracture specimen.	167
10	Orientation of test specimens in "As Received" forged plate.	169
11	Clip gage used to establish the load- displacement curves	171
12	Numerical constant " C_3 " as a function of the a/W ratio for the "X" type WOL toughness specimen.	174

LIST OF FIGURES (Cont.)

<u>Figure</u>		<u>Page</u>
13	Temperature dependence of 0.2% yield strength, charpy impact energy and K_{Ic} for HP-9-4-25 steel	177
14	Temperature dependence of 0.2% yield strength, charpy impact energy and K_{Ic} for Ti-6AL-4V titanium.	177
15	Temperature dependence of 0.2% yield strength, charpy impact energy, and K_{Ic} for 7079-T6 aluminum.	178
16	Numerical constant " C_3 " as a function of the a_0/W ratio for the "T" type WOL toughness specimen	179
17	Dimension designations for the "T" type WOL toughness specimen.	180
18	Typical load displacement curve indicating deviation prior to rapid failure.	181
19	Typical load displacement curve indicating deviation prior to "Pop-In"	182
20	Load displacement curve indicating "Pop-In" prior to deviation	183
21	Room temperature fracture appearance of HP-9-4-25 steel WOL toughness specimens	186
22	Room temperature fracture appearance of Ti-6AL-4V titanium WOL toughness specimens.	187
23	Room temperature fracture appearance of 7079-T6 aluminum WOL toughness specimens.	188

SECTION 7.3

1	Equipment used to ultrasonically monitor crack growth.	208
---	--	-----

LIST OF FIGURES (Cont.)

<u>Figure</u>		<u>Page</u>
2	Crack growth rate as a function of stress intensity factor for HP-9-4-25 steel as determined on the "1T" WOL fracture toughness specimen	211
3	Crack growth rate as a function of stress intensity factor for 7079-T6 aluminum toughness specimen.	211
4	Crack growth rate as a function of stress intensity for HP-9-4-25 steel (log-log plot). .	212
5	Crack growth rate as a function of stress intensity for 7079-T6 aluminum (log-log plot) .	212
6	Combined cyclic flaw growth data for HP-9-4-25 steel plate	213
7	Combined cyclic flaw growth data for 7079-T6 aluminum plate.	213

SECTION 8.1

1	The relationship of fracture strength to crack size for different levels of fracture toughness	224
2	Typical crack growth rate properties under cyclic loading.	225
3	Typical cyclic flaw growth data	225

SECTION 8.2

1	A crack in an infinite sheet with uniform normal stress at infinity	240
2	A crack in an infinite sheet subject to centrally applied wedge forces.	240
3	An infinite sheet with a semi-infinite crack subject to a concentrated force	241

LIST OF FIGURES (Cont.)

<u>Figure</u>		<u>Page</u>
4	An infinite sheet with colinear semi-infinite cracks with a concentrated force . . .	241
5	An infinite sheet with load transmitted across a neck between two semi-infinite colinear cracks	241
6	Semi-infinite notch approaching the free edge of a half plane.	242
7	An edge crack in a semi-infinite sheet subject to tension.	242
8	An elliptical crack in an infinite body subject to uniform normal tension	243
9	Concentrated forces applied to the axis of a circular disk crack in an infinite body	243
10	Two equal colinear cracks in an infinite sheet subject to uniform normal stress.	244
11	An infinite array of colinear cracks in an infinite sheet.	244
12	Double-symmetric edge cracks in strip of infinite length subject to uniform tension. . .	245
13	A crack (or cracks) emanating from a circular hole in a sheet.	246
14	Stress intensity factor K at center of the approaching edge of two adjacent coplanar elliptical flaws subject to a uniform normal stress field	247

SECTION 8.3

1	Crack growth rate as a function of stress intensity factor for HP-9-4-25 steel.	267
2	Crack growth rate as a function of stress intensity for 7079-T6 aluminum.	267

LIST OF FIGURES (Cont.)

<u>Figure</u>		<u>Page</u>
3	Combined flaw growth data for HP-9-4-25 steel plate	271
4	Combined cyclic flaw growth data for 7079-T6 aluminum plate.	271
5	Crack growth rate as a function of stress intensity for HP-9-4-25 steel (log-log plot). .	277
6	Crack growth rate as a function of stress intensity for 7079-T6 aluminum (log-log plot) .	277
7	Cyclic life as a function of initial crack size for Materials A and B (Case 1)	278
8	Cyclic life as a function of initial crack length for Materials A and B (Case 2)	278
9	Cyclic life as a function of initial crack length for Materials A and B (Case 3)	279
10	Schematic representation of crack growth rate plotted as a function of ΔK for fixed values of $\gamma = K_{\text{mean}}/\Delta K$	288
11	Variations of external load with time	291
12	Schematic representation of cyclic flaw growth.	293
13	Combined cyclic flaw growth for 7079-T6 aluminum plate.	293
14	Schematic representation of sustained stress flaw.	294
15	Sustained stress data for room-temperature tests of 17-7PH steel	294

SECTION 8.4

1	Hypothetical pressure vessel.	305
2	Graphical solution for ϕ^2 for use with elliptical shaped defects	308

LIST OF FIGURES (Cont.)

<u>Figure</u>		<u>Page</u>
3	Cyclic flaw growth data for aluminum alloy. . . .	312
4	Cyclic flaw growth data for Material B, 200 ksi yield strength steel.	314
5	Cyclic flaw growth data for Material E, a 150 ksi yield strength steel (HY150).	317
6	Crack growth and failure times under sustained loading, HY150 steel.	317
7	Acceptable external flaw sizes.	328
8	Acceptable internal flaw sizes.	329

LIST OF TABLES

SECTION 6.2

<u>Table</u>		<u>Page</u>
I	Comparison of Various Fracture Toughness Specimens	114
II	Recommended Minimum Specimen Dimensions and Ratios of Required Loads.	114

SECTION 7.1

I	Materials for Which K_{Ic} Data are Presented in Appendix I	147
---	---	-----

SECTION 7.2

I	Chemical Analysis of Alloys	157
II	Heat Treatment and Room Temperature Tensile Properties.	158
III	Measurement Capacity Associated with the WOL Fracture Toughness Specimen	165
IV	Cyclic Load Used to Precrack WOL Type Fracture Toughness Specimen	168
V	Room Temperature Tensile Properties and Toughness	172
VI-A	Transverse Tensile Properties of HP-9-4-25 Steel	192
VI-B	Transverse Charpy V-Notch Properties of HP-9-4-25 Steel	193
VI-C	Transverse Toughness Properties of HP-9-4-25 Steel	194

LIST OF TABLES (Cont.)

<u>Table</u>		<u>Page</u>
VII-A	Transverse Tensile Properties of Ti-6AL-4V Titanium	196
VII-B	Transverse Charpy V-Notch Properties of Ti-6AL-4V Titanium	197
VII-C	Transverse Toughness Properties of Ti-6AL-4V Titanium	198
VIII-A	Longitudinal Tensile Properties of 7079-T6 Aluminum	200
VIII-B	Longitudinal Charpy V-Notch Properties of 7079-T6 Aluminum	201
VIII-C	Longitudinal Toughness Properties of 7079-T6 Aluminum	202

SECTION 7.3

I	Cyclic Loading Data.	215
---	------------------------------	-----

SECTION 8.4

I	Materials Initially Considered	303
II	Stresses in the Pressure Vessel for Various Materials.	304
III	Critical Defect Sizes for Catastrophic Fracture During Proof Tests for Various Materials and Types of Defects (Hypothetical Pressure Vessel)	307

TABLE OF CONTENTS

Sections 1 to 5

	<u>Page</u>
1. INTRODUCTION	2
1.1 General Background and Problem.	2
1.2 Phases of the Program	3
1.3 Authorization for the Program	3
2. OBJECT	4
3. SUMMARY.	5
4. CONCLUSIONS.	7
5. RECOMMENDATIONS.	9

Section 1

INTRODUCTION

1.1 GENERAL BACKGROUND AND PROBLEM AREAS

The potential of brittle failure is inherent in the use of high-strength, low-toughness materials which are subjected to high stresses. The present trend toward higher strength materials, higher applied stresses, larger structures and thicker sections further serves to aggravate the brittle fracture problem. In order to minimize weight, the design safety factors in many applications are, by necessity, relatively low. In effect, then, modern applications demand that the utmost performance be exacted from the available materials. This type of situation, therefore, requires an intimate knowledge of the capabilities and limitations of the materials that are contemplated or employed, as well as the use of a modern design philosophy.

Although not currently experiencing any significant amount of brittle fracture problems, the U.S. Army Tank-Automotive Center, anticipating the need for light-weight, highly mobile vehicles, initiated this program to circumvent fracture problems that could arise when the higher strength materials are used in future applications. The objective of the program was to provide the materials and design engineers with the basic information, procedures, criteria, and data that are necessary to properly coordinate material application and design considerations for the prevention of brittle fracture. In effect, this final report is intended not only to provide a comprehensive review of the state of the art, but also to serve as a primer in the use of a modern approach to the combined problem of selection of materials and design against brittle failure.

1.2 PHASES OF THE PROGRAM

The program consisted of three phases. Phase I involved a review and evaluation of available information concerning the various approaches to design against failure, a comparison of the general applicability of the approaches, the selection of the most universal approach, and a summary of the current state of the art for the approach selected. Phase II consisted of tabulating all of the pertinent, valid data available from the literature, identifying the areas of missing data, and performing tests to obtain some necessary data. Phase III developed procedures and criteria and illustrates the application of the selected approach and data to the solution of engineering problems involving selection of materials and design against fracture.

The materials of interest are intermediate- to high-strength steels, and high-strength aluminum and titanium alloys. The application is related to heavy-section tank and automotive components other than armor.

1.3 AUTHORIZATION FOR THE PROGRAM

The work described in this report was authorized by the U.S. Army Tank-Automotive Center (ATAC), Warren, Michigan, under contract DA-30-069-AMC-602(T), Department of the Army Project Number 1, DO-24401-A-105, Ordnance Management Structure (OMS) Code Number 5025.11.26800.01.01. Technical administration of the contract was the responsibility of V. H. Pagano, Section Chief, Metals Section, Materials Laboratory, ATAC. The original ATAC project engineer was C. J. Kropf, and Mr. Kropf was subsequently replaced by E. Moritz.

Section 2

OBJECT

The overall objective of the program is to provide materials and design engineers with data, criteria, and procedures which can be employed to circumvent brittle failure, with particular emphasis on the future use of high-strength materials. Each of the three phases of the investigation have associated sub-objectives as follows:

Phase I - Review and evaluate the available approaches, and select that approach which is most universally applicable to ATAC's requirements.

Phase II - Review, evaluate, and tabulate pertinent data available in the literature, and conduct tests to generate missing data.

Phase III - Develop criteria and procedures for material selection and design against brittle fracture, and illustrate their use in the solution of realistic engineering problems.

Section 3

SUMMARY

In Phase I, several approaches to the brittle fracture problem were reviewed and evaluated in terms of their applicability to ATAC's future need for high-strength materials. The various criteria and approaches are divided into two general categories: (1) the transition temperature approaches and (2) the stress analysis approaches. Several other specific criteria are also described and evaluated.

The linear-elastic fracture mechanics approach was selected as being most universally applicable to the future use of high-strength materials. Therefore, a comprehensive state-of-the-art review of this approach is provided in the report. Although the transition temperature approach was judged to be inadequate for satisfying ATAC's needs involving high-strength materials, a comprehensive review of this approach was also provided, insofar as it may be usefully applied, to the lower-strength materials currently in use.

The first task in Phase II consisted of a comprehensive review of the literature to obtain valid linear-elastic fracture mechanics data. Metals of possible interest to ATAC were included, e.g. steels, aluminum, and titanium alloys. Approximately 100 references whose titles and abstracts suggested the use of some form of fracture mechanics were reviewed. The validity of these data was then evaluated using the most current published criteria for analyzing tests and data, and 27 were found to contain plane strain fracture toughness data which were judged to be valid. These data were extracted from the references and are presented in tabular or graphical form. Represented in these data are several steels of the quenched-and-tempered, maraged, or precipitation-hardened types; three titanium alloys; and three aluminum alloys.

The second task in Phase II consisted of conducting tests to obtain fracture-mechanics fracture toughness data. With the concurrence of ATAC, three materials of possible future interest were selected for testing--one alloy representative of each of three classes of materials (steel, aluminum, and titanium). These alloys were: HP 9-4-25 steel quenched and tempered to 175,000 psi yield strength, 7079-T6 aluminum at 65,000 psi yield strength, and 6Al-4V titanium solution treated and aged to 145,000 psi yield strength. In addition to K_{Ic} fracture toughness measurements,* the slow crack growth rates under cyclic loading were determined for the HP 9-4-25 steel and the 7079-T6 aluminum alloy. The growth rates were measured and the data are presented in terms of "K", the stress intensity factor.

Phase III describes the procedures and criteria that are employed in the utilization of the linear-elastic fracture mechanics approach to the brittle fracture problem. Both fracture toughness and slow crack growth parameters are used in the illustrations and in the discussions of the pertinent areas of material evaluation and selection, design, specifications, inspection and quality control, and performance and life expectancy evaluations.

Example solutions to realistic, hypothetical problems are provided. These involve considerations of such factors as: critical defect sizes, shapes and distributions; critical applied stresses for various defects, geometry and loading conditions; the slow growth of flaws under cyclic or sustained loading from a sub-critical size to a critical size; the relationship of nondestructive inspection capabilities to the defects of concern; and the establishment of specifications and acceptance criteria. Wherever possible, step-by-step procedures are outlined, and their application to materials selection and design are illustrated. All of the various considerations and their interreactions are illustrated by conducting a complete analysis of all of the factors involved in a hypothetical pressure vessel--from initial design considerations to evaluations of life expectancy in the finished product.

* K_{Ic} = Critical stress intensity factor for unstable crack propagation for the opening mode of fracture (I).

Section 4

CONCLUSIONS

Phase I

Of the approaches which were evaluated, the linear-elastic fracture mechanics type of stress analysis approach is deemed to be the most applicable for satisfying ATAC's need for design and material selection criteria for the prevention of fracture in the future use of high-strength materials. The approach is not limited to high-strength, low-toughness materials, but is applicable to any material for which proper fracture toughness parameters can be determined.

Phase II

A large portion of the fracture toughness (K_{Ic}) data which are available in the literature was judged to be either invalid or of questionable validity. The limited amount of published fracture toughness data which did conform to the general requirements for valid plane strain toughness testing is tabulated. The toughness of a given material can vary considerably with various metallurgical parameters; therefore, the material used to establish toughness data must be nearly identical to that used in any given application.

Tests conducted during this program provided additional fracture toughness data on HP 9-4-25 steel, 7079-T6 aluminum and 6Al-4V titanium for the temperature range of -75°F to 150°F . K_{Ic} for these alloys was found to be temperature insensitive, the respective average values being 110, 35, and 70 $\text{ksi}\sqrt{\text{in}}$. Crack growth rates as a function of K_I under cyclic loading were also determined for the steel and the aluminum alloys.

Phase III

When properly employed within the limits of the basic principles, linear-elastic fracture mechanics technology provides engineering procedures and criteria that can be used by designers and materials engineers to obtain quantitative answers to fracture problems. The technology is not restricted to considerations involving catastrophic failure upon a single application of load, but is also applicable to problems involving the slow growth of defects under cyclic or sustained loading conditions. The procedures and criteria are applicable to the areas of design, material evaluation and selection, establishment of specifications and acceptance criteria, quality control during fabrication, proof testing and life expectancy evaluations.

Section 5

RECOMMENDATIONS

As a result of this program, and in view of the continuing advancements in fracture mechanics technology, the following recommendations are provided:

1. A continuing program should be established whereby ATAC can keep abreast of the rapid advancements being made in fracture mechanics technology.
2. A development-type program should be initiated to study the potential of extending linear-elastic fracture mechanics technology, or elastic-plastic modifications thereof, to the low- and intermediate-strength materials of current and near-future interest.
3. Analytical and experimental work should be started to develop fracture mechanics expressions for any unique combined-loading and defect-geometry situations for which no current solutions exist.

Since the current and near-future interests of ATAC evolve around materials of intermediate strengths, consideration of the second recommendation appears appropriate. The applicability of linear-elastic fracture mechanics technology for the higher-toughness, intermediate-strength materials is relatively unexplored. Depending upon the actual section sizes and materials involved, it is possible that plane strain conditions will not prevail for some of the applications of interest. Hence, linear elastic principles will not be applicable in their present form, and some modifications in the direction of elastic-plastic considerations may be required. Therefore, some preliminary efforts to explore this area appears advisable.

The fourth recommendation concerns a problem area which needs some resolution before fracture mechanics technology can be fully utilized. Many of the components of interest, i.e., axles, drive shafts, torsion

bars, etc., are subjected to combined loading such as torsion and bending. At the present time there are no fracture mechanics expressions (relating K_{Ic} toughness, applied stress and defect size) that are applicable to these unique conditions of loading and to some unique combinations of defect and component geometry that are envisioned. Therefore, it appears highly desirable to initiate some effort to analyze these situations and to attempt to develop the required expressions.

TABLE OF CONTENTS

Section 6

PHASE I - GENERAL REVIEW AND SELECTION OF AN APPROACH

	<u>Page</u>
6.1 REVIEW OF GENERAL APPROACHES TO BRITTLE FRACTURE	
6.1.1 Introduction and ATAC Philosophy	15
6.1.2 Transition Temperature Approach.	16
6.1.2.1 Tests for Determining Transition Temperatures .	17
6.1.2.2 Significance and Application of the Transition Temperature Approach.	26
a. Considerations in the Selection of a Transition Temperature Criterion.	27
b. Applicability for Comparison Purposes . . .	29
c. Applicability to Design Situations.	30
d. Applications Where the Use of the Transition Temperature Approach is Uncertain	35
e. Transition Temperature Based Fracture Analysis Diagram.	36
f. General Summary of Applicability of Transition Temperature Approach	40
6.1.2.3 Applicability of Transition Temperature Approach to ATAC's Interest and Project Goals. .	40
6.1.3 Stress Analysis Approach	41
6.1.3.1 Stress Criteria	42
a. Use of Fracture Curve	42
b. Maximum Stress.	45
c. Stress Concentration Factor Approach. . . .	45
d. Use of Stress Gradient as a Parameter . . .	50
e. Applicability of Stress Criteria.	50

TABLE OF CONTENTS (Cont.)

	<u>Page</u>
6.1.3.2 Strain Criteria.	51
a. Exhaustion of Ductility.	51
b. Critically Strained Volume Criteria.	53
c. Use of Strain Hardening Exponent	53
d. Crack Opening Displacement Criteria.	54
e. Applicability of Strain Criteria	54
6.1.3.3 Linear Elastic Fracture Mechanics.	55
a. Energy Criteria.	55
b. Stress Intensity Criteria.	59
c. Applicability of Linear Elastic Fracture Mechanics.	63
6.1.3.4 Elastic-Plastic Analysis	63
6.1.3.5 Statistical Considerations	64
6.1.4 Selection of the Most Applicable Approach	65

LIST OF FIGURES

Section 6.1

REVIEW OF GENERAL APPROACHES TO BRITTLE FRACTURE

	<u>Page</u>
Figure 1. Schematic representation of the various transition temperatures obtainable from the results of Charpy "V"-notch impact tests . .	18
Figure 2. Schematic representation of the relative positions of the crack-starter transition temperatures on the Charpy "V"- notch energy curve.	21
Figure 3. The effect of temperature on the fracture stress and fracture appearance of sharply notched, high strength sheet specimens of a 12% Cr steel	22
Figure 4. The effect of temperature on the stress required for the propagation of a brittle crack.	24
Figure 5. Various transition temperatures obtained on a given plate of steel.	25
Figure 6. Schematic illustration of the Charpy "V"- notch impact behavior of two unlike materials.	30
Figure 7. The effect of temperature on the stress required for propagation of fracture (schematic).	33
Figure 8. Fracture analysis diagram.	38
Figure 9. Ludwik's fracture concept.	43

LIST OF FIGURES (Cont.)

	<u>Page</u>
Figure 10. Effect of change in strain rate $\dot{\epsilon}$ or temperature T on fracture stress	43
Figure 11. True stress-strain curves; after Beeuwkes	44
Figure 12. Elliptic crack in an infinite sheet subjected to normal uniaxial stress.	47
Figure 13. Influence of material and specimen geometry on notch strength behavior.	48
Figure 14. Effect of the equivalent particle size on the K_{tm} vs K curve of a brittle material. . .	49
Figure 15. Stress-strain curve for a small amount of strain hardening.	52
Figure 16. Effect of notch radius on apparent G_c . Schematic based on data for Aluminum 7075-T6 sheets 1/16 in. thick.	59
Figure 17. Coordinates measured from the leading edge of a crack and the stress components in the crack tip stress field.	61

Section 6

PHASE I - GENERAL REVIEW AND SELECTION OF AN APPROACH

6.1 REVIEW OF GENERAL APPROACHES TO BRITTLE FRACTURE

6.1.1 INTRODUCTION AND ATAC PHILOSOPHY

Prior to selecting an approach to be employed throughout the program, it was deemed advisable to review the various brittle fracture approaches that have been employed or suggested, and to evaluate these in terms of their applicability to ATAC's requirements. It was recognized that the most widely used approach is the ductile-to-brittle transition temperature approach. However, it was also recognized that the transition temperature approach lacked much of the quantitiveness that was required, and its applicability was questionable with respect to the use of the higher strength materials. The potential of the more recently developed linear elastic fracture mechanics approach (commonly referred to as "fracture mechanics", "fracture toughness", or "crack toughness") to provide quantitative answers was also recognized. While primary consideration was given to these two approaches, several other approaches were also evaluated. The following sections are devoted to discussions of the various approaches.

The first section (6.1.2) which follows provides a rather comprehensive review of the various types of approaches which fall into the general category of transition temperature approaches. While it was generally recognized that these approaches would not be applicable to the future use of high strength materials, it was believed that a thorough description and discussion of the transition temperature criteria would be of value in the use of the lower strength materials.

The other approaches are described in the next section (6.1.3) under the general heading of "stress analysis approaches". Included are

the various stress and strain criteria considered to be in the general fracture mechanics category. The linear elastic fracture mechanics approach, which is receiving much current attention, is one of the criteria considered.

6.1.2 THE DUCTILE-TO-BRITTLE TRANSITION TEMPERATURE APPROACH

Because of the vast experience and general usage of this approach, a relatively comprehensive discussion is presented. The transition temperature approach has been in use for many years. The basic philosophy is relatively simple - a material has a characteristic temperature below which it is susceptible to low-stress, brittle-fracture in the presence of sharp defects, and above which brittle fracture does not occur. Above the transition temperature the behavior of the material containing defects is controlled by the conventional plastic properties. Innumerable tests employing both static and dynamic loading are utilized to measure the transition temperature, but all of these have one common feature: In the presence of a sharp notch or defect the material undergoes an abrupt transition from a ductile to a brittle behavior over a narrow range of temperature as measured by the change in some property. The various tests, properties, and criteria can be grouped into one of the four general categories which follow.

1. The temperature at which the capacity of the material for gross plastic deformation in the presence of a very sharp notch or crack decreases rapidly to essentially zero (tough-frangible transition temperature).

2. The temperature at which the mode of fracture propagation readily changes with decreasing temperature from fibrous to cleavage, or from a full shear to a flat fracture surface (fracture mode transition temperature).

3. The temperature at which the fracture strength of a sharply notched or pre-cracked specimen decreases rapidly from values which are well above to values which are well below the conventional yield strength (fracture stress transition temperature).

4. The temperature above which a running crack will be arrested (crack arrest transition temperature).

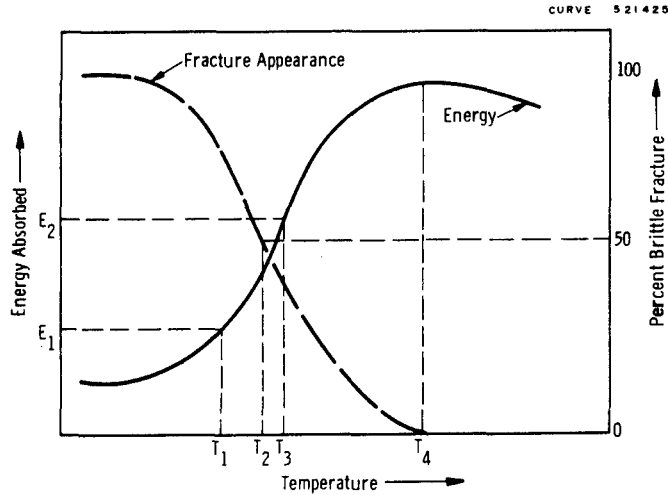
Of these four transition temperature definitions, the first two have undoubtedly received the most attention. One or more, generally several, test procedures may be used to obtain transition temperatures in each of the four categories. While the class of definition that is preferred dictates the basic type of test that may be used, the details of the test procedures and techniques may vary considerably. Usually the particular technique that is employed is based in large part on the type of application that is of concern and the personal preference of the investigator.

6.1.2.1 Tests for Determining Transition Temperatures

While it is impractical to describe all of the tests that have been employed, some of the more commonly used ones for each of the transition temperature definition categories warrant discussion. A much more comprehensive review of the various test techniques may be found in the literature.^{(1-3)*}

The Charpy "V" notch impact test is undoubtedly the most commonly used test. Several transition temperatures may be ascertained from any one given set of data obtained from these impact tests since several criteria may be employed. Both the tough-frangible and fracture mode types of transition temperatures are represented in this test. Some of the various criteria are illustrated in Figure 1. T_1 is the transition temperature as determined by some fixed level of impact energy, E_1 . The specific energy level is usually determined by correlations with other types of tests or service performance; occasionally it is defined on the basis of what can be anticipated from commercially available material. This fixed energy criterion is used fairly extensively, particularly for quality control evaluations and acceptance tests of structural steels. The FATT (T_2 , Figure 1) fracture appearance transition temperature

*Superscripts refer to the bibliography which is to be found at the end of each major division separated by dividers and tabs.



Sec. 6.1 Fig. 1— Schematic representation of the various transition temperatures obtainable from the results of Charpy "V" notch impact tests

(50% shear - 50% brittle) criterion is also used quite frequently. It is chiefly used in development work for comparative evaluations of materials. The basis of selecting FAT_T at 50% brittle fracture is somewhat arbitrary. Some correlations between FAT_T and service performance and/or other types of tests have been suggested.⁽⁴⁾ T_3 , or the mid-point of the energy transition, is another arbitrary choice based on ease of measurement. The temperature " T_4 ", above which the fracture appearance is entirely shear, represents the most conservative criterion in that it yields the highest transition temperature coupled with the maximum energy for fracture. Because of practical limitations this criterion is seldom used except in development investigations or applications requiring an extremely high degree of toughness.

There are several modifications of the Charpy impact tests which principally involve variations of the specimen geometry primarily the notch configuration; i.e., Charpy keyhole or U-notch, the Schnadt notch, the low-blow or pre-cracked test,⁽⁵⁾ and the brittle-boundary Charpy test.⁽⁴⁾ There are also modifications in the loading system from beam

(Charpy), to cantilever loaded (Izod). However, in general, the results of these tests are interpreted and applied in similar fashions.

The notched impact tests may also be interpreted in terms of the lateral expansion* which occurs in the test specimen opposite the root of the notch. This in essence is a measure of the ability of the material to accommodate plastic deformation in the presence of a notch and therefore belongs in the tough-frangible category of transition temperature classifications. An inflection in the temperature dependence of the lateral contraction or some arbitrary fixed value of contraction may be used to establish the transition temperature.

Another generally known type of transition temperature measurement belonging in the tough-frangible category is NDT, "nil-ductility transition temperature", which is determined using the "drop-weight" test technique.^(6,7) This is simply a "go-no-go" test which defines the temperature below which the capacity of the material to undergo a small amount of plastic deformation in the presence of a sharp notch is essentially nil under impact loading conditions. The test utilizes a plate-like specimen which is supported at the ends and subjected to a rapidly applied load by virtue of a weight being dropped at mid-span. A brittle weld bead on the underside (the tension side) of the plate serves as the crack starter since a brittle crack forms in this bead at a small value of strain. As the specimen continues to bend under the impact load, this crack may or may not propagate in a brittle manner throughout the section of the specimen. A stop under the specimen prevents excessive plastic bending; consequently the specimen remains unbroken unless a relatively high degree of brittleness exists. The highest temperature at which the specimen breaks is defined as the nil-ductility transition temperature. This test has been widely applied to structural steels, and in some instances forms the basis for acceptance and quality control tests. Quite often the NDT temperature is correlated with the Charpy V-notch impact energy at the corresponding temperature

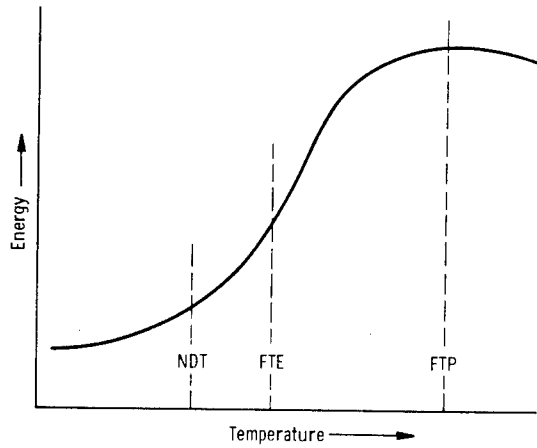
*Lateral contraction of the sides of the impact specimen is also employed for the same purpose.

thereby providing a secondary standard commonly referred to as a "fix". The Charpy impact energy corresponding to NDT can vary appreciably between materials being as low as 5 to 10 ft lbs in some mild structural steels to 50 to 60 ft lbs in heat treated alloy steels. Good correlations have been reported⁽⁸⁻¹¹⁾ between drop-weight test results and brittle service failures involving several types of steel.

Another form of crack-starter test, the explosion bulge^(5,7) has been used to evaluate primarily the crack propagation characteristics of materials. In this case the sample consists of a square plate (or weldment) with a brittle weld bead on the underside. The plate is placed on an open die and an explosive charge is detonated over the plate. The materials are rated with respect to the nature and extent of the resulting deformation and cracks. When tested over a range of temperatures, the performance of a given material changes from extensive plastic bulging at high temperatures, with or without some ductile shear tearing emanating from the brittle weld bead, to a flat, brittle, shattering type of fracture at low temperatures. The nature and degree of cracking varies between these extremes. The highest temperature where extensive deformation without brittle cracking occurs is referred to as F.T.P., fracture transition plastic, which is the order of 120^oF above the NDT temperature. The temperature below which the cracking begins to extend beyond the deformed material into the elastic loaded edge regions has been designated FTE, fracture transition elastic. FTE always occurs at a temperature higher (~60^oF) than NDT. A brittle shattering type of fracture is always obtained at temperatures corresponding to NDT. The relative positions of these transition temperatures superimposed on a Charpy V-notch impact energy curve for the general case is shown in Figure 2. Naturally, because of the practical considerations involved in conducting the explosion tests, it is not so widely used as the drop weight or Charpy impact tests.

Other more recently developed crack starter tests are the drop weight tear and the explosion tear tests.⁽¹¹⁾ The explosion tear test is a measure of the ability of the material to undergo plastic deformation in the presence of a through-the-thickness defect, whose length

CURVE 521426



Sec.
6.1 Fig. 2- Schematic representation of the relative positions of the crack-starter transition temperatures on the Charpy "V" notch energy curve.

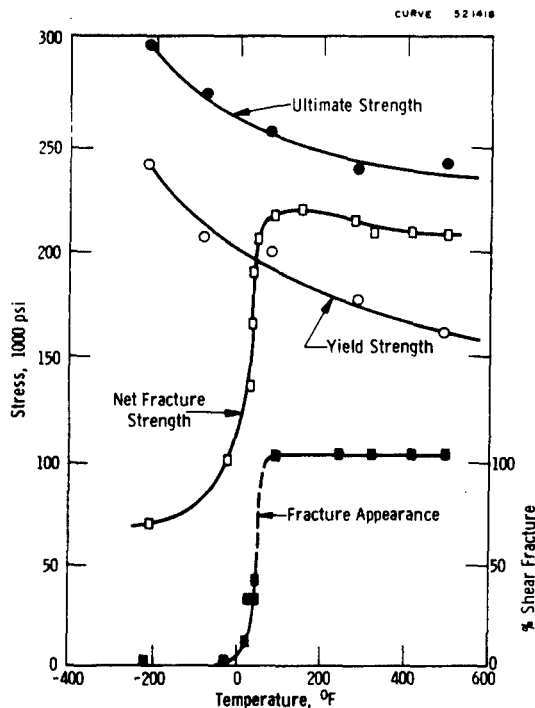
is twice the specimen thickness, without significant extension of the defect. The results of the explosion tear test are related to drop weight tear test results, which can in turn be related to Charpy V-notch test data. (11)

The foregoing test techniques have all been concerned with transition temperature measurements in the tough-frangible and fracture-mode categories. There are innumerable others which fall into these same categories. Among these are the slow bend tests, (12-15) the notched tensile tests, (16-20) the tear tests, (21-23) and others. In all these tests some property, ductility, energy, fracture appearance, etc., changes rapidly with decreased temperature and forms the basis for defining the transition temperature.

The work which has been conducted relative to the third category of transition temperature (fracture-stress transition) is not nearly as extensive or as well developed as for the previous categories.

In essence, this category includes those tests where the fracture stress is measured as a function of temperature and where it exhibits a relatively abrupt change from values which are greater than, to values that are less than, the normal yield strength at that equivalent temperature. This temperature, or range, may be considered as the transition temperature. Several specimen configuration and loading conditions may be used, all of which involve a sharp notch. ⁽²⁴⁻²⁹⁾

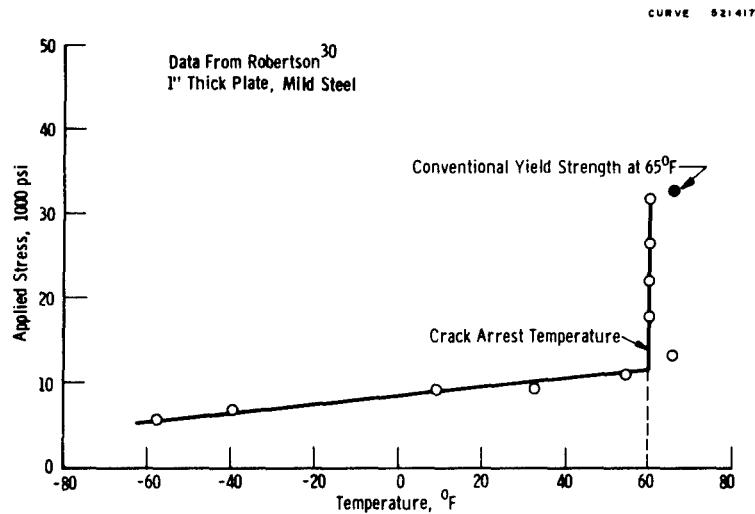
Generally, but not always, the transition in fracture stress is associated with a similar change in some other property; i.e., ductility, fracture mode, fracture appearance, etc. In some cases, the change in one of these other properties has proven to be a better criterion; for example, the "FST", full shear transition, defined by Srawley. ⁽¹⁹⁾ There seems to be a general difference between the behaviors of the low strength structural steels and higher strength materials. The lower strength materials fail to exhibit the fracture stress transition even though ductility and fracture mode transitions occurs. ^(17, 18, 25) In the higher strength materials, the transition in all properties appear to coincide. Figure 3 is a typical example.



Sec. 6.1 Fig. 3 — The effect of temperature on the fracture stress and fracture appearance of sharply notched, high strength, sheet specimens of a 12% Cr steel. Srawley & Beachem ¹⁹

Since the fracture stress, hence the fracture stress transition temperature, is dependent upon specimen size and notch acuity,⁽³⁰⁾ caution must be exercised in employing the fracture stress transition temperature. The primary application for this type of test is for comparative purposes. However, the test technique can be particularly useful in design for sheet materials where full thickness tests can be conducted. In this case, the results are directly applicable to design when proper consideration is given to the effects of defect size.⁽²⁹⁾

Another category of transition temperature definition is concerned with the temperature at which a running cleavage crack will be arrested, commonly referred to as the "crack arrest temperature". Tests to measure the crack arrest temperature generally involve developing a fast moving brittle crack and determining the stress-temperature conditions necessary to arrest the crack. Robertson has reported extensive work of this type.⁽³¹⁻³⁴⁾ In the Robertson test a relatively large plate is loaded to a uniform tensile stress with a temperature gradient across the width of the plate. A cleavage crack is started by an explosive charge on the side of the plate containing the cold end of the temperature gradient. The uniform tensile stress imposed on the plate keeps the crack growing across the specimen until it reaches a temperature that is high enough to permit sufficient plastic flow to stop the crack. By conducting a series of tests where stress is varied, one can obtain the relationship of stress and temperature. A typical set of Robertson's data is shown in Figure 4 for a 1" thick plate of ordinary mild steel.⁽³²⁾ Note that at about 60°F, the stress can be raised markedly (3 or 4 times) without any accompanying increase in the temperature at which the crack stops. This is termed the ductile-arrest temperature (fracture arrest transition temperature). The arrest temperature decreases with decreasing plate thickness, hence full thickness tests should be used in this type of evaluation. Because of the stress transition associated with the arrest temperature, this test could also be classified in the previously discussed fracture-stress transition temperature category.



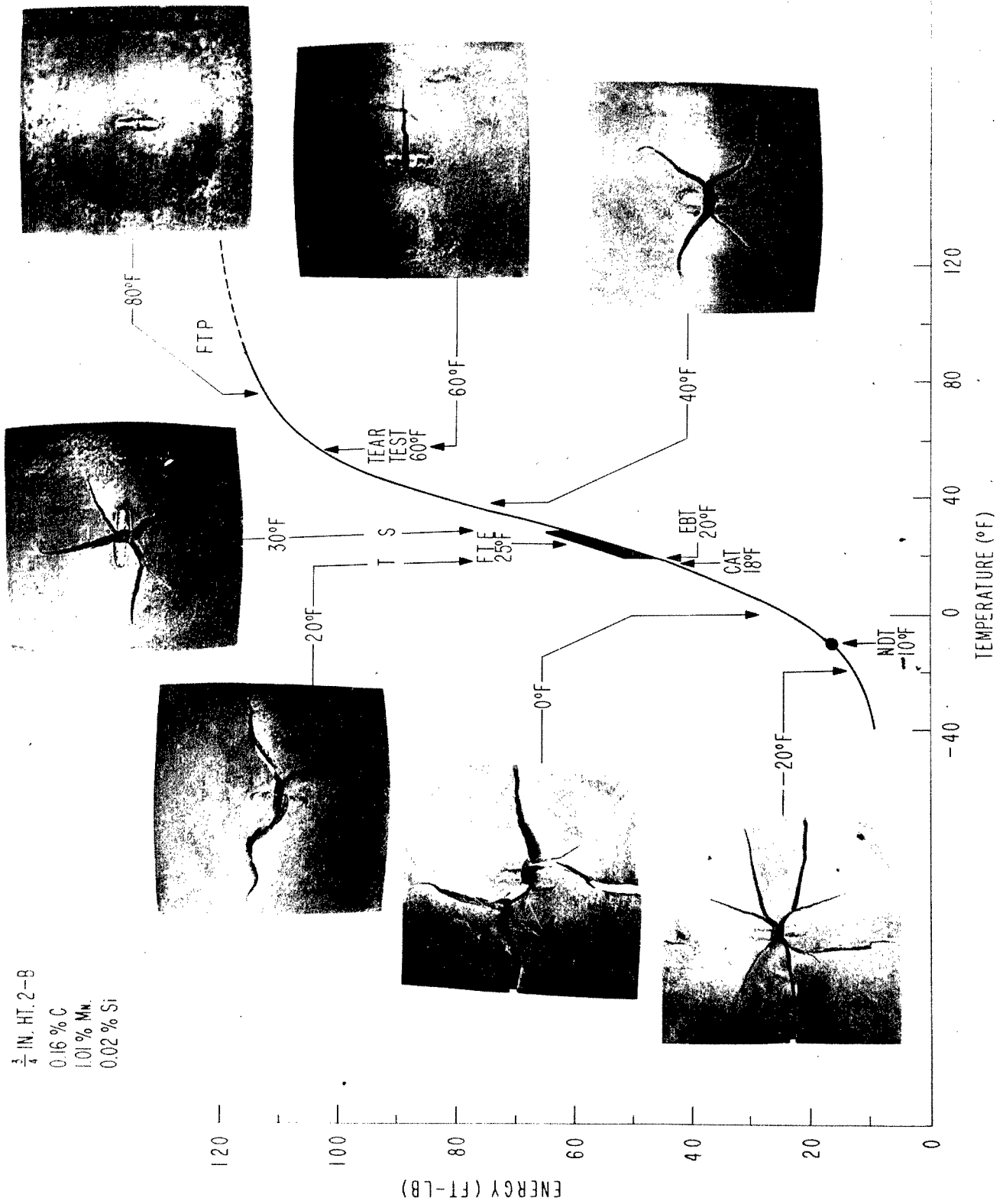
Sec. 6.1 Fig. 4 — The effect of temperature on the stress required for the propagation of a brittle crack³²

The Robertson test has subsequently been modified by others^(35,36) into a constant temperature type of test (SOD) in order to eliminate any uncertainties caused by the temperature gradient. Good agreement between service failures and the SOD tests have been obtained. Similar test techniques and the applications of the crack arrest temperature concepts, particularly with regard to welding, have been employed by Wells,⁽³⁷⁾ Mosborg,⁽³⁸⁾ and others.

The crack arrest transition temperature type of test, although somewhat bulky, it useful for development, comparison, quality control, and design purposes. It should be emphasized that full thickness tests are necessary to obtain representative data. Since a designer is accustomed to working with stresses, this approach is particularly attractive because it not only provides him with a transition temperature but also with a knowledge of the critical stress for propagation of cracks as a function of temperature. A significant feature is that the critical applied stresses for failure below the transition temperature are alarmingly low; thereby implying that a safe design is impractical in many cases.

The relative positions of several of the transition temperature criteria are shown superimposed on a Charpy V-notch impact energy curve for a given material in Figure 5. These data from Pellini and Srawley⁽³⁹⁾ are unique, for this is the only example in the literature of such a

$\frac{1}{4}$ IN. HT. 2-B
 0.16 % C
 1.01 % Mn.
 0.02 % Si



Sec. 6.1 Fig. 5 Various transition temperatures obtained on a given plate of steel.

comprehensive collection of transition temperatures for a specific plate of any given material. Such a picture is extremely useful in illustrating the relative degrees of toughness represented by the various transition temperature criteria. The maximum toughness, which may be required in extremely severe applications, is depicted by FTP (80°F) measured by the explosion crack starter test.^(6,7) A similar high level of toughness prevails at 60°F which is the Navy Tear Test⁽²¹⁻²³⁾ transition temperature. Good agreement is obtained between FTE (fracture transition elastic by explosion crack starter test), EBT (Esso brittle temperature from SOD test),^(35,36) and CAT (crack arrest temperature from Robertson test)^(31,34) at 18 to 25°F. All three of these transition temperature criteria pertain to crack propagation abilities and depict the temperature above which the propagation of cracks is relatively difficult. These criteria generally represent an adequate level of toughness for most all applications, except those where high applied stresses and the possibility of gross plastic deformation prevails. NDT, at -10°F, describes the minimum level of toughness that is acceptable* under nearly any circumstances where a sharp notch is present and the applied stresses are sufficient to cause yielding in the highly localized region at the tip of the notch. At temperatures below NDT, brittle fracture can initiate and readily propagate at average applied stresses that are only a small fraction of the conventional yield strength.

6.1.2.2 Significance and Application of the Transition Temperature Approach

The applicability of the transition temperature approach to the problem of brittle failure varies considerably depending upon the criterion that is used and the purpose to which it is applied. While it may be used directly in its simplest form for comparative evaluations of the fracture resistance of materials, its application to design may in many instances

*Some materials can be used safely below NDT, but this requires an intimate knowledge of their fracture characteristics in terms of the inter relationships of the magnitude and nature of the stresses; the size, shape and distribution of defects; and geometric considerations of the member.

be quite complex or even impractical. For comparative purposes, almost any one of the various transition criteria may be used directly with a reasonable degree of confidence that the material which exhibits the lowest transition temperature is likely to be the most fracture resistant. In some design situations the transition temperature may be very useful for establishing design parameters. On the other hand for some complex applications, the selection of an appropriate transition temperature criterion and its subsequent translation into useful design parameters can be extremely involved. In other applications, e.g., where a material must be used below any of the conventional transition temperatures, or where the material does not exhibit an abrupt ductile to brittle transition behavior, the approach is virtually useless as a design tool. In subsequent paragraphs the discussion will be directed towards providing an appraisal of the applicability and usefulness of the transition temperature approach to the various phases of the brittle fracture problem.

a. Considerations in the Selection of a Transition Temperature Criterion

While the basic concept of the transition temperature approach is quite simple, its implementation in practical situations can be complex. Some of the complexities arise primarily because of the existence of the different kinds of transition behavior and the many criteria of transition temperatures within any given behavior category. Ideally, if each test and each transition behavior yielded a common transition temperature there would be no problem. Obviously this is not the case. Therefore the choice of a criterion for transition temperature for a particular application involves the consideration of many factors, some of which are: What embrittling factors are present? Which behavior transition is most pertinent? What degree of assurance against brittle failure is required? What are the practical limitations regarding size, weight, cost, material availability, etc.?

Relative to embrittling factors, consideration must be given to such aspects as: the size, shape, distribution and acuity of the

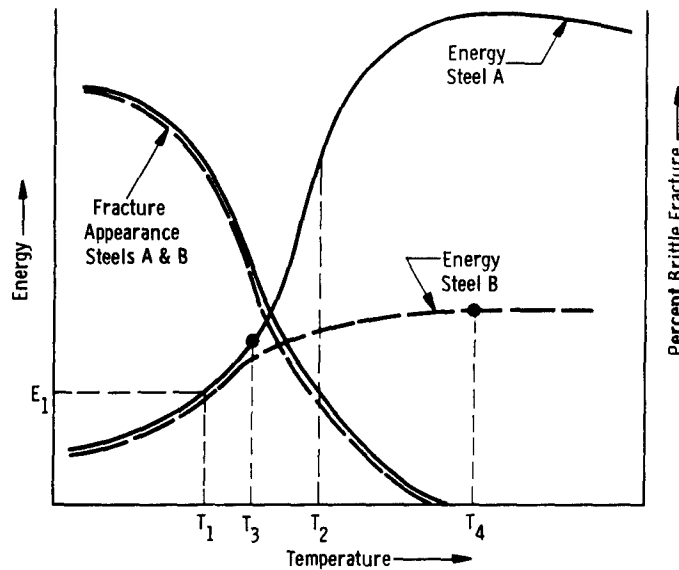
notches or defects that are assumed to be present; the level of the applied stresses; the type of loading, the size of the structural members, the minimum operating temperature, etc. Large complex structures, large sharp notches, high applied stresses and impact loading suggest the use of a conservative type of transition temperature, i.e., FTP as measured in the explosion tests.

With respect to behavior transitions, one may be concerned with either the initiation or propagation of fracture. In cases where, because of prevailing circumstances, it must be assumed that initiation of fracture will occur, it is then necessary to guard against propagation. This situation suggests the use of a crack arrest transition temperature such as determined by the Robertson or SOD test, or alternatively, the FTE measured in the explosion test. These transition temperatures may be interpreted in terms of stresses and temperatures which limit crack propagation. In some situations, this may not be practical, and it may be necessary to risk the chance of propagation and attempt to guard against initiation. The use of a less conservative transition temperature criterion such as NDT measured by the drop weight test may be applicable in this situation to guard against fracture initiation. However, for most materials and applications it must be realized that if fracture initiation does occur, subsequent propagation is quite likely since NDT is lower than the crack arrest temperatures of CAT, SOD, or FTE.

Considerations regarding the required degree of assurance against brittle failure are obvious. While all brittle failures are undesirable, certainly the dire consequences of the failure of a nuclear reactor pressure vessel, a submarine hull, a turbine generator rotor, etc., are far more serious than the isolated failure of some minor piece of equipment. These considerations quite naturally reflect in the degree of conservatism employed in the selection of a transition temperature criterion. Finally, practical limitations of size, cost, availability of material, etc. all add to the complexity of selecting a transition temperature criterion.

b. Applicability for Comparison Purposes

The transition temperature approach is used quite extensively for the purpose of comparison of materials. For this purpose, it is generally quite useful and reliable. However, depending upon the purpose for which the comparison is intended, there are some considerations which should not be neglected in interpreting the data. If the comparison is confined to a given class of materials of approximately the same strength level, the interpretation is quite straightforward. The material with the lowest transition temperature is most likely to be the most fracture resistant regardless of the transition temperature criterion employed. However, this generalization cannot be extended to the comparison of unlike materials, for example, steels of two different strength levels. Figure 6 is a schematic representation of the Charpy V-notch impact curves of two steels. Steels "A" and "B" could represent any one of several situations: markedly different strength levels with "B" being the stronger, the same strength level but different microstructures, "A" being fine tempered martensite and "B" being coarse bainite, the same steel from the same plate but with different orientations of the test specimens - "A" being longitudinal and "B" being transverse. On the basis of any of the fracture appearance transition temperature criterion these steels would have identical transition temperatures. Referring to Figure 6, at some fixed energy level such as E_1 again the transition temperatures (T_1) would be the same. Now assuming the minimum operating temperature is T_2 , which steel is the most fracture resistant at that temperature? It seems obvious that steel "A" which requires more energy for fracture would be the most fracture resistant at T_2 . A knowledge of the transition temperature alone would not show this. While some of the transition temperature criteria would fail to differentiate between the steels, some other criterion may be capable of doing so, i.e., the NDT temperatures of the steels could be T_3 and T_4 . Similarly, a crack-arrest criterion of transition temperature may also reveal the difference between the steels. Thus, it is apparent that even for simple comparative purposes proper consideration must be given to the proper choice of a transition temperature criterion and the subsequent interpretation of the results.



Sec. 6.1 Fig. 6— Schematic illustration of the Charpy "V" notch impact behavior of two unlike materials

c. Applicability to Design Situations

The application of the transition temperature approach to design becomes even more complex than for the simple comparison of materials. However in some cases, with proper consideration, the approach can be quite fruitful. In design, the ultimate question involves the load-bearing capacity of the structure or member for the prevailing circumstances and the relationship of transition temperature to the load-bearing capacity. For lack of something more specific to answer this question, a general concept has come into wide acceptance. In essence, this concept is that for temperatures above the transition temperature, stresses of the order of the normal yield stress may be tolerated, and below the transition temperature the applied stress must be kept to some unknown lower level. Although generally applicable in principle, this concept leaves much to be desired. However, with proper consideration, some transition temperature measurements can be used to obtain qualitative estimates concerning load-bearing capacity. On the other hand, there are also some situations where the transition

temperature approach is nearly useless in this respect. Both of these aspects will be considered in the discussion which follows.

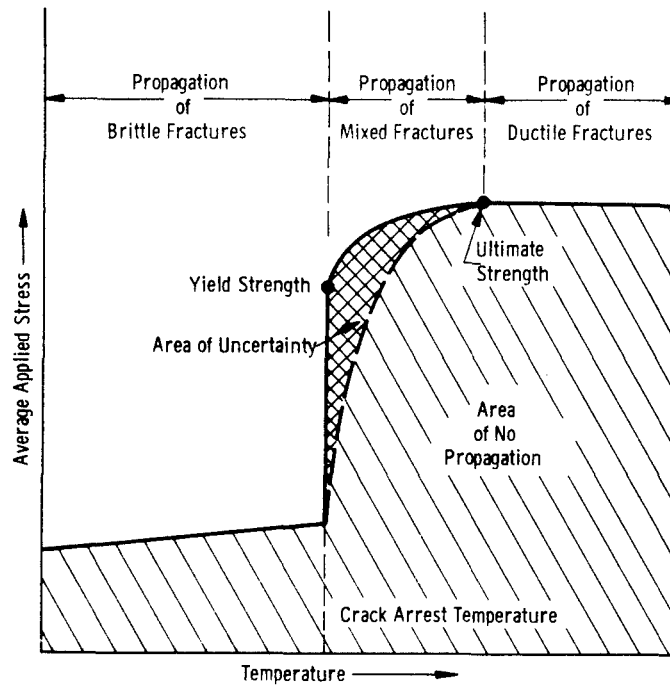
In utilizing the transition temperature approach in design, the first problem is determining which transition behavior and associated transition temperature criterion is most pertinent to the application. Then, after having established some preferred criterion, the problem becomes one of translating this transition temperature into load-bearing terms. The initial problem of selecting a transition temperature criterion has been discussed earlier in this report and in the literature.^(39,40) Primarily, it is a matter of deciding what degree of toughness is required for the application in question, and which of the criteria best describes the embrittling conditions that are of concern. A designer upon proper consideration of all of the factors involved, can generally choose the most representative criterion. Subsequent discussion will deal more specifically with the translation of a transition temperature into load-bearing terms.

One sound solution to the general design problem is based on the establishment of a correlation between service performance (preferably failures) and transition temperature. A well-established relationship of this kind has been obtained for one class of materials and application. A statistical study of steel plates from failed ships indicated that brittle catastrophic failure was very unlikely if the 15 ft lb., Charpy V-notch, impact energy transition temperature was below the minimum operating temperature.⁽⁴¹⁾ Hence for this particular class of material and this particular application, the 15 ft lb transition temperature criterion is very useful and reliable. Similar relationships between NDT and service failures have also been reported⁽⁸⁻¹¹⁾ for other steels and applications. When a sufficiently well established correlation between transition temperature and service performance exists, the transition temperature approach can be used with a reasonably high degree of confidence. While this type of correlation does not yield direct data concerning load-bearing capacity, it does through service experience provide some insight as to the general stress level that can be sustained above the transition temperature.

It must be appreciated that this approach to the brittle failure problem requires a correlation that is specific to the material and the particular application conditions. The results of such a correlation cannot be directly applied to another class of material or another application. Likewise, for a given situation, any change in material and/or the embrittling factors present in the application will necessitate reconsideration of the applicability of the correlation.

Another approach available to the designer involves the use of a transition temperature measurement which also incorporates a direct measurement of the load-bearing capacity. The Robertson⁽³¹⁻³⁴⁾ or the SOD^(35,36) crack arrest transition tests are good examples. These tests yield data of the type illustrated schematically in Figure 7. This approach is related specifically to the propagation of cracks. It is most applicable to those situations where a designer must assume that a fracture will be initiated in some manner or another but when initiated, the fracture must not be permitted to propagate catastrophically. The application of this criterion is straightforward. If the crack arrest temperature is below the minimum operating temperature, there is little concern about catastrophic brittle failure at normal design stresses; except perhaps for the small area of uncertainty shown in Figure 7. The probable limitations on applied stress above the crack arrest temperature are more directly related to plastic distortion or rupture. However, if the minimum operating temperature is below the crack arrest temperature, brittle catastrophic fracture can occur at alarmingly low values of applied stress. In many situations the allowable stresses for applications below the crack arrest temperature are so low that it becomes impractical to use this approach because of the large section sizes that would be necessary to keep the stresses low.

It must be emphasized that the reliability of the crack arrest transition temperature approach is directly related to the size of the plate used to determine the crack arrest temperature. The arrest temperature increases with increasing plate thickness.⁽³¹⁾ Therefore, for a high degree of reliability, a plate thickness corresponding to that of the application must be used in ascertaining the transition temperature.



Sec. 6.1 Fig. 7—The effect of temperature on the stress required for propagation of fracture (schematic)

Therein lies the major limitation for the use of this transition temperature criterion. While perfectly applicable to structures involving plates which can be conveniently tested in full thickness, it is of little direct value for heavy sections such as forgings.

There is another type of transition temperature criterion that yields at least semi-quantitative information relative to load-bearing capacity. This is confined principally to applications involving high strength sheet materials, and the use of pre-cracked tensile specimens to measure transition temperatures. These types of test yield transition temperatures based on a change of fracture stress, ductility, and/or fracture appearance as was described in Section 6.1.2.1 of this report. When full thickness specimens containing flaws simulation those that may prevail in the application are employed in the tests, the resulting data may be used for design with a reasonable degree of confidence. Such tests have also proven valuable as a screening device and in providing essential data for the "fracture mechanics" approach to brittle fracture. (29)

The transition temperature derived from the crack-starter types of tests (NDT from drop weight and FTE and FTP from explosion tests) also may be used to estimate allowable stresses. For example, at or above the FTP temperature the development of extensive plastic deformation and a high resistance to shear tearing in the explosion tests is certainly indicative that stresses well in excess of the yield strength can prevail without danger of brittle fracture*. At or above FTE cracks may be started by the high stresses which prevail in the plastically loaded region, but these cracks will not continue to propagate in areas that are elastically loaded. In essence then, the load-bearing capacity defined by FTE may be generalized as follows: at or above FTE applied stresses of the order of the yield strength are required to initiate and sustain fracture, while below FTE, fracture once initiated will propagate at applied stresses less than the yield strength.

The drop weight NDT is less useful for design purposes in terms of defining load-bearing capacity. At NDT, brittle fracture can be initiated in the presence of a sharp notch if the applied stresses are sufficient to develop yielding at the highly localized region near the tip of the crack. This really doesn't help the designer very much unless he is able to ascertain what level of applied stress will result in localized yielding at the tip of some flaw. Because of the many complicating factors, i.e., stress concentration, plastic restraint, residual stress, etc., the determination of this critical applied stress level is quite difficult. In those cases where a correlation of NDT and service failures exist, it may be possible to approximate the critical stress level from a knowledge of the existing stresses. A fracture once started at NDT or lower will most likely propagate catastrophically since in most applications the average applied stresses are undoubtedly in excess of the propagation requirement.

*In some materials a low energy form of catastrophic shear failure can develop at temperatures corresponding to FTP. This behavior is more characteristic of high strength materials that demonstrate a low energy shelf in the Charpy V-notch impact test. Because of its influence on load-bearing capacity, it too must be given proper consideration.

d. Applications Where the Use of the Transition Temperature Approach is Uncertain

The greatest difficulty in applying any of the transition temperature criteria to design is encountered in the application involving large section sizes, i.e., generator or turbine rotors, fly wheels and shafts, thick-walled pressure vessels, large forgings, etc. Tests for determining transition temperatures of full size large sections are not practical. There is a great deal of uncertainty regarding the applicability of any transition temperature criteria as determined in small section sizes to design situations involving large section sizes, and the uncertainty is becoming more prevalent with the increasing amount of fracture testing on large section sizes. Increasing the gross dimensions of the test specimen, or the notch size, or the notch acuity all tend to induce transition temperatures at higher temperatures, particularly with reference to load-bearing capacity. Several examples of this trend of behavior may be found in the literature. (20,31,42-48)

In addition to increasing the degree of uncertainty relative to the applicability to very large section sizes, thus the possible effects of size on transition temperature determinations casts of doubt regarding the reliability of all transition temperature criteria in cases where full section sizes are not employed in the determinations. This is the major area of uncertainty which is currently receiving much attention. There have been some attempts (45,46,49-52) to relate the results of other types of fracture toughness measurements obtained from tests of large sections to some of the conventional transition temperature criteria. But, as yet, the usefulness and reliability of these correlations remains unproven. Therefore, until some firm assurance can be obtained to the effect that the transition temperatures measured in small size tests are indicative of the behavior of the material in large section sizes, the usefulness of the transition temperature approach for applications involving very large sections is limited to the comparison of materials. In comparing materials, it seems reasonable to assume that the same relative degree of toughness will prevail at various section sizes. However, there is only a limited amount of experimental data to this effect.

There are also applications where, from the design viewpoint, the transition temperature approach is virtually of no value whatsoever. The most obvious of these is in the application of materials which do not exhibit a normal characteristic ductile-to-brittle transition behavior, but which may fail in a brittle manner*. Another involves those situations where there is no alternative but to use a material in the sub-transition temperature range. As discussed previously, the crack-arrest transition temperature criteria may be of value in this latter situation since these criteria do describe the sub-transition temperature dependence of the critical stress for the propagation of fracture. However, it may be impractical to design on the basis of the critical propagation stress because these stresses are generally quite low and large sections would be required. Likewise, it may not be possible to obtain reliable data of the crack arrest type if thick section sizes are involved or if the material is in some form other than plates. Current available data of this type are limited to carbon steel plates up to about 1" thick. Excluding then, the crack arrest transition temperature criteria, the transition temperature approach provides the designer with no means of predicting load-bearing capacity at sub-transition temperatures. In both these situations (the non-existence of a transition temperature or use below the transition temperature) some other approach which relates the load-bearing capacity to the material characteristics and prevailing embrittling factors must be utilized.

e. Fracture Analysis Diagram

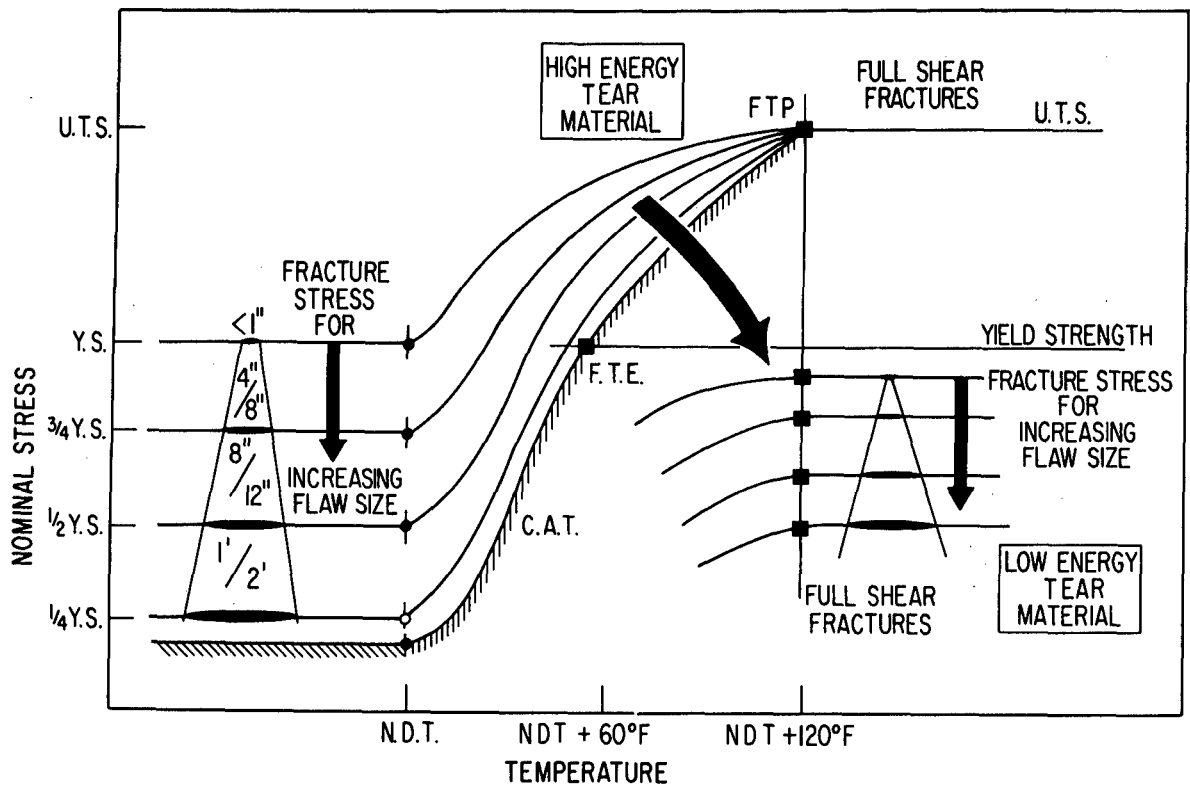
Through the correlation of the various laboratory and simulated service tests, and actual service failures, it has been possible⁽⁹⁻¹¹⁾ to construct a "Fracture Analysis Diagram" which represents the most sophisticated form of the transition temperature approach that is

*Fail in a brittle manner does not necessarily imply that cleavage (transgranular) fracture occurs. It is also possible to have failures at relatively low applied stresses and without any gross plastic deformation by other fracture mechanisms, i.e., catastrophic shear, intergranular failure, fatigue, stress corrosion, and other forms of environmental effects.

presently available. This diagram⁽⁹⁻¹¹⁾ relates the three parameters of applied stress, defect size, and temperature, Figure 8. It is applicable to the structural grades of steel which exhibit a pronounced temperature dependent ductile-to-brittle transition behavior, and to section sizes of the order of 1/2 to 2" thick. With this diagram and a knowledge of one the transition temperatures (preferably NDT) of the material to serve as a reference point, it is possible to approximate the critical combinations of stress and overall defect size which will cause catastrophic failure.

Detailed descriptions of the basis and development of the diagram, and its use, are available in the literature.⁽⁹⁻¹¹⁾ Therefore, only a brief explanation is required in this report. The diagram (Figure 8) is based on the results of laboratory tests of various transition temperature criteria and their correlation with one another, simulated service tests, and actual service experiences. The significance of the three transition criteria NDT, FTE, and FTP, shown in Figure 8 for the high-energy tear material was previously discussed. The CAT (crack arrest temperature) curve is based on the Robertson or SOD types of tests, and pertains to the propagation of cracks. It describes the critical stress-temperature combination for the arrest of a running, brittle crack. Cracks will not propagate at stress temperature combinations which lie below the CAT curve. The other curves lying above the CAT curve are constant flaw-size curves and pertain to the initiation of fracture. They may be related to stress-temperature combinations which will initiate fracture. The position and shape of these curves are based primarily upon service experience related to failures or components or structures.

The constant flaw size curves for the low energy tear material, shown to the right of $NDT + 120^{\circ}F$ in Figure 8, are more schematic in nature. These provide a qualitative idea of how some of the higher strength materials, which generally exhibit a relatively low energy in the Charpy impact test, behave in the presence of defects. Of significance is the fact that catastrophic shear failures can occur at nominal stresses below the yield strength if defects are present and the material has low tear energy characteristics.



Sec. 6.1 Fig. 8—Fracture analysis diagram

The application of the fracture analysis diagram (high energy tear material portion below $NDT + 120^{\circ}F$) is quite straightforward. The minimum operating temperature relative to one of the transition temperatures, preferably NDT, is established for the material. Then, knowing the nominal applied stress, it is possible to estimate the size of defect that is required to initiate brittle fracture. Conversely, knowing the operating temperature relative to NDT and the size of a defect that may exist in the structure, it is possible to estimate the level of nominal applied stress that will cause fracture initiation. Similarly, by using the CAT curve, estimates can be made regarding the stress limits for arresting a running brittle crack at the temperature of interest.

While the fracture analysis diagram is a useful engineering tool for some materials and applications, some limitations and uncertainties restrict its general use. It was based on and developed from test data and service failures on the structural grades of steel which exhibit an abrupt ductile-to-brittle transition behavior. Its use therefore should be restricted to these kinds of materials. It is not applicable to the high strength steels, aluminum and titanium alloys because these materials do not have an abrupt transition behavior. There are also some uncertainties inherent in the diagram. The diagram predicts a constant flaw size stress relationship for temperatures below NDT. There are strong indications that the nominal stress for fracture for a constant flaw size should decrease with decreasing temperature below NDT^(20,31,40,45). Another uncertainty is concerned with the effects of section size on the position of the CAT and constant flaw size curves. It is possible that for many materials these curves would be shifted to higher temperatures and lower nominal stresses as the section thickness is increased. Shifts of this type in the CAT curves have been reported.⁽³¹⁾ Because of these limitations and uncertainties the fracture analysis diagram can only be considered as a qualitative tool for making engineering judgments where the materials are the structural grades of steel.

f. General Summary of Applicability Transition Temperature Approach

To summarize the transition temperature approach, the basic concept is simple, but its application to specific design problems can be quite complex and therefore requires careful consideration of all of the factors involved. There are two primary steps in these considerations. The first is to select a transition temperature criterion that is appropriate to the needs of the application and that is truly representative of the embrittling factors that are present. Then, the selected transition temperature criterion must be translated into terms related to defect size and load-bearing capacity; for ultimately this is the terminology which the designer can understand and apply. In those situations where both of these steps can be satisfactorily accomplished, the transition temperature approach can be successfully applied.

The most useful, comprehensive summary of the transition temperature approach is provided in the form of a Fracture Analysis Diagram. This diagram illustrates the general relationships between defect size, applied stress, and temperature. Where applicable, in terms of the material and intended use, the diagram is useful for purposes of making engineering judgments.

6.1.2.3 Applicability of Transition Temperature Approach to ATAC's Interest and Project Goals

While the general transition temperature approach may be applicable to presently used, low-strength materials for purposes of comparing materials and for rough design approximations, it is not satisfactory for the high-strength materials that are expected to be used in the future. Therefore the approach cannot satisfy the project goals. The first and primary reason is that the high-strength steels, aluminum and titanium alloys do not exhibit a characteristic abrupt ductile-to-brittle transition behavior. Secondly, even if it were possible to establish the various transition temperature criteria for these materials, the approaches lacks the basic quantitiveness that

is required to solve specific problems. For example, the fracture analysis diagram deals with only one dimension (length) of a defect and does not recognize that the critical stress for fracture can vary markedly, depending upon the type of loading and the geometry of the defect, i.e., semi-elliptical surface cracks of various lengths and depths, internal defects of various shapes, through the thickness edge or center cracks, etc. The establishment of design stress levels and realistic inspection and acceptance standards, requires specific consideration of the effects of all the effects of all the possible types of flaws and loading conditions. Thirdly, the slow growth of an initial sub-critical size defect to a critical size defect during the operational life time of a cyclic or sustained loaded component is another important consideration which cannot be handled with the transition temperature approach. Thus it is apparent that an alternate approach must be applied to achieve the ultimate objectives of this project. The subsequent sections of this report discuss and evaluate possible alternate approaches.

6.1.3 STRESS ANALYSIS APPROACH

In the stress analysis approach to the prediction of catastrophic fracture some property of the stress-strain distribution is used as the prediction criterion. A number of different properties have been used as the criterion and in general they can be placed in one of three categories: (1) stress criteria, (2) strain criteria, and (3) energy release rate criteria. Some of the approaches can be placed in more than one of the above categories since there is considerable overlap among them.

The stress analysis approach requires that the stress-strain distribution, or at least a reasonable estimate of this distribution, in the structural component be known. If the component contains notches or sharp flaws, the stress analysis must take this into account. The effects of plastic flow around these stress risers on the stress-strain distribution should also be considered when possible. Due to the mathematical difficulty involved in determining the exact stress-strain distribution of a body, most all of the methods involve a compromise with

exactness. These compromises in turn bound the limits of applicability of each specific approach.

In general, the critical value of the criteria parameter (maximum stress, etc.), which signifies failure, for each specific stress analysis approach is determined for each material from a relatively simple test specimen. The metallurgical and mechanical variables of the test specimen should be as similar as possible to those in the structure for which failure is to be predicted.

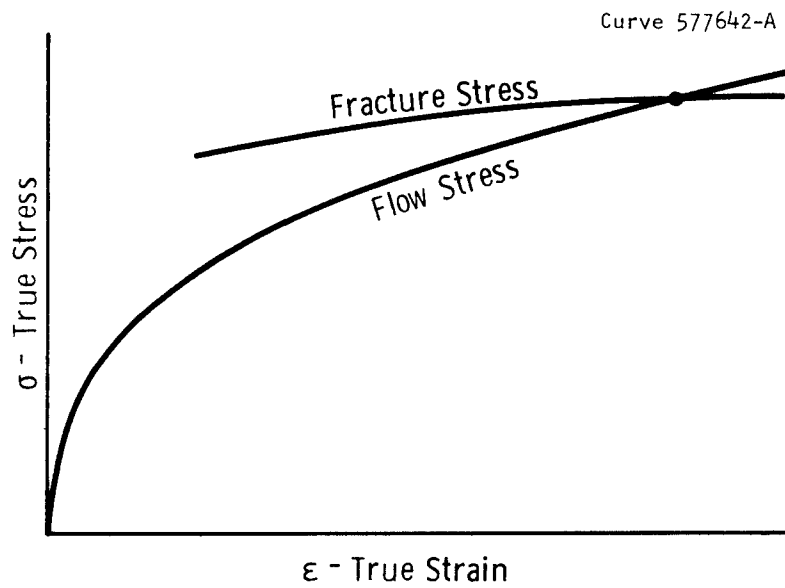
Some of the more significant approaches in the stress, strain, and energy categories will now be considered.

6.1.3.1 Stress Criteria

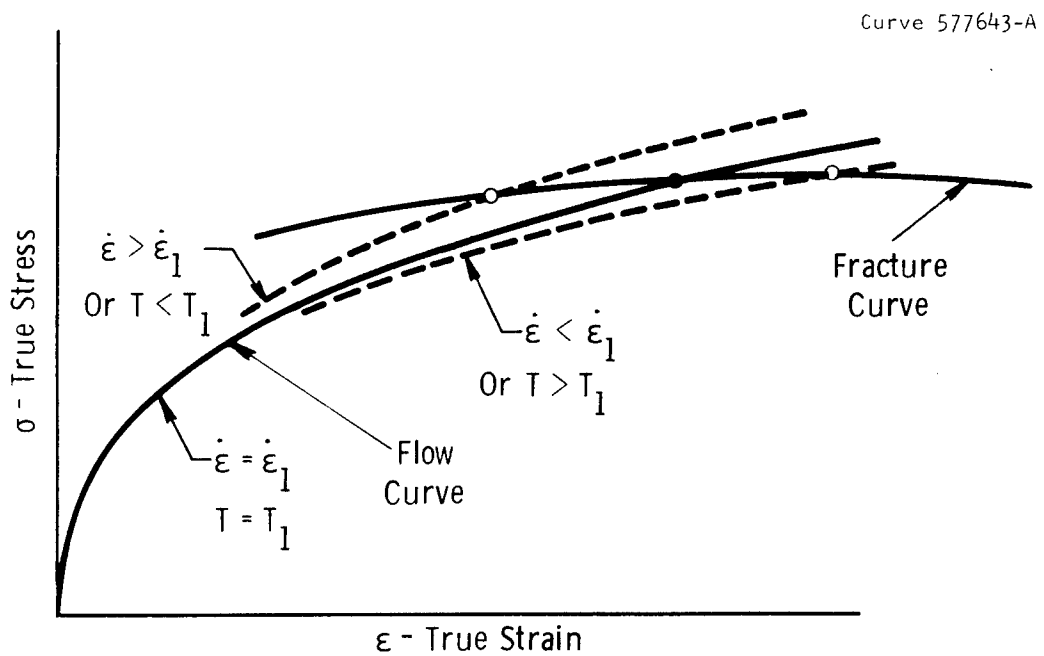
Perhaps the oldest criterion used to predict fracture is that of stress. Many variations of the stress criteria have been suggested through the years. Most of the approaches are related to the maximum stress criterion or some modification of it. Some of the more noteworthy modifications are the critically stressed volume criterion and the stress gradient influence. A number of the more significant stress approaches will now be considered.

a. Use of Fracture Curve

It was originally hypothesized by Ludwik, ⁽⁵³⁾ that not only could a flow stress curve be represented on a stress-strain diagram but also a fracture stress curve could be represented on such a diagram (Figure 9). He suggested that fracture occurs at the stress where the two curves intersect. Others ^(54,55) proposed that the effects of temperature, strain rate, and triaxiality on fracture stress and mode of fracture could be accounted for by the shifting of relative positions of the two curves due to the changes in these conditions. An example of this effect is shown in Figure 10. Due to the difficulty in experimentally verifying the existence of fracture curves, the Ludwik approach and its various modifications have not been pursued very earnestly.

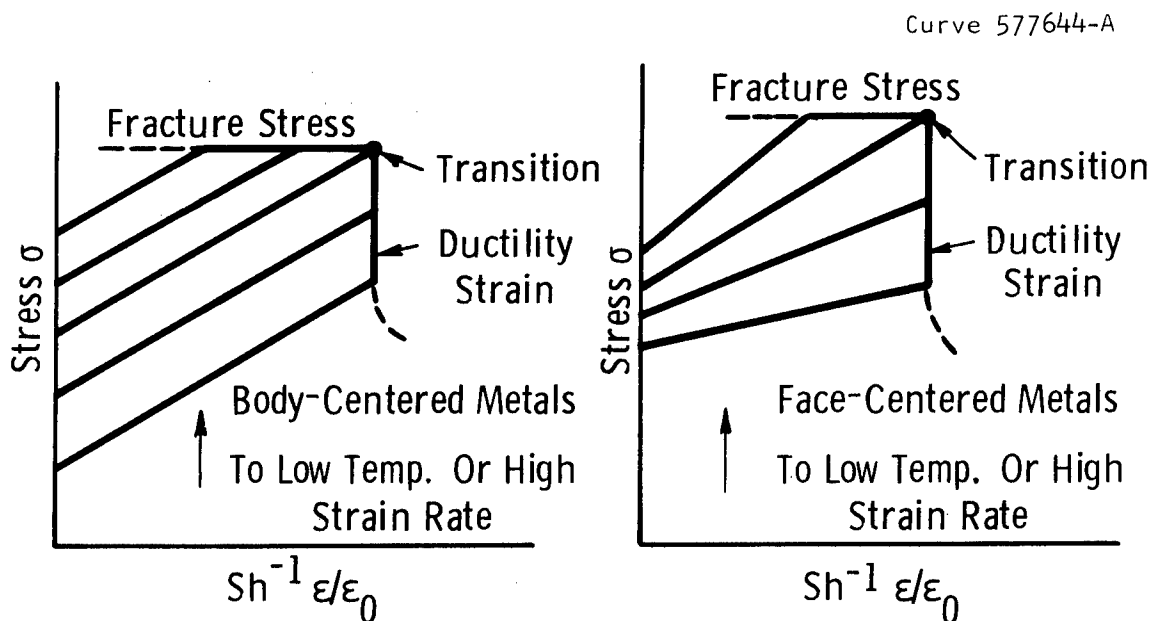


Sec. 6.1 Fig. 9 - Ludwik's fracture concept



Sec. 6.1 Fig. 10 - Effect of change in strain rate $\dot{\epsilon}$ or temperature T on fracture stress (55)

More recently a fracture concept somewhat similar to Ludwik's has been proposed by Beeuwkes.⁽⁵⁶⁾ He suggests that on a true stress-hyperbolic true strain diagram, the fracture curve has the shape of a "corner" (Figure 11). Beeuwkes has shown that flow curves for different temperatures and strain rates will appear as straight lines on this type of diagram. For the materials he investigated, the face centered cubic metals had flow curves which were parallel to each other, while the flow curves for body center cubic metals had flow curves which intersected at one point. Beeuwkes defines fracture which occurs on the constant stress surface of the "fracture corner" as being brittle and fracture which occurs on the constant strain surface as being ductile. This concept has the same limitation as the Ludwik approach. That is, the necessary experimental work needed to verify the existence of the "fracture corner" has not been performed. In addition, in their present forms, Ludwik's and Beeuwkes's concepts are not usable in design considerations.



Sec. 6.1 Fig. 11 - True stress-strain curves; after Beeuwkes (56)

b. Maximum Stress

Hendrickson and coworkers⁽⁵⁷⁾ showed that a maximum stress criterion could be used to predict failure of notched round tensile specimens made of mild steel. An approximate elastic-plastic analytic solution was used to estimate the maximum stresses in the specimens at failure. It was shown that regardless of test temperature and rate of loading, the maximum stress reached in each specimen was approximately the same. Further work⁽⁵⁸⁾ by these same investigators was encouraging, but later studies^(59,60) indicated that for most materials the maximum stress at fracture varies with temperature, rate of loading, the stress gradient at the point of initial fracture, and the state of stress in the notched area where fracture initiates. The state of stress at the notch can be one of plane stress, plane strain, or some state between these two limiting cases.

The congruency principle⁽⁶¹⁾ proposed by Lubahn takes into account the effect of the stress gradient at the notch, and also the state of stress at the notch. The congruency principle states that fracture will occur at the same nominal stress in two different notched objects if the nominal stress gradient at the notch root is the same in both objects and if the notches are geometrically congruent to each other. Lubahn experimentally checked this principle by correlating fracture data from notched bend tests and notched disk bursting tests. Subject to the above conditions, the correlation between the two types of test was found to be within 8%. The major drawback of the congruency principle is that each fracture situation of interest must be evaluated by an individual laboratory test on a specimen whose ratio of maximum stress to stress gradient at the notch is equal to that of the structure of interest and whose notch geometry is congruent with that of the structure.

c. Stress Concentration Factor Approach

Most of the recent work^(60,62,63,64) associated with the maximum stress concept has been closely related to Neuber's previously developed theory of notch stresses.⁽⁶⁵⁾ The notch theory as originally developed makes it possible to express the maximum stress, σ_{\max} , at the

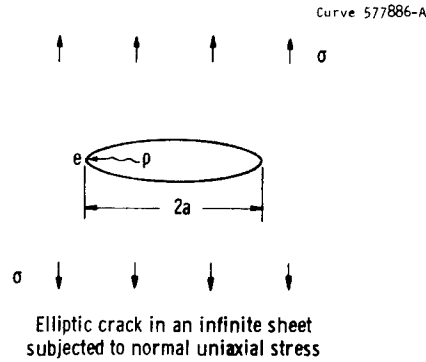
root of a notch or crack in an elastic body as a linear function of the nominal stress, σ_{nom} , in the body containing the notch or crack. The relation between these two stresses in the form $\sigma_{\text{max}} = K_t \sigma_{\text{nom}}$ where the constant proportionality factor, K_t , is defined as the theoretical elastic stress concentration factor. The stress concentration factor is a function of the geometry of the body containing the notch, of the size, location, and orientation of notch, and of the external load distribution on the body. The magnitude of K_t for a specific geometry and loading condition can be determined theoretically by employing the basic principles of the theory of elasticity⁽⁶⁶⁾ or experimentally by a number of methods.

For example, an elliptical crack of length $2a$ in an infinite plate subject to a uniform uniaxial tension field perpendicular to the plane of the crack (Figure 12) has a theoretical elastic stress concentration factor expressed by the equation

$$K_t = 1 + 2 \sqrt{\frac{a}{r}} \quad (1)$$

where r is the crack tip root radius. In this example the nominal stress is equal to the uniaxial stress away from the crack. The elastic stress concentration factors for a number of other geometries and loading conditions are available.⁽⁶⁷⁾

Attempts have been made to combine the elastic stress concentration factor concept with the maximum stress concept so that the nominal fracture stress of notched bodies can be accurately predicted. The simplest and most direct method used is to assume that at failure σ_{max} is equal to the uniaxial ultimate strength of the material, σ_u , and that the actual stress concentration factor is equal to the elastic stress concentration factor. This method predicts that the nominal stress will be inversely proportional to the elastic stress concentration factor. When experimental results are compared with those predicted by this method a number of the shortcomings of the method become apparent.



Sec. 6.1 Fig. 12

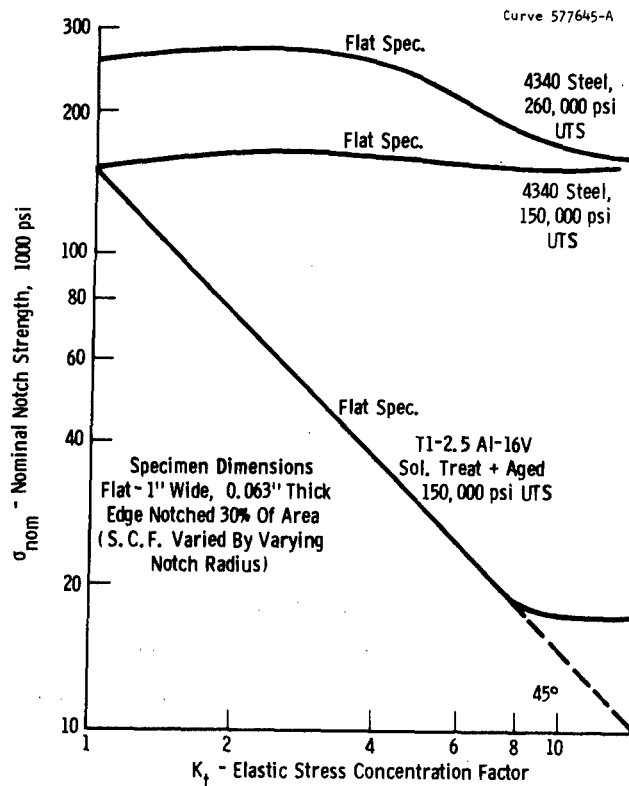
1. For relatively brittle materials the method underestimates the nominal fracture stress when the elastic stress concentration factors become large. This is demonstrated by the curve shown for a titanium alloy in Figure 13.

2. For some ductile materials the theoretically predicted nominal fracture stresses are completely misleading as is shown by the curve for 4340 steel in Figure 13. This material is insensitive to the presence of notches.

3. This method doesn't predict a variation in the fracture stress for geometrically similar notched specimens differing in absolute size only. That is, this method doesn't account for a size effect. Experimental results indicate that for many materials containing sharp notches the size effect is significant.

4. Finally, this approach doesn't predict the difference in fracture stress which occurs in going from a state of plane stress to one of plane strain at the notch tip.

These limitations of the linear elastic stress concentration factor approach are to a large degree the result of two factors. First, since the theory of elasticity, which is used in determining the stress concentration factors, is valid for a continuum only, deviation would be expected between theory and test results for extremely sharp notches where the use of a continuum becomes invalid. Secondly, due to the high stress concentration at the root of the notch, the material in the



Sec. 6.1 Fig. 13 - Influence of material and specimen geometry on notch strength behavior (60) (88)

vicinity of the notch tip will flow plastically and therefore, the stresses predicted by elastic theory will be in error. To correct for these deficiencies various means of correcting the values of the elastic stress concentration factors have been proposed.

To correct for the breakdown in the continuum aspects of the elasticity theory at the roots of sharp notches Neuber introduced⁽⁶⁵⁾ the "finite particle" concept as a means of modifying the elastic stress concentration factors. In this modification an effective root radius is used in the analytic expressions for the elastic stress concentration factors instead of the physical root radius which was originally used. The effective radius, r_e , is equal to the sum of the physical root radius, r , plus twice the "particle size" 2η . The particle size can be physically interpreted as representing the size of some basic structural unit of the material. That is, η is considered as a material constant which can be determined experimentally along with σ_{max} . For example, the modified form of equation (1) is

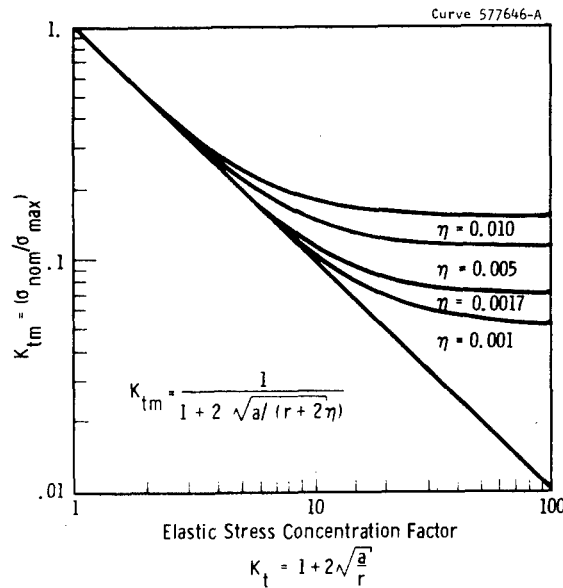
$$K_{tm} = 1 + 2 \sqrt{\frac{a}{r + 2\eta}} \quad (2)$$

where K_{tm} is defined as the modified stress concentration factor. A plot⁽⁷¹⁾ of K_{tm} as a function of K_t is shown in Figure 14 for various values of η . For this case the nominal stress at fracture becomes

$$\sigma_{nom} = \frac{\sigma_{max}}{1 + 2 \sqrt{\frac{a}{r + 2\eta}}} \quad (3)$$

As equation (3) indicates, this approach involves the use of two parameters, η and σ_{max} . It is of interest to note that for very small root radii equation (3) can be reduced to the following form:

$$\sigma_{nom} = \frac{\sqrt{\eta} \sigma_{max}}{\sqrt{2a}} \quad (4)$$



Sec. 6.1 Fig. 14—Effect of the equivalent particle size η on the K_{tm} vs. K_t curve of a brittle material - (calculated) (71)

Since $\sqrt{\eta} \sigma_{\max}$ is in effect one parameter, equation (4) shows that for sharp cracks the "finite particle" concept is a single parameter method. This equation also predicts a size effect. The equation states that the nominal fracture stress is inversely proportional to the square root of the crack length. This same inverse square root relation will be obtained for sharp cracks when the energy approach is considered and also when a particular form of the strain criteria is used.

To account for the plastic flow at the tips of notches, a number of other methods for modifying the elastic stress concentration factors have been suggested.^(68,69,70,71) Most methods have a form similar to that presented by Stowell⁽⁶⁸⁾:

$$K_p = 1 + (K_t - 1) \frac{E_s}{E_\infty} \quad (5)$$

where K_p is the corrected stress concentration factor, E_s is the secant modulus of the material at the point of the maximum stress, and E_∞ is the secant modulus of the material at a large distance from the notch. Using this modification, fracture would be predicted when $\sigma_{\text{nom}} = \sigma_{\max} / K_p$ where σ_{\max} is determined from a uniaxial unnotched specimen and K_p , which can be determined from equation (5), is a function of geometry, external load, and the flow properties of the material.

d. Use of Stress Gradient as a Parameter

Based on previous test results, Weiss⁽⁷¹⁾ has suggested that for some materials the criteria for fracture might be a function of maximum stress gradient at the root of the notch. This would make the stress criteria a two parameter one. The consideration of the stress gradient would make it possible to account for the size effect noted^(62,71) for some materials in the presence of relatively blunt notches.

e. Applicability of Stress Criteria

For general engineering design purposes the stress concentration factor approach is the most applicable of the stress methods considered. By applying the various correction factors (finite particle size, plasticity correction) to the elastically determined stress concentration

factors and by using the stress gradient as an additional parameter, a reasonable correlation between experimental results and theory can be obtained in a somewhat empirical manner for each material. The problem of estimating the magnitude of the various parameters from a uniaxial stress-strain curve still exists. At present the magnitude of the various prediction parameters must be determined by rather extensive testing. With an increasing availability of elastic-plastic solutions for notched and cracked geometries, the need of these correction factors can be eliminated.

6.1.3.2 Strain Criteria

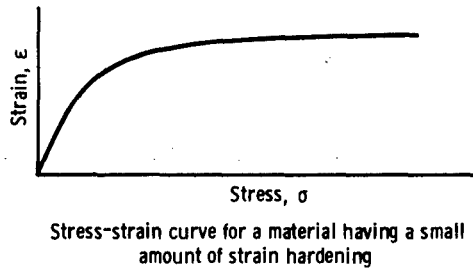
For the methods involving a strain criteria for the prediction of fracture loads, the maximum strain or some critically strained volume is usually used as the critical parameter. In general the strain criteria methods are very similar in form to those which were listed as stress criteria methods in the previous section. In fact some of the methods discussed in the stress section could also be considered as strain methods. In particular, the congruency principle,⁽⁶¹⁾ Ludwik's hypothesis,⁽⁵³⁾ and the "fracture corner" concept of Beeuwkes⁽⁵⁶⁾ could also be interpreted as approaches based on a strain criteria.

An advantage of a strain criteria over a stress criteria is the increased sensitivity of strain compared to stress in the plastic range. For example, for a material which has a very moderate amount of strain hardening (Figure 15), the strain is a much more meaningful criterion for fracture than the stress in a smooth specimen fracture test.

A number of fracture analysis methods involving strain criterion have been introduced in the last few years. Most of these approaches are now in the development stage. These methods will not be considered.

a. Exhaustion of Ductility

The exhaustion of ductility approach is based on the premise that fracture occurs when the available ductility of the material is less



Sec. 6.1 Fig. 15

than the ductility required under the local constraint at the notch. Supporters^(55,72,73) of this approach attempt to validate this premise by showing that the net fracture stress of precompressed notch plates is much less than that of plates which were not precompressed. It is stated that this large reduction in fracture strength is due to the fact that ductility of the material is substantially reduced (exhausted) by the precompression working. It has been pointed out by others⁽⁷⁵⁾ that the reduction in fracture stress caused by the precompression of the notched plates is due to the effect of the residual stress which is produced at the notch tip by the precompression process and not due to a reduction in the ductility of the material. Some limited studies⁽⁷⁵⁾ on plate specimens in which the precompression operation was performed before the notches were machined in the plate have indicated a substantial reduction in net fracture stress when the precompressive strain exceeded some minimum value. Under these conditions the possibility of appreciable residual stress at the notch was eliminated. Besides the question concerning the significance of the residual stress at the notch root, the major drawback of this approach is that in its present state it is very qualitative and doesn't lend itself to be used with quantitative analytical expressions which are useful in engineering design.

b. Critically Strained Volume Criteria

McClintock⁽⁷⁶⁾ has suggested a two parameter strain criteria for the prediction of rapid propagation of sharp cracks. He suggests that propagation will take place when the strain at some distance, ρ , from the crack tip exceeds a magnitude of ϵ_f . That is, fracture is assumed to occur when all the material for a distance ρ directly ahead of the crack has reached a cumulative value of plastic strain equal to a critical value ϵ_f . The two parameters, ρ and ϵ_f , are considered to be material properties which can be determined for each material by simple tests.

McClintock's suggestion of a two parameter criterion was a result of his analysis⁽⁷⁷⁾ of the stress-strain distribution of a sharp crack subject to a longitudinal shear stress field. The analysis applied to an elastic-perfectly-plastic material. It is of interest to note that for large cracks, the stress for fracture is inversely proportional to the square root of the crack length and the criterion for rapid crack propagation reduced to that of effectively one parameter. This type of a relationship is the same as that obtained from Neuber's "particle size" concept when applied to sharp cracks is the same as that which is obtained by using fracture mechanics concepts as will be shown.

c. Use of Strain Hardening Exponent

One of the more recent strain concepts has been proposed and studied by Kraft.⁽⁷⁸⁾ Although it is similar to McClintock's approach in some aspects, it is actually an outgrowth of the fracture mechanics approach which will be discussed later.

Kraft states that when the strain at a particular distance "d" from the crack tip reaches a value equal to the strain hardening exponent of the true stress-strain curve, catastrophic crack propagation will begin. The distance "d" is considered to be a function of material only and is independent of strain rate and temperature. The strain hardening exponent is a function of material, strain rate and temperature. Therefore ideally the quantity "d" can be determined from a single fracture test and then from a knowledge of the magnitude of the strain

hardening exponent as a function of temperature and strain rate, the fracture load at various temperatures and strain rates can be predetermined. In its present form the approach is applicable to sharp cracks only.

d. Crack Opening Displacement Criteria

Wells⁽⁷⁹⁾ suggests that the crack opening displacement at some fixed but short distance from the crack tip could be used as a fracture criterion. The local crack opening displacement will be related to the strain distribution around the crack, and, therefore, the method can be classified as a strain criteria. Thus the use of this criterion temporarily avoids the need of an exact elastic-plastic solutions and also avoids the problem of attempting to measure strains in the vicinity of the crack tip.

This approach is also an outgrowth of linear fracture mechanics. Wells states that the crack opening displacement approach can be used when widespread yielding has occurred around the crack tip whereas the linear fracture mechanics approach is restricted to situations in which a very limited amount of yielding has occurred. At present the methods are still in the development stages and has had only limited use in design applications.

e. Applicability of Strain Criteria

All of the strain concepts considered here have, in general, not been used in design considerations and are still in the development stage. While McClintock's critically strained volume analysis gives a better understanding of the relative role played by the various material properties in the fracture process, in its present form it is not very applicable to design considerations. The "exhaustion of ductility" approach has many of the limitations of the transition temperature approach, in that it is more qualitative than quantitative in nature and therefore does not lend itself directly to design considerations. Although Kraft's "strain hardening exponent" approach is based on a strain criterion, it is directly related to linear elastic fracture mechanics and has the same limitations. These limitations will be

considered in Section 6.2. The "crack opening displacement" criteria is an extension of the linear elastic fracture mechanics approach which promises to extend the areas of applicability of the present linear theory.

6.1.3.3 Linear Elastic Fracture Mechanics

In recent years there has been a marked increase in the number of publications concerned with linear elastic fracture mechanics. The increase involves both basic experimental data and analytic solutions concerned with application. Simultaneously, the number of actual design applications of fracture mechanics has also sharply increased. The formulation and limitations of this approach will now be discussed.

The theory of linear elastic fracture mechanics provides a means of predicting the fracture load of structures containing sharp flaws of known size and location. The theory can be based on either an energy approach or on a stress intensity approach. Both approaches are closely related and lead to the same results. The approaches will be considered individually in Sections 6.1.3.3.a and 6.1.3.3.b, respectively.

a. Energy Criterion

The energy approach to fracture was originally presented by Griffith⁽⁸⁰⁾ and later re-emphasized and broadened by Irwin⁽⁸¹⁾ and Orowan.⁽⁸²⁾ Some of the historical background of the approach will be discussed later (Section 6.2.1), but now the basic concepts involved will be considered.

The energy approach to fracture instability is one in which the criterion for propagation of a crack in a body is stated in terms of the rates of change with respect to crack extension of the various energy components involved in the process. The criterion is that crack propagation will occur if the amount of energy which could be supplied to the crack tip during an incremental crack extension is greater than or equal to the energy which would be absorbed at the crack tip during an incremental extension of the crack. Before this criterion for fracture can be expressed in mathematical terms the changes in the

various energy components involved in an incremental crack extension must be considered. The five energy components involved in the crack extension process are: (1) strain energy, (2) energy supplied to the body by external work, (3) kinetic energy, (4) free energy required to form the new surfaces, and (5) the energy required to perform the plastic work at the crack tip. For materials which exhibit some ductility the surface energy component is exceedingly small compared to the other forms of energy and can be neglected.⁽⁸²⁾ Also, normally the kinetic energy component is small compared to the others and can be neglected. Therefore just the energy due to external work, the strain energy, and plastic work need to be considered.

If the size of the plastic zone at the tip of the crack is very small compared to the total volume of the body containing the crack, then the strain energy of the body can be set equal to the elastic strain energy which would be determined for the body if it is assumed that no yielding occurred. The strain energy will be represented by the symbol U.

The work performed on the body by external forces will be represented by W_e and the energy absorbed by plastic work will be represented by E_p . Now if "A" represents crack area, the energy criterion for crack extension, as stated above, can be expressed mathematically as

$$\frac{dW_e}{dA} \delta A \geq \frac{dU}{dA} \delta A + \frac{dW_p}{dA} \delta A \quad (6)$$

This means that crack extension begins when

$$\frac{dW_e}{dA} - \frac{dU}{dA} = \frac{dW_p}{dA} \quad (7)$$

The left hand side of equation (7) is defined as the energy release rate, G

$$G = \frac{dW_e}{dA} - \frac{dU}{dA} \quad (8)$$

Still using the restriction that the plastic zone is very small compared to the total volume of the body, it can be shown⁽⁸³⁾ that

$$G = \left(\frac{\partial U}{\partial A} \right)_{\delta} \quad (9)$$

That is, the energy release rate is equal to the rate of change of strain energy with respect to crack area when the displacements of the externally applied loads are held constant during incremental crack extension. The energy release rate is a function of the geometry of the body under consideration and of the loads applied to it.

It has been shown experimentally, that, within limits which will be stated later, dW_p/dA is a function of the material, temperature, strain rate and of the state of stress at the crack tip is either one of plane stress, plane strain, or of some degree between these two limits. At present no means of determining dW_p/dA from the standard material properties has been determined. The magnitude of dW_p/dA must be determined from at least one fracture test on a cracked body for which an expression for the energy release rate is known. The body must be made from the material under investigation, and the state of stress at the crack tip of the body must be the same as that in the body to which the test result will be applied. The energy release rate at fracture is defined as G_c , that is $G_c = dW_p/dA$.

Since this criterion for predicting fracture of a body due to the presence of a crack is not as intuitive as a stress or a strain criteria, a simple example will be used to demonstrate the approach. An infinite plate of unit thickness containing a crack of finite length, $2a$, perpendicular to an uniaxial stress field, σ , will be considered. The presence of the crack in the body reduces the elastic energy (assuming elastic conditions) by $\pi\sigma^2 a^2/E$. If U_0 is defined as the elastic strain energy of the uncracked plate then the strain energy of the cracked plate is

$$U = U_0 - \frac{\pi\sigma^2 a^2}{E} \quad (10)$$

By substituting this expression into equation (9), the energy release rate of the plate can be shown to be

$$G = \frac{\pi \sigma^2 a}{E} \quad (11)$$

where the crack area $A = 2a$. The theory predicts that the fracture of the plate will occur when

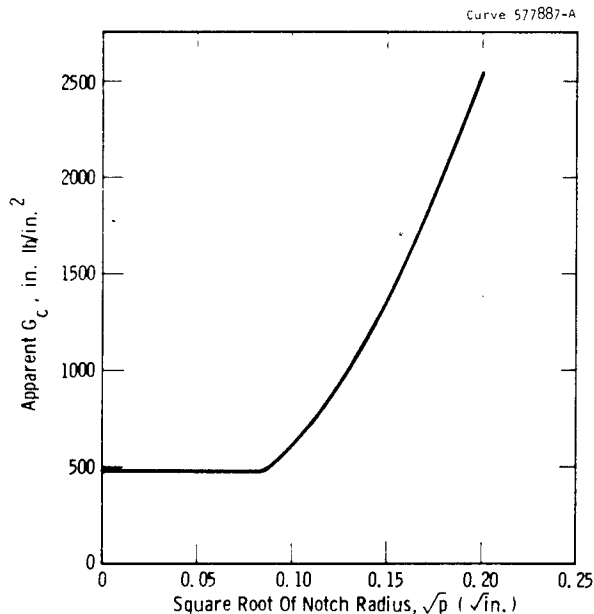
$$\sigma_c = \sqrt{\frac{G_c E}{\pi a}} \quad (12)$$

where ideally G_c can be determined from at least one fracture test performed on this geometry at some known crack length. As can be seen the fracture stress is a function of the inverse square root of the crack length. This inverse square root relation is the same as that obtained from the Neuber "finite particle" approach and from McClintock's critically strained volume approach.

This approach has a number of limitations. As mentioned in the above derivation the derived equations were restricted to conditions in which the plastic zone at the crack tip is very small compared to the other dimensions of the body. This limits the use of the energy approach as just formulated to materials which are relatively brittle in the presence of cracks.

Another limitation of this approach is that it fails to adequately handle the effect of small crack root radius. The energy approach doesn't predict a difference in the fracture stress of two similar cracked specimens differing only in the crack tip root radius (assuming both are small), but it has been shown experimentally that the fracture stress levels do differ under such circumstances as shown⁽⁶⁴⁾ in Figure 16.

The root radius limitation could be related to what some consider a basic weakness of the energy approach.⁽⁵⁵⁾ It has been stated that the relations obtained by an energy approach are necessary for fracture to occur, but not sufficient. That is, for crack extension to occur it is necessary that enough energy be available to supply the work



Sec. 6.1 Fig. 16 -Effect of notch radius on apparent G_c . Schematic based on data for Aluminum 7075-T6 sheets 1/16 in. thick.

dissipated in the fracture processes, but just because the necessary energy is available doesn't mean that crack propagation must occur. In addition to the energy requirement it has been suggested that there is another criterion which must also be met before crack extension will occur. For example, the other criterion could be one of maximum stress or strain.

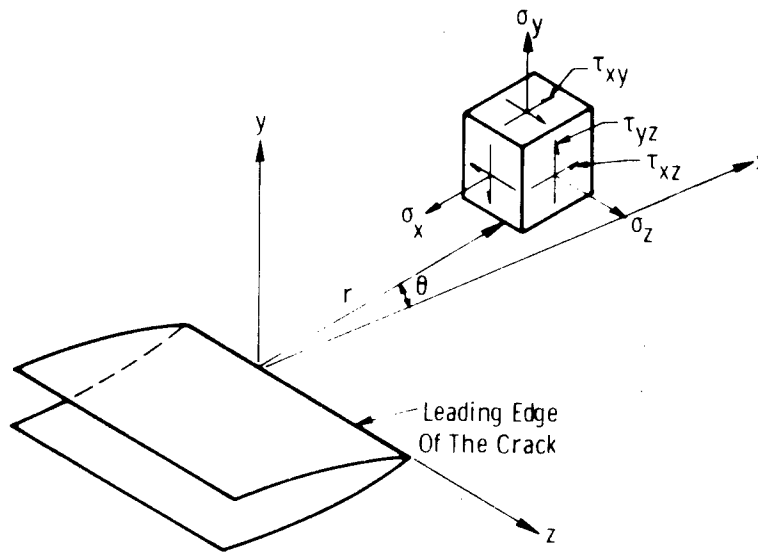
b. Stress Intensity Criterion

Over the last few years, the energy approach has transformed into what is called the stress intensity approach. This transformation has resulted in a de-emphasis of the energy considerations of the fracture process. The shift is probably due to three factors. First it side steps some of the problems just mentioned above which are inherent in the energy approach. Secondly, since the stress intensity places more emphasis on the stress-strain distribution at the crack tip than on the energy balance, it generally has more appeal to the engineer since he is more familiar with stress-strain concepts than with energy ones. Finally the relations between crack size and fracture load for all geometries are exactly the same for the two concepts.

The stress intensity approach to fracture can best be introduced by describing the general form of the elastic stress field at the tip of a crack. For a through-the-thickness crack of zero root radius in a plate subject to in-plane loads which are uniformly distributed through the thickness of the plate and symmetric with respect to the plane of the crack, the elastic stress field in the vicinity of the crack tip ($r \rightarrow 0$) has the general form. (84)

$$\begin{aligned}\sigma_x &= \frac{K}{(2\pi r)^{1/2}} \cos \frac{\theta}{2} \left[1 - \sin \frac{\theta}{2} \sin \frac{3\theta}{2} \right] \\ \sigma_y &= \frac{K}{(2\pi r)^{1/2}} \cos \frac{\theta}{2} \left[1 + \sin \frac{\theta}{2} \sin \frac{3\theta}{2} \right] \\ \tau_{xy} &= \frac{K}{(2\pi r)^{1/2}} \sin \frac{\theta}{2} \sin \frac{\theta}{2} \cos \frac{\theta}{2} \cos \frac{3\theta}{2}\end{aligned} \quad (13)$$

where the coordinate system (r, θ) is shown in Figure 17. The stress intensity factor, K (not to be confused with the stress concentration factor K_t , etc.) is a function of the plate geometry, the applied loads, size, location, and orientation of the crack. In effect, equation (13) states that the crack tip elastic stress and strain fields for different geometries and loading conditions differ by only a multiple constant equal to the ratio of the stress intensity factors. This fact is the basis for the stress intensity approach to fracture. The approach is based on the assumption that crack propagation will occur when the stress intensity at a crack tip reaches a critical level K_c . Once the magnitude of K_c has been determined experimentally, the fracture load for a structure containing a crack can be predicted, within certain limitations, if the stress intensity at the crack tip is known as a function of the applied load for that structure. At present the value of K_c must be determined experimentally. The state of stress (plane stress, plane strain, etc.) at the crack tip in the specimen used to



Sec. 6.1 Fig. 17 - Coordinates measured from the leading edge of a crack and the stress components in the crack tip stress field (84)

determine K_c must be the same as that at the tip of the crack in the structure for which the fracture load is being predicted. There are a number of other conditions which also must be satisfied before such a prediction can be made, and they will be discussed later.

As an example, the case of the infinite plate containing a finite crack of length $2a$, perpendicular to a uniaxial stress field σ , will be considered again. The stress intensity factor for this case is $K = \sqrt{\pi a} \sigma$. Therefore fracture would be predicted at the critical stress $\sigma_c = K_c / \sqrt{\pi a}$, where K_c could be obtained from a small and reasonably simple laboratory test specimen. Here again we have the size effect equal to the inverse square root of the crack length.

Since the stress intensity factor describes the elastic stress and strain distribution at the tip of the crack it would be expected that there should be some relationship between K and the energy release G . It has been shown by Irwin⁽⁸⁵⁾ that the following relations exists:

$$K = \sqrt{GE} \quad (\text{for plane stress}) \quad (14)$$

$$K = \sqrt{\frac{GE}{(1 - \nu^2)}} \quad (\text{for plane strain}) \quad (15)$$

Where E is the elastic Modulus and ν is Poissons ratio. These relationships show that the two approaches (stress intensity and energy release rate) are equivalent.

The theory of elasticity is used in the determination of the stress intensity factors for various geometries and loading conditions, and in the analysis it is assumed that the root radius of the crack is equal to zero. These two facts place rather significant restrictions on the use of a critical stress intensity factor as a criterion for failure of an initially cracked body. Due to the extremely high stress concentration at the crack tip, plastic flow will occur in a zone around the crack tip. If the zone of plastic flow is small compared to area around the crack tip in which the elastic stresses are accurately described by equation (13), then the stress intensity factor will adequately represent the elastic-plastic stress and strain conditions at the crack tip. Therefore, the requirement is imposed that the size of the plastic zone at fracture must be very small compared to the total volume of the cracked body. This same restriction was imposed on the energy approach.

It has also been shown⁽⁶⁴⁾ that the value of K_c is sensitive to the size of the crack root radius (Figure 15). For many materials the value of K_c decreases in proportion to the decrease in the square root of the root radius until the root radius reaches some minimum value. As the root radius decreases below this value the magnitude of K_c remains constant. To eliminate the effect of the root radius, K_c is determined by using a fatigue crack in the test specimen and therefore can only be accurately applied to structure cracks of similar sharpness.

c. Applicability of Linear Elastic Fracture Mechanics

Even though the use of linear elastic fracture mechanics is limited to sharp flaws for which the size of the plastic zone at fracture is small, it still has a wide area of application. Due to the analytical character of the method, it can quite readily be incorporated into design procedures. Since it is a single parameter criterion it is very convenient to use in materials evaluations. The ever increasing availability of valid experimentally determined fracture data expressed in terms of fracture mechanics parameters also makes the use of this approach advantageous. A similar statement can also be made with respect to the availability of analytic solutions for the stress intensity factors of various geometries. In addition it has been demonstrated that slow crack growth rates caused by low stress level cyclic loading and stress corrosion can be related to the crack tip stress intensity.

6.1.3.4 Elastic-Plastic Analysis

If any of the previously discussed stress analysis approaches are to be extended beyond their present limitations, it is apparent that rather rigorous elastic-plastic solutions must be obtained for at least a few simple geometries containing cracks. Such solutions are needed to properly interpret test data. Careful studies of test results obtained from specimens for which the exact stress-strain distribution is known would be of significant aid in determining what parameter or parameters might best be used to predict the onset of fracture.

Of course after these parameters have been established by such an investigation, it would be desirable to have elastic-plastic solutions available for many other geometries containing cracks and notches so that reasonable estimates of the elastic-plastic stress and strain distributions around cracks in more complex structures can be estimated.

The major obstacle to such an investigation is the availability of elastic-plastic solutions. Although the presently accepted fundamental equations of plasticity⁽⁸⁶⁾ are already based on some simplifying assumptions, the mathematical difficulty which the solutions to these equations creates is quite extreme. Therefore, only a limited number of

elastic-plastic solutions for cracked bodies and notches are available. But presently a great deal of effort is being directed toward the solution of elastic-plastic problems, and in the future it appears that a significant number of solutions will be available.

This more sophisticated approach should also reveal whether the same fracture criteria can be used for all materials. For example, the fracture of one material could be dictated by the maximum strain criteria, but for another material, fracture may be dictated by a maximum stress criteria. It cannot necessarily be assumed that the same macroscopic criteria will apply to all materials, for plasticity theory is applied to a macroscopic continuum whereas fracture occurs on a microscopic level.

6.1.3.5 Statistical Considerations

All of the stress analysis methods discussed above predict a geometric size effect for equally proportioned specimens containing sharp cracks. In addition to this type of size effect, there is a statistical size effect which must be considered. This effect is most easily described by considering smooth specimens. For the smooth specimens the statistical size effect is due to the fact that the probability of the presence of a flaw large enough to cause fracture increases with the size of the specimen. Weibull⁽⁸⁷⁾ has shown that for inhomogeneous smooth specimens the statistical size effect may be expressed as

$$\frac{\sigma_2}{\sigma_1} = \left(\frac{V_1}{V_2} \right)^{\frac{1}{n}} \quad (16)$$

where σ_1 and σ_2 are fracture strengths of two geometrically similar specimens having volumes V_1 and V_2 and n is known as Weibull's coefficient. The coefficient n represents the density of the flaw distribution. At present n cannot be related to any physical characteristic of materials and must be determined experimentally for each

material. In using equation (16) it is assumed that the density of flaws in each volume under consideration is equal. But this is usually not the case due to the differences in the manufacturing processes used for structures of different sizes.

When the statistical size effect is considered for a notched structure or for one that contains a comparatively large sharp crack the situation becomes much more complicated. The presence of smaller cracks of an inhomogeneous material in the vicinity of the root of the notch or of the large crack will cause the strength of the structure to be less than it would be if the small cracks were not present. Therefore under these conditions it would be expected the size effect would be a combination of the geometric size effect and the statistical size effect. Usually in the presence of severe notches or cracks the statistical size effect is small compared to the geometric size effect. The results of a study of the interaction of these two size factors is presented in Reference 62.

6.1.4 SELECTION OF THE MOST APPLICABLE APPROACH

The linear elastic fracture mechanics type of stress analysis approach is selected as being most applicable to satisfying ATAC's need for design and material selection criteria for the prevention of brittle fracture in the future use of high-strength materials. While linear elastic fracture mechanics is an engineering method within the discipline of continuum mechanics, the subject is broad and interdisciplinary. In essence this approach represents the most sophisticated, yet the most simple, direct and quantitative method currently available for attacking the problems associated with the brittle fracture of high-strength materials. The procedures and criteria developed from the technology provide a sound basis for dealing with the interrelated aspects of material properties, defects and applied stresses, and ultimately, determining the load-bearing capacity of components or structures. None of the transition temperature approaches the desired quantitative capability that is required, particularly with regard to the high-strength materials of interest in this program.

Of all the stress analysis approaches considered in Section 6.1.3, only the fracture mechanics approach and the stress concentration approach appear at present to be applicable for both design considerations and materials evaluation. Both are analytically compatible with design procedures. In addition, a substantial amount of basic experimental data has been accumulated for each approach. In the case of sharp cracks with zero root radius, the case for which we are specifically concerned, both approaches lead to the same relations between geometric parameters and external fracture loads. The choice of the fracture mechanics approach over the stress concentration approach was made because the major emphasis in the field of brittle fracture at present and in the recent past has been on fracture mechanics. In addition, fracture mechanics readily lends itself to the development of engineering procedures and criteria. Most experimental data and technical advancements published in the field of brittle fracture are presented from a fracture mechanics viewpoint. These advancements are typified by Kraft's strain hardening exponent approach to the effects of strain rate on fracture, and Well's crack opening approach to fracture occurring with substantial yielding.

While the employment of fracture mechanics concepts, expressions, and data may initially appear to be quite complex to the uninitiated designer or materials engineer, a familiarity with the subject coupled with proper consideration of all the factors in a logical, systematic fashion can evolve into relatively simple and quantitative engineering procedures and design criteria. A brief description of the basis of the approach and its capabilities follows.

The basis of the concept is that the fracture toughness of a material in the presence of a sharp crack can be expressed as a material parameter, analogous to yield strength. This parameter is usually described in terms of " G_{Ic} " (critical crack extension force, in lbs/in.^2) or K_{Ic} (critical stress intensity factor, $\text{psi } \sqrt{\text{in.}}$). Both G_{Ic} and K_{Ic} are commonly referred to as "fracture toughness." Being a material parameter, the fracture toughness, once properly determined under one set of conditions, is applicable to other conditions, i.e., geometry, flaw size, and loading conditions. The values for G_{Ic} or K_{Ic} must be

determined experimentally and several types of specimens and loading conditions have been successfully employed to obtain these measurements of fracture toughness.

Once properly determined, the fracture toughness parameters, used in conjunction with appropriate mathematical expressions relating toughness, defect size, applied stress, and a geometrical factor for the relative geometries of the defect and component, can be employed to make quantitative determinations of the effects of specific defects in specific situations. Expressions relating the fracture toughness and the load-bearing capacity of defect-containing structures or components are available for a number of geometries, loading conditions, and types of defects. Such expressions nearly always involve the following terms: the fracture toughness, the applied stress, the elastic modulus, the yield strength of the material, a linear dimension of the crack or defect, and a proportionality term dependent only on the manner of loading and the relative geometry of the defect and structural component.

The implementation of the fracture toughness approach for determining load-bearing capacity is rather straightforward. Knowing the fracture toughness of the material in question for the temperature range of interest, and the size of the defects from a nondestructive evaluation, it is possible to evaluate the load-bearing capacity of the structure by inserting the G_{Ic} or K_{Ic} and defect size numbers in the appropriate expressions and solving for the stress. Conversely, knowing the toughness and applied stress, it is possible to estimate the critical defect sizes that are required for catastrophic failure. These, in turn, can be compared with performance capabilities of the nondestructive test techniques that may be employed to detect flaws. For a given level of toughness, the applied stress that is required for catastrophic fracture decreases as the crack size increases; the stress is proportional to the inverse square root of the defect size. For a given defect size, a decrease in toughness results in a lower applied stress for fracture. Thus, an estimate of the critical combination of defect size and applied stress that is required for fracture

may be readily determined if one knows the toughness of the material and either one of the other two variables.

It should be realized that the foregoing paragraph is intended only to provide a general idea of the application of the fracture toughness approach, and to emphasize the interplay between toughness and defect size in determining the load-bearing capacity of a structure. For a precise evaluation of any specific situation, considerably more detailed information is required regarding the following: the temperature dependence of the fracture toughness (K_{Ic} or G_{Ic}) in the range of interest; the location, size, shape, orientation, and type of defect; the direction and magnitude of the applied (plus possible residual) stresses acting on the defect; the slow growth characteristics of a sub-critical size flaw under sustained or cyclic loading at the application temperatures; the relative geometry of the structural member and the defect; and the proper criterion of fracture toughness to be employed. These factors are discussed in detail in subsequent sections of this report.

By properly combining evaluations of crack growth characteristics with linear elastic fracture mechanics technology, engineering procedures and criteria are established whereby one can answer questions such as: What type and size of defect can be tolerated under the design load? Conversely, what stress levels can be tolerated in the presence of some known defects? What is the maximum size flaw that can be initially accepted with the assurance that it will not grow to a critical size during the desired life of the structure? What size defects must be removed and repair made? How do metallurgical and fabrication variables affect the maximum allowable initial flaw size, the flaw growth characteristics, and the critical size flaw for catastrophic failure? What are the capabilities of the available, practical, nondestructive inspection techniques relative to these sub-critical and critical flaw sizes? If an unexpected failure should occur during proof testing or operation of a pressure vessel, what will be the nature of the failure - a localized splitting and leakage or an extensive bursting with fragmentation? What fracture toughness and crack growth characteristics

are required in a material for a given application in terms of practical methods of testing, fabrication, welding, and inspection? What are the realistic operational limitations of structures containing defects?

Linear elastic fracture mechanics technology, combined with appropriate information concerning stresses, defect size, and slow crack growth rates can be and has been employed to provide answers to the above type questions. At present the application of the technology is limited to those materials for which valid fracture toughness parameters can be determined, and to applications where sufficient section size and restraint prevail so that an essentially plane strain state of stress exists in the region of the defect. In those situations where gross plastic deformation occurs in the region of the defect because of extremely high toughness and/or thin sections where a plane stress state of stress exists, further developments are required before the technology can be successfully applied.

The next section (6.2) of this report provides a comprehensive review of the state of the art of fracture mechanics.

Section 6.1 References

1. W. D. Biggs, "The Brittle Fracture of Steel," Pitman Publishing Corp., New York City (1960).
2. C. F. Tipper, "Testing for Brittleness in Structural Steels," Cambridge Conference on Brittle Fracture, September, 1959.
3. E. R. Parker, "Brittle Behavior of Engineering Structures," John Wiley and Sons, Inc., New York City (1957).
4. D. L. Newhouse and B. M. Wundt, "A New Fracture Test for Alloy Steels," ASM, Metals Progress, Vol. 48, No. 1, July, 1960, p. 81.
5. C. E. Hartbower, "Crack Initiation and Propagation in the V-Notch Charpy Impact Specimen," Welding, J., Res. Suppl. Vol. 36, No. 11, November, 1957, p. 494s.
6. P. P. Puzak, E. W. Eschbacher and W. S. Pellini, "Initiation and Propagation of Brittle Fracture in Structural Steels," Welding J., Res. Suppl., Vol. 31, No. 12, December, 1952, p. 561s.
7. P. P. Puzak, M. E. Schuster and W. S. Pellini, "Crack-Starter Tests of Ship Fracture and Project Steels," Welding J., Res. Suppl., Vol. 33, No. 10, October, 1954, p. 481s.
8. P. P. Puzak, A. J. Babecki and W. S. Pellini, "Correlation of Brittle-Fracture Service Failures with Laboratory Notch-Ductility Tests," Welding J., Res. Suppl., Vol. 37, No. 9, September 1958, p. 391s.
9. W. S. Pellini and P. P. Puzak, "Practical Considerations in Applying Laboratory Fracture Test Criteria to the Fracture Safe Design of Pressure Vessels," Trans. ASME, J. of Basic Engrg. for Power, October 1964, p. 429-443.
10. ASTM E208-63T, "Tentative Method for Conducting Drop-Weight Test to Determine Nil-Ductility Transition Temperature of Ferritic Steels," 1963 (also Nav Ships 250-634-3, August 21, 1963).
11. W. S. Pellini, et al., "Review of Concepts and Status of Procedures for Fracture-Safe Design of Complex Welded Structures Involving Metals of Low to Ultra-High Strength Levels," U.S. Naval Research Laboratory Report #6300, June 1965.
12. K. J. Stodden and E. P. Klier, "Brittle Failure and Size Effect in a Mild Steel," Welding J., Res. Suppl., Vol. 29 (1950) p. 303s.

13. N. Grossman, "Pearlitic Structure Effect on Brittle Transition Temperature," *Welding J., Res. Suppl.*, Vol. 28 (1949) p. 265s.
14. A. B. Kinzel, "Ductility of Steels for Welded Structures," *Welding J., Res. Suppl.*, Vol. 27 (1948), P. 217s.
15. J. E. DeGraaf and J. H. Van Der Veen, "The Notched Slow Bench Test as a Brittle Fracture Test," *J. Iron and Steel Inst.*, Vol. 173 (1953) p. 19.
16. C. F. Tipper, "Brittle Fracture of Metals at Atmospheric and Sub-Zero Temperatures," *Metallurgical Reviews*, Vol. 2, No. 7, (1957) p. 195.
17. J. F. Baker and C. F. Tipper, "The Value of the Notch Tensile Test," *Proc. Inst. Mech. Eng.*, London, Vol. 170 (1956) p. 65.
18. W. M. Wilson, R. A. Hechtman and W. H. Bruckner, "Cleavage Fracture of Ship Plates as Influenced by Size Effect," *Welding J., Res. Suppl.*, Vol. 27 (1948) p. 200s.
19. J. E. Srawley and C. D. Beachem, "Crack Propagation Tests of High Strength Sheet Materials," Parts I to V, *NRL Reports* 5127, 5263, 5348, 5460, and 5507 (1958, 1959, 1960).
20. E. T. Wessel, "The Influences of Pre-Existing Sharp Cracks and the Brittle Fracture of a Ni Mo V Forging Steel," *Trans. ASM*, Vol. 52 (1960) p. 277.
21. N. A. Kahn and E. A. Imbembo, "Notch Sensitivity of Steel Evaluated by Tear Test," *Welding J., Res. Suppl.*, Vol. 28 (1949) p. 153s.
22. H. M. Banta, R. H. Frazier and C. H. Loring, "Some Metallurgical Aspects of Ship Steel Quality," *Welding J., Res. Suppl.*, Vol. 30 (1951) p. 79s.
23. A. B. Bagsar, "Notch Sensitivity of Mild Steel Plates," *Welding J., Res. Suppl.*, Vol. 28, (1949) p. 484s.
24. T. M. Norin, *Trans. N. E. Coast Inst. Eng. and Shipbuilders*, Vol. 73 (1956) p. 87.
25. E. T. Wessel and W. H. Pryle, "Brittle Fracture Characteristics of a Reactor Pressure Vessel Steel," *Welding J., Res. Suppl.*, Vol. 40, January 1961, p. 41s.
26. G. B. Espey, M. H. Jones and W. F. Brown, Jr., "The Sharp Notch Strength of Several High Strength Sheet Alloys," *Proc. ASTM*, Vol. 59 (1959) p. 837.

27. G. Sacks and J. G. Sessler, "Effect of Stress Concentration on Tensile Strength of Titanium and Steel Alloy Sheet at Various Temperatures," ASTM Preprint 76a (1960).
28. V. Wein and J. G. Sessler, "Analysis of the Effects of Test Temperature on the Notch Strength of High Strength Sheet Alloys," ASTM Preprint 80d, (1961).
29. ASTM Special Committee, "Fracture Testing of High Strength Sheet Materials," ASTM Bulletin, January 1960, p. 29, February 1960, p. 18.
30. E. T. Wessel, "Brittle Fracture Strength of Metals," ASTM, S.T.P. No. 283, "Properties of Crystalline Solids," (1960) p. 99.
31. T. S. Robertson, "Brittle Fracture of Mild Steel," Engineering, (London) Vol. 172 (1951) p. 445.
32. T. S. Robertson, "Propagation of Brittle Fracture in Steel," J. Iron and Steel Inst., Vol. 175 (1953) p. 361.
33. T. S. Robertson and D. Hunt, and J. W. Scot. Iron and Steel Inst., Vol. 60 (1953) p. 259.
34. T. S. Robertson, "Conference on Properties at High Rates of Strain," Inst. Mech. Eng. (1957).
35. F. J. Feely, D. Hrtko, S. R. Kleppe and M. S. Northrup, "Report on Brittle Fracture Studies," Welding J., Res. Suppl., Vol. 33 (1954) p. 99s.
36. F. J. Feely, et al, "Studies on the Brittle Failure of Tankage Steel Plates," Welding J., Res. Suppl., Vol. 34, No. 12 (1955) p. 596s.
37. A. A. Wells, P.H.R. Lane and G. Coates, "Experiments on the Arrest of Brittle Cracks in 36" Wide Steel Plates," British Welding J., December, 1956, p. 554.
38. R. J. Mosborg, "An Investigation of Welded Crack Arresters," Welding J., Res. Suppl., Vol. 39, No. 1, (1960) p. 40s.
39. W. S. Pellini and J. E. Srawley, "Procedures for the Evaluation of Fracture Toughness of Pressure-Vessel Materials," NRL Report No. 5609, June 8, 1961, p. 10.
40. S. Yukawa, "Testing and Design Considerations in Brittle Fracture," Presented at 64th Annual Meeting ASTM, Atlantic City, New Jersey, June, 1961.

41. M. L. Williams, "Analysis of Brittle Behavior in Ship Plate," ASTM, S.T.P. No. 158, "Metallic Materials at Low Temperatures," (1954), p. 11.
42. S. Yukawa, "Temperature and Microstructure Dependence of Size Effects in Notched Bend Tests of Some Alloy Steels," ASM Preprint No. 238 (1960).
43. L. E. Benson and S. J. Watson, "The Brittle Fracture Problem and the Local Carrying Capacity of Structures," Metallurgia, April, 1960 p. 145.
44. B. M. Wundt, "A Unified Interpretation of Room-Temperature Strength of Notched Specimens as Influenced by Their Size," ASME Paper 59 Met 9 (1959).
45. G. O. Sankey, "Spin Fracture Tests of Ni Mo V Rotor Steels in the Brittle Fracture Range," Proceedings, ASTM, Vol. 60 (1960) p. 721.
46. D. H. Winne and B. M. Wundt, "Application of Griffith-Irwin Theory of Crack Propagation to the Bursting Behavior of Disks Including Analytical and Experimental Studies," Trans. ASME, Vol. 80 (1958), p. 1643.
47. G. R. Irwin, "Relation of Crack Toughness Measurements to Practical Applications," Welding J., Res. Suppl., Vol. 41, No. 11, November 1962, p. 519s.
48. R. W. Nichols, et al, "A Limit Approach to the Prevention of Pressure Vessel Failure," Preprint of International Conference on Fracture, No. 3 (Chap. C, D, E) Sendai, Japan, September 1965, p. DII-19.
49. D. R. DeForest, D. L. Newhouse and B. R. Seguin, "Progress in the Development of Steam Turbine Generator Rotor Materials," ASME Paper 57A280, December 1957.
50. E. T. Wessel and L. E. Hays, "Fracture Characteristics of Some High-Strength Weldable Structural Steels," Welding J., Res. Suppl., Vol. 42, No. 11, November 1963, p. 512s.
51. C. J. Boyle, et al, "Further Progress in the Development of Large Steam Turbine and Generator Rotors," GEP Paper 2216, Presented at ASTM 68th Annual Meeting, Purdue University, June 1965.
52. ASME Subcommittee on Brittle Fracture, "A Review of Engineering Approaches to Design Against Brittle Fracture," ASME Special Publication, May 1965.

53. Ludwik, "Die Bedeutung des Gleit-Und Reissividerstandes für die Werkstoffprüfung," Z. Ver. deut. Ing., Vol. 71, No. 2, 1927, pp. 1532-1538.
54. E. Parker, "Brittle Fracture of Engineering Structures," John Wiley & Sons, 1957.
55. D. C. Drucker, "A Continuum Approach to the Fracture of Metals," Brown University Report, ARPA-E4.
56. R. Beeuwkes, Jr., "Plasticity and Fracture," Proc. Third Sagamore Ordnance Materials Research Conference, Duke University, Durham, North Carolina, 1956.
57. J. A. Hendrickson, D. S. Wood, and D. S. Clark, "The Initiation of Brittle Fracture in Mild Steel," Trans. ASM, Vol. 50, 1958, p. 656.
58. J. A. Hendrickson, D. S. Wood, and D. S. Clark, "Prediction of Transition Temperature in a Notched Bar Impact Test," Trans. ASM, Vol. 51, 1959, p. 629.
59. D. J. Krause, "An Influence of Grain Size on the Initiation of Brittle Fracture in Mild Steel," Calif. Institute of Tech., 8th Interim Tech. Report, Army Res. Off. DA-04-495-ORD-1631.
60. J. G. Sessler, "Behavior of a Brittle Metal," presented at Seventh Sagamore Ord. Materials. Res. Conf., August, 1960.
61. J. D. Lubahn, "Correlation of Tests Using Congruency Principle," Proc. ASTM, Vol. 58, 1958, p. 678.
62. G. T. Schaeffer, V. Weiss, "Effect of Section Size on Notch Strength," Syracuse University Research Institute Report MET. E-1078-1064-FR.
63. P. Kuhn, "A Comparison of Fracture Mechanics and Notch Analysis," presented at the ASTM Special Committee on Fracture Testing.
64. J. Mulherin, D. Armiento, H. Markus, "The Relationship Between Fracture Toughness and Stress Concentration Factors for Several High-Strength Aluminum Alloys," ASME Paper No. 63-WA-306.
65. H. Neuber, "Kerbspannungslehre," Springer, Berlin, 1937 and 1958; English Translation available from Edwards Bros., Ann Arbor, Michigan.
66. A. S. Sokolnikoff, "Mathematical Theory of Elasticity," McGraw-Hill Book Company, Inc., New York, New York, 1956.

67. R. E. Peterson, "Stress Concentration Design Factors," John Wiley & Sons, Inc., New York, New York, 1953.
68. E. L. Stowell, "Stress and Strain Concentration at a Circular Hole in an Infinite Plate", NACA TN 2073, 1950.
69. H. F. Hardrath and L. Ohman, "A Study of Elastic and Plastic Stress Concentration Factors Due to Notches and Fillets in Flat Plates," NACA Report 1117, 1953.
70. H. Neuber, "Theory of Stress Concentration for Shear Strained Prismatical Bodies with Arbitrary Non-Linear Stress-Strain Law," Trans. ASME, Vol. 28, Series E, 1961, p. 544
71. V. Weiss, "Current Views and Theories on Fracture, Crack Initiation and Propagation," presented at Seventh Sagamore Ord. Materials Res. Conf. Aug., 1960.
72. C. Mylonas, "Exhaustion of Ductility and Brittle Fracture of E-Steel Caused by Prestrain and Aging," Second Progress Report of Project, SR-158, SSC, Bureau of Ships.
73. D. C. Drucker, C. Mylonas, G. Lianis, "Exhaustion of Ductility of E-Steel in Tension Following Compressive Prestrain," Welding J. Res. Suppl., Volt. 39, 1960, p. 117s.
74. H. Kihara and K. Masubuchi, "Effect of Residual Stress on Brittle Fracture," Weld. Res. Suppl. Vol. 38, 1959, p. 159s.
75. J. E. Jobaris, "The Influence of Compressive Prestrain on the Fracture Toughness of S.A.E. 4340 Steel," University of Illinois, TAM Report No. 219. 1962.
76. F. A. McClintock, discussion of paper by G. R. Irwin entitled, "Fracture Mode Transition for a Crack Traversing a Plate," Trans. ASME, J. of Basic Engrg., Vol. 82, 1960, p. 417.
77. F. A. McClintock, "Ductile Fracture Instability in Shear," J. of Applied Mechanics, Dec., 1958, p. 582.
78. J. Krafft and G. Irwin, "Crack-Velocity Considerations," Fracture Toughness Testing and its Applications, ASTM Special Technical Publication No. 381.
79. A. A. Wells, Proc. Roy. Soc. A, 285, 34 (Paper II), 1965.
80. A. A. Griffith, "The Phenomena of Rupture and Flow in Solids," Royal Soc. (London) Phil. Trans. Series A, V. 221, (1920), pp. 163-198.

81. G. R. Irwin, "Fracture Dynamics," Fracturing of Metals, Am. Soc. Metals, Cleveland, 1948, pp. 147-166.
82. E. Orowan, "Fracture and Strength of Solids," Report on Progress in Physics, Phys. Soc. London, 12, p. 185 (1949).
83. H. F. Bueckner, "The Propagation of Cracks and the Energy of Elastic Deformation," Trans. ASME, Journal of Applied Mechanics, 1958.
84. P. C. Paris, G. Sih, "Stress Analysis of Cracks, Fracture Toughness Testing and Its Applications," ASTM Special Technical Publication No. 381.
85. G. R. Irwin, "Analysis of Stresses and Strains Near the End of a Crack Traversing a Plate," Trans. ASME, Journal of Applied Mechanics, 1957.
86. R. Hill, "The Mathematical Theory of Plasticity," Oxford Press, 1950.
87. W. Weibull, "A Statistical Theory of Strength of Metals," Proc. Roy. Swedish Inst. Engr. Research, V. 193 (1939), No. 151.
88. Subcommittee on Brittle Fracture of the ASME Research Committee on Prevention of Fracture in Metals, "A Review of Engineering Approaches to Design Against Fracture," an ASME publication, 1964.

TABLE OF CONTENTS

Section 6.2

	<u>Page</u>
6.2 SUMMARY OF THE STATE OF THE ART OF FRACTURE MECHANICS	82
6.2.1 Description of the Evolution of the Approach	82
6.2.2 Description of Basic Terminology	83
6.2.2.1 Fracture Appearance	83
6.2.2.2 Brittle Fracture and Ductile Fracture	85
6.2.2.3 Frangible and Tough	86
6.2.2.4 Modes of Fracture	86
6.2.2.5 Energy Release Rate	88
6.2.2.6 Stress Intensity Factor	88
6.2.2.7 Plane Stress and Plane Strain	91
6.2.2.8 Plastic Zone Size	92
6.2.2.9 Fracture Mode Transition with Variation in Plate Thickness	93
6.2.2.10 Effect of Plate Width	96
6.2.2.11 Plastic Zone Size Correction Factor	97
6.2.2.12 Slow Crack Growth	98
6.2.3 Influence of Mechanical and Metallurgical Variables. . .	101
6.2.3.1 Mechanical Variables.	101
6.2.3.2 Metallurgical Variables	105
6.2.4 Summary of Tests for Plane Strain Fracture Toughness (K_{Ic} or G_{Ic})	111
6.2.4.1 Types of Specimens.	111
6.2.4.2 Calibration of Specimens.	113
6.2.4.3 Fatigue Cracking of Test Specimens.	113
6.2.4.4 Instrumentation for K_{Ic} Testing	130

TABLE OF CONTENTS (Cont.)

	<u>Page</u>
6.2.4.5 Summary and Comparison of Specimens	131
6.2.4.6 Summary	132
6.2.5 General Experience in Applying Fracture Mechanics.	132
6.2.6 Limitations of Fracture Mechanics.	133

LIST OF TABLES

Section 6.2

SUMMARY OF THE STATE-OF-THE-ART OF FRACTURE MECHANICS

	<u>Page</u>
Table I Comparison of Various Fracture Toughness Specimens	114
Table II Recommended Minimum Specimen Dimensions and Ratios of Required Loads.	114

LIST OF FIGURES

Figure 1. Modes of fracture.	84
Figure 2. (a) Brittle fracture at component level	86
(b) Ductile fracture at component level	86
Figure 3. Basic modes of crack surface displacements	87
Figure 4. Coordinates measured from the leading edge of a crack and the stress components in the crack tip stress field	90
Figure 5. Approximation of plastic zone sizes under plane strain and plane stress conditions	94
Figure 6. Three-dimensional schematic diagram of the crack surface, the crack front and the plastic zone	94
Figure 7. Dependence of K_c and fracture appearance on thickness of plate specimens	95
Figure 8. Effect of specimen width on K_c	97
Figure 9. Correlation of crack growth rates 7075-T6 aluminum alloy under sinusoidal loading with cyclic change in stress intensity, ΔK	99

LIST OF FIGURES (Cont.)

	<u>Page</u>
Figure 10. Crack growth rate versus field parameter for 100 percent R.H. at 80°F. Data for H-11 steel at 230 ksi yield strength.	100
Figure 11. Summary plot: crack growth rates versus stress field parameter for several relative humidities at 80°F	100
Figure 12. The effect of strain rate on the K_{Ic} fracture toughness of an 18 Ni maraging steel-300 grade	103
Figure 13. Fracture toughness as a function of strain rate for mild steel at several temperatures.	103
Figure 14. Expected general behavior of K_{Ic} as a function of strain rate	106
Figure 15. Temperature dependence of K_{Ic} fracture toughness of annealed A302B steel, WOL specimen	106
Figure 16. Temperature dependence of the fracture toughness of a Ni Mov forging steel	107
Figure 17. Temperature dependence of fracture toughness for ship plate	107
Figure 18. The effect of tempering temperature on the yield strength and fracture toughness of SAE 4340 steel plate	109
Figure 19. Temperature dependence of K_{Ic} fracture toughness of various lots of A302B steel.	110
Figure 20. Variability of room temperature fracture toughness with yield strength for 18 Ni maraging steel	112
Figure 21. K_{Ic} as a function of yield strength for 18 Ni maraging steel (various aging treatments).	112
Figure 22. Symmetrical center - cracked plate	115
Figure 23. Symmetrical edge - cracked plate	116
Figure 24. Single-edge-notched plate (tension).	117

LIST OF FIGURES (Cont.)

	<u>Page</u>
Figure 25. Notched bend specimen (three-point loaded) . . .	118
Figure 26. Notched bend specimen (four-point loaded). . . .	119
Figure 27. Surface cracked plate.	120
Figure 28. Circumferentially notched and fatigue - cracked round bar	121
Figure 29. Symmetrical center notched disc (rotor or spin specimen).	122
Figure 30. Wedge-opening-loading (WOL) type center- line loaded specimen	123
Figure 31. K calibration for the center-cracked plate specimen	124
Figure 32. K calibration for the single-edge crack tension specimen	125
Figure 33. K calibrations for bend specimens	126
Figure 34. K calibration for circumferentially cracked- notched round bar.	127
Figure 35. K calibrations for compact crack-line loaded specimens	128
Figure 36. Calibration - numerical constant " C_3 " as a function of the a/\sqrt{W} ratio for the "T" type WOL specimen	129

Section 6.2

SUMMARY OF THE STATE-OF-THE ART OF FRACTURE MECHANICS

6.2.1 BRIEF DESCRIPTION OF THE EVOLUTION OF THE APPROACH

The fracture mechanics approach which is now being extensively used has grown from a concept presented by Griffith⁽¹⁾ in 1920. Griffith suggested that the fracture strength of very brittle materials (glass) would be limited by the largest of a distribution of tiny cracks always present in the material at the time of testing. He suggested that the strength could be calculated from solid state surface energy and crack size by a critical instability relation. Instability was assumed to occur when the strain energy release rate with crack extension exceeded the rate of increase of surface energy. Griffith's experimental results obtained from glass were high compared to those predicted by his theory, but the results were encouraging.

Due to the increased occurrence of brittle fracture failures during the World War II period, Griffith's energy concept was re-examined. In 1948 Irwin⁽²⁾ proposed that the Griffith theory could be modified and applied to metals which are not as brittle as glass by considering the energy balance between the strain energy release rate and the plastic strain work rate required for crack extension. At approximately the same time Orowan⁽³⁾ (1949) suggested a modification of the Griffith theory very similar to that proposed by Irwin but inferred that the theory could be used only for relatively brittle materials. In 1952 Irwin and Kies⁽⁴⁾ showed that the modified form of the Griffith concept in which the plastic strain work is considered could be widely employed in fracture strength analysis in the presence of substantial amounts of plastic strain so long as fracture occurred prior to general yielding. This subsequently led to the extension of the modified Griffith approach to design applications.

In 1957 it was shown⁽⁵⁾ that the energy release rate G , could be directly related to the stress intensity factor K . Subsequently the stress intensity factor approach to brittle fracture has surpassed the energy release rate approach in general acceptance and use.

In 1959 the ASTM Special Committee on Fracture Testing of High Strength Metallic Materials was formed. The committee has provided tentative recommendations on crack toughness measurement procedures which have received extensive use. In general the recommendations of the committee have been based on fracture mechanics concepts. A significant recommendation made by the committee has been that test specimens should have fatigue cracked flaws and plane strain conditions at the crack tip.

In 1963 it was shown by Paris and Erdogan⁽⁶⁾ that cyclic crack growth could be expressed as a function of the stress intensity factor. Later, 1965, it was also demonstrated by Johnson and Willner⁽⁷⁾ that slow corrosive crack growth could be expressed as a function of the stress intensity factor. Since about 1960 the number of publications dealing with fracture mechanics concepts and applications has increased at an extremely high rate.

6.2.2 DESCRIPTION OF BASIC CONCEPTS AND TERMINOLOGY

An understanding of the various aspects of fracture mechanics requires a knowledge of the related terminology and concepts. The necessary terminology consists of that which is common to fracture mechanics only and that which is related to fracture in general. Some of the terms used in the field of fracture mechanics have a number of somewhat different meaning and the exact interpretation will depend upon the context of the terms. Some of the more significant concepts and terminology will be defined and discussed in this section.

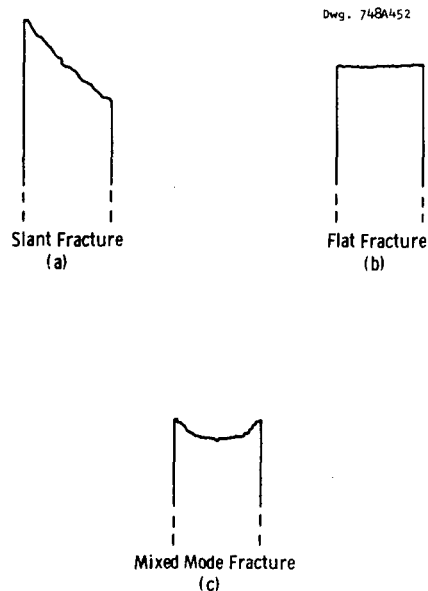
6.2.2.1 Fracture Appearance⁽⁸⁾

The fracture surface of a body can be described in macroscopic terms or in microscopic terms. The macroscopic viewpoint usually involves a description of the orientation of the fracture plane and an unaided eye description of the texture of the fracture surface. In general the orientation of the fracture surface can be placed in one of two categories: (1) flat fracture or (2) slant fracture as indicated in Figure 1 (a) and (b).

The term flat fracture is used when the plane of the fracture surface is perpendicular to the axis of a high tensile stress. Flat fracture is also commonly referred to as square fracture. In general this orientation of the fracture surface accompanies fracture which occurs with relatively little plastic flow at the fracture surface. This type of fracture usually has a granular or crystalline appearance.

When the plane of the fracture surface is oblique to an axis of high tensile stress, the term slant fracture is used. This type of fracture is usually accompanied by large amounts of plastic flow in the fracture area and occurs on planes of high shear stress. Slant fracture is usually accompanied by scratches and striations on the fracture surface and is fibrous in appearance.

In most cases the fracture surface is composed of both a slanted segment and a flat segment as shown in Figure 1(c). This condition will be discussed further in the section of thickness transition (6.2.2.9).



Sec. 6.2 Fig. 1 - Modes of fracture

Surfaces observed through a light microscope are sometimes classified as brittle if the fracture path is transcrystalline (through the grains) or intercrystalline (along the grain boundaries). A ductile fracture is generally characterized by a fibrous tearing of the grains.

Observation by the electron microscope reveals another level of fracture surface description. The descriptive terminology used at the level will not be discussed here because of its limited use in engineering design at the present time. Electron microscope studies of fracture surfaces are providing quite valuable in investigations aimed at determining the microscopic parameters which govern the fracture process.

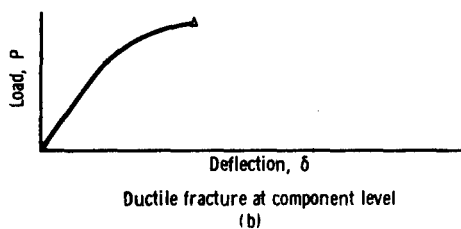
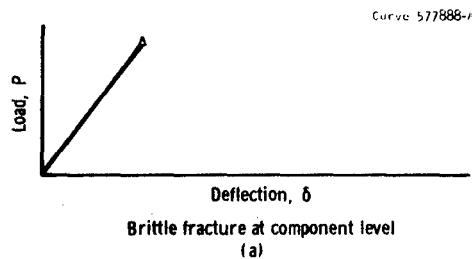
6.2.2.2 Brittle Fracture and Ductile Fracture

Due to their extensive use the terms brittle fracture and ductile fracture have accumulated a number of somewhat different interpretations. This difference in interpretation can be related to the different viewpoints which are being considered when the terms are used. When discussing brittle and ductile fracture, three levels of consideration can be used: (1) the component level, (2) the level corresponding to the area local to the crack tip, and (3) the microscopic level.

At the component level, the interpretation of brittle fracture and ductile fracture is related to the load deflection curve of the component. If the load-deflection curve has remained relatively linear up to the fracture point as shown in Figure 2(a) then the fracture is defined as brittle. If the load-deflection curve became appreciably non-linear before fracture as shown in Figure 2(b) then the fracture is referred to as ductile.

On the level corresponding to the local macroscopic fracture surface the fracture is referred to as brittle if the fracture is flat and accompanied by a minimum of plastic flow. The term ductile fracture is used if the fracture surface is slanted and large amounts of plastic flow are observed at the fracture surface.

At the microscopic level fracture is considered brittle if the fracture surface is granular or crystalline in appearance. At this level ductile fracture is defined as that which has a fibrous jagged appearance and is usually accompanied by striations and scratches.



Sec. 6.2 Fig. 2

6.2.2.3 Frangible and Tough

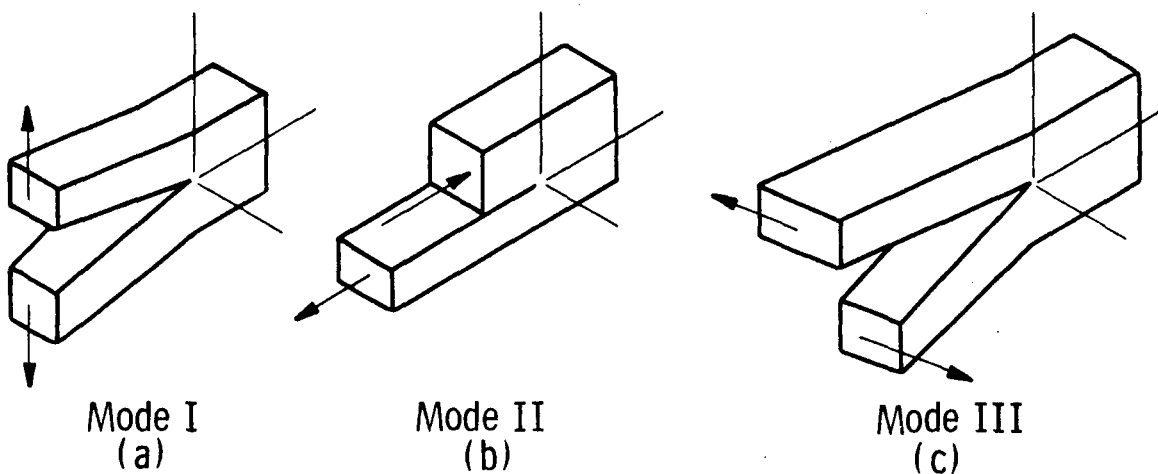
Frangible and tough are terms which are now being used instead of brittle and ductile in certain situations. As just discussed, brittle and ductile can have a number of somewhat different meanings, and the particular meaning intended in each situation is not always clear. The terms frangible and tough are used to eliminate some of this confusion. When fracture occurs at a nominal stress below the yield stress of the material and the amount of plastic flow at the fracture surface is small the fracture is referred to as frangible rather than brittle. Similarly, when the fracture stress is greater than the yield stress and gross plastic deformations have occurred the behavior is referred to as tough instead of ductile.

6.2.2.4 Modes of Fracture

The mode of fracture refers to the direction of the relative motion between the two corresponding crack surfaces during the fracture process. The relative crack surface movements can be resolved into three basic modes. In mode I, the opening mode, the crack surfaces move opposite

and perpendicular to each other as shown in Figure 3(a). In mode II, the forward sliding mode as shown in Figure 3(b), the two crack surfaces move in approximately the same plane and in a direction perpendicular to the line of the crack tip. Mode III, the tearing mode as shown in Figure 3(c), is the mode in which the two corresponding crack surfaces move in approximately the same plane and in a direction which is parallel to the line of the crack front. These three modes are sufficient to describe all forms of crack surface displacements. The flat fracture described previously is equivalent to mode I. Also the slant fracture can usually be related to mode II. Normally the fracture of flat specimens involves both a flat and a slant surface so that both modes I and II are involved. Most fracture mechanics studies are predominantly mode I although some limited studies⁽⁹⁾ of mode II and III have been performed.

Dwg. 748A456



Sec. 6.2 Fig. 3 - Basic modes of crack surface displacements

6.2.2.5 Energy Release Rate

The energy release rate, G , of an elastic body subject to external loads and containing a crack is the energy, per unit of new crack area, provided by the body for the crack-extension process. This concept was discussed in some detail in Section 6.1.3.3.a. In brief, it was shown that the released energy was provided by the work of the external forces acting on the body and the change in the elastic strain energy of the body during the crack extension. Neglecting small order terms, the energy absorbed by the fracture process is that needed to perform the plastic work at the crack tip as it extends.

If the size of the plastic zone at the crack tip of an actual specimen is very small compared to the total volume of the specimen, then the elastically determined energy release rate can be considered to be approximately equal to the actual energy release rate of the specimen.

The energy release rate of the cracked body is a function of the mode of crack extension. The energy release rates corresponding to modes I, II, and III are defined as G_I , G_{II} , and G_{III} , respectively.

Once the elastic stress and strain distribution of a body containing a crack are known the energy release rate of the body can be determined by means of equation (9) of Section 6.1.3.3.a.

$$G = - \left(\frac{\partial U}{\partial A} \right)_{\delta}$$

6.2.2.6 Stress Intensity Factor

The crack tip elastic stress fields, of all bodies which are loaded such that the crack surfaces have a mode I type of displacement, differ by a multiple constant only. As presented in Section 6.1.3.3.b the general stress distribution for this class is

$$\begin{aligned}\sigma_x &= \frac{K_I}{(2\pi r)^{1/2}} \cos \frac{\theta}{2} \left[1 - \sin \frac{\theta}{2} \sin \frac{3\theta}{2} \right] \\ \sigma_y &= \frac{K_I}{(2\pi r)^{1/2}} \cos \frac{\theta}{2} \left[1 + \sin \frac{\theta}{2} \sin \frac{3\theta}{2} \right] \\ \tau_{xy} &= \frac{K_I}{(2\pi r)^{1/2}} \sin \frac{\theta}{2} \cos \frac{\theta}{2} \cos \frac{3\theta}{2}\end{aligned}\quad (1)$$

$$\sigma_z = \nu (\sigma_x + \sigma_y) \quad (\text{plane strain})$$

$$\sigma_z = 0 \quad (\text{plane stress})$$

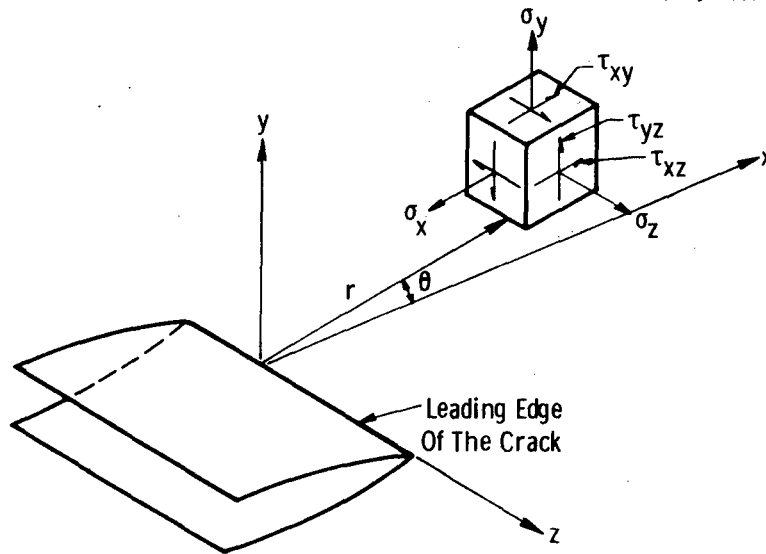
$$\tau_{xy} = \tau_{yz} = 0$$

where the coordinate system is shown in Figure 4 and K_I is defined as the mode I stress intensity factor. The displacement fields also differ by only a multiple constant and have the form (for plane strain conditions):

$$\begin{aligned}u &= \frac{2(1+\nu)K_I}{E} \left[\frac{r}{2\pi} \right]^{1/2} \cos \frac{\theta}{2} \left[1 - 2\nu + \sin^2 \frac{\theta}{2} \right] \\ v &= \frac{2(1+\nu)K_I}{E} \left[\frac{r}{2\pi} \right]^{1/2} \sin \frac{\theta}{2} \left[2 - 2\nu - \cos^2 \frac{\theta}{2} \right]\end{aligned}\quad (2)$$

$$w = 0 \quad (\text{plane strain})$$

where u , v , and w are the displacements in the x , y , and z directions respectively. Equations (1) and (2) are only exact as $r \rightarrow 0$. That is, the stress intensity factor only parametrically describes the stress field in a vicinity local to the crack tip. The stress intensity factor for each crack is a function of the geometry of the body containing the crack, size and location of the crack, and of the distribution of the external loads on the body. The means of determining the stress intensity factor for various geometries and loading conditions will be discussed in Section 8.2.4.



Sec. 6.2 Fig. 4 -Coordinates measured from the leading edge of a crack and the stress components in the crack tip stress field.

The stress and displacement fields around the tip of cracks, whose surfaces have the mode II type of relative displacement, also differ by only a multiple constant. The constant is defined as the mode II stress intensity factor K_{II} . The general distribution of the mode II stress and strain fields at the crack tip are given in reference (10). Similarly, the stress and strain distribution around the tips of mode III type cracks differ by only a multiple constant, K_{III} , and have a general form which is also given in reference (10).

The stress intensity factors for the various crack displacement modes act as a single parameter representation of the conditions at the crack tip. Since the stress intensity factors are determined by use of elastic conditions, the size of the plastic zone must be small compared to the zone at the crack tip in which the stress intensity factor accurately describes the elastic stress field. If the relative size of the plastic zone just prior to fracture is not small, then it cannot be expected that the elastically determined stress intensity factor will give single parameter representation of the fracture processes at the crack tip.

The stress intensity factors and the energy release rates for the various modes are directly related. The relationships⁽¹⁰⁾ are

$$\begin{aligned}
 G_I &= \frac{(1-\nu^2)}{E} K_I^2 \quad (\text{plane strain}) \\
 G_{II} &= \frac{(1-\nu^2)}{E} K_{II}^2 \quad (\text{plane strain}) \\
 G_{III} &= \frac{(1+\nu)}{E} K_{III}^2
 \end{aligned} \tag{19}$$

and for the case of plane stress:

$$\begin{aligned}
 G_I &= \frac{K_I^2}{E} \quad (\text{plane stress}) \\
 G_{II} &= \frac{K_{II}^2}{E} \quad (\text{plane stress})
 \end{aligned}$$

6.2.2.7 Plane Stress and Plane Strain

The state of stress throughout most bodies usually fall between the limits defined by the states of plane stress and plane strain. In a few limiting cases a body will be completely in a state of plane stress or completely in a state of plane strain. But normally it will consist of sections which are in a plane stress state, sections which are in a plane strain state, and sections whose state is somewhere between these two limits. In the mathematical theories of elasticity and plasticity the terms plane stress and plane strain are defined in a rather rigorous manner, but when the terms are used in the field of fracture mechanics these rigorous definitions are sometimes relaxed somewhat.

In the mathematical theory of elasticity and plasticity, a state of plane stress exists when the following conditions are satisfied:

$\sigma_z = \tau_{xz} = \tau_{yz} = 0$. An example of a plane stress condition is a very thin sheet which is subject to in-plane external loads which do not vary in intensity through the thickness of the sheet.

Similarly, a state of plane strain exists when the following conditions are satisfied: $\epsilon_z = \tau_{xz} = \tau_{yz} = 0$. For elastic conditions these relations insure that $\sigma_z = \nu(\sigma_x + \sigma_y)$. A long cylinder which is restrained at its ends and whose external load distribution doesn't vary in the axial direction is an example of a body in a plane strain state.

Another state of stress which is commonly referred to is that of relative plane strain. This state is defined as one in which $\epsilon_z = \epsilon_0$ and $\tau_{xy} = \tau_{yz} = 0$ where ϵ_0 is a constant. Under these conditions $\sigma_z = E\epsilon_0 + \nu(\sigma_x + \sigma_y)$ in the elastic range. A cylinder whose ends are not restrained and whose external load distribution doesn't vary in the axial direction is in a state of relative plane strain.

As stated above most bodies have regions which are in a state of plane stress, regions which are in a state of plane strain, and also regions whose state falls somewhere between the two limits. For instance a relatively thick plate subject to in-plane loading has a plane strain region at mid-thickness and a plane stress region at the two lateral surfaces.

6.2.2.8 Plastic Zone Size

Equations (1) of Section 6.2.2.6 indicate that the elastically determined stresses approach infinity as the crack tip is approached ($r \rightarrow 0$). Therefore, since most engineering materials have finite yield stresses plastic flow will occur in a zone surrounding the crack tip prior to fracture. This plastic zone has been experimentally observed on the outside surface of specimens and experimental attempts⁽¹¹⁾ have been made to determine the size of the zone away from the surface area. From an analytical point of view the size of the plastic zone could be determined by a rigorous solution of the appropriate plasticity equations. Due to the mathematical difficulty involved in such an approach an exact solution has only been obtained for a mode III crack.⁽¹²⁾ Numerical solutions have been used to obtain the size of the plastic zone in the more interesting mode I type of crack configuration.⁽¹³⁾

A rough estimate of the size and shape of the plastic zone for mode I cracks can be obtained by assuming that the elastic stress dis-

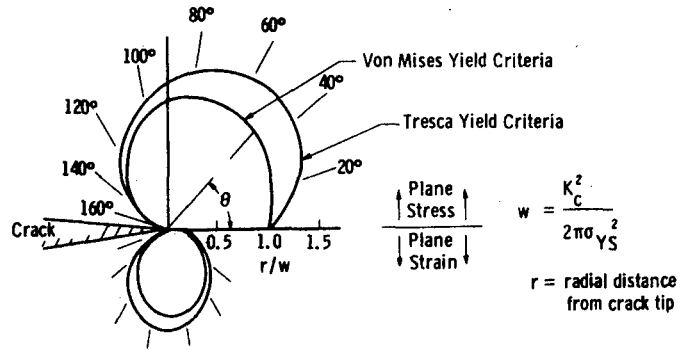
tribution given in equations (1) of Section 6.2.2.6 is valid up to the plastic zone boundary. The plastic zone sizes obtained by this method are shown in Figure 5. The shape of the zone for conditions of plane strain and plane stress are shown for both the von Mises yield condition and the Tresca yield condition. The zones will actually be larger than those shown for the various conditions because of the relaxation of the elastic stresses caused by the yielding. The higher the amount of material strain hardening the more exact this approximation becomes. Also the size of the plastic zone must be small compared to the zone in which the elastic stresses can be described by equations (1). If this situation doesn't exist then the size and shape shown in Figure 5 will not be realistic.

In a relatively thick plate the size of the plastic zone at mid thickness would be approximately equal to the zone size shown for the plane strain condition in Figure 5. The size of the zone at the lateral surfaces would be roughly equal to that shown for the plane stress case in Figure 5. The variation in zone size between the mid-thickness and lateral surfaces would be expected to be similar to that shown in Figure 6.

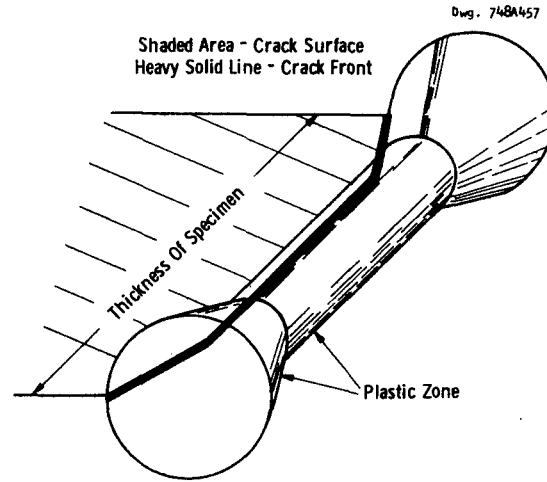
It should be noted that for a plate of fixed thickness the dimensions of the plastic zone are approximately proportional to $(K_c/\sigma_{YS})^2$ and the volume of the plastic zone is approximately proportional to $(K_c/\sigma_{YS})^4$. This conclusion can be arrived at from a study of Figure 5.

6.2.2.9 Fracture Mode Transition with Variation in Plate Thickness

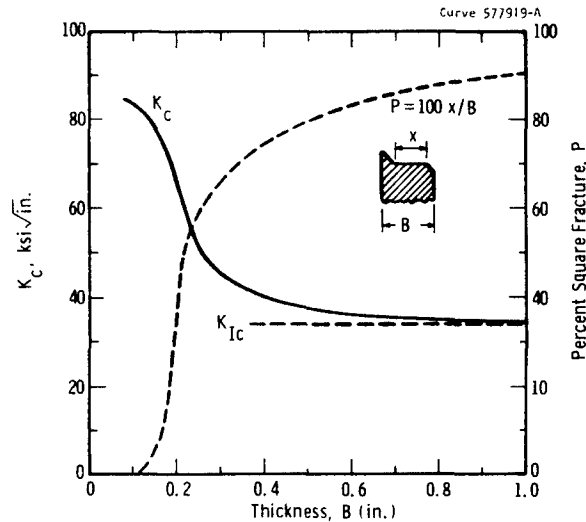
The effect of plate thickness on the critical stress intensity, K_c , of a material is illustrated in Figure 7. The results shown here were obtained from specimens which were tested at the same temperature and loading rate and which were independent of metallurgical processing variables. The specimens were also of sufficient width to give valid results at each thickness (6.2.2.10). Also shown as a function of thickness is the percent of square fracture. In general most high strength metals have the same trends and features as are demonstrated in Figure 7. As the mode of fracture changes with increasing plate thickness from 100% slant fracture to approximately 100% square fracture, the stress intensity



Sec. 6.2 Fig. 5 - Approximation of plastic zone sizes under plane strain and plane stress conditions



Sec. 6.2 Fig. 6 - Three-dimensional schematic diagram of the crack surface, the crack front and the plastic zone (21)



Sec. 6.2 Fig. 7—Dependence of K_c and fracture appearance (in terms of percentage of square fracture) on thickness of plate specimens. Schematic, but based on data for aluminum 7075-T6 (Ref. 15)

factor decreases in magnitude and asymptotically approaches a lower limit defined as K_{Ic} and referred to as the plane strain critical stress intensity factor. Of course a similar plot in which G_c is used instead of K_c will have the same features. In this case the lower limiting value is defined as G_{Ic} and refer to as the plane strain fracture toughness.

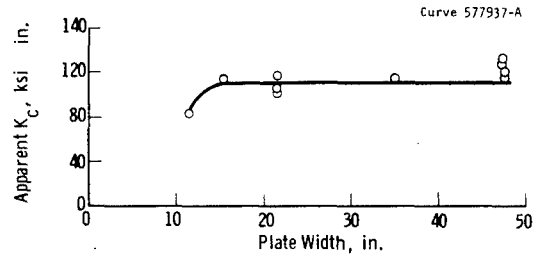
The transition in the fracture mode and decrease in K_c with increasing plate thickness have been qualitatively related to the change in the size of the plastic zone at the crack tip with increasing thickness.⁽¹⁴⁾ Also quantitative estimates have been made of the thickness needed to measure K_{Ic} values. These estimates usually require that the plate thickness be equal to or greater than some multiple of the plastic zone size and are expressed in the form $B = \alpha (K_{Ic}/\sigma_{YS})^2$ where B is plate thickness, σ_{YS} is the uniaxial yield stress of the material and α is a numerical constant. The value of α varies from material to material. Therefore, an estimate of the plate thickness needed to obtain a valid K_{Ic} value involves an initial guess as to the value of α and K_{Ic} for that material. For many materials an initial guess of α would be

between 2.0 and 3.0. The only reliable way of determining K_{Ic} is to test specimens at increasing thicknesses until the K_c values approach the lower limiting value.

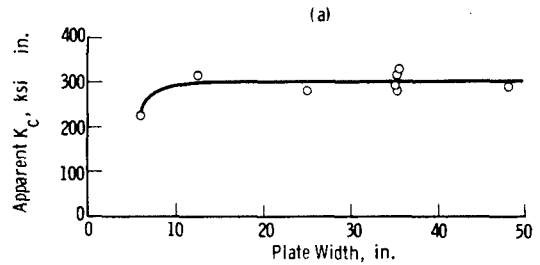
The plane strain critical stress intensity factor K_{Ic} is of particular importance because it represents a lower limit of the toughness of a material. Since K_{Ic} represents the toughness of a material under the most severe conditions, it can be used as a basis for rating the relative susceptibility of materials containing cracks to fail by catastrophic fracture. But in design situations in which plane strain conditions do not exist, a comparison of K_{Ic} values could lead to erroneous conclusions concerning the choice of the toughest material for an application.

6.2.2.10 Effect of Plate Width

As stated previously, the use of the stress intensity factor, which is determined from elastic conditions, as a single parameter representation of conditions at the crack tip requires that the plastic zone at the crack tip be small compared to the area in which the elastic crack tip stress field is accurately described by equations (17). The limitations of the use of K_c as the fracture parameter with respect to this consideration are demonstrated in Figure 8. In this figure critical stress intensity factors obtained from center cracked specimens, differing in absolute size, are shown. As the size of the specimens decreases below a certain size, it is observed that K_c no longer remains constant, and, therefore, the use of K as a single parameter fracture criteria in this size range becomes invalid. Since the size of the plastic zone at failure in each of these specimens is approximately the same, it is apparent that the decrease in K_c is due to the increase in the size of the plastic zone compared to the other dimensions of the specimens. Therefore if K_c is to be independent of geometry for a fixed thickness, temperature, and loading rate, the absolute size of the specimen must be greater than some "minimum size". For each geometric configuration the "minimum size" must be determined experimentally or estimated by use of previously determined experimental information. No analytic method for determining "minimum size" is presently available.



2219-T87 Aluminum plate ($B = 0.10$ in., $2a$ from 5 in. to 15 in.)



4330M Low alloy steel plate ($B = 0.14$ in., $2a$ from 3 in. to 12 in.)

Sec. 6.2 Fig. 8 - Effect of specimen width on K_c

6.2.2.11 Plastic Zone Size Correction Factor

The size requirements needed to obtain valid K_c measurements at various thicknesses can be relaxed somewhat by use of a plastic zone correction factor. Based on a suggestion made by Irwin,⁽¹⁵⁾ the effect of a limited amount of plastic flow at the crack tip can be corrected for by adding a fictitious incremental length, r_Y , to the physical crack length a_0 , and then using this corrected crack length, $a = a_0 + r_Y$ in calculating K_c . For plane stress conditions the correction term⁽¹⁶⁾ is $r_Y = K_I^2 / 2\pi\sigma_{YS}^2$ and for plane strain conditions the term is $r_{IY} = K_{Ic}^2 / 6\pi\sigma_{YS}^2$.

The theoretical basis for this correction is related to an elastic-perfectly plastic solution obtained by McClintock and Hult,⁽¹⁷⁾ for a mode III crack configuration. The solution showed that the elastic stress field surrounding the small plastic zone was exactly the same as the stress field of a totally elastic body whose crack tip was placed at the center of the plastic zone. This meant that the effective crack length was equal to the physical crack length plus half the diameter of the plastic zone.⁽¹⁵⁾ By use of an analogy between mode III and I the above correction factors were obtained.

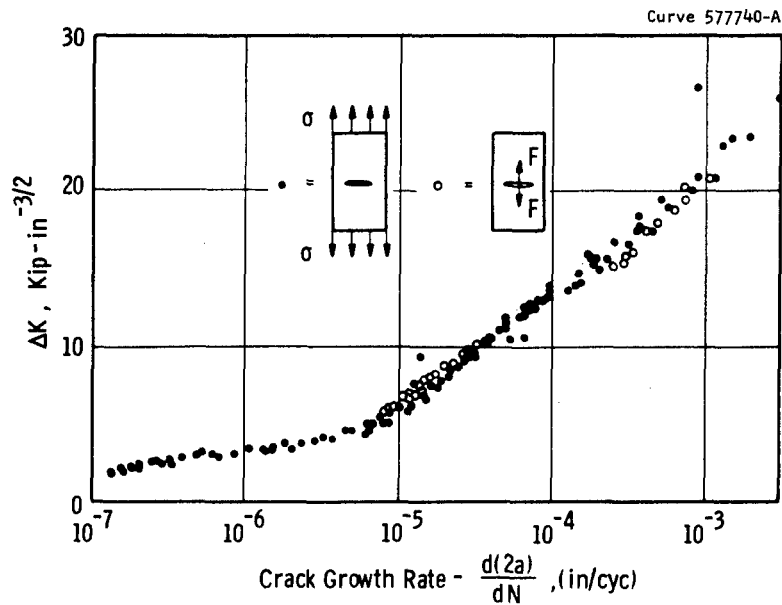
Use of the plastic zone correction factor is valid when the amount of yielding at the crack tip is small. If gross yielding occurs, then the use of the correction factor is of no aid, and linear elastic fracture mechanics cannot be used under these conditions.

6.2.2.12 Slow Crack Growth

All of the previous considerations of fracture mechanics in this text have been concerned with the prediction of the loads at which the onset of rapid catastrophic crack growth will occur. There are also many other areas in which the principles of linear fracture mechanics can be applied. One of the most promising is that of stable slow crack growth due to either cyclic loading or sustained loading in a corrosive environment. Since the stress intensity factor, K , defines the stress-strain distribution at the crack tip, under previously indicated conditions (sufficient size, etc.), it would be expected that the crack growth rates under similar conditions should be a function of the K parameter.

The general applicability of the stress intensity factor as a fatigue crack growth parameter is demonstrated by the results reported by Paris⁽¹⁸⁾ and shown in Figure 9. The correlation of the crack growth rates of these two different geometries by use of the stress intensity factor is quite good. Correlations similar to this for other geometries and materials led to the conclusion that within specific limitations, the rate of crack growth of a fatigue crack in a given material and environment depends, uniquely, on the local time-history of the stress intensity factor at the crack tip. This conclusion makes it possible to predict the fatigue life of various precrack geometries subject to known loading time-histories by use of data obtained from crack growth studies on a single specimen geometry.

Under the more restricted conditions of constant environmental conditions and sinusoidal loading, it has been shown that the stress intensity crack growth law can be put in the mathematical form^(18,19)
 $da/dN = f(\Delta K)$ where N is number of cycles. That is, the crack growth rate, da/dN , is a function of the change in stress intensity, ΔK , per cycle. Paris⁽¹⁸⁾ has shown that for many materials the law has the more specific

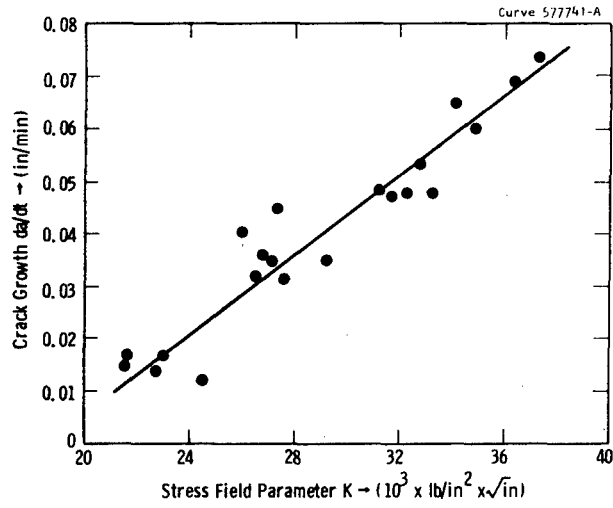


Sec. 6.2 Fig. 9 -Correlation of crack growth rates 7075-T6 aluminum alloy under sinusoidal loading with cyclic change in stress intensity, ΔK (18)

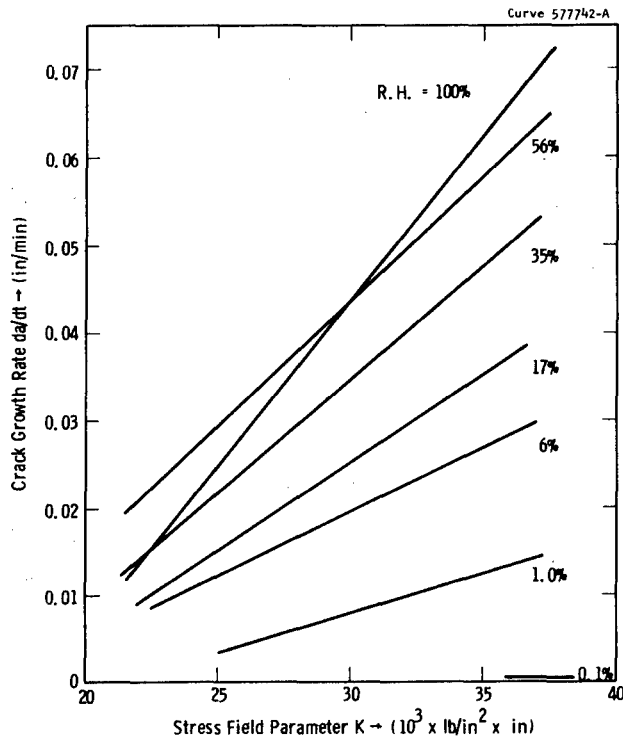
form $da/dN = C_0 (\Delta K)^4$ where C_0 is a material constant. Also a second power law, $da/dN = C_0 (\Delta K)^2$, has been developed by Liu⁽¹⁹⁾ from analytic considerations and has been shown to fit test results from some materials. Of course, the general use of the stress intensity approach to fatigue crack growth is not dependent on the validity of either of these specific relations.

Experimental results from work by Johnson and Willner⁽²⁰⁾ demonstrate that stable slow crack growth under static loading in high strength steels subject to high humidities can also be expressed as a function of the stress intensity factor. As shown in Figures 10 and 11, for the materials considered the crack growth rates for fixed environmental conditions are linear functions of the stress intensity. Investigators are presently considering the effects of fatigue crack growth in a corrosive environment from a stress intensity point of view.

In addition to not being applicable to crack initiation considerations, the use of the stress intensity factor as a crack growth parameter has the same limitations as those which have been discussed in



Sec. 6.2 Fig. 10.—Crack growth rate versus field parameter for 100 per cent R. H. at 80 °F. Data for H-11 steel, at 230,000 lb/in² yield strength. (20)



Sec. 6.2 Fig. 11.—Summary plot: crack growth rate versus stress field parameter for several relative humidities at 80 °F. Data for H-11 steel, at 230,000 lb/in² yield stress (20)

rapid catastrophic crack growth considerations. In brief this means that the size of the plastic zone must be small and gross yielding must not be present. Such limitations in general restrict the use of the stress intensity concept to low-stress high-cycle crack growth situations.

6.2.3 INFLUENCE OF MECHANICAL AND METALLURGICAL VARIABLES

6.2.3.1 Mechanical Variables

The two variables of temperature and strain rate (or loading rate) are the predominate mechanical variables which can have a strong influence on K_{Ic} -- the plane strain fracture toughness parameter for the opening mode of fracture. In considering these variables, it is convenient to divide the materials into two categories; the high strength steels, aluminum and titanium alloys which are relatively insensitive to variations in temperature and strain rate, and the low-strength, strain rate and temperature sensitive materials. It must be realized that the degree of sensitivity is relative, and therefore no sharp distinction between a sensitive and insensitive behavior can be made. As a guide, the Special ASTM Committee on Fracture Toughness Testing of Metallic Materials* has suggested⁽²²⁾ that materials with a strain rate sensitivity that does not exceed that found in martensitic steels heat treated to 200 ksi yield strength be considered as insensitive.

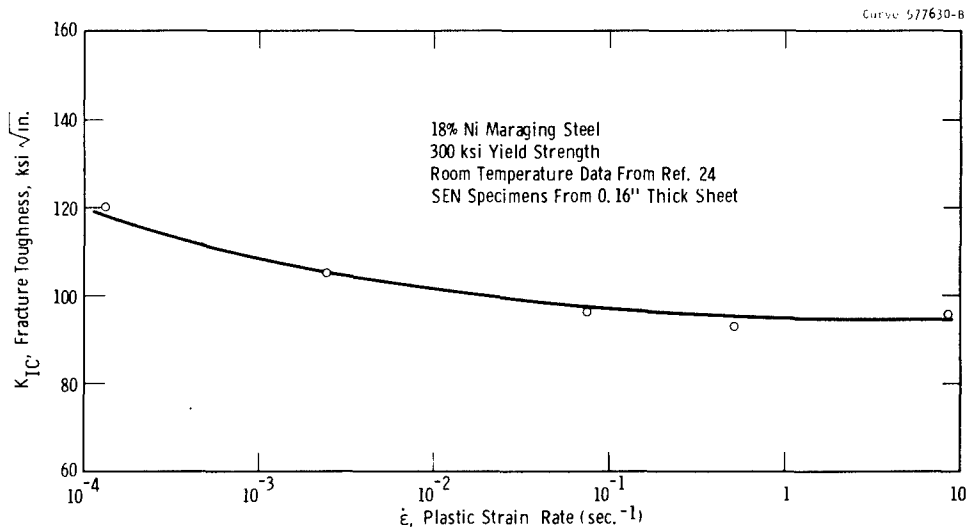
In considering the high strength materials, it should be realized that there can be exceptions to the general insensitive behavior pattern which has been reported.⁽²²⁻²⁴⁾ Some of the valid K_{Ic} data accumulated during the literature search (Appendix I) conducted in this project indicate an inconsistent behavior in the temperature dependence of the high strength materials. For example, the D6AC, H-11, AM355, and HP 9-4-25 quenched and tempered steels exhibit an appreciable increase in K_{Ic} with increased temperature.⁽²⁵⁻²⁷⁾ In SAE 4340 steel, the data from two investigations^(26,27) show K_{Ic} to be temperature dependent, whereas a third study⁽²⁵⁾ reports a temperature independent behavior. A similar difference in behavior is

* Now designated as ASTM Committee E24 on Fracture Testing of Metals with four Subcommittees.

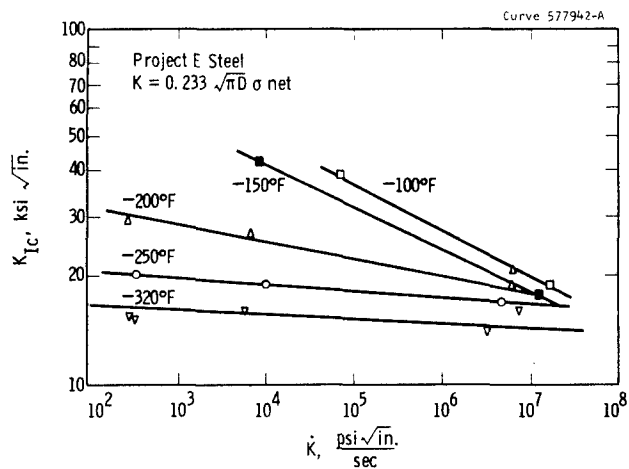
observed for the various investigations of 18% Ni maraging steels. (25,26,28) Strain rate experiments were not included in these studies, but based on the temperature dependence behavior, a corresponding effect of strain rate could be anticipated. In another study, Krafft⁽²⁴⁾ investigated strain rate effects at various temperatures in a 300 ksi yield strength maraging steel and observed only minor effects compared to lower strength steels. Figure 12 illustrates the strain rate sensitivity of the maraging steel. Because of these inconsistencies in the temperature dependence of K_{Ic} of high strength materials, it seems advisable that no generalizations be made when considering a specific material for a specific application. In this case, it is recommended that the temperatures and strain rates employed in the determinations of K_{Ic} correspond to those prevailing in the intended application. As a first approximation, however, those materials which exhibit an increase in yield strength with decreasing temperature or increasing strain rate can be expected to exhibit a decrease in K_{Ic} for those conditions which produce an increase in yield strength.

The temperature and strain rate dependence of K_{Ic} of the lower strength materials, such as the structural steels, have received much more attention than the high strength materials because these materials are known to exhibit pronounced changes in strength and toughness as a function of temperature or strain rate. Krafft has conducted several investigations^(23,24,29,30) with low strength steels in attempts to relate K_{Ic} and temperature, strain rate, yield strength, and work hardening exponent. The results of Krafft's investigations show marked strain rate dependence on K_{Ic} in ship plate, ASTM A302B steel, and a 150 ksi yield strength quenched and tempered steel. Some typical results for a mild steel are shown in Figure 13. Note that the rate of decrease of K_{Ic} with increasing strain rate becomes more pronounced at the higher temperatures where the yield strength is lower.

The general behavior of K_{Ic} as a function of strain rate is illustrated in Figure 14. While the data shown^(23,30) are specific to mild steel tested at -12°F , the basic form of the curve is believed to be representative of the general behavior of strain rate sensitive materials.



Sec. 6.2 Fig. 12 —The effect of strain rate on the K_{IC} fracture toughness of 18 Ni maraging steel-300 grade



Sec. 6.2 Fig. 13 —Fracture toughness as a function of strain rate (\dot{K}) for mild steel at several temperatures. Ref. 24

The data on the left side are estimated values of K_{Ic} for initial crack extension as a function of loading rate. The data on the right are values of K_{Ic} estimated for running cracks in wide plates. Between the two sets of data the curve is believed to be continuous as indicated by the dashed portion of the curve. Several rate effect criteria are provided (Figures 12-14); loading rate \dot{K} , strain rate $\dot{\epsilon}$, and crack velocity.

Referring to the left side of the diagram, K_{Ic} is seen to decrease as the rate is increased, eventually reaching a minimum at a crack velocity of about 10 ft/sec. After passing through a minimum, the K_{Ic} is seen to increase very rapidly with increased rates. This rapid increase in K_{Ic} is associated with adiabatic heating⁽³¹⁾ of the material in the vicinity of the crack tip. Because the heat being generated by plastic work at the advancing tip of the crack cannot be dissipated at a fast enough rate, a local rise in temperature occurs, thereby resulting in an increase of K_{Ic} to a value corresponding to the higher temperature.

In applying K_{Ic} data to applications where loading or strain rates are of concern, but the actual rates are ill defined, it appears advisable to use the minimum in the K_{Ic} vs strain rate curve. It should also be recognized that the minimum operating temperature should also be considered in conjunction with the minimum in the K_{Ic} rate curve.

The temperature dependence of K_{Ic} (at a constant strain rate) for the low strength materials is an area which is currently being investigated.⁽³²⁻³⁴⁾ Some of the available data are shown in Figures 15-17. Of significance is the fact that all of these materials, ranging from about 30-110 ksi yield strength, exhibit a significant (2 to 3 times) increase in K_{Ic} with increased temperature.

One of the controversial questions yet to be resolved is whether or not K_{Ic} undergoes an abrupt transition from low to high values over a very narrow temperature range, e.g., similar to energy absorption behavior in a Charpy impact test. The data in Figure 15 for annealed A302B steel do not indicate an abrupt rise in K_{Ic} . However, the validity of the K_{Ic} values above about 0°F are questionable (too high) in view of very recent changes suggested by ASTM E24 Committee⁽³⁵⁾; hence the dashed line. On the other hand, the data for the Ni MoV steel (Figure 16) suggest a rather

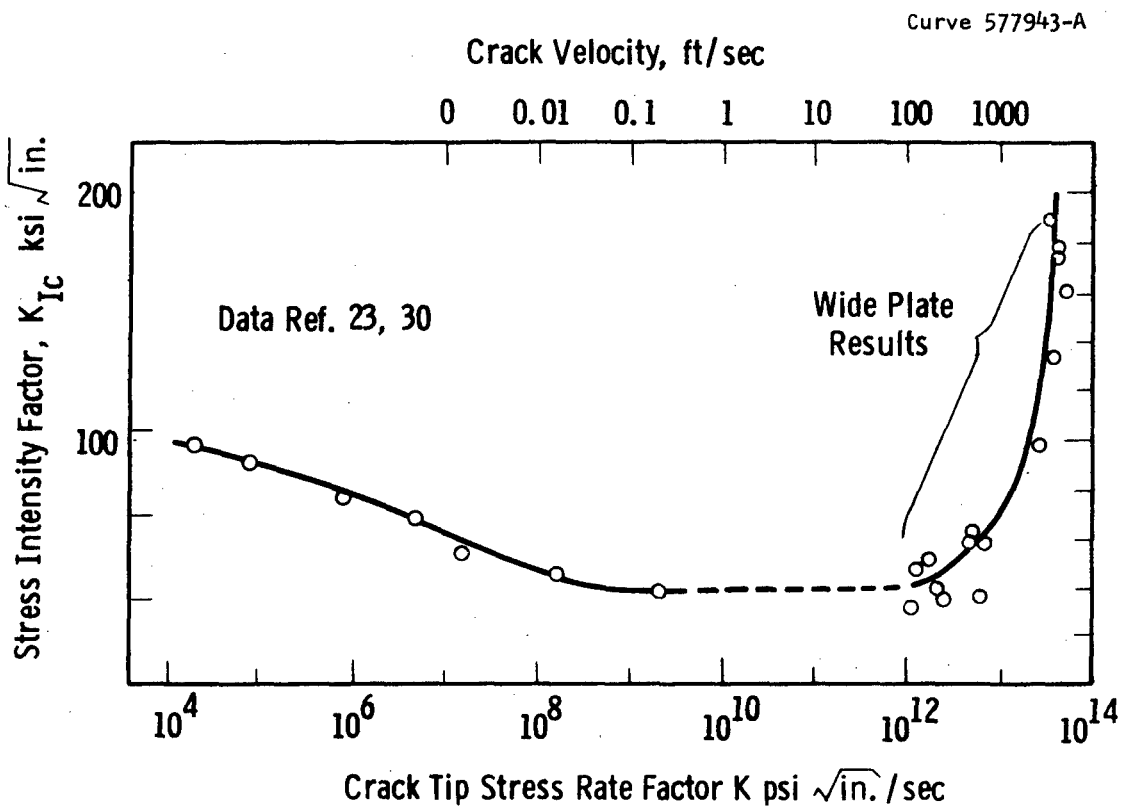
abrupt rise in K_{Ic} between 100 to 200°F. The authors⁽³⁴⁾ report these data to be valid K_{Ic} measurements at all temperatures. However, as was the case for the A302B steel, the validity is questionable for the data at the higher temperatures when considered in terms of the recent suggestions.⁽³⁵⁾ The 1020 type steel (Figure 17) also suggests a rather abrupt increase in K_{Ic} , but these data also are of questionable validity.

The problem of obtaining valid data in these steels at high temperatures, where the K_{Ic} value exceeds the yield strength, is primarily an experimental one. In order to maintain plane strain conditions very large test specimens are required. As yet data from very large specimens are very meager, however, there is considerable work in progress, and the question of the true K_{Ic} temperature dependence of low strength materials should be resolved in the near future. Until a resolution is forthcoming, it appears advisable to take a conservative approach where very heavy sections are involved and assume that the low temperature K_{Ic} data can be extrapolated to high temperatures along a smooth, rather than an abruptly increasing, curve.

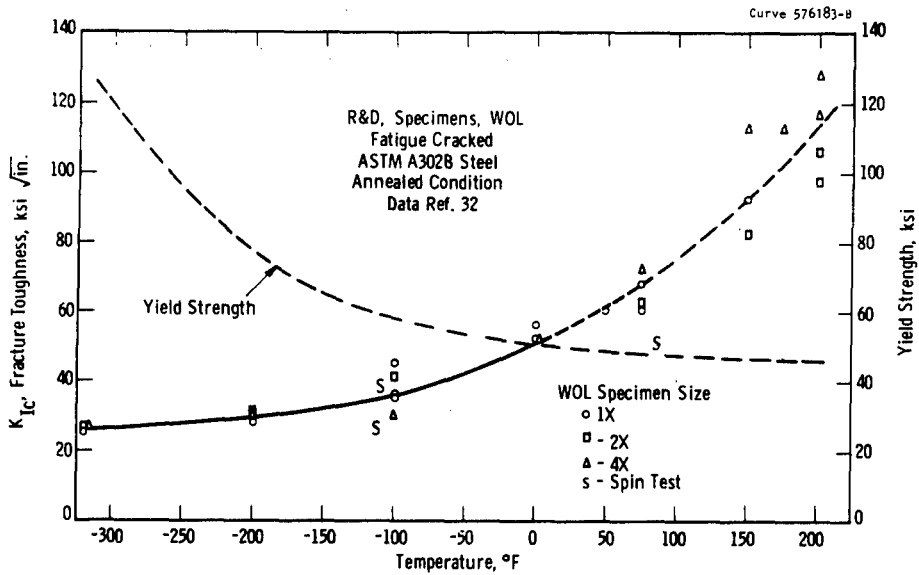
The data currently available on strain rate and temperature effects, although not fully adequate in some respects, indicate that in general the lower strength materials can be expected to exhibit a much more pronounced sensitivity than the high strength materials. However, when evaluating a specific material for a specific application, it would be good practice to take both strain rate and temperature effects into consideration, regardless of the strength level.

6.2.3.2 Metallurgical Variables

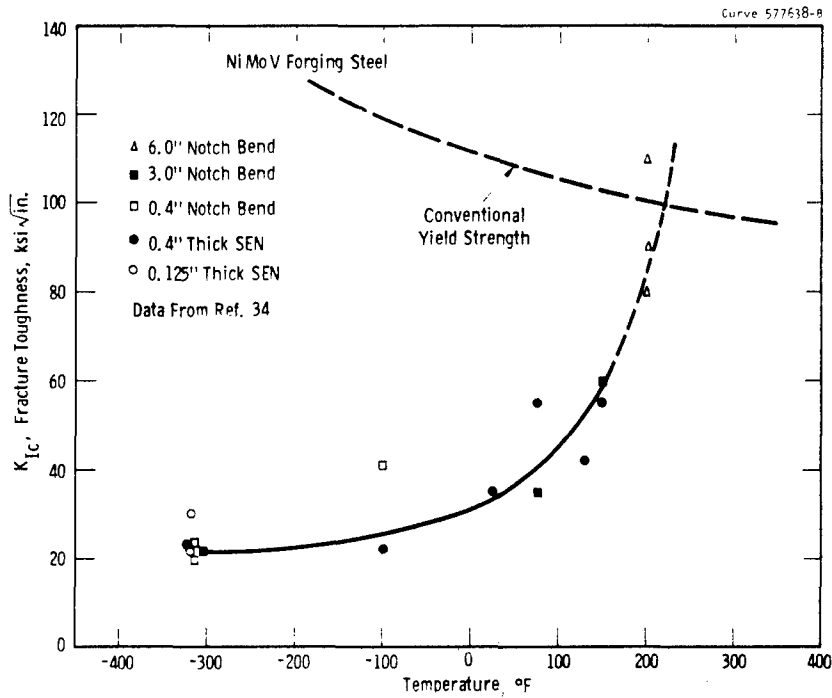
The fracture toughness parameter, K_{Ic} , is sensitive to variations in metallurgical factors just as many of the other strength or toughness properties are. Among the more significant factors are: melting practice, fabrication, chemistry, impurities, microstructure, heat treatment, service environment. The embrittling factor which reduces toughness as measured by other criteria, i.e., Charpy impact, energy or transition temperature, notched tension, tensile ductility, etc., also reduce K_{Ic} . Considerable data are available in the literature citing the effects of metallurgical variables on fracture, a few examples of which are given in references (32,36-44).



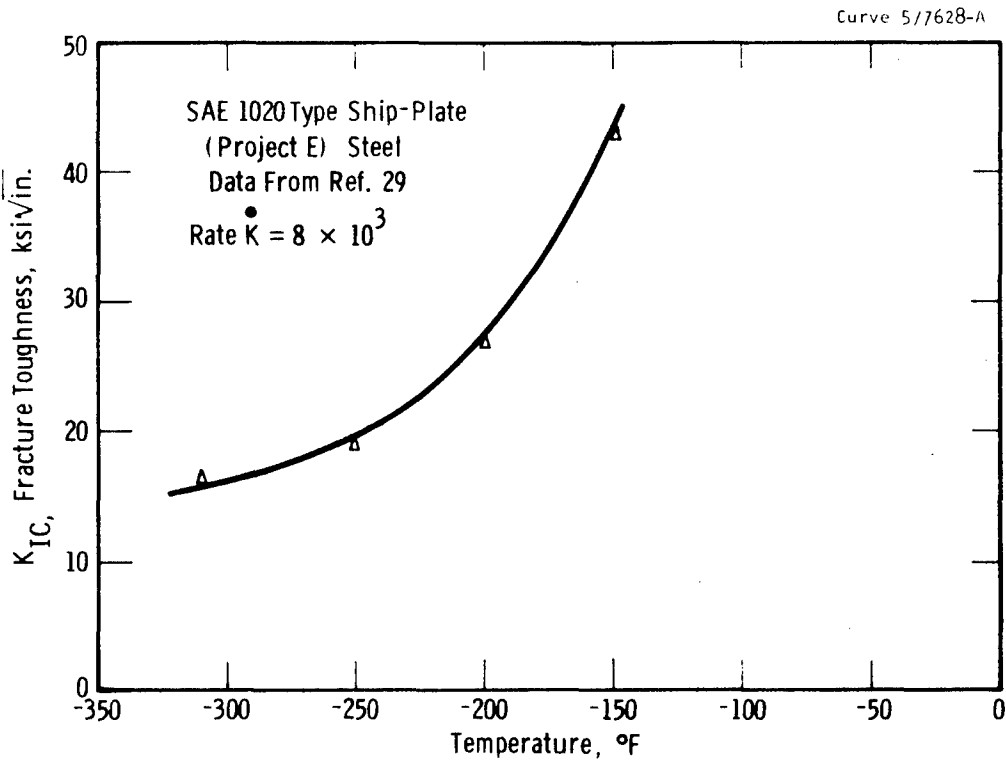
Sec. 6.2 Fig. 14—Expected general behavior of K_{Ic} as a function of strain rate



Sec. 6.2 Fig. 15—Temperature dependence of K_{Ic} fracture toughness of annealed A302B steel, WOL specimen, fatigue cracked



Sec. 6.2 Fig. 16 —Temperature dependence of the fracture toughness of a Ni Mo V forging steel

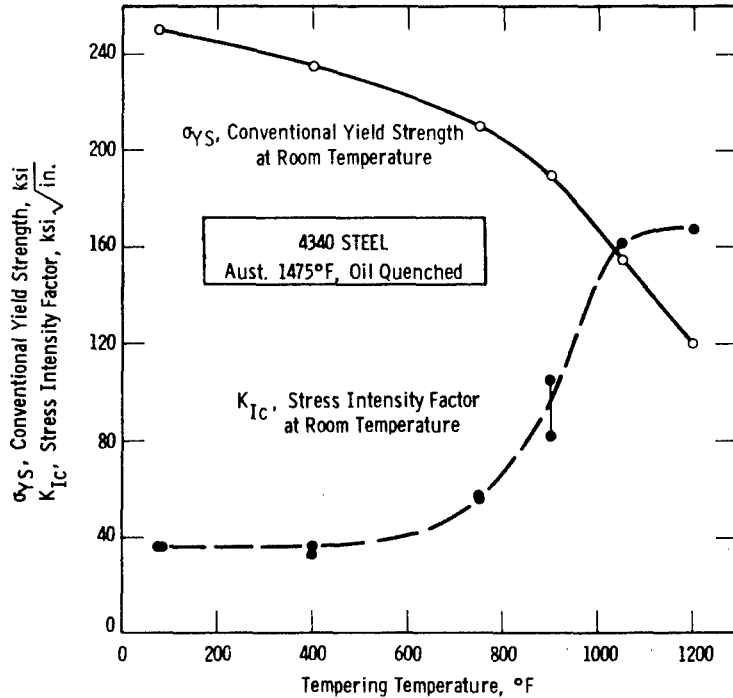


Sec. 6.2 Fig. 17 —Temperature dependence of fracture toughness for ship plate

In recent years it has become apparent, that for many materials, the melting practice can have a considerable effect on toughness. For example, upgrading from conventional air melting to double slag electric furnace air melting, to vacuum degassing, and to consumable electrode vacuum arc remelting, tends to improve toughness for a given material in a given metallurgical condition. The improvements are attributed to increased cleanliness (decrease in nonmetallic inclusions) and reductions in impurities such as hydrogen, oxygen, nitrogen, sulfur, and phosphorous.

Similarly, the factors associated with fabrication, i.e., ingot breakdown, rolling, forging, hot and cold work, welding, etc., can also result in variations in the fracture toughness. For example, a plate or forging which has undergone a large amount of work (hot or cold) in one direction relative to another can be expected to have a significantly lower toughness in the transverse direction -- that is when the notch or plane of fracture propagation coincides with the primary working direction. Fabrication by welding is another example where there can be significant effects on fracture toughness. While the base metal may exhibit adequate toughness, the heat-affected-zone and/or the weld metal could have much lower values of K_{Ic} . Although this is the general trend, it is also possible in some instances that the weld metal and heat-affected-zone toughness may be superior to the base metal.

Heat treatment and the resulting microstructure also have significant effects on fracture toughness. An example is provided in Figure 18 for SAE 4340 plate tempered to various yield strengths.⁽³⁹⁾ Figure 19 also illustrates the effects of heat treatment and microstructures on K_{Ic} .⁽³²⁾ The quenched and tempered and the annealed heat A material were taken from the same original large 7" thick plate of A302B steel. The quenched and tempered B was a large plate from another heat of steel produced to the same specification. As seen, the annealed Heat A has a much more coarse microstructure and poorer fracture toughness than Heat A quenched and tempered. The quenched and tempered microstructure of Heats A and B were nearly identical and so are their toughness. The yield strength of all three lots was essentially the same. Thus it is apparent that large differences in heat treatment and microstructure in a given

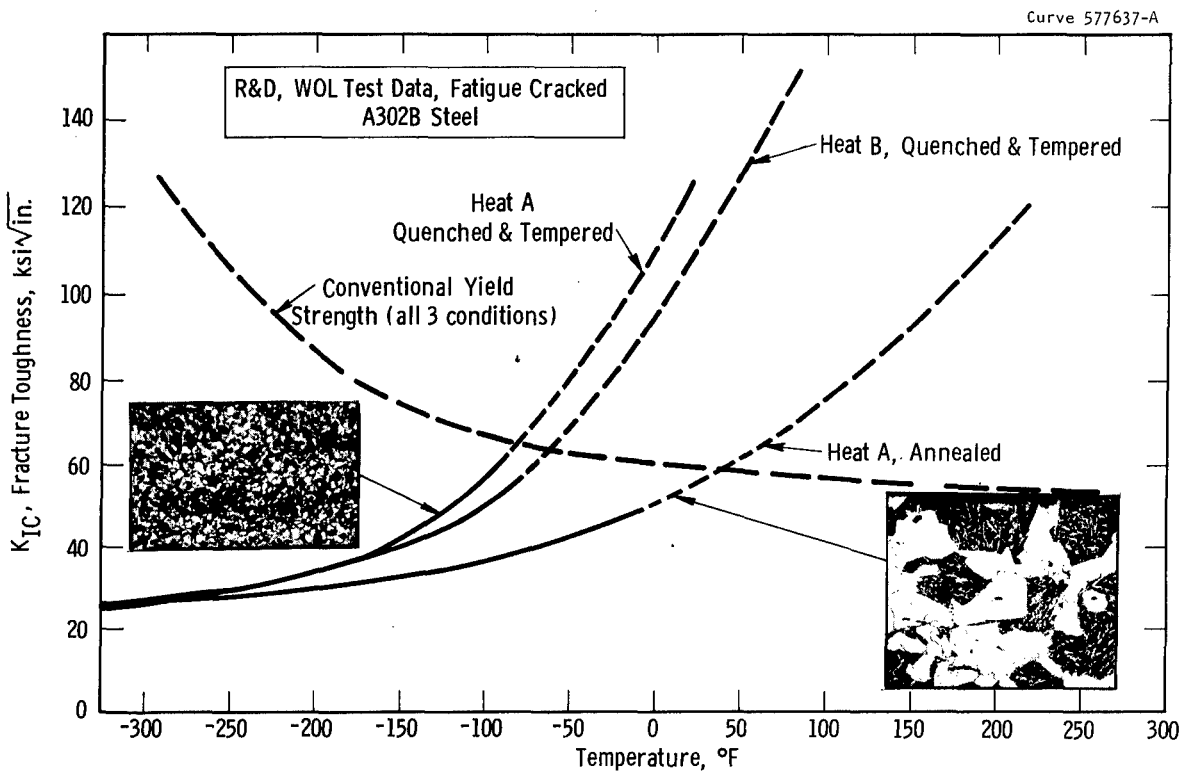


Sec. 6.2 Fig. 18 —The effect of tempering temperature on the yield strength and toughness of SAE 4340 steel plate. Ref.

material, at a given strength, can result in large differences in toughness -- much more than observed in two different heats that had the same heat treatment and similar microstructures.

The service or testing environment can also have pronounced effects on fracture toughness. When tested or used in a hostile environment, many materials exhibit considerably lower apparent values of fracture toughness. Most of these effects are related to the influence of stress corrosion⁽⁴⁵⁻⁴⁷⁾ on the rate of crack propagation, but other types of environment such as irradiation⁽⁴⁸⁾ can have a direct effect on K_{Ic} . Therefore, environmental effects must be considered, and efforts should be considered, and efforts should be made to expose test specimens to the same environment that the component experiences in service.

A dramatic illustration of the effects of metallurgical variables is provided in Figure 20. This graph contains all of the valid data for the room temperature K_{Ic} of 18% Ni maraging steels which were accumulated during the literature search task of Phase II of this project. In this figure, no consideration is given to the metallurgical factors such as composition, heat treatment, specimen orientation, processing, etc., hence



Sec. 6.2 Fig. 19 —Temperature dependence of K_{IC} fracture toughness for various lots of A302B steel. R&D-fatigue cracked, WOL specimen. Ref. 32

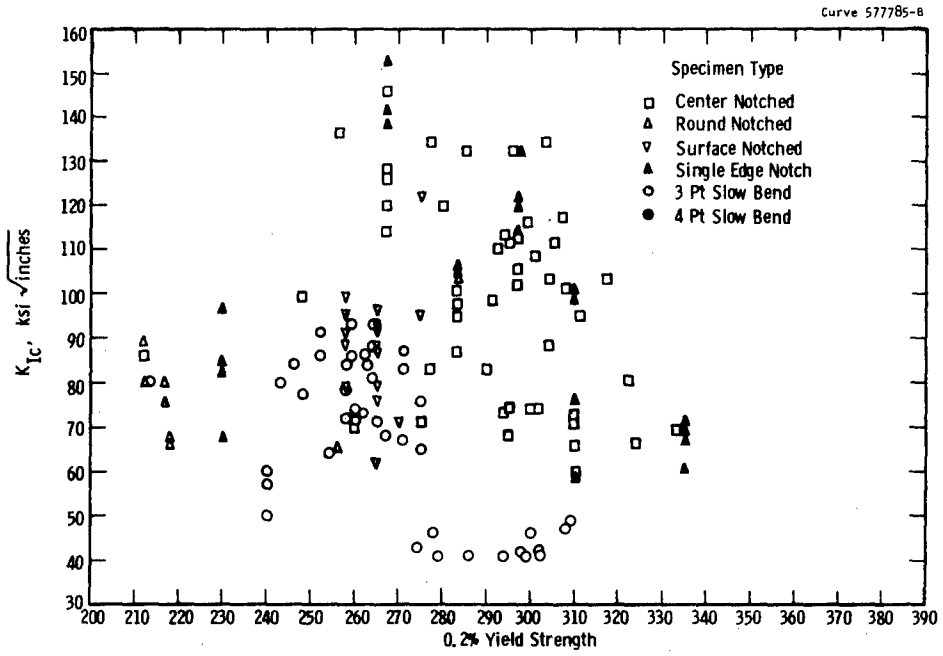
the vast amount of scatter in data. When a specific set of data representing the variation in only one metallurgical factor is extracted from these data, a much more consistent behavior is observed as seen in Figure 21. The foregoing example clearly illustrates that the 18% Ni maraging steel, or any other material, cannot be expected to have a single unique value of K_{Ic} independent of metallurgical variables. Obviously then, in order to insure satisfactory measurement of fracture toughness, the test material should be as nearly identical as possible to that in the component of interest. Also, the notch orientation in the specimen should coincide with the direction of the defect known or anticipated in the component.

6.2.4 SUMMARY OF TESTS FOR PLANE STRAIN FRACTURE TOUGHNESS

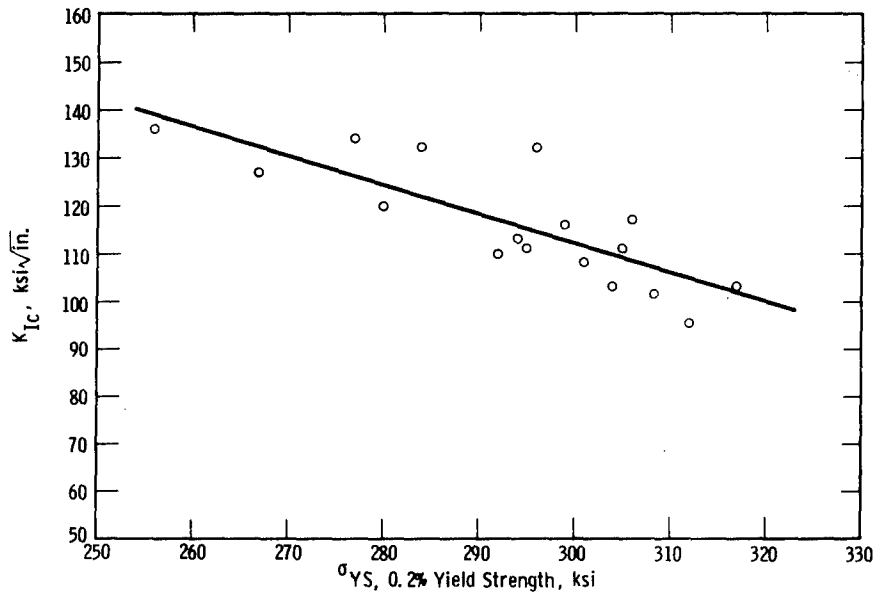
Several types of test specimens have been successfully employed to measure K_{Ic} or G_{Ic} . The details of specimen design, preparation, testing, and analysis of test records have been reported in the literature.⁽⁴⁹⁻⁵³⁾ Therefore, the discussion in this report will be confined to a summary of the state-of-the-art. As yet, there is no recognized standard for fracture toughness testing. However, the ASTM Committee E24 on Fracture Testing of Metals is striving hard to prepare a TRP (Tentative Recommended Practice) for plane strain fracture toughness testing of high-strength metals.⁽⁵⁴⁾ At the present it appears that a formal TRP may be a year or more away.

6.2.4.1 Types of Specimens

The basic types of specimens that have been described in the published literature,⁽⁴⁹⁻⁵³⁾ their relative dimensions and the expressions used to calculate toughness from test results are provided in Figures 22-30. It must be appreciated that the overall size of each of these types of specimens is dependent upon the level of toughness of the material being tested. In order to maintain a plane strain state of stress at the notch front, and thereby assure a valid measurement of K_{Ic} , the specimen size must increase with increased toughness. Table I provides a comparison of the dimensions required^(49,51) for three levels of toughness ($\frac{K_{Ic}}{\sigma_{YS}} = 0.5, 1.0$ and 1.6) for several different specimens.



Sec. 6.2 Fig. 20—Variability of room temperature toughness with yield strength for 18% Ni maraging steel



Sec. 6.2 Fig. 21— K_{IC} as a function of yield strength for 18% Ni maraging steel (various aging treatments)

While the foregoing information is representative of the most recent published information,⁽⁴⁹⁻⁵³⁾ it should be recognized that specimen design and dimensions may not be optimum. Because of the rapid advancement of the technology of fracture mechanics, changes may become necessary. For example, recent suggestions⁽⁵⁴⁾ are that neither the crack length "a" or the thickness "B", should be less than $2.5 \left(\frac{K_{Ic}}{\sigma_{YS}} \right)^2$ for any test specimen to be capable of valid K_{Ic} measurements. Therefore it is possible that future recommendations will necessitate larger test specimens than those shown in Table I. It is also possible that the relative dimensions of some of the specimen types shown in Figures 22-30 may be modified. Table II shows some of the new dimensions which have been suggested⁽⁵⁴⁾ for some of the basic types of specimens. For those who are interested in planning or conducting fracture toughness test programs, it is highly recommended that thorough consideration be given to the changes in dimension which are currently being suggested.⁽⁵⁴⁾

6.2.4.2 Calibrations of Specimens

A relation between the stress intensity factor K, the applied load P, and the specimen dimensions is conventionally referred to as a K calibration. Precise calibrations which permit a ready calculation of K_{Ic} from test results over a wide range of crack lengths (a/W ratio) are now available for a number of specimens. The most current and accurate calibration curves^(54,59,65) for several specimen types are given in Figures 31-36. The simplicity of calculating K_{Ic} from the expressions given in the calibration curves versus those given earlier in Figures 22-30 is readily apparent.

6.2.4.3 Fatigue Cracking of Test Specimens

All of the test specimens require that the notch be extended by fatigue cracking prior to K_{Ic} testing. Methods of fatigue cracking are described in the literature.^(49-51,54) Precaution must be taken during fatigue cracking to keep the stresses sufficiently low so as to avoid influencing the K_{Ic} value by virtue of excessive plastic deformation at the crack tip. As a rule of thumb, the nominal net section stresses

Sec. 6.2 Table I - Comparison of Various Fracture Toughness Specimens

Symmetrically Cracked Plate	Single Edge Notch			Surface Crack	Notch Round	WOL	
	Tension	3pt Bend	4pt Bend				
$K_{IC}/\sigma_{YS}^* = 0.5$							
W = width or dia (in.)	1.25	1	1	0.875	1.5	1.25	(1X) 1.44
B = thickness (in.)	0.16	0.16	0.16	0.16	0.25	-	1.00
L = length (in.)	5	4	9	8	6	5	1.00
Volume (in. ³)	1	.64	1.44	1.12	2.25	6.15	1.44
P/ σ_{YS} load/yield strength	0.11	0.05	0.009	0.01	0.33	0.7	0.072
$K_{IC}/\sigma_{YS}^* = 1.00$							
W	5.0	4.0	4.0	3.5	6.0	5.0	(2T) 6.2
B	0.65	0.65	0.65	0.65	1.0	-	2.0
L	20	16	36	32	24	20	5.0
Volume	65	41.6	94	73	144	392	61.5
P/ σ_{YS}	1.8	0.8	0.14	0.16	5.4	11.2	0.64
$K_{IC}/\sigma_{YS}^* = 1.6$							
W	12.5	10	10	8.75	15	12.5	(4T) 12
B	1.6	1.6	1.6	1.6	2.5	-	4
L	50	40	90	80	60	50	10
Volume	1000	640	1440	1120	2250	6150	476
P/ σ_{YS}	11.7	5.2	0.91	1.00	35	73	2.74

* Maximum measurement capacity for plane strain conditions
 Dimensions for all specimens except WOL are from Ref. 1,3

SEC. 6.2

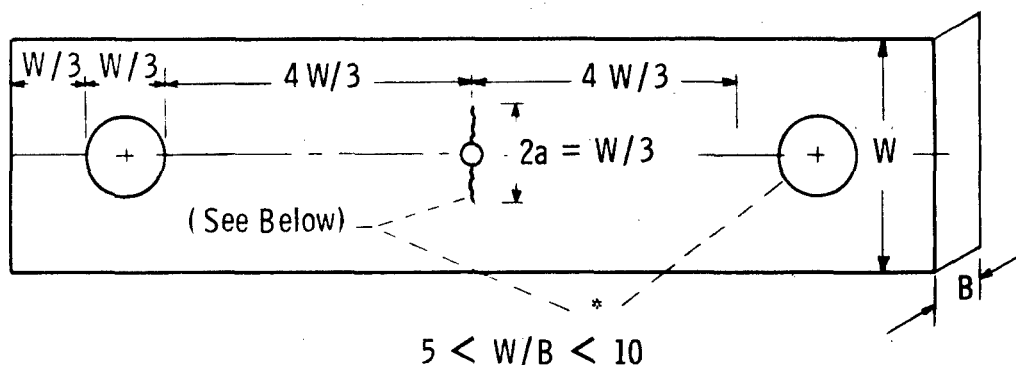
TABLE II - RECOMMENDED MINIMUM SPECIMEN DIMENSIONS AND RATIOS OF REQUIRED LOAD TO YIELD STRENGTH FOR $(K_{IC}/\sigma_{YS})^2 = 1$

Specimen Type	Thickness (inch)	Crack Length (inch)	Width Or Diameter (inch)	Specimen Length (inch)	Load Yield Strength (square inch)
Crack-Notched Round Bar	---	2.5 (D/2-d/2)	10 (D)	40	14.7
Center-Crack Plate	2.5	5.0 (2a)	10	40	7.5
Double-Edge-Crack Plate	2.5	2.5	10	40	7.9
Single-Edge-Crack Plate, Tension	2.5	2.5	5	20	1.6
Single-Edge-Crack Plate, 4-Point Bend (8:1:: Span: Depth) (2:1:: Minor Span: Depth)	2.5	2.5	5	41	0.33
Single-Edge Crack Plate, 3-Point Bend (4:1:: Span: Depth)	2.5	2.5	5	21	0.50
Crackline Loaded Plate (WOL)	2.5	(2.5)	(5)	(5)	(0.37)

(For other values of $(K_{IC}/\sigma_{YS})^2$, the dimensions should be in proportion to this factor, and the loads in proportion to its square.)

Data Taken From Reference 6

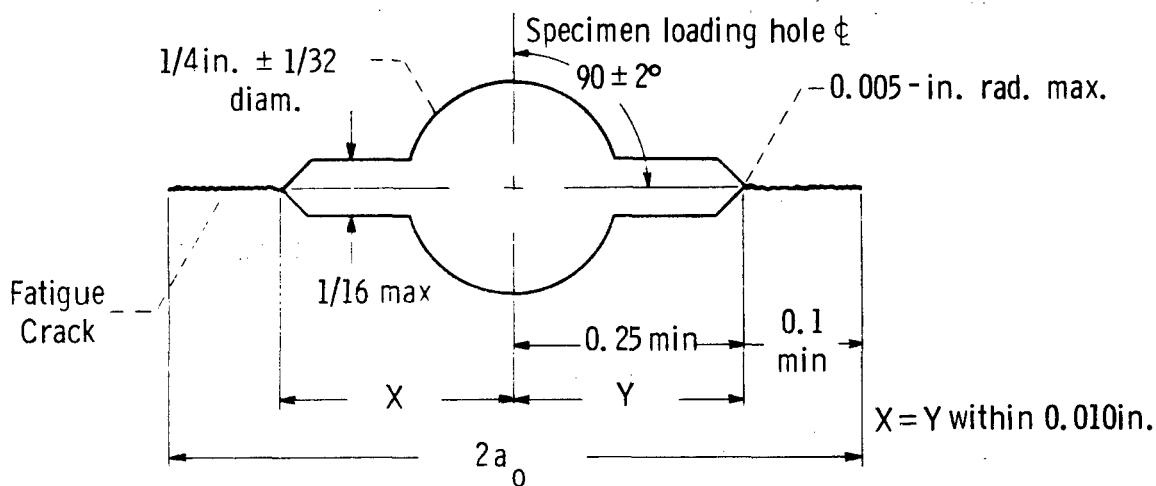
Sec. 6.2 Fig. 22 — Symmetrical center-cracked plate



$$K_I = \frac{P}{B} \frac{a^{1/2}}{W} \left[1.77 + 0.227 \left(\frac{2a}{W}\right) - 0.510 \left(\frac{2a}{W}\right)^2 + 2.7 \left(\frac{2a}{W}\right)^3 \right]$$

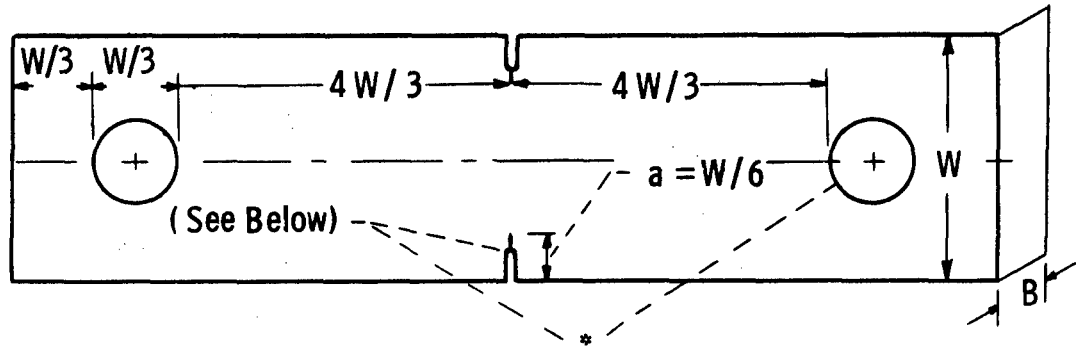
for range $\frac{2a}{W} = 0$ to 0.7

* -Surfaces must be symmetric to specimen center line within $W/1000$



Fatigue crack starter for center-cracked plate specimens ($W \geq 2$ in.)

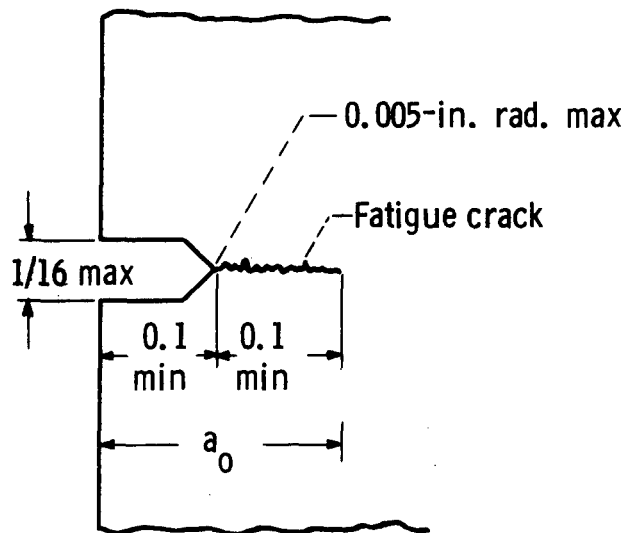
Sec. 6.2 Fig. 23 - Symmetrical edge-cracked plate



$$5 < W/B < 10$$

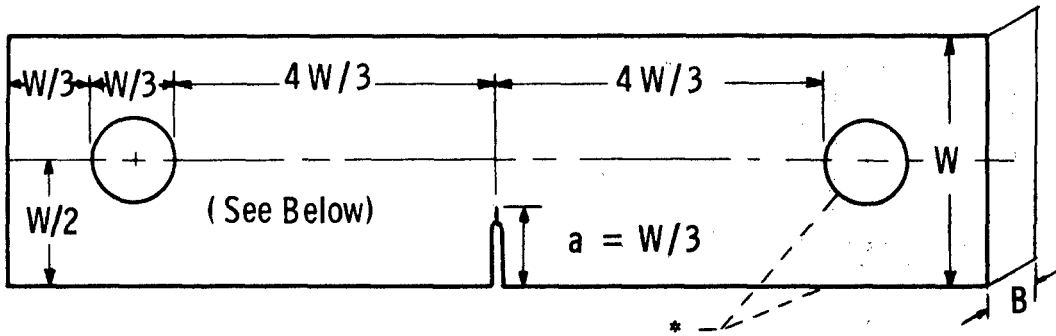
$$K_I = \frac{P(\pi a)^{1/2}}{BW} \left[\frac{W}{\pi a} \left(\tan \frac{\pi a}{W} + 0.1 \sin \frac{2\pi a}{W} \right) \right]^{1/2}$$

* -Surfaces must be symmetric to specimen center line within W/1000



Fatigue crack starter for edge-notched plate specimens

Sec. 6.2 Fig. 24 - Single-edge-notched plate (tension)

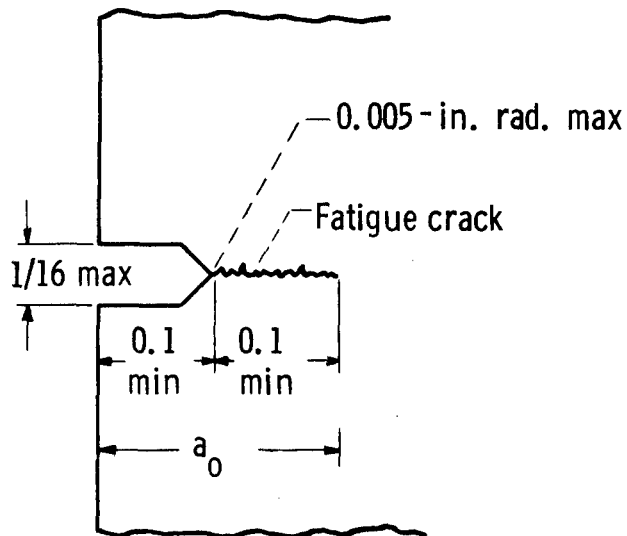


$$4 < W/B < 8$$

$$K_I = \frac{P}{B} \frac{a^{1/2}}{W} \left[1.99 - 0.4124 \left(\frac{a}{W}\right) + 18.70 \left(\frac{a}{W}\right)^2 - 38.48 \left(\frac{a}{W}\right)^3 + 53.85 \left(\frac{a}{W}\right)^4 \right]$$

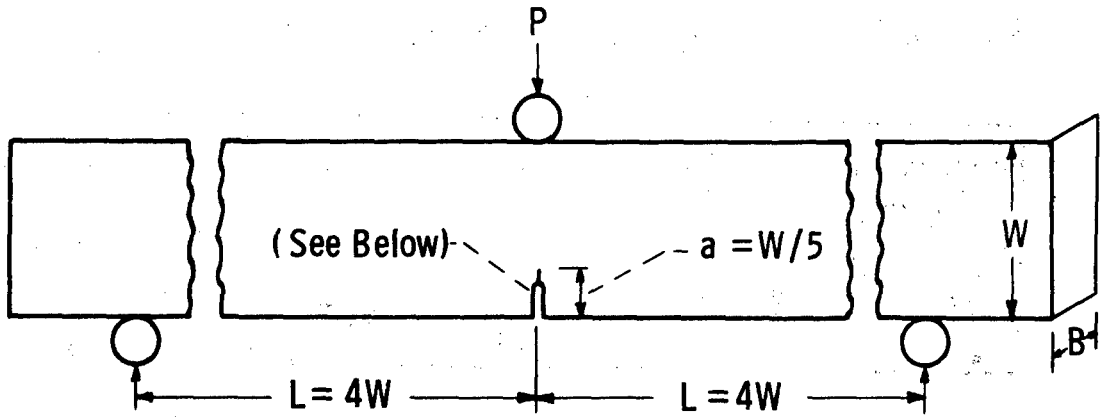
for range $\frac{a}{W} = 0$ to 0.6

* -Surfaces must be true to specimen center line within $W/1000$



Fatigue crack starter for edge-notched plate specimens

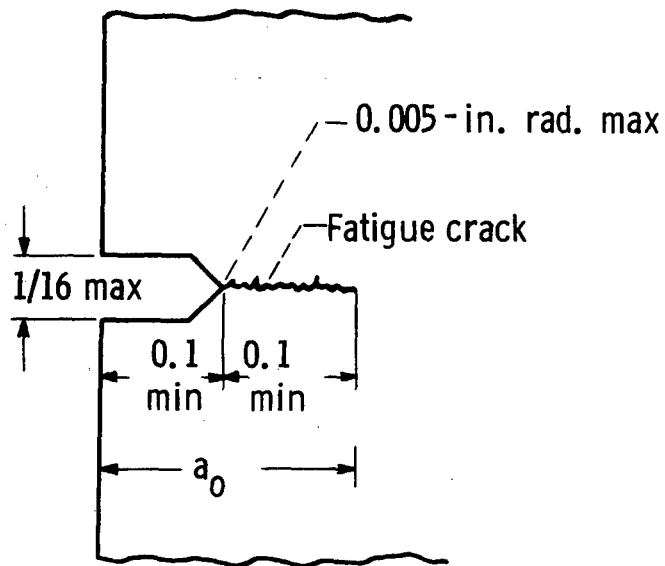
Sec. 6.2 Fig. 25 —Notch bend specimen (three-point loaded)



$$2 < W/B < 8$$

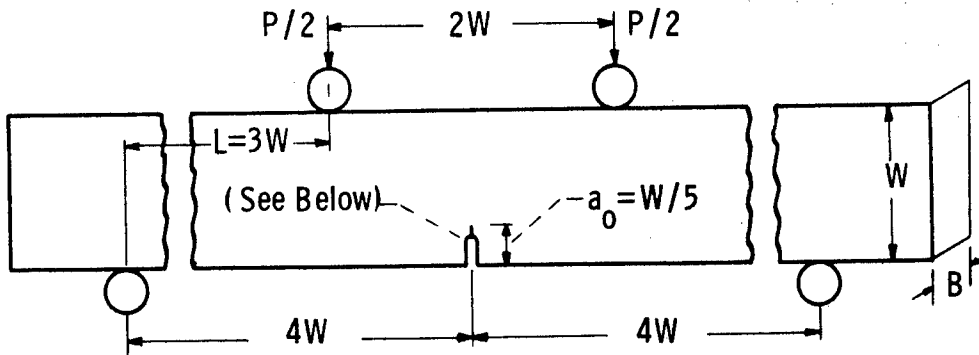
$$K_I = \frac{6M}{B} \frac{a^{1/2}}{W^2} \left[1.96 - 2.75 \left(\frac{a}{W}\right) + 13.66 \left(\frac{a}{W}\right)^2 - 23.98 \left(\frac{a}{W}\right)^3 + 25.22 \left(\frac{a}{W}\right)^4 \right]$$

for $\frac{a}{W} = 0$ to 0.6



Fatigue crack starter for edge-notched plate specimens

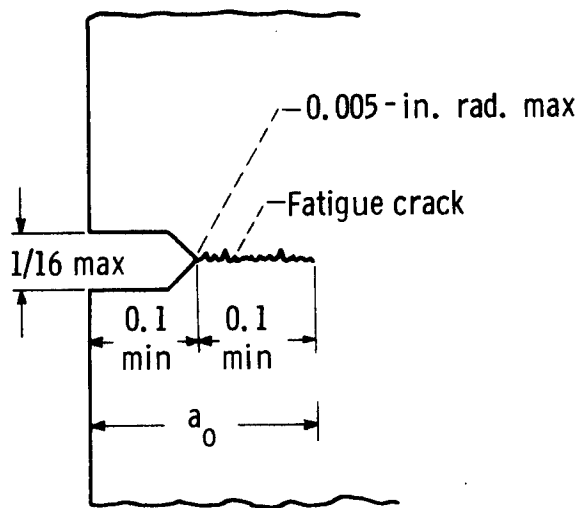
Sec. 6.2 Fig. 26 -Notch bend specimen (four-point loaded)



$$K_I = \frac{6M}{B} \frac{a^{1/2}}{W^2} \left[1.99 - 2.47 \left(\frac{a}{W}\right) + 12.97 \left(\frac{a}{W}\right)^2 - 23.17 \left(\frac{a}{W}\right)^3 + 24.80 \left(\frac{a}{W}\right)^4 \right]$$

for $\frac{a}{W} = 0$ to 0.6

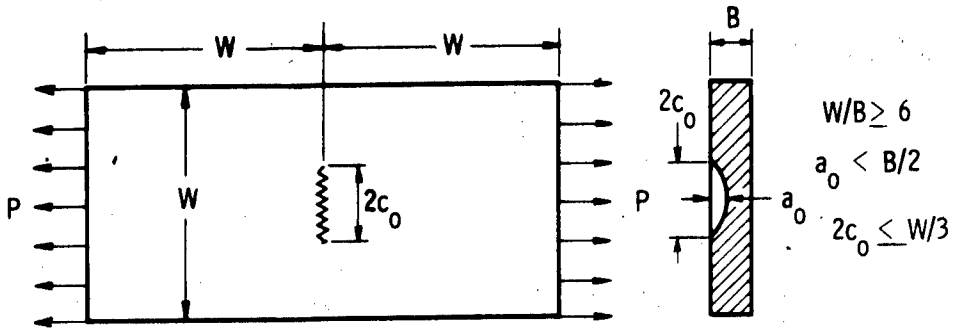
where $M = \frac{PL}{2}$



Fatigue crack starter for edge-notched plate specimens

Sec. 6.2 Fig. 27 — Surface-cracked plate

Dwg. 748A417

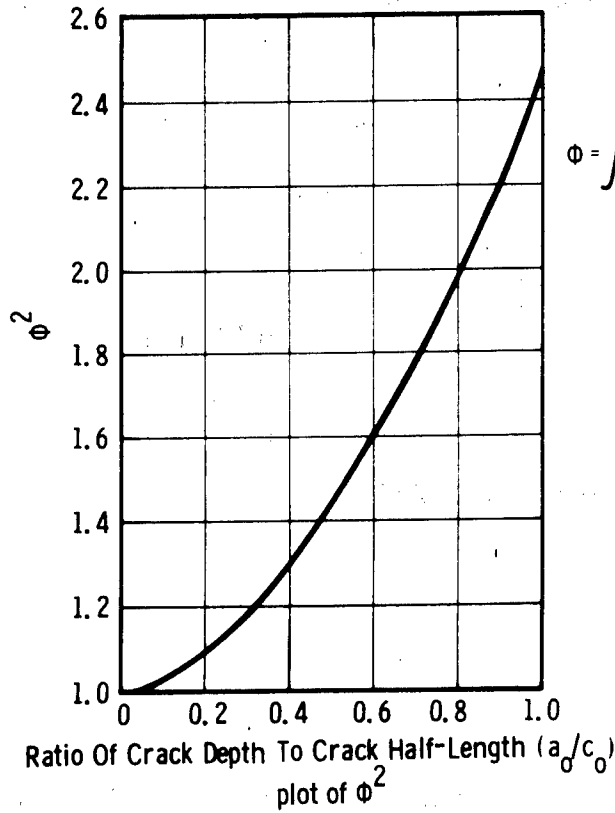


$$W/B \geq 6$$

$$a_0 < B/2$$

$$2c_0 \leq W/3$$

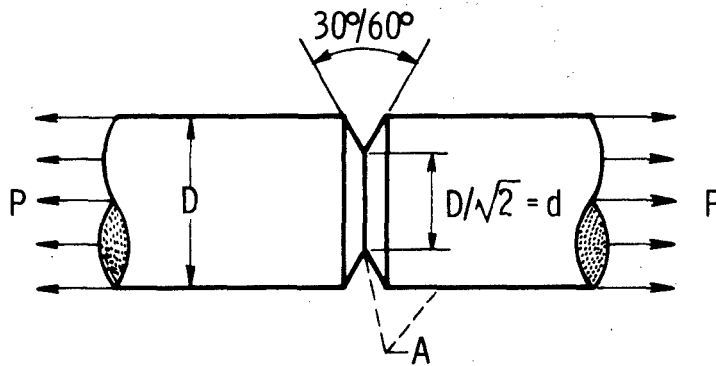
$$K_I^2 = \frac{1.2\pi P^2 a_0^2}{W^2 B^2} \left[\frac{1}{\Phi^2 - 0.2 \left(\frac{P^2}{W^2 B^2 \sigma_{YS}^2} \right)} \right]$$



$$\Phi = \int_0^{\pi/2} \sqrt{1 - \frac{c_0^2 - a_0^2}{c_0^2} \sin^2 \theta} d\theta$$

Dwg. 748A418

Sec. 6.2 Fig. 28 '—Circumferentially notched and fatigue-cracked round bar



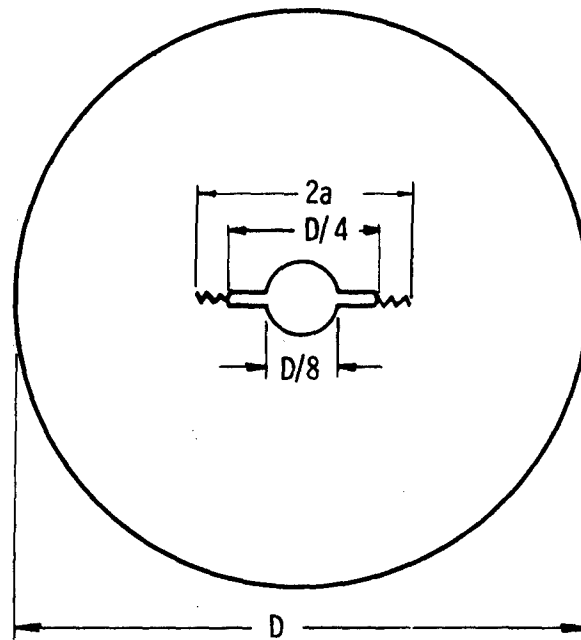
$$K_I = \frac{P}{D^{3/2}} \left[1.72 \left(\frac{D}{d} \right) - 1.27 \right]$$

for d/D of 0.5 to 0.8

A-surfaces must be concentric to within $D/1000$

Sec. 6.2 Fig. 29 – Symmetrical center notched disc (rotor or spin)

Dwg. 748A415



$$B \geq 2a$$

$$\frac{2a}{D} \text{ range of } 0.1 \text{ to } 0.3$$

$$K_I = \sqrt{\pi a} \sigma_0$$

Where σ_0 = nominal fracture stress-tangential stress at the center of a solid rotor, corresponding to a fracture speed of test rotor, (similar to use of gross section stress for plates)

Where ν = Poissons Ratio

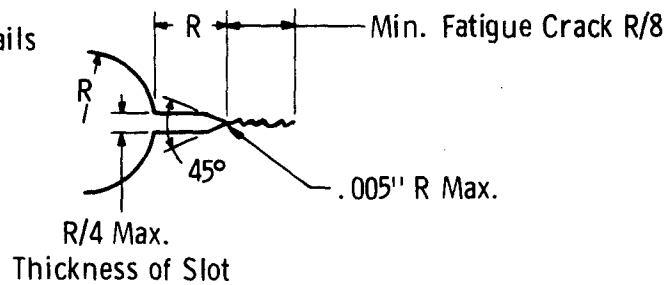
$$\sigma_0 = \left(\frac{3 + \nu}{8}\right) \rho \omega R_0^2$$

ρ = Mass Density (lb sec²/in⁴)

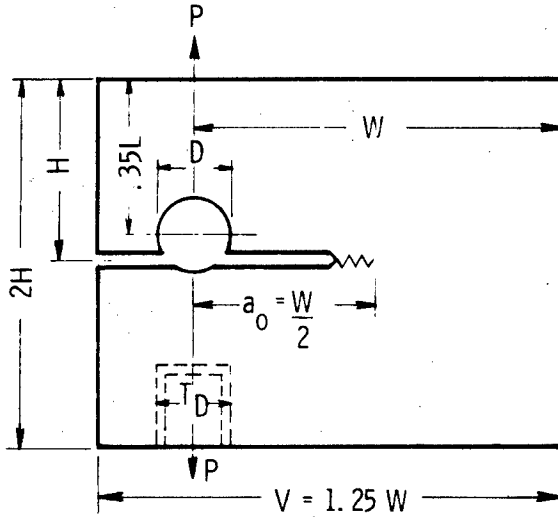
R_0 = Outer Radius (D/2) inches

ω = Angular Velocity (rad/sec)

Notch Details



Sec. 6.2 Fig. 30—Wedge-opening-loading (WOL type center-line loading)



$$B = a_0$$

$$W = 2H = 2.0B$$

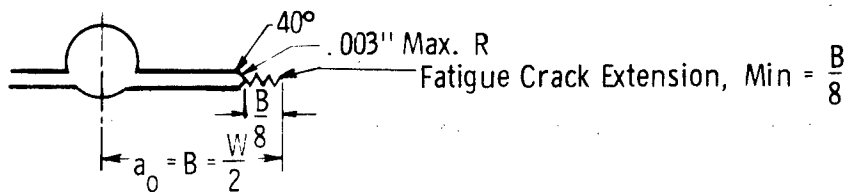
$$D = .6B$$

$$T_D = .5B$$

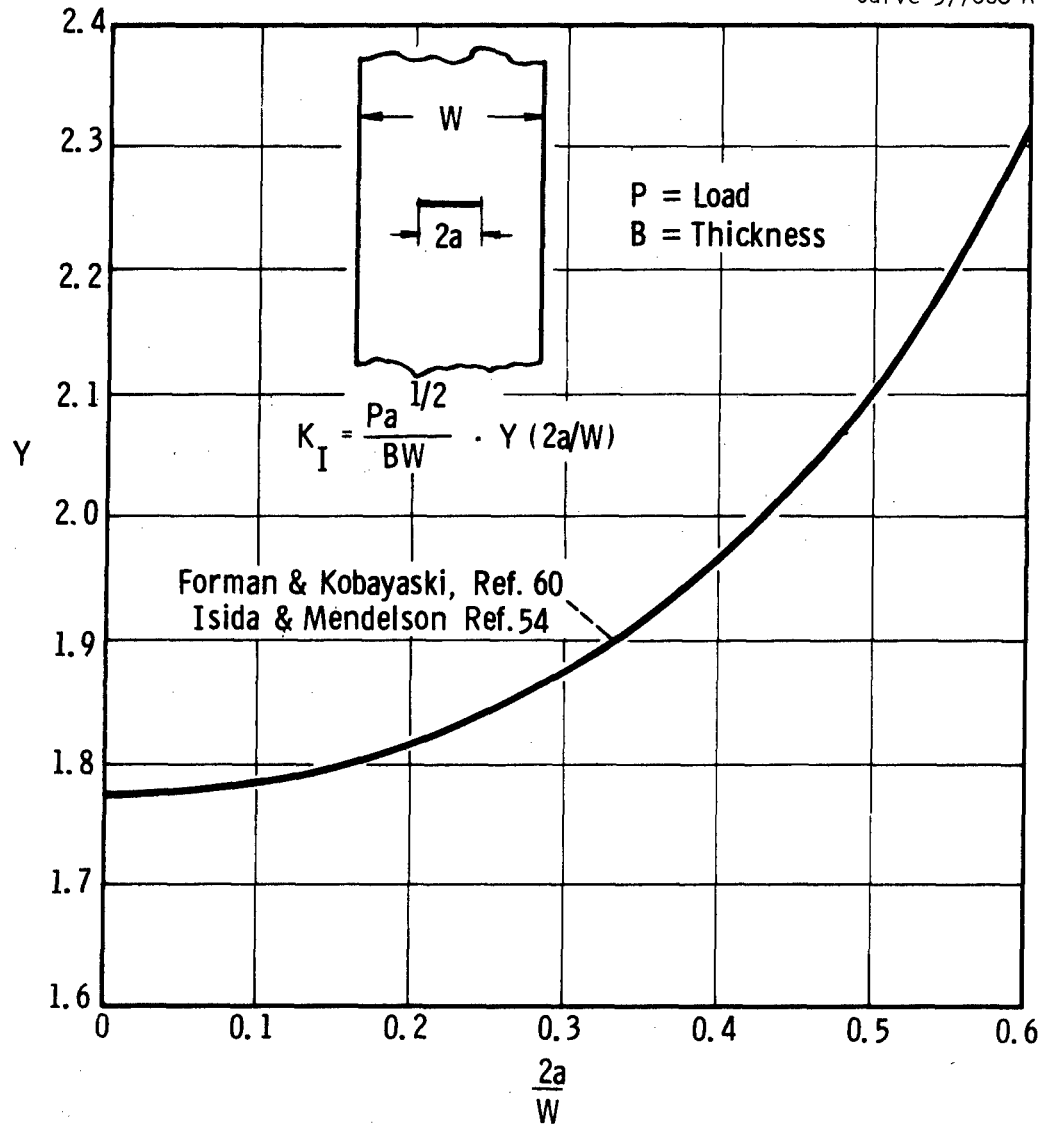
For a/W from 0.25 to 0.65

$$K_I = \frac{P}{B} \frac{a^{1/2}}{W} \left[39.70 - 294.2 \left(\frac{a}{W}\right) + 1118 \left(\frac{a}{W}\right)^2 - 1842 \left(\frac{a}{W}\right)^3 + 1159 \left(\frac{a}{W}\right)^4 \right]$$

Notch Details

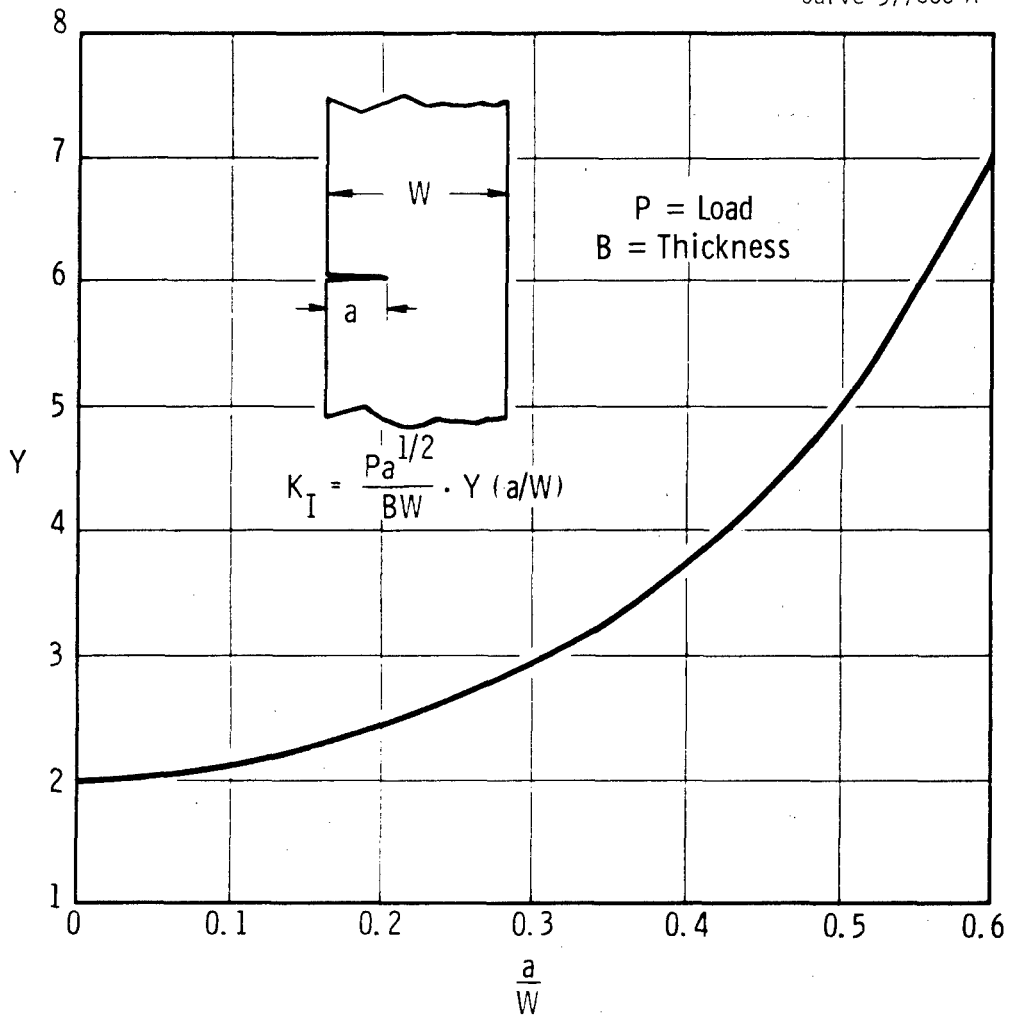


Curve 577668-A

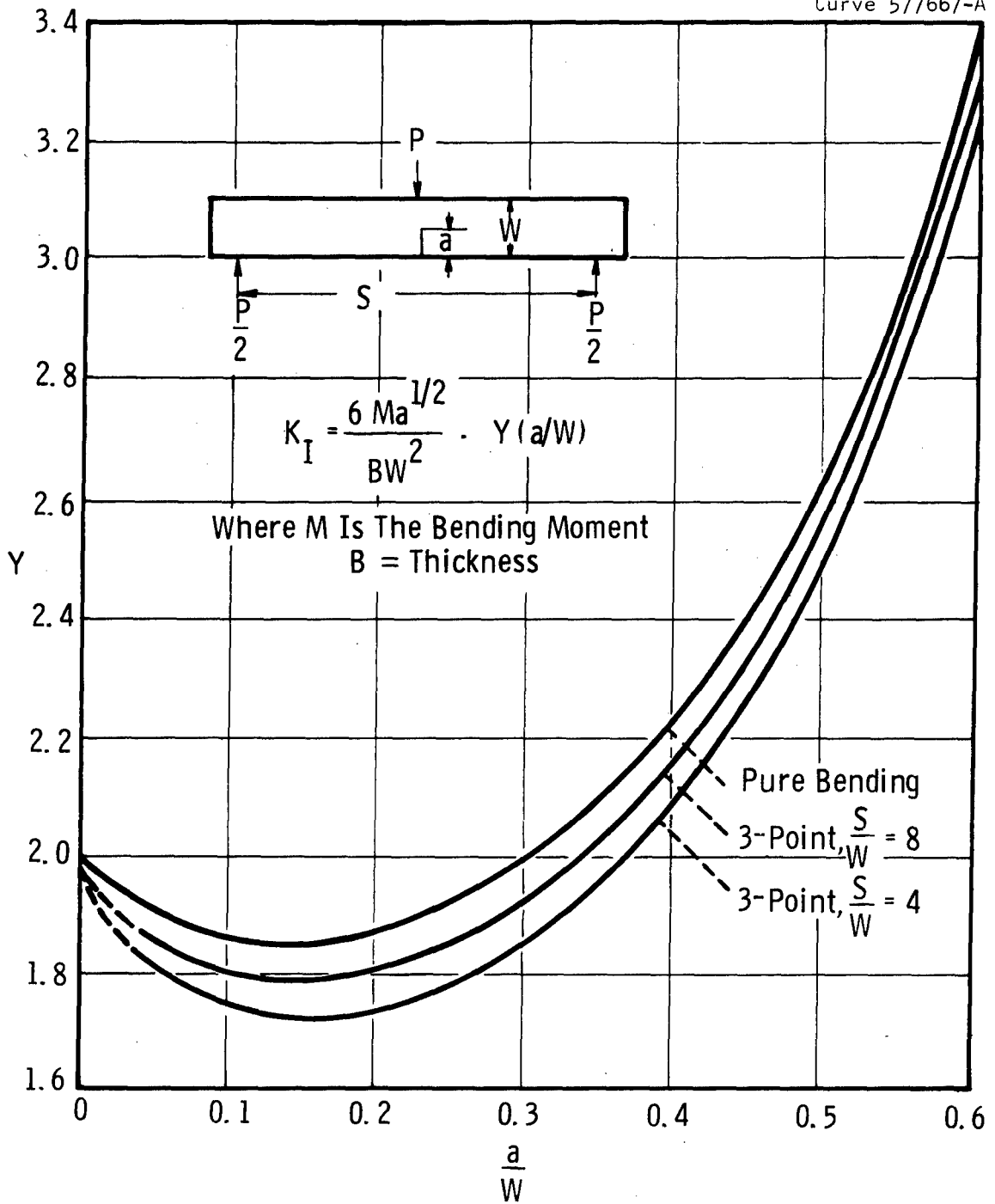


Sec. 6.2 Fig. 31 -K calibration for the center-cracked plate specimen

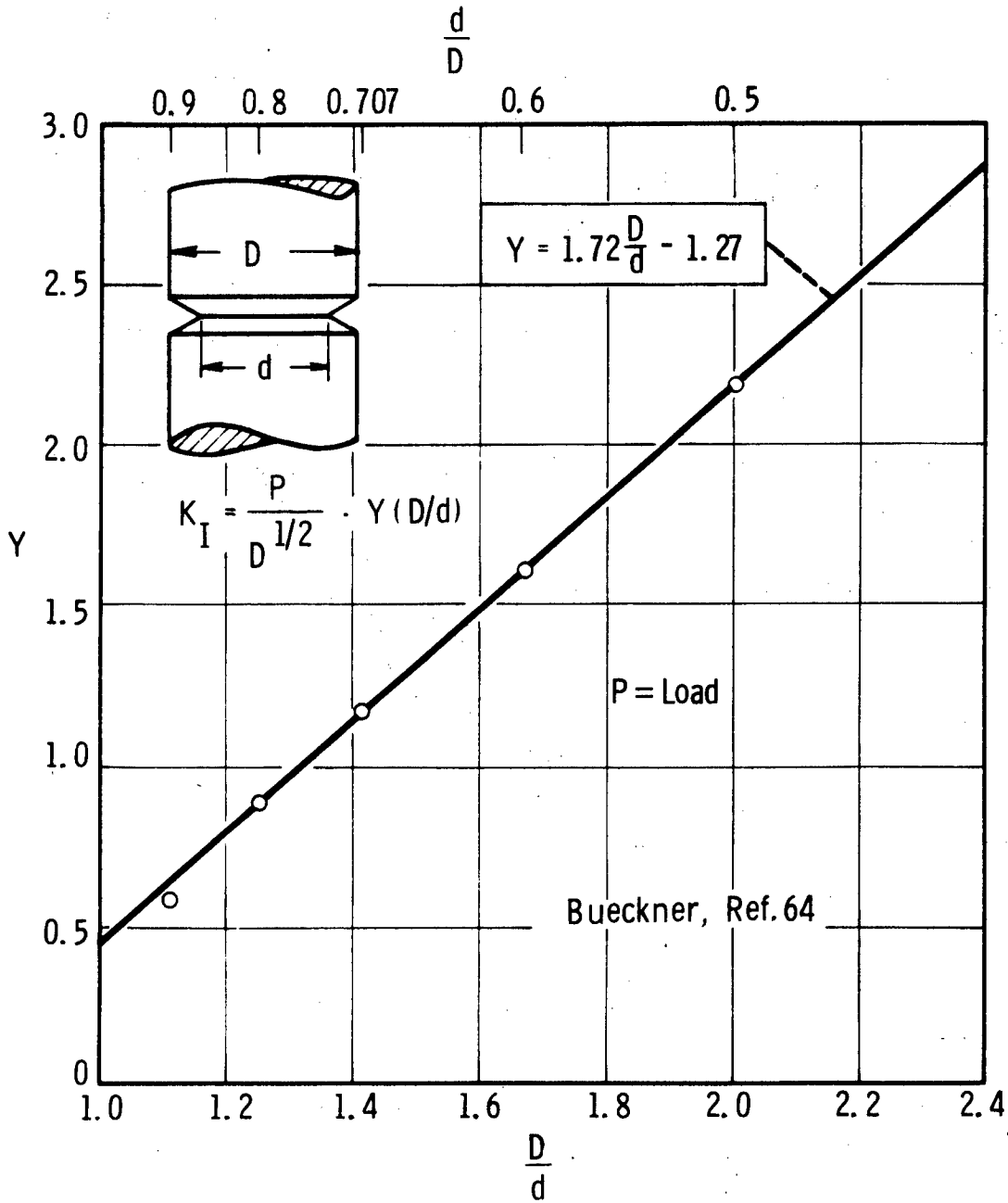
Curve 577666-A



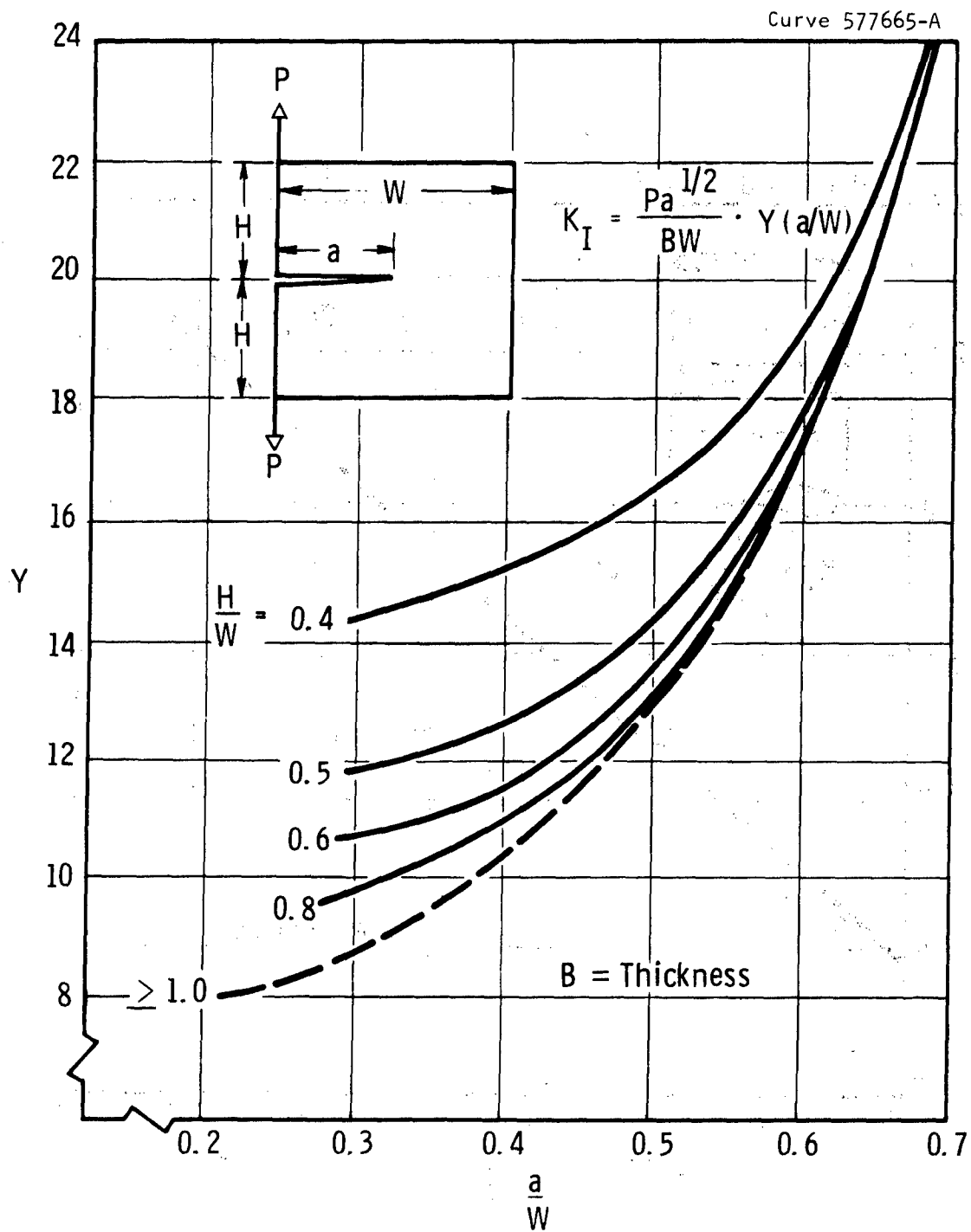
Sec. 6.2 Fig. 32 -K calibration for single-edge crack tension specimen. Ref. 61



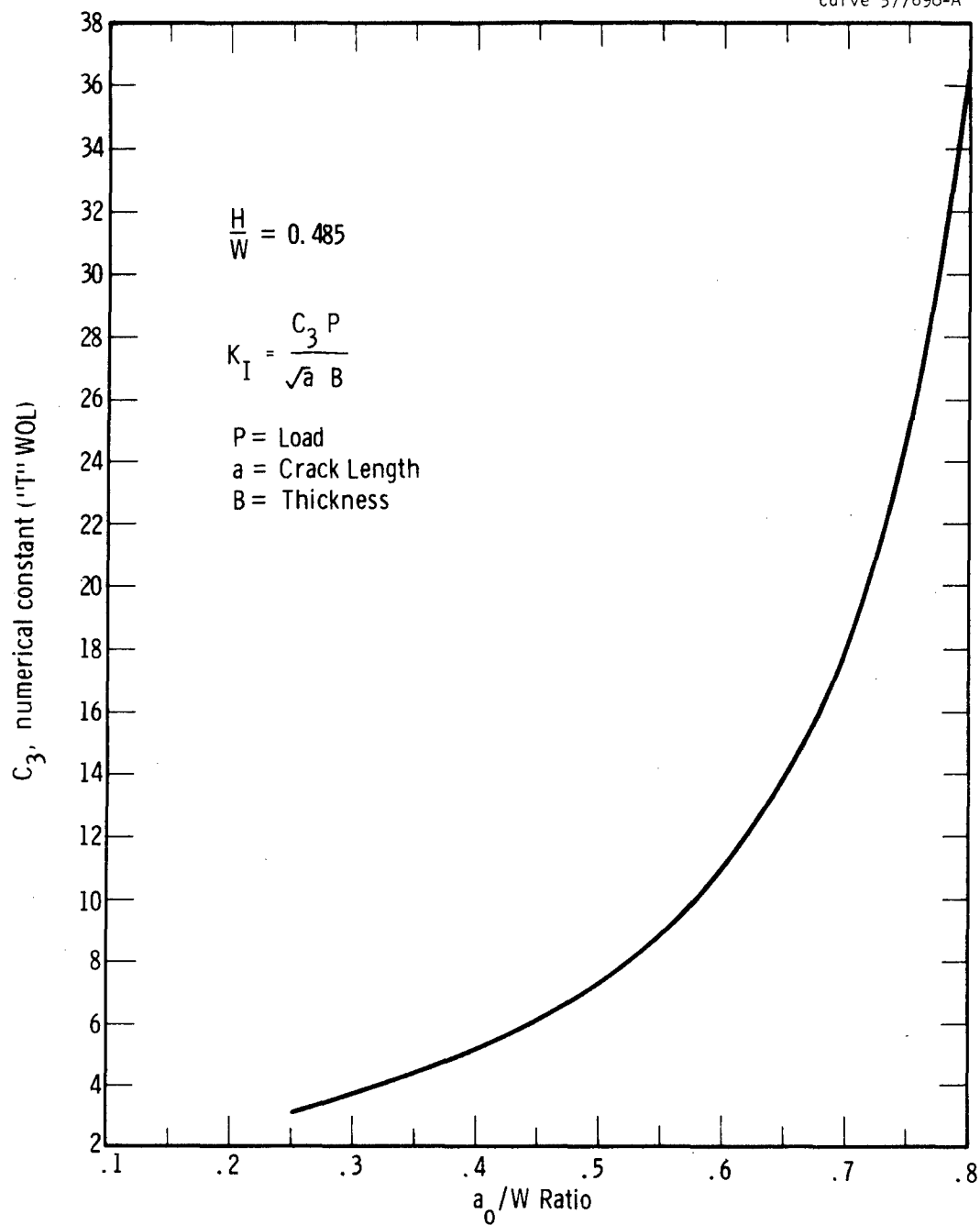
Sec. 6.2 Fig. 33 -K calibrations for bend specimens. Ref. 62, 63



Sec. 6.2 Fig. 34 -K calibration for circumferentially crack-notched round bar



Sec. 6.2 Fig. 35 -K calibrations for compact crackline loaded specimens
Ref. 54



Sec. 6.2 Fig. 36—Numerical constant " C_3 " as a function of the a_0/W ratio for the "T" type WOL toughness specimen Ref. 65

during fatiguing should not exceed 1/2 the yield strength of the material. In no case should the load for fatiguing exceed that anticipated for fracture in the K_{Ic} test.

6.2.4.4 Instrumentation for K_{Ic} Testing

Proper instrumentation of the test specimen is essential for K_{Ic} testing. ^(49-51,54) The determination of K_{Ic} or G_{Ic} requires a knowledge of the crack length corresponding to the load at the time of fracture instability. There are two possibilities for the onset of fracture instability during the K_{Ic} test. It can occur immediately from the initial crack front, or some amount of slow crack extension may occur prior to instability. The instrumentation must be capable of distinguishing which behavior occurs, and if instability is preceded by some slow crack growth, the length of the crack at instability must be definable by the instrumentation. The slow crack growth preceding instability may either be a slow continuous extension from the original fatigue crack front, or it may occur in the form of intermittent, discontinuous crack movement.

Several instrumentation techniques have been employed to measure crack extension. An autographic load-deflection record is commonly used with all the various type specimens. Ideally, the load-deflection curve should remain linear until instability occurs. Observations of deviation from linearity prior to fracture could arise from two sources: extensive plastic deformation at the crack tip or elsewhere in the specimen, or slow crack extension. It is also possible that both could occur simultaneously. Excessive plastic deformation at the crack tip cannot be tolerated in a plane strain fracture toughness test.* If observed, deviation due to plastic flow is a good indication that the specimen size that is being employed is too small for the toughness of the material. On the other hand, if the deviation can be definitely associated with slow crack

* If the amount of plastic deformation (plastic zone size) at the tip of the crack is small compared to the total crack length and specimen thickness, it is possible to apply a correction⁽⁵⁵⁾ (see Section 6.2.2.8) which will permit the calculation of the value for K_{Ic} . The limitations regarding the allowable plastic zone size have been discussed in the literature. ^(49-51,54,55)

extension prior to fracture, it is possible to obtain a valid test result if the crack length and load at the onset of instability can be determined. The load and, more particularly, the crack length at instability can be determined from the autographic load-deflection curve provided a suitable compliance calibration is available for the specimen. The amount of crack extension between the original length and that at the time of fracture is related to the change in compliance of the specimen as signified by the change in slope of the load deflection curve. Several types of compliance gages have been used for this purpose.

Other instrumentation, in addition to load-deflection recordings, are often employed to measure slow crack extension which may occur during K_{Ic} tests. One of these is the electrical potential method. (49,51) When a specimen carrying a current contains a crack (discontinuity) there will be a disturbance of the potential field in the region of the crack. The potential difference between two fixed points spanning the crack will increase as the crack extends (total current must remain constant). The potential change is generally recorded against load on an X-Y recorder. For any specific geometry, a calibration curve relating crack length to potential change is required.

Other techniques that have been employed to detect or measure crack extension are acoustic, photography, and ultrasonics, and discussions of these techniques may be found in the literature. (49-51,54,56,57) Each of the techniques has its own advantages and limitations. The use of any one technique depends in large part upon the material, its form and the type of test specimen being used. When employed in conjunction with the WOL specimen the ultrasonic technique has been very useful (see sections 7.2, 7.3 and Appendix II).

6.2.4.5 Summary and Comparison of Specimens

Several factors must be considered when selecting a particular type of specimen for a fracture toughness test program. Foremost among these are: the expected toughness of the material to be tested, the size and shape of the available test material, the loading capacity of the available test facilities, the economical usage of test material, and the accuracy desired in the toughness measurements.

As previously discussed, materials with high toughness ($\frac{K_{Ic}}{\sigma_{YS}} > 1$) require the use of large, thick specimens as can be seen from Tables I and II. In this case where material availability and test capacity become limiting factors, the crack-line-loaded, WOL, or notched bend specimens are most attractive. Quite often the type of specimen will be dictated by the form of the material. Tests of high strength thin sheet are obviously limited to specimens like the single edge notched plate or the symmetrical center or edge cracked plates. On the other hand, bar stock or cylindrical forgings necessitate the use of notched round, WOL, or notched bend tests. The texture of the material and the orientation of probable defects relative to the principal stress in the component of interest also limit the type of specimen which can be employed. In addition to being limited in the amount of available material, the cost of the material, e.g., titanium alloys at \$6 to \$8 a pound, could be an important consideration. The accuracy of the expressions used with the various specimens has been discussed in detail^(49,51,58) and, in general is quite satisfactory. The error introduced from the expression is considerably less than the normal scatter inherent in the material and the possible errors arising from test procedures. If the recommended^(49,51,54) procedures are employed during specimen preparation, testing, and interpretation of the test results, the accuracy of the K_{Ic} measurements should be quite adequate for engineering purposes.

6.2.4.6 Summary

Even though the subject of fracture toughness testing has not been finalized and standards specified, meaningful data can be obtained by proper use of the existing testing technology. It is recommended that a thorough study of the existing information and experience be conducted before embarking on any large scale test programs.

6.2.5 GENERAL EXPERIENCE IN APPLYING FRACTURE MECHANICS

In recent years considerable progress has been made in applying fracture mechanics principles, concepts, expressions, and test data to solutions of practical problems. Although most of the early experience

with fracture mechanics dealt with materials and applications of interest to the aerospace industry, the applicability of the approach to other areas has been recognized and some experience acquired. The concept is not limited to the high-strength metals of low or intermediate toughness, but may be applied to any material for which a valid K_{Ic} fracture toughness parameter can be determined.

A number of examples of the application of fracture mechanics to engineering problems are available in the literature.⁽⁶⁶⁻⁷⁹⁾ By combining fracture mechanics technology and slow crack growth (fatigue) characteristics, answers to the following type questions have been found. What type and size of defect can be tolerated under the design load: Conversely, what stress levels can be tolerated in the presence of some known defects? What is the maximum size flaw that can be initially accepted with the assurance that it will not grow to a critical size during the desired operating life of the component? How do metallurgical variables affect the maximum allowable initial flaw size, the flaw growth characteristics, and the critical flaw size for catastrophic failure? What are the capabilities of the available, practical, non-destructive inspection techniques relative to these subcritical and critical flaw sizes? If an unexpected failure should occur during prooftesting or operation of a structure, what will be the nature of the failure -- a localized rupture and spitting or a catastrophic bursting with fragmentation? What fracture toughness and crack growth characteristics are required of the material employed in specific components, and how are these requirements spelled-out in material specifications in terms of practical testing and inspection techniques? Some specific examples of how these questions can be answered are provided in Section 8 of this report.

6.2.6 LIMITATIONS OF FRACTURE MECHANICS

Although linear elastic fracture mechanics is very useful in material selection and other design considerations, it does have a bounded area of use. At present the bounds of the areas of application have not been distinctly determined, but in applying the theory one should be aware of its general limitations. Most of these limitations have been discussed previously and will now be reviewed and summarized.

The stress intensity factor which is used as a single parameter fracture criterion for sharp cracks is determined (experimentally or analytically) under elastic conditions. But, of course, the extremely high stress concentration at the crack tip will cause plastic flow around it. Therefore, if the stress intensity factor K is to parametrically represent the plastic flow and eventually fracture conditions at the crack tip, the size of the plastic zone at fracture must be very small compared to the area over which K adequately describes the elastic stresses. In other words, the size of the plastic zone at the crack tip must be small compared to the other dimensions of the body containing the crack. At present a specific statement as to just how small the plastic zone must be cannot be made, but some reasonable guidelines can be obtained by using the experimentally determined restrictions imposed on the various plane strain fracture mechanics test specimens which were described in Section 6.2.4.2. These restrictions are usually in terms of keeping the nominal stress in the plane of the crack at fracture equal to or less than some percent of the uniaxial yield stress. Such restrictions require that the dimensions of geometrically similar structures containing flaws, which are proportional to some other dimension of the structure, be proportional to $(K_c/\sigma_{YS})^2$. This means that both the size of structures and the size of the cracks in materials having high K_c and low σ_{YS} must be very large before linear elastic fracture mechanics can be applied. For this reason, the application of fracture mechanics to high-toughness low-yield-stress materials is very limited. The use of the plastic zone correction factor extends the use of the linear elastic stress intensity factor a little further.

As was shown previously (Section 6.1.3.3), the apparent critical stress intensity factor of a material is a function of the crack tip root radius. To eliminate this additional variable in material selection and design considerations, all valid critical stress intensities are now obtained from specimens whose machined notches are extended by fatigue crack growth prior to testing, thus giving a zero crack tip root radius. Therefore, the application of such data to blunt crack tips of finite root radius may lead to conservative results. But in many cases a crack large enough to cause catastrophic failure has grown to its critical size by the

fatigue process, and thus the application of data obtained from fatigue-cracked test specimens is directly applicable.

The particular value of critical stress intensity used in each application should correspond to the state of stress at the tip of the crack under consideration. For plate this means that the K_c used in each application should be the value corresponding to the plate thickness being considered. At present most valid critical stress intensity data reported are for plane strain conditions (K_{Ic}). The use of K_{Ic} values in design considerations for thicknesses less than those actually required for plane strain fracture will normally result in a conservative design, the exception being when the thicknesses become very small. But for material selections the comparison of the K_{Ic} 's of materials for uses at thicknesses for which K_{Ic} isn't applicable could easily lead to an improper choice.

As discussed in Section 6.2.2.12, fracture mechanics principles can also be used in the analysis of slow crack growth caused by cyclic loading or sustained loading. Here again the use of the linear elastic fracture mechanics theory must be restricted to cases in which the size of the plastic zone is small compared to the other dimensions of the structure. Although distinct limits of the areas of applicability cannot be given at present, the following general statements can be made. The limits of applicability for sustained slow crack growth should be approximately the same as those considered at the beginning of this section for the case of fracture due to monotonically increasing loading in which no slow crack growth occurs prior to catastrophic failure. The area of applicability for cyclic loading slow crack growth should be even larger than that for sustained load slow crack growth because of the smaller crack tip plastic zones for corresponding external loads. These smaller plastic zones are a result of the strain hardening of the material at the crack tip caused by strain cycling. Of course the strain hardening may also have an effect on the K_{Ic} of the material and if so this influence must be taken into account.

Section 6.2 References

1. A. A. Griffith, "The Phenomena of Rupture and Flow in Solids," Royal Soc. (London) Phil. Trans., Series A, Vol. 221 (1920) pp. 163-198.
2. G. R. Irwin, "Fracture Dynamics," Fracturing of Metals, Amer. Soc. Metals, Cleveland, 1948, pp. 147-166.
3. E. Orowan, "Fracture and Strength of Solids," Report on Progress in Physics, Phys. Soc. (London) Vol. 12, p. 185 (1949).
4. G. R. Irwin and J. A. Kies, "Fracturing and Fracture Dynamics," Welding J. Res. Suppl. pp. 95s-100s, (1952).
5. G. R. Irwin, "Analysis of Stresses and Strains Near the End of a Crack," J. of Applied Mechanics, Vol. 24, p. 361, (1957).
6. P. Paris and F. Erdogan, "A Critical Analysis of Crack Propagation Laws," J. of Basic Engineering, Dec. 1963.
7. H. H. Johnson and A. M. Willner, "Moisture and Stable Growth in a High Strength Steel, Applied Materials Research, Jan. 1965.
8. Subcommittee on Brittle Fracture of the ASME Research Committee on Prevention of Fracture in Metals, "A Review of Engineering Approaches to Design Against Fracture," an ASME publication.
9. E. Ripling, S. Mostovoy, and R. Patrick, "The Application of Fracture Mechanics to Adhesive Joints," Mats. Res. and Standards, Vol. 4, p. 29, (1964).
10. P. C. Paris, G. Sih, "Stress Analysis of Cracks," Fracture Toughness Testing and Its Applications, "ASTM Special Technical Publications No. 381.
11. G. Hahn and A. Rosenfield, "Local Yielding and Extension of a Crack Under Plane Stress," Ship Structure Committee, SSC-165.
12. J. R. Rice, "Stresses Due to a Sharp Notch in a Work Hardening Elastic-Plastic Material Loaded by Longitudinal Shear," Brown University Report NSF-GK286/1.
13. I. S. Tuba, "A Method of Elastic-Plastic Plane Stress and Strain Analysis," J. of Strain Analysis, Vol. 1, No. 2, (1966).
14. G. R. Irwin, "Fracture Mode Transition for a Crack Traversing a Plate," J. of Basic Engineering, June 1960.
15. N. F. Brown, Jr. and J. E. Srawley, "Fracture Toughness Testing," from "Fracture Toughness Testing and Its Applications," ASTM Special Technical Publication No. 381.

16. F. A. McClintock and J. Hult, "Elastic-Plastic Stress and Strain Distribution Around Sharp Notches in Repeated Shear," Ninth International Congress of Applied Mechanics, (1956).
17. G. R. Irwin, "Plastic Zone Near a Crack and Fracture Toughness," 1960 Sagamore Ordnance Materials Conference, Syracuse University, (1961).
18. P. C. Paris, "The Fracture Mechanics Approach to Fatigue," Proceedings of the 10th Sagamore Army Materials Research Conference, (1963).
19. H. W. Liu, "Fatigue Crack Propagation and Applied Stress Range -- an Energy Approach," J. Basic Eng., Trans. ASME, March 1963.
20. H. H. Johnson and A. M. Willner, "Moisture and Stable Crack Growth in a High Strength Steel," Applied Materials Research, January 1965.
21. V. Weiss and S. Yukawa, "Critical Appraisal of Fracture Mechanics," from Fracture Toughness Testing and Its Applications, "ASTM Special Technical Publication No. 381.
22. ASTM Special Committee on Fracture Testing of High Strength Materials, "Progress in Measuring Fracture Toughness and Using Fracture Mechanics," Fifth Report, ASTM Materials and Research Standards, March 1964, p. 107.
23. J. M. Krafft and G. R. Irwin, "Crack Velocity Consideration," from "Fracture Toughness Testing," ASTM STP No. 381, (1965).
24. J. M. Krafft, "Correlations of Plane Strain Crack Toughness With Strain Hardening, Characteristics of a Low, a Medium, and a High Strength Steel," Applied Materials Research, April 1964, p. 88.
25. Hanna and Steigerwald, "Fracture Characteristics of Structural Metals," AD411509, ER-5426 Thompson-Ramo-Wouldridge, June 1963.
26. "Thick Section Fracture Toughness," AD452824L, Tech. Doc. Report No. ML-TDR-64-236, Boeing-North American, October 1964.
27. Amateau and Steigerwald, "Fracture Characteristics of Structural Metals," AD611873, ER-5937-3 Thompson-Ramo-Wouldridge, January 1965.
28. Brisbane, Hawn, & Ault, "Fracture Toughness and Delayed Failure Behavior of 18% Nickel Maraging Steel," Materials Research and Standards, Vol. 5, No. 8, August 1965, p. 395.
29. J. M. Krafft and A. M. Sullivan, "Effects of Speed and Temperature on Crack Toughness and Yield Strength in Mild Steel," Trans. ASM, Vol. 36, (1963), p. 160.
30. J. Eftis and J. M. Krafft, "A Comparison of the Initiation With the Rapid Propagation of a Crack in a Mild Steel Plate," ASME J. of Basic Engineering, March 1965.

31. G. R. Irwin, "Crack Toughness Testing of Strain Rate Sensitive Materials," ASME Paper 63-WA-217, (1963).
32. E. T. Wessel and W. H. Pryle, "Investigation of the Applicability of the Biaxial Brittle Fracture Test for Determining Fracture Toughness," AEC Research and Development Report WERL 8844-11, August 1965.
33. A. J. Brothers, D. L. Newhouse, and B. M. Wernott, "Results of Bursting Tests of Alloy Steel Disks and Their Application to Design Against Brittle Fracture," ASTM Preprint, Presented at 68th Annual Meeting ASTM, Lafayette, Indiana, June 13-18, 1965.
34. D. F. Mowbray, A. J. Brothers, and S. Yukawa, "Fracture Toughness Determination of A302B and NiMoV Steels with Various Size Specimens," ASME Paper 66-Met-1, Presented at ASME Metals Engineering Conference, Cleveland, Ohio, April 18-22, 1966.
35. W. F. Brown and J. E. Srawley, "Task Group ASTM E24 Sub I, "Plane Strain Crack Toughness Testing," Draft of 6th Committee Report, Distributed at E34 Sub I Committee Meeting, Washington, D.C., February 1, 1966.
36. G. R. Sippel, "Metallurgical Factors Affecting Fracture Toughness," Presented at ASM, Pittsburgh Chapter Educational Series Lecture, Pittsburgh, Pa., April 1965.
37. D. R. Poirier, M. L. Ebner, M. C. Flemings and W. A. Backofen, "Effect of Processing History on Fracture of Materials at High Strength Levels," ASD-TDR-63-819 Part 1, September 1963, Air Force Materials Lab, Wright-Patterson Air Force Base, Ohio.
38. C. E. Hartbower and G. M. Orner, "Metallurgical Variables Affecting Fracture Toughness in High-Strength Sheet Alloys," ASD-TDR-62-868, June 1963, Air Force Materials Lab, Wright-Patterson Air Force Base, Ohio.
39. L. E. Hays and E. T. Wessel, "The Fracture Toughness of 4340 Steel At Various Yield Strength Levels," Applied Materials Research, Vol. 2, No. 2, April 1963, p. 99.
40. E. T. Wessel, "Brittle Fracture Strength of Metals," from "Properties of Crystalline Solids," ASTM STP No. 283, (1960), p. 99.
41. W. A. Backofen and M. L. Ebner, "Metallurgical Aspects of Fracture at High Strength Levels," WAL TR310.24/5-4, May 1963, (also N64-10245; AD-406167).
42. "Third Maraging Steel Project Review," RTD-TDR-63-4048, Air Force Materials Lab, Wright-Patterson Air Force Base, Ohio.
43. "Fourth Maraging Steel Project Review," ML-TDR-64-225, Air Force Materials Laboratory, Wright-Patterson Air Force Base, Ohio.

44. "A Review of Engineering Approaches to Design Against Failure," Subcommittee on Brittle Fracture of the ASME Research Committee on Prevention of Fracture in Metals, Special ASME Booklet, (1965).
45. G. R. Irwin, "Relatively Unexplored Aspects of Fracture Mechanics," Univ. of Illinois, T. and A.M. Report No. 240, February 1963 (also N63-14097).
46. C. F. Tiffany and J. N. Masters, "Applied Fracture Mechanics," from "Fracture Toughness Testing," ASTM STP #381, (1965).
47. B. F. Brown, et al, "A New Stress Corrosion - Cracking Test Procedure for High-Strength Alloys," Presented at 68th Annual Meeting, ASTM, Lafayette, Indiana, June 1965.
48. R. E. Johnson, "Fracture Mechanics: A Basis for Brittle Fracture Prevention," WAPD-TM-505, AEC Research and Development Report, November 1965.
49. J. E. Srawley and W. F. Brown, Jr., "Fracture Toughness Testing," NASA TN D 2599, January 1965.
50. Battelle Memorial Institute "Current Methods of Fracture-Toughness Testing of High Strength Alloys with Emphasis on Plane Strain," DMIC Report 207, August 31, 1964.
51. "Fracture Toughness Testing and Its Applications," ASTM STP 381, April 1965..
52. R. E. Johnson, "Fracture Mechanics: A Basis for Brittle Fracture Prevention," AEC Research and Development Report, WAPD TM 505, Bettis Atomic Power Laboratory, November 1965.
53. M. B. Reynolds, "Fracture Mechanics and the Stability of Engineering Structures," AEC Research and Development Report GEAP-4678, September 1965.
54. W. F. Brown, Jr. and J. E. Srawley, A Task Group of ASTM Committee E24, Sub. I, "Plane Strain Crack Toughness Testing," Draft of 6th Committee Report distributed at Committee meeting, Washington, D. C., February 1, 1966.
55. ASTM Special Committee, Fifth Report, "Progress in Measuring Fracture Toughness and Using Fracture Mechanics," ASTM Materials Research and Standards, March 1964, p. 107.
56. Klima, Lesco and Freche, "Ultrasonic Technique for Detection and Measurement of Fatigue Cracks," NASA TN TND 3007, September 1965.
57. W. G. Clark, Jr., "Ultrasonic Detection of Fracture Initiation and Extension," Westinghouse Research Lab. Memo 66-1B4-BTLFR-M1, January 1966, distributed to ASTM Committee E24, Sub. III, Washington, D. C., January 31, 1966.

58. P. C. Paris and G. C. Sih, "Stress Analysis of Cracks" from "Fracture Toughness Testing and Its Applications," ASTM STP 381, p. 30.
59. W. K. Wilson, "Analytic Determinations of Stress Intensity Factors for the Manjoine (WOL) Brittle Fracture Test Specimen," AEC Research and Development Report WERL-0029-3, Westinghouse Research Laboratories, August 26, 1965.
60. R. G. Forman and A. S. Kobayashi, "On the Axial Rigidity of a Perforated Strip and the Strain Energy Release Rate In a Centrally Notched Strip Subjected to Uniaxial Tension," ASME Paper 63-WA-29, 1963.
61. B. Gross, J. E. Srawley and W. F. Brown, Jr., "Stress Intensity Factors for a Single Edge Notch Tension Specimen by Boundary Collocation of a Stress Function," NASA TN D-2395, August 1964.
62. B. Gross and J. E. Srawley, "Stress Intensity Factors for Single Edge Notch Specimens in Bending or Combined Bending and Tension by Boundary Collocation of a Stress Function," NASA TN D-2603, January 1965.
63. B. Gross and J. E. Srawley, "Stress Intensity Factors for Three-Point Bend Specimens by Boundary Collocation," NASA TN D-3092, December 1965.
64. H. F. Buechler, "Coefficients for Computation of the Stress Intensity Factor, K_I , for a Notched Round Bar," ASTM STP 381 (Discussion of "Stress Analysis of Cracks," p. 82-83).
65. W. K. Wilson, "Optimization of WOL Brittle Fracture Test Specimen," Westinghouse Research Laboratories Report 66-LB4-BTLFR-R1, January 5, 1966 (For unlimited distribution).
66. ASTM Committee on FTSM, "Progress in Measuring Fracture Toughness and using Fracture Mechanics," Fifth Committee Report, ASTM Materials and Research Standards, March, 1964.
67. W. E. Anderson and P. C. Paris, "Evaluation of Aircraft Material by Fracture," ASM Metals Engineering Quarterly, V. 1, No. 2, May, 1961.
68. G. R. Irwin, "Relation of Crack Toughness Measurements to Practical Applications," Welding Journal Research Supplement, V. 41, No. 11, November, 1962, pp 519s-528s.
69. C. J. Boyle, et al., "Further Progress In the Development of Large Steam Turbine and Generator Rotors," Paper GER-2216 presented at 68th Annual Meeting of ASTM, Purdue University, June, 1965.
70. C. F. Tiffany & F. A. Poll, "An Approach to the Prediction of Pressure Vessel Minimum Fatigue Life Based On Applied Fracture Mechanics," Boeing Document D2-22437, The Boeing Company, 1963 (unlimited distribution).

71. R. E. Johnson, "Fracture Mechanics: A Basis for Brittle Fracture Prevention," AEC Research and Development Report WAPD-TM-505, Bettis Atomic Power Laboratory, November, 1965.
72. R. A. Davis & W. E. Quist, "Fracture Toughness" Materials In Design Engineering, November, 1965, pp 92-97.
73. P. C. Paris, "The Fracture Mechanics Approach to Fatigue," Proceedings 10th Sagamore Army Materials Research Conference, August, 1963, Syracuse University Press, 1964.
74. C. F. Tiffany and J. N. Masters, "Applied Fracture Mechanics" from "Fracture Toughness Testing," ASTM-STP-381, April 1965, pp 133-198.
75. W. F. Payne, "Incorporation of Fracture Information In Specifications," from "Fracture Toughness Testing," ASTM-STP-381, April, 1965, pp 357-372.
76. E. T. Wessel, "Correlation of Laboratory Determinations of Fracture Toughness With the Performance of Large Steel Pressure Vessels," Welding Journal Research Supplement, V. 43, No. 9, September, 1964, p 415s.
77. J. E. Srawley and J. B. Esgar, "Investigation of Hydrotest Failure of Thiokol Chemical Corporation 260-Inch Diameter SL-1 Motor Case," NASA TM X-1194, January, 1966.
78. C. M. Carman, D. F. Armiento and H. Markus, "Fracture Toughness and Pressure Vessel Performance," ASME Paper 63-WA-138, Presented at ASME Annual Meeting, November, 1963, Philadelphia, Pennsylvania.
79. H. D. Greenberg, "An Engineering Basis for Establishing Radiographic Acceptance Standards for Porosity In Steel Weldments," Trans. ASME, J. Basic Engineering, V. 87 Series D, No. 4, December, 1965, p 879.

TABLE OF CONTENTS

Section 7.1

PHASE II - DATA COLLECTION

	<u>Page</u>
7.1 LITERATURE SURVEY	
7.1.1 Introduction	144
7.1.2 Evaluation Criteria.	144
7.1.3 Compilation of Data.	146
7.1.4 Discussion	148
7.1.5 Summary.	152

LIST OF TABLES

Section 7.1

PHASE II - DATA COLLECTION

	<u>Page</u>
TABLE I Materials For Which Valid K_{Ic} Data Are Presented In Appendix I	147

LIST OF FIGURES

Figure 1. Variability of room temperature toughness with yield strength for 18% Ni Maraging steel . .	150
Figure 2. K_{Ic} as a function of yield strength for 18% Ni maraging steel (various amounts of cold work) . .	151
Figure 3. K_{Ic} as a function of yield strength for 18% Ni maraging steel (various aging treatments)	151

Section 7

PHASE II - DATA COLLECTION

7.1 LITERATURE SURVEY

7.1.1 INTRODUCTION

During the last five years, an extensive amount of fracture toughness data have been developed and published for a variety of structural materials. However, due to recent advances in the state of the art of fracture toughness testing, much of the published data are presently considered invalid. Therefore, a literature survey was conducted in order to establish the availability of valid plane strain fracture toughness data and to provide a basis for the selection of material for subsequent investigation. The survey was limited to the review of published data containing notch toughness properties expressed in terms of fracture mechanics parameters. The available data were re-evaluated in accordance with the latest ASTM recommended criteria for valid plane strain toughness testing, and those established as valid are tabulated in handbook form.

7.1.2 EVALUATION CRITERIA

Several test specimens are available for the determination of the plane strain fracture toughness parameter, K_{Ic} . Those encountered as the result of the literature survey were: notched rounds, single-edge-notched plates, surface-cracked plates, notched bend bars (3- and 4-point loading), center-notched plates, and center-line-loaded specimens. Although the available toughness specimens vary considerably in appearance they are each subject to the same general test requirements. The criteria used to establish the validity of the reported K_{Ic} data were based upon the latest requirements recommended by the ASTM Special Committee on

Fracture Testing.^(1,2) The general criteria common to each test specimen require: the extension of machined notches to fatigue crack severity by low-stress, $<0.5 \sigma_{Y.S.}$ ($\sigma_{Y.S.} = 0.2\%$ yield strength), fatigue cycling; limiting the net section stress (σ_N) at the onset of fast fracture to $0.8 \sigma_{Y.S.}$ except for notched rounds, slow bend, and center-line-loaded specimens, in which case $\sigma_N < 1.1 Y.S.$; and satisfactory instrumentation to evaluate crack behavior (yielding or slow growth) prior to rapid failure. The recommended minimum specimen size and relative dimension proportions necessary to satisfy the general toughness testing criteria for the various specimen geometries are summarized below.^(2,3)

1. Notched round bar where $d =$ diameter at root of notch

$D =$ outside diameter of bar

$$D \geq 4.4 \left(\frac{K_{Ic}}{\sigma_{Y.S.}} \right)^2 \quad d = 0.707 D \quad \text{Length} = 10 D$$

2. Single-edge-notch plate where $a_o =$ crack length $W =$ width
 $B =$ thickness $L =$ length

$$B \geq \left(\frac{K_{Ic}}{\sigma_{Y.S.}} \right)^2 \quad 4 < W/B < 8 \quad a_o = W/3 \quad L = 4 W$$

3. Notch bend (three-point loading)

$$B \geq 2.1 \left(\frac{K_{Ic}}{\sigma_{Y.S.}} \right)^2 \quad 2 < W/B < 8 \quad \text{span} = 8 W \quad a_o = W/5$$

4. Notch bend (four-point loading)

$$B \geq 2.1 \left(\frac{K_{Ic}}{\sigma_{Y.S.}} \right)^2 \quad 2 < W/B < 8 \quad \text{span} = 8 W \text{ and } 2 W \quad a_o = W/5$$

5. Center-Cracked plate specimen

$$B \geq 0.75 \left(\frac{K_{Ic}}{\sigma_{Y.S.}} \right)^2 \quad 5 < W/B < 10 \quad L = 4 W \quad a_o = W/6$$

6. Symmetrical edge-cracked plate

$$B \geq 0.65 \left(\frac{K_{Ic}}{\sigma_{Y.S.}} \right)^2 \quad 4 < W/B < 8 \quad L = 4 W \quad a_o = W/6$$

7. Surface-cracked plate

$$B \geq 0.85 \left(\frac{K_{Ic}}{\sigma_{Y.S.}} \right)^2 \quad W/B \geq 6 \quad \text{crack length } 2 C_o \leq W/3 \\ L = 2 W \quad \text{crack depth } a_o < B/2$$

8. Wedge-opening-loading specimen (X-type geometry)

$$B = 4 \left(\frac{K_{Ic}}{\sigma_{Y.S.}} \right)^2 \quad W/B = 1.125 \quad B = L \quad a_o/W = 0.25 \text{ to } 0.80 \\ W = \text{width from centerline of loading}$$

9. Wedge-opening-loading specimen (T-type geometry)

$$B = 2 \left(\frac{K_{Ic}}{\sigma_{Y.S.}} \right)^2 \quad W/B = 2.5 \quad L = 2.5 B \quad a_o/W = 0.25 \text{ to } 0.80 \\ W = \text{width from centerline of loading}$$

The most stringent requirement for proof of failure under plane strain conditions involves the evaluation of crack behavior prior to final failure. Yielding at the crack tip (beyond the established plastic zone) prior to failure indicates non-plane-strain conditions; therefore, satisfactory instrumentation for monitoring crack behavior during testing is required. Those data presented in the literature which indicated specimen failure prior to deviation of the load displacement curve (pop-in) were considered valid and no additional instrumentation aside from the displacement gauge was necessary. However, those data which indicated deviation of the load displacement curve prior to failure were considered invalid unless some technique was used to attribute the reason for deviation to slow crack growth rather than plastic yielding.

7.1.3 COMPILATION OF DATA

Approximately 100 references were reviewed during the literature survey, and 29 were found to contain valid plane strain fracture toughness

data. Table I lists the materials for which some valid K_{Ic} data exist and also provides an indication of the amount of data available. A

Section 7.1 Table I

MATERIALS FOR WHICH VALID K_{Ic} DATA ARE PRESENTED IN APPENDIX I

<u>Material</u>	<u>Strength Level 0.2% Yield Strength (ksi)</u>	<u>Temperature Range, °F</u>	<u>Volume of Data*</u>	<u>Location in Appendix I</u>
<u>Ferrous Alloys</u>				
18% Ni Maraging Steel	180 - 350	-110 to 650	(A)	Table I-A
4340	130 - 300	-110 to 750	(A)	Table I-B
D6ac	200 - 260	-200 to 75	(B)	Table I-C
H-11	160 - 240	-100 to 300	(B)	Table I-D
HP-9-4	140 - 250	-200 to 400	(D)	Table I-E
12Ni-5Cr-3Mo	180 - 190	R.T.	(D)	Table I-F
AM 355	160 - 200	-110 to 650	(D)	Table I-G
4335+V	210	-100 to 0	(D)	Table I-H
20% Ni Maraging Steel	300	R.T.	(D)	Table I-I
300 M	230	R.T.	(D)	Table I-J
PH-13Cr-8Ni	180 - 220	-110 to 400	(D)	Table I-K
A302B	50 - 130	-320 to 0	(D)	Table I-L
Ni-Mo-V Forging Steel	80 - 140	-320 to 25	(D)	Table I-M
<u>Titanium Alloys</u>				
Ti-6Al-6V-6Sn	140 - 190	-320 to 400	(B)	Table II-A
Ti-6Al-4V	140 - 170	-320 to 300	(C)	Table II-B
Beta Titanium	170	-100 to 300	(D)	Table II-C
<u>Aluminum Alloys</u>				
7075-T6 & T651	70	R.T.	(A)	Table III-A
7079-T6	70	- 75 to 150	(B)	Table III-B
7001-T75	77	R.T.	(D)	Table III-C

* (A) Extensive data available; (B) Moderate amount of data available; (C) Little data available; (D) Data very sparse.

compilation of the valid K_{Ic} data as well as the associated material and test parameters is presented in Appendix I. The materials have been classified into three categories--ferrous, aluminum, and titanium alloys--and are presented in order of increasing section size. The data have been arranged in such a manner as to provide the most efficient tabular form for both design and fracture mechanics reference information.

The references reviewed during the literature survey are presented in the bibliography associated with Appendix I. Those references containing valid K_{Ic} data are presented in that portion of the bibliography noted as "References Cited." References which do not contain valid data and also those which do not present sufficient information to permit evaluation are tabulated in reverse chronological order as "References Not Cited."

7.1.4 DISCUSSION

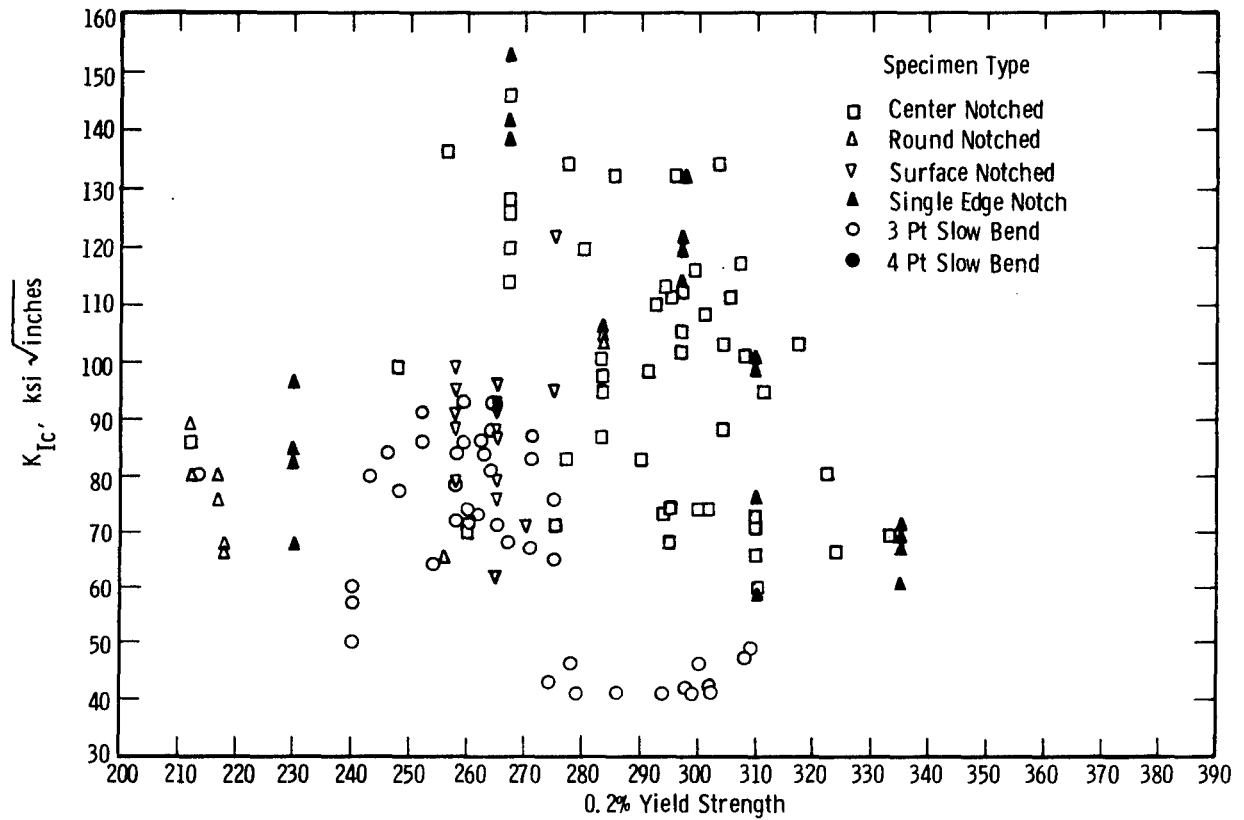
As indicated by the results of the literature survey, a limited amount of published data is available which conforms to the latest requirements for valid plane strain fracture toughness testing. In addition, those data presently considered valid may be modified as the fracture mechanics concepts associated with toughness testing change with advancing technology. Fracture toughness testing is a relatively recent development which requires the testing of rather large, expensive specimens; as a result, the amount of experimental data available to confirm existing concepts is limited and as more data become available for examination the recommended testing procedures may become modified. Even at the time of this writing an ASTM committee (Subcommittee I of ASTM Committee E-24) is reviewing the recommended procedures for plane strain toughness testing in order to establish the best approach.⁽⁴⁾

The published toughness data encountered during the literature survey were limited to relatively high-strength structural materials. Data are available for ferrous materials in the 0.2% yield strength range of 50-300 ksi, titanium alloys ranging in yield strength from 130 to 190 ksi, and aluminum alloys with yield strengths of 60 to 90 ksi. The majority of the data were determined at room temperature; however, a

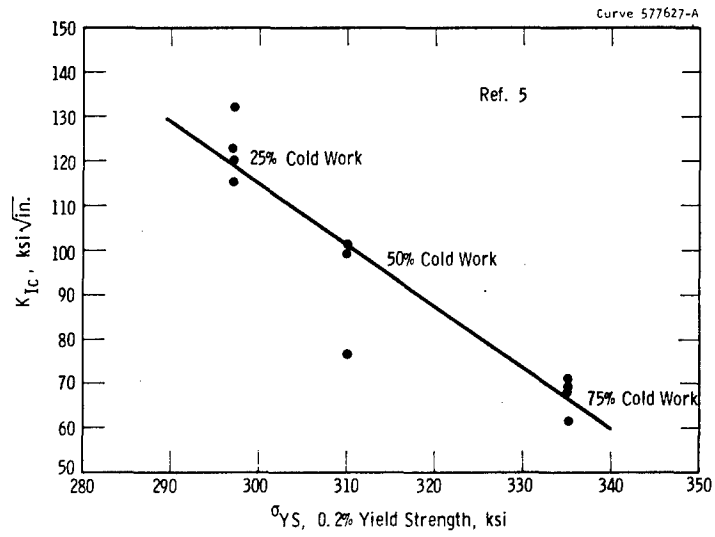
considerable amount of data obtained at other test temperatures is available.

Examination of the data presented in Appendix I clearly illustrates the possible variability of constant temperature fracture toughness measurements for a given material. This variability is further exemplified by the room temperature K_{Ic} versus 0.2% yield strength plot for 18% Ni maraging steel shown in Figure 1. Included in Figure 1 are all of the room temperature toughness data accumulated for 18% Ni maraging steel with no consideration given metallurgical parameters such as form, composition, heat treatment, and test orientation. Figures 2 and 3 illustrate the variation in room temperature K_{Ic} with yield strength for 18% Ni maraging steel where the only metallurgical variables are the percent cold work and the aging treatment, respectively.^(5,6) Although the plane strain stress intensity factor, K_{Ic} , is assumed to be a materials property which varies inversely with yield strength, it is obvious that this assumption is applicable only to materials of the same metallurgical history. The effect of metallurgical parameters upon yield strength and other conventional strength criteria is much less variable than the effect of the same parameters upon fracture toughness.⁽⁷⁾ Yield strength measurements are affected only by those variables which result in a change in the degree of material yielding, whereas fracture toughness is basically an energy measurement at fracture instability and is affected by all variables which affect the micromechanisms of failure. As a result, fracture toughness measurements must be conducted with test specimens representative of the material to be used in component fabrication. The chemistry, heat treatment, working history and test orientation must be nearly identical to that of the component in order to ensure satisfactory toughness measurements.

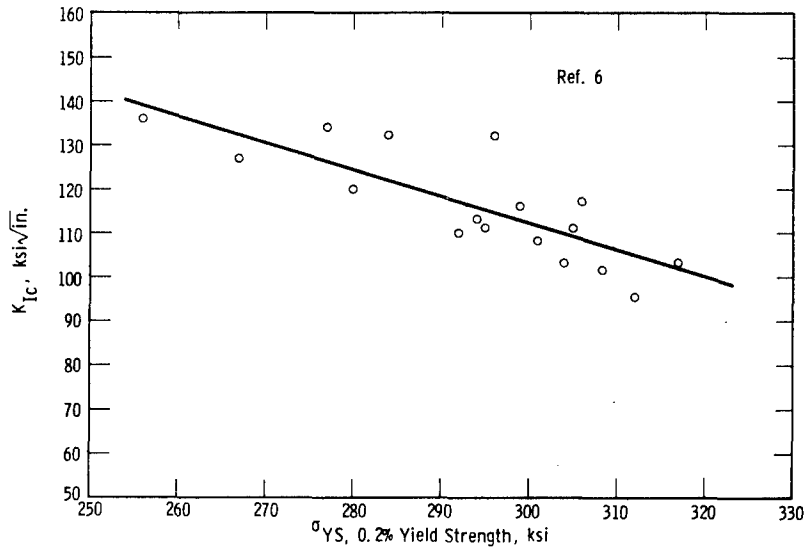
Tabulated K_{Ic} data arranged in handbook form for design reference must provide sufficient information to adequately describe the material tested. All variables known to affect K_{Ic} measurements must be included. Only then can the data be utilized for the design against brittle failure.



Sec. 7.1 Fig. 1 -Variability of room temperature toughness with yield strength for 18% Ni maraging steel



Sec. 7.1 Fig. 2 — K_{IC} as a function of yield strength for 18% Ni maraging steel (various amounts of cold work)



Sec. 7.1 Fig. 3 — K_{IC} as a function of yield strength for 18% Ni maraging steel (various aging treatments)

7.1.5 SUMMARY

A limited amount of published K_{Ic} data is available which conforms to the latest requirements for valid plane strain fracture toughness testing. These data are confined to relatively high-strength structural materials.

The reported toughness of a given material can vary considerably with various metallurgical parameters; therefore, the material used to establish toughness data must be nearly identical to that used for component fabrication.

Section 7.1 References

1. "Progress in Measuring Fracture Toughness and Using Fracture Mechanics," Fifth Report of the ASTM Special Committee on Fracture Testing of High-Strength Materials, Materials Research and Standards, March 1964, p. 113.
2. J. E. Srawley and W. F. Brown, "Fracture Toughness Testing Methods," Fracture Toughness Testing, STP 381 (1965).
3. W. F. Payne, "Incorporation of Fracture Information in Specifications," ASTM Meeting, Chicago, June 23-24, 1964.
4. W. F. Brown, "Plane Strain Crack Toughness Testing," Tentative draft submitted to Subcommittee I of ASTM Committee E-24, January 1966.
5. H. W. Maynor and C. C. Busch, " K_{Ic} of a 300-Grade 18-Nickel Maraging Steel as Influenced by Specimen Type and Thermal and Mechanical Treatment," AD 601537, Auburn Research Foundation, May 1964.
6. W. F. Payne, "Analysis of Surface-Cracked Fracture Toughness Information," Fourth Maraging Steel Project Review, Vol. 1, Air Force Materials Labs Report No. ML-TDR-64-225, July 1964.
7. R. E. Johnson, "Fracture Mechanics: A Basis for Brittle Fracture Prevention," AEC Research and Development Report WAPD-TM-505, November 1965.

TABLE OF CONTENTS

Section 7.2

	<u>Page</u>
7.2 GENERATION OF K_{Ic} DATA	
7.2.1 Material	157
7.2.2 Specimen Preparation	160
7.2.3 Test Procedure	163
7.2.4 Results and Discussion	170
7.2.5 Summary.	189

LIST OF TABLES

Section 7.2

GENERATION OF K_{Ic} DATA

		<u>Page</u>
TABLE	I Chemical Analysis of Alloys	157
TABLE	II Heat Treatment and Room Temperature Tensile Properties.	158
TABLE	III Measurement Capacity Associated with the WOL Fracture Toughness Specimen	165
TABLE	IV Cyclic Load Used to Precrack WOL Type Fracture Toughness Specimen	168
TABLE	V Room Temperature Tensile Properties and Toughness	172
TABLE	VI-A Transverse Tensile Properties of HP-9-4-25 Steel	192
TABLE	VI-B Transverse Charpy V-Notch Properties of HP-9-4-25 Steel	193
TABLE	VI-C Transverse Toughness Properties of HP-9-4-25 Steel	194
TABLE	VII-A Transverse Tensile Properties of Ti-6AL-4V Titanium.	196
TABLE	VII-B Transverse Charpy V-Notch Properties of Ti-6AL-4V Titanium.	197
TABLE	VII-C Transverse Toughness Properties of Ti-6AL-4V Titanium.	198
TABLE	VIII-A Longitudinal Tensile Properties of 7079-T6 Aluminum.	200

LIST OF TABLES (Cont.)

	<u>Page</u>
TABLE VIII-B Longitudinal Charpy V-Notch Properties of 7079-T6 Aluminum	201
TABLE VIII-C Longitudinal Toughness Properties of 7079-T6 Aluminum.	202

LIST OF FIGURES

Figure 1. "As Received" Microstructure of each alloy system investigated.	159
Figure 2. Tensile specimens used in this investigation. . .	161
Figure 3. Charpy V-notch impact test specimen.	162
Figure 4. Wedge-opening-loading (WOL) "X" type fracture toughness specimens	164
Figure 5. Wedge-opening-loading (WOL) "T" type fracture toughness specimens	164
Figure 6. WOL fracture toughness specimen ("2X" Geometry).	165
Figure 7. WOL fracture toughness specimen ("1T" Geometry).	166
Figure 8. WOL fracture toughness specimen ("2T" Geometry).	166
Figure 9. 25,000 lb. Westinghouse crank machine for fatigue cracking fracture specimen	167
Figure 10. Orientation of test specimens in "As Received" forged plate	169
Figure 11. Clip gage used to establish the load- displacement curves.	171
Figure 12. Numerical constant "C ₃ " as a function of the a ₀ /W ratio for the "X" type WOL tough- ness specimen.	174

LIST OF FIGURES (Cont.)

	<u>Page</u>
Figure 13. Temperature dependence of 0.2% yield strength, charpy impact energy and K_{Ic} for HP-9-4-25 steel	177
Figure 14. Temperature dependence of 0.2% yield strength, charpy impact energy and K_{Ic} for Ti-6AL-4V titanium.	177
Figure 15. Temperature dependence of 0.2% yield strength, charpy impact energy, and K_{Ic} for 7079-T6 aluminum.	178
Figure 16. Numerical constant " C_3 " as a function of the a_0/W ratio for the "T" type WOL toughness specimen	179
Figure 17. Dimension designations for the "T" type WOL toughness specimen.	180
Figure 18. Typical load displacement curve indicating deviation prior to rapid failure	181
Figure 19. Typical load displacement curve indicating deviation prior to "Pop-In".	182
Figure 20. Load displacement curve indicating "Pop-In" prior to deviation	183
Figure 21. Room temperature fracture appearance of HP-9-4-25 steel WOL toughness specimens	186
Figure 22. Room temperature fracture appearance of Ti-6AL-4V titanium WOL toughness specimens.	187
Figure 23. Room temperature fracture appearance of 7079-T6 aluminum WOL toughness specimens	188

Section 7.2

GENERATION OF K_{Ic} DATA

7.2.1 MATERIAL

In order to supplement the fracture toughness data accumulated as a result of the literature survey, three high-strength forging alloy systems representative of those materials which appear promising for future military vehicle applications were selected for further investigation. These materials represent relatively new alloys for which a very limited amount of valid fracture toughness data are available. The alloys selected for the experimental program were:

HP-9Ni-4Co-.25C Steel

7079-T6 Aluminum

Ti-6Al-4V Titanium

The HP-9-4-25 steel was selected as representative of the high-strength, high-alloy martensitic steels presently receiving considerable attention for many critical applications. The titanium-base alloy, Ti-6Al-4V, was selected to represent the more commonly used heat-treatable alpha-beta titanium high-strength alloys; and aluminum alloy 7079-T6 was selected as representative of the high-strength, heat-treatable aluminum alloys.

The chemical compositions of each alloy heat involved in the investigation are given in Table I.

Section 7.2 Table I
CHEMICAL ANALYSIS OF ALLOYS

	<u>C</u>	<u>Mn</u>	<u>P</u>	<u>S</u>	<u>Si</u>	<u>Ni</u>	<u>Cr</u>	<u>Mo</u>	<u>V</u>	<u>Co</u>
HP-9-4-25	0.26	0.33	0.008	0.008	0.01	8.41	0.40	0.48	0.07	3.9
	<u>Cu</u>	<u>Fe</u>	<u>Si</u>	<u>Mn</u>	<u>Mg</u>	<u>Zn</u>	<u>Cr</u>	<u>Ti</u>	<u>Al</u>	
7079-T6 Al (Nominal)	0.4- 0.8	0.4	0.3	0.10- 0.30	0.29- 0.37	3.8- 4.8	0.10- 0.25	0.10	Bal.	
	<u>C</u>	<u>Fe</u>	<u>N</u>	<u>Al</u>	<u>Va</u>	<u>H</u>	<u>O₂</u>			
Ti-6Al-4V	0.023	0.13	0.014	6.3	4.1	0.004	0.17			

The steel (HP-9-4-25) was supplied as two pieces, 18" x 24", and one piece, 8" x 12", of three-inch-thick consumable electrode vacuum melted forged plate in the quenched and tempered condition. The heat treatment involved austenitizing at 1550°F for one hour, oil quenching, and double tempering two hours at 1000°F followed by an air cool.

The 7079-T6 aluminum alloy was supplied as three pieces, 18" x 24", of three-inch-thick forged plate in the solution treated and aged condition. The heat treatment consisted of solution treating at 830°F for four hours, water quenching, and aging at room temperature for five days plus 48 hours at 240°F.

The titanium (Ti-6Al-4V) was supplied as one piece, 12" x 36", of three-inch-thick forged plate in the solution treated and aged condition. Heat treatment involved solution treating at 1750°F for one hour, water quenching and aging at 1000°F for four hours. A summary of the alloy heat treatments and the resulting room temperature tensile properties are given in Table II. Figure 1 shows the typical as-received microstructure of each alloy.

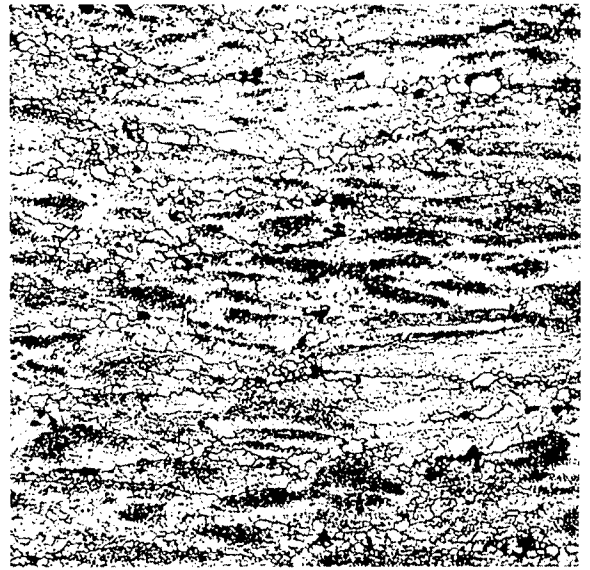
Section 7.2 Table II
HEAT TREATMENT AND ROOM TEMPERATURE TENSILE PROPERTIES
(3"-Thick Forged Plate)

<u>Alloy</u>	<u>Heat Treatment</u>	<u>Test Direction</u>	<u>0.2% Yield Strength psi</u>	<u>Ultimate Tensile Strength psi</u>
HP-9-4-25	Austenitized 1 hr - 1550°F. Oil quenched, double tempered 2 hr 1000°F. Air cooled.	Longitudinal	176,000	184,000
		Transverse	177,000	186,000
		Short Trans.	175,000	185,000
Ti-6Al-4V	Solution treated 1 hr 1750°F, water quench. Aged 4 hr 1000°F	Longitudinal	143,000	150,000
		Transverse	145,000	154,000
Al-7079-T6	Solution treated 4 hr 830°F, water quench. Aged 5 days 75°F plus 48 hr 240°F	Longitudinal	65,500	76,900
		Transverse	62,000	74,000



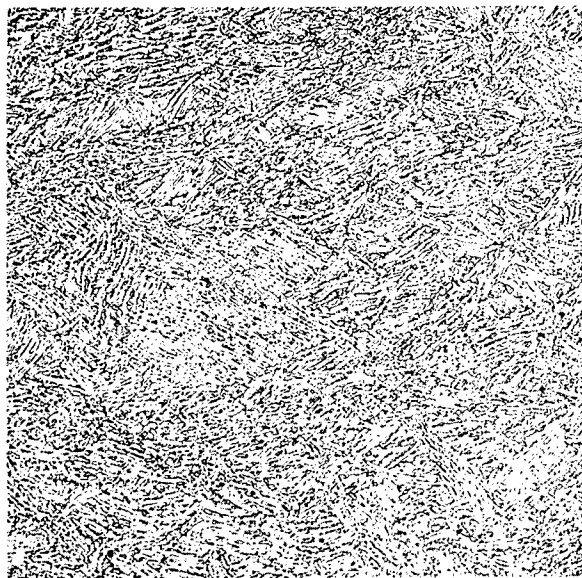
500X

HP-9-4-25 Steel



200X

7079-T6 Aluminum



100X

Ti-6AL-4V Titanium

Sec. 7.2 - Figure 1 "As Received" Microstructure of Each Alloy System Investigated

7.2.2 SPECIMEN PREPARATION

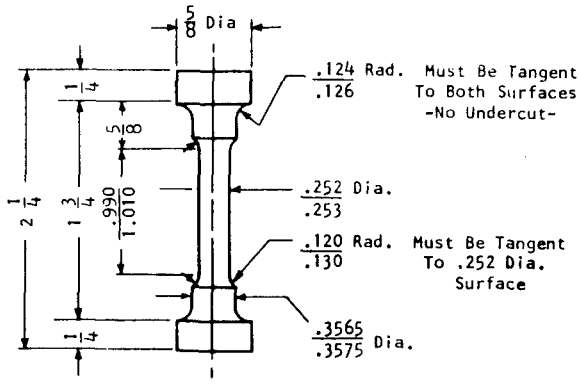
The experimental investigation conducted in conjunction with the overall program involved the determination of the major strength and toughness parameters for the steel (HP-9-4-25), aluminum (7079-T6), and titanium (Ti-6Al-4V) alloys described above. The parameters investigated included the tensile properties, the Charpy V-notch impact properties, the plane strain fracture toughness and the slow crack growth characteristics under cyclic loading (Sec. 7.3).

The tensile properties were determined using the smooth tensile specimens shown in Figure 2. The steel (HP-9-4-25) tensile specimens were prepared in accordance with Figure 2(a) (0.252" diameter); the titanium specimens with Figure 2(b) (0.356" diameter) and the aluminum specimens with Figure 2(c) (0.505" diameter).

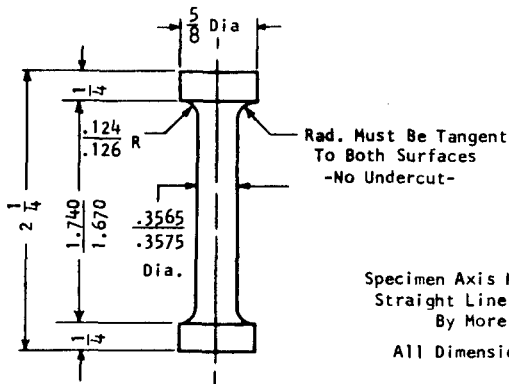
All of the Charpy V-notch impact data were determined using the standard Charpy specimens shown in Figure 3.

In view of the number of fracture toughness specimen designs available capable of providing satisfactory plane strain toughness data, it was necessary to review each design as to its relative merits with respect to the proposed investigation prior to selecting a specimen. The basic criteria for the selection of the most efficient specimen design were established as follows: (a) availability of a satisfactory fracture mechanics analysis; (b) demonstrated capability for valid K_{Ic} determination; (c) minimum volume of material required; and (d) relatively low load requirements. In addition, some consideration was given to the applicability of the specimen for slow crack growth measurements under cyclic loading.

A comparison of the available specimen designs resulted in the selection of the Wedge-Opening-Loading (W.O.L.) type fracture toughness specimen. This specimen quite adequately satisfies the established specimen requirements with no exceptions. Extensive stress analysis, photo-elastic studies and demonstrated capability ensure the reliability of the specimen to plane strain fracture toughness testing.^(1,2,3,4,5) The compact geometry of the specimen provides a minimum material volume requirement along with relatively low loads and the specimen is particularly applicable to slow crack growth measurement (see Appendix II).

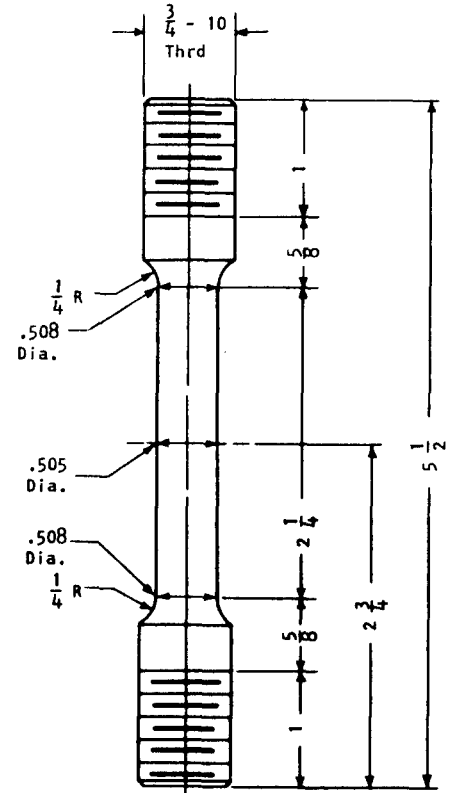


(a)



(b)

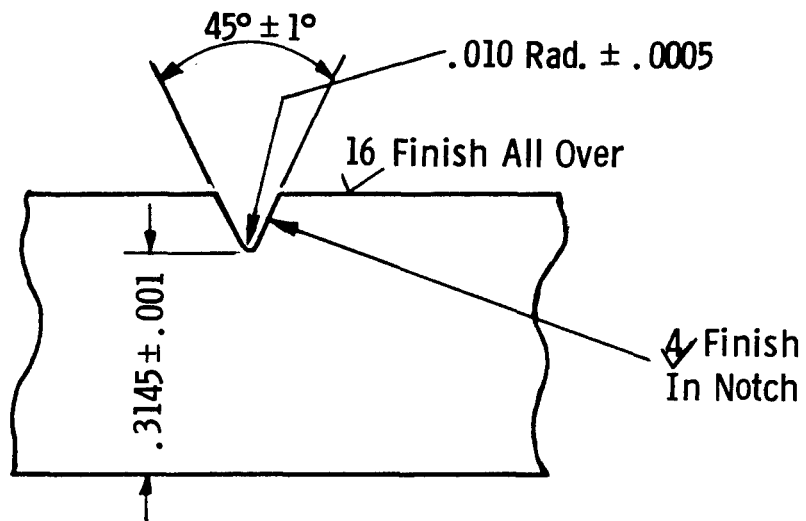
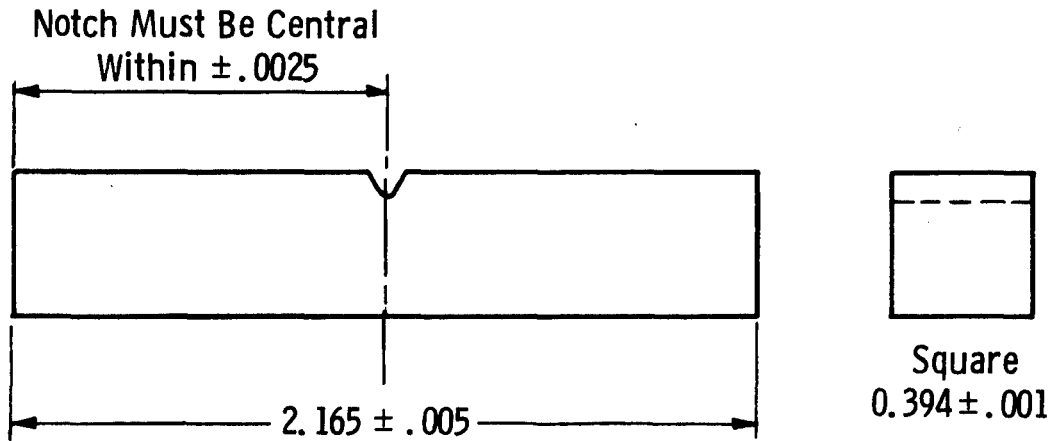
Specimen Axis Must Not Deviate From
Straight Line Through End Centers
By More Than 0.0005
All Dimensions Are In Inches



(c)

Sec. 7.2 Fig. 2 --Tensile specimens used in this investigation

Dwg. 851A622



Sec. 7.2 Fig. 3 -Charpy "V" notch impact test specimen

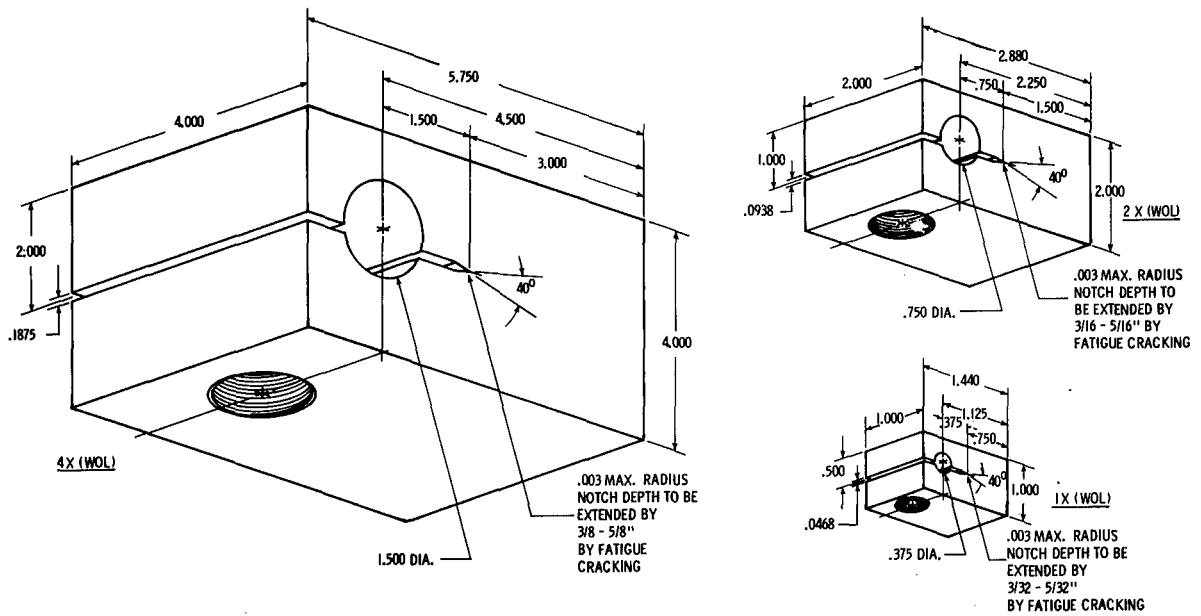
Two geometries and several sizes of the W.O.L. specimen are available. Figure 4 shows the "X" type W.O.L. geometry and Figure 5 shows the "T" geometry.

The specimen size is dictated by the maximum specimen capacity for plane strain fracture toughness measurement and ultimately by the properties of the material to be tested. Specimen capacity is represented by the ratio of the material toughness parameter to the 0.2% yield strength and is expressed as $K_{Ic}/\sigma_{Y.S.}$. As this ratio increases the specimen size required to satisfy plane strain conditions also increases. The maximum measurement capacity associated with various W.O.L. specimen sizes is given in Table III for both the "X" and "T" series geometry. The fracture toughness specimens used in conjunction with this investigation were of the "2X", "1T" and "2T" configurations. The specimens were prepared in accordance with the drawings shown in Figures 6, 7, and 8.

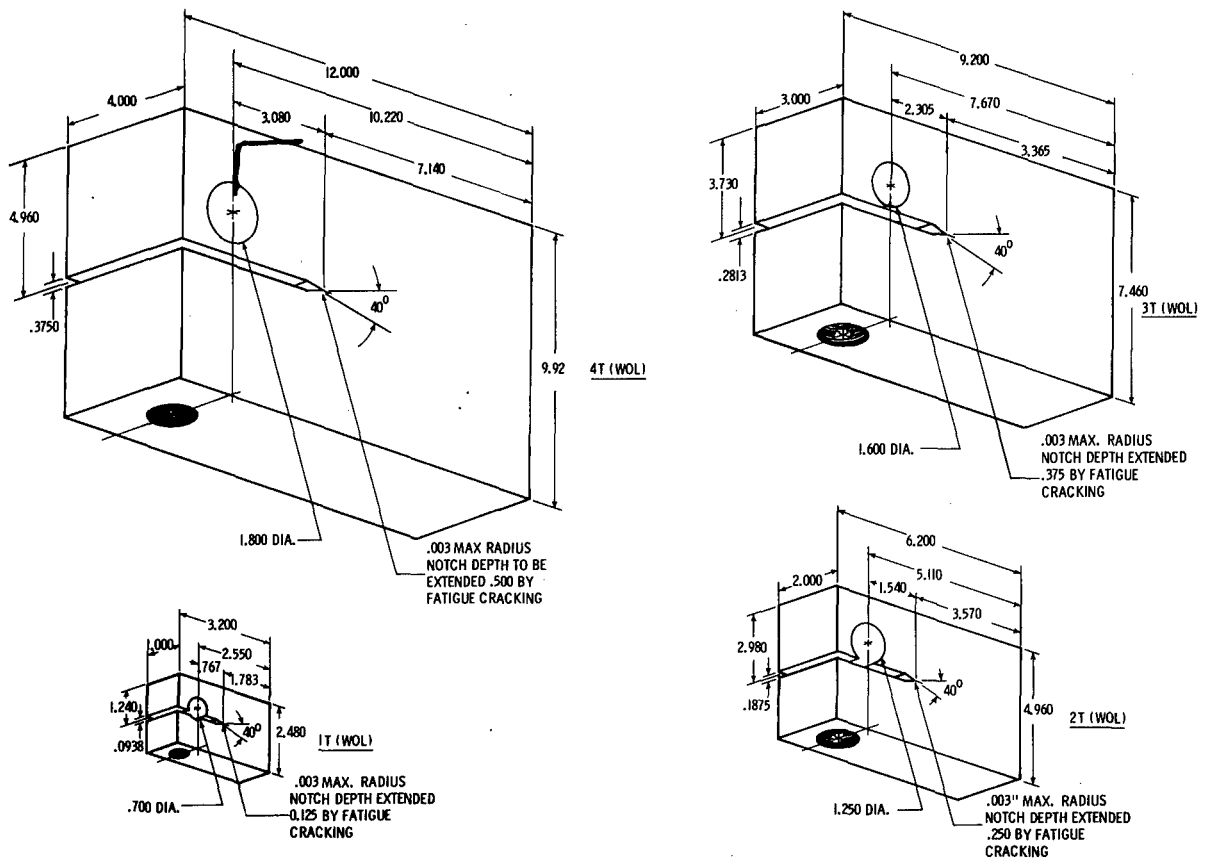
The machined notches were extended to fatigue crack severity by subjecting the specimens to low-stress cyclic loading at room temperature prior to tension testing. The precracking operation was conducted using a variety of commercial fatigue testing machines as well as several specially built 0-25,000-lb. constant deflection machines. Figure 9 shows the 25,000-lb. crank machine built for precracking the larger ("2X" and larger) W.O.L. type specimens. Table IV gives the initial nominal stress at the tip of the machined notch (no fatigue crack) and the maximum cyclic load involved in precracking the specimens used in this investigation. In order to facilitate the precracking of the "2T" steel specimens, a compression load equivalent to the maximum cyclic load was applied prior to precracking.

7.2.3 TEST PROCEDURE

The effect of test direction upon the room temperature tensile properties and toughness was determined for each alloy system under investigation. A minimum of three smooth tensile specimens and three "2X" type W.O.L. toughness specimens were tested in the longitudinal and long transverse directions. Figure 10 illustrates the orientation of the test specimens in the as-received three-inch-thick forged plate. (The location of Charpy bars is also indicated.)



Sec. 7.2 Figure 4 - Wedge opening loading (WOL) "X" type fracture toughness specimens

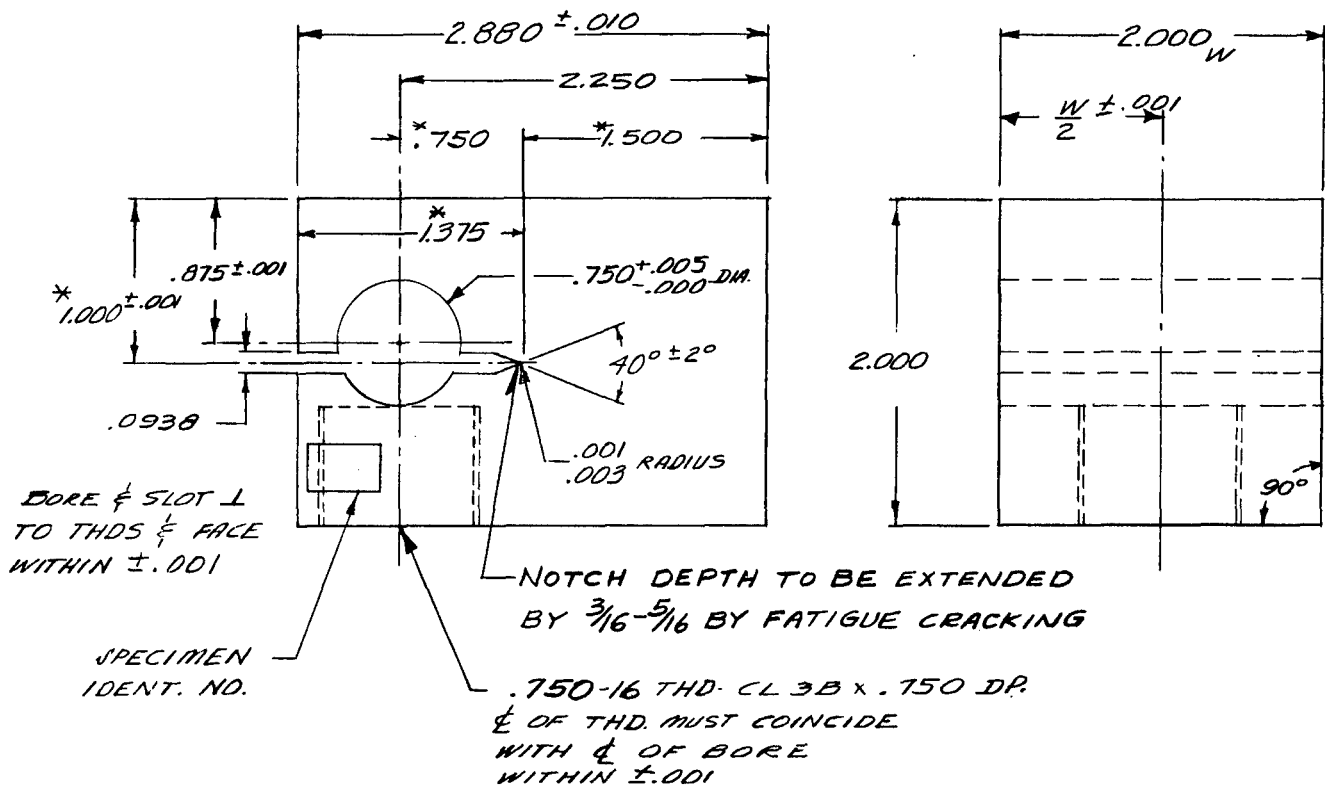


Sec. 7.2 Figure 5 - Wedge opening loading (WOL) "T" type fracture toughness specimens

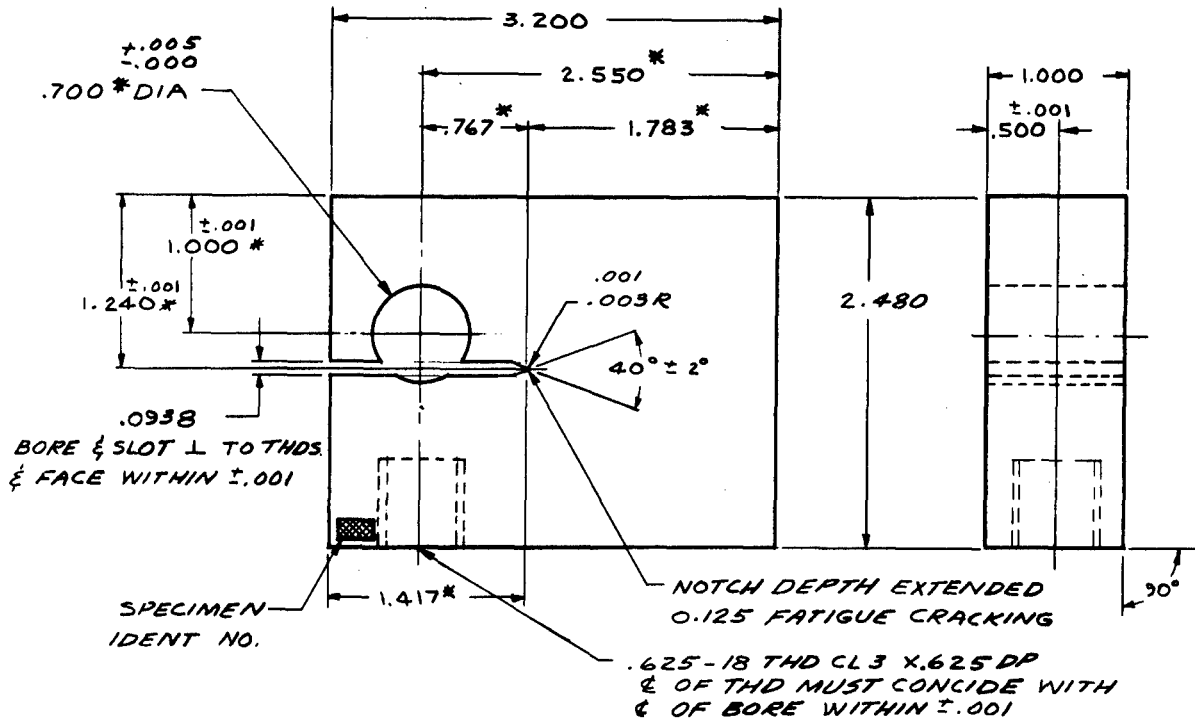
Sec. 7.2 Table III—Measurement Capacity Associated With The WOL Fracture Toughness Specimen

Identification	Dimensions						
	Square Design "x" Type			Optimum Design "T" Type			
	1x	2x	4x	1T	2T	3T	4T
B (thickness)	1.0	2.0	4.0	1.0	2.0	3.0	4.0
W (width)	1.44	2.88	5.75	3.2	6.2	9.2	12.0
L (length)	1.0	2.0	4.0	2.5	5.0	7.5	9.9
a (crack length)	0.5	1.0	2.0	0.9	1.8	2.7	3.6
$\frac{K_{Ic}}{\sigma_{YS}}$ (measurement capacity)	0.48	0.67	0.95	0.79	1.12	1.37	1.58

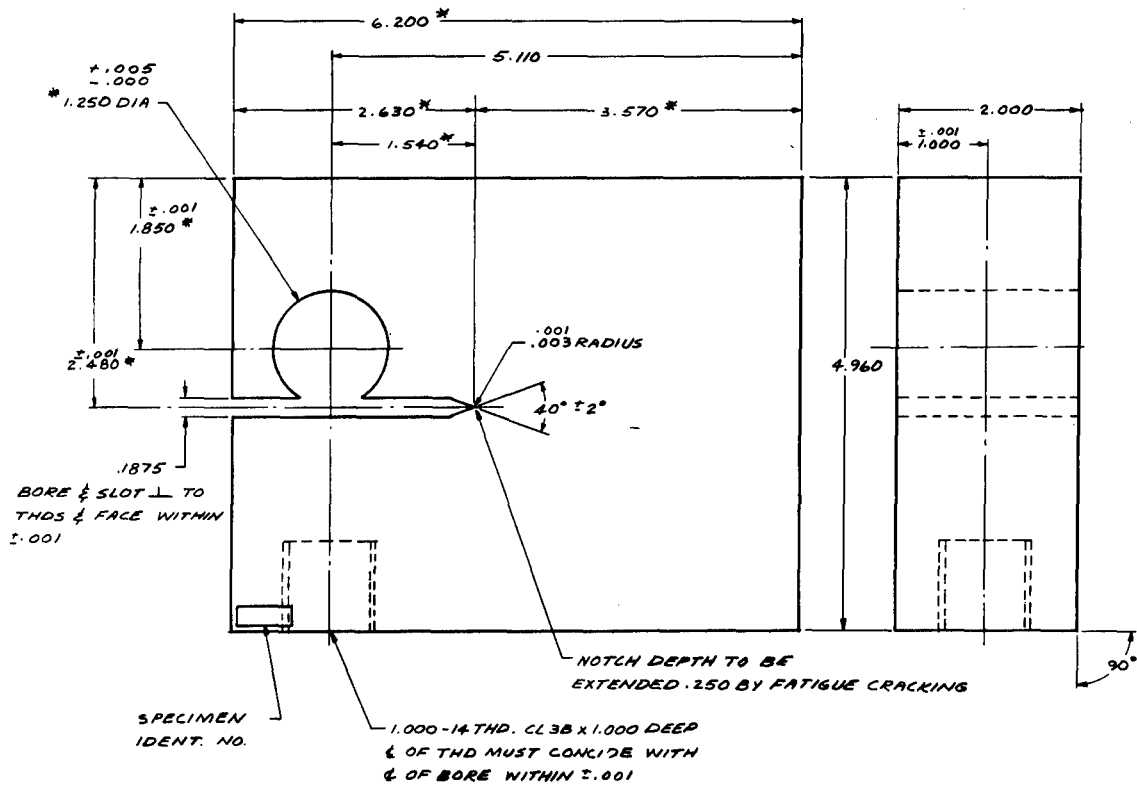
* For: Minimum volume of material required
 Where: $\sigma_N / \sigma_Y \leq 0.75$
 Plastic zone size $r_y \leq B/30$ (plane strain)
 No plastic bending in arms at $\sigma_N \leq 1.2 \sigma_{YS}$



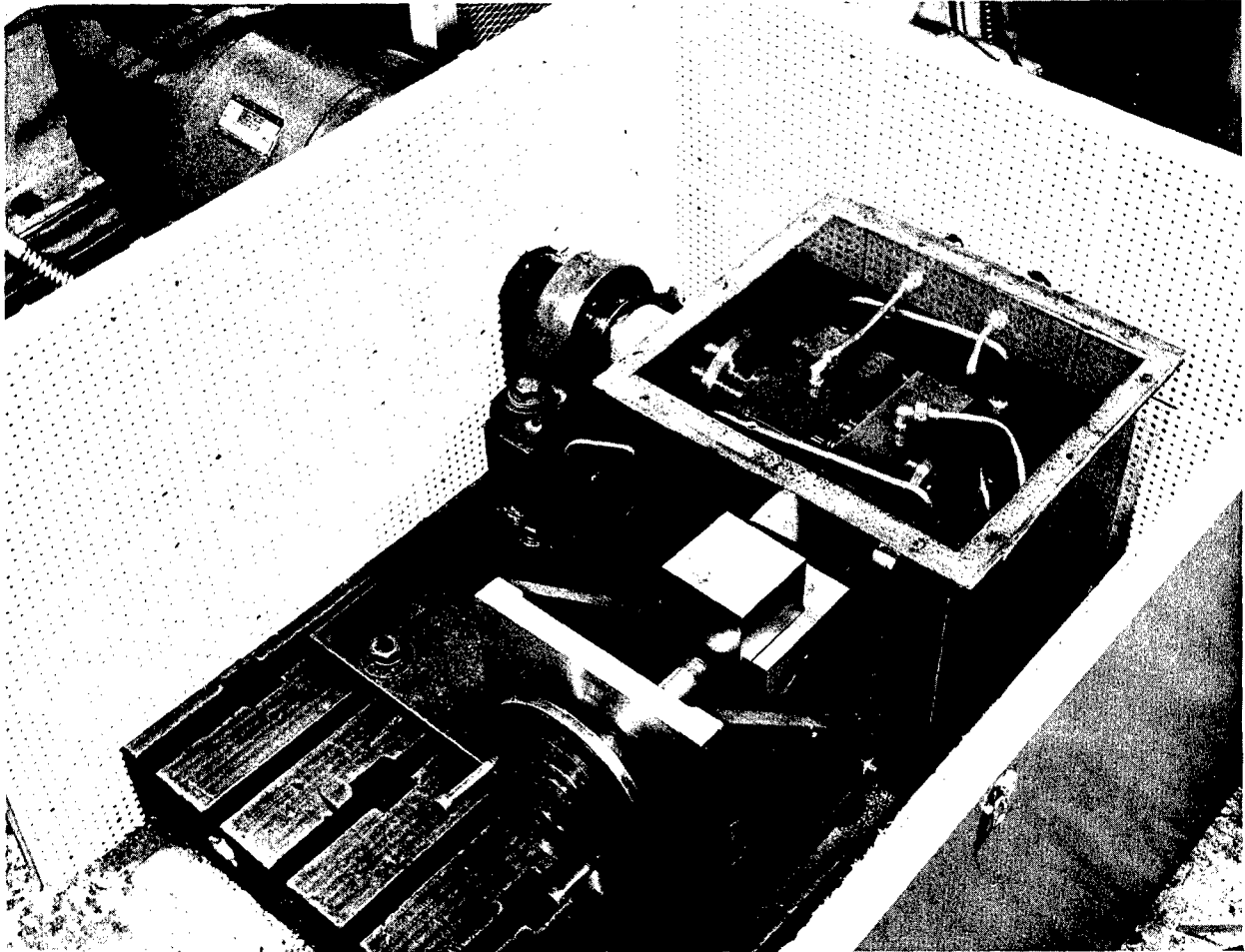
Sec. 7.2 Fig. 6 -W. O. L. fracture toughness specimen ("2X" geometry)



Sec. 7.2 Fig. 7 -W. O. L. fracture toughness specimen ("1T" geometry)



Sec. 7.2 Fig. 8 -W. O. L. fracture toughness specimen ("2T" geometry)

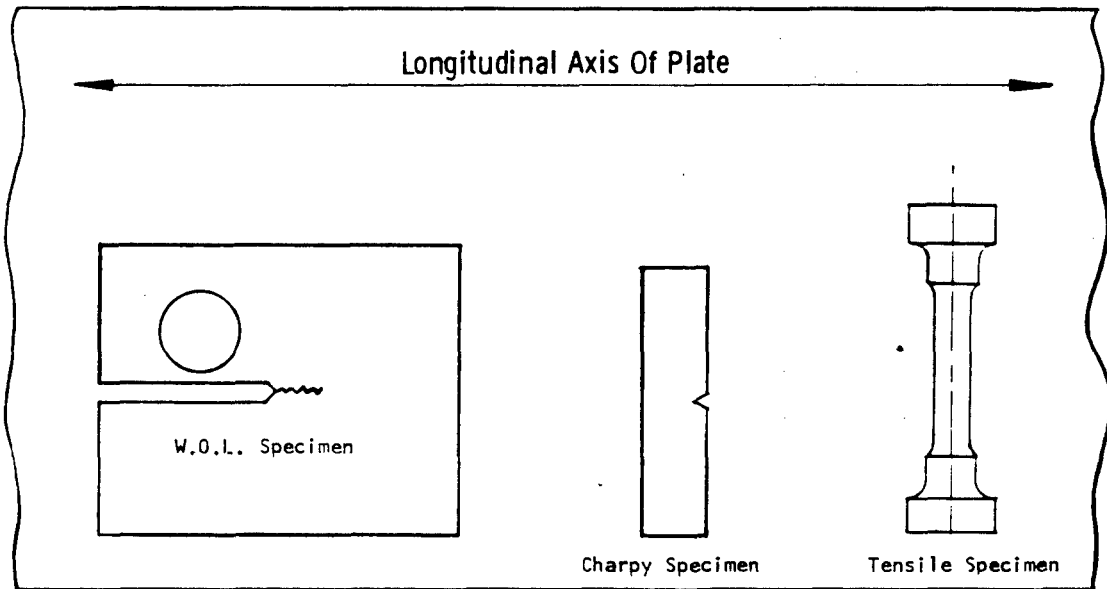


Sec. 7.2 Figure 9 - 25,000 lb Westinghouse crank machine for fatigue cracking fracture specimens

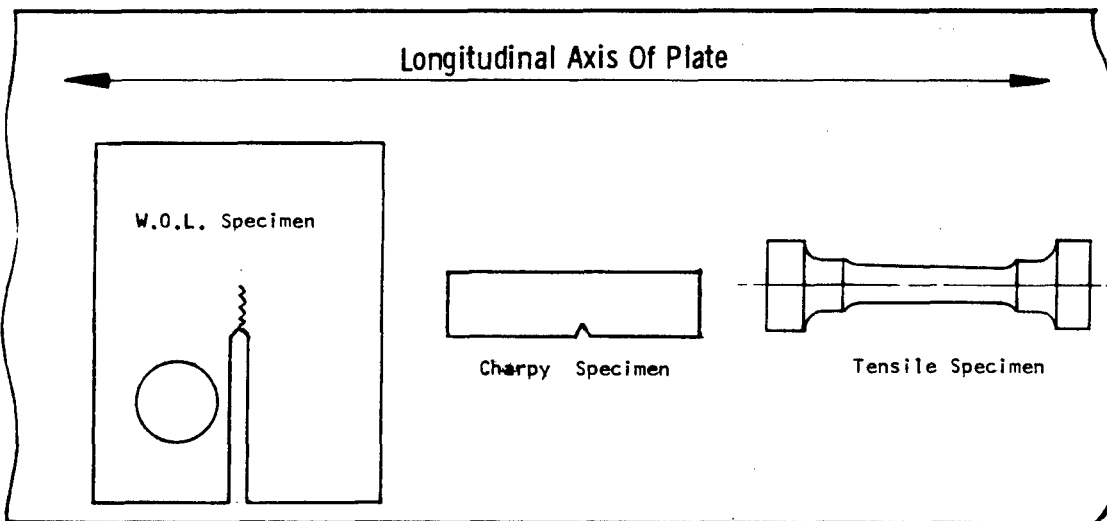
Section 7.2 Table IV

CYCLIC LOADS USED TO PRECRACK W.O.L. TYPE FRACTURE TOUGHNESS SPECIMENS

<u>Specimen Geometry</u>	<u>Cyclic Load (lbs.)</u>	<u>Nominal Stress σ_N at tip of Machined Notch</u>	<u>σ_N/σ_{YS}</u>	<u>No. Cycles Required to Propagate Crack to Desired Length</u>
<u>HP-9-4-25 Steel</u>				
1T	0- 5,000	18,400 psi	0.11	70,000 - 100,000
2X	0- 6,000	14,000 psi	0.08	180,000 - 680,000
2T	0-16,000	14,800 psi	0.08	42,000 - 115,000
<u>Ti-6Al-4V Titanium</u>				
1T	0- 4,000	14,700 psi	0.10	31,000 - 431,000
2X	0- 5,500	13,000 psi	0.09	128,000-1,500,000
2T	0-16,000	14,800 psi	0.11	21,000 - 50,000
<u>7079-T6 Aluminum</u>				
1T	0- 1,300	4,780 psi	0.08	126,000 - 695,000
2X	0- 2,500	5,800 psi	0.09	36,000 - 225,000



Transverse Test Specimens



Longitudinal Test Specimens

Sec. 7.2 Fig. 10 -Orientation of test specimens in "as-received" forged plate

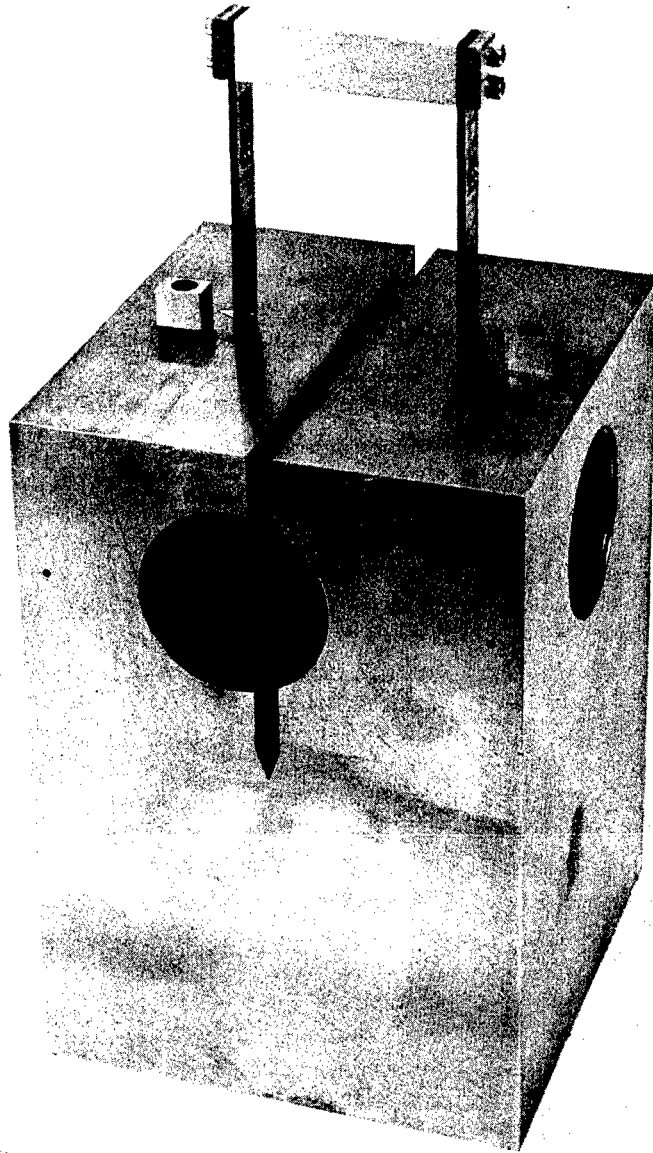
The "2X" W.O.L. toughness specimens were tested in direct tension at a loading rate of 0.040 inch/minute using a 400,000-lb. maximum load universal hydraulic test machine. The load-displacement characteristics of the specimen under test were recorded using the clip gauge instrumentation shown in Figure 11. The clip gauge was calibrated to 40 microinches of strain per 1 mil (0.001 inch) of displacement and the output fed into an autographic x-y recorder. The resulting load-displacement curve was used along with an ultrasonic crack growth detection technique (Appendix II) to evaluate the validity of the test. The combination of displacement gauge and ultrasonic instrumentation provided a technique capable of distinguishing between slow crack growth and general yielding at the fatigue crack tip prior to rapid failure.

Upon determining the effect of test orientation on the room temperature toughness, additional test specimens (tensile specimens, Charpy bars and W.O.L. specimens of various sizes) were prepared in order to evaluate the effect of temperature upon the strength parameters in that test direction yielding the lower toughness. This approach was used to provide a conservative evaluation of each material. Testing was conducted over a temperature range of -75°F to 150°F (a few specimens were tested at 200°F).

The determination of the toughness parameters for the steel and titanium alloys at various test temperatures was conducted using "1T" and "2T" type W.O.L. specimens. The toughness characteristics of the aluminum alloy were determined using "2X" and "1T" W.O.L. specimens.

7.2.4 RESULTS AND DISCUSSION

The results of the effect of specimen orientation upon the room temperature tensile properties and toughness of those alloys under investigation are given in Table V. The toughness data were determined using "2X" type W.O.L. specimens and the plane strain stress intensity factor determined using the following method and expressions.



Sec. 7.2 Figure 11 - Clip gage used to establish the load-displacement curves

Section 7.2 Table V

ROOM TEMPERATURE TENSILE PROPERTIES AND TOUGHNESS

<u>Alloy</u>	<u>Test Direction</u>	<u>0.2% Yield Strength (ksi)</u>	<u>Ultimate Strength (ksi)</u>	<u>Elongation %</u>	<u>Reduction in Area %</u>	<u>Critical Stress Intensity* ksi $\sqrt{\text{in.}}$</u>
HP-9-4-25	Longitudinal	176	184	19.3	63	151**
	Transverse	177	186	17	53	142.3**
Ti-6Al-4V	Longitudinal	143	150	14.5	37	80.9**
	Transverse	145	154	13	40	77.6**
Al-7079-T6	Longitudinal	65.5	76.9	12	27	29.3
	Transverse	62.0	74	7.5	22	29.1

* Determined using the "2X" W.O.L. specimen

** Apparent values

- (1) Determine nominal plane strain stress intensity factor

$$K_I = \frac{C_3 P}{\sqrt{a_o B}} = \begin{array}{l} \text{Nominal value of plane strain stress} \\ \text{intensity factor for opening mode of} \\ \text{crack extension} \end{array}$$

C_3 = Numerical constant obtained from Figure 12
using appropriate a_o/W

P = Load (lbs) from test - the load at fracture instability

a_o = Original crack length (inches) measured from center
line of loading

B = Specimen thickness measured from specimen

- (2) Compute plastic zone size

$$r_{IY} = \frac{K_I^2}{6\pi \sigma_{YS}^2} = \text{Plastic zone correction (plane strain)}$$

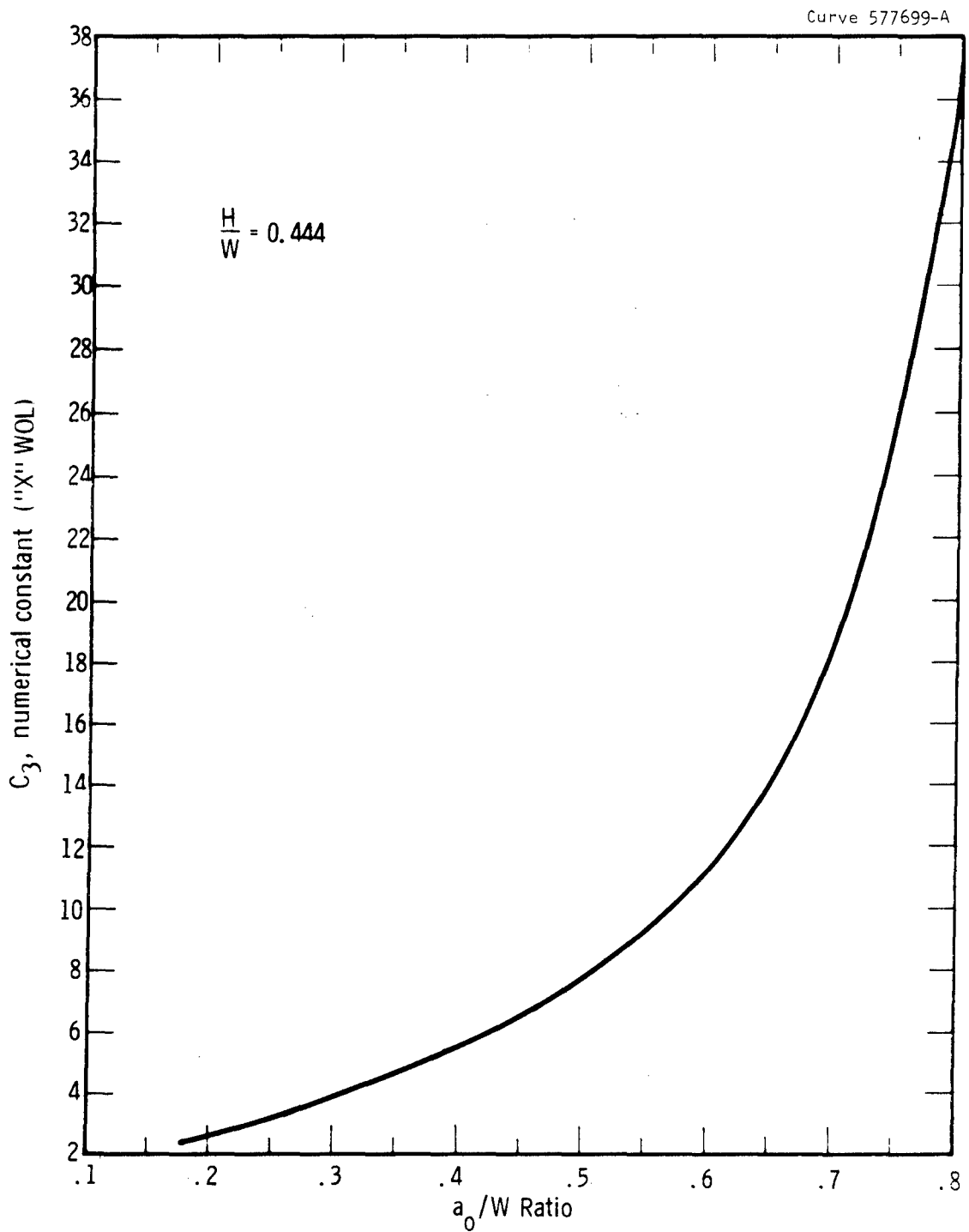
σ_{YS} = 0.2% yield strength

- (3) Add plastic zone correction to original crack length and
recalculate K_I

$$K_I' = \frac{C_3' P}{\sqrt{a_o' B}} = K_I \text{ corrected for plastic zone}$$

C_3' = Numerical constant obtained from Figure 12 using
 a_o'/W

a_o' = $a_o + r_{IY}$ = Corrected crack length



Sec. 7.2 Fig. 12 - Numerical constant " C_3 " as a function of the a_0/W ratio for the "X" type WOL toughness specimen

- (4) Apply iteration procedure to obtain K_{Ic} - usually one iteration is sufficient

$$K_I'' = \frac{C_3'' P}{\sqrt{a_o''} B} = K_I \text{ after iteration. } a_o'' = a_o' + r_{IY}'$$

$$K_I'' = K_{Ic} = \text{Plane strain stress intensity factor}$$

If desired K_{Ic} can be converted to the critical strain energy release rate as follows:

$$G_{Ic} = \frac{K_{Ic}^2 (1 - \nu^2)}{E} = \text{Critical strain energy release rate}$$

ν = Poisson's ratio

E = Young's modulus

Examination of the load-displacement curves and the corresponding ultrasonic presentation indicated that the K_{Ic} values calculated for the steel and titanium alloys using the "2X" specimens were not entirely plane strain since the load-displacement curve deviated from linearity with no indication of crack growth prior to rapid failure. The aluminum alloy specimens exhibited pronounced "pop-in" prior to deviation indicating the existence of plane strain conditions. Although the preliminary toughness testing resulted in apparent K_{Ic} values for the steel and titanium, these data were considered satisfactory for determining the test orientation yielding the lower toughness. Based upon the preliminary toughness data, additional testing was conducted in the transverse direction for the steel and titanium alloys and in the longitudinal test direction for the aluminum alloys.

In view of the inability to obtain plane strain toughness data for the steel and titanium alloys with the "2X" type W.O.L. specimen it

was necessary to use test specimens which exhibited a greater toughness measurement capacity. The theoretical measurement capacity of the "2X" WOL as expressed by K_{Ic}/σ_{YS} , is 0.67; that of the "1T" and "2T" is 0.8 and 1.12 respectively. Therefore, the investigation of the HP-9-4-25 steel and Ti-6Al-4V titanium alloys was continued with "1T" and "2T" WOL specimens. Additional "2X" and "1T" WOL specimens were prepared from the aluminum in order to establish the temperature dependence of the critical stress intensity factor.

HP-9-4-25 Steel

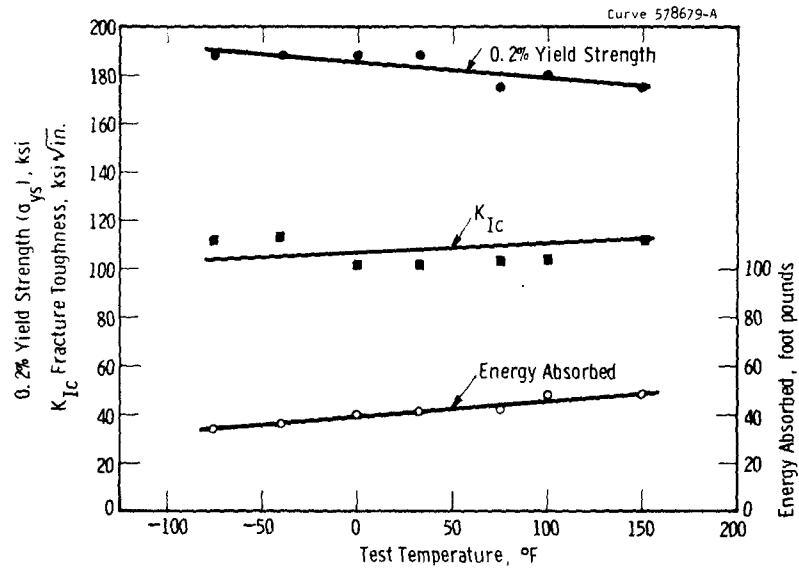
The results of the temperature dependence investigation of HP-9-4-25 alloy steel are presented in Table VI. The tensile data, Charpy impact data, and toughness at various test temperatures along with the other pertinent test parameters are tabulated in Tables VI -A, -B, and -C, respectively. These data were determined in the transverse test direction. The effects of test temperature upon the 0.2% yield strength and Charpy impact energy and the corresponding fracture toughness is illustrated in Figure 13.

TI-6Al-4V Titanium

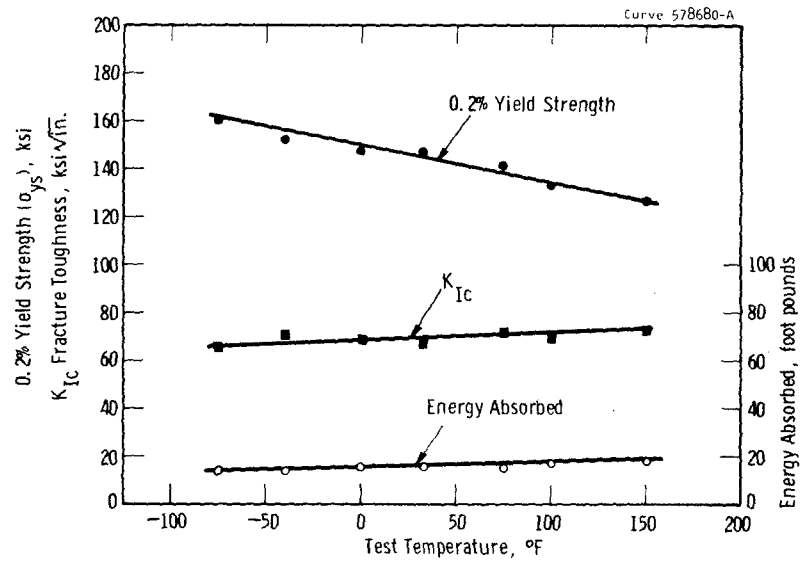
The individual test results generated during the temperature dependence investigation are presented in Table VII. The pertinent tensile data, Charpy impact data and fracture toughness characteristics are presented in Tables VII -A, -B, and -C, respectively. These data were developed in the transverse test direction. Figure 14 presents the effect of test temperature upon the K_{Ic} , Charpy impact energy, and the 0.2% yield strength for titanium alloy Ti-6Al-4V.

7079-T6 Aluminum

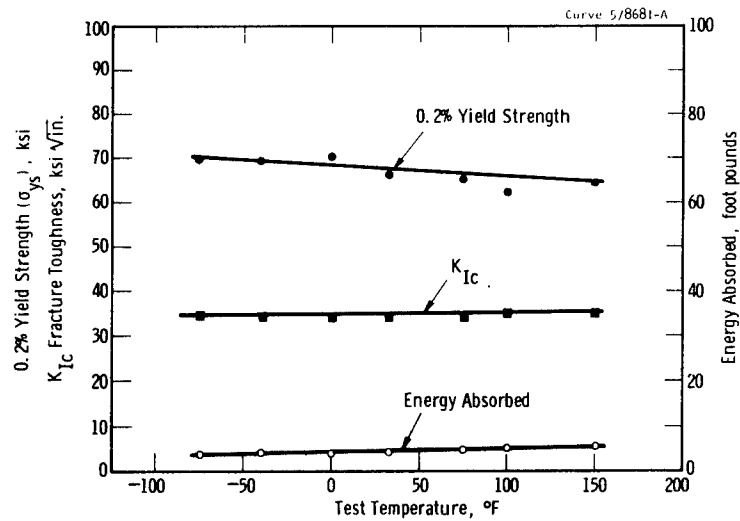
Table VIII presents the results of the temperature dependence of the strength parameters for 7079-T6 aluminum determined in the longitudinal test direction. The tensile data, Charpy impact data, and toughness at various test temperatures are tabulated in Tables VIII -A, -B, and -C. Figure 15 illustrates the temperature dependence of the 0.2% yield strength and Charpy "V" notch impact energy along with the corresponding toughness.



Sec. 7.2 Fig. 13—Temperature dependence of 0.2% yield strength, Charpy impact energy, and K_{Ic} for HP-9-4-25 steel



Sec. 7.2 Fig. 14—Temperature dependence of 0.2% yield strength, Charpy impact energy, and K_{Ic} for Ti-6Al-4V titanium



Sec. 7.2 Fig. 15—Temperature dependence of 0.2% yield strength, Charpy impact energy, and K_{Ic} for 7079-T6 aluminum

The expressions and method used to determine the critical plane strain stress intensity factor for the "1T" and "2T" WOL type toughness specimens were identical to those used for the "2X" specimens with the exception of the numerical constant, C_3 , involved. Due to differences in the specimen geometry the compliance characteristics vary; as a result, each geometry requires a different numerical constant versus a_0/W curve. Figure 16 shows the numerical constant curve used to determine the K_{Ic} for the "T" type WOL specimen geometry.

The nominal stress reported in the tabulated data was determined using the following equation:

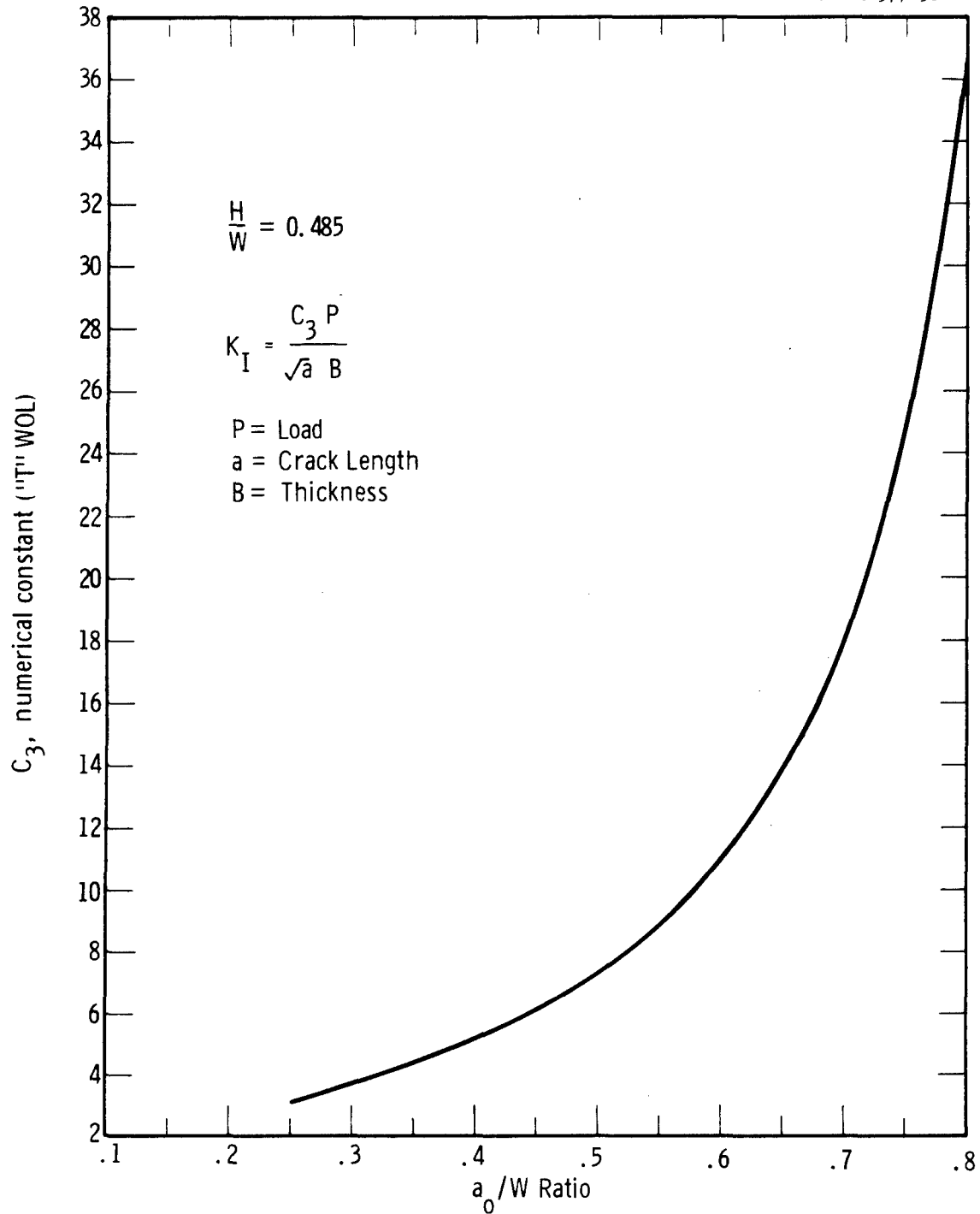
$$\sigma_N = \frac{P}{Bh} \left[\frac{6(a_0 + h/2)}{h} + 1 \right] = \text{nominal stress}$$

where: P = load (pounds) at fracture instability

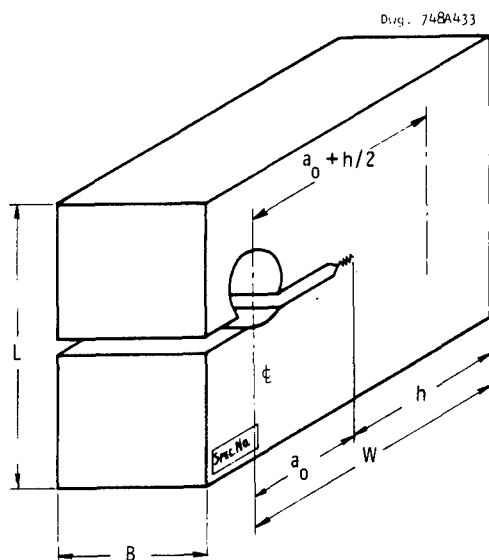
B = specimen thickness

h = ligament length (inches)

a_0 = initial crack length (inches)



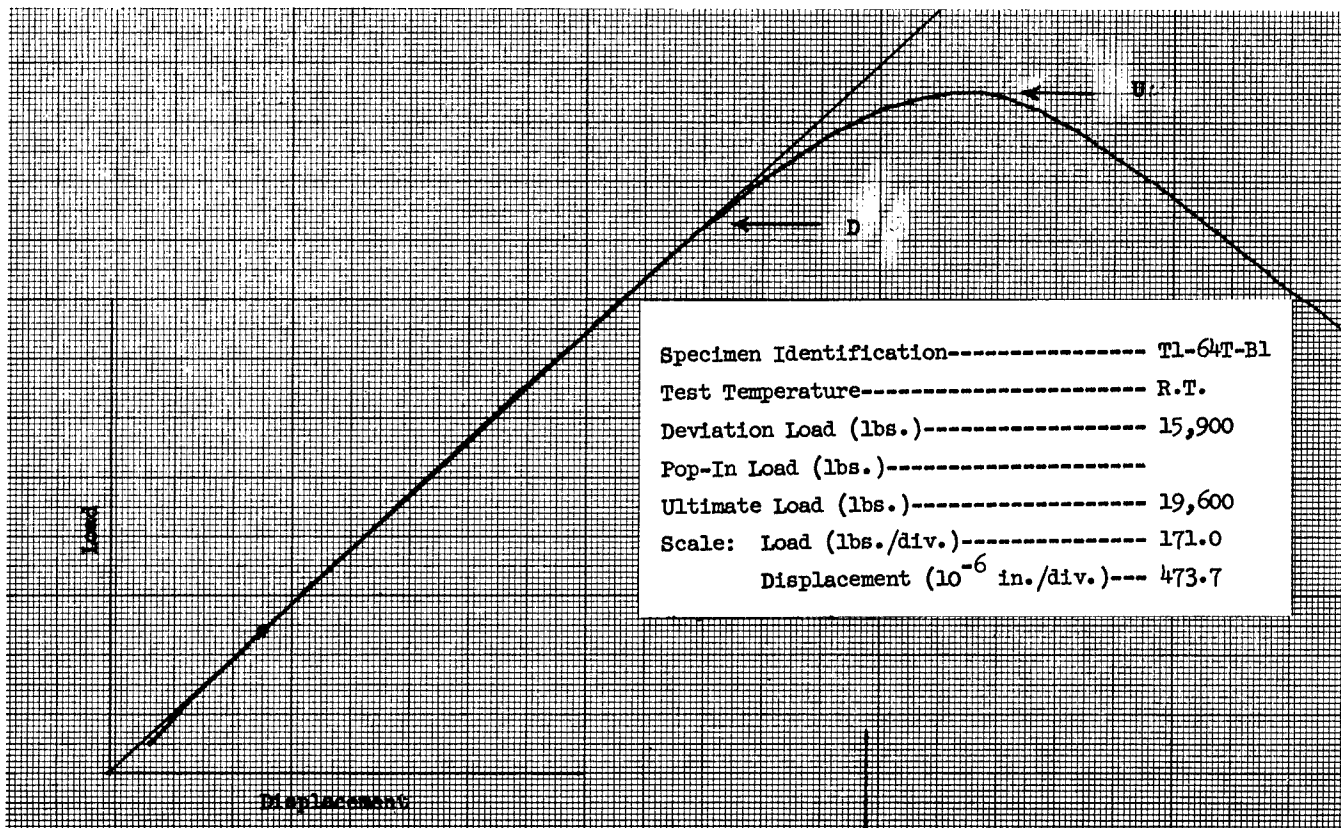
Sec. 7.2 Fig. 16-Numerical constant " C_3 " as a function of the a_0/W ratio for the "T" type WOL toughness specimen



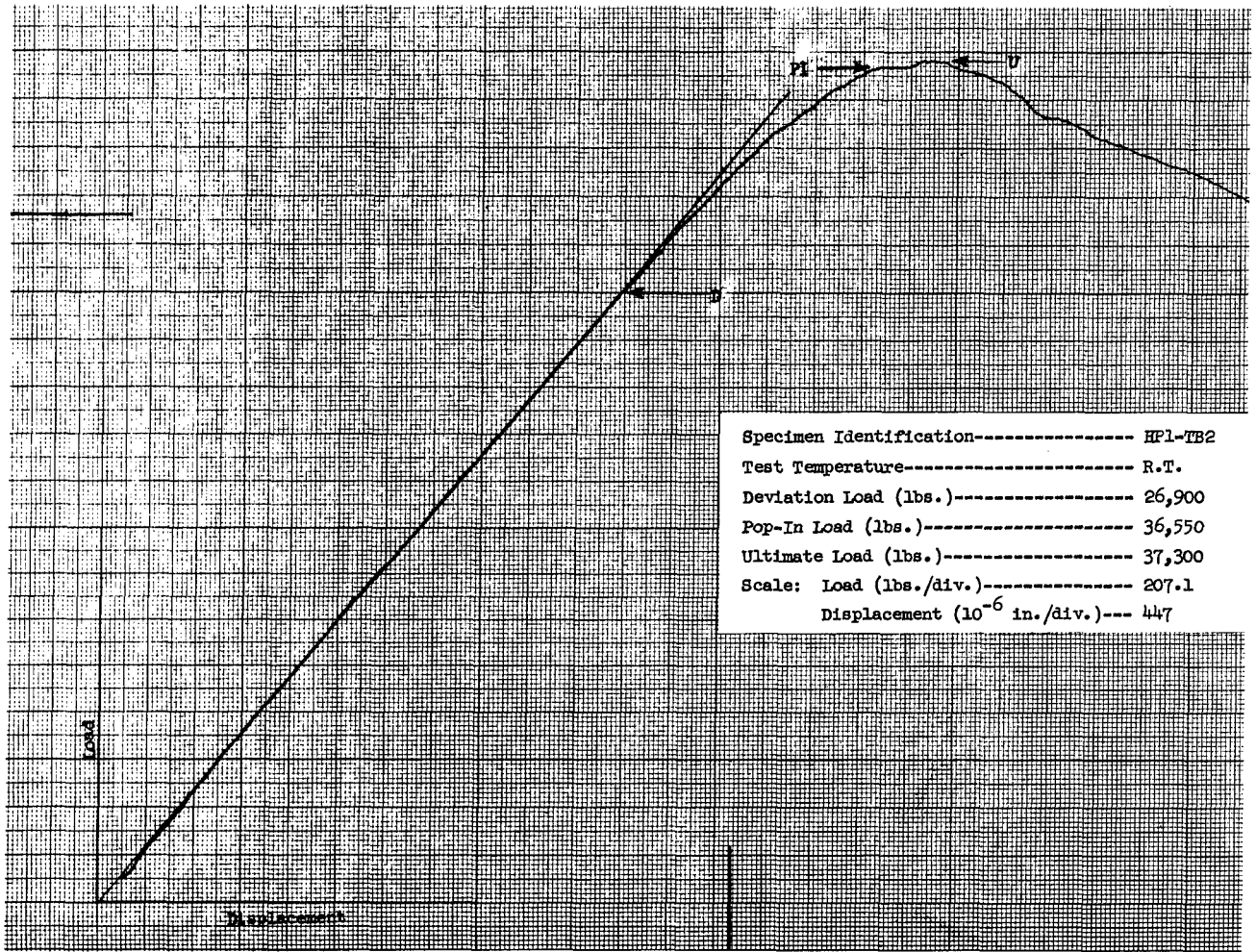
Sec. 7.2 Fig. 17 -Dimension designations for the "T" type WOL toughness specimen

Figure 17 illustrates the WOL specimen dimensions and corresponding designations involved in the calculations.

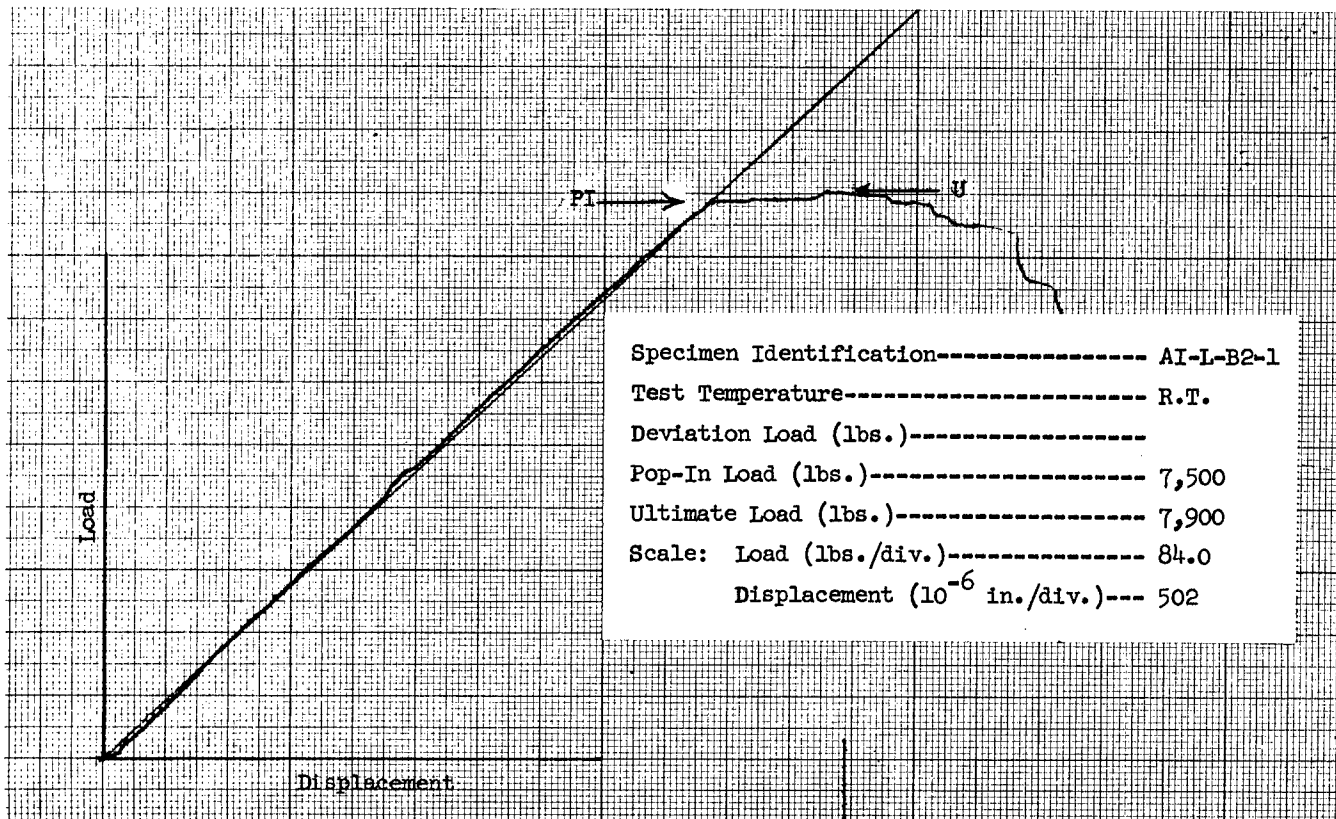
Examination of the load-displacement curves associated with the fracture toughness testing portion of the temperature dependence investigation indicated that deviation from linearity occurred prior to "pop-in" or rapid failure for all tests conducted on the steel and titanium alloys. Ultrasonic examinations of the crack behavior during loading indicated that the point of deviation on the load-displacement curves corresponded to slow crack extension; however, the extent of crack growth could not be accurately measured due to the texture of the cleavage surface (Appendix II). Figures 18 and 19 illustrate typical load-displacement curves encountered during the toughness testing of the steel and titanium alloys. Figure 18 indicates deviation prior to rapid failure and Figure 19 illustrates deviation prior to "pop-in". The load-displacement curves associated with the toughness testing of the aluminum alloy (7079-T6) all exhibited distinct "pop-in"; however, in some cases deviation was encountered prior to "pop-in", resulting in a curve similar to Figure 19. Figure 20 shows a typical load-displacement curve recorded for 7079-T6



Sec. 7.2 Fig. 18 -Typical load displacement curve indicating deviation prior to rapid failure



Sec. 7.2 Fig. 19 Typical load displacement curve indicating deviation prior to "Pop-In"



Sec. 7.2 Fig. 20 -Load displacement curve indicating "Pop-In" prior to deviation (Aluminum 7079-T6)

aluminum in which no deviation occurred prior to "pop-in". In those cases where deviation did occur the ultrasonic instrumentation indicated that it was due to slow crack growth. Ultrasonic measurement of the extent of the slow growth in the aluminum specimens prior to "pop-in" indicated that the maximum amount of crack extension did not exceed 0.015 inches; therefore, no correction for crack extension was necessary since a change in the crack length of 0.015 inches had little effect upon the calculated K_{Ic} value at the a_o/W ratio involved. ($a_o/W = 0.389$ versus 0.395.)

In order to establish the significance of the slow crack growth encountered during the testing of the steel and titanium alloys several "2T" type WOL specimens were loaded under direct tension until evidence of crack extension was indicated by the displacement and ultrasonic instrumentation. The load was then held constant. Crack propagation in the titanium alloy continued until failure occurred; the time involved was a matter of seconds. The crack in the steel specimen did not continue to grow to the critical crack length, but instead grew an undetermined amount and stopped. These test results were indicative of the crack behavior under continuous loading. The steel (HP-9-4-25) was more subject to "pop-in" behavior than the titanium.

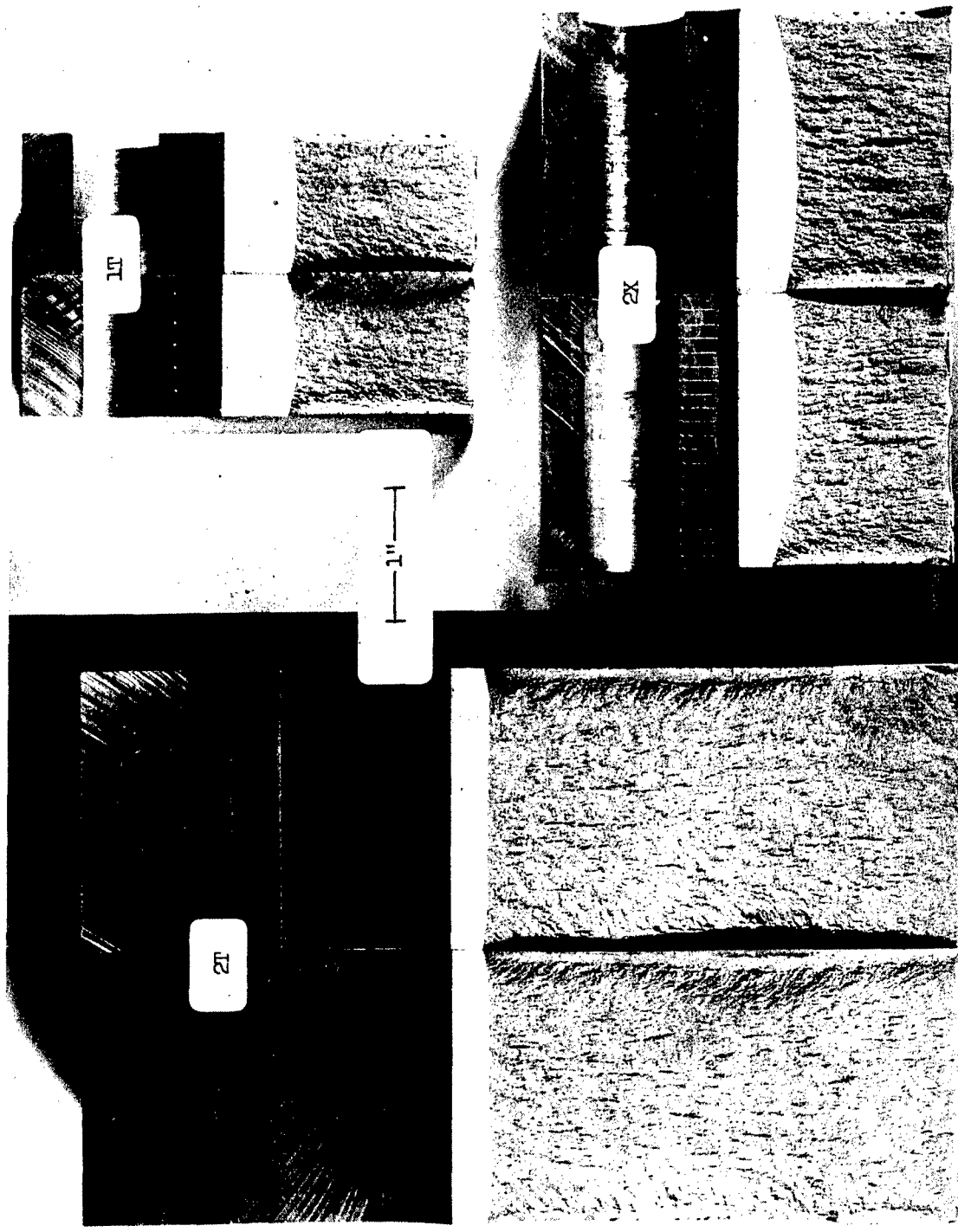
As defined, the critical stress intensity factor, K_{Ic} , describes the stress intensity at the tip of a crack at fracture instability. This definition presents a problem as to what crack growth rate corresponds to fracture instability. The constant load-crack growth experiments indicate that an existing crack can grow to critical size at a constant load in one cycle. The crack growth rate involved is not equivalent to that at catastrophic failure; however, the rates are such that no structure can be used at those stresses since the "slow crack growth" is quite rapid. Slow crack growth is a relative term and the amount of time necessary for an existing crack to grow to the critical size at a given applied load can vary considerably, depending upon the material and test parameters. Therefore, the actual value of the K_{Ic} , described as the stress intensity at catastrophic failure, may be an unrealistic design criterion unless the crack growth behavior of the material is well established.

In view of the above considerations, the determination of the critical stress intensity factor for the purpose of this investigation was based upon the crack length and load at the point of crack extension (deviation on the load displacement curve). Although the stress intensity determined in this manner may not correspond to the actual K_{Ic} , it does provide a realistic design criterion.

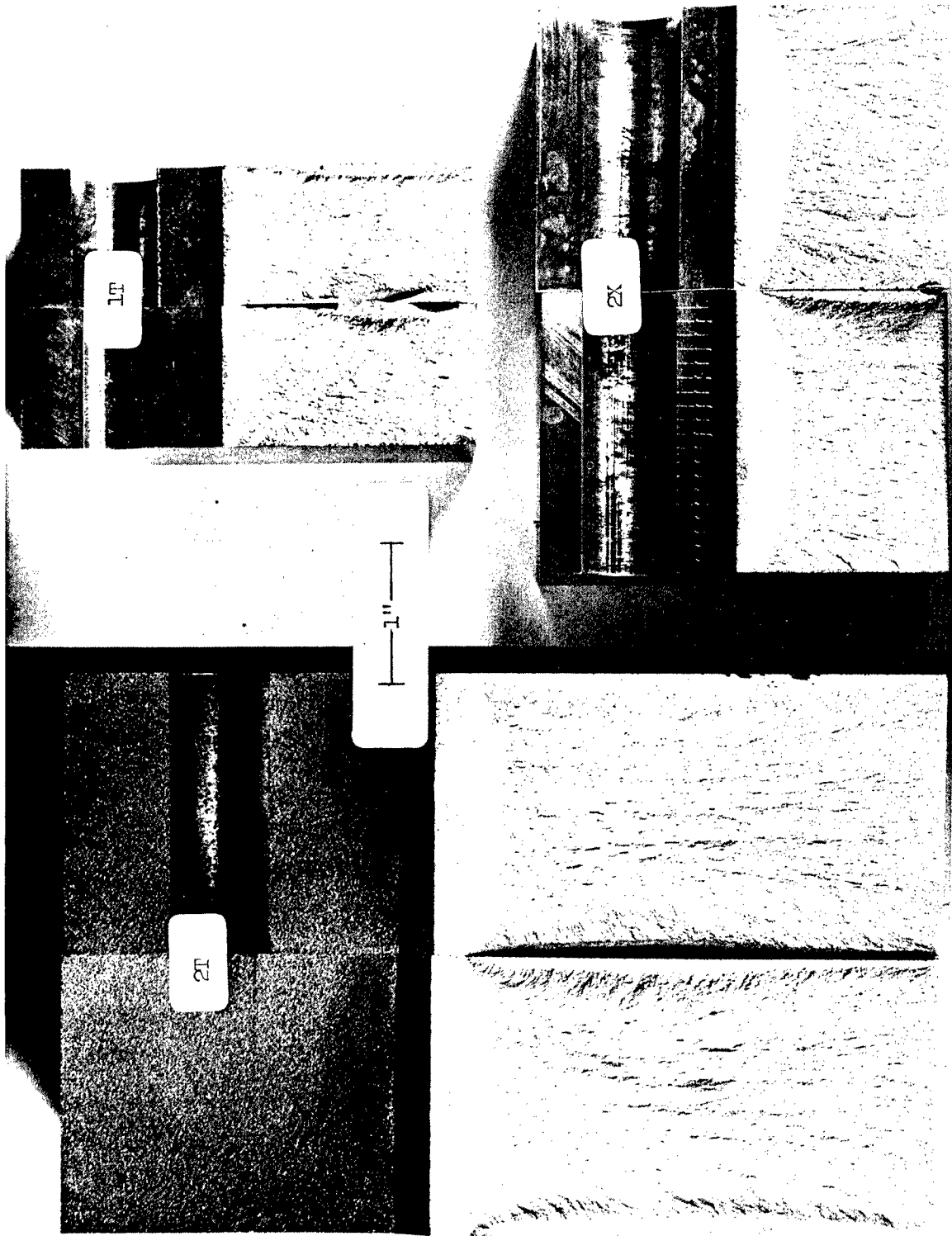
The crack length involved in the stress intensity calculations was taken as the precrack (fatigue crack) length readily determined by measuring the extent of the fatigue crack on fractured specimens. Figures 21, 22, and 23 show the room temperature fracture appearance of the WOL toughness specimens prepared from HP-9-4-25 steel, Ti-6Al,4V titanium, and 7079-T6 aluminum, respectively. Note the ease with which the precrack can be distinguished from the cleavage fracture. In those cases where the precracking operation produced a concave crack front, the crack length was measured at the center of the specimen.

Examination of the results of the temperature dependence investigation indicates relatively little effect of test temperature (-75° to 150°F) upon the strength parameters for those alloys investigated. Test temperature appears to have the most effect upon the toughness and tensile properties of the steel and titanium alloys (Figures 13 and 14) and the least effect upon the aluminum alloy (Figure 15). This behavior is to be expected, since metals which exhibit a body-centered lattice structure (steel) and some which exhibit the hexagonal-close-packed structure (alpha titanium) exhibit a marked increase in their resistance to plastic deformation with decreasing temperature.⁽⁶⁾ This behavior is much less pronounced in face-centered-cubic metals (aluminum), and as a result the effect of test temperature upon the measured strength parameters is less pronounced. Temperature appears to have the most effect upon the toughness and tensile properties of the titanium alloy (Ti-6Al-4V) as compared to the steel and aluminum.

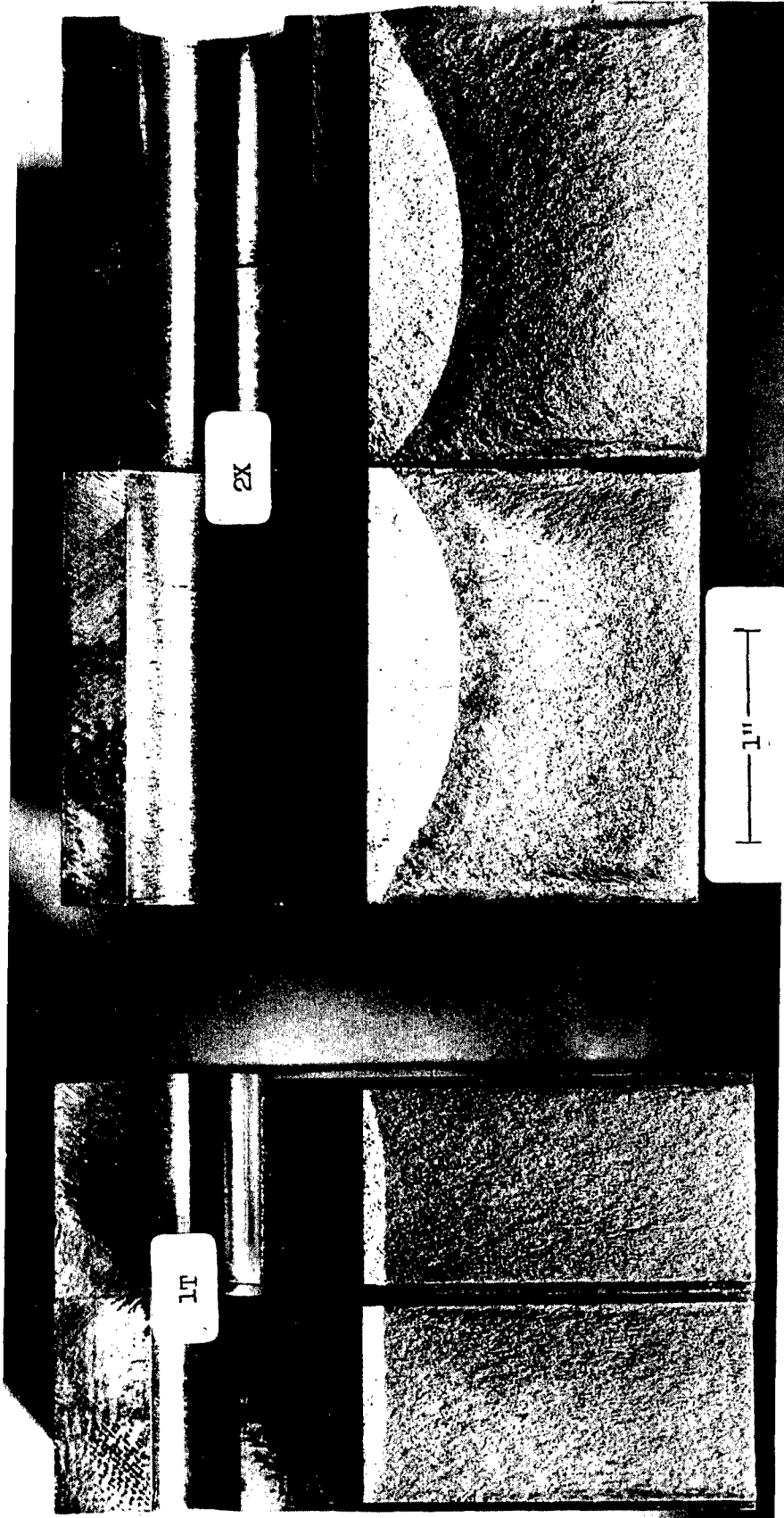
The variation in K_{Ic} with yield strength (at various temperature) for each alloy system investigated illustrates the inverse relationship generally expected to exist. As the yield strength of a given material increases, one can expect a corresponding decrease in the measured



Sec. 7.2 Figure 21 Room Temperature Fracture Appearance of
HP-9-4-25 Steel WOL Toughness Specimens



Sec. 7.2 Figure 22 Room Temperature Fracture Appearance of
Ti-6Al-4V Titanium WOL Toughness Specimens



Sec. 7.2 Figure 23 Room Temperature Fracture Appearance of
7079-T6 Aluminum WOL Toughness Specimens

toughness since the controlling stress-relieving mechanism at the tip of an existing crack approaches new surface formation (cracking) rather than plastic yielding as the yield strength increases.

The relationship between the Charpy impact energy and the K_{Ic} at various test temperatures as illustrated in Figures 13, 14, and 15 provides the most favorable correlation between toughness and those strength parameters measured during this investigation. As expected, the K_{Ic} and Charpy impact energy exhibit a regular trend since the material property -- fracture resistance -- is common to both types of test.

Comparison of the critical stress intensity factors determined for the steel and titanium alloys using the "1T" and "2T" type WOL specimens and for the aluminum alloy using "2X" and "1T" specimens illustrates the consistency and reproducibility of the test results with variations in specimen size and geometry. The consistency of the test results at the various test temperatures is evidence that the stress intensity was determined under plane strain conditions. The plane strain critical stress intensity factor K_{Ic} , is a materials property which does not vary with specimen size or geometry provided the specimen is of sufficient size to ensure plane strain conditions. As indicated earlier, the "2X" type WOL toughness specimen could not be used to determine the K_{Ic} for the steel and titanium alloys since it does not provide adequate plane strain conditions; as a result, the measured stress intensity is higher than that obtained on specimens with greater measurement capacity.

7.2.5 SUMMARY

The major strength parameters of three high-strength forging alloy systems (HP-9-4-25 steel, Ti-6Al-4V titanium, and 7079-T6 aluminum) were determined over a temperature range of -75° to 150° F in order to establish the applicability of these alloys for future military vehicle construction. The strength parameters investigated included the tensile properties, the Charpy "V" notch properties, and the plane strain

fracture toughness. Due to the limited amount of toughness data presently available for these alloys, adequate evaluation of the toughness characteristics was of primary concern.

All of the toughness testing was conducted with Wedge-Opening-Loading (WOL) type toughness specimens of various sizes. The K_{Ic} was determined at that load and crack length corresponding to fracture instability as indicated by load-deflection and ultrasonic instrumentation. A considerable amount of continuous slow crack growth was encountered prior to "pop-in" or catastrophic failure in the steel and titanium alloys. Further investigation indicated that this crack growth constituted fracture instability since once initiated, the crack continued to grow at a constant load.

Test temperature (-75° to 150° F) was found to have relatively little effect upon the measured strength parameters. The toughness values exhibited the least temperature dependence.

Section 7.2 References

1. W. K. Wilson, "Optimization of WOL Brittle Fracture Test Specimen," Westinghouse Research Report 66-1B4-BTLFR-R1, January 1966.
2. E. T. Wessel and W. H. Pryle, "Investigation of the Applicability of the Biaxial Brittle Fracture Test for Determining Fracture Toughness," AEC Research and Development Report WERL-8844-11, August 1965.
3. M. M. Leven, "Stress Distribution in the M4 Biaxial Fracture Specimen," Westinghouse Research Report 65-1D7-STRSS-R1, March 1965.
4. W. K. Wilson, "Analytic Determination of Stress Intensity Factors for the Manjoine Brittle Fracture Test Specimen," AEC Research and Development Report WERL-0029-3, August 1965.
5. A. J. Bush and W. K. Wilson, "Determination of Energy Release Rate for Biaxial Brittle Fracture Specimen," AEC Research and Development WERL-8844-2, August 1965.
6. J. J. Gilman, "Dislocation Motions and the Yield Strength of Solids," Properties of Crystalline Solids, ASTM STP 283, 1960, p. 69.

Section 7.2 - Table VI-A Transverse Tensile Properties of HP-9-4-25 Steel

Spec. No.	Test Temp. Of	Proportional Limit		Strength (PSI)		Ultimate Tensile Stress	Unif. Elong. %	Total Elong. %	Reduction in Area %
		0.01%	0.2% Yield	0.5% Yield					
HP3T-T6	200	154200	171300	178300	186400	327500	4.9	18.0	64.1
HP3T-T4	150	158200	173000	180700	188700	326000	4.6	18.4	63.1
HP3T-T5	150	162200	176200	183500	190300	329000	4.9	18.6	64.1
HP3T-T2	100	161300	180000	185700	192300	328000	5.1	18.5	63.5
HP3T-T3	100	164300	180300	186500	193200	333500	4.8	18.5	64.1
HP1T-T4	75	169000	177000	179700	184600	307500	5.2	18.9	61.8
HP1T-T5	75	163000	175700	179500	184600	317200	5.4	19.4	64.1
HP1T-T6	75	162300	173500	178400	183700	314200	5.4	19.3	64.1
HP2T-T4	32	172300	186200	190300	195200	339000	4.7	18.9	64.5
HP3T-T1	32	171000	188000	192800	198000	337000	5.0	18.4	63.1
HP2T-T2	0	172200	186700	191500	196400	331000	5.1	18.4	61.7
HP2T-T3	0	172400	186700	191500	196800	341000	4.9	18.5	64.1
HP1T-T9	-40	169200	184300	189200	194300	331000	5.6	18.1	62.1
HP2T-T1	-40	176300	191500	195000	199700	345000	4.8	18.3	63.5
HP1T-T7	-75	168300	186700	190300	195600	324500	5.7	17.9	60.1
HP1T-T8	-75	172300	186700	190700	196000	330000	5.3	17.9	61.8

Section 7.2 - Table VI-B Transverse Charpy "V" Notch Properties of HP-9-4-25 Steel

Specimen No.	Test Temp. °F	Energy Absorbed Foot Pounds	Brittle Fracture Percent	Lateral Expansion Inches
HP2-C7	150	47.0	0	0.022
HP2-C6	100	46.5	0	0.022
HP2-C8	100	46.0	0	0.023
HP2-C1	75	45.5	0	0.020
HP3-C5	75	40.5	0	0.016
HP2-C5	32	43.0	0	0.020
HP3-C1	32	38.5	0	0.017
HP2-C4	0	39.0	0	0.018
HP3-C2	0	38.0	5	0.016
HP2-C3	-40	38.0	10	0.016
HP3-C3	-40	34.0	20	0.015
HP2-C2	-75	37.0	35	0.013
HP3-C4	-75	31.5	55	0.010

Section 7.2 - Table VI-C Transverse Toughness Properties of HP-9-4-25 Steel

Spec. No.	Test Temp. °F	0.2% Yield Strength σ_{ys} (Ksi)	Specimen Type	Initial Crack Length a_0 (in)	Plastic Zone Size r_{Iy} (in)	Nominal Stress σ_N (Ksi)	σ_N/σ_{ys}	K_{Ic} $\frac{Ksi\sqrt{in}}{(1)}$	Comments (2)
HP3T-B27	150	174.6	1TWOL	1.019	0.026	119.4	.68	119.2	Fracture
HP2T-B28	150	174.6	2TWOL	1.834	0.021	74.5	.43	110.7	Pop In
HP2T-B34	150	174.6	2TWOL	1.824	0.019	70.8	.41	105.7	Pop In
HP3T-B26	100	180.1	1TWOL	1.001	0.020	110.8	.62	110.7	Fracture
HP3T-B8	100	180.1	2TWOL	1.853	0.017	70.8	.39	104.0	Pop In
HP2T-B33	100	180.1	2TWOL	1.855	0.017	68.1	.38	100.7	Fracture
HP3T-B15	75	175.4	1TWOL	0.964	0.019	104.2	.59	107.0	Pop In
HP3T-B17	75	175.4	1TWOL	1.281	0.021	136.0	.78	114.4	Fracture
HP3T-B4	75	175.4	2TWOL	1.808	0.017	68.3	.39	102.3	Fracture
HP3T-B5	75	175.4	2TWOL	1.822	0.015	64.3	.37	95.7	Fracture
HP1T-B1	75	175.4	2XWOL	1.093	0.031	164.5	.94	145.3*	Fracture
HP1T-B2	75	175.4	2XWOL	1.104	0.027	155.5	.89	135.2*	Pop In
HP1T-B3	75	175.4	2XWOL	1.174	0.032	180.0	1.03	146.3*	Fracture
HP3T-B24	32	187.1	1TWOL	1.033	0.016	104.8	.56	102.8	Pop In
HP3T-B11	32	187.1	2TWOL	1.868	0.016	71.4	.38	104.5	Pop In
HP2T-B32	32	187.1	2TWOL	1.954	0.015	69.5	.37	99.4	Pop In

(1) K_{Ic} Determined at First Indication of Unstable Crack Extension

(2) Crack Behavior

* Apparent K_{Ic}

Section 7.2 - Table VI-C Transverse Toughness Properties of HP-9-4-25 Steel (cont.)

Spec. No.	Test Temp. Of	0.2% Yield Strength σ_{ys} (Ksi)	Specimen Type	Initial Crack Length a_0 (in)	Plastic Zone Size r_{ly} (in)	Nominal Stress σ_N (Ksi)	σ_N/σ_{ys}	K_{Ic} Ksi \sqrt{in} (1)	Comments (2)
HP3T-B23	0	186.8	1TWOL	0.981	0.016	102.5	.55	103.0	Pop In
HP3T-B10	0	186.8	2TWOL	1.837	0.017	72.3	.39	107.3	Pop In
HP2T-B31	0	186.8	2TWOL	1.879	0.017	72.1	.39	105.2	Pop In
HP3T-B18	-40	187.9	1TWOL	1.047	0.020	120.8	.64	117.6	Pop In
HP2T-B30	-40	187.9	2TWOL	1.863	0.019	76.0	.40	112.2	Pop In
HP3T-B7	-40	187.9	2TWOL	1.886	0.018	75.0	.40	109.8	Pop In
HP3T-B12	-75	186.7	1TWOL	0.930	0.017	101.3	.54	105.8	Pop In
HP3T-B6	-75	186.7	2TWOL	1.864	0.017	72.5	.39	107.0	Pop In
HP2T-B29	-75	186.7	2TWOL	1.834	0.022	82.8	.44	123.0	Pop In

(1) K_{Ic} Determined at First Indication of Unstable Crack Extension

(2) Crack Behavior

Section 7.2 - Table VII-A Transverse Tensile Properties of Ti-6Al-4V Titanium

Spec. No.	Test Temp. Of	P. L.		Strength (PSI)		Ultimate Tensile	Fracture Stress	Unif. Elong. %	Total Elong. %	Reduction in Area %
		0.01%	0.2%	0.5% Yield	Yield					
278T-T5	150	111400	124400	128200	134800	182300	4.5	12.7	38.8	
278T-T6	150	112800	128200	131400	139600	183400	7.1	14.6	36.1	
278T-T7	150	117700	127700	130700	137800	181300	6.4	14.4	35.0	
278T-T8	100	118000	132600	135800	141200	186500	4.9	12.1	35.3	
278T-T9	100	120200	132200	135000	141400	187500	5.6	12.8	34.7	
278T-T10	100	120600	133400	136200	141400	181800	5.1	12.7	31.0	
278T-T11	75	130000	140000	142600	147800	187800	3.4	11.5	31.2	
278T-T12	75	128200	136600	140200	144600	192700	4.1	12.2	36.1	
278T-T13	75	132200	144600	147600	152200	200100	4.1	12.7	37.0	
278T-T14	32	134200	147000	150200	154200	196700	3.3	11.7	33.8	
278T-T15	32	138200	148200	151400	156200	194700	2.4	9.4	29.7	
278T-T16	32	136200	147200	151000	155000	193200	2.5	8.8	29.2	
278T-T17	0	134800	146400	150200	154600	186500	3.5	10.7	25.8	
278T-T18	0	136200	146600	150400	155000	187500	3.9	10.3	24.3	
278T-T19	0	138200	147400	151000	155800	186000	3.7	10.5	23.8	
278T-T20	-40	142600	155400	159400	163600	199600	3.1	10.4	25.3	
278T-T21	-40	142000	152600	156600	160200	204300	2.4	7.5	28.8	
278T-T22	-40	138400	150200	154200	158200	196000	3.2	9.8	28.2	
278T-T23	-75	148200	160600	164200	167400	209500	2.1	8.0	28.2	
278T-T24	-75	150200	159200	162400	164800	212500	1.9	7.7	30.1	
278T-T25	-75	150200	157400	161000	164000	204000	2.2	9.0	28.2	

Section 7.2 - Table VII-B Transverse Charpy "V" Notch Properties of Ti-6Al-4V Titanium

Specimen No.	Test Temp.	Energy Absorbed Foot Pounds	Brittle Fracture Percent	Lateral Expansion Inches
278T-C3	150	17.5	----	0.009
278T-C2	100	16.0	----	0.007
278T-C1	75	15.0	----	0.006
278T-C4	32	15.0	----	0.004
278T-C5	0	15.0	----	0.007
278T-C6	-40	14.0	----	0.003
278T-C7	-75	14.0	----	0.003

Section 7.2 - Table VII-C Transverse Toughness Properties of Ti-6AL-4V Titanium

Spec. No.	Test Temp. °F	0.2% Yield Strength σ _y (Ksi)	Specimen Type	Initial Crack Length a _o (in)	Plastic Zone Size r _{Iy} (in)	Nominal Stress σN (Ksi)	σN/σ _y	K _{Ic}	
								Ksi	√in ⁽¹⁾
									Comments (2)
278T-B19	150	126.8	1TWOL	0.970	0.012	61.1	.48	63.4	Fracture
278T-B24	150	126.8	2TWOL	2.033	0.021	57.6	.45	82.0	Fracture
278T-B25	150	126.8	2TWOL	1.970	0.016	50.8	.40	74.0	Fracture
278T-B18	100	132.7	1TWOL	0.944	0.011	59.7	.45	63.2	Pop In
278T-B22	100	132.7	2TWOL	2.049	0.013	48.4	.36	69.3	Fracture
278T-B23	100	132.7	2TWOL	1.969	0.014	49.8	.38	72.9	Fracture
278T-B12	75	140.4	1TWOL	0.904	0.008	53.9	.38	58.4	Fracture
278T-B13	75	140.4	1TWOL	0.958	0.009	57.5	.41	60.9	Fracture
278T-B4	75	140.4	2TWOL	2.019	0.015	54.7	.39	76.6	Fracture
278T-B5	75	140.4	2TWOL	2.010	0.014	52.1	.37	76.3	Fracture
278T-B27	75	140.4	2TWOL	1.986	0.017	58.3	.42	84.9	Fracture
Ti64T-B1	75	140.4	2XWOL	1.141	0.012	87.5	.62	75.2*	Fracture
Ti64T-B2	75	140.4	2XWOL	1.151	0.013	94.0	.67	77.9*	Fracture
Ti64T-B3	75	140.4	2XWOL	1.180	0.014	100.0	.71	79.7*	Fracture
278T-B17	32	147.5	1TWOL	0.920	0.010	63.8	.43	68.3*	Fracture
278T-B20	32	147.5	2TWOL	2.041	0.009	45.3	.30	64.4	Fracture
278T-B21	32	147.5	2TWOL	2.011	0.009	45.7	.31	65.5	Fracture

(1) K_{Ic} Determined at First Indication of Unstable Crack Extension

(2) Crack Behavior

* Apparent K_{Ic}

Section 7.2 - Table VII-C Transverse Toughness Properties of Ti-6AL-4V Titanium (cont.)

Spec. No.	Test Temp. °F	0.2% Yield Strength σ _y (Ksi)	Specimen Type	Initial Crack Length a ₀ (in)	Plastic Zone Size r _{1y} (in)	Nominal Stress σ _N (Ksi)	σ _N /σ _y	K _{Ic}	
								Ksi	√in(1) Comments (2)
278T-B16	0	146.8	1TWOL	0.950	0.010	61.2	.42	64.8	Fracture
278T-B10	0	146.8	2TWOL	2.081	0.012	51.5	.35	72.9	Fracture
278T-B11	0	146.8	2TWOL	1.998	0.010	45.9	.31	66.4	Fracture
278T-B15	-40	152.7	1TWOL	0.975	0.008	61.2	.40	63.2	Fracture
278T-B8	-40	152.7	2TWOL	2.088	0.013	54.6	.36	76.8	Fracture
278T-B9	-40	152.7	2TWOL	2.059	0.009	46.5	.30	66.2	Fracture
278T-B14	-75	159.1	1TWOL	0.965	0.007	59.1	.37	61.2	Pop In
278T-B6	-75	159.1	2TWOL	2.091	0.010	50.1	.31	70.0	Fracture
278T-B7	-75	159.1	2TWOL	1.998	0.009	46.1	.29	66.3	Fracture

(1) K_{Ic} Determined at First Indication of Unstable Crack Extension

(2) Crack Behavior

Section 7.2 - Table VIII-A Longitudinal Tensile Properties of 7079-T6 Aluminum

Spec. No.	Test Temp. °F	Proportional Limit 0.01%	Strength (PSI)		Fracture Stress	Unif. Elong. %	Total Elong. %	Reduction in Area %
			0.2% Yield	0.5% Yield				
ALL-T1	200	54200	61100	63400	71400	8.5	15.9	37.8
ALL-T14	150	55900	62100	64400	73300	9.0	14.8	28.8
ALL-T15	150	55900	63900	66400	74200	7.7	12.1	28.8
ALL-T12	100	54900	61500	64100	74400	8.9	12.3	24.0
ALL-T13	100	55700	62600	65100	74300	9.3	13.0	26.4
ALL-T2	75	58399	65400	67700	76900	8.1	11.8	27.1
ALL-T3	75	59300	65500	67700	76900	8.8	12.2	26.8
ALL-T10	32	61900	70500	72600	80700	7.7	8.4	17.0
ALL-T11	32	55300	60800	62900	73400	8.8	11.4	22.7
ALL-T8	0	61900	69000	70800	79200	7.4	9.5	22.0
ALL-T9	0	61900	69400	71400	79500	7.1	8.6	20.6
ALL-T6	-40	62200	67400	69600	78000	7.6	9.3	21.6
ALL-T7	-40	61400	69400	70450	78900	7.8	9.8	22.0
ALL-T4	-75	61900	68600	70800	79100	9.3	11.7	20.6
ALL-T5	-75	61900	68600	71200	78700	7.9		21.6

Section 7.2 - Table VIII-B Longitudinal Charpy "V" Notch Properties of 7079-T6 Aluminum

Specimen No.	Test Temp. °F	Energy Absorbed Foot Pounds	Brittle Fracture Percent	Lateral Expansion Inches
Al C7	150	5.0	---	0.007
Al C8	150	4.5	---	0.006
Al C6	100	4.5	---	0.004
Al C9	100	5.0	---	0.006
Al C1	75	4.5	---	0.005
Al C14	75	4.5	---	0.004
Al C5	32	3.5	---	0.004
Al C10	32	4.0	---	0.004
Al C4	0	4.0	---	0.003
Al C11	0	4.0	---	0.004
Al C3	-40	4.0	---	0.003
Al C12	-40	4.0	---	0.004
Al C2	-75	3.5	---	0.003
Al C13	-75	3.5	---	0.002

Section 7.2 - Table VIII-C Longitudinal Toughness Properties of 7079-T6 Aluminum

Spec. No.	Test Temp. °F	0.2% Yield Strength σ _y (Ksi)	Specimen Type	Initial Crack Length, a ₀ (in)	Plastic Zone Size, r _{py} (in)	Nominal Stress σ _N (Ksi)	σ _N /σ _y	K _{Ic} Ksi√in	Comments
ALL-B9	150	63.0	1TWOL	0.978	0.016	34.9	.55	35.6	Pop In
ALL-B45	150	63.0	2XWOL	1.163	0.014	42.5	.67	34.9	Pop In
ALL-B46	150	63.0	2XWOL	1.179	0.015	44.6	.70	36.0	Pop In
ALL-B5	100	62.1	1TWOL	0.977	0.014	32.7	.52	33.4	Pop In
ALL-B42	100	62.1	2XWOL	1.249	0.012	44.0	.70	32.4	Pop In
ALL-B44	100	62.1	2XWOL	1.280	0.016	52.6	.84	37.1	Pop In
ALL-B7	75	65.0	1TWOL	0.958	0.010	28.9	.44	29.5	Pop In
ALL-B18	75	65.0	1TWOL	0.911	0.011	29.1	.44	30.4	Pop In
ALL-B18-1	75	65.0	1TWOL	0.966	0.014	33.6	.51	34.3	Fracture
ALL-B24	75	65.0	1TWOL	0.875	0.011	28.7	.44	30.7	Fracture
ALL-B28	75	65.0	1TWOL	1.107	0.011	32.8	.50	32.8	Pop In
ALL-B29	75	65.0	1TWOL	0.932	0.014	32.3	.49	33.5	Fracture
ALL-B30	75	65.0	1TWOL	1.080	0.014	36.2	.55	34.5	Pop In
ALL-B10-1	75	65.0	1TWOL	1.058	0.018	40.4	.62	38.5	Pop In
ALL-B1	75	65.0	2XWOL	1.205	0.010	39.3	.60	30.5	Pop In
ALL-B1-1	75	65.0	2XWOL	1.265	0.012	41.3	.63	32.5	Pop In
ALL-B2	75	65.0	2XWOL	1.148	0.009	34.0	.52	28.2	Pop In
ALL-B2-1	75	65.0	2XWOL	1.348	0.013	53.9	.83	33.9	Pop In
ALL-B47	75	65.0	2XWOL	1.169	0.012	40.9	.63	33.3	Pop In
ALL-B49	75	65.0	2XWOL	1.129	0.015	52.9	.81	36.7	Pop In

Section 7.2 - Table VIII-C Longitudinal Toughness Properties of 7079-T6 Aluminum (cont.)

Spec. No.	Test Temp. °F	0.2% Yield Strength σ_{ys} (Ksi)	Specimen Type	Initial Crack Length, a_0 (in)	Plastic Zone Size r_{Iy} (in)	Nominal Stress σ_N (Ksi)	σ_N/σ_{ys}	K_{Ic} Ksi \sqrt{in}	Comments
ALL-B10	32	65.7	1TWOL	0.918	0.012	30.4	.46	32.2	Pop In
ALL-B38	32	65.7	2XWOL	1.206	0.012	43.8	.67	33.9	Pop In
AL-B39	32	65.7	2XWOL	1.218	0.012	43.2	.66	33.7	Pop In
ALL-B11	0	69.2	1TWOL	1.017	0.013	35.2	.51	35.0	Pop In
ALL-B36	0	69.2	2XWOL	1.315	0.012	52.2	.75	34.7	Pop In
ALL-B37	0	69.2	2XWOL	1.229	0.009	41.4	.60	30.7	Pop In
ALL-B15	-40	68.5	1TWOL	0.896	0.009	27.2	.40	28.8	Pop In
ALL-B34	-40	68.5	2XWOL	1.280	0.012	41.9	.61	34.5	Pop In
ALL-B35	-40	68.5	2XWOL	1.276	0.009	43.7	.64	30.8	Pop In
ALL-B6	-75	68.6	1TWOL	0.881	0.012	30.2	.44	32.3	Pop In
ALL-B3	-75	68.6	2XWOL	1.260	0.008	39.4	.57	28.4	Pop In
ALL-B33	-75	68.6	2XWOL	1.251	0.015	53.4	.78	39.5	Pop In

TABLE OF CONTENTS

Section 7.3

GENERATION OF SLOW CRACK GROWTH DATA

	<u>Page</u>
7.3.1 Introduction	206
7.3.2 Material and Specimen Preparation	207
7.3.3 Test Procedure	207
7.3.4 Results and Discussion	209
7.3.5 Summary	217

LIST OF TABLES

Section 7.3

GENERATION OF SLOW CRACK GROWTH DATA

	<u>Page</u>
Table I Cyclic Loading Data	215

List of Figures

Figure 1 Equipment used to ultrasonically monitor crack growth	208
Figure 2 Crack growth rate as a function of stress intensity factor for HP-9-4-25 steel as determined on the "1T" WOL fracture toughness specimen	211
Figure 3 Crack growth rate as a function of stress intensity factor for 7079-T6 aluminum toughness specimen	211
Figure 4 Crack growth rate as a function of stress intensity for HP-9-4-25 steel (log-log plot) . . .	212
Figure 5 Crack growth rate as a function of stress intensity for 7079-T6 aluminum (log-log plot) . .	212
Figure 6 Combined cyclic flaw growth data for HP-9-4-25 steel plate	213
Figure 7 Combined cyclic flaw growth data for 7079-T6 aluminum plate	213

Section 7.3

GENERATION OF SLOW CRACK GROWTH DATA

7.3.1 INTRODUCTION

The relationship between the applied stress and flaw size necessary to cause catastrophic failure of a structural component is adequately expressed by the plane strain fracture toughness parameter K_{Ic} . This relationship provides a satisfactory design criterion which can be used to establish the critical flaw size for catastrophic failure; however, knowledge of the critical stress intensity does not indicate the useful life of the component. The component life is dependent upon the rate of growth of existing subcritical flaws to the critical size. Therefore, an understanding of the slow crack growth characteristics of the material under application conditions is essential to satisfactory design.

Fatigue (slow) crack propagation is a localized phenomenon dependent upon the temperature, environment and stress conditions at the crack front. The stress intensity factor "K" provides a desirable means of describing the stress conditions at the tip of an advancing crack; as a result, the crack growth is dependent upon the stress intensity at the crack tip. As the crack grown under constant cyclic loading the stress intensity, expressed as $K = f(\sigma, a)$, increases due to the increase in the applied stress σ and crack length a . Eventually the crack grows to a sufficient length such that the stress intensity K increases to a level equivalent to the material characteristic K_{Ic} , the plane strain critical stress intensity factor at fracture instability.

Consideration of the ratio of the initial stress intensity to the critical stress intensity, K_{Ii}/K_{Ic} for a given structure provides a technique for estimating how close conditions are to catastrophic

failure. Determination of the number of cycles to failure required for a specimen loaded to a specific K_{Ii}/K_{Ic} ratio provides a technique whereby the life of a component can be predicted. Conversely, knowing the desired life of the component and K_{Ic} of the material, the maximum allowable initial stress intensity, K_{Ii} can be determined. It is then possible to compute either the initial allowable flaw size for a given stress, or the allowable stress for some given initial size. As a result, consideration of slow crack growth behavior in terms of the stress intensity provides a powerful tool for studying and applying slow crack growth data.

In order to adequately evaluate the materials involved in this investigation for possible use under severe service conditions involving cyclic loading, it was desirable to develop additional insight into the relationship between material toughness and crack characteristics.

7.3.2 MATERIAL AND SPECIMEN PREPARATION

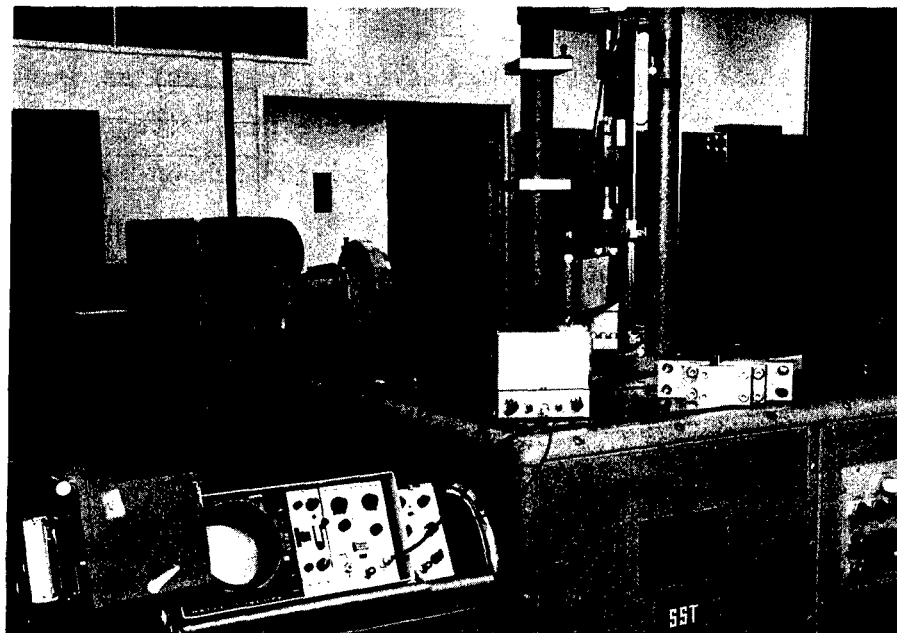
The determination of slow crack growth characteristics as related to fracture toughness parameters was limited to the investigation of the steel (HP-9-4-25) and aluminum (7079-T6) alloys. Wedge-opening-loading type "1T" fracture toughness specimens were prepared from the as-received 3 inch forged plate (Transverse Direction) as described earlier in Section 7.2.2. The specimens were side notched (45° included angle, 0.010" root radius) to a depth of 0.050 inch on each side prior to precracking in order to ensure crack propagation parallel to the specimen surface. Side notching was necessary to permit accurate ultrasonic measurement of crack extension.

7.3.3 TEST PROCEDURE

The side-notched "1T" WOL toughness specimens were subjected to sinusoidal cyclic loading and the associated crack propagation continuously measured and recorded. A constant-load type universal fatigue machine operating at 1800 cycles per minute was used for cyclic loading and all tests conducted at room temperature. An ultrasonic flaw

detection technique involving the use of a 10 MHz, 3/8"-diameter ceramic transducer was used to measure and record the extent of the fatigue crack propagation during cyclic loading. The ultrasonic instrumentation was calibrated to a sensitivity capable of detecting 0.005" of crack extension. A detailed description of the ultrasonic monitoring technique is given in Appendix II. Figure 1 shows the equipment used to ultrasonically monitor crack growth under cyclic loading conditions.

The toughness specimens were precracked in the same manner as those used for the conventional K_{Ic} tests with the exception that the extent of the precracking was accurately monitored using the ultrasonic equipment. Upon inducing a fatigue crack 0.150 inch long, cyclic loading was continued to a constant maximum load corresponding to a given initial stress intensity factor. Since the crack length was accurately known at all times it was possible to determine the maximum cyclic load necessary to produce the desired initial stress intensity at the crack tip. Table I shows the pertinent data associated with the cyclic loading of each specimen. Cyclic loading (0 to maximum load - 1800 cpm) was continued until failure and the associated crack extension continuously measured and recorded against the number of elapsed cycles. The crack growth rate was determined by dividing the change in crack length Δa by the



Sec. 7.3.3 Figure 1 - Equipment used to ultrasonically monitor crack growth

change in the number of elapsed cycles, ΔN at a convenient interval of crack growth. Continuous monitoring of the crack length made possible the determination of the stress intensity at any point between the initial and critical stress intensity as well as the corresponding crack growth rate.

7.3.4 RESULTS AND DISCUSSION

The relationship between the slow crack growth characteristics and the stress intensity factor for the steel (HP 9-4-25) and aluminum (7079-T6) alloys under investigation is illustrated in Figures 2 and 3 respectively. These data present the basic crack growth behavior under plane strain conditions and clearly illustrate the dependency of the crack growth rate on the stress conditions at the tip of the crack. As the stress intensity approaches the K_{IC} of the material, the crack growth rate increases accordingly, approaching a maximum at the K_{IC} .

The maximum cyclic load appears to have little effect upon the relationship between the K_{IC} and crack growth rate as indicated by the consistent data; however, the variations in maximum load involved in this investigation were relatively small and some effect may be encountered at higher loads.

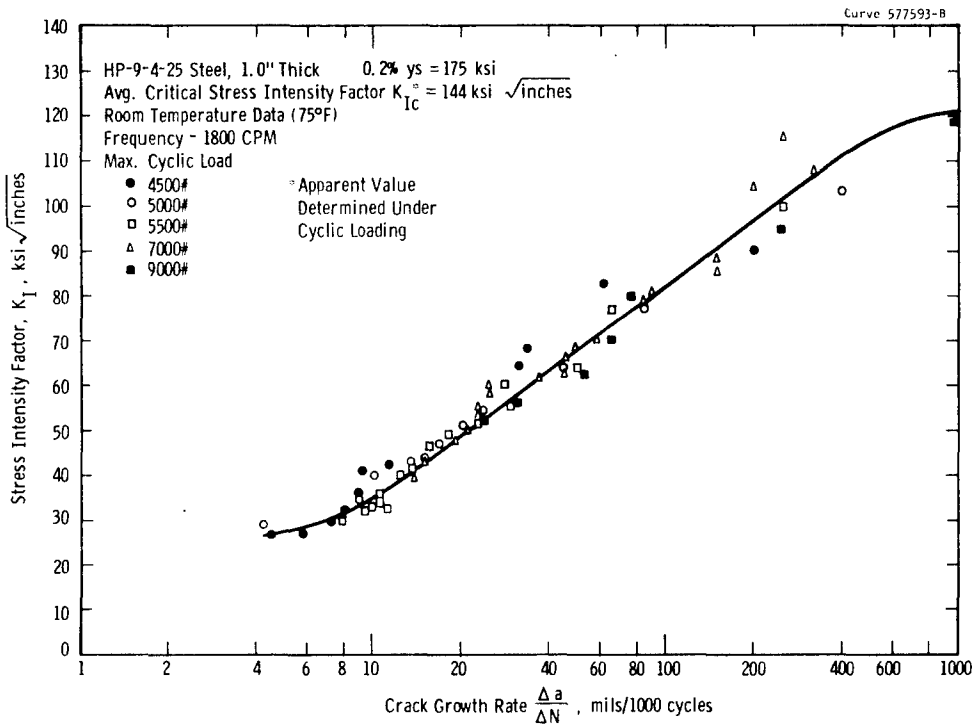
In order to more thoroughly evaluate the crack growth data presented in Figures 2 and 3, the data were replotted on a log-log basis and are shown in Figures 4 and 5, respectively. Presentation of the data in this form readily provides an evaluation of the crack propagation power law involved. The general form of the propagation law used to express cumulative damage under sinusoidal loading is given as⁽¹⁾

$$\frac{\Delta a}{\Delta N} = C \cdot (\Delta K)^n$$

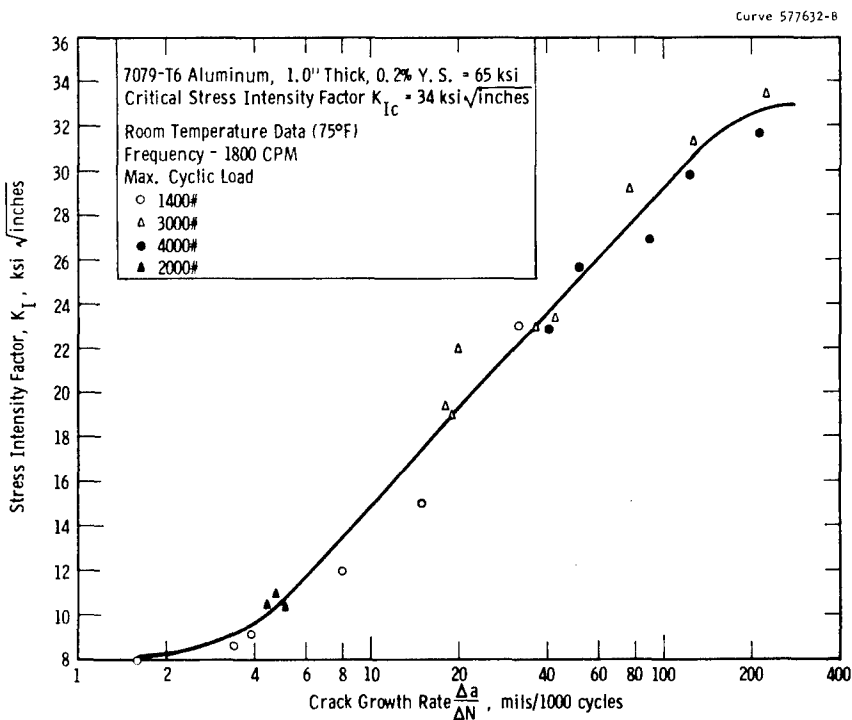
where $\Delta a / \Delta N$ is the crack growth rate, inch/cycle; C is a constant which depends upon the relative mean load, the material, and the frequency; and ΔK is the change in stress intensity during cyclic loading which for the purpose of this investigation is equivalent to K_I since the load

varied from zero to the maximum in one cycle. The exponent "n" readily describes the linear slope of the log-log plot of the test data and is the descriptive parameter of the propagation law. The straight lines drawn through the data points in Figures 4 and 5 correspond to $n = 3.0$ for the aluminum 7079-T6 and $n = 2.5$ for HP-9-4-25 steel. Crack propagation behavior under plane strain conditions expressed in terms of the power law is reported to yield a constant exponent.^(1,2) However, the reported value of the exponent varies among investigators; Paris⁽¹⁾ reports $n = 4$ and Liu⁽²⁾ reports $n = 2$. The results of this investigation yield intermediate values.

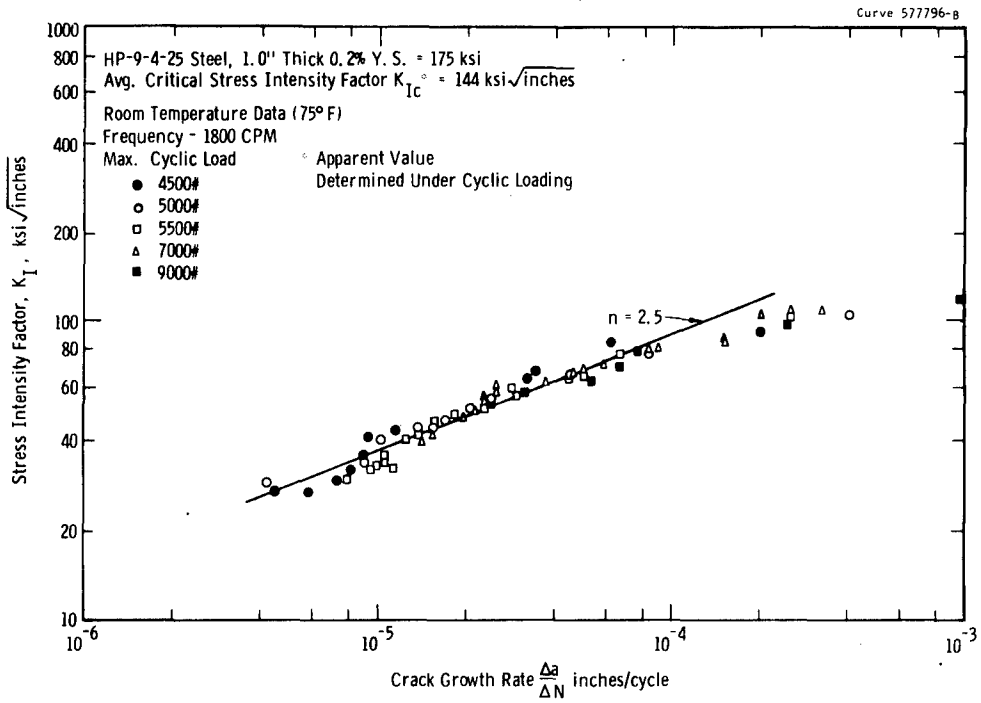
Although the data presented in Figures 2 and 3 illustrate the basic relationship between crack growth rate and stress intensity, these data do not provide a convenient method of predicting the service life under cyclic loading. As pointed out earlier, the number of cycles required for an existing flaw to grow to critical size at a constant loading rate can be expressed by the relationship between K_{Ii}/K_{Ic} and N , the number of cycles to failure. One method to develop this relationship would be to take a specimen containing a flaw of known size, subject this to a constant loading rate corresponding to a given initial K_{Ii} , continue the cyclic loading until failure, and recording the number of elapsed cycles. However, this technique would require testing several specimens at each stress intensity level in order to establish a reliable K_{Ii}/K_{Ic} vs. N relationship. A better method, and the one used here, is to automatically record the crack length and number of elapsed cycles during cyclic loading; this permits the determination of the stress intensity and associated number of elapsed cycles at any point during the test. Therefore, one specimen can be used to establish the K_{Ii}/K_{Ic} vs. N curve since the number of cycles to failure corresponding to the stress intensity at any point during the test is readily determined by subtracting the number of cycles required to propagate the crack to the given K_{Ii} level from the number of elapsed cycles at catastrophic failure. This technique was used to establish the K_{Ii}/K_{Ic} vs. N curves for the steel and aluminum alloys illustrated in Figures 6 and 7, respectively. Crack growth data presented in this form provide a usable technique for predicting the service life of a component under cyclic loading.



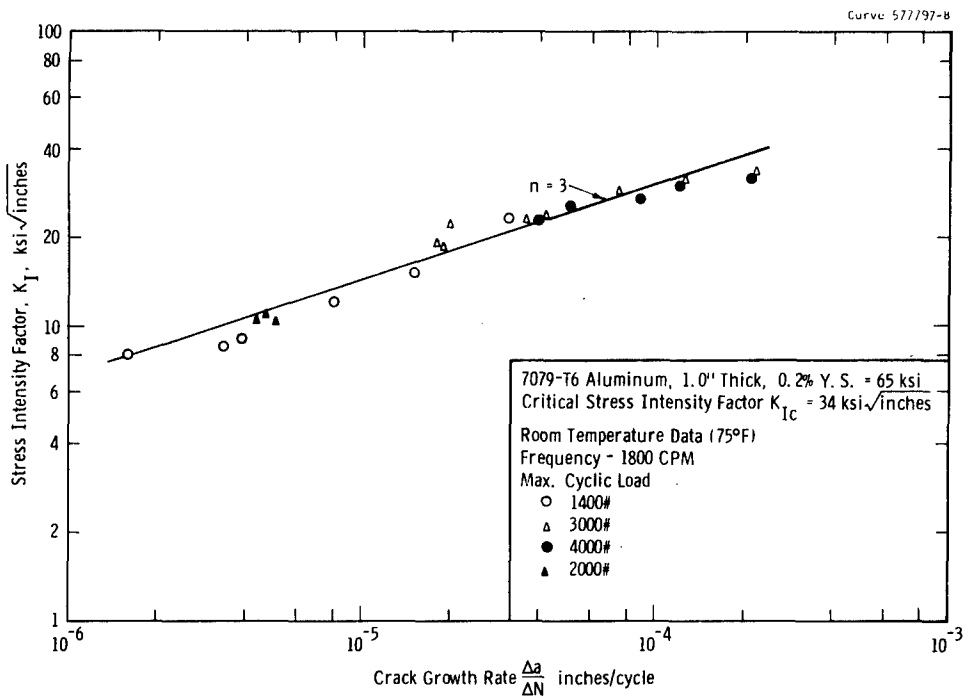
Sec. 7.3 Fig. 2 —Crack growth rate as a function of stress intensity factor for HP-9-4-25 steel as determined on the "IT" WOL fracture toughness specimen



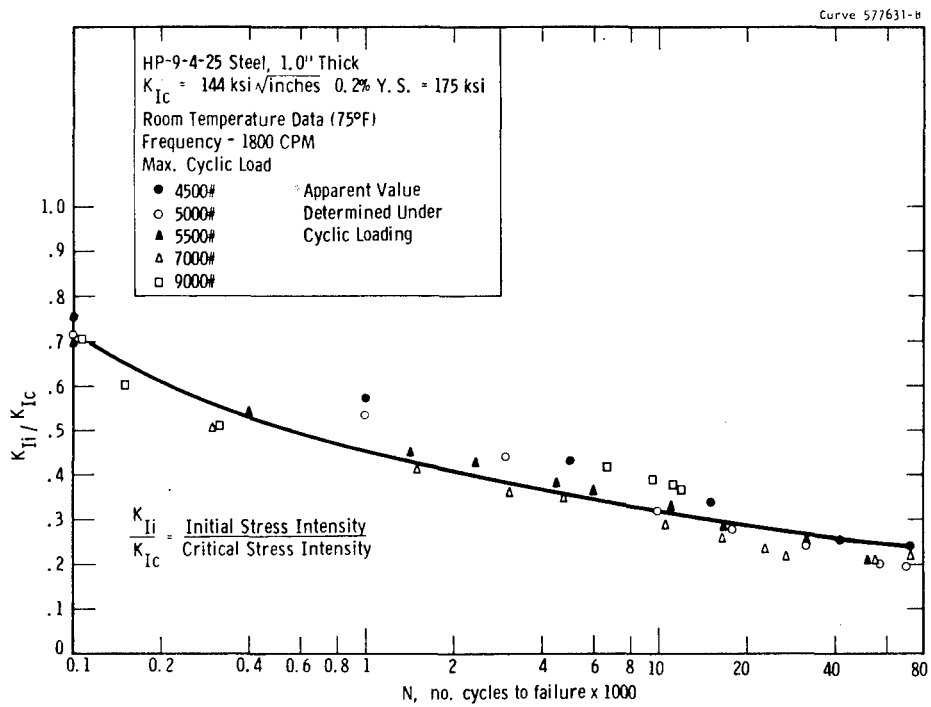
Sec. 7.3 Fig. 3 —Crack growth rate as a function of stress intensity factor for 7079-T6 aluminum as determined on the "IT" WOL fracture toughness specimen



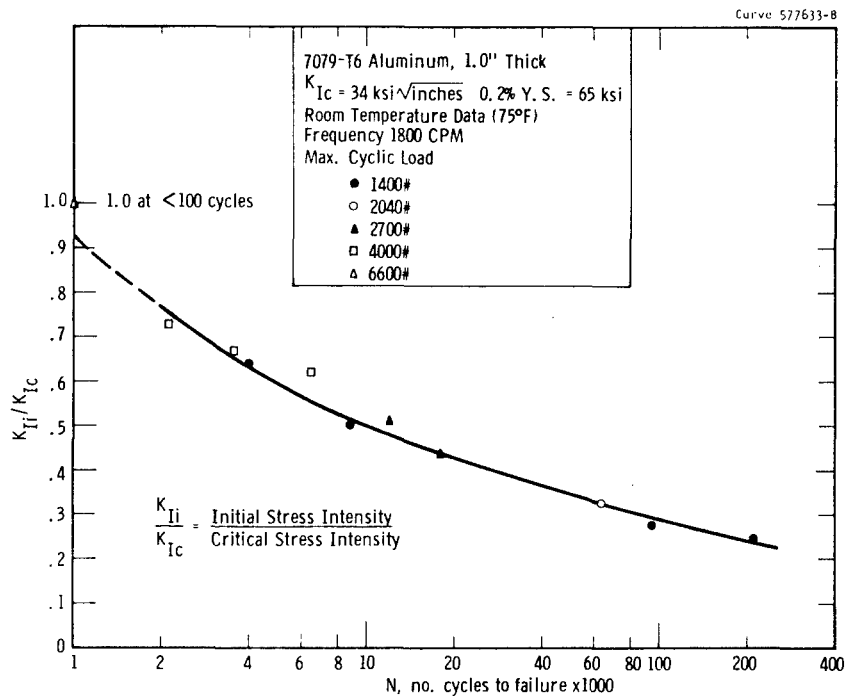
Sec. 7.3 Fig. 4 —Crack growth rate as a function of stress intensity for HP-9-4-25 steel (log-log plot)



Sec. 7.3 Fig. 5 —Crack growth rate as a function of stress intensity for 7079-T6 aluminum (log-log plot)



Sec. 7.3 Fig. 6 — Combined cyclic flaw growth data for HP-9-4-25 steel plate



Sec. 7.3 Fig. 7 — Combined cyclic flaw growth data for 7079-T6 aluminum plate

From the above considerations it is obvious that the crack growth characteristics of a material under cyclic loading are of utmost importance for the determination of satisfactory design criteria. The rate at which a subcritical flaw grows to critical size under cyclic loading can be of primary concern in the determination of the useful service life of a structural component.

The stress intensity factors reported in Table I (Section 7.3.3) were determined from data collected under cyclic loading conditions and will be referred to as the apparent critical stress intensity. The crack length and maximum cyclic load at catastrophic failure (failure of the specimen under cyclic loading) were used to compute the stress intensity. The apparent K_{Ic} determined for the aluminum alloy (7079-T6) based upon cyclic data corresponds to that determined using the conventional direct tension continuous loading toughness testing technique. However, the stress intensity values reported for the steel alloy (HP-9-4-25) as the result of conventional toughness testing do not correspond with the values determined under cyclic loading. The apparent discrepancy is due to the fact that the K_{Ic} values reported for the steel as a result of conventional testing (Section 7.2.4) were determined on the basis of unstable crack propagation whereas those values established under cyclic loading conditions were based upon catastrophic failure. The stress intensity at catastrophic failure is not expected to correspond to the stress intensity at unstable crack propagation if "slow crack growth" occurs prior to failure. As a result, the stress intensity measured for the steel at unstable crack growth is lower than the value at catastrophic failure.

The stress intensity at catastrophic failure can readily be determined under low-stress cyclic loading at a constant maximum load since the crack length at failure can easily be measured by examining the fracture surface - a beach mark clearly indicates the transition from fatigue failure to cleavage fracture. However, the ability to determine the stress intensity at unstable crack growth from data collected under low-stress cyclic loading has not been well established.

Section 7.3 Table I

CYCLIC LOADING DATA

<u>Specimen Identification</u>	<u>Maximum Cyclic Load</u>	<u>Initial Stress Intensity K_{Ti} ksi\sqrt{in}</u>	<u>Apparent Critical Stress Intensity* K_{Ti} ksi\sqrt{in}</u>	<u>Cycles to Failure</u>
<u>HP-9-4-25 Steel</u>				
HP-3T-B13	7000#	41.25	176	23,000
HP-3T-B14	5500#	29.6	142	53,000
HP-3T-B16	9000#	49.5	134	12,100
HP-3T-B20	7000#	38.0	169	27,500
HP-3T-B21	4500#	27.0	119	73,000
HP-3T-B25	5000#	28.7	146	70,300
<u>7079-T6 Aluminum</u>				
A11 B-13	2040#	11	34.0	63,000
A11 B-16	4300#	23	34.2	3,500
A11 B-17	3000#	19	36.2	12,000
A11 B-21	2700#	15	34.8	18,000
A11 B-22	2000#		Irregular fatigue crack	
A11 B-23	1400#	8	34	210,000
A11 B-25	4000#	21.8	34.8	6,400
A11 B-26	6600#	34	34	<100

* Apparent value-determined under cyclic loading.

Cyclic loading induces a specific amount of crack extension per cycle depending upon the stress intensity at the tip of the crack (Figures 2 and 3). When the stress intensity at the maximum cyclic load approaches that level at which unstable crack extension normally occurs under direct tension loading, the amount of crack growth per cycle becomes a function of both the fatigue characteristics and continuous crack growth. At this point, the amount of continuous crack growth depends upon the test frequency since continuous crack growth occurs as long as the stress intensity at the crack tip is high enough. Therefore, at lower frequencies more crack growth per cycle can be expected. From this consideration, it is reasonable to expect that some indication of the transition from fatigue crack growth effects to combine fatigue and continuous growth effects should exist on the stress intensity versus crack growth rate curve. Examination of the crack growth rate characteristics established for the steel alloy (Figure 2) indicates a linear relationship between the stress intensity and the log of the crack growth rate over a stress intensity range from about 30 to 110 ksi $\sqrt{\text{in}}$.

The deviation from a linear relationship at a stress intensity of 30 ksi $\sqrt{\text{in}}$ may represent a threshold level below which fatigue crack growth does not occur. The upper point of deviation ($K_I = 110 \text{ ksi } \sqrt{\text{in}}$) corresponds to the average room temperature critical stress intensity factor at unstable crack propagation determined for the steel using the conventional toughness testing technique ($K_{Ic} = 105 \text{ ksi } \sqrt{\text{in}}$). The log-log plot of the K vs. Δ_a/Δ_N data (Figure 4) also indicates deviation from linearity at a stress intensity of approximately 100 ksi $\sqrt{\text{in}}$. This deviation may also be caused by the effect of continuous crack growth.

Examination of the crack growth rate curves established for the aluminum alloy (Figures 3 and 5), which does not exhibit significant crack growth prior to "pop-in" or failure, indicates deviation just prior to the established critical stress intensity factor ($K_{Ic} = 34 \text{ ksi } \sqrt{\text{in}}$). Therefore, it appears that a careful evaluation of the crack growth rate versus stress intensity curve established for a given material may

permit determinations of the stress intensity at unstable crack propagation; however, additional experimental evidence is necessary.

7.3.5 SUMMARY

The slow crack growth characteristics of two high-strength forging alloys (HP-9-4-25 steel and 7079-T6 aluminum) were determined at room temperature and the test results expressed in terms of fracture mechanics parameters. All testing was conducted with "IT" Wedge-Opening-Loading type toughness specimens under sinusoidal loading. Crack extension during loading was measured and recorded using the ultrasonic instrumentation described in Appendix II.

The rate of crack propagation prior to catastrophic failure is directly related to the stress intensity at the tip of an existing crack; as a result, the ratio of the initial stress intensity to the critical stress intensity provides a quantitative method of predicting component life. As the initial stress intensity approaches K_{IC} the crack growth rate increases accordingly, approaching a maximum at the K_{IC} . Expressed in terms of the generalized crack propagation power law, $\frac{\Delta a}{\Delta N} = C(\Delta K)^n$, n was found to be 2.5 for the HP-9-4-25 alloy steel and $n = 3.0$ for the 7079-T6 aluminum.

Variations in the maximum applied cyclic load corresponding to a given stress intensity appear to have little effect upon the crack growth rate.

The stress intensity at catastrophic failure as determined under cyclic loading does not necessarily correspond to the material property K_{IC} , critical stress intensity at fracture instability, as determined in a conventional toughness test under direct tension. Toughness testing under cyclic loading conditions does not readily provide a technique whereby the stress intensity at unstable crack propagation (crack growth at a constant load) can be detected since continuous crack growth is essentially masked by the cyclic nature of the applied load.

The relationship between linear elastic fracture mechanics and slow crack growth characteristics as demonstrated by the results

of this investigation provides a quantitative basis for evaluating life expectancy under cyclic loading.

Section 7.3 References

1. P. C. Paris, "The Fracture Mechanics Approach to Fatigue," Fatigue - An Interdisciplinary Approach, Proceedings of the 10th Sagamore Army Materials Research Conference, 1964, p. 117.
2. Ibid., H. W. Liu, Discussion, p. 127.

TABLE OF CONTENTS

Section 8.1

PHASE III - APPLICATION OF FRACTURE MECHANICS TECHNOLOGY

	<u>Page</u>
8.1 INTRODUCTION	221
8.1.1 Generalized Description of the Use of Fracture Mechanics Technology.	221
8.1.1.1 Brittle Fracture During Static Loading	222
8.1.1.2 Slow Crack Growth During Cyclic Loading. . . .	224
8.1.1.3 Summary.	226

LIST OF FIGURES

Section 8.1

PHASE III - APPLICATION OF FRACTURE MECHANICS TECHNOLOGY

	<u>Page</u>
Figure 1. The relationship of fracture strength to crack size for different levels of fracture toughness	224
Figure 2. Typical crack growth rate properties under cyclic loading.	225
Figure 3. Typical cyclic flaw growth data	225

Section 8

PHASE III - APPLICATION OF FRACTURE MECHANICS TECHNOLOGY

8.1 INTRODUCTION

To educe the utmost performance from available or contemplated materials requires an intimate knowledge of their capabilities and limitations as well as the application of that knowledge in design, testing, and specifications. In designing against fracture and selecting appropriate materials, the fracture mechanics or "fracture toughness" approach provides the needed knowledge and permits its application in situations involving plane strain or nearly plane strain conditions. Appropriate fracture mechanics data for both the slow growth and catastrophic propagation phases of fracture, and the proper consideration of these data can be successfully applied in the following areas: quantitative evaluations of the brittle fracture potential of components and structures in specific situations; the design of components or structures, including the selection of appropriate materials to provide the desired reliability against fracture; evaluation of pertinent nondestructive inspection procedures; predictions of life expectancy of components under sustained or cyclic loading conditions; and the establishment of quantitative material specifications and associated realistic standards for inspection and acceptance that will assure the desired degree of immunity from brittle failure for the desired life of the component.

8.1.1 GENERALIZED DESCRIPTION OF THE USE OF FRACTURE MECHANICS TECHNOLOGY

A detailed discussion of fracture mechanics technology was provided in previous section (6.2). However, a brief review of the

approach would appear to be helpful before delving into the application features in detail.

8.1.1.1 Brittle Fracture During Static Loading

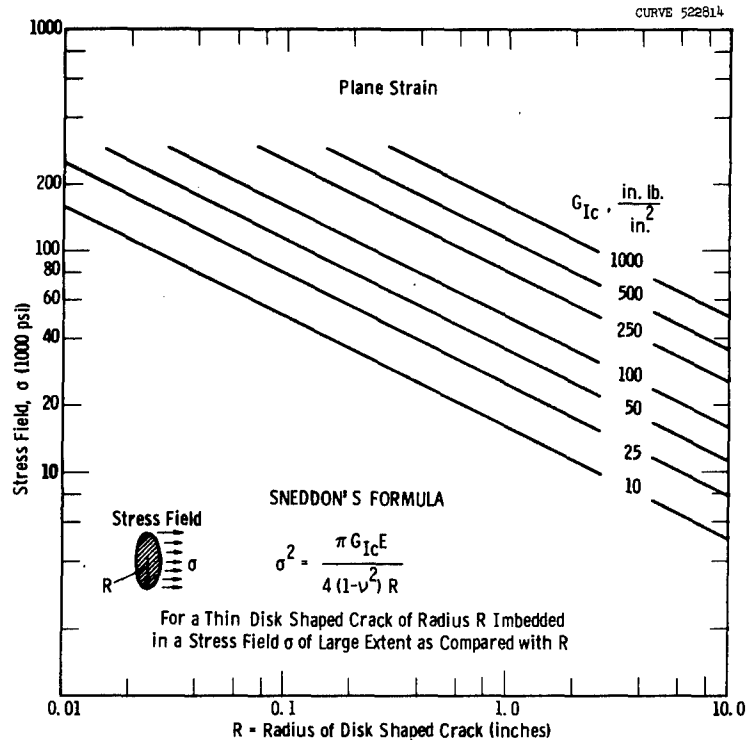
The basis of the concept is that for essentially plane strain conditions the fracture toughness of a material can be expressed as a material parameter*, analogous to yield strength. This parameter is usually described in terms of " G_{Ic} " (critical crack extension force, in-lbs/in²) or K_{Ic} (critical stress intensity factor, psi $\sqrt{\text{in.}}$). Either G_{Ic} or K_{Ic} are commonly referred to as "fracture toughness"**. Being a material parameter the fracture toughness, once properly determined under one set of conditions, is applicable to other conditions, i.e., geometry, flaw size, and loading conditions. The values for G_{Ic} or K_{Ic} must be determined experimentally, and several types of specimens and loading conditions have been successfully employed to obtain these measurements of fracture toughness (Section 6.2.4). Considerable data are available from the literature (Section 7.1). For a given application, temperatures and strain rates equivalent to the service use should be employed in the fracture toughness determinations. Once properly determined the fracture toughness parameters, used in conjunction with appropriate mathematical expressions relating toughness, defect size, applied stress, and a geometrical factor for the relative geometries of the defect and component, can be employed to make quantitative determinations of the effects of specific defects in specific situations. Detailed examples will be provided in subsequent sections.

*The evidence to date substantiates that the fracture toughness, when properly measured, can be considered as a material constant for practical engineering purposes.

**There are many subscripts used to denote various aspects of G_{Ic} or K_{Ic} , and therefore an intimate knowledge of this terminology is essential to the proper use of these parameters (Section 6.2.2).

Expressions relating the fracture toughness and the load bearing capacity of defect containing structures or components are available for a number of geometries, loading conditions, and types of defects. Such expressions nearly always involve the following terms: the fracture toughness, the applied stress, the elastic modulus, the yield strength of the material, a linear dimension of the crack or defect, and a proportionality term dependent only on the manner of loading and the relative geometry of the defect and structural component. The expressions which are available for many types of defects and loading conditions are provided in Section 8.2.4.

The implementation of the fracture toughness approach for determining load bearing capacity is rather straightforward. Knowing the fracture toughness of the material in question for the temperature range of interest, and the size of the defects from a nondestructive evaluation, it is possible to evaluate the load bearing capacity of the structure by inserting the G_{Ic} or K_{Ic} and defect size numbers in the appropriate expressions and solving for the critical value of the stress which will cause catastrophic fracture. Conversely, knowing the toughness and applied stress, it is possible to estimate the critical defect sizes that are required for catastrophic failure. These, in turn, can be compared with performance capabilities of the nondestructive test techniques that may be employed to detect flaws. For a given level of toughness, the applied stress that is required for catastrophic fracture decreases as the crack size increases; the stress is proportional to the inverse square root of the defect size. For a given defect size, a decrease in toughness results in a lower applied stress for fracture. Thus an estimate of the critical combination of defect size and applied stress that is required for fracture may be readily determined if one knows the toughness of the material and either one of the other two variables. Figure 1 provides a graphical illustration of the relationships of stress, defect size, and toughness for the case of a small disk shaped crack imbedded in a large tensile stress field.

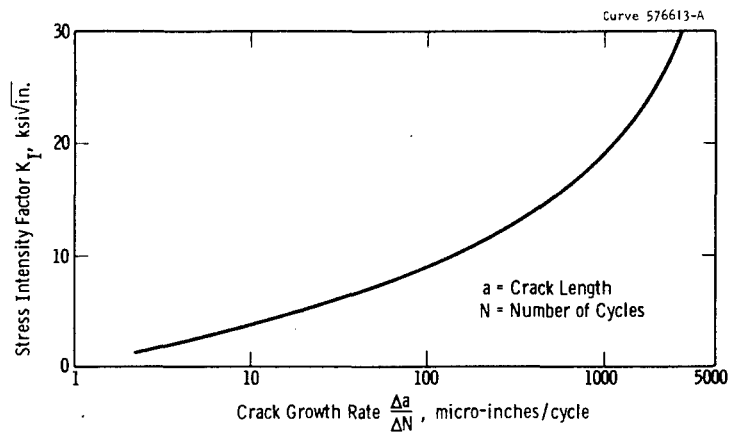


Sec. 8.1 Fig. 1—The relationship of fracture strength to crack size for different levels of fracture toughness

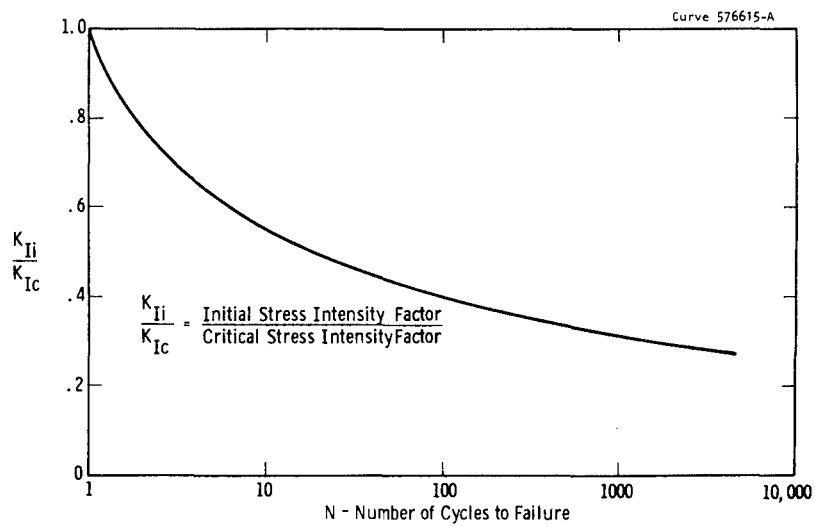
8.1.1.2 Slow Crack Growth During Cyclic Loading

While the termination of the life of a structure or component may be based on the critical flaw size for catastrophic failure, it must be recognized that the total useful life of a cyclic-loaded component is dependent upon the rate of growth of flaws from a sub-critical size to a critical size. Therefore, both an understanding of the critical combination of stress and defect size for catastrophic fracture, and the measurement of crack growth characteristics of the material under application conditions are essential to determining the useful life of a component.

Fatigue (slow) crack propagation is a localized phenomenon dependent upon the temperature, environment, and stress conditions at the crack front. The stress intensity factor "K" provides one of the best means available for describing the stress conditions at the tip of the advancing crack. For a given geometry (flaw and component) and given loading conditions, the crack growth rate is dependent upon the stress intensity at the tip of the crack, as shown schematically in Figure 2.



Sec. 8.1 Fig. 2 -Typical crack growth rate properties under cyclic loading



Sec. 8.1 Fig. 3 -Typical cyclic flaw growth data

For given conditions, the stress intensity factor K is a function of the applied load (stress) and the crack length "a"; that is, $K = f(\sigma a)$. As the crack grows under constant load cycling the stress intensity increases since both "a" and σ are increasing. Eventually the crack grows to a sufficient length that the stress intensity K increases to a level equivalent to the material characteristic K_{Ic} , the critical stress intensity factor. At this point, brittle fracture (rapid crack propagation) occurs.

Consideration of the ratio K_{Ii}/K_{Ic} (where K_{Ii} is the initial stress intensity factor) provides a technique for estimating how close conditions are to fracture. The data are quite useful when shown in the form illustrated schematically in Figure 3. For example, knowing the ratio K_{Ii} to K_{Ic} , the number of cycles to failure can be predicted. Conversely, knowing the desired life of the component and K_{Ic} of the material, the maximum allowable initial stress intensity K_{Ii} can be determined. Since K_{Ii} is a function of the applied stress and the flaw size, it is then possible to compute either the initial allowable flaw size for a given stress or, conversely, the allowable stress for some given initial flaw size.

Clearly, consideration of slow crack growth behavior in terms of the stress intensity K provides a powerful tool for studying and applying slow crack growth. Much recent progress has been made using the stress intensity concept^(1,2,3) and a good agreement between laboratory and full-scale tests has been obtained.^(4,5) The subject of sub-critical crack growth is described in more detail in Sections 8.2 and 8.3.

8.1.1.3 Summary

It should be realized that the foregoing discussion is intended only to provide a general idea of the application of the fracture toughness approach, and to emphasize the interplay between toughness and defect size in determining the load bearing capacity of a structure. For a precise evaluation of any specific situation, more

detailed information is required regarding: the temperature dependence of the fracture toughness (K_{Ic} or G_{Ic}) in the temperature and strain rate range of interest; the location, size, shape, orientation, and type of defect; the direction and magnitude of the applied (plus possible residual) stresses acting on the defect; the slow growth characteristics of a sub-critical size flaw under sustained or cyclic loading at the application temperatures; the relative geometry of the structural member and the defect; and the proper criterion of fracture toughness to be employed. At the present, the application of the technology is limited to those materials for which valid fracture toughness (K_{Ic} or G_{Ic}) parameters can be determined, and to applications where sufficient section size and restraint prevail so that an essentially plane strain state of stress exists in the region of the defect. In those situations where gross plastic deformation occurs in the region of the defect prior to fracture because of extremely high temperature and/or thin sections, further developments are required before the technology can be successfully applied.

Section 8.1 References

1. P. C. Paris, "Fatigue Crack Growth," Chapter IV Fracture Mechanics Workshop, Denver, August, 1965.
2. P. C. Paris, "The Fracture Mechanics Approach to Fatigue," Fatigue--An Interdisciplinary Approach, Syracuse University Press, 1964, p. 107.
3. Che-Yu Li, P. M. Tolda, and R. P. Wei, "The Effect of Environments on Fatigue Crack Propagation in a Quenched-and-Tempered High-Strength Steel," Presented at ASTM Committee on Fracture Toughness Testing of Metals (E24 Sub IV) Meeting, Washington, D. C., February 3, 1966.
4. C. F. Tiffany and P. M. Lorenz, "An Investigation of Low-Cycle Fatigue Failures using Applied Fracture Mechanics," ML-TDR-65-53, Air Force Materials Laboratory, Wright-Patterson Air Force Base (May 1964).
5. P. C. Paris, M. P. Gomez, and W. E. Anderson, "A Rational Analytical Theory of Fatigue," The Trend in Engineering, 13:9 (January 1961).

TABLE OF CONTENTS

Section 8.2

	Page
8.2 INFORMATION REQUIRED IN UTILIZING FRACTURE MECHANICS TECHNOLOGY	231
8.2.1 Material Properties	231
8.2.2 Stress Information	234
8.2.3 Defect Characterization	235
8.2.4 Expressions Appropriate to Geometry and Loading Conditions.	237
8.2.5 Type of Loading	248

LIST OF FIGURES

Section 8.2

		Page
Figure 1.	A crack in an infinite sheet with uniform normal stress at infinity	240
Figure 2.	A crack in an infinite sheet subject to centrally applied wedge forces.	240
Figure 3.	An infinite sheet with a semi-infinite crack subject to a concentrated force	241
Figure 4.	An infinite sheet with colinear semi-infinite cracks with a concentrated force	241
Figure 5.	An infinite sheet with load transmitted across a neck between two semi-infinite colinear cracks	241
Figure 6.	Semi-infinite notch approaching the free edge of a half plane.	242
Figure 7.	An edge crack in a semi-infinite sheet subject to tension.	242
Figure 8.	An elliptical crack in an infinite body subjected to uniform normal tension	243
Figure 9.	Concentrated forces applied to the axis of a circular disk crack in an infinite body	243
Figure 10.	Two equal colinear cracks in an infinite sheet subject to uniform normal stress.	244
Figure 11.	An infinite array of colinear cracks in an infinite sheet.	244
Figure 12.	Double-symmetric edge cracks in strip of infinite length subject to uniform tension.	245
Figure 13.	A crack (or cracks) emanating from a circular hole in a sheet.	246
Figure 14.	Stress intensity factor K at center of the approaching edge of two adjacent coplanar elliptical flaws subject to a uniform normal stress field	247

Section 8.2

INFORMATION REQUIRED IN UTILIZING FRACTURE MECHANICS TECHNOLOGY

The successful employment of fracture mechanics technology is dependent upon having adequate basic information concerning material properties, existing defects and stresses. In addition, an appropriate expression, relating these factors for the prevailing loading conditions and the relative geometries of the defect and structural component, must be available in order to utilize the information. The following sections discuss these areas of required information.

8.2.1 MATERIAL PROPERTIES INFORMATION REQUIRED

The following material properties are necessary for various aspects of fracture mechanics considerations.

- (1) K_{Ic} or G_{Ic} - the inherent fracture toughness
- (2) σ_{YS} - the conventional tensile yield strength, generally the 0.2% offset criterion
- (3) E - Young's modulus of elasticity
- (4) ν - Poisson's ratio
- (5) $\frac{\Delta a}{\Delta N}$ - the crack growth rate (increase in length per cycle) as a function of the stress intensity K_I during cyclic loading
- (6) - crack growth rates as a function of K_I during sustained loading

The basic material parameter of K_{Ic} or G_{Ic} is essential in all considerations, from a simple comparison of materials to complex calculations of allowable defect sizes. It should be recognized that while K_{Ic} is a basic material parameter, it is dependent upon certain mechanical and metallurgical variables as discussed in Section 6.2.3. Strain rate and temperature effects are the most significant mechanical

variables which require consideration. For materials which have a strong strain rate and temperature sensitivity, K_{Ic} generally decreases with decreased temperature and increased strain or loading rate. In the specific application of these kinds of materials, caution should be taken to use K_{Ic} or G_{Ic} values corresponding to those prevailing in the application. Similar considerations are necessary with respect to metallurgical variables such as heat treatment, microstructure, rolling (working) texture, steel making practice, impurities, etc. It must be realized that the K_{Ic} fracture toughness of a given type of metal or alloy can vary markedly as a result of the effect of metallurgical variables. Therefore, it is essential that the designer or materials engineer be certain that the test material condition and notch orientation employed in the fracture toughness measurements correspond with that of the component of interest. Also sufficient K_{Ic} tests should be conducted to provide a basis for allowance of data scatter due to material inhomogeneities.

The conventional engineering yield strength, σ_{YS} , (0.2% offset tensile yield strength) is another material parameter which is commonly involved in fracture toughness considerations and calculations. It appears as one of the terms in many of the expressions relating toughness, defect size, and stresses. The ratio of $\frac{K_{Ic}}{\sigma_{YS}}$ is often used as a convenient method of expressing and comparing the relative toughness of materials. For example, if two candidate materials have the same yield strength, the one with the higher $\frac{K_{Ic}}{\sigma_{YS}}$ ratio is obviously the more tough. The $\frac{K_{Ic}}{\sigma_{YS}}$ ratio is also employed as a criterion for selecting an appropriate specimen size for K_{Ic} testing. The most recent suggestion⁽¹⁾ is that for any type of test specimen, the minimum crack length "a" and minimum thickness "B" be $2.5 \left(\frac{K_{Ic}}{\sigma_{YS}}\right)^2$. In setting up a test program, an estimate of K_{Ic} is made and the test specimen size is chosen accordingly. For initial tests it is usually expedient to assume a K_{Ic} value representing the high side of the estimated range.

The conventional 0.2% offset tensile yield strength as determined in a standard test is generally adequate for most fracture mechanics considerations. However, as was the case for K_{Ic} measurements,

the σ_{YS} should be determined using the temperature and strain rate, and the material condition, corresponding to the intended application.

Young's modulus E appears as a term in the expression involving the G_{Ic} parameter, defect size and stress. It is also a term used in converting from G_{Ic} to K_{Ic} and vice versa, $K_{Ic}^2 = G_{Ic}E/(1-\nu^2)$, where ν is Poisson's ratio. Handbook values for E and ν are generally sufficiently accurate for most purposes, so long as the temperature is considered.

In cyclic loaded applications, the crack growth rate ($\frac{\Delta a}{\Delta N}$, change in length per cycle) characteristic is another material parameter of concern as apparent from the discussion in Sections 6.2, 7.3 and 8.3. The crack growth rate of a given material under given conditions can be described in terms of the driving force, K_I (the stress intensity factor), the particular growth rate at any cycle being related to the K_I at that cycle. For a given value of K_I , different material can exhibit considerable differences in growth rates. Similarly, a given type of material can have a different growth rate at a given K_I depending upon the metallurgical condition, the plane of crack extension, the texture, the cleanliness (non-metallic inclusions and impurities), etc. Mechanical variables of temperature, environment, and cyclic spectrum also affect the growth rate in a given material at a given value of K_I . Therefore, these factors must be considered when determining growth rate as a function of K_I , and conditions (metallurgical and mechanical) corresponding to practice should be employed.

In making preliminary judgments of the relative crack growth rates of various materials, it is convenient to consider the material in terms of their relative K_{Ic} values. For any given stress intensity, K_I , the material with the lower fracture resistance, K_{Ic} , can be expected to have the faster crack growth rate. For specific applications, the crack growth rate should be determined as a function of K_I over the range from the initial stress intensity factor envisioned (K_{Ii}) to where K_I is equivalent to the material fracture toughness parameter, K_{Ic} . Having these basic data, it is then possible to make quantitative evaluations of life expectancy as will be described in detail in Section 8.3.

In some applications it is also necessary to have crack growth rate data for sustained loading conditions, particularly if a hostile environment is present. The most convenient form of data is a plot of $\frac{K_{Tt}}{K_{Ic}}$ as a function of time to failure. These data are employed in the same manner as the data for cyclic loading. For complex loading spectrums, it is possible that both cyclic and sustained loading conditions will prevail, and appropriate materials data will be required.

8.2.2 STRESS INFORMATION

From a fracture mechanics viewpoint the stress analysis of a structure must result in a relationship between the external loads applied to the structure and the stress intensity, K , at the tips of cracks known or hypothesized to exist in the structure. Due to mathematical difficulty exact expressions for crack tip stress intensity factors are known only for a limited number of geometries. For this reason various approximations may have to be made in obtaining a relationship between external loads and crack tip stress intensity factors in complex structures.

In general an approximation of the desired relationship can be obtained by means of a two-step procedure. In the first step the presence of a crack or cracks in the structure is ignored, and a typical stress analysis in which the principles of force equilibrium and displacement compatibility are applied is carried out. As a result of this step a reasonable estimate of the relation between the externally applied loads and the nominal stresses in any part of the structure will have been obtained. Next, it is assumed that the stresses at a moderate distance from each crack are unaffected by the presence of that crack or other cracks. That is, it is assumed that the stresses at a moderate distance from the crack are equal to those calculated for the case in which the cracks were ignored. The second step is then to find the existing stress intensity solution (8.2.4) which best resembles the actual situation with respect to (a) geometric boundaries near the crack and (b) stress distribution at a moderate distance away from the crack. By use of this existing solution an approximate relation

between the stress field local to the crack and the stress intensity of the crack tip can be obtained. Finally, by combining the relations obtained in the two steps, a mathematical relation between the external loads and the crack tip stress intensities can be obtained.

In using this method of analysis a reasonable amount of judgment must be used in determining whether the local stress field of the crack which was determined in step one by ignoring the presence of the crack is significantly affected by the actual presence of the crack. In tough materials in which the size of non-critical cracks can become significant, the presence of the crack could affect the general flexibility of the structure and thus in turn affect the stress distribution at moderate distances from the crack. This situation would make the accuracy of the above procedure questionable. An example of such a situation is a thin cylindrical vessel containing a longitudinal crack. From step one of the above procedure the conclusion would be reached that in effect the crack is subject to a plane biaxial uniform stress field. But actually, if the crack is large enough, bulging of the cylinder wall will occur in the vicinity of the crack, thus subjecting the crack to additional bending stresses.⁽²⁾

In general the non-critical crack sizes in materials for which the fracture mechanics principles are valid will be small enough such that the two-step procedure described above will give a valid estimate of the relation between external loads and the stress intensity factors of the cracks in the body. As in any stress analysis the effects of thermal stresses and residual stresses must also be taken into account. The relation between these additional stresses and the crack stress intensity factors can be obtained by using the same two-step procedure described above for external loads.

8.2.3 DEFECT CHARACTERIZATION

The detection, description, and dimensional measurements of defects is another area essential to the proper utilization of fracture mechanics technology. Information concerning the location, size, shape, orientation, and distribution of defects is vital to all considerations

and computations of critical or allowable stresses for either the slow crack growth or catastrophic stages of fracture. Expressions relating toughness, stress, and defect size are available for a number of types of defects, loading conditions, and relative geometries of the defect and the component. These are described in detail in the next section (8.2.4). A knowledge of the location and shape of the defect is essential to the choice of the appropriate expression. The orientation of the defect relative to the stresses which prevail in the application will define the principle stress of concern. All of the expressions for various geometries and loading conditions contain a term involving some linear dimension of the defect; hence, the defect dimensions must be known. This basic information relative to the shape, orientation, and size of the defect, coupled with a knowledge of the K_{Ic} fracture toughness, then permits the selection of an appropriate expression and the calculation of the critical applied stress for fracture.

The above discussion is pertinent to the situation of establishing allowable stresses for known defects. In many instances the toughness of the material and the applied stresses are fixed, and the situation is then one of determining what size, shape and orientation of defects are critical. By inserting the toughness and stress into the appropriate expressions it is possible to calculate the critical size defects for various shapes and orientations. The problem then reduces to being able to detect and describe the defects that may exist in the component, and subsequently relating these observed defects to the calculated critical conditions.

The distribution of defects is of concern both the catastrophic and slow crack growth phases of fracture. If the neighboring defects are sufficiently close to one another; i.e., a cluster of non-metallic inclusions, pores, cracks, etc., so that there is an interaction between them, ⁽³⁻⁵⁾ it may be necessary to treat the whole cluster as a single defect. This would apply to either catastrophic or slow crack growth considerations. On the other hand, if the defects are sufficiently far apart, they would be treated as individual defects for catastrophic fracture evaluations. However, it is possible that in this latter

situation, the neighboring defects would have an effect on the slow crack growth rates, particularly if the defects were aligned in the same plane. The growth rate through a region of relatively small, neighboring, planer defects could be substantially greater than that for a clean region in the same material.

In many cases, particularly in large, heavy sections produced from large ingots or in large weldments, there may be relatively large areas of segregates, foreign matter, or non-metallic inclusions. The inherent fracture toughness of the material in the region associated with these defects may be considerably less than that of clean areas. Therefore to properly assess these kinds of defects the effective K_{Ic} and crack growth rate values should be representative of the material in the regions adjacent to the defects. Otherwise the effectiveness of the defects in causing fracture may be underestimated. In situations involving more isolated defects, it may not be possible to obtain K_{Ic} and growth rate data representative of the material immediately adjacent to the defects. In this case, some extra conservatism should be employed to protect against possible lower, local toughness in the surrounding material.

The following section (8.3) will illustrate how the matter of defects is handled in practical situations. The present discussion is intended only to emphasize that defect detection and description is a vital part of the basic information required in the application of fracture mechanics. The important defect characteristics that require definition are location, shape, size, orientation, and distribution. Acuity of the tip of the defect does not require definition since the use of fracture mechanics incorporates the basic assumption that all defects have an acuity (sharpness) equivalent to a crack. In so far as actual defects may be blunter than a crack, the calculated allowable stress will be on the conservative side.

8.2.4 EXPRESSIONS APPROPRIATE TO GEOMETRY AND LOADING CONDITIONS

The number of geometries and loading conditions for which solutions for the stress-intensity factors is known is rather limited.

But there are a sufficient number of solutions available to cover a great many design configurations, and the number of available solutions is rapidly increasing. These solutions are obtained by both analytic and experimental methods.

The experimental method of determining K consists of determining the energy release rate G first and then determining K by use of the relationship between the two quantities. The method was originally proposed by Irwin and Kies⁽⁶⁾ and is described in detail in Reference 7. In brief, the compliance λ (deflection/unit load) of the body is determined as a function of crack length, a, by experimentally determining the compliance at a number of different crack lengths. The energy release rate is then determined by use of the relation

$$G = \frac{P^2}{2} \left(\frac{\partial \lambda}{\partial a} \right)_{\delta}$$

where P represents the load applied to the structure and the partial derivative is evaluated by holding the displacement, δ , of the external load constant.

The analytic methods for determining K can be subdivided into exact methods and approximate methods. In the exact methods the necessary partial differential equations and boundary conditions of elasticity theory are exactly satisfied. In the approximate method^(8,9) the partial differential equations are satisfied exactly, but the boundary conditions are satisfied only approximately. Due to the mathematical rigor involved in an exact solution, the boundary conditions must usually be rather simple, and, thus, in many cases the solutions do not represent practical situations. Due to the versatility of the approximate methods, they can be applied to many practical geometries and loading conditions.

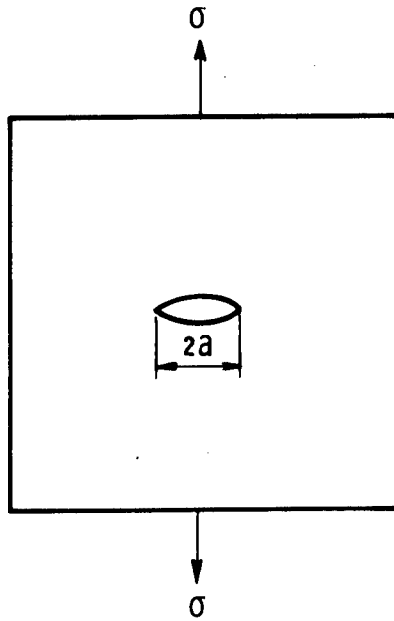
An excellent collection of available solutions for stress intensity factors has been given by Paris and Sih.⁽¹⁰⁾ Many of the solutions listed in their paper which are applicable to Mode I design are presented in Figures 1 through 13 of this section. Further information on these solutions can be obtained from the references indicated

on the figures or in the Paris and Sih paper. The Paris and Sih paper also contains a number of Mode II and II solutions. The stress-intensity solutions given for the various fracture mechanics specimens in (6.2.4.3) are also very useful in design considerations and can be used to approximate the stress-intensity factors of cracks in many standard design configurations.

As stated in (8.2.2), it is desirable to find an available solution which resembles as closely as possible the geometry and loading conditions of the actual physical situation under consideration. In many cases the difference between the actual conditions of interest and the closest conditions for which a solution exists is significant. For example, the crack front shapes may be different or the proximity of free surfaces to the crack may differ. If these differences are not appreciable it is possible to modify the existing solutions by means of correction factors so that they become more nearly applicable to the actual conditions. A number of simple methods for modifying these solutions are discussed by Paris and Sih in Reference 5.

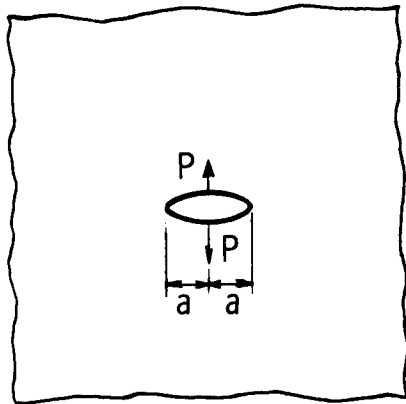
The interaction of the crack tip stress fields of adjacent cracks is an additional situation which may complicate the determination of stress intensity factors. As the tips of adjacent cracks approach each other, the influence of the geometry of each crack on the crack tip stress intensity of the other crack increases. Only a limited number of solutions for the interaction of cracks are available. One such solution is shown in Figure 14. This approximate solution for two embedded coplanar elliptical flaws subject to a uniform normal stress field was determined by Hall and Kobayashi.⁽²¹⁾ As is observed there is little interaction for the larger values of b/a until the cracks are quite close to each other. This same solution is used by Tiffany and Masters⁽²²⁾ for the case of two coplanar elliptical surface flaws in a plate. Some other solutions for the interaction of cracks are shown in Figure 10 and 11.

Besides the difficulty in determining the magnitude of the stress intensity factors, the interaction of adjacent flaws causes additional difficulties. As the distance between two adjacent cracks



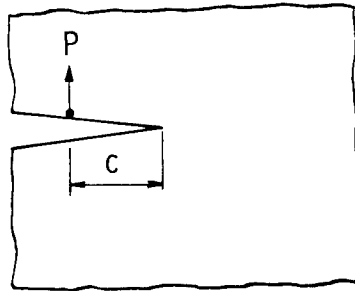
$$K_I = \sigma (\pi a)^{1/2}$$

Sec. 8.2 Fig. 1 —A crack in an infinite sheet with uniform normal stress at infinity



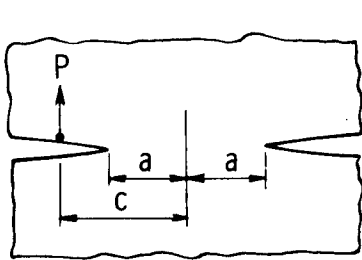
$$K_I = \frac{P}{(\pi a)^{1/2}}$$

Sec. 8.2 Fig. 2 —A crack in an infinite sheet subject to centrally applied wedge forces



$$K_I = \frac{P}{(2\pi c)^{1/2}}$$

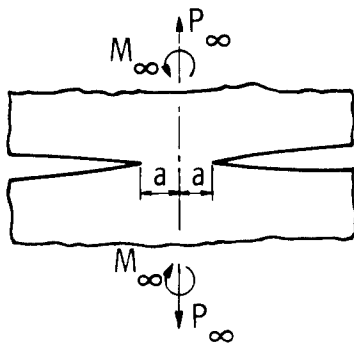
Sec. 8.2 Fig. 3 —An infinite sheet with a semi-infinite crack subject to a concentrated force (1)



$$K_I = \frac{P(c^2 - a^2)^{1/2}}{2(\pi a)^{1/2}(c - a)} \quad \text{(Left Crack Tip)}$$

$$K_I = \frac{P(c^2 - a^2)^{1/2}}{2(\pi a)^{1/2}(c + a)} \quad \text{(Right Crack Tip)}$$

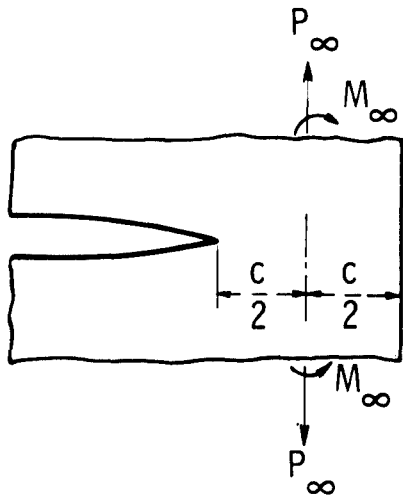
Sec. 8.2 Fig. 4 —An infinite sheet with colinear semi-infinite cracks with a concentrated force (1)



$$K_I = \frac{P_\infty}{(\pi a)^{1/2}} + \frac{2M_\infty}{\pi^{1/2} a^{3/2}}$$

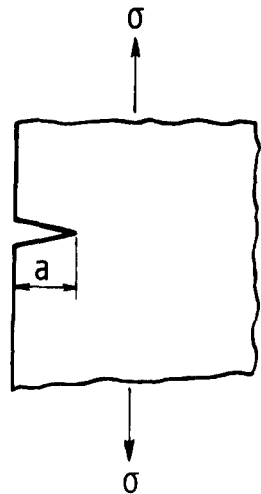
(Right Crack Tip)

Sec. 8.2 Fig. 5 —An infinite sheet with load transmitted across a neck between two semi-infinite colinear cracks (2)



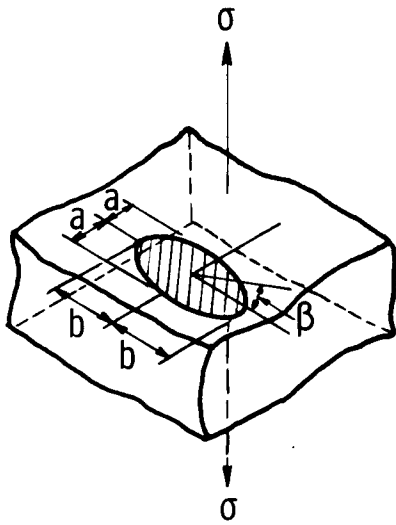
$$K_I = \pi^{1/2} \left(\frac{4\pi - 12}{\pi^2 - 8} \right) \frac{P_\infty}{c^{1/2}} + \pi^{1/2} \left(\frac{4\pi - 8}{\pi^2 - 8} \right) \frac{M_\infty}{c^{3/2}}$$

Sec. 8.2 Fig. 6 – Semi-infinite notch approaching the free edge of a half plane (2, 3)



$$K_I = 1.12 \sigma (\pi a)^{1/2}$$

Sec. 8.2 Fig. 7 – An edge crack in a semi-infinite sheet subject to tension (4)

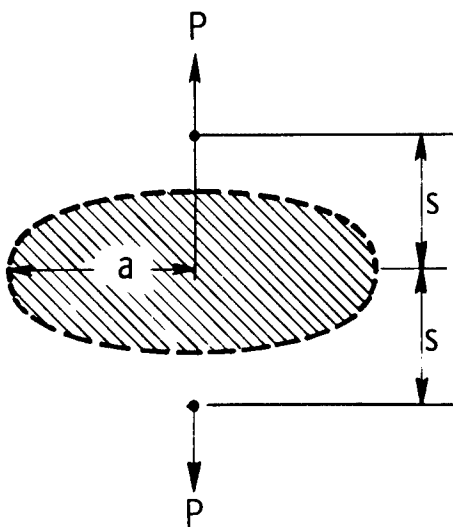


$$K_I = \frac{\sigma (\pi a)^{1/2}}{\Phi_0} \left(\sin^2 \beta + \frac{a^2}{b^2} \cos^2 \beta \right)^{1/4}$$

$$\Phi_0 = \int_0^{\pi/2} \left[1 - \left(\frac{b^2 - a^2}{b^2} \right) \sin^2 \theta \right]^{1/2} d\theta$$

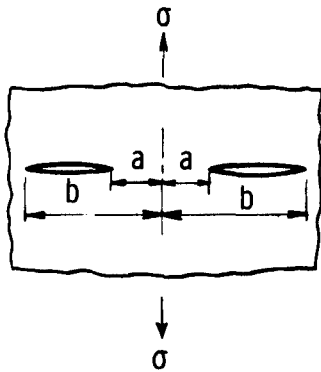
Where Φ_0 is the Elliptic Integral

Sec. 8.2 Fig. 8 -An elliptical crack in an infinite body subjected to uniform normal tension (5)



$$K_I = \frac{P}{(\pi a)^{3/2}} \frac{\left[1 + \left(\frac{2-\nu}{1-\nu} \right) \frac{s^2}{a^2} \right]}{\left[1 + \frac{s^2}{a^2} \right]^2}$$

Sec. 8.2 Fig. 9 -Concentrated forces applied to the axis of a circular disk crack in an infinite body

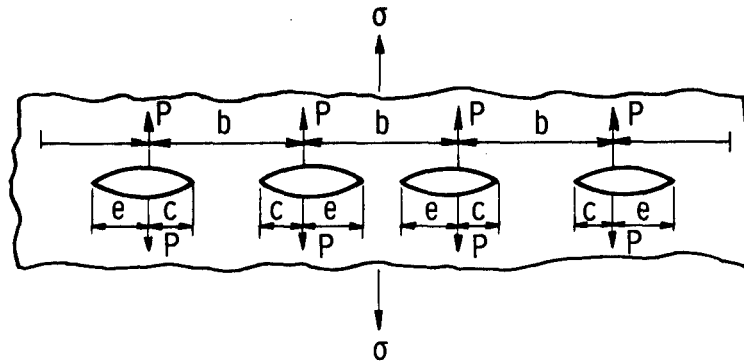


$$K_I = \sigma (\pi/a)^{1/2} \frac{b^2 \frac{E(k)}{K(k)} - a^2}{(b^2 - a^2)^{1/2}} \quad (\text{At Near Ends})$$

$$K_I = \sigma (\pi/b)^{1/2} \left(\frac{1}{k} - \frac{E(k)}{k K(k)} \right) \quad (\text{At Far Ends})$$

Where $k = [1 - (a/b)^2]^{1/2}$ is the modulus of the complete elliptic integrals $E(k)$ and $K(k)$ of the first and second kind, respectively

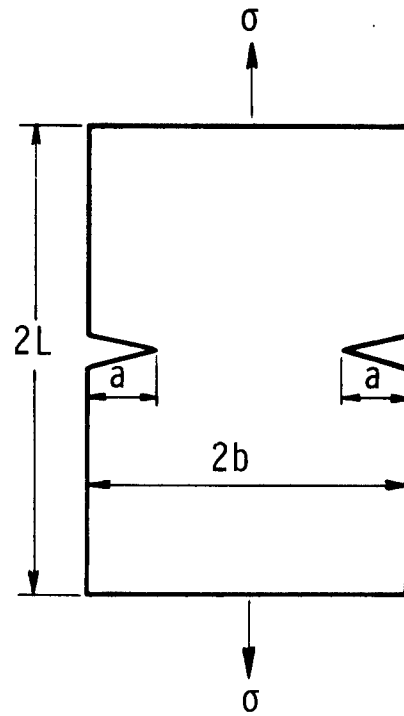
Sec. 8.2 Fig. 10 - Two equal colinear cracks in an infinite sheet subject to uniform normal stress (6, 7)



$$K_I = \frac{\sigma (4b)^{1/2} \sin \frac{\pi c}{2b}}{\left(\cos \frac{\pi e}{2b} \left(\sin \frac{\pi e}{2b} + \sin \frac{\pi c}{2b} \right) \right)^{1/2}} + \frac{P \left(\sin \frac{\pi c}{2b} \right)^{1/2}}{\left(b \sin \frac{\pi e}{2b} \cos \frac{\pi e}{2b} \left(\sin \frac{\pi e}{2b} + \sin \frac{\pi c}{2b} \right) \right)^{1/2}}$$

(At Crack Tips at Ends Denoted by e)

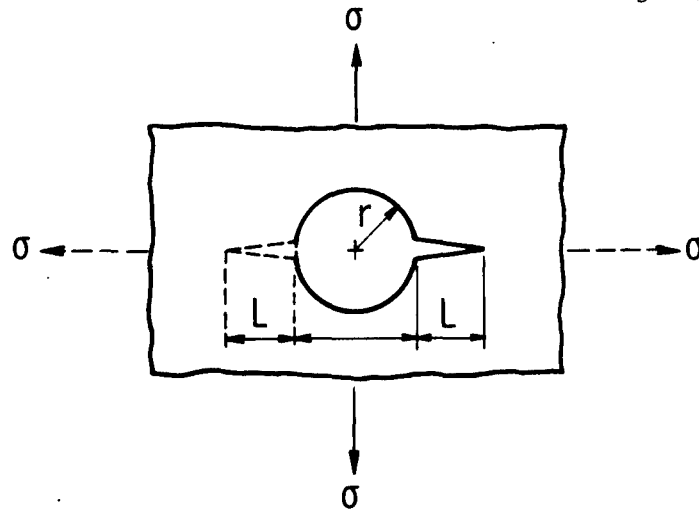
Sec. 8.2 Fig. 11 - An infinite array of colinear cracks in an infinite sheet (8, 9)



$$K_I = \sigma (\pi a)^{1/2} \left[\frac{2b}{\pi a} \tan \frac{\pi a}{2b} \right]^{1/2} h\left(\frac{a}{b}\right)$$

a/b	h(a/b)		
	L/b = 1.00	L/b = 3.00	L/b = ∞
0.1	1.13	1.12	1.12
0.2	1.13	1.11	1.10
0.3	1.14	1.09	1.09
0.4	1.16	1.06	1.06
0.5	1.14	1.02	1.02
0.6	1.10	1.01	1.01
0.7	1.02	1.00	1.00
0.8	1.01	1.00	1.00
0.9	1.00	1.00	1.00

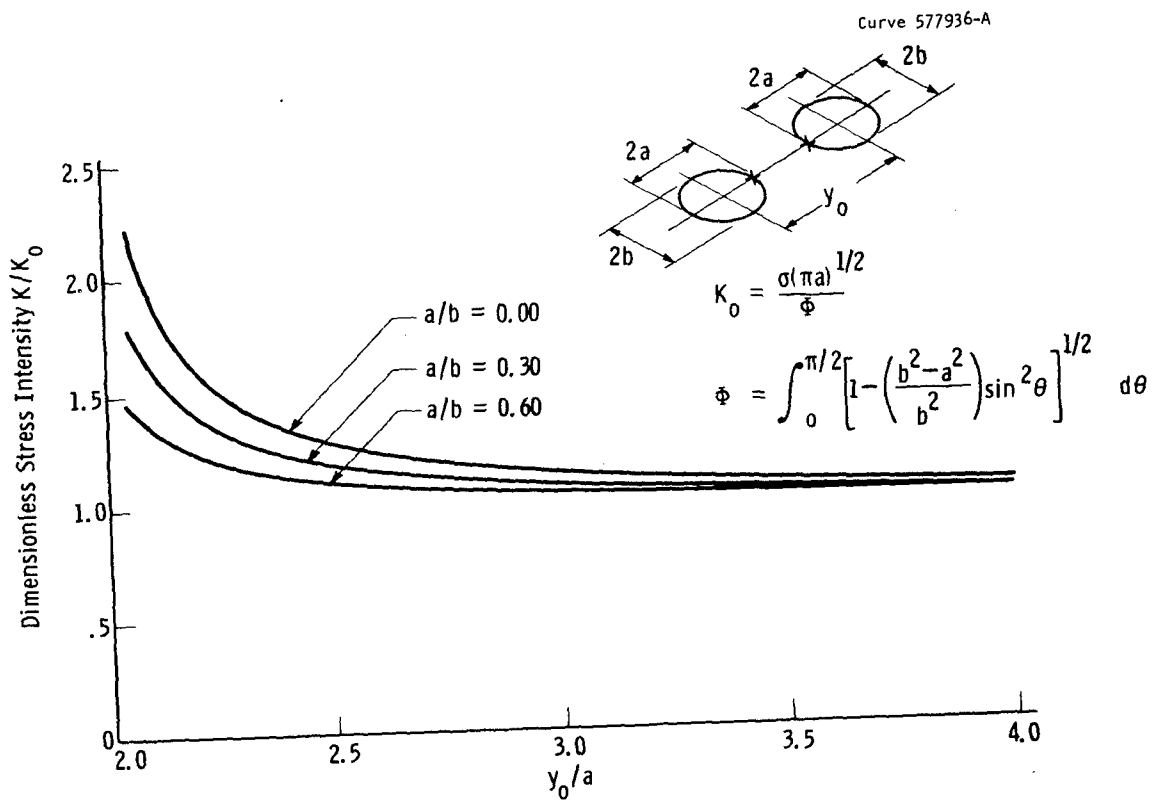
Sec. 8.2 Fig. 12 —Double-symmetric edge cracks in strip of infinite length subject to uniform tension (20)



$$K_I = \sigma (\pi L)^{1/2} F(L/r)$$

L/r	F(L/r), One Crack		F(L/r), Two Cracks	
	(uniaxial stress)	(biaxial stress)	(uniaxial stress)	(biaxial stress)
0.00	3.39	2.26	3.39	2.26
0.10	2.73	1.98	2.73	1.98
0.20	2.30	1.82	2.41	1.83
0.30	2.04	1.67	2.15	1.70
0.40	1.86	1.58	1.96	1.61
0.50	1.73	1.49	1.83	1.57
0.60	1.64	1.42	1.71	1.52
0.80	1.47	1.32	1.58	1.43
1.0	1.37	1.22	1.45	1.38
1.5	1.18	1.06	1.29	1.26
2.0	1.06	1.01	1.21	1.20
3.0	0.94	0.93	1.14	1.13
5.0	0.81	0.81	1.07	1.06
10.0	0.75	0.75	1.03	1.03
∞	0.707	0.707	1.00	1.00

Sec. 8.2 Fig. 13 —A crack (or cracks) emanating from a circular hole in a sheet (16)



Sec. 8.2 Fig. 14 — Stress intensity factor K at center of the approaching edge of two adjacent coplanar elliptical flaws subject to a uniform normal stress field (6)

decreases the stress intensity at the approaching edges of the cracks becomes significantly greater than at the remote edges and therefore initial fracture will occur across the ligament between the cracks. Now if the size of the large crack produced by the joining of the smaller cracks is significantly smaller than the theoretically calculated critical size for the applied loads then catastrophic questionable. The difficulty in determining whether or not the crack will continue growing or not after the ligament has fractured is related to the fact that the stress intensity required to sustain a running crack can be smaller than that required for initial crack extension. This is particularly true for temperature and strain rate sensitive materials. At present the understanding of this effect has not progressed to the point where it can be used in design considerations.

8.2.5 TYPE OF LOADING

A reasonable approximation of the expected time-history of the external loads on a structure must be available if the life of the structure is to be estimated. Combining this information with (1) information of initial crack sizes and locations obtained from inspection or proof testing (8.2.3), and (2) the relationship between external loads and crack tip stress intensities (8.2.2), the time-history of the stress intensity factors of cracks in the structure can be estimated. From a knowledge of the variation of the crack tip stress-intensity with time and by use of slow crack growth information the size of the crack can be predicted as a function of time (8.3.4). And, of course, a knowledge of K_c or K_{Ic} makes it possible to determine when failure can be expected.

If the external load is cyclic, the mean loads, range of loading, and length of cycle must be known. In cases where the material is susceptible to slow crack growth under sustained loading, the time periods at various loads must be considered in the life calculations. When strain rate sensitive materials are used the time rate of load application becomes a significant factor.

The expected thermal time history of the structure should also be known. The variation of the crack tip stress intensities due to thermal stresses contributes to crack growth and failure to the same degree as variation caused by external loads. In addition, since the crack growth rates and critical stress intensities are functions of material temperature, the expected temperature history around known and suspected cracks must be considered when life estimates are being made.

Section 8.2 References

1. W. F. Brown, Jr. and J. E. Srawley--Task Group of ASTM Committee E24, Sub I, "Plane Strain Crack Toughness Testing," Draft of 6th Committee Report distributed at E24 meeting, Washington, D. C., February 1, 1966.
2. R. B. Anderson and F. L. Sullivan, "Fracture Mechanics of Through-Cracked Cylindrical Pressure Vessels," NASA Technical Note D-3252.
3. R. E. Peterson, "Interreaction Effects of Neighboring Holes and Cavities with Particular Reference to Pressure Vessels and Rocket Motor Cases," Trans. ASME, J. Basic Engineering, V. 87, Series D, No. 4, December, 1965, p 879.
4. H. D. Greenberg, "An Engineering Basis for Establishing Radiographic Acceptance Standards for Porosity In Steel Weldments," Trans. ASME, J. Basic Engineering, V. 87, Series D, No. 4 December, 1965, p 887.
5. W. F. Payne, "Incorporation of Fracture Information In Specifications," From Fracture Toughness Testing," ASTM STP 381, May, 1965, p 357.
6. G. R. Irwin and J. A. Kies, "Fracture and Fracture Dynamics," Welding Journal Res. Suppl., p 95s - 100s, February, 1952.
7. J. E. Srawley, M. H. Jones, B. Gross, "Experimental Determination of the Dependence of Crack Extension Force on Crack Length for a Single-Edge-Notch Tension Specimen," NASA Technical Note D-2396.
8. B. Gross, J. E. Srawley, and W. F. Brown, Jr., "Stress Intensity Factors for a Single-Edge-Notch Tension Specimen by Boundary Collocation of a Stress Function," NASA Technical Note D-2395, 1964.
9. O. L. Bowie, "Rectangular Tensile Sheet with Symmetric Edge Cracks," Journal of Applied Mechanics, June, 1964.
10. P. C. Paris and G. Sih, "Stress Analysis of Cracks," ASTM Special Technical Publication No. 381.
11. F. E. Erdogan, "On the Stress Distribution in Plates with Colinear Cuts Under Arbitrary Loads," Proceedings, Fourth U. S. National Congress of Applied Mechanics, 1962.
12. H. Neuber, "Kerbspannungslehre," Springer, Berlin, 1937 and 1958; English translation available from Edwards Bros., Ann Arbor, Mich.

13. D. H. Winne and B. M. Wundt, "Application of the Griffith-Irwin Theory of Crack Propagation to Bursting Behavior of Disks," Transactions ASME, Vol. 80, 1958.
14. L. A. Wigglesworth, "Stress Distribution in a Notched Plate," Mathematika, Vol. 4, 1957.
15. G. R. Irwin, "The Crack Extension Force for a Part Through Crack in a Plate," Transactions ASME, J. of Applied Mechanics, 1962.
16. O. L. Bowie, "Analysis of an Infinite Plate Containing Radial Cracks Originating from the Boundary of an Internal Circular Hole," J. of Mathematics and Physics, Vol. 35, 1956.
17. G. E. Barenblatt, "Mathematical Theory of Equilibrium Cracks in Brittle Fracture Theory," Advances in Applied Mechanics, Vol. VII, Academic Press, New York, 1962.
18. G. R. Irwin, "Analysis of Stresses and Strains Near the End of a Crack Traversing a Plate," Transactions ASME, J. of Applied Mechanics, 1957.
19. G. R. Irwin, "Fracture," Handbuch der Physik, Vol. VI, Springer, Berlin, 1958.
20. O. L. Bowie, "Rectangular Tensile Sheet with Symmetric Edge Cracks," Transactions ASME, J. of Applied Mechanics, Vol. 31, Ser. E, No. 2, June, 1964.
21. L. R. Hall and A. S. Kobayashi, "On the Correction of Stress Intensity Factors for Two Embedded Cracks," Boeing Structural Development Research Memorandum No. 9, The Boeing Co., 1963
22. C. F. Tiffany and J. N. Masters, "Applied Fracture Mechanics," ASTM Special Technical Publication No. 381.

TABLE OF CONTENTS

Section 8.3

	<u>Page</u>
8.3 Application of Information, Procedures and Data	256
8.3.1 Design Considerations.	256
8.3.2 Evaluation and Selection of Materials.	257
8.3.2.1 Evaluating Resistance to Catastrophic Failure for Static Loading.	257
a. Acquiring Basic Design Information and Material Requirements	257
b. Selection of Basic Type of Fracture Toughness Specimen.	258
c. Selection of Size of Test Specimen and Testing for K_{Ic}	258
d. Evaluation of Materials Based on K_{Ic} Data and Design Requirements	259
e. Summary	263
8.3.2.2 Evaluation and Selection of Materials for Resis- tance to Fracture Under Cyclic or Sustained Loading Conditions.	264
a. Obtaining Crack Growth Rate Data.	265
b. Evaluation of Crack Growth Rate Data.	265
c. Summary of Possible Crack Growth Behaviors.	273
8.3.3 Quality Control Inspection and Specifications.	280
8.3.3.1 Inspection and Quality Control.	281
8.3.3.2 Quality Control Specifications.	283
8.3.3.3 Summary	284
8.3.4 Performance and Life Expectancy Evaluation	285
8.3.4.1 Information Needed to Make Life Evaluation.	286
8.3.4.2 Procedure for Estimating Life Under Cyclic Loading Condition	288
8.3.4.3 Limitations of Procedure.	290

TABLE OF CONTENTS (Cont.)

	<u>Page</u>
8.3.4.4 Simplified Method of Predicting Cyclic Life . .	292
8.3.4.5 Life Predictions When Slow Crack Growth Occurs Under Sustained Loading.	295
8.3.5 Summary.	297

LIST OF FIGURES

Section 8.3

	<u>Page</u>
Figure 1. Crack growth rate as a function of stress intensity factor for HP9-4-25 steel.....	267
Figure 2. Crack growth rate as a function of stress intensity for 7079-T6 aluminum.....	267
Figure 3. Combined flaw growth data for HP9-4-25 steel plate.	271
Figure 4. Combined cyclic flaw growth data for 7079-T6 aluminum plate.....	271
Figure 5. Crack growth rate as a function of stress intensity for HP9-4-25 steel (log-log plot).....	277
Figure 6. Crack growth rate as a function of stress intensity for 7079-T6 aluminum (log-log plot).....	277
Figure 7. Cyclic life as a function of initial crack size for Materials A and B (Case 1).....	278
Figure 8. Cyclic life as a function of initial crack length for Materials A and B (Case 2).....	278
Figure 9. Cyclic life as a function of initial crack length for Materials A and B (Case 3).....	279
Figure 10. Schematic representation of crack growth rate plotted as a function of ΔK for fixed values of $\gamma = K_{\text{mean}}/\Delta K$	288
Figure 11. Variations of external load with time.....	291
Figure 12. Schematic representation of cyclic flaw growth.....	293
Figure 13. Combined cyclic flaw growth for 7079-T6 aluminum plate.....	293

LIST OF FIGURES (Cont.)

	<u>Page</u>
Figure 14. Schematic representation of sustained stress flaw growth.....	294
Figure 15. Sustained stress data for room-temperature tests of 17-7PH steel.....	294

Section 8.3

APPLICATION OF INFORMATION, PROCEDURES AND DATA

The preceding sections 8.1. and 8.2. have described the general use of fracture mechanics technology and the type of information which is necessary for its application. In this section attention will be centered on the application of the technology in the various areas which must be considered when designing and selecting a material against fracture. The areas of consideration are as follows:

1. Basic design features and requirements
2. Evaluation and selection of materials
3. Establishment of specifications and quality control criteria
4. Performance and life expectancy evaluations

The interreaction of the considerations in these various areas are emphasized.

8.3.1 DESIGN CONSIDERATION

In general the resulting shape and size of an engineered structure is a function of the intended functional purpose of the structure, available materials, means of fabricating, available inspection technique, and cost. Fracture considerations play a role in each of these interrelated design considerations. The degree of the role played by fracture considerations, of course, varies greatly from case to case but a few typical situations will be mentioned. If a relatively brittle material must be used for a component, then one fabricating process may be preferred over another because of the relative size of defects which may be produced by the respective fabricating procedure. If the shape of the structure must be such that specific areas can't be properly

inspected, then some balance must be obtained between toughness of material and minimizing size of initial cracks produced in fabrication. The toughness of the material used will also depend upon the degree to which failures can be tolerated. Similarly, the life requirements of the structure will influence the crack growth rate requirements of the material used. These and many other examples of the influence of the fracture considerations can be given, but of course each design situation must be uniquely considered.

The use of fracture mechanics concepts in design makes it possible to handle fracture considerations in a quantitative manner whereas most other methods are very qualitative. Some specific illustrations are provided in the sections which follow.

8.3.2 EVALUATION AND SELECTION OF MATERIALS

One of the most fruitful areas in which fracture mechanics technology can and is being employed concerns the comparison, evaluation and selection of materials. The technology provides the materials engineer and designer with a tool for making direct, quantitative assessments of the relative merits of various materials in terms of resistance to catastrophic fracture, resistance to slow (fatigue) crack propagation, tolerance for defects, applicability for inspection, and overall costs of acquiring a satisfactory component.

8.3.2.1 Evaluating Resistance to Catastrophic Fracture (K_{Ic}) for Static Loading

a. Acquiring Basic Design Information and Material Requirements

Evaluation of the resistance to catastrophic brittle fracture (K_{Ic}) require the consideration of several factors. The first step involves cooperation between the materials engineer and designer. Before the materials engineer plans an evaluation program he must obtain basic information from the designer relative to the size and shape of the component, the type of loading involved, the magnitude and orientation of the primary stresses, environmental conditions, etc. From this information the materials engineer can make judgments about how the component

will be fabricated, i.e., rolled, forged, welded, etc., and what the final condition of the material will be. Then it is possible to estimate what type, size, shape and orientation of defects are likely to be present, i.e., inclusion stringers, weld cracks, fatigue cracks which may develop during operation, etc. The anticipated defects and their orientation relative to the primary stresses can then be established.

b. Selection of the Basic Type of Fracture Toughness Specimen

The next step is to select the type of fracture toughness (K_{Ic}) test specimen that will be employed in the evaluation program. The basic form of the material as it is used in the component (sheet, plate, bar stock, forgings, etc.) will in most cases dictate the type of specimen that can be employed. Consideration must also be given to the type of defect to be employed with the specimen; i.e., edge cracks, center cracks, internal defects, surface defects, etc. In some of the basic specimen forms, the type of notch configuration is fixed, e.g., notched round. However, in others there is some option, for example, sheet or plate specimens can have edge, center, internal or surface types of notches. Wherever possible the type of notch to be employed should correspond to that envisioned in service. The test specimen should be oriented such that the plane of the notch in the specimen corresponds to that of the most likely defect in the component. Consideration must also be given to the relative orientations of the stresses and the notches in the test specimen and component. In situations when there may be some conflict of these considerations, it is good general practice to use the worst possible combination of conditions and thereby produce conservative data.

c. Selection of Size of Test Specimen and Testing for K_{Ic}

After the basic form of test specimen notch and orientation have been determined, the next problem is deciding how large the specimen should be. The most current general rule⁽¹⁾ that can be used in estimating the minimum size of specimen that will provide plane strain conditions is that the thickness "B" and crack length "a" should be $\geq 2.5 \left(\frac{K_{Ic}}{\sigma_{ys}} \right)^2$. Once "a" and "B" are determined the rest of the specimen

dimensions are also established since the other dimensions are in direct proportion to "a" or "B". For most materials it is generally possible to make an approximate estimate of $\frac{K_{Ic}}{\sigma_{ys}}$, and for the preliminary tests it is advisable to choose a value on the high side of the anticipated range. If, after the preliminary tests have established the K_{Ic} level, it is seen that the estimate was too high an appropriate reduction in specimen size can be made for subsequent tests. After the optimum specimen size has been established for each of the materials being evaluated, the test program can proceed. Proper test procedures and techniques, as described in Section 6.2.4, should be employed to insure the attainment of valid K_{Ic} data at the temperature, strain rate and environment of interest. A sufficient number of tests should be conducted to establish the scatter due to material inhomogeneities, and to define the minimum K_{Ic} level that could be expected in the material.

d. Evaluation of Materials Based on K_{Ic} Data and Design Requirements

The remaining task is to evaluate the materials based on the data accumulated from the test program. This can best be illustrated by the use of a hypothetical example. Three materials--a steel, a titanium and an aluminum alloy --are initially selected as potential candidate materials for an application where one of the foremost design considerations is minimum weight. The yield strength of each is chosen so that the three materials have nearly equivalent strength/weight ratios. The yield strengths and the K_{Ic} values from the test programs are as follows:

<u>Alloy</u>	<u>Density</u> #/in ³	<u>σ_{ys}</u> ksi	<u>$\sigma_{ys}/\text{Density}$</u> x1000 in	<u>K_{Ic}</u> ksi√in.
Steel	.284	250	880	100
Aluminum	.098	85	870	30
Titanium	.163	140	860	80

The most deleterious type of defect that could prevail in the application is judged to be a semi-elliptical surface flaw with a depth "a" to length "c" ratio of 0.2. (Other depth to length ratios can be handled most

conveniently using the flaw shape parameter "Q" described in reference 2.) It is located in a thick plate loaded in tension. From the initial design consideration the average applied stress normal to the defect is 1/2 of the yield strength in the case of each material. Now the materials engineers must decide which material provides the most fracture resistance. One way to approach this question is to establish which material requires the largest critical flaw size for catastrophic fracture for the prevailing conditions. As a result of the design and the materials test program the following factors are known.

	Steel	Ti	Al
1. K_{Ic} value of each material (ksi $\sqrt{\text{in}}$)	100	80	30
2. σ_{ys} of each material (ksi)	250	140	85
3. Type defect-semi-elliptical surface flaw whose depth is 1/5 of its length			
4. Loading - tension (static)			
5. Applied Stress - 1/2 σ_{ys} (ksi)	125	70	42.5
6. Equation for this type of flaw and loading geometry as illustrated in Figure 1			

$$a_{cr} = \frac{K_{Ic}^2 \left[\phi^2 - .212 \left(\frac{\sigma}{\sigma_{ys}} \right)^2 \right]}{1.21 \pi \sigma^2}$$

a_{cr} = unknown critical crack depth-inches

ϕ^2 = 1.3 (for $a/c = .4$ from graph Figure) (same for each material)

σ = applied stress = 1/2 yield strength for each material (ksi)

σ_{ys} = 0.2% yield strength each material (ksi)

K_{Ic} = fracture toughness each material (ksi $\sqrt{\text{in}}$.)

By inserting the appropriate numbers for σ_{ys} , σ and K_{Ic} into the equation, the critical crack depth can be determined for each material. The results are as follows:

	Depth (inches) a_{cr}	Length (inches) $2c$
Steel	.212	1.06
Al	.165	0.83
Ti	.432	2.16

Thus, it is apparent that for the conditions imposed, the titanium alloy is most fracture resistant in terms of requiring the largest critical size defect for catastrophic fracture.

This conclusion could also have been reached by a less tedious method by considering the K_{Ic}/σ_{YS} ratios for the various materials which are as follows:

	$\frac{K_{Ic}}{\sigma_{YS}}$	$\left(\frac{K_{Ic}}{\sigma_{YS}}\right)^2$
Steel	.400	.160
Aluminum	.353	.125
Titanium	.572	.327

The titanium, having the highest $\frac{K_{Ic}}{\sigma_{YS}}$ ratio, could be expected to be the most tough material for the given application. Since the applied stress is a fixed percentage of the yield strength in all materials, the critical defect size will be proportional to the ratio of $\left(\frac{K_{Ic}}{\sigma_{YS}}\right)^2$. This is apparent if one considers the terms in the equation used above.

ϕ^2 and $\frac{\sigma}{\sigma_{YS}}$ are constants for all three materials. The σ in the denominator is fixed at $\sigma_{YS}/2$ for each material. Therefore a_{cr} is proportional to $\frac{K_{Ic}}{(.5\sigma_{YS})^2}$. So long as the applied stress is fixed at a given percentage of the yield strength for each material, the ratio of $\left(\frac{K_{Ic}}{\sigma_{YS}}\right)^2$ will provide an accurate index of the relative critical defect sizes.

The resistance to catastrophic fracture could also be evaluated by calculating the maximum allowable applied stress for equivalent defects in each material. The defect chosen for these calculations should correspond to the worst possible combination of type, shape, orientation and size, and to the minimum size that could readily be found with the available nondestructive inspection techniques. While it is obvious that the same ranking of the fracture resistance of the materials will

be maintained, there are some additional benefits that can be derived from these computations.

Again the most harmful type of defect is envisioned as a semi-elliptical surface flaw with a depth to length ratio of 0.2. Based on considerations of the practical capability of available nondestructive inspection tools, the minimum detectable flaw is 0.15 deep by 0.75 long. The same basic equation is employed to calculate the critical applied stress for fracture.

$$\sigma^2 = \frac{K_{Ic}^2 \left[\phi^2 - .212 \left(\frac{\sigma}{\sigma_{YS}} \right)^2 \right]}{1.21 \pi a}$$

$a = 0.15''$ the assumed crack depth, with a length $0.75''$. The critical fracture stresses for the various materials are shown below.

<u>Material</u>	<u>σ Critical Stress</u>
	ksi
Steel	144
Aluminum	43
Titanium	112

With this information the designer can now re-evaluate his original choice of a design stress equivalent to $1/2$ of the yield strength. Having assurance that a defect of the type and size used in the calculations of fracture stress (semi-elliptical surface flaw $0.15''$ deep by $0.75''$ long) can consistently and reliably be detected in the component, the designer can proceed to establish the safety factor in his design. At first appearance, it may seem that the steel is the best material since it requires the highest stress for fracture in the presence of the given defect. However, to properly assess the safety factor, it is necessary to consider the ratio of the fracture stress to the design stress ($1/2$ of yield strength). The pertinent data for the three materials for the given type and size of defect are shown below:

<u>Material</u>	<u>Yield Strength σ_{YS} ksi</u>	<u>Design Stress .5σ_{YS} ksi</u>	<u>Fracture Stress σ ksi</u>	<u>Safety Factor $\sigma/.5\sigma_{YS}$</u>
Steel	250	125	144	1.15
Aluminum	85	42.5	43	1.01
Titanium	140	70	112	1.60

From these data it is readily apparent that the titanium provided the greatest safety factor and resistance to fracture. The steel and aluminum alloys would be quite marginal since their fracture strengths do not exceed the design stress by any significant amount. At this point the designer could alter his design stress for each of the materials to provide whatever safety factor is desired. However, it must be recognized that any decrease in design stress to raise the safety factor would necessitate an undesirable increase in weight (one of the original requirements was minimum weight.)

Economic considerations are also an important factor in the final evaluation of the fracture resistance of candidate materials for a given application. In the previous example the titanium alloy exhibited a marked superiority over the steel and aluminum alloys. However, the cost of the titanium alloy is approximately twice that of steel and six times that of the aluminum alloy. Thus, costs would have to be factored into the overall design and material selection consideration. The fracture toughness data (K_{IC}), used in conjunction with appropriate information concerning design stresses and defects and costs thus provides the basis for quantitative considerations of all of the factors involved.

e. Summary

The type of fracture toughness evaluations for plane strain failure under static loading that were described in the preceding paragraphs can be applied equally as well to various types of applications, materials, loading, geometry, and defect types and sizes. The same type of logic and the same sequence of considerations are necessary as summarized below.

1. Obtain basic information
 - a. Design requirements
 - b. Methods of fabrication and metallurgical condition
 - c. Anticipated types of defects
2. Select basic type of fracture toughness specimen
3. Select the absolute size of the specimens
4. Obtain the necessary K_{Ic} fracture toughness data
5. Evaluate the materials based on K_{Ic} data and the design requirements
 - a. Calculations of critical size defects for given design stresses
 - b. Calculations of critical fracture stresses for various types and sizes of defects
 - c. Relationship of defects to nondestructive inspection capabilities
 - d. Establishing safety factors for various given conditions
 - e. Re-evaluation of original design stipulations
 - f. Modifications based on composite considerations of all factors involved including economics
6. Finalize design and material selection

8.3.2.2 Evaluation and Selection of Materials for Resistance to Fracture Under Cyclic or Sustained Loading Conditions

If an application involves cyclic or sustained loading, some additional steps must be taken when evaluating materials resistance to fracture. These involve consideration of the crack growth rate characteristics of the materials. While the K_{Ic} data facilitate a quantitative assessment of the critical combinations of defects and stresses for catastrophic failure, the useful life of a component under cyclic loading is governed by the rate of growth of defects from a sub-critical to critical size. As discussed in earlier sections (7.3.1 and 6.2.2.12) the cracks growth rates are related to K , the stress intensity factor at the crack tip. Therefore, a comparison of the crack

growth rates of materials in terms of K provides a convenient method of assessing their relative resistance to the propagation of cracks. In evaluating materials for a specific application, the relative crack growth rates must be considered in conjunction with other factors; i.e., the size of the defects initially present in the material, the critical defect size for catastrophic fracture, the applied stresses, nondestructive inspection capabilities, environmental effects, type of loading, cycle spectrum, etc. These aspects are discussed in subsequent paragraphs.

a. Obtaining Crack Growth Rate Data

The selection of a suitable test specimen for acquiring crack growth rate data for the purpose of comparing materials involves many of the same considerations as were necessary in selecting a specimen for K_{Ic} testing. The material should be in the same metallurgical condition as it is in the component. The orientation of the starting defect and the plane of crack propagation should coincide with those anticipated in service. In testing, the environment, loads, and cyclic spectrum should simulate insofar as possible those of the application. Any of the K_{Ic} fracture toughness specimens, whose basic shape is suitable to the form of the available test material, and to the defect and component geometry, can be employed to obtain crack growth rate data so long as a precise analysis for the variation of K with crack length is available for a suitable range of crack lengths. Instrumentation capable of measuring the crack length as a function of number of cycles (or time for sustained loading) is also essential.

Knowing the maximum load, the crack length, and the total number of cycles for any given point during the test, and having an expression describing K , it is possible to construct curves of the basic crack growth rates from test results. Some examples of data obtained from tests conducted in Phase II of this project (Section 7.3) are shown in Figs. 1 and 2.

b. Evaluating Crack Growth Rate Data

One's first reaction is that these data (Figs. 1 and 2) provide a basis for comparing the crack growth rates of the two materials at

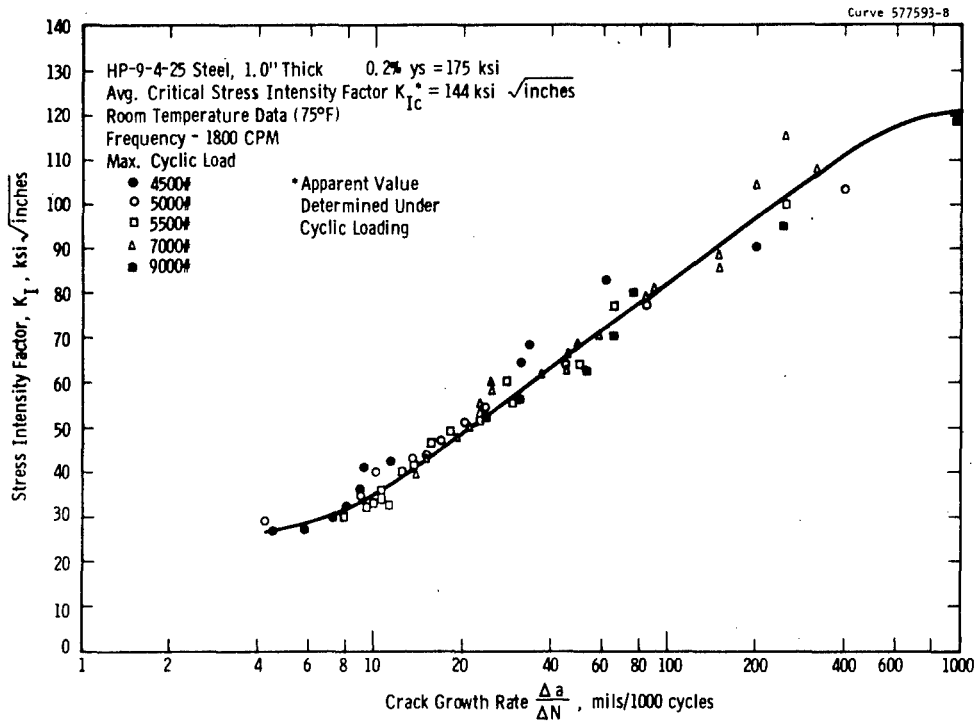
equivalent values of K . For example, at a K_I value of 30 ksi $\sqrt{\text{in.}}$, the relative crack growth rates are aluminum 0.12 mils/cycle and steel 0.008 mils/cycle. Thus, one might conclude the steel is obviously the most fracture resistant material since its growth rate at a given K is only 7% of that for the aluminum.

However, a comparison based on the growth rates at an equivalent K value is not a very realistic way to evaluate materials, particularly those having drastic differences in strength and fracture toughness. In any specific application it is very unlikely that the two materials would be exposed to equivalent K 's since the design stresses would undoubtedly be considerably different; e.g., assuming a design stress of 1/2 the yield strength for both materials, the steel is subjected to 87,500 psi and the aluminum to 32,500 psi. Therefore, in order to have an equivalent K_I in each material, the size of a given type of defect would have to be much larger in the aluminum because of the lower stress.

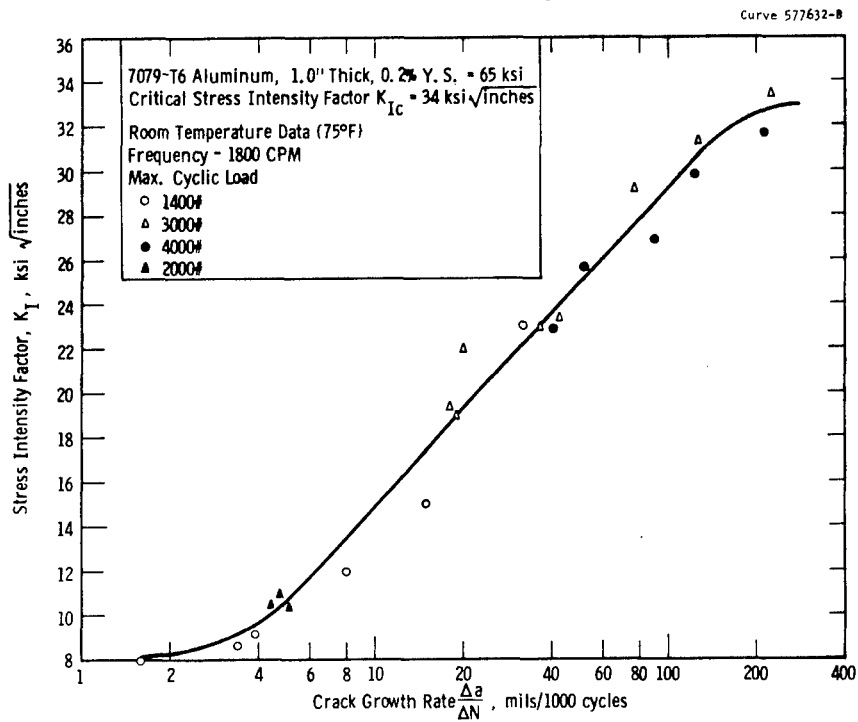
A more realistic and practical approach for comparing materials is to evaluate their crack growth characteristics under given application conditions. As a hypothetical example, let us consider the steel and aluminum alloys for which the data are given in Figs. 1 and 2. The component of interest is a thick plate cyclic loaded in tension. The cyclic loading is sinusoidal, and the stress varies from zero to maximum tension during each cycle. The design fixes σ_{max} as 1/2 the yield strength for each material: 88 ksi for steel and 32 ksi for aluminum. The worst possible type of flaw that is envisioned is a semi-elliptical surface flaw with a depth to length ratio of 0.2. The minimum size flaw that could be detected in either material by available nondestructive inspection techniques is 0.15" deep by 0.75" long. Therefore, each material is assumed to contain a flaw of this size at the beginning of life. Under these prevailing circumstances, which material has the longest life?

Solution:

Step 1. The first step is to compute the value of the initial stress intensity, K_{Ii} , for each material for the prevailing conditions of defect



Sec. 8.3 Fig. 1 -Crack growth rate as a function of stress intensity factor for HP-9-4-25 steel as determined on the "IT" WOL fracture toughness specimen



Sec. 8.3 Fig. 2 -Crack growth rate as a function of stress intensity factor for 7079-T6 aluminum as determined on the "IT" WOL fracture toughness specimen

size and stress. The appropriate expression for K_{Ii} for the stipulated defect and component geometry is:

$$K_{Ii}^2 = 1.2 \pi a \sigma^2 \left[\frac{1}{\phi^2 - 0.212 \left(\frac{\sigma}{\sigma_{YS}} \right)^2} \right]$$

where: $a = \text{crack} = 0.15'' = \text{specified}$

$\sigma = \text{applied stress (max during cycle)} = 1/2 \sigma_{YS}$ each material

steel = 88 ksi aluminum = 32 ksi

$\sigma_{YS} = \text{yield strength, steel} = 175 \text{ ksi, aluminum} = 65 \text{ ksi}$

$\phi^2 = 1.3$ for specified flaw geometry

The calculations reveal the following:

Steel

$$K_{Ii}^2 = \frac{1.2 \pi (.15) (88,000)^2}{1.3 - .212 \left(\frac{88,000}{175,000} \right)^2}$$

$$K_{Ii} = 59,000 \text{ psi } \sqrt{\text{in.}}$$

Aluminum

$$K_{Ii}^2 = \frac{1.2 \pi (.15) (32,000)^2}{1.3 - .212 \left(\frac{32,000}{65,000} \right)^2}$$

$$K_{Ii} = 21,500 \text{ psi } \sqrt{\text{in.}}$$

The crack growth rates for the two materials at the beginning of life can now be determined from Figs. 1 and 2 using their respective K_I values for the imposed conditions. The results are as follows:

	K_I (psi $\sqrt{\text{in.}}$)	Crack Growth Rate (mils/cycle)
Steel	59,900	.035
Aluminum	21,500	.030

However, a knowledge of the crack growth rates at the beginning of life is not sufficient to determine the respective life expectancy of each material. One must consider the change in K_I and the associated change in crack growth rates for each material as the crack grows during service. Step 2. Growth rate data illustrated in the form shown in Figs. 3 and 4 provide a convenient method for evaluating life expectancy without becoming intimately involved with changes in K_{Ic} and growth rates. Figures 3 and 4 are constructed from the same basic test data as used to construct Figs. 1 and 2. To utilize Figs. 3 and 4 it is necessary to know the ratio of K_{Ii} to K_{Ic} . The previous calculations in Step 1 showed that K_{Ii} is 59 ksi $\sqrt{\text{in.}}$ for steel and 21.5 ksi $\sqrt{\text{in.}}$ for aluminum. Since the K_{Ic} values for each material were known from static fracture toughness tests, the $\frac{K_{Ii}}{K_{Ic}}$ ratios are readily determined.

$$\text{Steel} \quad \frac{K_{Ii}}{K_{Ic}} = \frac{59,000}{144,000} = .41$$

$$\text{Aluminum} \quad \frac{K_{Ii}}{K_{Ic}} = \frac{21,500}{34,000} = .63$$

The cyclic life corresponding to these $\frac{K_{Ii}}{K_{Ic}}$ values may be determined directly from Figs. 3 and 4 - steel 1800 cycles and aluminum 4000 cycles.

Thus, for this specific example where both materials contained the same given size and type of defect, and were both stressed to 1/2 their yield strengths, the aluminum has the greatest life expectancy.

It should be emphasized at this point that the result of this example cannot be used to generalize the relative behavior of the two materials. For other conditions of initial defect sizes and/or applied stresses, it is possible that the steel could have the greater life

expectancy. This is demonstrated in the following table which shows the life expectancy of the two materials for a wide range of initial defect sizes and for a constant applied stress of $\sigma_{YS}/^2$.

Initial Defect Depth a_i (inches)	Initial Stress Intensity Factor K_{Ii} (ksi $\sqrt{\text{in.}}$)		$\frac{K_{Ii}}{K_{Ic}}$		Cycles to Failure N (Life Expectancy)	
	Steel	Aluminum	Steel	Aluminum	Steel	Aluminum
	.05	19.6	7.2	.136	.210	$>>300 \times 10^3$
.07	27.5	10.1	.191	.297	$>100 \times 10^3$	100×10^3
.10	39.4	14.3	.274	.420	30×10^3	21×10^3
.15	59.0	21.5	.410	.632	1.8×10^3	4×10^3
.20	78.8	28.7	.540	.845	$.37 \times 10^3$	1.5×10^3
.25	98.4	35.9	.683	$>1.$	$.25 \times 10^3$	---

From the table it may be seen that when the initial defect depth is 0.15 inches or larger, the aluminum will have the longer life N. However, when the initial defect depth is 0.10 inches or smaller, the steel will have the greater life expectancy. Although the steel has the larger absolute value of fracture toughness, K_{Ic} , and therefore has the largest critical crack size for catastrophic failure, it also has a greater crack growth rate for a given change in K as seen from the differences in slope of the growth rate curves shown in Figs. 5 and 6. Therefore, it is possible to have a "cross-over" situation between the life expectancies of steel and aluminum, as noted in the table.

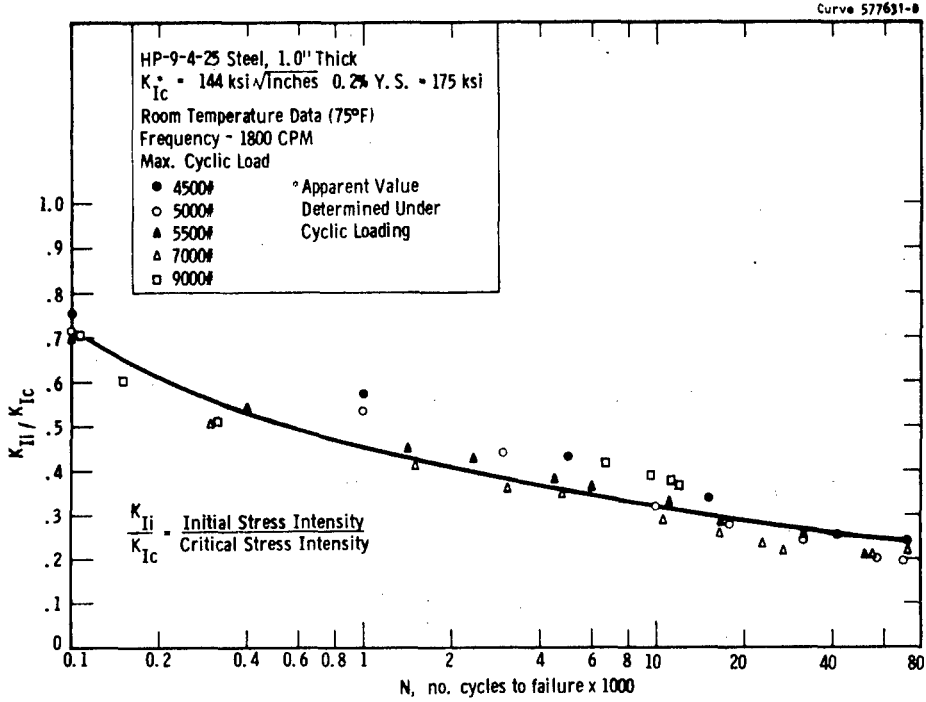
The materials could also be compared in another manner by using the data provided in Figs. 3 and 4 to answer the question of which material could tolerate the largest initial defect (of a given type) that would not grow to a critical size during some given minimum lifetime for the component.

Example

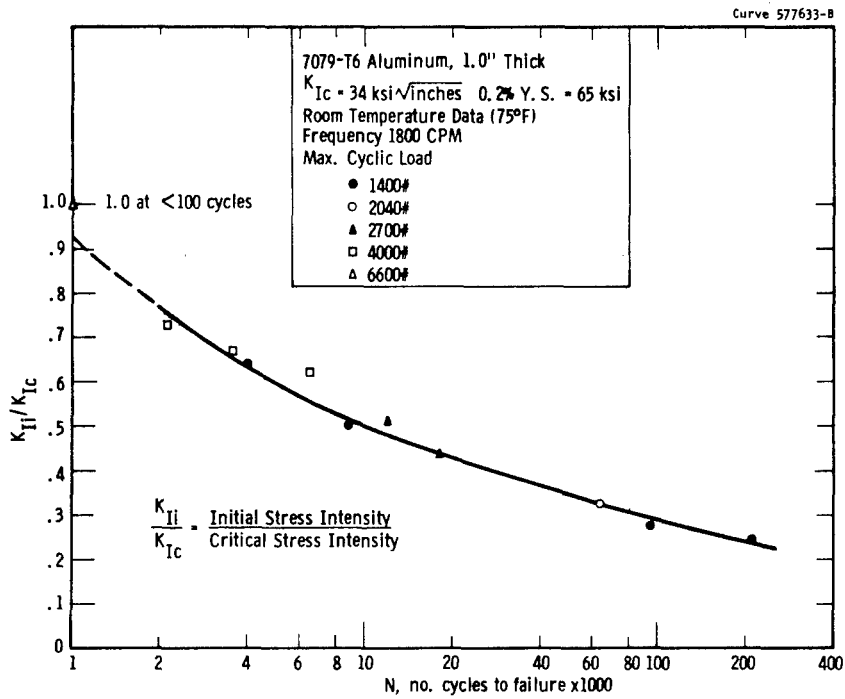
Known Information

Plate cyclic loaded (sinusoidal) in tension

Required life 50,000 cycles



Sec. 8.3 Fig. 3 — Combined cyclic flaw growth data for HP-9-4-25 steel plate



Sec. 8.3 Fig. 4 — Combined cyclic flaw growth data for 7079-T6 aluminum plate

Applied stress (max stress during cycle) = 1/2 yield strength

Steel = 88,000 psi

Aluminum = 32,000 psi

Type Defect - semi-elliptical surface flaw with $a/c = .4$

Fracture toughness, K_{Ic}

Steel = 144,000 psi $\sqrt{\text{in.}}$

Aluminum = 34,000 psi $\sqrt{\text{in.}}$

Unknown

Which material can tolerate the largest initial defect?

Solution

Step 1. From Figs. 3 and 4 find the $\frac{K_{Ii}}{K_{Ic}}$ ratio corresponding to the desired life of 50,000 cycles

Steel $\frac{K_{Ii}}{K_{Ic}}$ at 50,000 cycles = 0.25

Aluminum $\frac{K_{Ii}}{K_{Ic}}$ at 50,000 cycles = 0.34

Step 2. Knowing K_{Ic} and $\frac{K_{Ii}}{K_{Ic}}$ ratio corresponding to 50,000 cycles solve for K_{Ii} .

Steel $K_{Ii} = 0.25 K_{Ic} = 0.25 (144,000 \text{ psi}\sqrt{\text{in.}}) = 36,000 \text{ psi } \sqrt{\text{in.}}$

Aluminum $K_{Ii} = 0.34 K_{Ic} = 0.34 (34,000 \text{ psi } \sqrt{\text{in.}}) = 11,500 \text{ psi } \sqrt{\text{in.}}$

Step 3. Since K_{Ii} is dependent upon stress and defect size, it is now possible to solve for defect size knowing stress. For semi-elliptical surface defect with $a/c = 0.4$ the following expression is appropriate

$$a_i = \frac{K_{Ii}^2 \left[\phi^2 - 0.212 \left(\frac{\sigma}{\sigma_{YS}} \right)^2 \right]}{1.21 \pi \sigma^2}$$

Steel

$$a_i = \frac{(36,000)^2 \left[1.3 - 0.212 \left(\frac{88,000}{175,000} \right)^2 \right]}{1.2 \pi (88,000)^2}$$

$$a_i = 0.056''$$

defect = 0.056" deep by 0.28" long

Aluminum

$$a_i = \frac{(11,500)^2 \left[1.3 - 0.212 \left(\frac{32,000}{65,000} \right)^2 \right]}{1.21 \pi (32,000)^2}$$

$$a_i = 0.043''$$

defect = 0.043" deep by 0.215" long

Thus, it is apparent that for the conditions imposed the steel could tolerate a slightly larger initial defect than could the aluminum. Since the difference in the maximum allowable initial defect size is not great, the ultimate choice of a material for this situation may depend more heavily on other comparative factors; i.e., the applicability and capability of nondestructive inspection techniques, the type and size of insidious defects as related to the maximum allowable initial defect size, availability, ease of fabrication, costs, etc.

c. Summary of Possible Crack Growth Behaviors

In many cases involving cyclic loading, the choice of the best material for a particular application is not only dependent on critical stress intensity, cyclic stress level, crack growth rate, and desired cyclic life, but also on the size of the maximum possible expected initial flaws. This situation was demonstrated in one of the examples given in the previous section (8.3.2.2.b). Some understanding of the interaction of all these effects can be gained by studying an idealized analytic solution for a particular crack growth situation. By assuming a simple crack growth rate law, an analytic relation can be obtained between initial crack size, applied cyclic load, critical stress intensity, crack growth rate parameters, and expected life.

For cyclic conditions in which the applied stress level varies between zero and a positive value most slow crack growth data, obtained to date under conditions for which fracture mechanics concepts apply, can be reasonably represented by a growth law of the form

$$\frac{dA}{dN} = C_0 K^n \quad (1)$$

where K is the range of the magnitude of stress intensity at the crack tip and C_0 and n are material constants. This type of law usually fits experimental data well over a wide range of K for each material, but normally deviation occurs at relatively low K 's and at K 's approaching K_{Ic} .

To obtain the desired analytic relationship between the parameters influencing cyclic life, the relation between applied stress, crack size, and crack tip, stress intensity must be known. It will be assumed that the relation has the form

$$K = \sigma \sqrt{Ma} \quad (2)$$

where for the cases to be considered in this analysis M is a constant. For the case of a through crack of length $2a$ in an infinite plate subject to a uniform stress field σ perpendicular to the plane of the crack, M is equal to π . For the example considered in Section 8.3.2.2.c (semi-elliptical surface flaw with depth to length ratio of 0.2) M equals 3.0, and a is flaw depth.

If the expression for K given by equation (2) is substituted into equation (1) and the necessary integration

$$\int_{a_i}^{a_{cr}} a^{-n/2} da = C_0 \sigma^n M^{n/2} \int_0^N dN \quad (3)$$

is performed between the initial crack size, a_i , at zero cycles, and crack size, a_{cr} , at fracture, the resulting expression for cyclic life N becomes

$$N = \frac{2}{(n-2) C_o M^{n/2} \sigma^n} \left[\frac{1}{(a_i)^{\frac{n-2}{2}}} - \frac{1}{(a_{cr})^{\frac{n-2}{2}}} \right] \quad \text{for } n \neq 2 \quad (4)$$

$$N = \frac{1}{C_o M \sigma^2} \ln \frac{a_{cr}}{a_i} \quad \text{for } n = 2$$

In obtaining these equations, it is assumed that the range of the cyclic applied stress σ remains constant through the life of the structure. If the design stress, σ , is established as a fraction, m , of the yield stress ($m = \sigma/\sigma_{YS}$) and use is again made of equation (2), then the equation for cyclic life can be put in the following convenient form.

$$N = \frac{2(K_{Ic}/\sigma_{YS})^2}{(n-2)m^2 M C_o K_{Ic}^n} \left\{ \left[\frac{(K_{Ic}/\sigma_{YS})^2}{m^2 M a_i} \right]^{\frac{n-2}{2}} - 1 \right\} \quad \text{for } n \neq 2 \quad (5)$$

$$N = \frac{1}{m^2 M C_o \sigma_{YS}^2} \ln \left[\frac{(K_{Ic}/\sigma_{YS})^2}{m^2 M a_i} \right] \quad \text{for } n = 2$$

These equations show the relationship between initial crack size, critical stress intensity, cyclic stress level, crack growth rate parameters, and expected cyclic life for the assumed conditions.

By use of equation (5), it will be beneficial to consider the effect of the variation of crack growth parameters (C_o, n) and initial crack size on the choice between two materials having specific plane strain critical stress intensities and yield stresses. The nominal stress level in both materials is assumed to be one-half of the yield stress ($m = 0.5$), and the presence of a semi-elliptical surface crack having a

depth to length ratio of 0.2 is assumed ($M = 3.0$). The toughness and yield strengths of the two materials considered are:

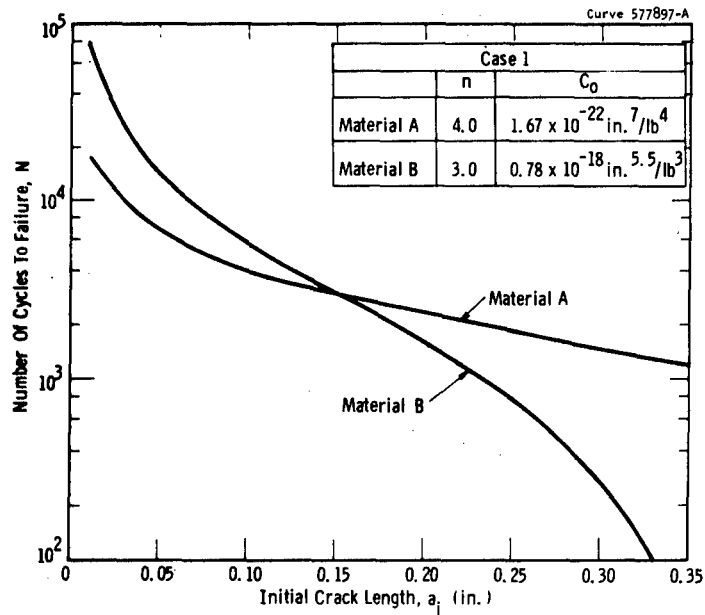
Material	K_{Ic}	σ_{YS}	(K_{Ic}/σ_{YS})
A	30,000 psi $\sqrt{\text{in.}}$	60,000 psi	0.50 $\sqrt{\text{in.}}$
B	100,000 psi $\sqrt{\text{in.}}$	125,000 psi	0.80 $\sqrt{\text{in.}}$

For the indicated stress levels the critical crack depth are $a_{cr} = 0.333$ in. for material A and $a_{cr} = 0.852$ in. for material B. The curves of cyclic life vs. initial crack depth for the two materials will be compared for three different combination of cyclic slow crack growth parameters. The growth parameters for the three cases are given in the following table.

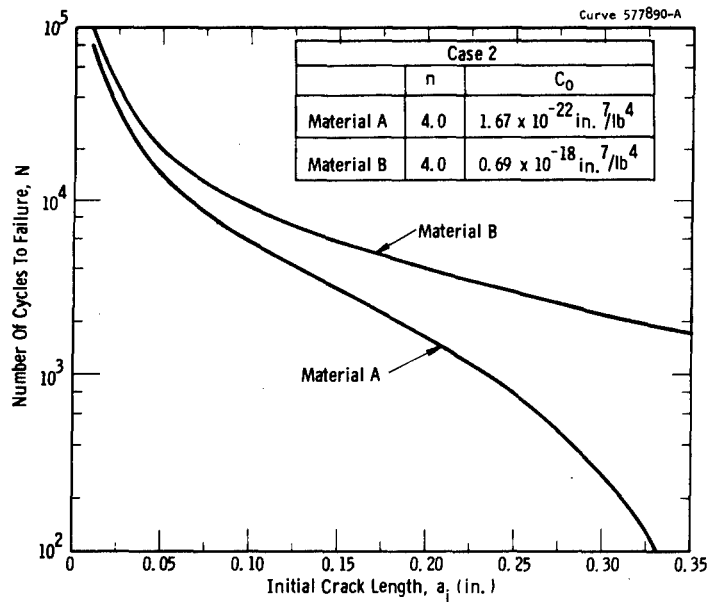
Case	Material A		Material B	
	n	C_o	n	C_o
1	4.0	$1.67 \times 10^{-22} \text{ in}^7/\text{lb}^4$	3.0	$0.78 \times 10^{-18} \text{ in}^{5.5}/\text{lb}^3$
2	4.0	$1.67 \times 10^{-22} \text{ in}^7/\text{lb}^4$	4.0	$0.69 \times 10^{-18} \text{ in}^7/\text{lb}^4$
3	2.5	$1.20 \times 10^{-22} \text{ in}^{4.75}/\text{lb}^{2.5}$	4.0	$1.47 \times 10^{-18} \text{ in}^7/\text{lb}^4$

The comparisons for the three cases are shown in Figures 7, 8, and 9.

As shown in Fig. 7, the assumed growth rates for case 1 result in a "cross-over" of the cyclic life curves at an initial crack depth $a_i = 0.15$ in. and a cyclic life of $N = 3000$ cycles. It can be concluded, that for this case, material A will have a greater cyclic life for initial crack depths less than $a_i = 0.15$ in., and material B will have a greater life for initial crack depths greater than this value. Or from a different viewpoint, larger surface flaws can be tolerated in material A than material B for each value of expected life greater than $N = 3000$ cycles, whereas the opposite is true for values of N less than 3000 cycles. Therefore, in this case, the choice of the better material from a cyclic life point of view is not only dependent on the material properties but also on the maximum size of initially expected flaws.



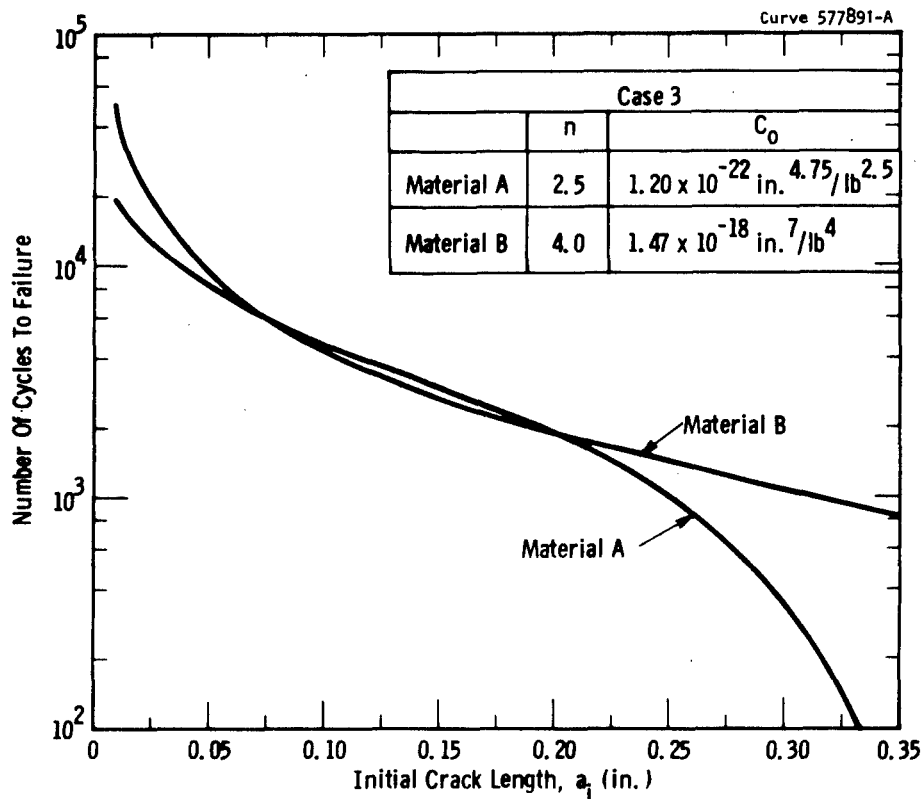
Sec. 8.3 Fig. 7 -Cyclic life as a function of initial crack size for Materials A and B (Case 1)



Sec. 8.3 Fig. 8 -Cyclic life as a function of initial crack length for Materials A and B (Case 2)

The resulting cyclic life vs. initial crack depth curves for the crack growth properties assumed for case 2 are shown in Fig. 8. As is observed, the two curves do not "cross-over" and for any initial crack depth the life of material B is always greater than that of A. Therefore, for the same size initial crack in the two materials, material B would always be the most desirable material from a cyclic life point of view. Of course, the comparison is not as simple as demonstrated in this somewhat idealized case since we can't expect the same size of maximum initial flaw in the two materials because of the differences in means of production and metallurgical make-up.

The case 3 cyclic life vs. initial crack depth curves for material A and B are shown in Fig. 9. In this case the curves "cross-over" twice. The cyclic life of material B is greater than that of material



Sec. 8.3 Fig. 9 -Cyclic life as a function of initial crack length for Materials A and B (Case 3)

A for all initial crack lengths except those in the interval $a_i = 0.07$ in. to $a_i = 0.20$ in. In this range the cyclic life of material A is slightly greater than that of material B. Again as in case 1, the better material from a cyclic life point of view is a function of initial crack size, but in this case there are three distinct regions instead of two. But for practical engineering purposes it can be stated that material B has an equal or greater life than material A for all initial crack size. It should be realized that for some conditions the cyclic life difference between two materials for initial cracks lengths between two "cross-over" points could be appreciable.

These three examples demonstrate that the selection of the material which will have the greater cyclic life is not only dependent on the crack growth properties, critical stress intensity factor, and cyclic stress level, but also in many cases on the maximum initial flaw size which can be expected in the structure. In addition equation 5 or equations similar to it but applicable to other geometric conditions can be used to estimate expected cyclic life when the crack grow rate can be represented by the power law of the form of equation 1.

8.3.3 QUALITY CONTROL INSPECTION AND SPECIFICATIONS

Many of the preliminary considerations leading to the establishment of quality control inspection techniques and the development of acceptance standards have been described in the preceding section. These considerations involve parameters developed as the result of fracture toughness determinations and include the types and sizes of defects which lead to brittle fracture, the maximum allowable initial defect size for cyclic or sustained loading, and crack growth characteristics. In addition to the above considerations, knowledge of the capabilities of the available nondestructive inspection techniques is necessary to permit the development of realistic inspection specifications. Since the determination of the factors related to toughness parameters have already been discussed in considerable detail, this section will be confined to a summary of the applications of the knowledge to quality control considerations.

8.3.3.1 Inspection and Quality Control

In order to adequately employ fracture mechanics technology, nondestructive inspection techniques capable of detecting and describing existing defects which affect the fracture behavior of a material under service conditions are necessary. A knowledge of the K_{Ic} fracture toughness of the material combined with a knowledge of the prevailing stresses, permits the calculation of the size of defect which will cause catastrophic brittle fracture. Such predictions are possible for a wide assortment of defect types and shapes, loading conditions, and relative geometric relationships between the defect and the component. To utilize any structural material it must be possible to locate and describe defects which are smaller than those established as critical. The required detectable defect size will depend upon the critical size for failure and the applied design safety factor. For example, the maximum allowable initial defect size may be set at 1/2 the critical size; therefore, the inspection procedure must be capable of detecting this size flaw. In those loading situations where crack growth is encountered prior to catastrophic failure, the inspection requirements become much more rigorous since it now becomes necessary to detect those flaws which can grow to critical size under service conditions. As an example, consider the case of a semi-elliptical surface defect in the steel (HP-9-4-25) and aluminum (7079-T6) alloys under cyclic loading described in Section 8.2.2.2.b. The pertinent flaw size data are given below.

<u>Material</u>	<u>Maximum Allowable Defect Size at the Start of Life</u>	<u>Critical Defect Size at Catastrophic Failure</u>
Aluminum Alloy (7079-T6)	0.043" deep 0.215" long	0.372" deep 1.860" deep
Steel Alloy (HP-9-4-25)	0.056" deep 0.280" long	0.882" deep 4.400" long

The critical defect size for catastrophic failure is relatively large for each material and the detection of such flaws is very likely within available inspection capabilities even if a safety factor of 1/2 were employed. However, the maximum allowable initial defect sizes are

relatively small, particularly if a safety factor is employed, and such flaw sensitivity may not be within the capabilities of available inspection techniques. Assuming that such defects cannot be reliably detected, what alternatives are available for consideration by the designer or materials engineer? The applied stresses could be lowered to a level which would permit a maximum allowable initial defect size that is within the inspection capabilities. Another material with more resistance to slow crack growth, hence a larger allowable initial defect size, could be substituted for the steel or aluminum.

Considering this same example, it is also possible that one material could be more readily inspected than the other. For example, the steel would lend itself to magnetic particle inspection for the semi-elliptical surface crack, whereas the aluminum would not. Considerations such as this may then strongly influence the final selection of a material.

Consideration of inspection techniques should not be limited to those applicable to the in-plant inspection of structural components prior to service application. Field inspection capability must also be considered. It is not always possible to disassemble a large, complex structure to remove the component of interest such that it can be shipped to a suitable inspection facility; therefore, "on-site" inspection capable of detecting defects or increases in defect size incurred during service are necessary. Considerations may involve such aspects as determining when a major overhaul or repair is necessary, the removal of a component from service, unusual flaw growth characteristics, trouble shooting, field failures, etc.

The nondestructive inspection techniques to be used in conjunction with the fracture mechanics approach to component design must exhibit certain capabilities. The general shape and size (all three dimensions) of a defect must be defined. The location and orientation of the flaw relative to the dimensions of the component is equally important. In the case of multiple defects, the location of one defect to another and the distance between them should be known. In some instances, the change in flaw size with increased service time must also be definable. The inspection capability must extend from the case of

very tight cracks to spherical voids. The ability to determine the acuity at the tip of defects is not required, since all defects are assumed to have a crack-like sharpness, thus providing a conservative approach to the effect of discontinuities upon fracture behavior.

Each nondestructive test has certain advantages and disadvantages; some are particularly applicable to certain materials and others are insensitive to special types of defects. The various methods are complementary rather than competitive and it is advantageous for the engineer to have some knowledge of the limitations of all methods available. It is very unlikely that any one inspection technique has the capability to meet all of the requirements. In most situations, two or more supplementary techniques are required to obtain all of the required information. For example, radiography may be capable of providing a two-dimensional picture of an internal defect, however, ultrasonic inspection may be necessary to locate the depth and to establish the orientation of the flaw with respect to the test surface. Similarly, magnetic particle inspection can be used to reveal the length of a surface flaw in a ferromagnetic material, but radiography or ultrasonics may be necessary to establish its depth. The sensitivity requirements for the inspection technique will naturally depend upon the particular situation and the safety factor involved. In a questionable situation it is good practice to favor the direction which will introduce conservatism into the application.

8.3.3.2 Quality Control Specifications

Incorporation of fracture toughness considerations into material acceptance specifications requires a thorough understanding of the stresses involved under the proposed service conditions and the corresponding toughness properties necessary to satisfy these conditions. Once these data have been well established, satisfactory acceptance criteria can be developed in terms of a quality control specification. Knowledge of the critical defect size determined from fracture toughness testing provides a basis for the maximum acceptable defect size which may be encountered in "as-received" material. In addition, toughness testing

conducted in various test directions limits the acceptable defect size with respect to orientation. The nondestructive inspection technique used to evaluate the "as-received" material must be capable of reliably detecting flaws equivalent to the maximum acceptable limit in the test direction in question. A typical acceptance specification established for a forged plate to be used in a direct tension static loading situation would require, in addition to the conventional acceptance criteria-chemical analysis, tensile properties, etc; a minimum K_{Ic} fracture toughness value as determined on a series of toughness specimens removed from a predetermined location within the plate and the nondestructive inspection of the plate using a technique and sensitivity level capable of detecting the presence of defects larger than the maximum allowable size. Some distinction must also be made regarding the location of the flaws in the "as-received" plate since an internal flaw which is located near the surface of the plate may be uncovered during fabrication resulting in a more detrimental stress situation.

Material to be used for cyclic loading conditions would require similar acceptance criteria based upon toughness testing and slow crack growth characteristics. The inspection technique would be required to detect the presence of those defects larger than the initial acceptable flaw size which will not grow to critical size under cyclic loading conditions.

8.3.3.3 Summary

With proper consideration of all of the factors described above, fracture mechanics technology can provide a sound basis for the establishment of realistic inspection procedures and standards that can be used for specification, inspection, and quality control. The effects of types, sizes, shapes, location, and orientation of defects can be determined in a quantitative fashion. These results can subsequently be translated into terms of those defects which can be tolerated and those which are unacceptable for the materials and application in question. Then meaningful standards for specifications, inspection, and quality control can be

established and applied to production. Careful coordination of the inspection considerations with the early stages of the design and selection of a material is very desirable, and can be very helpful in achieving a satisfactory product in an efficient and effective manner.

8.3.4 PERFORMANCE AND LIFE EXPECTANCY EVALUATION

Fracture mechanics concepts can be used to estimate the expected life of a structure. By using crack growth rate data expressed as a function of crack tip stress-intensity and similarly expressed fracture toughness data, the time history of the crack size up to critical size can be determined. The use of fracture mechanics principles presupposes the existence of cracks or defects which may behave as cracks in the body. Sometimes small cracks are initially present due to metallurgical imperfections, or fabrication. If such initial cracks are not present then the subject of crack initiation must be considered. The subject of crack initiation will not be covered in this text, but it is extensively covered in available literature. For the purposes of this discussion it will be assumed that either a crack of known size is initially present or that some upper bound on possible initial crack size is known. If the actual initial crack size is known then an estimate of the actual life of the structure can be calculated. If an upper bound of crack size is used in the calculation then the life calculated will be an estimate of a lower limit of the life of the structure.

In estimating expected life by the fracture mechanics approach the general limitations of fracture mechanics must not be exceeded. The limitations of fracture mechanics with respect to predicting catastrophic failure were considered in Sec. 6.2.6. The limitations with respect to cyclic slow crack growth rates are less severe. If conditions are such that fracture mechanics concepts can be used to predict the fracture load, then the fracture mechanic cyclic growth rate concepts can be validly applied since the area of applicability of fracture mechanics to cyclic crack growth is greater. This is true since the size of the plastic zone connected with the fatigue process is much smaller than that

connected with the fracture process due to the lower stress intensities associate with fatigue and due to the decrease in plastic zone size caused by strain hardening.

8.3.4.1 Information Needed to Make Life Evaluation⁽³⁾

The following information is needed to estimate the expected life of a structure by the fracture mechanics approach.

1. A knowledge of the critical stress intensity of the material is necessary. The value used should be representative of the actual conditions with respect to mechanical variables, metallurgical variables, and environmental conditions.

2. An estimate of the initial sizes of the cracks present in the structure or an estimate of the size of the largest possible crack present in the structure should be available. Under some conditions the actual size, shape, and orientation of cracks can be determined by the various nondestructive inspection techniques. In some cases the inspection techniques are not sufficient to determine actual crack sizes but they can be used to obtain an upper bound of crack sizes.

Besides the use of inspection techniques, the proof test method is also a means of determining an upper bound of crack sizes in a structure. In a proof test the structure is initially subject to a single cycle load higher in magnitude than the normal operating load. If failure doesn't occur at this load, the maximum possible flaw size in various locations of the structure can be determined from a knowledge of the stress distribution. For example if a large thick plate of known toughness, K_{Ic} , is subject to a uniaxial proof stress, σ_p , and failure by catastrophic fracture does not occur, then it will be known that any through the thickness cracks present in the plate cannot have a length greater than approximately $(K_{Ic}/\sigma_p)^2/\pi$. For more complex structures the estimation of maximum possible crack size by proof testing becomes more difficult and involves many of the considerations presented in (8.2.2).

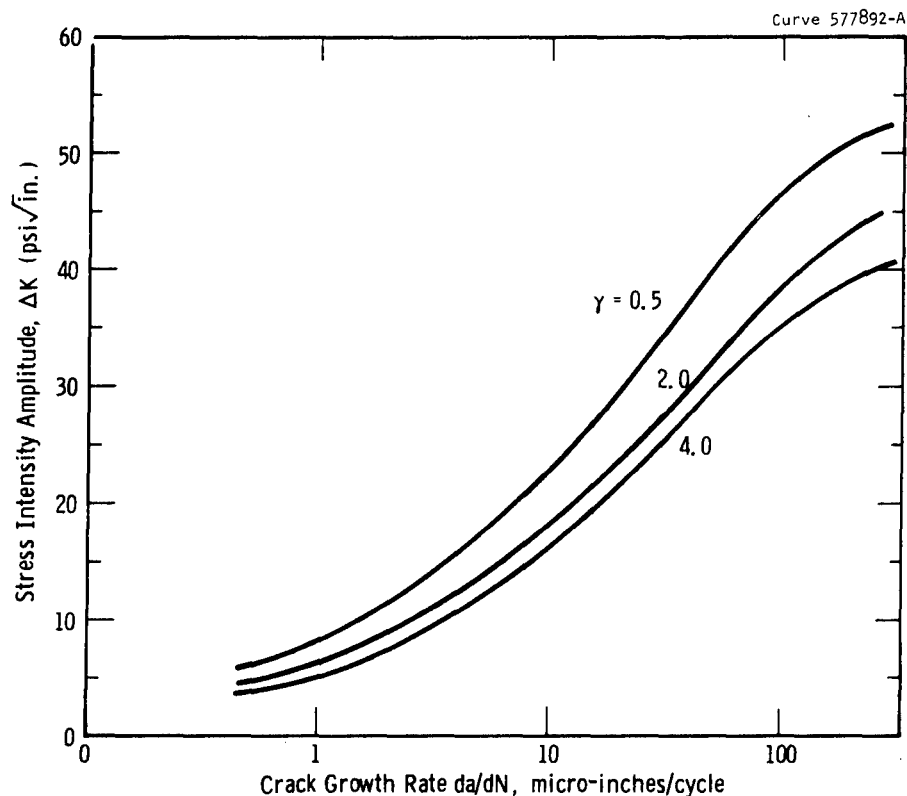
3. The relationship between external load, P , and the stress intensity factors, K , of detected cracks of known size and shape or of

cracks of assumed size and shape (based on proof testing, etc.) must be known as a function of crack length, $K = F(a) P$. If thermal stresses are a significant factor, then the relation between the thermal stresses and stress-intensity factors must be known. This subject was considered in (8.2.2).

4. The expected time history of the external loads and thermal conditions must be available (8.2.5).

5. The cyclic crack growth rate of the material as a function of cyclic variation of the crack tip stress intensity must be available. At present the relation between crack growth rate and cyclic stress intensity must be determined experimentally. Normally the crack growth data are obtained for conditions of sinusoidal variation in stress intensity. The most convenient parameters for describing the sinusoidal variation of stress intensity are the range of fluctuation $\Delta K = K_{\max} - K_{\min}$ and the relative mean of the $\gamma = K_{\text{mean}}/\Delta K$ where K_{mean} is the mean value of the stress intensity. By use of these two parameters the crack growth rate data can be plotted as a function of ΔK for various fixed values of γ as schematically shown in Figure 10. For most materials such a plot indicates that γ has only a secondary effect on the crack growth rate⁽⁴⁾ if its variation is not too great and, therefore, for such materials the growth rate is a function of ΔK only for most engineering purposes.

The growth data can be obtained from any of the specimens described in Section 6.2.4 by cycling the applied loads to produce the desired variation in the crack tip stress intensity and by closely monitoring the crack length (Section 7.3.3). It is desirable to obtain the data from specimens whose thickness (or state stress at the crack tip) is the same as that of the structural component to which the data will be applied. At present the effect of thickness on slow crack growth rate due to cyclic loading has not been rigorously determined. But for most materials it would appear that for conditions in which the cyclic K_{\max} is somewhat less than K_{Ic} , the growth rate is independent of thickness, but for cyclic conditions in which K_{\max} approaches K_{Ic} (or for thin sheet, exceeds K_{Ic}) the rate will be dependent on plate thickness.



Sec. 8.3 Fig. 10 — Schematic representation of crack growth rate plotted as a function of ΔK for fixed values of $\gamma = K_{\text{mean}} / \Delta K$

8.3.4.2 Procedure for Estimating Life Under Cyclic Loading Conditions

After the above (8.3.4.1) information has been accumulated an estimate of the expected life of the component can be made. In the procedure used for estimating life, crack growth is considered to be quasi-static with respect to time compared to the variation of the external load. That is, if the relationship between stress intensity, crack length and load under static conditions is $K = F(a) \cdot P$ then for conditions varying with time over some local time interval in which crack length doesn't change appreciably with respect to time the relation is considered to have the functional form $K(t) = F(a) P(t)$.

The cyclic life can be estimated by use of a procedure in which the total number of applied cycles is analytically divided up into a number of small cyclic increments. The number of cycles in each increment must be small enough such that both the relative change in the magnitude of the function $F(a)$ due to change in crack length during the increment and the change in the mean and range of the external loading during the increment is very small. For each such cyclic increment the following three step procedure, described for the n -th increment, is carried out.

1. Using the crack length, a_n , present at the beginning of the n -th cyclic increment and the expected sinusoidal variations in external load, ΔP_n and $\Delta P/P_{\text{mean}}$, during the increment, the values of ΔK_n and α_n acting on the crack tip during the increment are determined from the relations $\Delta K_n = F(a_n) \Delta P_n$ and $\alpha_n = \Delta K/K_{\text{mean}} = \Delta P/P_{\text{mean}}$.

2. From the curves based on experimental data the crack growth rate, (da/dN) , corresponding to ΔK_n and α_n is obtained.

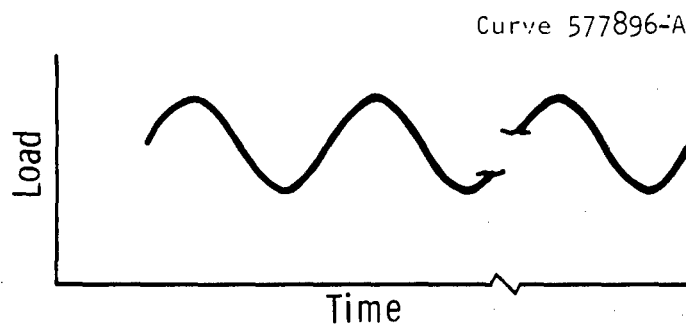
3. The change in crack length Δa_n during the n -th increment is then calculated as $\Delta a_n = (da/dN)_n (\Delta N_n)$ where ΔN_n is the number cycles in the n -th increment. The crack length at the end of the n -th increment and therefore at the beginning of the $(n + 1)$ th increment is $a_{n+1} = a_n + \Delta a_n$. Steps (1) through (3) are again carried out for the $(n + 1)$ th time interval. This cyclic procedure is carried out until the analytically determine crack size has grown to the critical length were $K_{\text{max}} = K_c$. The total number of cycles accumulated to this point then is the estimated cyclic life of the body.

The crack size used in the calculations during the first time increment is that which has actually been detected or some upper limit of the size of possible cracks. The upper limit can be determined by proof testing or by some detection technique. In the case where the upper limit of crack size is used in the calculations the resulting calculated life is an estimate of the minimum possible life of the structure.

8.3.4.3 Limitations of Procedure

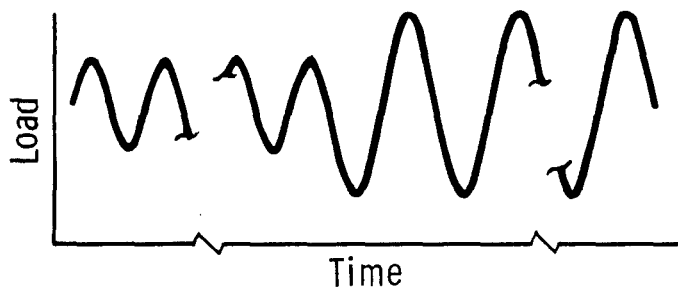
In general the life estimating procedure described in (8.3.4.2) should give reasonable results if fracture mechanics concepts can be validly applied (Section 6.2.2) and if the mean and amplitude of the applied loads vary in a continuous and reasonably smooth manner as demonstrated in Figures 11(a) and 11(b). If the variation of external load with respect to time is random as shown in Figure 11(c), then the above procedure cannot be used. Work is presently being done on methods for predicting slow crack growth due to random loading by use of growth data obtained for sinusoidal loading conditions.^(3,5) But at present the proposed methods for handling random loading have not been experimentally verified.

One aspect of this procedure which should be studied further is the effect of crack growth at high stress intensities on the critical stress intensity. In the method presented above failure is predicted when the maximum stress intensity reaches a magnitude equal to that of the critical stress intensity determined from a test in which the load was monotonically increased until failure occurred. In a structure which is subject to cyclic loading and fails when the crack has grown to critical size, the crack has actually been subject to alternating stress intensities of large magnitude prior to failure. Some test results⁽¹⁾ indicate that alternating stress intensities of high magnitude have a significant effect on the critical stress intensity factor. But results so far indicate that use of monotonic loading critical stress intensity factors in predicting life expectancy under cyclic loading conditions will give conservative results.



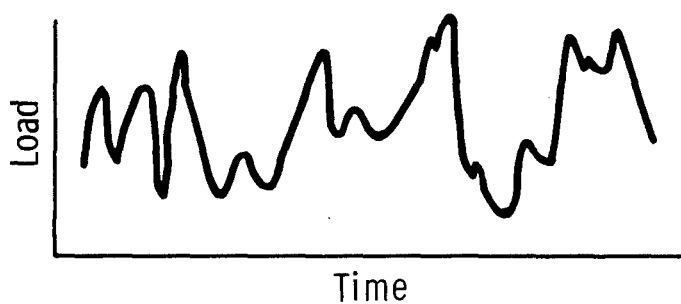
Constant Sinusoidal Loading

(a)



Varying Sinusoidal Loading

(b)



Random Loading

(c)

Sec. 8.3 Fig. 11 -Variations of external load with time

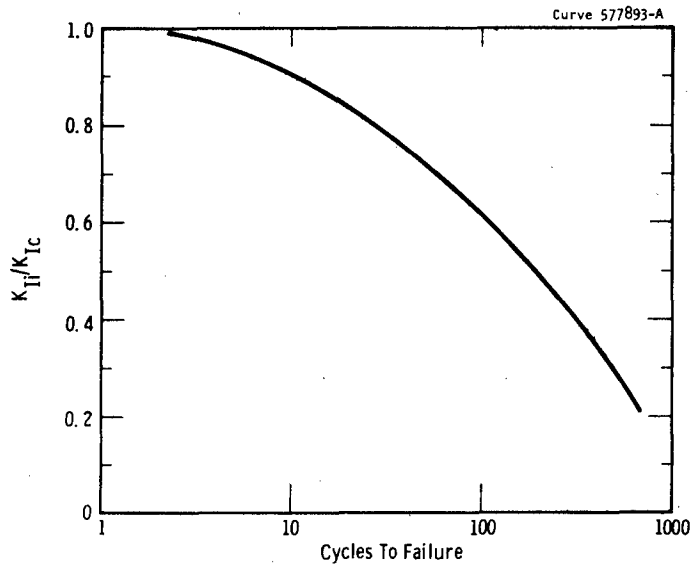
8.3.4.4 Simplified Method for Predicting Cyclic Life

Under somewhat restricted conditions cyclic life can be quickly estimated for plane strain fracture conditions by use of curves similar to that shown in Figure 12 instead of going through the tedious procedure described in (8.3.4.2). From this type of a plot cyclic life can be determined as a function of K_{Ii}/K_{Ic} where K_{Ic} is the plane strain critical stress intensity of the material and K_{Ii} is initial maximum stress intensity. The initial maximum stress intensity is calculated from the initial crack size and from the maximum external load. The Boeing Company, Aero-Space Division, makes extensive use of plots similar to that shown in Figure 12 and the method is considered in detail in Reference 6.

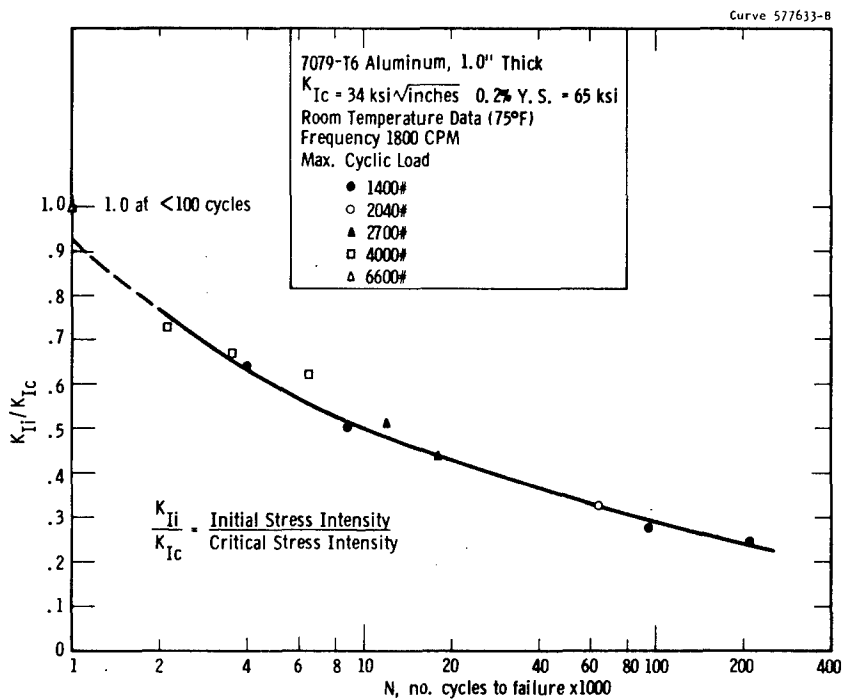
Curves like the one shown in Figure 12 can only be used to estimate cyclic life of structures whose pattern of loading history is somewhat similar to that used on the laboratory test specimens used to obtain the curves. Normally these curves are obtained by cycling specimens under a load of constant mean and amplitude through out the life of the specimen. Therefore, curves obtained under such conditions can only be expected to apply to structures subject to a similar loading pattern. The method described in (8.3.4.2) for estimating cyclic life has a distinct advantage over this method in that it is also directly applicable to conditions in which the cyclic mean and amplitude of the external load vary with time in a smooth manner.

The functional relation between cyclic life and the ratio K_{Ii}/K_{Ic} as shown in Figure 12 is dependent on cyclic stress level and the geometry of the structure containing the crack. Therefore a curve of this type should be constructed for conditions close to those actually existing in the structure to which it will be applied.

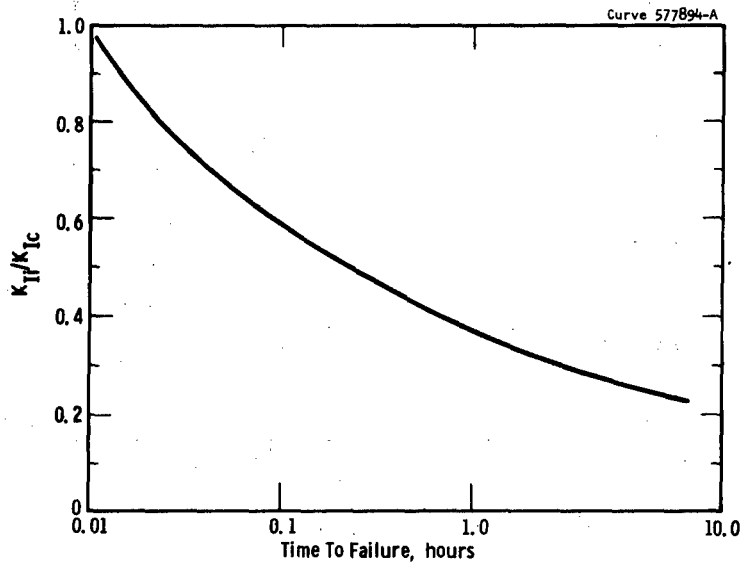
Curves of this type can be constructed directly from experimental data as demonstrated by Figure 13, or indirectly from fundamental crack growth rate data by the method presented in (8.3.4.2).



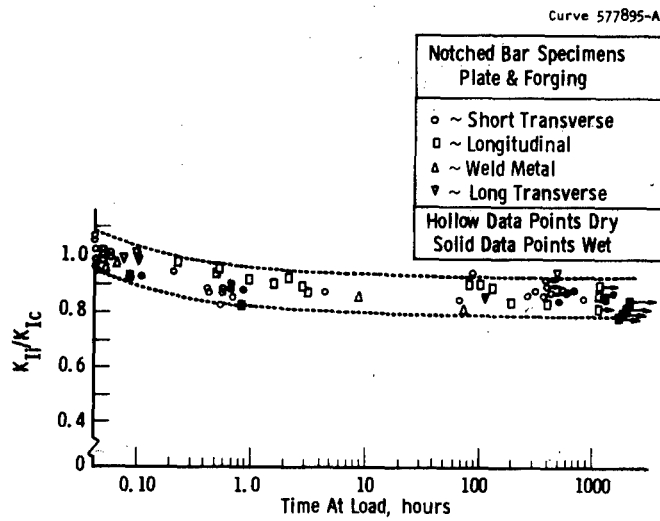
Sec. 8.3 Fig. 12 - Schematic representation of cyclic flaw growth



Sec. 8.3 Fig. 13 - Combined cyclic flaw growth data for 7079-T6 aluminum plate



Sec. 8.3 Fig. 14 —Schematic representation of sustained stress flaw growth



Sec. 8.3 Fig. 15 —Sustained stress data for room-temperature tests of 17-7PH Steel (Ref. 6)

A curve which expresses cyclic life as a function of K_{Ii}/K_{Ic} can be used in a number of ways. For example, if the initial crack size is known, then the K_{Ii} can be determined and the expected life can be quickly obtained for the corresponding ratio of K_{Ii}/K_{Ic} . Also if an upper bound on crack size is known then the same procedure can be carried out to give a lower limit on expected life. Finally, for a particular life requirement, the maximum value of K_{Ii} necessary to give this life can be easily determined from such a curve. Once the maximum allowable value of K_{Ii} is known the maximum tolerable crack size can be determined.

8.3.4.5 Life Predictions When Slow Crack Growth Occurs Under Sustained Loading

If conditions are such that slow crack growth will occur under sustained loading, the estimated time to failure can be calculated by procedures analogous to those used in the case of slow crack growth due to cyclic loading. For cases in which a rather estimate of life is desired or in which the magnitude of the sustained load varies with time, the procedure used is analogous to that described in (8.3.4.2). When the sustained load remains constant throughout the life of the structure and an estimate of the life is required, curves analogous to those considered in (8.3.4.4) for cyclic growth conditions can be constructed and used.

When the procedure analogous to that presented in (8.3.4.2) is used to determine the life expectancy of a structure subject to sustained load crack growth, the information necessary to make the estimate is the similar to that listed in (8.3.4.1). The only difference is that an experimentally determined curve expressing crack growth rate, da/dt , as a function of crack tip stress intensity K is used (Figure 11, Section 6.2) instead of one expressing cyclic crack growth rate da/dN as function ΔK . Also incremental time intervals Δt are now considered instead of cyclic intervals ΔN . The length of each incremental time interval is chosen small enough such that the relative change in the crack tip stress intensity due to crack growth and change in external load during each

interval is small. The three step numerical procedure described next for the n-th time increment is carried out for each increment.

1. Using the crack length, a_n , present at the beginning of the n-th increment and the average external load acting during the increment, the average stress intensity acting at the crack tip during the increment is calculated.

2. From the curve showing da/dt as a function K , the crack growth rate $(da/dt)_n$ corresponding to the stress intensity calculated in (1) is determined.

3. The change in crack length, Δa_n , during the n-th increment is then calculated as $\Delta a_n = (da/dt)_n \Delta t_n$ where Δt_n is the length of the time increment. The crack length at the end of the n-th increment and at the beginning of the (n + 1)-th increment is $a_{n+1} = a_n + \Delta a_n$. This procedure is now carried out for the (n + 1)-th time interval and for each succeeding interval until the analytical calculated crack length has increased to critical size. The crack length used during the first increment is either the length of an actually detected crack or an upper bound of possible crack length.

If the external load remains constant, the life of a structure can be simply estimated by the use of a curve similar to that shown in Figure 14. Here the time to failure is given as a function of the ratio K_{Ii}/K_{Ic} where K_{Ii} is the stress intensity present at the crack tip at zero time. As with the corresponding type of approach to cyclic life predictions, this technique is extensively used by the Boeing Company.⁽⁶⁾ Also, as is the case in cyclic life estimates, the curves can be constructed directly from experimental data as indicated in Figure 15 or indirectly from experimental data which is given in the form of crack growth rate as a function of stress intensity. As stated in Section 8.3.4.4 curves of this type are a function of stress level and geometry, and therefore should be constructed for conditions similar to those to which they will be applied.

8.3.5 SUMMARY

The preceding sections have demonstrated the complexities and interactions between design, materials, fabrication, inspection and performance considerations. It is apparent that the use of a modern technology, such as fracture mechanics, and an advanced design philosophy no longer permit each of the areas of consideration to be treated as separate identities. Rather, the considerations in each area must be carefully evaluated with respect to the possible effects on other areas, and optimum compromises must be established in any conflicting areas. Ultimately, this type of approach will result in a product of the desired level of integrity, and it will be produced in an effective and efficient manner.

Section 8.3 References

1. W. F. Brown, Jr. and J. E. Srawley, Task Group of ASTM Committee E24-Sub I, "Plane Strain Crack Toughness Testing" Draft of forthcoming 6th Committee Report, Distributed at E24 Meeting, Washington, D.C., February 1, 1966.
2. ASTM Special Committee on Fracture Testing of High Strength Material "Progress in Measuring Fracture Toughness and Using Fracture Mechanics, Fifth Report" ASTM Materials Research and Standards, March 1964, p. 107.
3. P. C. Paris, "The Fracture Mechanics Approach to Fatigue," Proceedings of the 10th Sagamore Army Materials Research Conference, (1963).
4. P. C. Paris, notes from Fracture Mechanics Workshop held at the University of Denver, (1964).
5. S. H. Smith, "Fatigue Crack Growth Under Uniaxial Narrow and Broadband Random Loading," proceedings of the 2nd International Conference on Acoustic Fatigue, Syracuse University Press, (1965).
6. C. F. Tiffany and J. N. Masters, "Applied Fracture Mechanics," ASTM Special Technical Publication No. 381.

TABLE OF CONTENTS

Section 3.4

	<u>Page</u>
8.4 APPLICATION OF FRACTURE MECHANICS TECHNOLOGY IN A HYPOTHETICAL PRESSURE VESSEL	301
8.4.1 Operational Requirements and Initial Design Consideration.	301
8.4.2 Evaluation and Selection of a Material	304
8.4.2.1 Consideration of Fabrication Techniques	304
8.4.2.2 Initial Evaluation of Materials	305
a. Critical Defect Sizes for Failure During Proof Testing.	306
b. Nondestructive Inspection Capabilities.	308
c. Considerations of Cyclic Life and Initial Flaw Sizes.	311
8.4.2.3 Reconsideration of Material Selection	313
a. Reduction in Design Stresses.	314
8.4.2.4 Using a Lower-Strength, Higher-Toughness Steel	316
a. Critical Defect Sizes for Failure	316
b. Cyclic and Sustained Loading Crack Growth.	318
c. Reducing the Weight of the Vessel	319
8.4.2.5 Summary of Final Selection of a Material.	322
8.4.3 Establishing Specifications, Inspection and Acceptance Criteria	324
8.4.4 Proof Testing and Life Expectancy Evaluation	327
8.4.4.1 Proof Testing	327
a. Crack Growth Under Sustained Loading.	330
b. Leak or Failure During Proof Testing.	332

TABLE OF CONTENTS (Cont.)

	<u>Page</u>
8.4.4.2 Evaluation of Life Expectancy	333
a. Minimum Life Resulting from Undected Flaws	333
b. Maximum Life for No Detectable Flaws.	334
c. Realistic Life Expectancy Based on Maximum Allowable Size Flaws.	335
8.4.5 Summary.	337

LIST OF TABLES

Section 8.4

	<u>Page</u>
TABLE I Materials Initially Considered	303
TABLE II Stresses In The Pressure Vessel For Various Materials.	304
TABLE III Critical Defect Sizes For Catastrophic Fracture During Proof Tests For Various Materials And Types of Defects (Hypothetical Pressure Vessel).	307

LIST OF FIGURES

Figure 1. Hypothetical pressure vessel	305
Figure 2. Graphical Solution for ϕ^2 for use with elliptical shaped defects.	308
Figure 3. Cyclic flaw growth data for aluminum alloy.	312
Figure 4. Cyclic flaw growth data for Material B, 200 ksi yield strength steel	314
Figure 5. Cyclic flaw growth data for Material E, a 150 ksi yield strength steel (HY150)	317
Figure 6. Crack growth and failure times under sustained loading, HY150 steel	317
Figure 7. Acceptable external flaw sizes	328
Figure 8. Acceptable internal flaw sizes	329

Section 8.4

APPLICATION OF FRACTURE MECHANICS TECHNOLOGY, IN A HYPOTHETICAL PRESSURE VESSEL

The application of fracture mechanics concepts, expressions and data are most readily illustrated by solving realistic problems associated with a hypothetical situation which involves consideration of all of the interrelated aspects. The areas involved in the considerations and application of fracture mechanics are:

- (1) Operational requirements and initial design
- (2) Selecting a material
- (3) Establishing criteria for specifications and inspection
- (4) Quality control during fabrication
- (5) Evaluating finished product
- (6) Proof testing
- (7) Final evaluation of expected performance characteristics

To illustrate the use of fracture mechanics a realistic hypothetical example is selected, and the detailed considerations in each of the areas are described. The example is a thin-walled, cyclic-loaded pressure vessel used to contain hydraulic fluid at high pressures. A total of 2000 high integrity units are required.

8.4.1 OPERATIONAL REQUIREMENTS AND INITIAL DESIGN CONSIDERATIONS

The following requirements are involved in the application:

- (1) High pressure, 10,000 psig maximum operating pressure
- (2) Hydrostatic proof test at 150% of operating pressure, for 60 minutes holding time
- (3) Minimum cyclic life, 40,000 cycles to maximum operation pressure

- (4) Environment, internal-hydraulic fluid, external-moist air
- (5) Minimum weight consistent with requirements (maximum for vessel, 350 lbs.)
- (6) Minimum size consistent with requirements (maximum available space 18" square by 42" long)
- (7) Operating temperature range, -20^oF to 100^oF
- (8) Minimum volume of hydraulic fluid consistent with requirements.

The initial design considerations indicate that a simple cylindrical vessel with hemispherical heads is the most satisfactory geometry. The internal dimensions required for the necessary volume of fluid are 12.5" ID by 36.5" overall length. The design is such that bending stresses at the intersection of the heads with the cylindrical body, or elsewhere in the vessel, are less than 10% of the nominal stresses. Two small diameter openings for attachment of lines are provided at each end of the vessel. For the stipulated conditions, the wall thicknesses and weight of the vessel are naturally dependent upon the material and the design stresses which are allowed. The designer chooses 1/2 of the yield strength of the material as an initial selection of an operating stress (maximum stress-hoop stress in cylindrical section). In cooperation with a materials engineer, the initial materials considerations are directed to four materials:

- (a) Maraging steel at 300,000 psi yield strength
- (b) A quenched and tempered steel at 200,000 psi yield strength
- (c) A titanium alloy at 140,000 psi yield strength
- (d) An aluminum alloy at 70,000 psi yield strength

The corresponding wall thickness, weight and approximate overall dimensions are determined as follows:

$$\sigma = \frac{PD}{2T}$$

σ = hoop stress in cylindrical section = $1/2 \sigma_{YS}$ of material

P = pressure

D = diameter of vessel

T = wall thickness*

And the results given in Table I.

Section 8.4 Table I

MATERIALS INITIALLY CONSIDERED

<u>Material</u>	<u>σ_{YS} (ksi)</u>	<u>Wall Thickness (inches)</u>	<u>Total Outside Diameter (inches)</u>	<u>Total Length of Vessel (inches)</u>	<u>Total Weight Vessel Panels</u>
Steel A	300	.42	13.4	37.3	192
Steel B	200	.63	13.8	37.8	284
Titanium C	140	.90	14.3	38.3	281
Aluminum D	70	1.80	16.1	40.1	287

As may be seen, all of the materials are capable of producing a vessel which will fit into the allotted space requirements of 18" square by 42" long. Because of its greater strength, Steel A provides the most desirable combination of minimum weight and size.

The nominal stresses in the vessels for the various materials are given in Table II. **

* For convenience, the required wall thickness of the heads and the cylindrical sections are assumed to be equivalent.

** For the purpose of this example, it is assumed that the design is such that the stresses in the head sections are smaller than those in the cylindrical section. The joint between the heads and the cylinder is assumed to have the same stresses as the cylinder.

Section 8.4 Table II

STRESSES IN THE PRESSURE VESSEL FOR VARIOUS MATERIALS

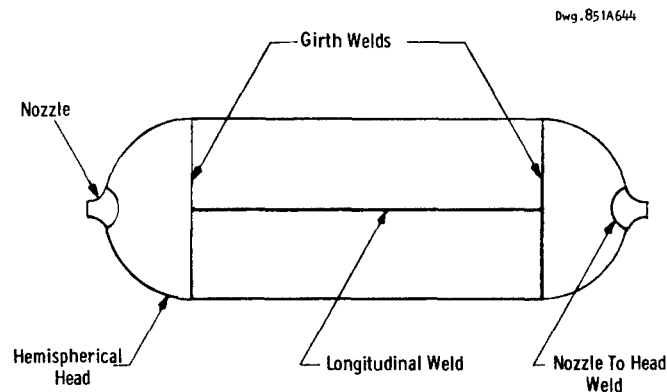
Cylindrical Section				
Material	Transverse (Hoop) Stress ksi		Longitudinal (Axial) Stress ksi	
	σ_H		σ_A	
	Operational	Proof	Operational	Proof
A	150	225	75	112.5
B	100	150	50	75
C	70	105	35	52.5
D	35	52.5	17.5	26.2

At this point the basic shape and size of the vessel have been determined, and first approximation of design stresses has been established for four candidate materials. The next step in the considerations involves a more thorough evaluation of the potential of these materials.

8.4.2 EVALUATION AND SELECTION OF A MATERIAL

8.4.2.1 Consideration of Fabrication Techniques

One of the first factors which must be considered concerns how the vessel is to be fabricated. The most economic approach would be to roll the cylinder from plate and weld with one longitudinal seam as seen in Figure 1. The hemispherical heads could be hot spun, pressed or forged. The entry ports in each head could be welded inserts. The hemispherical ends would be welded to the cylinder with a single girth weld at each end. Alternatively, to minimize welding, the cylinder could be made as a one piece forging or extrusion; the hemispheres could be forged with the entry port as an integral part, and the heads welded to the cylinder. Bolting of the heads to the cylinder would necessitate large flanges, adding to the weight and complicating the entire structure. Thus, it appears that rolling and welding is the most convenient and economic method of fabrication. The final heat treatment could be performed before or after welding depending upon the base material and weldment considerations.



Cylinder with Hemispherical Heads

Cylinder

Inside Diameter 12.5"

Inside Length 24.0"

Head

Inside Radius 6.25"

Outside dimensions dependent on material and design stress

Sec. 8.4 Fig. 1 — Hypothetical pressure vessel

Materials A and D (Table I) would require post weld heat treatment to bring the weld strength up to that of the base material. Materials B and C could be used either way, but a post weld stress relief to remove residual stresses appears desirable.

8.4.2.2 Initial Evaluation of Materials

The next step in the material considerations involves obtaining basic fracture mechanics data for the materials. Ultimately, both K_{Ic} and slow crack growth data are required. However, K_{Ic} data will suffice for initial evaluations. In addition to these fracture toughness parameters, some preliminary judgments concerning the type and size of anticipated defects are necessary. Since this is a welded application it must also be remembered that the required data and defect considerations should include base metal, heat-affected-zone and weld metal. If used in the as-welded condition, the residual stresses must also be considered in addition to the applied stresses.

It is very unlikely that the literature will contain sufficient K_{Ic} and slow crack growth data for all of the materials and for the

conditions of temperature, strain rate, heat treatment, environment and cyclic conditions specific to the application. To obtain all of these data for all of the materials would require an extensive testing program. However, the preliminary material evaluations do not require extensive data. K_{Ic} data for each material are sufficient to obtain an initial estimate of the defect tolerance of the materials in terms of the critical defect size for catastrophic failure upon one cycle of loading. For the problem at hand, the K_{Ic} data available from the literature or from a modest test program are shown in Table III. Also shown in Table III are the various types of possible defects that are envisioned in the pressure vessel. Type I is a relatively short, deep semi-elliptical surface flaw characteristic of a transverse weld crack or a crack occurring during heat treatment. Type II is long, shallow surface defect that could be a longitudinal weld or heat treatment crack in the weld-heat affected zone, or it could be a gouge, seam or lap in the base material. A spherical internal defect, Type III, represents a pore in a weld, an inclusion such as a tungsten globule from the welding electrode, or a nonmetallic inclusion. Type IV, an elliptical internal flaw represents the envelope which could be drawn around a cluster of small inclusions, pores, etc., which are sufficiently close to one another to have an interaction, or around a single, irregular shaped flaw. This type is most conveniently handled by considering it as one large flaw represented by the envelope.

a. Critical Defect Sizes for Failure During Proof Testing

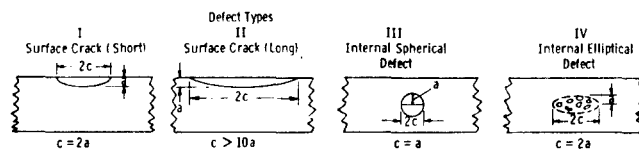
Using the K_{Ic} data for the materials and the envisioned types of flaws, the critical defect size which would cause failure during the 150% over pressure proof test ($\sigma = .75 \sigma_{YS}$) can be calculated. The worst condition is envisioned; that is, the defect is located in the the cylindrical section and is oriented normal to the largest (hoop) stress, and is located in the region of the weldment having the lowest K_{Ic} value. The results are shown in Table III, and the expressions used in the calculations are shown below.

Type I Short, deep surface crack ($c = 2a$)

$$a_{cr} = \frac{K_{Ic}^2 \left[\phi^2 - .212 \left(\frac{\sigma}{\sigma_{YS}} \right)^2 \right]}{1.21 \pi \sigma^2}$$

Sec. 8.4 Table III - Critical Defect Sizes for Catastrophic Fracture during Proof Tests for Various Materials and Types of Defects (Hypothetical Pressure Vessel) Curve 577917-8

Material	Yield Strength (ksi)	K _{Ic} (ksi√in)	Critical Defect Size* (Inches)							
			Type I		Type II		Type III	Type IV		
			Depth "a"	Length "2c"	Depth "a"	Length "2c"	Diameter 2a=2c	Minor Axis "2a"	Major Axis "2c"	
A. Maraging Steel Base Metal (BM) Weld Metal (WM) Heat-affected-zone (HAZ) (Welded and Aged)	300	50								
		45								
		40	.011	.044	.0073	>.073	.048	.026	.052	
B. Quench and Temper Steel BM WM HAZ (Welded and Stress Relieved)	200	90								
		90								
		70	.076	.304	.050	>.50	.330	.184	.368	
C. Titanium Alloy BM WM HAZ (Welded and Stress Relieved)	140	70								
		60								
		40	.051	.204	.034	>.34	.220	.124	.248	
D. Aluminum Alloy BM WM HAZ (Welded and Aged)	70	28								
		15								
		20	.029	.116	.019	>.19	.124	.070	.140	



* Defect is located in a longitudinal weld and is oriented normal to the hoop (primary) stress. The hoop stress during the proof test equals .75 σ_{ys} for each material

K_{Ic} = for appropriate region of weldment for each material

$\sigma = .75 \sigma_{ys}$ - stress during over pressure proof test

σ_{ys} = yield strength

$\Phi^2 = 1.45$ for defect geometry (from Figure 2)

Type II Long, shallow surface crack ($c > 10a$)

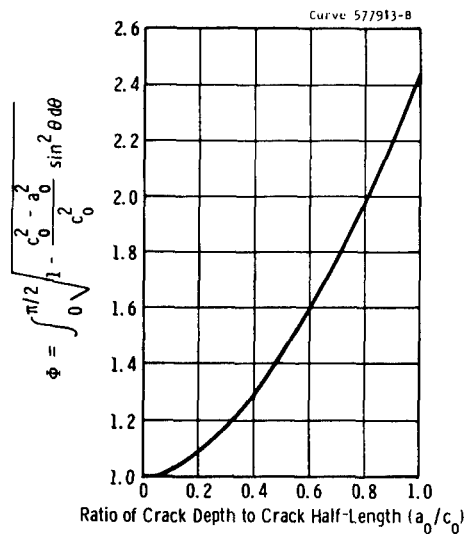
Same as Type I except

$$\Phi^2 = 1 \text{ (from Figure 2)}$$

Type III Internal sphere ($c = a$)

$$a_{cr} = \frac{K_{Ic}^2 \left[\Phi^2 - .212 \left(\frac{\sigma}{\sigma_{ys}} \right)^2 \right]}{\pi \sigma^2}$$

$$\Phi^2 = 2.5 \text{ (from Figure 2)}$$



Sec. 8.4 Fig. 2 -Graphical solution for ϕ^2 for use with elliptical shaped defects

Type IV Internal elliptical defect ($c = 2a$)

Same as Type III

$$\phi^2 = 1.45 \text{ (from Figure 2)}$$

As apparent from Table III, the surface defects (Types I and II) are the most crucial in that the critical defect size is the smallest in these types. For any given type and size of defect the fracture resistance of the four materials decreases in the following order: material B, C, D, A.

b. Nondestructive Inspection Capabilities

It is now necessary to consider these flaw sizes in terms of the inspection capability. The critical flaw sizes in the poorest material "A" are quite small, and the detection of such flaws would require non-destructive test capabilities which do not currently exist. The situation becomes even more realistic when a flaw detection safety factor is considered. The critical flaw sizes associated with material "B" (the toughest material of the group) are also quite small, and the detection of such flaws would tax the available nondestructive test techniques beyond these capabilities.

An ultrasonic inspection technique may be capable of detecting internal void similar in size and type to that shown in Table III (Type III and IV) however, such a technique would not permit the reliable detection of shallow surface flaws (Type I and II). Radiographic inspection would also be severely limited for the detection of surface cracks due to the proposed orientation and width (hair line cracks) of the flaws. Magnetic particle inspection could adequately reveal surface cracks over 1/8" in length but would provide no indication of the crack depth. As a result, a satisfactory nondestructive inspection procedure based upon the proposed critical flaw sizes shown in Table III could not be established for the materials under consideration.

A satisfactory inspection technique requires the capability of detecting the type of flaw which exhibits the smallest critical dimensions as well as the other type flaws which may be encountered in the structure. In view of this consideration it is obvious that a combination of inspection techniques may be required to adequately evaluate the structure. Prior to selecting the inspection technique and subsequent inspection specifications, a careful evaluation of the type and possible orientation of the flaws which may exist must be conducted. Once this is done the available inspection techniques can be evaluated as to the maximum flaw sensitivity based upon flaw type and testing orientation. The maximum flaw sensitivity can then be established and a limit set for the flaw size which can be reliably detected.

Considering the design and fabrication of the pressure vessel described above, the minimum critical flaw size which can be detected with a maximum degree of assurance using available nondestructive inspection techniques would be established as follows. The most critical flaw type and orientation would be a long shallow surface flaw (Type II) oriented with the length parallel to the major axis of the vessel. The most economical approach to the inspection of this vessel, provided it were fabricated from a ferromagnetic material, would be magnetic particle inspection. However, this inspection technique would be limited to the detection of the length of existing surface defects and would provide no indication of the depth. Another approach to consider would be radiographic

inspection but again this technique is limited. Radiography is capable of detecting flaws to a thickness sensitivity of 2% in the direction the x-ray beam is traveling. Assuming a vessel wall thickness of 3/4" this would mean a sensitivity capable of detecting a flaw 0.015" deep provided of course that the flaw was oriented parallel to the x-ray beam. Slight variations in orientation would reduce the sensitivity considerably. The apparent radiographic sensitivity appears quite adequate; however, no consideration of flaw cross-section with respect to the x-ray beam has been considered. The most stringent radiographic standards are limited to the detection of flaws which exhibit a width equivalent to twice the thickness sensitivity. Thus, a surface crack (Type II) would have to be about 0.030" wide regardless of its length to be detected. Since hair line type surface cracks (< < 0.030" wide) can occur during the welding operation, radiography cannot be used to accurately detect surface crack. However, the sensitivity to internal voids and inclusion similar to Types III and IV is quite adequate. Another alternative inspection procedure involves ultrasonic inspection. In order to detect surface cracks using an ultrasonic inspection techniques an angle beam test procedure is required. Sensitivities capable of detecting flaws which exhibit reflecting areas on the order of 0.005 sq. in. are normally readily obtainable when testing on flat surfaces.

However, considering the relatively small diameter of the pressure vessel under consideration (13" diameter) transducer contact problems result in a reduction in maximum sensitivity. A realistic detection capability to surface flaws would be limited to flaws about 0.045" deep and 0.180" long (reflecting area 0.008 sq. in.). As the flaws become deeper the length requirement would obviously decrease. In addition, ultrasonic inspection is limited in that it reveals the reflecting area of a flaw and not the flaw shape. As a result, ultrasonic inspection alone would not be sufficient to evaluate an existing surface flaw as to its critical nature. Ultrasonic inspection is also unable to detect tungsten inclusions which may exist in the weld.

Based upon the above considerations it is obvious that the non-destructive inspection specifications used to evaluate the vessel must

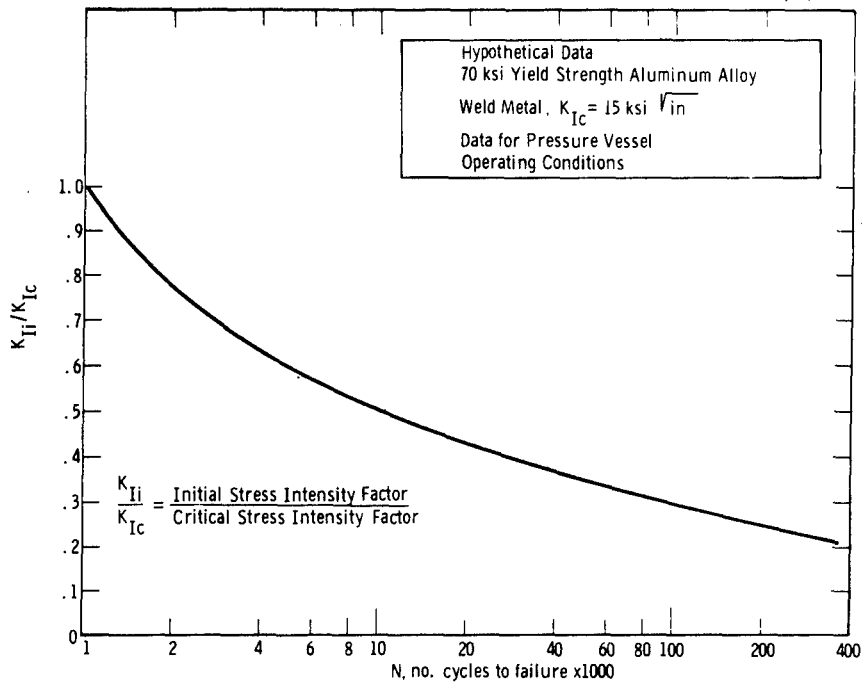
include a combination of inspection techniques. Ultrasonic and magnetic particle (dye-penetrant test in the case of non-magnetic materials) inspection could be used to evaluate surface flaws since the magnetic particle examination would reveal the crack length and ultrasonics would reveal the reflecting area (based upon a known notch-size reference standard) as a result, the crack depth could be determined. A radiographic examination would also be required to permit the detection of tungsten inclusions.

The maximum sensitivity of the combined inspection procedure would be limited to the detection of surface cracks larger than 0.045" deep and 0.180" long and internal flaws approximately 0.03" in diameter.

c. Considerations of Cyclic Life and Initial Flaw Sizes

In view of the NDT capabilities, it is apparent that none of the four materials would be satisfactory for the application and the initial design requirements which were imposed. This is most apparent when the cyclic life is considered. Detailed data on the slow crack growth characteristics of the materials under the specific application conditions are not available in the literature. However, for the situation of concern specific data for quantitative consideration are not required since it can be stated without doubt that the allowable size of an initial defect at the start of life will be much smaller than the critical flaw sizes for catastrophic failure during proof testing that are shown in Table III. Therefore, since the capability of the available NDT techniques to detect flaws of the critical size is questionable, it is certain that the much smaller initial size defects that would not grow to a critical size could not be found.

This conclusion can be substantiated by considering the situation for the case of the Aluminum alloy and the Type I defect. Although no crack growth data specific to the application conditions exist for the alloy, there are some data available (Figure 3) for the alloy for similar conditions. These will suffice for a qualitative estimate of the allowable size for the initial defect.



Sec. 8.4 Fig. 3 -Cyclic flaw growth data for aluminum alloy

Referring to the original design conditions the following information is known:

- (1) Required minimum life 40,000 cycles
- (2) Maximum stress in a cycle $1/2 \sigma_{YS} = 35,000$ psi
- (3) K_{Ic} of material (weld metal = 15,000 psi in.
- (4) Semi-elliptical surface defect (length 4x depth)

From Figure 2, the $\frac{K_{Ii}}{K_{Ic}}$ ratio corresponding to 40,000 cycles of life is 0.36. The initial stress intensity can now be determined

$$K_{Ii}/K_{Ic} = .36 = \frac{K_{Ii}}{15,000 \text{ psi in.}}$$

$$K_{Ii} = .36 (15,000 \text{ psi in.}) = 5400 \text{ psi in.}$$

Knowing the design stress of 35,000 psi and the expression of the type of defect, it is now possible to find the defect size corresponding to a K_{Ii} of 5400 psi in.

The approach now is to reduce the design stress to a level so that the initial allowable defect size for a Type II defect is no less than the minimum detectable depth of 0.045" plus a detection safety factor arbitrarily set at 1.5. The operating stress for cyclic loading to a minimum life of 40,000 cycles with this initial flaw size ($a_i = 0.067"$) can be computed as follows: the K_{Ii}/K_{Ic} ratio for material B for 40,000 cycles is 0.38 from Figure 4.

$$K_{Ii} = .38 K_{Ic} = .38 (70,000 \text{ psi } \sqrt{\text{in.}}) = 26,600 \text{ psi } \sqrt{\text{in.}}$$

Substituting into the proper expression for the semi-elliptical surface flaw and solving for σ :

$$a_i = \frac{K_{Ii}^2 \left[\phi^2 - .212 \left(\frac{\sigma}{\sigma_{YS}} \right)^2 \right]}{1.21 \pi \sigma^2}$$

$$.067 = \frac{(26,600)^2 \left[1.0 - .212 \left(\frac{\sigma}{200,000} \right)^2 \right]}{1.21 \pi \sigma^2}$$

$$\sigma = 55,500 \text{ psi}$$

Therefore, a reduction in the operating stress from 100,000 to 55,500 psi would make it possible for Steel B to tolerate an initial defect of 0.067" deep. If a larger safety factor is deemed necessary for detection of this size flaw, the design stress would have to be further reduced.

The size and weight of the vessel based on this design stress of 55,500 psi are:

- Total Outside Diameter = 14.7"
- Total Outside Length = 38.7"
- Total Weight of Vessel = 498 lbs.

Although the overall dimensions are within the allotted space requirements, the weight of the vessel is unacceptably high. Thus, material B is eliminated from any further consideration.

8.4.2.4 Using a Lower-Strength, Higher-Toughness Steel

a. Critical Defect Sizes for Failure

The other alternative of using a lower strength but higher toughness material must now be considered. Considerations of potential lower strength materials reveal that a quenched and tempered steel called HY150 (Material E) can develop high toughness at a yield strength of 150,000 psi. No aluminum or titanium alloys with a satisfactory combination of strength and toughness were found to be available. The following fracture toughness data are available from the supplier for this steel E in the welded and stress relieved condition.

	<u>K_{Ic} (psi $\sqrt{\text{in.}}$)</u>
Base Metal	150,000
Weld Metal	140,000
Heat Affected Zone	120,000

A limited test program using the application conditions is conducted and confirms the supplier's data given above. Slow crack growth information are also generated for both cyclic and sustained loading with the results shown in Figures 5 and 6.

With these data it is now possible to quantitatively evaluate the potential of this new material "E". Using the same design conditions as employed for the other materials (A-D) and Type II defect, the critical flaw sizes for catastrophic failure during proof testing or operation are calculated in the same manner previously illustrated. The critical defect sizes are found to be:

for operating stress of $.5 \sigma_{YS}$, depth 0.63" length > 12.8"

for proof test stress of $.75 \sigma_{YS}$, depth 0.267" length > 5.34"

These flaw sizes are well within the inspection capability. Combinations

The approach now is to reduce the design stress to a level so that the initial allowable defect size for a Type II defect is no less than the minimum detectable depth of 0.045" plus a detection safety factor arbitrarily set at 1.5. The operating stress for cyclic loading to a minimum life of 40,000 cycles with this initial flaw size ($a_i = 0.67''$) can be computed as follows: the K_{Ii}/K_{Ic} ratio for material B for 40,000 cycles is 0.38 from Figure 4.

$$K_{Ii} = .38 K_{Ic} = .38 (70,000 \text{ psi } \sqrt{\text{in.}}) = 26,600 \text{ psi } \sqrt{\text{in.}}$$

Substituting into the proper expression for the semi-elliptical surface flaw and solving for σ :

$$a_i = \frac{K_{Ii}^2 \left[\phi^2 - .212 \left(\frac{\sigma}{\sigma_{YS}} \right)^2 \right]}{1.21 \pi \sigma^2}$$

$$.067 = \frac{(26,600)^2 \left[1.0 - .212 \left(\frac{\sigma}{200,000} \right)^2 \right]}{1.21 \pi \sigma^2}$$

$$\sigma = 55,500 \text{ psi}$$

Therefore, a reduction in the operating stress from 100,000 to 55,500 psi would make it possible for Steel B to tolerate an initial defect of 0.067" deep. If a larger safety factor is deemed necessary for detection of this size flaw, the design stress would have to be further reduced.

The size and weight of the vessel based on this design stress of 55,500 psi are:

- Total Outside Diameter = 14.7'
- Total Outside Length = 38.7'
- Total Weight of Vessel = 498 lbs.

Although the overall dimensions are within the allotted space requirements, the weight of the vessel is unacceptably high. Thus, material B is eliminated from any further consideration.

8.4.2.4 Using a Lower-Strength, Higher-Toughness Steel

a. Critical Defect Sizes for Failure

The other alternative of using a lower strength but higher toughness material must now be considered. Considerations of potential lower strength materials reveal that a quenched and tempered steel called HY150 (Material E) can develop high toughness at a yield strength of 150,000 psi. No aluminum or titanium alloys with a satisfactory combination of strength and toughness were found to be available. The following fracture toughness data are available from the supplier for this steel E in the welded and stress relieved condition.

	<u>K_{Ic} (psi $\sqrt{\text{in.}}$)</u>
Base Metal	150,000
Weld Metal	140,000
Heat Affected Zone	120,000

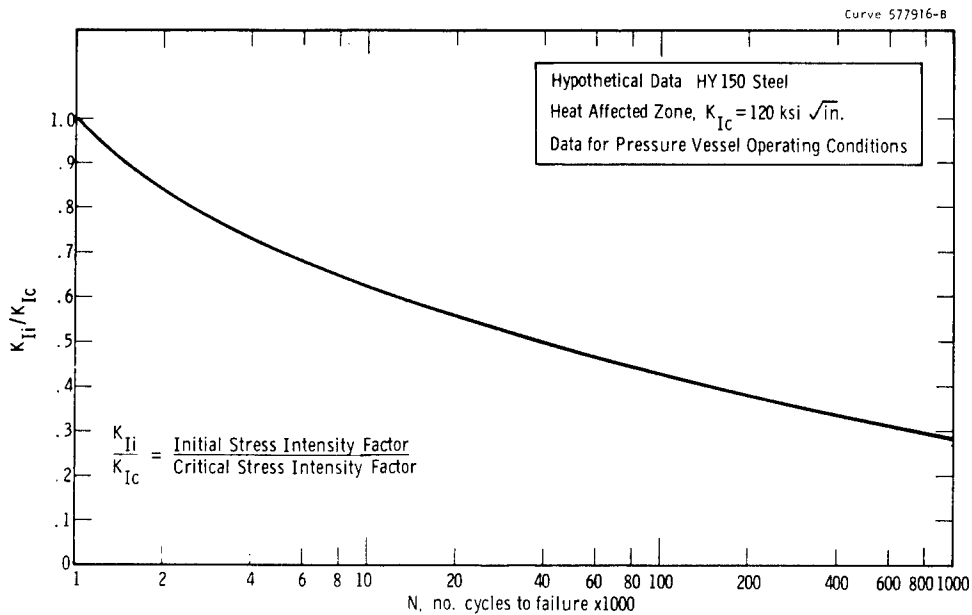
A limited test program using the application conditions is conducted and confirms the supplier's data given above. Slow crack growth information are also generated for both cyclic and sustained loading with the results shown in Figures 5 and 6.

With these data it is now possible to quantitatively evaluate the potential of this new material "E". Using the same design conditions as employed for the other materials (A-D) and Type II defect, the critical flaw sizes for catastrophic failure during proof testing or operation are calculated in the same manner previously illustrated. The critical defect sizes are found to be:

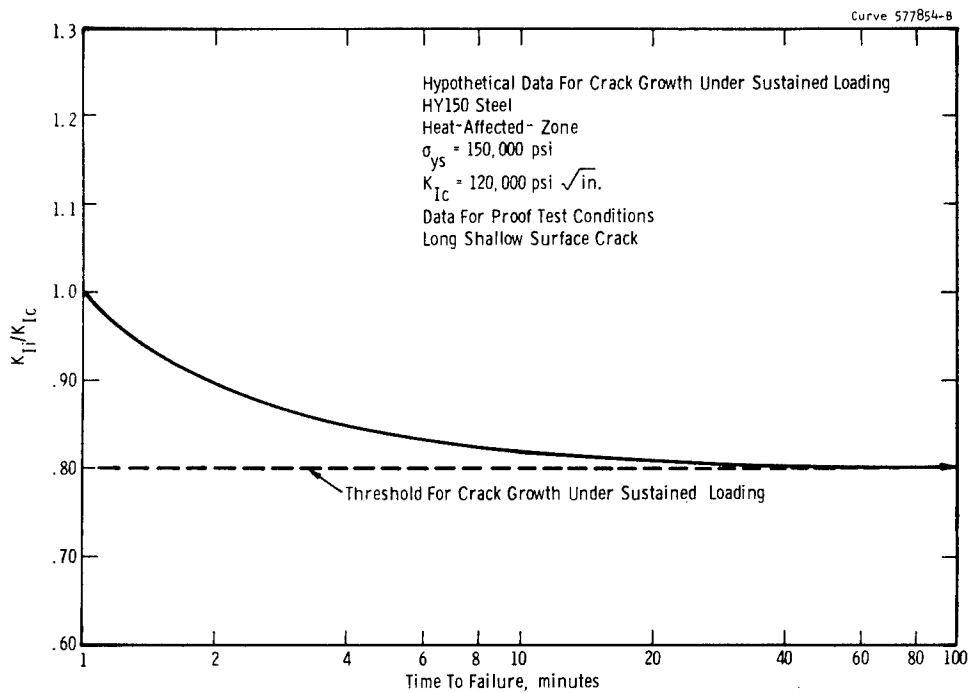
for operating stress of $.5 \sigma_{YS}$, depth 0.63" length > 12.8"

for proof test stress of $.75 \sigma_{YS}$, depth 0.267" length > 5.34"

These flaw sizes are well within the inspection capability. Combinations



Sec. 8.4 Fig. 5 -Cyclic flaw growth data for material E, a 150 ksi yield strength steel (HY 150)



Sec. 8.4 Fig. 6 -Crack growth and failure times under sustained loading

of shorter, deeper flaws could also be critical, but these also would be within detection limits because their depth will always be increasing beyond the already detectable limit represented by the shallow flaw.

b. Cyclic and Sustained Loading Crack Growth

In considering the cyclic behavior the critical initial defect size (Type II) is found in the manner described below using the data from Figure 5 and the known values of K_{Ic} and operating stress of $.5\sigma_{YS}$.

Determining the maximum allowable initial defect size from Figure 5 $\frac{K_{Ii}}{K_{Ic}}$ at 40,000 cycles = 0.5

$$K_{Ii} = 5 K_{Ic} = 60 \text{ ksi in.}$$

$$a_i = \frac{K_{Ii}^2 \left[\phi^2 - .212 \left(\frac{\sigma}{\sigma_{YS}} \right)^2 \right]}{1.21 T \pi \sigma^2}$$

$$a_i = \frac{(60,000)^2 \left[1.0 - .212 \left(\frac{75000}{150000} \right)^2 \right]}{1.21 \pi (75000)^2}$$

$$a_i = .160$$

For steel E the maximum allowable initial defect size (Type II) which will not grow to a critical size in 40,000 cycles is 0.16" deep by 3.2" long. Again other combinations of shorter and deeper flaws could result in the same cyclic life. However, since the most shallow flaw represented by Type II already has a depth of 0.16" which is greater than the detection limit of $> .045"$, all of the initial size defects for shorter, deeper cracks which would grow to a critical size are within detection limits.

It is also necessary to determine the size of defect which can initially exist and not grow to a critical size under sustained loading during the proof test. Again considerations will be confined to the worst case, a long shallow surface flaw in the heat-affected-zone of the longitudinal weld, thus normal to the hoop stress. Data (Figure 6) for the heat-affected-zone

and other conditions appropriate to the hydro test conditions, e.g. a water environment, are available from a test program. These data indicate that the threshold for slow crack growth under sustained loading is $K_{Ii}/K_{Ic} = 0.8$. The holding time specified in the proof test is 60 minutes and the pressure is 150% of the operating pressure. Based on the data (Figure 6) the vessel will not fail during proof test so long as the defect size at the beginning of the test did not exceed a value corresponding to a K_{Ii} greater than $0.8 K_{Ic}$. It is possible to determine this defect size using the worst case of a long shallow surface crack

$$a_i = \frac{K_{Ii}^2 \left[\phi^2 - .212 \left(\frac{\sigma}{\sigma_{YS}} \right)^2 \right]}{1.21 \pi \sigma^2}$$

$$a_i = \frac{[.8(120,000)]^2 \left[1.0 - .212 \left(\frac{112500}{150000} \right)^2 \right]}{1.21 \pi (112,500)^2}$$

$$a_i = .170 \text{ length} = 3.40''$$

This defect size is well within the inspection capability, therefore the material is adequate from the proof test viewpoint.

It is also necessary to determine the weight and size of the pressure vessel made from this steel. Using the same procedure as employed previously for the other materials, the following results are obtained:

Wall Thickness = 0.58"
 Total Outside Diameter = 14.2"
 Total Outside Length = 38.2"
 Total Weight of Vessel = 378 pounds

c. Reducing the Weight of the Vessel

The size of this pressure vessel would permit its use in the allotted space. However, the weight is undesirably high. In view of the good toughness and the associated large defects for a design stress of $.5 \sigma_{YS}$, it may be possible to reduce weight by increasing the design stress to a higher level, thereby reducing the necessary wall thickness.

The best way to determine how much the design stress can be raised is to center attention on the smallest defect of concern, which is the initial allowable defect. The maximum allowable initial size for the severe Type II defect that would not grow to a critical size during the desired life of the vessel was 0.160" deep and 3.2" long for a design stress of $1/2 \sigma_{YS}$. The minimum size defect that could be consistently detected is 0.045" deep by 0.180" long. This allows a safety factor of nearly 4 in terms of the available detection capability for depth and a much larger factor for length. After thorough consideration of the inspection techniques it is decided that such a large safety factor is too conservative, and that a factor of 2 based on depth would be quite adequate to allow for any uncertainties in inspection procedures. Applying a safety factor of 2 to the detection limits of 0.045" deep raises the maximum allowable initial defect size to 0.090" deep.

It is now possible to compute the allowable stress for this depth of initial defect. From the crack growth data of Figure 5, the $\frac{K_{Ii}}{K_{Ic}}$ ratio for a life of 40,000 cycles is 0.5. K_{Ii} is $0.5 K_{Ic}$ or $.5 (120 \text{ ksi in.}) = 60 \text{ ksi } \sqrt{\text{in.}}$. The allowable stress is determined using the expression

$$a_i = \frac{K_{Ii}^2 \left[\phi^2 - .212 \left(\frac{\sigma}{\sigma_{YS}} \right)^2 \right]}{1.21 \pi \sigma^2}$$

by substituting the appropriate numbers and solving for σ .

$$\begin{aligned} a_i &= 0.090" \\ K_{Ii} &= 60 \text{ ksi } \sqrt{\text{in.}} \\ \sigma_{YS} &= 150 \text{ ksi} \\ \phi^2 &= 1.0 \text{ for limiting case flaw geometry where } c \geq 10a \end{aligned}$$

The calculated value of σ is 98,000 psi.

Now it is necessary to determine the critical flaw depths for catastrophic failure for this operating stress and its corresponding proof stress. Using

$$\text{defect depths are: } a_{cr} = \frac{K_{Ic}^2 \left[\phi^2 - .212 \left(\frac{\sigma}{\sigma_{YS}} \right)^2 \right]}{1.21 \pi \sigma^2} \quad \text{the critical}$$

$$a_{cr} = 0.14'' \text{ deep} \quad \text{for proof test pressure}$$

$$a_{cr} = 0.36'' \text{ deep} \quad \text{for operating pressure}$$

The critical defect size for catastrophic failure during cyclic operation or proof testing must obviously be larger than the initial defect size that will not grow to be critical in 40,000 cycles. As seen above, their respective values for defect depth are well in excess of the initial allowable depth of .090".

The initial defect depth which will not grow to a critical size for failure on 1 cycle of loading during the 150% overpressure proof test must also be larger than the allowable initial defect in order to prevent premature failure during proof test. This defect size is calculated in the same manner as used above for the critical size for catastrophic failure, but the K_{Ic} value used must be reduced to $.8 K_{Ic}$ to be below the threshold for crack growth under sustained loading (Figure 6). The resulting depth is 0.112", which is larger than the .090" initial depth so there are no problems in this area. Therefore, all of the defects of concern, both the initial and critical for operating stress of 98,000 psi, and the initial and critical for the proof test at 147,000 psi, are sufficiently large to be within the detection capability of 0.045 deep by 0.180" long.

The foregoing data indicate that from the fracture viewpoint a design stress of 98,000 psi could be employed for operation. Similarly the stress of 147,000 psi during the 150% overpressure proof test could also be tolerated with a flaw considerably larger than the minimum detectable size. However, the proof stress of 147,000 psi is working too close to the yield strength of the material (150,000 psi) and could cause trouble from a plastic deformation viewpoint. Therefore a conservation design stress of 90,000 psi with a corresponding proof stress of 135,000 is deemed more reasonable. The design stress is now fixed at $.6 \sigma_{YS}$ and the proof stress at $.9 \sigma_{YS}$.

It is now possible to determine the size and weight of the vessel based on use of this steel (Material E) and a new design stress of 90,000 psi. The wall thickness is determined from the conventional expression:

$$T = \frac{PD}{2\sigma} = \frac{(10,000 \text{ psig}) (12.0'')}{2 (90,000 \text{ psi})}$$

$$T = .694 \text{ or } .70''$$

The vessel dimensions are:

$$\text{Inside Diameter} = 12.5''$$

$$\text{Outside Diameter} = 13.9''$$

$$\text{Wall Thickness} = 0.7''$$

$$\text{Overall Length} = 37.9''$$

The weight of the vessel is 306 pounds and represents a considerable reduction from the 378 pounds required if the lower design stress of 75,000 psi were used.

8.4.2.5 Summary of Final Selection of a Material

The material and design considerations have now reached essentially optimum conditions. With the available materials no further weight reductions are possible without jeopardizing the integrity of the pressure vessel. Based on the previous considerations, the HY150 steel (E) used in conjunction with an operating stress of $0.6 \sigma_{YS}$ has adequate toughness and crack growth resistance to provide a high degree of assurance against brittle fracture. All of the allowable defect sizes are well within inspection capabilities. While a higher operating stress could be tolerated from the fracture viewpoint, it would result in proof test stresses in excess of the yield strength. Therefore, the limiting criterion for the use of this steel is now related to preventing plastic distortion during the 150% overpressure proof test.

The pertinent information for the material and the application conditions are summarized below.

A. Material properties under application conditions

- (1) K_{Ic} - base material = 150,000 psi $\sqrt{\text{in.}}$
 - weld metal = 140,000 psi $\sqrt{\text{in.}}$
 - heat-affected zone = 120,000 psi $\sqrt{\text{in.}}$

- (2) σ_{YS} - yield strength = 150,000 psi
(lower limit for either base, weld, or heat-affect zone)

- (3) Slow crack growth characteristics as per Figure 5 (Material E)
(Upper limit for growth rate)

B. Maximum stresses at any location in the vessel

(Hoop stress in the cylindrical section)

σ - operating = 90,000 psi = 0.6 σ_{YS}

σ - proof test = 135,000 psi = 0.9 σ_{YS}

C. Critical defect sizes for most detrimental defects*

(1) Semi-elliptical surface defect where $c > 10a$ (limiting case for shallow defect)

	<u>Operating Conditions ($\sigma = 90,000$ psi)</u>		<u>Proof Test ($\sigma = 135,000$)</u>	
	<u>Depth "a" (inches)</u>	<u>Length "2c" (inches)</u>	<u>Depth "a" (inches)</u>	<u>Length "2c" (inches)</u>
Initial	0.11	2.20	-----	-----
Critical	0.44	9.00	0.18	3.60

(2) Semi-circular surface defect where $c = a$ (limiting case for short, deep defect)

	<u>Operating Conditions ($\sigma = 90,000$ psi)</u>		<u>Proof Test ($\sigma = 135,000$)</u>	
	<u>Depth "a" (inches)</u>	<u>Length "2c" (inches)</u>	<u>Depth "a" (inches)</u>	<u>Length "2c" (inches)</u>
Initial	0.28	0.56	-----	-----
Critical	1.11	2.22	0.48	0.97

D. Minimum detectable size of surface defects is 0.045" deep and 0.180" long.

- (1) All of the defect sizes shown above for the most detrimental case are well within the inspection capability.
- (2) There is a more than adequate difference in size between detectable and critical flaws to permit the use of a generous safety factor in establishing allowable flaw sizes.

* Most detrimental because:

- Defect geometry is the most critical type
- Defect is located in the region of poorest toughness (heat-affect-zone)
- Defect is located in the region of highest stress (longitudinal weld of cylinder)
- Defect is oriented normal to the highest (hoop) stress

Based on all of the foregoing considerations the HY150 quenched and tempered steel (Material E) has the capability of providing the desired assurance against brittle failure. It is therefore selected as the optimum material for use in the pressure vessels.

The material "E" (HY150) steel was chosen as a hypothetical material to use in this example. For the sake of clarity and brevity no other materials of lower strength-higher toughness were considered in this problem. In a real situation, there may be several alternative materials that should be considered. However, the procedures that would be employed would be the same as used for HY150 in the foregoing example.

8.4.3 ESTABLISHING SPECIFICATION, INSPECTION AND ACCEPTANCE CRITERIA

Once the application and design requirements have been well established and a satisfactory material selected, it becomes necessary to incorporate the pertinent acceptance criteria into quality control specifications. In terms of material requirements, the HY150 plate and spun heads supplied for vessel fabrication must exhibit tensile and toughness properties equivalent to those used for design purposes. In addition, the supplied material must satisfy the conventional acceptance criteria associated with chemistry, heat treatment, hardness, etc. Since the vessels in questions are to be fabricated using welding techniques, acceptance criteria must also be established for the weld and heat-affected zone. Therefore, material acceptance testing must be conducted on weld-prepared samples fabricated in the same manner as the proposed vessels using full thickness plate. Testing must be conducted under the environmental service conditions (temperature, atmosphere, etc.) most likely to induce brittle failure.

Although the allowable flaw size criteria are based upon the lowest toughness expected to be encountered in the fabricated vessel ($K_{Ic} = 120 \text{ ksi } \sqrt{\text{in.}}$ for heat-affected-zone), the minimum allowable toughness prior to fabrication must also be considered. Assuming that the welding operation degrades the plate toughness (HAZ), the acceptance criterion for the "as-received" plate must require sufficient toughness to permit the

allowable degradation. For the purpose of this example assume that the base plate (and spun heads) must exhibit a K_{Ic} of 150 ksi $\sqrt{\text{in.}}$ prior to welding in order to yield a K_{Ic} of 120 ksi $\sqrt{\text{in.}}$ in the heat-affected-zone. As a result, the material acceptance specifications for the 0.750" thick HY150 plate and hot sup heads to be used for vessel fabrication should stipulate the following requirements:

1. The supplied HY150 alloy steel (both plate and heads) must exhibit a minimum 0.2% off-set yield strength of 150,000 psi in the temperature range of -20°F to 100°F .
2. The minimum plane strain fracture toughness, K_{Ic} must be 150 ksi $\sqrt{\text{in.}}$ at any temperature from -20 and 100°F .

Provided the parent material satisfies the yield strength and toughness criteria as well as other related criteria (heat treatment, chemistry, etc.), weldment specimens must then be prepared and evaluated against the following criteria.

1. The 0.2% yield strength of the stress-relieved weldments (weld metal and heat-affected-zone) must exhibit a minimum value of 150,000 psi at any temperature from -20 and 100°F .
2. The minimum K_{Ic} value exhibited by the weldment over the temperature range of -20°F to 100°F must be 120 ksi $\sqrt{\text{in.}}$

Once it has been established that the supplied material and resulting weld structure exhibit the required yield strength and toughness criteria it is then necessary to provide adequate inspection specifications.

The nondestructive inspection specifications must require inspection techniques which are capable of evaluating the material or structure at any point during fabrication from the inspection of the "as-received" material to the inspection of a vessel removed from service.

The critical flaw sizes associated with failure under both static and cyclic loading conditions have been defined earlier during the preliminary design considerations involving the selection of HY150 as a satisfactory fabrication material. It was also shown that these flaw sizes were well within the detection capability of available inspection techniques. Knowledge of the minimum flaw sizes which can result in failure provides the basis for determining the nondestructive inspection acceptance criteria. Since the

fabricated pressure vessels are required to exhibit a life expectancy of 40,000 cycles at a stress of 90,000 psi, the existing flaw size at the beginning of life (initial size) which can grow to critical size in 40,000 cycles becomes the limiting flaw detectability consideration. Both surface flaws and internal flaws of geometric extremes (long shallow flaws to circular flaws) must be considered since the geometry of the flaw as well as its size determines its critical nature. In addition, the flaws must be considered to exist within the most highly stressed portion of the vessel, in this case, in the body cylinder of the vessel with the major flaw axis parallel to the seam weld. Figure 7 shows the size (length and depth) associated with the minimum initial surface flaw which will result in catastrophic failure in 40,000 cycles. Figure 8 presents similar information for internal defects. Considering the limitations of the available nondestructive test techniques described earlier (Section 8.4.2.2.b)--minimum detectable surface flaw depth 0.045", length 0.180", minimum detectable internal flaw 0.030" diameter--it is obvious that detection capabilities are well within the acceptance limits as illustrated in Figures 7 and 8. It now becomes necessary to establish a realistic limit for the maximum acceptable flaw size which becomes the basis for the acceptance-rejection inspection criteria.

The most critical inspection criterion is the evaluation of surface flaw depth since the minimum depth for failure (0.110") is the flaw dimension nearest the limits of detectability (0.045"). The minimum rejectable surface flaw depth was selected as 0.060" since this provides a safety factor of realistic magnitude (0.050"). The rejectable limits involving the surface flaw length as well as the length and depth of internal flaws were established using a safety factor of 1.5. The limits of acceptable flaw sizes are also illustrated in Figures 7 and 8 for surface flaws and internal flaws respectively. In addition, in establishing the rejection level, the mathematical limits of the expressions used to determine the critical flaw sizes must be considered. These expressions are reliable provided the flaw depths involved do not exceed one-half the plate thickness. Therefore, any flaw which exhibits a depth greater than one-half the plate thickness must be rejected. Based upon

Figures 7 and 8, such a limitation also provides assurance that an existing flaw will not grow through the vessel wall resulting in leakage.

The acceptable flaw size curves illustrated in Figures 7 and 8 must be used to evaluate the critical nature of each flaw detected as the result of nondestructive inspection. These curves apply equally well to the inspection of the "as-received" plate and at any stage of fabrication or service.

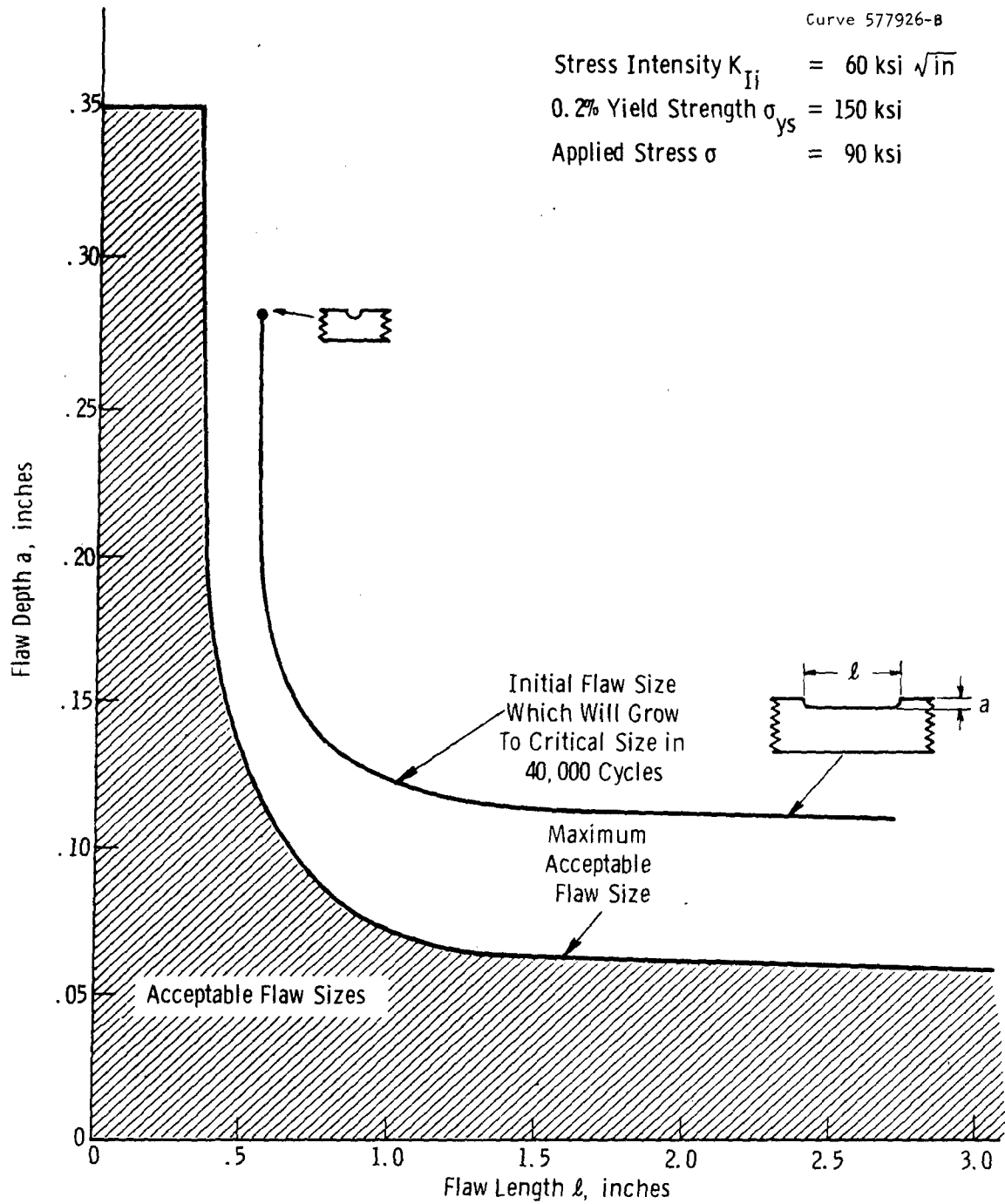
As pointed out in Section 8.4.1.2, a combination of magnetic particle, ultrasonic, and radiographic inspection techniques are required to provide an adequate inspection procedure. Magnetic particle and ultrasonic inspection of the supplied plate and heads in accordance with the flaw size acceptance criteria in Figures 7 and 8 would be sufficient for material acceptance criteria. However, radiographic inspection in addition to ultrasonics and magnetic particle inspection is required to evaluate the welds associated with vessel fabrication.

Summarizing the pertinent specifications and acceptance criteria it is obvious that the yield strength, toughness, and allowable flaw sizes provide the basic information required to permit the use of the fracture mechanic approach to design. The minimum allowable yield strength associated with any portion of the vessel including the weldments is 150,000 psi at any temperature within the operating range of -20 to 100°F. The acceptable K_{Ic} toughness level corresponding to the 150,000 psi yield strength is 150 ksi $\sqrt{\text{in}}$ for the plate and heads, and 120 ksi $\sqrt{\text{in}}$ for the weldment. The allowable defect sizes are adequately defined in Figures 7 and 8 and a sufficient safety factor included. This safety factor should take into account those possible flaw geometries and types not considered. Only when each of these factors are adequately considered can fracture mechanics provide a reliable quantitative basis to the design against brittle failure.

8.4.4 PROOF TESTING AND LIFE EXPECTANCY EVALUATION

8.4.4.1 Proof Testing

Proof testing of pressure vessels has been a common practice that has been employed for many years to demonstrate the integrity of the finished product. In effect it could be considered as a 100% inspection



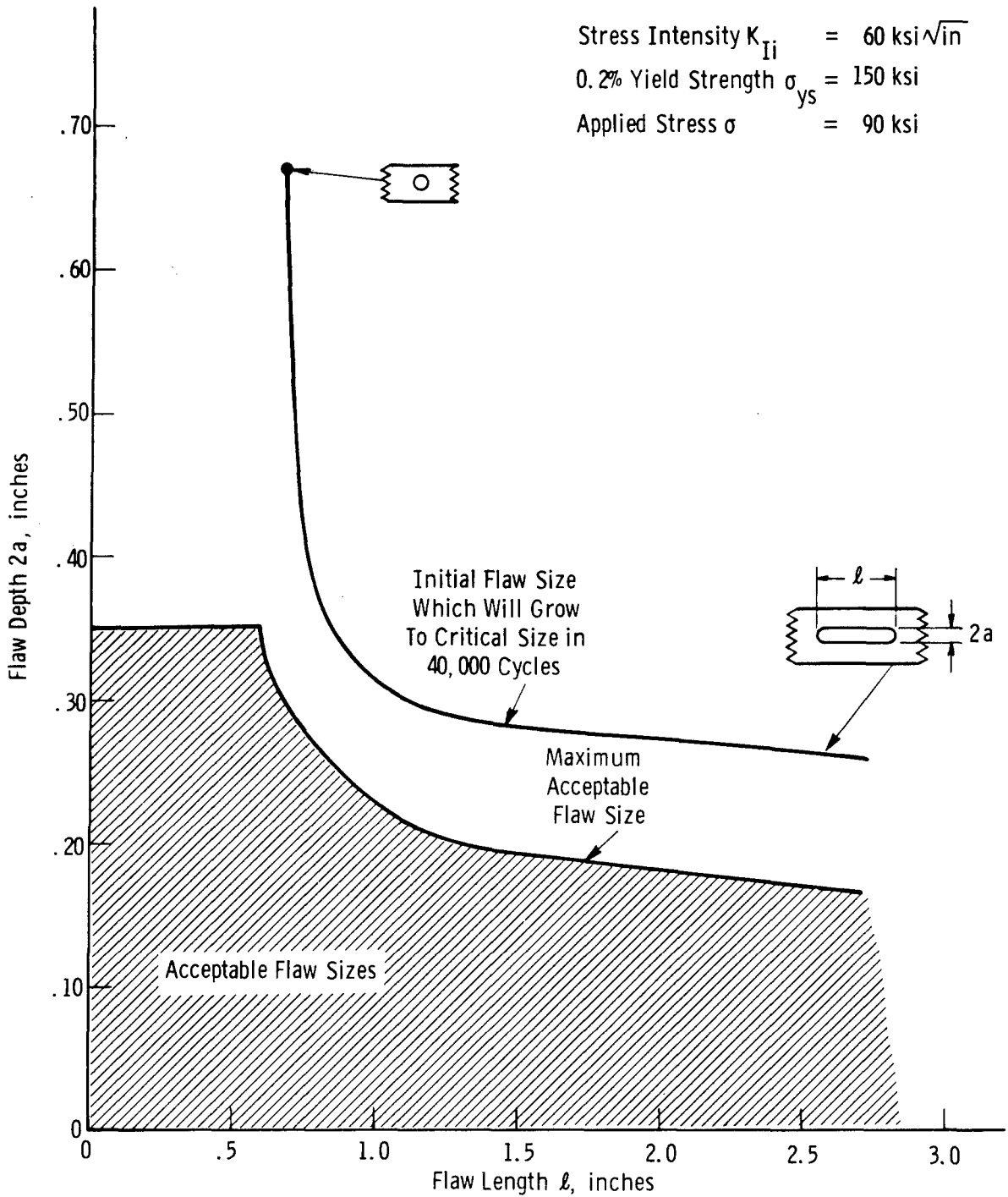
Sec. 8.4 Fig. 7 —Acceptable external flaw sizes

Curve 577927-8

Stress Intensity K_{Ii} = 60 ksi $\sqrt{\text{in}}$

0.2% Yield Strength σ_{ys} = 150 ksi

Applied Stress σ = 90 ksi



Sec. 8.4 Fig. 8 - Acceptable internal flaw sizes

technique. Fracture mechanics technology has made it possible to obtain even more quantitative information pertaining to the integrity and expected performance characteristics of pressure vessels from proof testing.

With respect to the example pressure vessel, surviving the proof test at 150% of operating pressure for a 60-minute holding period, provides assurance that any defects that may exist anywhere in the vessel are smaller than the critical size for failure at the proof stress. Naturally, the critical size for any given defect is dependent upon not only the material toughness but also upon the type of defect, its location or orientation, and the stresses prevailing in the section of the vessel where it is located. For purposes of this example, considerations will be confined primarily to the worst case, a long shallow surface flaw in the heat affected zone of the longitudinal weld and normal to the hoop stress. The same considerations that will be given to this defect will apply equally as well to other types of flaws and/or other locations within the vessel.

a. Crack Growth Under Sustained Loading

Slow crack growth under sustained loading during the proof test must be considered. One situation that can be envisioned concerns the possibility that an undetected flaw could grow to a critical size during the 60-minute sustained loading period and cause failure during the proof test. Another possibility is that a known defect of an initially acceptable size could grow to an unacceptable size for subsequent operating conditions or even to a critical size during proof testing. Let us consider these possibilities in more detail.

To properly assess the situation, data on the slow crack growth characteristics under sustained loading for the hydro test environment are required. A convenient form of these data is K_{Ii}/K_{Ic} vs time to failure. Data (Figure 6) for the poorest material condition (heat-affected-zone) and the other conditions appropriate to the application are available from the test program conducted during the initial evaluation of material E (Section 8.4.2.4.b). These data indicate that the threshold for slow crack growth under sustained loading in a water environment simulating the hydro test condition is $K_{Ii}/K_{Ic} = 0.8$. The holding time specified in the proof test is 60 minutes. Based on the data in Figure 6, the vessel would not fail

during proof test so long as the defect size at the beginning of the test did not exceed a value corresponding to a K_{Ii} greater than $.8 K_{Ic}$. It is possible to determine this defect size for various types of flaws. For an example, consider the case of a long shallow surface crack.

$$a_i = \frac{K_{Ii}^2 \left[\phi^2 - .212 \left(\frac{\sigma}{\sigma_{YS}} \right)^2 \right]}{1.21 \pi \sigma^2}$$

$$a_i = \frac{[.8(120,000)]^2 \left[1.0 - .212 \left(\frac{135000}{150000} \right)^2 \right]}{1.21 \pi (135,000)^2}$$

$$a_i = 0.110'' \quad \text{length} = 2.20''$$

If an undetected flaw of this size or larger in either dimension would be present at the start of the 60 minute proof test, the vessel would fail during test. However, in view of the detection capability of .045" deep by 0.180" long, it would appear unlikely that such a defect could go undetected, and the probability of an unexpected failure during proof testing is quite low.

Now consider the case where a known defect of an acceptable size for operating conditions exists prior to proof testing. The maximum allowable size flaw (for the type being used in this example) is .060" deep by 2.5" long as may be seen in Figure 7. This size is considerably smaller than the 0.110" by 2.2" flaw size which must prevail initially in order to grow to the critical size necessary to cause failure in the proof test. Viewed in other terms, the K_{Ii} for the specified maximum allowable defect size (for operating conditions) at the proof test stress is $.59 K_{Ic}$. As seen in Figure 6 this is considerably below the threshold level of $.8 K_{Ic}$ that is required for crack growth during the proof test. Therefore a defect of an initially acceptable size (Figure 7) would not grow at all during the proof test. Hence, there is no possibility during proof testing that a defect of an initially acceptable size will grow to an unacceptable size for subsequent operating condition.

b. Leak or Failure During Proof Testing

Fracture mechanics can also be employed to consider the question of leak before failure during proof testing. If an unexpected defect existed or developed during the proof test (hydrostatic) what would be the nature of the failure--a local rupture and leakage, or catastrophic failure with extensive splitting and/or fragmentation? Consideration of the critical size defect for failure provides the basis for answering this question. If for the prevailing proof test conditions the material has sufficient toughness to tolerate a defect large enough to extend through the wall thickness without failure, there is a possibility of leak before failure. On the other hand if the critical flaw size for failure is less than the wall thickness, catastrophic failure is almost a certainty. For the example pressure vessel, the critical size for the various defects envisioned are as follows:

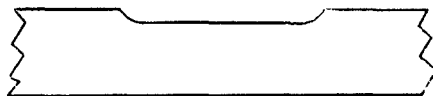
(For heat affected zone of longitudinal weld and normal to hoop stress)

1. Semi-circular surface defect



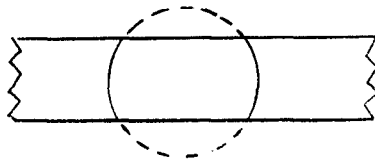
0.48" deep by 0.97" long

2. Long semi-elliptical surface defect



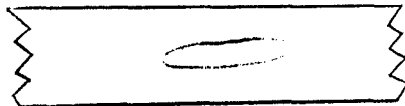
0.18" deep by 3.6" long

3. Disk-shaped internal defect



1.15" diameter

4. Long elliptical internal defect



0.42" by 4.16" long

When compared to the wall thickness of the pressure vessel which is 0.70", all of the types of defects shown above would result in catastrophic failure except possibly the disk shaped internal defect. Its critical diameter is greater than the wall thickness. Therefore, it would now have to be considered a through-the-thickness defect and a corresponding critical crack length determined.

For through-the-thickness defect:

$$a = \frac{K_{Ic}^2 \left[1 - .5 \left(\frac{\sigma}{\sigma_{YS}} \right)^2 \right]}{\pi \sigma^2}$$

where $a = 1/2$ the critical crack length

$$a = 0.15, \text{ or } a_{cr} = 2(.15) = 0.30$$

Therefore, if a disk shaped flaw did extend through the wall thickness and was .30" long, the failure would still be catastrophic in nature. Therefore, if a failure does occur during the proof test of the pressure vessel it can be expected to be of the catastrophic type.

8.4.4.2 Evaluations of Life Expectancy

a Minimum Life Resulting from Undetected Flaws

The proof test also provides a means of estimating the minimum life expectancy of the pressure vessel. As previously cited the critical size of defect for catastrophic failure during the proof test is 0.18" deep by 3.60" long for the case of a shallow surface crack. It is possible, although not probable, that an undetected defect just slightly smaller than this critical size could have existed at the termination of the proof test, and the vessel would have survived the test. If this defect still remains undetected in the post-proof test inspection, the vessel could be put into service and begin its life with a defect 0.179" deep by 3.60" long. Under the operating stress this initial defect would have to grow to the critical size of .445" deep by 9" long (Table 3,

Section 8.4.1.2) before failure would occur. The life expectancy will be determined by the number of cycles that are required to grow the crack from the initial to critical size. This cyclic life is determined as follows:

Step 1 Determine K_{Ii} for the initial size flaw and the operating stress

$$K_{Ii}^2 = \frac{a_i (1.21) \pi (\sigma^2)}{\phi^2 - .212 \left(\frac{\sigma}{\sigma_{YS}}\right)^2} = \frac{.179 (1.21) \pi (90,000)^2}{1 - .212 \left(\frac{90000}{150000}\right)^2}$$

$$K_{Ii} = 77000 \text{ psi in.}$$

Step 2 Determine ratio of $\frac{K_{Ii}}{K_{Ic}} = \frac{77000}{120000} = .64$

Step 3 From cyclic data of Figure 5 determine life for $\frac{K_{Ii}}{K_{Ic}} = .64$

$$N\text{-cycles to failure} = 8500$$

This is the minimum cyclic life that could be expected in the pressure vessel under the worst possible circumstances. That is, the vessel starts its life with an undetected defect which is just slightly smaller than the critical size for failure during proof test. The possibility of failing to detect a 0.179" deep by 3.60" long defect in the pre and post-proof test inspection is quite remote, considering that the detection capability is good to .045" deep by .180" and that the defect would tend to open up during proof testing making it more readily detectable in the post-test inspection. However, the existence of this remote possibility of premature failure in service must be acknowledged, and the probability of this situation occurring in the production of 2,000 units would have to be considered.

b. Maximum Life for no Detectable Flaws

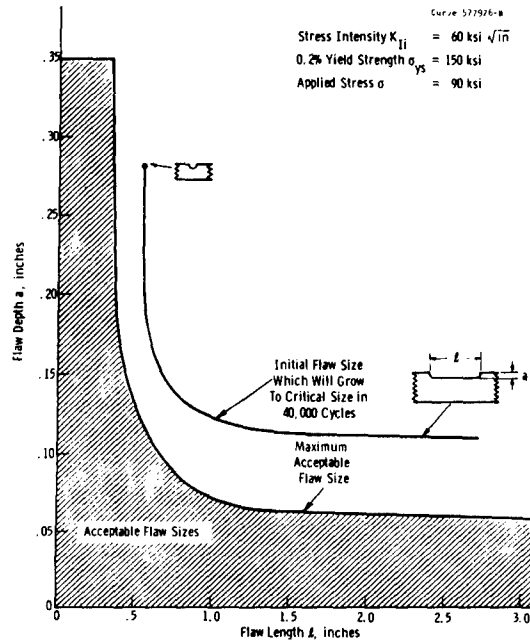
Let us now examine the case which will yield the most optimistic life expectancy. Inspection after proof testing indicates that there are no defects of a detectable size in terms of either depth or length.

The life expectancy is then based on an initial flaw size just under the detectable limits of 0.045" deep by 0.180" long. Following the same steps previously used, the estimated life expectancy is greater than 1,000,000 cycles. The probability of obtaining vessels in this category will depend upon the material and the processes used in fabrication and inspection.

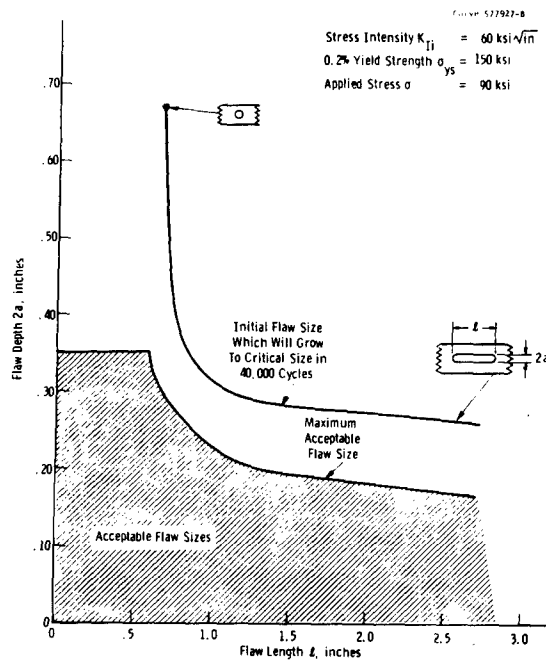
c. Realistic Life Expectancy Based on Maximum Allowable Size Flaws

Now that both extremes of life expectancy have been determined, let us consider the more realistic situations based on the allowable defect sizes which are cited in the specifications, Figures 7 and 8. The lower curve in Figure 7 defines the maximum allowable flaw sizes for the case of a surface defect with a geometry variation from short, deep flaws to long, shallow flaws. The life expectancy can be computed for any point along this curve, and since these represent the maximum allowable initial flaw sizes, the corresponding life-times would be the minimum expected (assuming there are no larger, undetected flaws). The basis for the establishment of this curve depended heavily on safety factors related to the non-destructive inspection capabilities as described previously in Section 8.4.3.

Considering the left-hand side of the minimum flaw size curve (Figure 7) for the region of short deep flaws, the life expectancy averages about 80,000 cycles. Moving to the right-hand side towards the long, shallow type of defect the life expectancy increases to a maximum of about 240,000 cycles. Interpreted in terms of safety factors ($\frac{\text{predicted life}}{\text{required life}}$) the short deep type of crack has a factor of 2 and this increases to 6 for the long, shallow crack. The larger safety factor for the shallow crack is consistent with the greater difficulty in measuring small differences in the depth during inspection (Section 8.4.3). Thus the minimum life expectancy that is assured by the specified maximum allowable flaw sizes varies from 80,000 to 240,000 cycles depending upon the geometry of the surface crack. Actually, the mean life expectancies would be greater since the defects would generally always be smaller than the maximum allowable sizes that are specified as upper limits.



Sec. 8.4 Fig. 7 — Acceptable external flaw sizes



Sec. 8.4 Fig. 8 — Acceptable internal flaw sizes

The same type of considerations also apply to the internal defects, Figure 8. As defined by the curve for maximum allowable defect sizes, the minimum life expectancy ranges from 70,000 cycles for the spherical hole to 150,000 cycles for the long, internal elliptical defect. Again the average life expectancy would be greater than these minimum values since the vessels are not likely to contain defects of a maximum allowable size. On the average it is reasonable to expect that the actual defect sizes will lie between the detectable limits and the maximum acceptable size.

The life expectancy of each vessel could be determined using the same procedures as employed in these example cases in conjunction with specific information concerning the prevailing defects as established from the post-proof test inspection. Any vessels containing defects of a border line type (with reference to the specified maximum allowable size) could be subjected to periodic inspections during service to provide assurance that these initial defects were not approaching the critical size for catastrophic failure. If any abnormal growth is detected, the vessel should be removed from service and repaired or replaced.

8.4.5 SUMMARY

In the foregoing example of a hypothetical pressure vessel, an attempt has been made to illustrate the usefulness of fracture mechanics technology for design and the selection of materials against fracture. The interactions of considerations in the areas of design, evaluation of materials, selection of a material, establishment of specifications and acceptance criteria, proof testing and life expectancy evaluations were demonstrated by solving various problems which develop in these areas. For convenience of illustration some simplifications were made, particularly in the areas concerning the design and stresses in the vessel. However, the procedures, technique and data which were employed are just as applicable to the situation where more precise information would be available concerning the stresses in the various

regions of the vessel. Similarly, the technology employed in this example of a pressure vessel can be applied to other types of structures and components, so long as all of the basic information that is required for the use of fracture mechanics is available.

APPENDIX I

TABULATION OF PLANE STRAIN FRACTURE TOUGHNESS DATA

Tables I-A through III-C of this Appendix include a tabulation of the plane strain fracture toughness data accumulated as the result of an extensive literature survey and also that data generated during this investigation. Tables IV through VI give the chemical composition (wt. %) of the alloys involved. The materials for which valid toughness data exist have been classified into three categories - Ferrous Alloys, Table I; Titanium Alloys, Table II; and Aluminum Alloys, Table III - and the data presented in order of increasing form size. The validity of the reported toughness data encountered during the literature survey was established in accordance with the latest ASTM criteria for toughness testing.* The tabulated data include the measured K_{Ic} values as well as the pertinent material and test parameters. The references from which the K_{Ic} data were obtained are presented in the Bibliography as "References Cited." Those references reviewed which do not contain K_{Ic} data established in accordance with the latest ASTM criteria and also those which do not contain sufficient information for evaluation are presented in the Bibliography as "References Not Cited."

*"Progress in Measuring Fracture Toughness and Using Fracture Mechanics," Fifth Report of the ASTM Special Committee on Fracture Testing of High-Strength Materials, Materials Research and Standards, March 1964, p. 113.

MATERIALS FOR WHICH VALID K_{Ic} DATA ARE PRESENTED IN APPENDIX I

<u>Material</u>	<u>Strength Level 0.2% Yield Strength (ksi)</u>	<u>Temperature Range, °F</u>	<u>Volume Of Data*</u>	<u>Location In Appendix I</u>
<u>Ferrous Alloys</u>				
18% Ni Maraging Steel	180 - 350	-110 to 650	(A)	Table I-A
4340	130 - 300	-110 to 750	(A)	Table I-B
D6ac	200 - 260	-200 to 75	(B)	Table I-C
H-11	160 - 240	-100 to 300	(B)	Table I-D
HP-9-4	140 - 250	-200 to 400	(D)	Table I-E
12Ni-5Cr-2Mo	180 - 190	R.T.	(D)	Table I-F
AM 355	160 - 200	-110 to 650	(D)	Table I-G
4335+V	210	-100 to 0	(D)	Table I-H
20% Ni Maraging Steel	300	R.T.	(D)	Table I-I
300 M	230	R.T.	(D)	Table I-J
PH-13Cr-8Ni	180 - 220	-110 to 400	(D)	Table I-K
A302 B	50 - 130	-320 to 0	(D)	Table I-L
Ni-Mo-V Forging Steel	80 - 140	-320 to 25	(D)	Table I-M
<u>Titanium Alloys</u>				
Ti-6Al-6V-6Sn	140 - 190	-320 to 400	(B)	Table II-A
Ti-6Al-4V	140 - 170	-320 to 300	(C)	Table II-B
Beta Titanium	170	-100 to 300	(D)	Table II-C
<u>Aluminum Alloys</u>				
7075-T6 & T651	70	R.T.	(A)	Table III-A
7079-T6	70	- 75 to 150	(B)	Table III-B
7001-T75	77	R.T.	(D)	Table III-C

* (A) Extensive data available; (B) Moderate amount of data available;
(C) Little data available; (D) Data very sparse.

BIBLIOGRAPHY

References Cited

1. A. W. Brisbane, J. M. Hawn, R. T. Ault, "Fracture Toughness and Delayed Failure Behavior of 18 Percent Nickel Maraging Steel," Materials Research and Standards, Volume 5, No. 8, August 1965, p. 395.
2. H. W. Maynor and C. C. Busch, " K_{Tc} of a 300-Grade 18-Nickel Maraging Steel as Influenced by Specimen Type and Thermal and Mechanical Treatment," AD 601537, Auburn Research Foundation, May 1964.
3. W. F. Payne, "Analysis of Surface Crack Fracture Toughness Information," Fourth Maraging Steel Project Review, Air Force Materials Lab Report No. ML-TDR-64-225, Volume 1, July 1964, p. 307.
4. C. F. Tiffany and P. M. Lorenz, "An Investigation of Low-Cycle Fatigue Failures Using Applied Fracture Mechanics," Tech. Doc. Report ML-TDR-64-53, Boeing Company, May 1964.
5. C. F. Tiffany, et al., "Large Motor Case Technology Evaluation," Progress Report - Contract AF 33(615)-1623, Boeing Company, September 1964.
6. Al Melville, "Metallurgical Evaluation of 18% Nickel Maraging Steel," p. 327, Third Maraging Steel Project Review, Tech. Doc. Report No. RTD-TDR-63-4048.
7. "Evaluation of High Nickel Steel for Application in Large Booster Motor Fabrication," ML-TDR-64-115, Aerojet-General Corporation, April 1964.
8. J. A. Kies, H. L. Smith, H. E. Romine and H. Bernstein, "Fracture Testing of Weldments," NASA Report NASACR-140, December 1964.
9. Aerospace Structural Metals Handbook, Volume I and II, Aeronautical Systems Division, Syracuse University Press, Review March 1964.
10. G. L. Hanna and E. A. Steingerwald, "Fracture Characteristics of Structural Metals," AD 411509, ER-5426, Thompson-Ramo-Wooldridge, June 1963.

References Cited (Cont.)

11. R. A. Brand and S. T. Rolfe, "Procedures for Determining K_{Ic} for 180/210 ksi Yield Strength Steels, "United States Steel Applied Research Lab, 40.018-002(23), December 1964.
12. "Thick Section Fracture Toughness," AD 452824L, Tech. Doc. Report No. ML-TDR-64-236, Boeing-North American, October 1964.
13. M. F. Amateau and E. A. Steigerwald, "Fracture Characteristics of Structural Metals," AD 611873, ER-5937-3, Thompson-Ramo-Wooldridge, January 1965.
14. W. A. Backofen and M. L. Ebner, "Metallurgical Aspects of Fracture at High Strength Level," AD 406167, Tech. Report No. WAL-TR-310.24/5-4, Watertown Arsenal Laboratories, May 1963.
15. C. F. Carman, D. F. Armiento and H. Markus, "Fracture Toughness and Pressure Vessel Performance," ASME Paper 63-WA-138, Transactions of the ASME, November 1963.
16. G. L. Hanna and E. A. Steigerwald, "Development of Standardized Test Methods to Determine Plane Strain Fracture Toughness," Report AFML-TR-65-213, Air Force Materials Lab, September 1965.
17. "Plane Strain Fracture Toughness of Large D6ac Steel Specimens Heat Treated to 220-240 and 260-280 ksi Strength Level," DDC No. 437887, General Dynamics, April 1964.
18. R. J. Urban, "Plane Strain Fracture Toughness of Large D6ac Steel Specimens," AD 437250, FGT-3064, General Dynamics, April 1964.
19. S. J. Matas and J. S. Pascover, "Properties of HP-9-4X Alloy Steels," Fourth Maraging Steel Project Review, Tech. Doc. Report No. ML-TDR-64-225, Volume 1, Air Force Materials Laboratory, July 1964.
20. T. S. DeSisto and C. F. Hickey, "The Influence of Microstructure and Testing Temperature on the Mechanical Properties and Fracture Toughness of Ti-6Al-6V-2Sn," U.S. Army Research Agency, presented at 68th Annual Meeting of the ASTM, Lafayette, Indiana, June 1965.
21. W. F. Brown and J. E. Srawley, Data presented at Subcommittee III Meeting of ASTM Committee E-24, April 24, 1964.
22. W. F. Brown, Progress Report on NASA-NRL Cooperative Plane Strain Testing Program, ASTM Committee E-24 Meeting, January 14, 1965.
23. J. G. Kaufman, Data presented at Subcommittee III Meeting of ASTM Committee E-24, April 24, 1964.

References Cited (Cont.)

24. J. G. Kaufman and H. Y. Hunsicker, "Fracture Toughness Testing at Alcoa Research Laboratories," Alcoa Research Laboratories, presented at 67th Annual Meeting of the ASTM, Chicago, Illinois, June 1963.
25. E. T. Wessel, Data presented at Subcommittee III Meeting of ASTM Committee E-24, January 13, 1965.
26. S. O. Davis, "Wedge Opening Loading Fracture Toughness Test Specimen," Air Force Materials Lab, Evaluation Report No. MAA 65-30, August 1965.
27. S. O. Davis, N. G. Tupper and R. M. Niemi, "Plane Strain Fracture Toughness Properties of Three Aluminum Alloys as a Function of Specimen Geometry," Air Force Materials Lab, Report No. AFML-TR-65-150, July 1965.
28. E. T. Wessel and W. H. Pryle, "Investigation of the Applicability of the Biaxial Brittle Fracture Test for Determining Fracture Toughness," AEC Research and Development Report WERL 8844-11, August 1965.
29. Unpublished Westinghouse Data.

References Not Cited

30. P. H. Denke, C. W. Bently and R. T. Hunt, "Fracture Toughness and Crack Propagation Properties of Candidate Mach 3 Transport Materials," SAE Report 650794, October 1965.
31. R. J. Goode and R. W. Huber, "Fracture Toughness Characteristics of Some Titanium Alloys for Deep-Diving Vehicles," U.S. Naval Research Laboratory, Report No. 6255, July 1965.
32. R. P. Wei and F. J. Lauta, "Measuring Plane Strain Fracture Toughness with Carbonitrided Single-Edge-Notched Specimens," Materials Research and Standards, Volume 5, No. 6, July 1965.
33. S. W. McClaren and C. R. Foreman, "Cryogenic Design Data for Materials Subjected to Uniaxial and Multi-Axial Stress Field," Tech. Report AFML-TR-65-140, LTV Aerospace Corporation, May 1965.
34. "Emerging Aerospace Materials," Tech. Report No. ML-TDR-65-114, Air Force Materials Laboratory, April 1965.

References Not Cited (Cont.)

35. S. T. Rolfe, "Development of a K_{IC} Stress-Corrosion Test Specimen," United States Steel Applied Research Lab, March 1965.
36. J. H. Bucher, et al.; "The Relationship of Microstructure to Strength and Toughness in High-Strength Steel," AFML-TR-65-60, Ohio State University Research Foundation, March 1965.
37. G. K. Bhat and J. B. Tobias, "Correlation of Weld Microstructures with Fracture Toughness of 18% Nickel (250) Grade Maraging Steel," AD 615425, Mellon Institute, February 1965.
38. M. Azrin, et al., "Effects of Processing History on Fracture at High Strength Levels," AD 459453, Tech. Report No. AFML-TR-64-376, Massachusetts Institute of Tech., February 1965.
39. Paul Kahn, "A Comparison of Fracture Mechanics and Notch Analysis," NASA-Langley Research Center, presented to the ASTM Special Committee on Fracture Testing, January 1965.
40. H. E. Romine, "Plane Strain Fracture Toughness of 18 Ni (250) and 18 Ni (200) Maraging Welded Steel Plate," U.S. Naval Weapons Lab, NWL Report No. 1959, January 1965.
41. A. R. Willner and M. L. Salive, "The Effect of Tempered Non-martensitic Products on the Notch Toughness and Mechanical Properties of an HY-80 Steel," David Taylor Model Basin, Report No. 1605, January 1965.
42. W. S. Pellini, et al., "Metallurgical Characteristics of High-Strength Structural Materials," NRL Report 6258, U.S. Naval Research Laboratory, December 1964.
43. "Physical and Mechanical Properties of Pressure Vessel Materials for Application in a Cryogenic Environment," Tech. Doc. Report No. ASD-TDR-62-258, Part III, General Dynamics/Astronautics, December 1964.
44. W. H. Munse, et al., "Studies of the Fatigue Behavior of Butt-Welded Joints in HY-80 and HY-100 Steels," AD 452191, University of Illinois, November 1964.
45. "18% Nickel Maraging Steels," Data Bulletin, The International Nickel Company, Inc., November 1964.
46. S. F. Frederick, "A Comparison of the Fracture-Toughness Properties of Two Motor Case Steels," Los Angeles Air Force Station, Report No. TDR-469(5250-10)-2, October 1964.

References Not Cited (Cont.)

47. A. J. Skalican, "Investigation of the Fracture Toughness of Thick Plate Metallic Materials," AD 449664, MEL R&D Report 202/64, U.S. Navy Marine Engineering Laboratory, October 1964.
48. "Problems in the Load-Carrying Application of High-Strength Steels," DMIC Report 210, Defense Metals Information Center, October 1964.
49. P. A. Farrar and H. Margolin, "Development of Tough, High-Strength Alpha-Beta Titanium-Base Alloys at 240,000-260,000 psi Yield Strength Level," AD 431680, Tech. Report No. WAL TR 401/303-4, New York University, September 1964.
50. J. H. Mulherin, "Fracture Characteristics of Several High-Strength Aluminum Alloys Using Variable Notch Root Radii," AD 452318, Report No. R-1734, Frankford Arsenal, September 1964.
51. J. L. Cavallaro, "Heat Treatment and Mechanical Properties of Near-Alpha Titanium Alloys," MEL R&D Phase Report 220/64, U.S. Navy Marine Engineering Laboratory, September 1964.
52. T. W. Eichenberger, "Mechanical Property and Fracture Toughness Evaluation of 2219-T6E46 for Cryogenic Applications," Boeing Company, Report No. D2-81287, August 1964.
53. I. R. Lane, Jr., "Development of Titanium Alloys for Hulls of Deep-Diving Vehicles," U.S. Naval Marine Engineering Laboratory, Report No. 194/647, August 1964.
54. W. J. Martin, T. Matsuda and E. F. Kaluza, "Study of Titanium Alloy Tankage at Cryogenic Temperatures," AD 604053, Report SM-43116, Douglas Aircraft Company, Inc., August 1964.
55. A. T. D'Annessa, "Fracture Toughness of X7006-T6351 Aluminum Alloy Plate Weldments," Lockheed Missile & Space Company, Report No. 6-62-64-10, July 1964.
56. R. N. Katz, "Fracture Toughness of D6ac Steel Shillelagh Rocket Motor Case," U.S. Army, AMRA TR No. 64-19, July 1964.
57. A. A. Iannelli and E. H. Swift, "Effect of Aging Temperature and Time on the Mechanical Properties of Titanium Alloy 6Al-6V-2Sn," AD 606567, U.S. Army Materials Research Agency, July 1964.
58. B. R. Banerjee and J. J. Hauser, "Fracture Micromechanics in High-Strength Steels and Titanium," AD 607048, Tech. Doc. Report No. ML-TDR-64-182, Crucible Steel Company of America, July 1964.

References Not Cited (Cont.)

59. R. H. Heyer, "Evaluation of Proposed Recommended Practice for Sharp Notch Tension Testing," Armco Steel Corporation, presented at 67th Annual Meeting of ASTM, Chicago, June 1964.
60. Morse Hill, J. S. Pascover and S. J. Matas, "The Application of Fracture Toughness Testing to the Development of a Family of Alloy Steels," Republic Steel Research Center, presented at 67th Annual Meeting of ASTM, Chicago, June 1964.
61. E. P. Gilewicz, et al., "Research on the Binary Iron-Nickel Alloys with 20 to 25 Percent Nickel," Tech. Doc. Report No. ASD-TDR-62-996, Curtiss-Wright Corporation, June 1964.
62. R. L. Jones and F. C. Nordquist, "An Evaluation of High-Strength Steel Forgings," AD 601446, Tech. Doc. Report No. RTD-TDR-63-4050, General Dynamics, May 1964.
63. M. S. Howeth, "Compilation of Unpublished Materials Information - Second Phase II Report," AD 437934, General Dynamics, May 1964.
64. J. L. Christian, C. T. Yang and W. E. Witzell, "Physical and Mechanical Properties of Pressure Vessel Material for Application in a Cryogenic Environment," Report No. GD/A 63-0818-3, General Dynamics/Astronautics, May 1964.
65. D. L. Corn and W. V. Mixon, "Interim Report on the Effect of Crack Shape on Fracture Toughness," Douglas Aircraft, Report SM-44671, April 1964.
66. R. A. Davis and L. Bakow, "Fracture Toughness and Tear Tests," AD 448752, Report No. BNJV-C-Q3, Boeing-North American, April 1964.
67. Saperstein and W. V. Mixon, "Evaluation of Maraging Steel for Application to Space Launch Vehicles," Douglas Missile and Space Systems, Report No. SM 43105, February 1964.
68. J. S. Pascover and S. J. Matas, "Some Relationships Between Structure and Properties in the 9Ni-4Co Alloy System," Republic Steel Research Center, presented as part of the AIME Symposium on "Steels with Yield Strengths over 200,000 psi," 1963 National Metal Congress, February 1964.
69. "Comparison of Various Test Specimens for the Determination of Notch Sensitivity and Fracture Toughness of High-Strength Sheet Materials," AD 601821, AMRA TR 64-04, U.S. Army Materials Research Agency, February, 1964.

References Not Cited (Cont.)

70. "Cracking in High-Strength Steel Weldments - A Critical Review," DMIC Report 197, Defense Metals Information Center, February 1964.
71. T. S. Desisto, F. L. Carr and F. R. Larson, "The Influence of Section Size on the Mechanical Properties and Fracture Toughness of 7075-T6 Aluminum, 6Al-6V-2Sn Titanium, and AISI 4340 Steel," AD 600846, Tech. Report No. AMRA-TR-64-05, U.S. Army Materials Research Agency, February 1964.
72. J. E. Campbell, F. J. Barone and B. P. Moon, "The Mechanical Properties of the 18 Percent Nickel Maraging Steels," AD 600427, DMIC Report 198, Defense Metals Information Center, February 1964.
73. G. L. Hanna and E. A. Steigerwald, "Influence of Environment on Crack Propagation and Delayed Failures in High-Strength Steels," AD 433286, Tech. Doc. Report No. RTD-TDR-63-4225, Thompson-Ramo-Wooldridge, January 1964.
74. R. N. Katz, "Effect of Tempering on Notch Properties of D6ac Alloy Steel Sheet," AD 431311, Tech. Report AMRA TR 63-35, U.S. Army Materials Research Agency, December 1963.
75. C. W. Bentley, "Notch Resistance and Fracture Toughness Characteristics of High-Strength Metals," AD 425573, Tech. Doc. Report No. ASD-TDR-63-494, Douglas Aircraft Company, Inc., September 1963.
76. S. J. Matas, Morse Hill and H. P. Munger, "Current and Future Trends for Steels with High Strength and Toughness," Metals Engineering Quarterly, Volume 3, No. 3, August 1963.
77. C. E. King, "Data Collection of Unpublished Materials Information," AD 416761, FPR-009, General Dynamics, August 1963.
78. R. A. Wood, "A Tabulation of Designations, Properties, and Treatments of Titanium and Titanium Alloys," AD 424412, DMIC Memorandum 171, Defense Metals Information Center, July 1963.
79. G. R. Sippel and G. L. Vonnegut, "Evaluation of 18% Ni-Co-Mo Maraging Steel for Heavy and Thin Wall Rocket Motor Case Applications," Engineering Department Report No. 3448, Allison Division of General Motors Corporation, July 1963.
80. H. W. Maynor and R. E. Blair, "The Effect of Thickness and Tempering Temperature on Fracture Appearance Transition Temperature and Critical Fracture Toughness of High-Strength Sheet Steel - Part II," AD 607314, Auburn Research Foundation, May 1963.

References Not Cited (Cont.)

81. H. A. Hauser and W. E. Helfrich, "Eleventh Quarterly Report on Research and Development of Titanium Rocket Motor Case," AD 420090, Tech. Report No. WAL 766.2/1-10, Pratt & Whitney Aircraft, April 1963.
82. B. R. Banerjee and J. J. Hauser, "Research and Application Engineering to Determine the Effect of Processing Variables on Crack Propagation of High-Strength Steels and Titanium," ASD-TDR-62-1034, Air Force Systems Cont., April 1963.
83. H. E. Romine, "Fracture Toughness Study of Ti-6Al-6V-2Sn Titanium Alloy Sheet 0.1 Inch Thick for Possible Application in the Construction of Welded Solid-Propellant Rocket Motor Cases," NWL Report No. 1839, U.S. Naval Weapons Laboratory, February 1963.
84. C. F. Hickey and F. R. Larson, "Comparison of Test Specimens for Notch Sensitivity and Fracture Toughness of High-Strength Sheet Materials," Proceedings of ASTM, Volume 63, 1963.
85. J. D. Morrison, P. C. Jenkins and J. R. Kattus, "An Investigation of the Crack-Propagation Resistance of High-Strength Alloys and Heat-Resistant Alloys, Contract NOW 61-0392-d, Southern Research Institute, Birmingham, Alabama, November 1962.
86. C. M. Carman and J. H. Mulherin, "Fracture Toughness of High-Strength Steels for Recoilless Rifles," AD 285677, Frankford Arsenal Report R-1648, July 1962.
87. "Background for the Development of Materials to be Used in High-Strength-Steel Structural Weldments," DMIC Report 172, Defense Metals Information Center, July 1962.
88. C. M. Carman, D. F. Armiento and H. Markus, "Plane Strain Fracture Toughness Measurements of High-Strength Steels," Frankford Arsenal, Paper No. 62-Met-8, presented at the AWSASME Metals Engineering Conference, Cleveland, April 1962.
89. R. H. Christensen and P. F. Denke, "Crack Strength and Crack Propagation Characteristics of High-Strength Metals," Tech. Report No. ASD-TR-60-207, U.S. Air Force, Wright-Patterson AFB, by Douglas Aircraft Company, Inc., January 1962.
90. G. K. Manning, "The Effect of Small Cracks on the Load-Carrying Ability of High-Strength Steel," Battelle Memorial Institute, presented at 64th Annual Meeting of the ASTM, Atlantic City, New Jersey, June 1961.

References Not Cited (Cont.)

91. Harold Bernstein and G. C. Young, "Progress Report on Fracture Toughness Tests of High-Strength Sheet Metals," NAVORD Report No. 6496, U.S. Naval Gun Factory, May 1959.

TABLE I-A - TABULATION OF K_{Ic} DATA
FERROUS ALLOYS - 18% Ni Maraging Steel

Form	Composition (1)	Heat Treatment			Test Orientation (2)	Test Temp. of	Yield Strength 0.2% (ksi)	K_{Ic} (3)	Specimen Type (4)	Specimen Size (in.)			σ_N/σ_{YS} (5)	Comments (6)	Ref. (7)	
		Solution Annealing Treatment		Aging Treatment						Thickness B	Width W	Length L				
		Time	Temp. of	Time												Temp. of
0.050" -thick Cold Rolled Sheet	A	1 hr	1500	3 hr	900	-103	348	(2) 71.6	CC	0.050	2.00	9.00	0.37	PI	1	
	A	1 hr	1500	3 hr	900	75	322	(2) 79.6	CC	0.050	2.00	9.00	0.42	PI	1	
	A	1 hr	1500	3 hr	900	200	311	(2) 88.6	CC	0.050	2.00	9.00	0.42	PI	1	
	A	1 hr	1500	3 hr	900	400	295	(2) 89.0	CC	0.050	2.00	9.00	0.41	Dev	1	
	A	1 hr	1500	3 hr	900	75	324	(2) 66.2	CC	0.050	2.00	9.00	0.32	PI	1	
	A	1 hr	1500	3 hr	800	800	-103	329	(2) 68.9	CC	0.050	2.00	9.00	0.42	PI	1
	A	1 hr	1500	3 hr	800	800	75	304	(2) 87.5	CC	0.050	2.00	9.00	0.57	PI	1
	A	1 hr	1500	3 hr	800	800	75	333	69.0	CC	0.050	2.00	9.00	0.33	PI	1
	A	1 hr	1500	4 hr	750	750	-103	288	73.6	CC	0.050	2.00	9.00	0.57	PI	1
	0.060" Cold Rolled Sheet	B	30 min	1500	2 hr	900	RT	267	146.0	SEN	0.060	1.00	4.00	0.34	PI	2
		B	30 min	1500	2 hr	900	RT	267	153.0	SEN	0.060	1.00	4.00	0.34	PI	2
		B	30 min	1500	2 hr	900	RT	267	142.0	SEN	0.060	1.00	4.00	0.32	PI	2
		B	30 min	1500	2 hr	900	RT	267	139.0	SEN	0.060	1.00	4.00	0.32	PI	2
		B	30 min	1500	9 hr	900	RT	283	105.1	SEN	0.060	1.00	4.00	0.23	PI	2
B		30 min	1500	9 hr	900	RT	283	106.8	SEN	0.060	1.00	4.00	0.19	PI	2	
B		30 min	1500	9 hr	900	RT	283	108.2	SEN	0.060	1.00	4.00	0.23	PI	2	
B		30 min	1500	9 hr	900	RT	283	106.7	SEN	0.060	1.00	4.00	0.22	PI	2	
B		30 min	1500	9 hr	900	RT	297	122.0	SEN	0.060	1.00	4.00	0.25	PI	2	
B		30 min	1500	9 hr	900	RT	297	132.0	SEN	0.060	1.00	4.00	0.27	PI	2	
B		30 min	1500	9 hr	900	RT	297	120.0	SEN	0.060	1.00	4.00	0.25	PI	2	
B		30 min	1500	9 hr	900	RT	297	114.0	SEN	0.060	1.00	4.00	0.24	PI	2	
B		30 min	1500	9 hr	900	RT	310	59.0	SEN	0.060	1.00	4.00	0.12	PI	2	
B		30 min	1500	9 hr	900	RT	310	101.0	SEN	0.060	1.00	4.00	0.20	PI	2	
B	30 min	1500	9 hr	900	RT	310	99.0	SEN	0.060	1.00	4.00	0.20	PI	2		
B	30 min	1500	9 hr	900	RT	310	76.0	SEN	0.060	1.00	4.00	0.15	PI	2		
B	30 min	1500	9 hr	900	RT	335	61.0	SEN	0.060	1.00	4.00	0.12	PI	2		
B	30 min	1500	9 hr	900	RT	335	69.0	SEN	0.060	1.00	4.00	0.13	FR	2		
B	30 min	1500	9 hr	900	RT	335	68.0	SEN	0.060	1.00	4.00	0.13	FR	2		
B	30 min	1500	9 hr	900	RT	335	71.0	SEN	0.060	1.00	4.00	0.13	FR	2		
B	30 min	1500	2 hr	900	RT	267	128.0	CC	0.060	3.00	12.00	0.55	PI	2		
B	30 min	1500	2 hr	900	RT	267	114.0	CC	0.060	3.00	12.00	0.53	PI	2		
B	30 min	1500	2 hr	900	RT	267	146.0	CC	0.060	3.00	12.00	0.47	PI	2		
B	30 min	1500	2 hr	900	RT	267	88.0	CC	0.060	3.00	12.00	0.60	PI	2		
B	30 min	1500	9 hr	900	RT	283	97.0	CC	0.060	3.00	12.00	0.39	PI	2		
B	30 min	1500	9 hr	900	RT	283	101.0	CC	0.060	3.00	12.00	0.38	PI	2		
B	30 min	1500	9 hr	900	RT	283	283	101.0	CC	0.060	3.00	12.00	0.40	PI	2	

(1) Alloy composition given in Table IV-A

(2) L - longitudinal - Test specimen axis parallel to rolling direction
T - transverse - Test specimen axis perpendicular to rolling direction

(3) Average of number of tests indicated in ()

(4) CC - Center-Cracked Plate

SEN - Single-Edge-Notched Plate

SC - Surface-Cracked Plate

NB3 - Notched Bend - 3-Point Loading

NB4 - Notched Bend - 4-Point Loading

NR - Notched Round

$$(5) \frac{\sigma_N}{\sigma_{YS}} = \frac{\text{Nominal Stress}}{0.2\% \text{ Yield Stress}}$$

(6) PI - Pop-in load
Dev - Load at deviation from linearity
FR - Ultimate load
CW - Cold worked

(7) References listed in Bibliography

TABLE I-A (Cont.)

Form	Composition	Heat Treatment				Test Orientation	Test Temp. °F	Yield Strength 0.2% (ksi)	K _{Ic} ksi√in	Specimen Type	Specimen Size (in.)			σ _N /σ _{YS}	Comments	Ref.	
		Solution Annealing Treatment		Aging Treatment							Thickness B	Width W	Length L				
		Time	Temp. °F	Time	Temp. °F												
0.060" Cold Rolled Sheet	B	30 min	1500	9 hr	900	T	RT	283	95.0	CC	0.060	3.00	12.00	0.35	PI	2	
	B	30 min	1500	9 hr	900	T	RT	297	102.0	CC	0.060	3.00	12.00	0.43	PI	2	
	B	30 min	1500	9 hr	900	T	RT	297	120.0	CC	0.060	3.00	12.00	0.45	PI	2	
	B	30 min	1500	9 hr	900	T	RT	297	112.0	CC	0.060	3.00	12.00	0.43	PI	2	
	B	30 min	1500	9 hr	900	T	RT	297	105.0	CC	0.060	3.00	12.00	0.45	PI	2	
	B	30 min	1500	9 hr	900	T	RT	310	71.0	CC	0.060	3.00	12.00	0.25	PI	2	
	B	30 min	1500	9 hr	900	T	RT	310	73.0	CC	0.060	3.00	12.00	0.084	PI	2	
	B	30 min	1500	9 hr	900	T	RT	310	66.0	CC	0.060	3.00	12.00	0.34	PI	2	
	B	30 min	1500	9 hr	900	T	RT	310	60.0	CC	0.060	3.00	12.00	0.31	PI	2	
	0.145" Cold Rolled Sheet	C	1 hr	1500	3 hr	850	L	RT	277.2	(3)134.0	CC	0.140	2.25	12.00	0.39	PI	3
		C	1 hr	1500	6 hr	850	L	RT	292	(2)110.0	CC	0.140	2.25	12.00	0.30	PI	3
		C	1 hr	1500	9 hr	850	L	RT	305	(3)111.0	CC	0.140	2.25	12.00	0.29	PI	3
C		1 hr	1500	12 hr	850	L	RT	311.6	(2) 95.0	CC	0.140	2.25	12.00	0.25	PI	3	
C		1 hr	1500	24 hr	850	L	RT	317.3	(3)103.0	CC	0.140	2.25	12.00	0.27	PI	3	
C		1 hr	1500	3 hr	900	L	RT	294.4	(4)113.0	CC	0.140	2.25	12.00	0.32	PI	3	
C		1 hr	1500	6 hr	900	L	RT	301.2	(2)108.0	CC	0.140	2.25	12.00	0.30	PI	3	
C		1 hr	1500	9 hr	900	L	RT	304.6	(3)103.0	CC	0.140	2.25	12.00	0.28	PI	3	
C		1 hr	1500	12 hr	900	L	RT	306	(2)117.0	CC	0.140	2.25	12.00	0.32	PI	3	
C		1 hr	1500	24 hr	900	L	RT	308.5	(3)101.0	CC	0.140	2.25	12.00	0.27	PI	3	
C		1 hr	1500	1 hr	950	L	RT	295.5	(2)111.0	CC	0.140	2.25	12.00	0.31	PI	3	
C		1 hr	1500	3 hr	950	L	RT	303.2	(2)134.0	CC	0.140	2.25	12.00	0.37	PI	3	
C		1 hr	1500	6 hr	950	L	RT	299.3	(2)116.0	CC	0.140	2.25	12.00	0.35	PI	3	
C		1 hr	1500	9 hr	950	L	RT	296.3	(2)132.0	CC	0.140	2.25	12.00	0.39	PI	3	
C		1 hr	1500	12 hr	950	L	RT	284	(2)132.0	CC	0.140	2.25	12.00	0.40	PI	3	
C		1 hr	1500	1 hr	1000	L	RT	291.3	98.0	CC	0.140	2.25	12.00	0.28	PI	3	
C		1 hr	1500	3 hr	1000	L	RT	280.8	(2)120.0	CC	0.140	2.25	12.00	0.34	PI	3	
C		1 hr	1500	6 hr	1000	L	RT	267.5	(2)127.0	CC	0.140	2.25	12.00	0.37	PI	3	
C	1 hr	1500	12 hr	1000	L	RT	256.3	(2)136.0	CC	0.140	2.25	12.00	0.44	PI	3		
0.145" Cold Rolled Sheet	D	1 hr	1500	6 hr	850	L	RT	295.5	(2) 74.0	CC	0.140	2.25	12.00	0.20	PI	3	
	D	1 hr	1500	12 hr	850	L	RT	295.6	(2) 68.0	CC	0.140	2.25	12.00	0.18	PI	3	
	D	1 hr	1500	3 hr	900	L	RT	293.8	(5) 73.0	CC	0.140	2.25	12.00	0.21	PI	3	
	D	1 hr	1500	6 hr	900	L	RT	301.8	(2) 74.0	CC	0.140	2.25	12.00	0.20	PI	3	
	D	1 hr	1500	12 hr	900	L	RT	299	(2) 74.0	CC	0.140	2.25	12.00	0.18	PI	3	
	D	1 hr	1500	3 hr	950	L	RT	289.5	(2) 83.0	CC	0.140	2.25	12.00	0.22	PI	3	
0.250" Cold Rolled Sheet	D	1 hr	1500	9 hr	950	L	RT	282	(2) 73.0	CC	0.140	2.25	12.00	0.20	PI	3	
	D	1 hr	1500	3 hr	1000	L	RT	276.8	(4) 83.0	CC	0.140	2.25	12.00	0.26	PI	3	
	E	1 hr	1500	3 hr	900	L	RT	248	99.2	CC	0.29	5.94	19.00	0.31	PI	4	
	E	1 hr	1500	3 hr	900	L	RT	260.3	70.1	CC	0.29	5.94	19.00	0.20	PI	4	
0.500" Plate	F	1 hr	1500	3 hr	900	L	RT	275	70.9	CC	0.29	5.94	19.00	0.20	PI	4	
	F	1 hr	1500	3 hr	900	L	RT	275.5	94.8	SC	0.25	6.00	27.00	0.63	PI	4	
	F	1 hr	1500	3 hr	900	L	RT	275.5	121.8	SC	0.25	6.00	27.00	0.80	PI	4	
	F	1 hr	1500	3 hr	900	L	RT	270	71.0	SC	0.400	2.00		0.46	PI	5	
0.500" Plate	F	1 hr	1500	3 hr	900	L	RT	265	76.4	SC	0.400	2.00		0.48	PI	5	
	F	1 hr	1500	3 hr	900	L	RT	265	62.2	SC	0.540	-2.00		0.40	PI	5	

TABLE I-A (Cont.)

Form	Composition	Heat Treatment				Test Orientation	Test Temp. T_p	Yield Strength $\sigma_{0.2}$ (ksi)	K_{Ic} ksi \sqrt{in}	Specimen Type	Specimen Size (in.)			σ_N/σ_{YS}	Comments	Ref.
		Solution Annealing Treatment		Aging Treatment							Thickness B	Width W	Length L			
		Time	Temp. T_p	Time	Temp. T_p											
0.500" Plate	G	1 hr	1500	3 hr	900	L	RT	252	(5) 91.0	NB3	0.500	0.500	4.00	FR	6	
		1 hr	1500	3 hr	900	L	RT	252	(5) 86.0	NB3	0.500	0.500	4.00	FR	6	
		1 hr	1500	3 hr	900	T	RT	259.4	(5) 93.0	NB3	0.500	0.500	4.00	FR	6	
		1 hr	1500	3 hr	900	T	RT	259.4	(4) 86.0	NB3	0.500	0.500	4.00	FR	6	
		1 hr	1500	3+3 hr	900	L	RT	262.5	(5) 86.0	NB3	0.500	0.500	4.00	FR	6	
		1 hr	1500	3+3 hr	900	L	RT	262.5	(5) 73.0	NB3	0.500	0.500	4.00	FR	6	
		1 hr	1500	3+3 hr	900	T	RT	264.1	(5) 93.0	NB3	0.500	0.500	4.00	FR	6	
		1 hr	1500	3+3 hr	900	T	RT	264.1	(5) 93.0	NB3	0.500	0.500	4.00	FR	6	
		30 min	1500	4 hr	900	L	RT	258	95.0	SC	0.500	4.000	26.00	FR	7	
		30 min	1500	4 hr	900	L	RT	258	99.0	SC	0.500	4.000	26.00	FR	7	
		30 min	1500	4 hr	900	L	RT	258	91.0	SC	0.500	4.000	26.00	FR	7	
		30 min	1500	4 hr	900	L	RT	258	85.0	SC	0.500	4.000	26.00	FR	7	
		30 min	1500	4 hr	900	L	RT	258	79.0	SC	0.500	4.000	26.00	FR	7	
		30 min	1500	4 hr	900	T	RT	265	91.0	SC	0.500	4.000	26.00	FR	7	
		30 min	1500	4 hr	900	T	RT	265	93.0	SC	0.500	4.000	26.00	FR	7	
30 min	1500	4 hr	900	T	RT	265	96.0	SC	0.500	4.000	26.00	FR	7			
30 min	1500	4 hr	900	T	RT	265	87.0	SC	0.500	4.000	26.00	FR	7			
30 min	1500	4 hr	900	T	RT	265	79.0	SC	0.500	4.000	26.00	FR	7			
30 min	1500	4 hr	900	L	RT	258	87.6	SC	0.125	0.500	8.00	FR	7			
30 min	1500	4 hr	900	L	RT	258	87.0	SC	0.125	0.500	8.00	FR	7			
30 min	1500	4 hr	900	L	RT	258	86.5	SC	0.125	0.500	8.00	FR	7			
30 min	1500	4 hr	900	T	RT	265	92.0	SC	0.125	0.500	8.00	FR	7			
30 min	1500	4 hr	900	T	RT	265	88.0	SC	0.125	0.500	8.00	FR	7			
30 min	1500	4 hr	900	T	RT	265	91.9	SC	0.125	0.500	8.00	FR	7			
30 min	1500	4 hr	900	L	RT	258	84.0	NB3	0.500	0.500	4.00	FR	7			
30 min	1500	4 hr	900	T	RT	271	(5) 87.0	NB3	0.500	0.500	4.00	FR	7			
30 min	1500	4 hr	900	L	RT	258	(5) 78.0	NB3	0.500	0.500	4.00	FR	7			
30 min	1500	4 hr	900	T	RT	271	(5) 83.0	NB3	0.500	0.500	4.00	FR	7			
30 min	1500	4 hr	900	L	RT	213	(5) 80.0	NB3	0.500	0.750	4.00	FR	7			
30 min	1500	4 hr	900	T	RT	246	(5) 84.0	NB3	0.500	0.750	4.00	FR	7			
0.500" Plate	I	8 hr	850	8 hr	850	L	RT	260	(5) 74.0	NB3	0.500	0.750	4.00	FR	7	
		8 hr	850	4 hr	900	T	RT	---	(5) 71.0	NB3	0.500	0.750	4.00	FR	7	
		4 hr	900	4 hr	900	L	RT	265	(5) 71.0	NB3	0.500	0.750	4.00	FR	7	
		4 hr	900	4 hr	900	L	RT	243	(5) 80.0	NB3	0.500	0.750	4.00	FR	7	
		2 hr	950	2 hr	950	L	RT	264	(2) 81.0	NB3	0.500	0.750	4.00	FR	7	
0.500" Plate	J	8 hr	850	8 hr	850	L	RT	254	(5) 64.0	NB3	0.500	0.750	4.00	FR	7	
		4 hr	900	4 hr	900	T	RT	271	(4) 72.0	NB3	0.500	0.750	4.00	FR	7	
		30 min	1500	8 hr	900	L	RT	267	(3) 68.0	NB3	0.500	0.750	4.00	FR	7	
		30 min	1500	8 hr	900	L	RT	275	(5) 65.0	NB3	0.500	0.750	4.00	FR	7	
		30 min	1500	2 hr	950	T	RT	---	(4) 76.0	NB3	0.500	0.750	4.00	FR	7	
		30 min	1500	8 hr	900	L	RT	---	(2) 37.0	NB3	0.500	0.750	4.00	FR	7	
0.500" Plate	K	4 hr	900	4 hr	900	L	RT	---	(3) 43.0	NB3	0.500	0.750	4.00	FR	7	
		4 hr	900	8 hr	900	T	RT	---	(2) 42.0	NB3	0.500	0.750	4.00	FR	7	
		8 hr	900	8 hr	900	L	RT	---	(2) 39.0	NB3	0.500	0.750	4.00	FR	7	
		8 hr	900	4 hr	900	T	RT	278	(2) 46.0	NB3	0.500	0.750	4.00	FR	7	
		30 min	1500	4 hr	900	L	RT	274	(5) 43.0	NB3	0.500	0.750	4.00	FR	7	
		30 min	1500	8 hr	900	T	RT	279	(4) 41.0	NB3	0.500	0.750	4.00	FR	7	
		30 min	1500	8 hr	900	L	RT	286	(5) 41.0	NB3	0.500	0.750	4.00	FR	7	
		30 min	1500	8 hr	900	T	RT	---	(2) 37.0	NB3	0.500	0.750	4.00	FR	7	

TABLE I-A (Cont.)

Form	Composition	Heat Treatment				Test Orientation	Yield Strength 0.2% (ksi)	K _{1c} ksi√in	Specimen Type	Specimen Size (in.)			σ _w /σ _{YS}	Comments	Ref.	
		Solution Annealing Treatment		Aging Treatment						Thick-ness B	Width W	Length L				
		Time	Temp. Of	Time	Temp. Of											
0.500" Plate	L	30 min	1500	8 hr	850	L	294	(3) 41.0	NB3	0.500	0.750	4.00		FR	7	
	L	30 min	1500	8 hr	900	L	300	(5) 46.0	NB3	0.500	0.750	4.00		FR	7	
	L	30 min	1500	8 hr	900	T	302	(4) 42.0	NB3	0.500	0.750	4.00		FR	7	
	L	30 min	1500	8 hr	850	L	298	(4) 42.0	NB3	0.500	0.750	4.00		FR	7	
	L	30 min	1500	8 hr	900	L	302	(4) 41.0	NB3	0.500	0.750	4.00		FR	7	
	L	30 min	1500	8 hr	900	T	299	(5) 41.0	NB3	0.500	0.750	4.00		FR	7	
	L	30 min	1500	8 hr	900	L	309	(3) 49.0	NB3	0.500	0.750	4.00		FR	7	
	L	30 min	1500	8 hr	900	T	308	(4) 47.0	NB3	0.500	0.750	4.00		FR	7	
	0.750" Plate	M	1 hr	1500	4 hr	915	T	248	(27) 77.0	NB3	0.750	0.750	6.00	<1.1	FR	8
		M	1 hr	1500	4 hr	915	L	263	(25) 84.3	NB3	0.750	0.750	6.00	<1.1	FR	8
	1.00" Plate	N	1 hr	1500	3 hr	900		230	85.0	SEN	0.140	1.000			PI	9
		N	1 hr	1500	3 hr	900		230	83.0	SEN	0.140	1.000			PI	9
N		1 hr	1500	3 hr	900		230	96.0	SEN	0.140	1.000			PI	9	
N		1 hr	1500	3 hr	900		230	68.0	SEN	0.140	1.000			PI	9	
O		1 hr	1500	3 hr	900	L	274.2	47.7	NR	D=.505	d=.375	3.00	0.55	FR	10	
1.00"-Dia. Bar	O	1 hr	1500	3 hr	900	L	261.5	(2) 39.4	NR	D=.505	d=.375	3.00	0.42	FR	10	
	O	1 hr	1500	3 hr	900	L	257.5	(2) 41.0	NR	D=.505	d=.375	3.00	0.51	FR	10	
	O	1 hr	1500	3 hr	900	L	256.1	(3) 64.4	NR	D=.505	d=.375	3.00	0.79	FR	10	
	O	1 hr	1500	3 hr	900	L	246.8	(3) 64.5	NR	D=.505	d=.375	3.00	0.82	FR	10	
	P		1500	3 hr	900	L	240	59.9	NB3	1.000	0.760	18.00	0.54	PI	11	
2.250" Plate	P		1500	3 hr	900	L	240	50.0	NB3	1.000	1.250	18.00	0.35	PI	11	
	P		1500	3 hr	900	L	240	59.9	NB3	1.000	1.520	18.00	0.38	PI	11	
	P		1500	3 hr	900	L	240	57.2	NB3	1.000	1.740	18.00	0.34	PI	11	
	Q	1 hr	1700	3 hr	1050	L	230.5	88.3	CN	0.375	6.000	9.00	0.44	PI	12	
	Q	1 hr	1700	3 hr	1050	L	230.5	84.0	CN	1.000	9.000	24.00	0.22	PI	12	
3.00"x9.00" Forging	Q	1 hr	1700	3 hr	1050	T	233	89.5	CN	0.190	3.000	9.00	0.67	PI	12	
	Q	1 hr	1700	3 hr	1050	L	230.5	76.6	NR	D=1.125	d=.750	3.00	0.74	FR	12	
	Q	1 hr	1700	3 hr	1050	L	230.5	78.7	NR	D=1.125	d=.750	3.00	0.76	FR	12	
	Q	1 hr	1700	3 hr	1050	L	212	86.1	CN	1.000	9.000	24.00	0.34	PI	12	
	Q	1 hr	1700	3 hr	1050	T	232.9	73.4	NR	D=1.125	d=.750	3.00	0.70	FR	12	
	Q	1 hr	1700	3 hr	1050	T	232.9	70.3	NR	D=1.125	d=.750	3.00	0.67	FR	12	
	Q	1 hr	1700	3 hr	1050	ST	232.5	65.4	NR	D=1.125	d=.750	3.00	0.63	FR	12	
	Q	1 hr	1700	3 hr	1050	ST	232.5	67.6	NR	D=1.125	d=.750	3.00	0.65	FR	12	
	Q	1 hr	1700	3 hr	1050	L	212.5	80.2	NR	D=1.125	d=.750	3.00	0.86	FR	12	
	Q	1 hr	1700	3 hr	1050	L	212.5	88.9	NR	D=1.125	d=.750	3.00	0.91	FR	12	
	Q	1 hr	1700	3 hr	1050	T	216.7	79.7	NR	D=1.125	d=.750	3.00	0.81	FR	12	
	Q	1 hr	1700	3 hr	1050	T	216.7	76.0	NR	D=1.125	d=.750	3.00	0.77	FR	12	
	Q	1 hr	1700	3 hr	1050	ST	218.3	67.1	NR	D=1.125	d=.750	3.00	0.68	FR	12	
	Q	1 hr	1700	3 hr	1050	ST	218.3	65.5	NR	D=1.125	d=.750	3.00	0.67	FR	12	
	Q	1 hr	1700	3 hr	1050	T	189.8	95.3	NR	D=1.125	d=.750	3.00	1.07	FR	12	
	Q	1 hr	1700	3 hr	1050	ST	198.2	87.0	NR	D=1.125	d=.750	3.00	0.95	FR	12	
	Q	1 hr	1700	3 hr	1050	ST	187.9	91.6	NR	D=1.125	d=.750	3.00	1.04	FR	12	
	Q	1 hr	1700	3 hr	1050	L	184	89.3	NR	D=2.750	d=1.91	12.00	0.68	FR	12	

TABLE I-B - TABULATION OF K_{Ic} DATA
FERROUS ALLOYS - 4340 STEEL

Form	Composition (1)	Heat Treatment			Test Orientation (2)	Yield Strength 0.2% (ksi)	K_{Ic} (3) ksi \sqrt{in}	Specimen Type (4)	Specimen Size (in.)			σ_N/σ_{YS} (5)	Comments (6)	Ref. (7)	
		Austenitizing Treatment	Temper	Time					Thick-ness B	Width W	Length L				
		Time	Temp. Of	Time	Temp. Of										
0.070" Cold Rolled Sheet	A	20 min	1550	1 hr + 1 hr	400	226.0	(3) 32.8	CN	0.070	1.750	8.00	0.31		10	
	A	20 min	1550	1 hr + 1 hr	400	224.5	(3) 36.0	CN	0.070	1.750	8.00	0.30		10	
	A	20 min	1550	1 hr + 1 hr	400	220.5	(3) 37.8	CN	0.070	1.750	8.00	0.38		10	
	A	20 min	1550	1 hr + 1 hr	400	223.6	(3) 35.2	CN	0.070	1.750	8.00	0.36		10	
	A	20 min	1550	1 hr + 1 hr	400	223.5	(3) 35.8	CN	0.070	1.750	8.00	0.40		10	
	A	20 min	1550	1 hr + 1 hr	400	221.5	(3) 34.0	CN	0.070	1.750	8.00	0.35		10	
	A	20 min	1550	1 hr + 1 hr	400	192.5	(3) 33.0	CN	0.070	1.750	8.00	0.35		10	
	A	20 min	1550	1 hr + 1 hr	400	227.3	(2) 35.8	CN	0.070	1.750	8.00	0.34		10	
	A	20 min	1550	1 hr + 1 hr	400	225.0	(3) 38.8	CN	0.070	1.750	8.00	0.37		10	
	A	20 min	1550	1 hr + 1 hr	400	222.5	(3) 39.0	CN	0.070	1.750	8.00	0.44		10	
	A	20 min	1550	1 hr + 1 hr	400	218.0	(3) 44.8	CN	0.070	1.750	8.00	0.49		10	
	A	20 min	1550	1 hr + 1 hr	400	224.0	(3) 40.0	CN	0.070	1.750	8.00	0.44		10	
	A	20 min	1550	1 hr + 1 hr	400	221.5	(3) 38.3	CN	0.070	1.750	8.00	0.45		10	
	A	20 min	1550	1 hr + 1 hr	400	189.0	(3) 38.9	CN	0.070	1.750	8.00	0.42		10	
	A	20 min	1550	1 hr + 1 hr	750	209.0	(3) 48.5	CN	0.070	1.750	8.00	0.43		10	
	A	20 min	1550	1 hr + 1 hr	750	205.0	(3) 61.0	CN	0.070	1.750	8.00	0.78		10	
	A	20 min	1550	1 hr + 1 hr	750	197.5	(3) 56.2	CN	0.070	1.750	8.00	0.80		10	
	A	20 min	1550	1 hr + 1 hr	750	198.6	(3) 62.4	CN	0.070	1.750	8.00	0.77		10	
	A	20 min	1550	1 hr + 1 hr	750	195.4	(3) 51.3	CN	0.070	1.750	8.00	0.68		10	
	A	20 min	1550	1 hr + 1 hr	750	183.6	(3) 63.9	CN	0.070	1.750	8.00	0.85		10	
	A	20 min	1550	1 hr + 1 hr	750	178.0	(3) 48.8	CN	0.070	1.750	8.00	0.79		10	
	A	20 min	1550	1 hr + 1 hr	750	211.7	(3) 64.9	CN	0.070	1.750	8.00	0.72		10	
	A	20 min	1550	1 hr + 1 hr	750	207.0	(3) 76.2	CN	0.070	1.750	8.00	0.82		10	
	A	20 min	1550	1 hr + 1 hr	750	197.5	(3) 79.2	CN	0.070	1.750	8.00	0.85		10	
	A	20 min	1550	1 hr + 1 hr	750	197.8	(3) 70.8	CN	0.070	1.750	8.00	0.86		10	
	A	20 min	1550	1 hr + 1 hr	750	198.1	(3) 51.6	CN	0.070	1.750	8.00	0.69		10	
	A	20 min	1550	1 hr + 1 hr	750	185.0	(3) 66.2	CN	0.070	1.750	8.00	0.80		10	
	A	20 min	1550	1 hr + 1 hr	750	176.2	(2) 63.6	CN	0.070	1.750	8.00	0.84		10	
	0.250" Sheet	B	1 hr	1500	1 hr + 1 hr	400	222.1	(3) 46.7	SC	0.500	1.000	8.00	0.52		13
		B	1 hr	1500	1 hr + 1 hr	600	216.0	50.0	SC	0.500	1.000	8.00	0.60		13
B		1 hr	1500	1 hr + 1 hr	600	216.0	46.8	SC	0.500	1.000	8.00	0.60		13	
B		1 hr	1500	1 hr + 1 hr	600	216.0	55.6	SC	0.500	1.000	8.00	0.61		13	
B		1 hr	1500	1 hr + 1 hr	400	216.8	53.2	SEN	0.147	1.000	4.00	0.47	PI	13	
B		1 hr	1500	1 hr + 1 hr	400	216.8	61.0	SEN	0.145	1.000	4.00	0.56	PI	13	
B		1 hr	1500	1 hr + 1 hr	500	221.2	60.8	SEN	0.147	1.000	4.00	0.53	PI	13	
B		1 hr	1500	1 hr + 1 hr	500	221.2	61.3	SEN	0.147	1.000	4.00	0.54	PI	13	
B		1 hr	1500	1 hr + 1 hr	600	208.9	54.9	SEN	0.150	1.000	4.00	0.50	PI	13	
B		1 hr	1500	1 hr + 1 hr	600	208.9	65.5	SEN	0.149	1.000	4.00	0.60	PI	13	
B		1 hr	1500	1 hr + 1 hr	600	208.9	66.1	SEN	0.148	1.000	4.00	0.60	PI	13	

(1) Alloy compositions given in Table IV-B

(2) L - longitudinal

T - transverse

ST - short transverse

(3) Average of number of tests indicated in ()

(4) CN - Center-Notched Plate

SC - Surface-Cracked Plate

SEN - Single-Edge-Notched Plate

MB3 - Notched Bend - 3-point loading

NR - Notched Round

(5) $\sigma_N/\sigma_{YS} = \frac{\text{Nominal Stress}}{0.2\% \text{ Yield Stress}}$

(6) PI - Pop-in load

FR - Ultimate load

(7) References listed in Bibliography

TABLE I-B (Cont.)

Form	Composition	Heat Treatment				Test Orientation	Yield Strength 0.2% (ksi)	K _{Ic} ksi√in	Specimen Type	Specimen Size (in.)			σ _N /σ _{YS}	Comments	Ref.	
		Austenitizing Treatment		Temper						Thick-ness B	Width W	Length L				
		Time	Temp. Of	Time	Temp. Of											
0.250" Sheet	B	1 hr	1500	1 hr + 1 hr	400	L	216.8	51.3	CN	0.150	2.000	8.00	0.32	PI	13	
	B	1 hr	1500	1 hr + 1 hr	400	L	216.8	39.1	CN	0.158	2.000	8.00	0.25	PI	13	
	B	1 hr	1500	1 hr + 1 hr	500	L	221.2	53.5	CN	0.150	2.000	8.00	0.33	PI	13	
	B	1 hr	1500	1 hr + 1 hr	600	L	208.9	55.5	CN	0.153	2.000	8.00	0.36	PI	13	
	B	1 hr	1500	1 hr + 1 hr	600	L	208.9	64.2	CN	0.148	2.000	8.00	0.42	PI	13	
	B	1 hr	1500	1 hr + 1 hr	600	L	208.9	58.3	CN	0.146	2.000	8.00	0.38	PI	13	
0.625" Sheet	B	1 hr	1500	1 hr + 1 hr	400	L	222.1	45.1	SEN	0.515	2.000	8.00	0.28	PI	13	
	B	1 hr	1500	1 hr + 1 hr	400	L	222.1	50.0	SEN	0.523	2.000	8.00	0.31	PI	13	
	B	1 hr	1500	1 hr + 1 hr	600	L	216.0	(3) 53.5	SEN	0.523	2.000	8.00	0.35	PI	13	
	B	1 hr	1500	1 hr + 1 hr	700	L	204.3	(3) 78.3	SEN	0.523	2.000	8.00	0.53	PI	13	
	B	1 hr	1500	1 hr + 1 hr	500	L	228.2	45.0	NB3	0.500	3.500	3.50	0.54	PI	13	
	B	1 hr	1500	1 hr + 1 hr	500	L	228.2	47.0	NB3	0.500	0.500	3.50	0.56	PI	13	
	B	1 hr	1500	1 hr + 1 hr	500	L	228.2	47.9	NB3	0.500	0.500	3.50	0.57	PI	13	
	B	1 hr	1500	1 hr + 1 hr	600	L	216.1	40.3	NB3	0.500	0.500	3.50	0.48	PI	13	
	B	1 hr	1500	1 hr + 1 hr	600	L	216.1	48.9	NB3	0.500	0.500	3.50	0.59	PI	13	
	B	1 hr	1500	1 hr + 1 hr	600	L	216.1	49.1	NB3	0.500	0.500	3.50	0.59	PI	13	
	1"-Dia. Bar	A			1 hr + 1 hr	400		225.4	40.6	NR	0.505	0.375	3.00	0.55		10
		A			1 hr + 1 hr	400		224.4	(3) 42.4	NR	0.505	0.375	3.00	0.58		10
A				1 hr + 1 hr	400		219.6	(3) 52.5	NR	0.505	0.375	3.00	0.74		10	
A				1 hr + 1 hr	400		221.0	(3) 55.5	NR	0.505	0.375	3.00	0.79		10	
A				1 hr + 1 hr	400		195.0	(3) 48.3	NR	0.505	0.375	3.00	0.67		10	
C				1 hr + 1 hr	400		180.0	(3) 41.8	NR	0.750	0.375	4.00	0.68		14	
C				1 hr	212		221.0	11.9	NR	0.750	0.375	4.00	0.17		14	
C				1 hr	212		221.0	13.0	NR	0.750	0.375	4.00	0.15		14	
C				1 hr	250		228.0	17.8	NR	0.750	0.375	4.00	0.16		14	
C				1 hr	300		232.0	24.4	NR	0.750	0.375	4.00	0.20		14	
C				1 hr	300		232.0	23.4	NR	0.750	0.375	4.00	0.26		14	
C				1 hr	400		238.0	26.7	NR	0.750	0.375	4.00	0.25		14	
C				1 hr	400		238.0	27.8	NR	0.750	0.375	4.00	0.28		14	
C				1 hr	500		236.0	39.0	NR	0.750	0.375	4.00	0.29		14	
C				1 hr	500		236.0	40.0	NR	0.750	0.375	4.00	0.42		14	
C				1 hr	600		229.0	47.0	NR	0.750	0.375	4.00	0.43		14	
C				1 hr	600		229.0	46.8	NR	0.750	0.375	4.00	0.52		14	
C				1 hr	700		217.0	61.5	NR	0.750	0.375	4.00	0.71		14	
C				1 hr	700		217.0	55.5	NR	0.750	0.375	4.00	0.65		14	
1.25" Plate		B	1 hr	1500	1 hr + 1 hr	500	L	228.2	50.4	NB3	1.000	1.000	5.00		FR	13
	B	1 hr	1500	1 hr + 1 hr	500	L	228.2	49.7	NB3	1.000	1.000	5.00		FR	13	
	B	1 hr	1500	1 hr + 1 hr	600	L	216.1	50.4	NB3	1.000	1.000	5.00		FR	13	
	B	1 hr	1550	1 hr + 1 hr	600	L	216.1	54.5	NB3	1.000	1.000	5.00		FR	13	
	B	1 hr	1550	1 hr + 1 hr	600	L	216.1	45.3	NB3	1.000	1.000	5.00		PI	13	
3.00" x 9.00" Forging	D	45 min	1525	1 1/2 hr + 1 1/2 hr	800	L	229.4	63.4	CN	0.197	6.000	9.00	0.350	PI	12	
	D	45 min	1525	1 1/2 hr + 1 1/2 hr	800	L	229.4	43.7	CN	0.375	6.000	24.00	0.153	PI	12	
	D	45 min	1525	1 1/2 hr + 1 1/2 hr	800	L	229.4	42.6	CN	1.000	9.000	24.00	0.359	PI	12	
	D	45 min	1525	1 1/2 hr + 1 1/2 hr	800	L	213.1	88.2	CN	0.375	6.000	24.00	0.413	PI	12	
	D	45 min	1525	1 1/2 hr + 1 1/2 hr	800	L	213.1	82.2	CN	0.375	6.000	24.00	0.383	PI	12	

TABLE I-B (Cont.)

Form	Composition	Heat Treatment				Test Orientation	Yield Strength (ksi)	K _{IC} ksi√in	Specimen Type	Specimen Size (in.)			σ _N /σ _{YS}	Comments	Ref.
		Austenitizing Treatment		Temper.						Thick-ness B	Width W	Length L			
		Time	Temp. of	Time	Temp. of										
3.00" x 9.00" Forging	D	45 min	1525	1 1/2	800	RT	213.1	CN	1.000	9.000	24.00	0.301	PI	12	
	D	45 min	1525	1 1/2	800	RT	213.1	CN	1.000	9.000	24.00	0.300	PI	12	
	D	45 min	1525	1 1/2	800	400	184.7	CN	1.000	9.000	24.00	0.463	PI	12	
	D	45 min	1525	800	1 1/2	800	213.9	-110	CN	0.197	3.000	9.00	0.367	PI	12
	D	45 min	1525	800	1 1/2	800	229.4	-110	NR	D=1.122	d=.846		0.640		12
	D	45 min	1525	800	1 1/2	800	229.4	-110	NR	D=1.122	d=.846		0.530		12
	D	45 min	1525	800	1 1/2	800	213.9	-110	NR	D=1.121	d=.844		0.570		12
	D	45 min	1525	800	1 1/2	800	213.9	-110	NR	D=1.123	d=.845		0.610		12
	D	45 min	1525	800	1 1/2	800	213.0	-110	NR	D=1.123	d=.846		0.460		12
	D	45 min	1525	800	1 1/2	800	202.2	75	NR	D=1.123	d=.846		0.890		12
	D	45 min	1525	800	1 1/2	800	196.9	75	NR	D=1.123	d=.846		0.80		12
	D	45 min	1525	800	1 1/2	800	184.7	400	NR	D=1.222	d=.847		0.97		12
	D	45 min	1525	800	1 1/2	800	184.4	400	NR	D=1.122	d=.846		0.80		12
	D	45 min	1525	800	1 1/2	800	156.7	650	NR	D=1.123	d=.845		0.96		12
	D	45 min	1525	800	1 1/2	800	213.0	75	SC	0.186	3.000	12.00	0.86		12
	D	45 min	1525	800	1 1/2	800	213.0	75	SC	0.192	3.000	12.00	0.87		12
	D	45 min	1525	800	1 1/2	800	213.0	75	SC	0.184	3.000	12.00	0.86		12
	D	45 min	1525	800	1 1/2	800	213.0	75	SC	0.187	3.000	12.00	0.67		12
	8.00" Square Forging	E	20 min	1550	1 hr + 1 hr	400	RT	221.9	NR	D	8.750	4.00	0.29		13
		E	20 min	1550	1 hr + 1 hr	400	RT	221.9	NR	D	8.750	4.00	0.36		13
		E	20 min	1550	1 hr + 1 hr	400	400	221.9	NR	D	8.750	4.00	0.23		13
		E	20 min	1550	1 hr + 1 hr	400	400	221.9	NR	D	8.750	4.00	0.32		13
		E	20 min	1550	1 hr + 1 hr	400	650	217.2	RT	NR	8.750	4.00	0.25		13
		E	20 min	1550	1 hr + 1 hr	650	650	217.2	RT	NR	8.750	4.00	0.67		13
		E	20 min	1550	1 hr + 1 hr	650	650	217.2	RT	NR	8.750	4.00	0.46		13
		E	20 min	1550	1 hr + 1 hr	650	650	217.2	RT	NR	8.750	4.00	0.65		13
		E	20 min	1550	1 hr + 1 hr	650	650	217.2	RT	NR	8.750	4.00	0.78		13
		E	20 min	1550	1 hr + 1 hr	650	650	217.2	RT	NR	8.750	4.00	0.75		13
		E	20 min	1550	1 hr + 1 hr	650	650	217.2	RT	NR	8.750	4.00	0.76		13
		E	20 min	1550	1 hr + 1 hr	650	650	217.2	RT	NR	8.750	4.00	0.69		13
		E	20 min	1550	1 hr + 1 hr	650	650	217.2	RT	NR	8.750	4.00	0.96		13
		E	20 min	1550	1 hr + 1 hr	400	400	195.0	300	NR	8.750	4.00	0.68		13
E		45 min	1525	1 hr + 1 hr	800	800	229.4	-110	NR	8.750	4.00	0.64		13	
E		45 min	1525	1 hr + 1 hr	800	800	229.4	-110	NR	8.750	4.00	0.52		13	
E		45 min	1525	1 hr + 1 hr	800	800	213.9	-110	NR	8.750	4.00	0.56		13	
E		45 min	1525	1 hr + 1 hr	800	800	213.9	-110	NR	8.750	4.00	0.61		13	
E		45 min	1525	1 hr + 1 hr	800	800	228.3	-110	NR	8.750	4.00	0.46		13	
E		45 min	1525	1 hr + 1 hr	800	800	202.0	-110	NR	8.750	4.00	0.89		13	
E		45 min	1525	1 hr + 1 hr	800	800	217.1	RT	NR	8.750	4.00	0.90		13	
E		45 min	1525	1 hr + 1 hr	800	800	196.9	RT	NR	8.750	4.00	0.80		13	
E		45 min	1525	1 hr + 1 hr	800	800	184.7	400	NR	8.750	4.00	0.83		13	
E		45 min	1525	1 hr + 1 hr	800	800	184.4	400	NR	8.750	4.00	0.81		13	
E		45 min	1525	1 hr + 1 hr	800	800	156.8	650	NR	8.750	4.00	0.96		13	
E		45 min	1525	1 hr + 1 hr	800	800	145.0	650	NR	8.750	4.00	0.90		13	
E		45 min	1525	1 hr + 1 hr	800	800	145.0	650	NR	8.750	4.00	0.65	PI	13	
E		45 min	1525	1 hr + 1 hr	800	800	145.0	650	CN	1.750	1.750	8.00	0.50	PI	13
E		45 min	1525	1 hr + 1 hr	800	800	145.0	650	CN	1.750	1.750	8.00	0.50	PI	13

TABLE I-C - TABULATION OF K_{Ic} DATA
FERROUS ALLOYS - D6ac Steel

Form	Composition (1)	Heat Treatment		Test Orientation (2)	Test Temp. of	Yield Strength 0.2% (ksi)	K_{Ic} ksi \sqrt{in}	Specimen Type (3)	Specimen Size			σ_N/σ_{YS} (4)	Comments (5)	Ref. (6)		
		Austenitizing Treatment	Temper						Thickness B	Width W	Length L					
		Time	Temp. of	Time	Temp. of											
0.095"-Thick Sheet	A	1 hr	1550	1 hr + 1 hr	500	235.7	50.6	CC	0.095	1.750	8.00	0.31	PI	13		
	A	1 hr	1550	1 hr + 1 hr	500	235.7	40.1	CC	0.095	1.750	8.00	0.25	PI	13		
	A	1 hr	1550	1 hr + 1 hr	500	235.7	48.1	CC	0.095	1.750	8.00	0.30	PI	13		
	A	1 hr	1550	1 hr + 1 hr	500	240.1	44.8	CC	0.095	1.750	8.00	0.28	PI	13		
	A	1 hr	1550	1 hr + 1 hr	500	240.1	43.1	CC	0.095	1.750	8.00	0.26	PI	13		
	A	1 hr	1550	1 hr + 1 hr	500	240.1	45.9	CC	0.095	1.750	8.00	0.28	PI	13		
	A	1 hr	1550	1 hr + 1 hr	500	252.7	36.1	CC	0.095	1.750	8.00	0.21	PI	13		
	A	1 hr	1550	1 hr + 1 hr	500	252.7	37.6	CC	0.095	1.750	8.00	0.22	PI	13		
	A	1 hr	1550	1 hr + 1 hr	500	252.7	38.0	CC	0.095	1.750	8.00	0.22	PI	13		
	A	1 hr	1550	1 hr + 1 hr	500	262.7	36.2	CC	0.095	1.750	8.00	0.20	FR	13		
	A	1 hr	1550	1 hr + 1 hr	500	262.7	37.9	CC	0.095	1.750	8.00	0.22	FR	13		
	A	1 hr	1550	1 hr + 1 hr	500	262.7	35.9	CC	0.095	1.750	8.00	0.20	FR	13		
	A	1 hr	1550	1 hr + 1 hr	1000	215.3	81.6	CC	0.095	1.750	8.00	0.56	FR	13		
	A	1 hr	1550	1 hr + 1 hr	1000	215.3	67.9	CC	0.095	1.750	8.00	0.46	FR	13		
	A	1 hr	1550	1 hr + 1 hr	1000	215.3	62.7	CC	0.095	1.750	8.00	0.43	FR	13		
	A	1 hr	1550	1 hr + 1 hr	1000	224.7	47.2	CC	0.095	1.750	8.00	0.31	FR	13		
	A	1 hr	1550	1 hr + 1 hr	1000	224.7	47.2	CC	0.095	1.750	8.00	0.31	FR	13		
	A	1 hr	1550	1 hr + 1 hr	1000	224.7	48.2	CC	0.095	1.750	8.00	0.32	FR	13		
	0.103"-Thick Sheet	NA*	1650F/30 min to 1550F/30 min, salt quench to 400F/5 min, AC, temper 4 hr/600F, AC and double temper at 1000F/2 hr and AC.				RT	199.2	60.7	CC	0.103	4.000	18.00	0.23	PI	15
		NA					RT	199.2	73.4	CC	0.103	4.000	18.00	0.28	PI	15
NA						RT	199.2	63.6	CC	0.103	4.000	18.00	0.24	PI	15	
0.500"-Thick Plate	B	1 hr	1550	1 hr + 1 hr	500	246.8	87.6	NB3	0.500	0.500	1.00	0.93	PI	16		
	B	1 hr	1550	1 hr + 1 hr	500	246.8	78.9	NB3	0.500	0.500	4.00	0.84	PI	16		
	B	1 hr	1550	1 hr + 1 hr	500	246.8	80.7	NB3	0.500	0.500	4.00	0.86	PI	16		
	B	1 hr	1550	1 hr + 1 hr	500	246.8	74.7	NB3	0.500	0.500	4.00	0.80	PI	16		
	B	1 hr	1550	1 hr + 1 hr	500	246.8	81.6	NB3	0.500	0.500	2.00	0.86	PI	16		
	B	1 hr	1550	1 hr + 1 hr	500	247.0	70.3	NB3	0.500	0.500	2.00	0.76	PI	16		
	B	1 hr	1550	1 hr + 1 hr	500	247.0	--	NB3	0.500	0.500	2.00	--	Dev	16		
	B	1 hr	1550	1 hr + 1 hr	500	247.0	74.1	NB3	0.500	0.500	3.00	0.42	PI	16		
	B	1 hr	1550	1 hr + 1 hr	500	247.0	70.1	NB4	0.500	0.500	2.00	0.70	PI	16		
	B	1 hr	1550	1 hr + 1 hr	500	247.0	68.1	NB4	0.500	0.500	2.00	0.68	PI	16		
	B	1 hr	1550	1 hr + 1 hr	500	247.0	84.6	NB4	0.500	0.500	3.00	0.93	PI	16		
	B	1 hr	1550	1 hr + 1 hr	500	247.0	68.7	NB4	0.500	0.500	3.00	0.72	PI	16		

* Not available

(1) Alloy compositions given in Table IV-C

(2) L - longitudinal

T - transverse

ST - short transverse

(3) CC - Center-Cracked Plate

NB3 - Notch Bend - 3-point loading

NB4 - Notch Bend - 4-point loading

NR - Notched Round

SC - Surface Cracked Plate

(4) $\sigma_N/\sigma_{YS} = \frac{\text{Nominal Stress}}{0.2\% \text{ Yield Stress}}$

(5) PI - Pop-in load

Dev - Load at deviation from linearity

FR - Ultimate load

(6) References listed in Bibliography

TABLE I-C (Cont.)

Form	Composition	Heat Treatment				Test Orientation	Yield Strength 0.2% (ksi)	K _{1c} ksi√in	Specimen Type	Specimen Size			σ _N /σ _{YS}	Comments	Ref.
		Austenitizing Temp. °F	Temper		Thickness B					Width W	Length L				
			Time	Temp. °F								Time			
0.500"-Thick Plate	C	1 hr 1550	400	2 hr + 2 hr	400	L	224.4	NR	NR	0.500	4.00	0.77		4	
	C	1 hr 1550	600	2 hr + 2 hr	600	L	246.0	NR	NR	0.500	4.00	0.85		4	
	C	1 hr 1550	800	2 hr + 2 hr	800	L	231.0	NR	NR	0.500	4.00	1.05		4	
	C	1 hr 1550	600	2 hr + 2 hr	600	L	247.0	NR	NR	0.500	4.00	0.66		4	
	C	1 hr 1550	600	2 hr + 2 hr	600	NA	247.0	NR	NR	0.332	4.00	0.71		4	
	C	1 hr 1550	600	2 hr + 2 hr	600	NA	247.0	NR	NR	0.351	4.00	0.55		4	
	C	1 hr 1550	600	2 hr + 2 hr	600	NA	247.0	NR	NR	0.329	4.00	0.61		4	
	C	1 hr 1550	600	2 hr + 2 hr	600	NA	247.0	NR	NR	0.348	4.00	0.67		4	
	C	1 hr 1550	600	2 hr + 2 hr	600	NA	247.0	NR	NR	0.346	4.00	0.63		4	
	C	1 hr 1550	600	2 hr + 2 hr	600	NA	247.0	NR	NR	0.316	4.00	0.54		4	
	C	1 hr 1550	600	2 hr + 2 hr	600	NA	247.0	NR	NR	0.342	4.00	0.72		4	
	C	1 hr 1550	600	2 hr + 2 hr	600	NA	247.0	NR	NR	0.323	4.00	0.52		4	
	C	1 hr 1550	600	2 hr + 2 hr	600	NA	247.0	NR	NR	0.290	4.00	0.55		4	
	C	1 hr 1550	600	2 hr + 2 hr	600	NA	247.0	NR	NR	0.306	4.00	0.58		4	
	C	1 hr 1550	600	2 hr + 2 hr	600	NA	247.0	NR	NR	0.350	4.00	0.75		4	
	C	1 hr 1550	600	2 hr + 2 hr	600	NA	247.0	NR	NR	0.343	4.00	0.59		4	
	C	1 hr 1550	600	2 hr + 2 hr	600	NA	247.0	NR	NR	0.335	4.00	0.62		4	
	C	1 hr 1550	600	2 hr + 2 hr	600	NA	247.0	NR	NR	0.325	4.00	0.55		4	
	C	1 hr 1550	600	2 hr + 2 hr	600	NA	247.0	NR	NR	0.347	4.00	0.48		4	
	0.750"-Thick Plate	B	1 hr 1550	500	1 hr + 1 hr	500		247.0	NB3	NB3	0.750	2.00	0.59	PI	16
B		1 hr 1550	500	1 hr + 1 hr	500		247.0	NB3	NB3	0.750	3.00	0.62	PI	16	
B		1 hr 1550	500	1 hr + 1 hr	500		247.0	NB3	NB3	0.750	3.00	---	Dev	16	
B		1 hr 1550	500	1 hr + 1 hr	500		247.0	NB3	NB3	0.750	1.00	0.70	PI	16	
B		1 hr 1550	500	1 hr + 1 hr	500		247.0	NB3	NB3	0.750	4.00	0.56	PI	16	
B		1 hr 1550	500	1 hr + 1 hr	500		247.0	NB4	NB4	0.750	2.00	0.60	PI	16	
B		1 hr 1550	500	1 hr + 1 hr	500		247.0	NB4	NB4	0.750	3.00	0.57	PI	16	
B		1 hr 1550	500	1 hr + 1 hr	500		247.0	NB4	NB4	0.750	3.00	0.49	PI	16	
B		1 hr 1550	500	1 hr + 1 hr	500		247.0	NB4	NB4	0.750	3.00	0.57	PI	16	
B		1 hr 1550	500	1 hr + 1 hr	500		247.0	NB4	NB4	0.750	1.00	0.84	PI	16	
B		1 hr 1550	500	1 hr + 1 hr	500		247.0	NB4	NB4	0.750	1.00	0.80	PI	16	
B		1 hr 1550	500	1 hr + 1 hr	500		247.0	NB4	NB4	0.750	1.00	0.67	PI	16	
B		1 hr 1550	500	1 hr + 1 hr	500		247.0	NB4	NB4	0.750	1.00	0.67	PI	16	
D		30 min 1650	650	2 hr + 2 hr	650	ST	266.0	NB4	NB4	2.000	24.00	0.28	PI	17	
D		30 min 1650	650	2 hr + 2 hr	650	ST	266.0	NB4	NB4	2.000	24.00	0.27	PI	17	
D		30 min 1650	650	2 hr + 2 hr	650	ST	266.0	NB4	NB4	2.000	24.00	0.21	PI	17	
D		30 min 1650	650	2 hr + 2 hr	650	ST	266.0	NB4	NB4	2.000	24.00	0.21	PI	17	
D		30 min 1650	650	2 hr + 2 hr	650	L	266.0	NB4	NB4	2.000	24.00	0.28	PI	17	
D		30 min 1650	650	2 hr + 2 hr	650	L	266.0	NB4	NB4	2.000	24.00	0.28	PI	17	
D		30 min 1650	650	2 hr + 2 hr	650	L	266.0	NB4	NB4	2.000	24.00	0.23	PI	17	
D	1750°F 1 hr → 1000°F, AC, Aust.				ST	209.0	NB4	NB4	2.000	24.00	0.64	PI	17		
D	1635°F 1 hr, q to 950°F 2 hr, AC				ST	209.0	NB4	NB4	2.000	24.00	0.64	PI	17		
D	to RT, double temper 2 hr at 1025°F				ST	209.0	NB4	NB4	2.000	24.00	0.54	PI	17		
D					ST	209.0	NB4	NB4	2.000	24.00	0.58	PI	17		
2.250"-Thick Plate	E	Norm. 1650°F 30 min, Aust. 1650°F				L	213.0	NB4	NB4	2.000	24.00	0.33	FR	18	
	E	30 min, held 950°F, 1 hr 400°F				L	213.0	NB4	NB4	2.000	24.00	0.33	FR	18	
	E	15 min AC, tempered 1 hr 400°F				ST	213.0	NB4	NB4	2.000	24.00	0.29	FR	18	
	E	Double temper at 1025°F 2 hr, air cool				ST	198.0	NB4	NB4	2.000	24.00	0.32	FR	18	
	E					ST	206.0	NB4	NB4	2.000	24.00	0.20	FR	18	

* Average of number of tests indicated in ()

TABLE I-D - TABULATION OF K_{Ic} DATA
FERROUS ALLOYS - H-11 Steel

Form	Composition (1)	Heat Treatment				Test Orientation (2)	Test Temp. T_p (°F)	Yield Strength 0.2% (ksi)	K_{Ic} (3) ksi $\sqrt{\text{in}}$	Specimen Type (4)	Specimen Size			σ_N/σ_{YS} (5)	Comments (6)	Ref. (7)
		Austenitizing Treatment		Temper							Thickness B	Width W	Length L			
		Time	Temp. T_p (°F)	Time	Temp. T_p (°F)											
0.085" Sheet	A	20 min	1850	2 hr + 2 hr	1000	L	-100	(3) 25.4	CC	0.085	1.750	8.00		10		
	A	20 min	1850	2 hr + 2 hr	1000	L	-45	(3) 24.5	CC	0.085	1.750	8.00		10		
	A	20 min	1850	2 hr + 2 hr	1000	L	40	(3) 29.5	CC	0.085	1.750	8.00		10		
	A	20 min	1850	2 hr + 2 hr	1000	L	75	(3) 242.9	CC	0.085	1.750	8.00		10		
	A	20 min	1850	2 hr + 2 hr	1000	T	75	(3) 235.2	CC	0.085	1.750	8.00		10		
	A	20 min	1850	2 hr + 2 hr	1000	L	200	(3) 231.6	CC	0.085	1.750	8.00		10		
	A	20 min	1850	2 hr + 2 hr	1050	L	-100	(3) 240.2	CC	0.085	1.750	8.00		10		
	A	20 min	1850	2 hr + 2 hr	1050	L	-45	(3) 231.4	CC	0.085	1.750	8.00		10		
	A	20 min	1850	2 hr + 2 hr	1050	L	40	(3) 225.4	CC	0.085	1.750	8.00		10		
	A	20 min	1850	2 hr + 2 hr	1050	L	75	(3) 223.0	CC	0.085	1.750	8.00		10		
	A	20 min	1850	2 hr + 2 hr	1050	T	200	(3) 214.6	CC	0.085	1.750	8.00		10		
	A	20 min	1850	2 hr + 2 hr	1050	L	300	(3) 212.0	CC	0.085	1.750	8.00		10		
	A	20 min	1850	2 hr + 2 hr	1150	L	-100	(3) 202.7	CC	0.085	1.750	8.00		10		
	A	20 min	1850	2 hr + 2 hr	1150	L	-45	(3) 196.2	CC	0.085	1.750	8.00		10		
	A	20 min	1850	2 hr + 2 hr	1150	L	-100	(3) 170.1	CC	0.085	1.750	8.00		10		
	1.00" Dia. Bar	A	20 min	1850	2 hr + 2 hr	1000	L	-45	(3) 21.7	NR	D=0.500	d=0.375	3.00		10	
		A	20 min	1850	2 hr + 2 hr	1000	L	40	(3) 26.6	NR	D=0.500	d=0.375	3.00		10	
		A	20 min	1850	2 hr + 2 hr	1000	L	75	(3) 25.0	NR	D=0.500	d=0.375	3.00		10	
		A	20 min	1850	2 hr + 2 hr	1000	L	200	(2) 226.0	NR	D=0.500	d=0.375	3.00		10	
		A	20 min	1850	2 hr + 2 hr	1000	L	300	(2) 228.0	NR	D=0.500	d=0.375	3.00		10	
A		20 min	1850	2 hr + 2 hr	1050	L	300	(4) 230.4	NR	D=0.500	d=0.375	3.00		10		
A		20 min	1850	2 hr + 2 hr	1050	L	-45	(3) 235.1	NR	D=0.500	d=0.375	3.00		10		
A		20 min	1850	2 hr + 2 hr	1050	L	40	(3) 228.2	NR	D=0.500	d=0.375	3.00		10		
A		20 min	1850	2 hr + 2 hr	1050	L	75	(3) 228.2	NR	D=0.500	d=0.375	3.00		10		
A		20 min	1850	2 hr + 2 hr	1050	L	200	(2) 219.7	NR	D=0.500	d=0.375	3.00		10		
A	20 min	1850	2 hr + 2 hr	1100	L	-45	(3) 207.7	NR	D=0.500	d=0.375	3.00		10			

(1) Alloy compositions given in Table IV-D

(2) L - longitudinal
T - transverse

(3) Average of number of tests indicated in ()

(4) CC - Center-Cracked Plate

NR - Notched Round

NB3 - Notched Bend - 3-point loading

(5) $\sigma_N/\sigma_{YS} = \frac{\text{Nominal Stress}}{0.2\% \text{ Yield Stress}}$

(6) PI - Pop-in load

(7) References listed in Bibliography

TABLE I-D (Cont.)

Form	Composition	Heat Treatment				Test Orientation	Test Temp. Of	Yield Strength 0.2% (ksi)	K _{1c} ksi√in	Specimen Type	Specimen Size			σ _w /σ _{YS}	Comments	Ref.
		Austenitizing Treatment		Temper							Thickness B	Width W	Length L			
		Time	Temp. Of	Time	Temp. Of											
8.00" Square Forged Billet	B	20 min	1850	2 hr + 2 hr	Double Temper 1050	T	RT	225.0	NB3	0.750	0.750	3.50	0.37	PI	13	
	B	20 min	1850	2 hr + 2 hr	1050	T	RT	225.0	NB3	0.750	0.750	3.50	0.38	PI	13	
	B	20 min	1850	2 hr + 2 hr	1050	T	RT	37.3	NB3	0.750	0.750	3.50	0.37	PI	13	
	B	20 min	1850	2 hr + 2 hr	1050	T	RT	225.0	NB3	0.750	0.750	3.50	0.41	PI	13	
	B	20 min	1850	2 hr + 2 hr	1050	T	RT	225.0	NB3	0.750	0.750	3.50	0.33	PI	13	
	B	20 min	1850	2 hr + 2 hr	1050	T	RT	225.0	NB3	0.750	0.750	3.50	0.36	PI	13	
	B	20 min	1850	2 hr + 2 hr	1050	T	RT	225.0	NB3	0.750	0.750	3.50	0.34	PI	13	
	B	20 min	1850	2 hr + 2 hr	1100	T	RT	225.0	NB3	0.750	0.750	3.50	0.38	PI	13	
	B	20 min	1850	2 hr + 2 hr	1100	T	RT	194.2	NB3	1.000	1.000	3.50	0.64	PI	13	
	B	20 min	1850	2 hr + 2 hr	1100	T	RT	194.2	NB3	1.000	1.000	3.50	0.70	PI	13	
	B	20 min	1850	2 hr + 2 hr	1100	T	RT	194.2	NB3	1.000	1.000	3.50	0.77	PI	13	
	B	20 min	1850	2 hr + 2 hr	1100	T	RT	194.2	NB3	1.000	1.000	3.50	0.69	PI	13	
	B	20 min	1850	2 hr + 2 hr	1100	T	RT	194.2	NB3	1.000	1.000	3.50	0.73	PI	13	
	B	20 min	1850	2 hr + 2 hr	1100	T	RT	194.2	NB3	1.000	1.000	3.50	0.76	PI	13	
	B	20 min	1850	2 hr + 2 hr	1100	T	RT	194.2	NB3	1.000	1.000	3.50	0.59	PI	13	
	B	20 min	1850	2 hr + 2 hr	1050	L	RT	221.2	NB3	0.750	0.750	3.50	0.74	PI	13	
	B	20 min	1850	2 hr + 2 hr	1050	L	RT	221.2	NB3	0.750	0.750	3.50	0.46	PI	13	
	B	20 min	1850	2 hr + 2 hr	1050	L	RT	221.2	NB3	0.750	0.750	3.50	0.38	PI	13	
	B	20 min	1850	2 hr + 2 hr	1050	L	RT	221.2	NB3	0.750	0.750	3.50	0.40	PI	13	
	B	20 min	1850	2 hr + 2 hr	1050	L	RT	221.2	NR	D=0.500	d=0.357	3.00	0.34	PI	13	
	B	20 min	1850	2 hr + 2 hr	1050	L	RT	221.2	NR	D=0.500	d=0.357	3.00	0.39	PI	13	
	B	20 min	1850	2 hr + 2 hr	1050	L	RT	221.2	NR	D=0.500	d=0.357	3.00	0.29	PI	13	
	B	20 min	1850	2 hr + 2 hr	1050	L	RT	221.2	NR	D=0.500	d=0.357	3.00	0.52	PI	13	
	B	20 min	1850	2 hr + 2 hr	1050	L	RT	27.4	NR	D=0.500	d=0.357	3.00	0.41	PI	13	
	B	20 min	1850	2 hr + 2 hr	1100	L	RT	193.8	NB3	0.750	0.750	3.50	0.69	PI	13	
	B	20 min	1850	2 hr + 2 hr	1100	L	RT	193.8	NB3	0.750	0.750	3.50	0.84	PI	13	
	B	20 min	1850	2 hr + 2 hr	1100	L	RT	193.8	NB3	0.750	0.750	3.50	0.70	PI	13	
	B	20 min	1850	2 hr + 2 hr	1100	L	RT	193.8	NB3	0.750	0.750	3.50	0.60	PI	13	
	B	20 min	1850	2 hr + 2 hr	1100	L	RT	193.8	NB3	0.750	0.750	3.50	0.79	PI	13	
	B	20 min	1850	2 hr + 2 hr	1100	L	RT	193.8	NB3	0.750	0.750	3.50	0.84	PI	13	

TABLE I-E - TABULATION OF K_{Ic} DATA
FERROUS ALLOYS - HP 9-4 Steel

Form	Composition (1)	Heat Treatment				Test Orientation (2)	Yield Strength 0.2% (ksi)	K_{Ic} ksi \sqrt{in}	Specimen Type (3)	Specimen Size			σ_N/σ_{YS} (4)	Comments (5)	Ref. (6)
		Austenitizing Temp. of	Temper		Thickness B					Width W	Length L				
			Time	Time								Temp. of			
0.095" Sheet	A	1450	1 hr + 1 hr	Double Temper	L	208.2	36.7	CC	0.095	1.750	8.00	0.26	PI	13	
	A	1450	1 hr + 1 hr		L	208.2	38.9	CC	0.095	1.750	8.00	0.28	PI	13	
	A	1450	1 hr + 1 hr	400	L	208.2	33.1	CC	0.095	1.750	8.00	0.23	PI	13	
	A	1450	1 hr + 1 hr	600	L	222.4	56.0	CC	0.095	1.750	8.00	0.37	PI	13	
	A	1450	1 hr + 1 hr	600	L	222.4	52.7	CC	0.095	1.750	8.00	0.35	PI	13	
	A	1450	1 hr + 1 hr	600	L	222.4	53.0	CC	0.095	1.750	8.00	0.35	PI	13	
	A	1450	1 hr + 1 hr	400	L	196.4	38.1	CC	0.095	1.750	8.00	0.28	PI	13	
	A	1450	1 hr + 1 hr	400	L	196.4	42.9	CC	0.095	1.750	8.00	0.32	PI	13	
	A	1450	1 hr + 1 hr	400	L	196.4	45.1	CC	0.095	1.750	8.00	0.34	PI	13	
	A	1450	1 hr + 1 hr	600	L	223.3	49.4	CC	0.095	1.750	8.00	0.33	PI	13	
	A	1450	1 hr + 1 hr	600	L	223.3	51.4	CC	0.095	1.750	8.00	0.34	PI	13	
	A	1450	1 hr + 1 hr	400	L	201.2	34.1	CC	0.095	1.750	8.00	0.25	PI	13	
	A	1450	1 hr + 1 hr	400	L	201.2	34.1	CC	0.095	1.750	8.00	0.25	PI	13	
	A	1450	1 hr + 1 hr	400	L	201.2	35.5	CC	0.095	1.750	8.00	0.26	PI	13	
	0.500" Plate	B	1450	1 hr + 1 hr		RT	250.0	50.0	SC						19
		B	1450	1 hr + 1 hr		RT	225.0	65.0	SC						19
	0.750" & 1.00" Rolled Plate	C	1500	2 hr + 2 hr		RT	192.7	110.8	SC	0.750	3.000	30.00	0.73		5
		C	1500	2 hr + 2 hr		RT	189.1	138.3	SC	1.000	3.000	30.00	0.96		5
9.00" x 9.00" x 24.00" Forged Block	D	1450			L	211.3	92.9	CN	0.375	6.000	24.00	0.42	PI	12	
	D	1450	700		L	211.3	55.0	CN	1.000	9.000	24.00	0.18	PI	12	
	D	1450	700		L	198.4	109.0	CN	1.000	9.000	24.00	0.35	PI	12	
	D	1450	700		L	169.1	37.7	CN	1.000	9.000	24.00	0.42		12	
	D	1450	700		T	220.6	101.8	NR	D=1.125	d=0.800	3.00	0.99		12	
	D	1450	700		T	220.6	105.8	NR	D=1.125	d=0.800	3.00	1.02		12	
	D	1450	700		L	130.5	130.5	NR	D=2.750	d=1.900	12.00	0.86		12	
	D	1450	700		T	204.7	155.5	NR	D=2.750	d=1.900	9.00	1.04		12	
	D	1450	700		L	198.4	160.0	NR	D=2.750	d=1.900	12.00	1.09		12	
	D	1450	700		T	165.1	123.0	NR	D=2.750	d=1.900	9.00	1.03		12	
	D	1450	700		L	169.1	117.0	NR	D=2.750	d=1.900	12.00	0.95		12	

(1) Alloy compositions given in Table IV-E

(2) L - longitudinal
T - transverse

(3) CC - Center-Cracked Plate
SC - Surface Cracked Plate
CN - Center-Notched Plate
NR - Notched Round
WOLX - Wedge-Opening-Loading "X" Type
WOLT - Wedge-Opening-Loading "T" Type

(4) $\sigma_N/\sigma_{YS} = \frac{\text{Nominal Stress}}{0.2\% \text{ Yield Stress}}$

(5) PI - Pop-in load

FR - Ultimate load

(6) References listed in Bibliography

TABLE I-E (Cont.)

Form	Composition	Heat Treatment				Test Orientation	Test Temp. Of	Yield Strength 0.2% (ksi)	K _{Ic} ksi√in	Specimen Type	Specimen Size			σ _N /σ _{YS}	Comments	Ref.
		Austenitizing Time	Temp. Of	Temper							Thickness B	Width W	Length L			
				Time	Temp. Of											
3" Forged Plate	E	2 hr	1550	2 hr + 2 hr	1000	L	RT	176.0	191.0	WOLX	2.000	2.25	1.085	Data Generated during this Investigation	FR	
		2 hr	1550	2 hr + 2 hr	1000	L	RT	176.0	112.3	WOLX	2.000	2.25	0.638			
		2 hr	1550	2 hr + 2 hr	1000	T	RT	177.0	145.3	WOLX	2.000	2.25	0.821			
		2 hr	1550	2 hr + 2 hr	1000	T	RT	177.0	135.2	WOLX	2.000	2.25	0.764			
		2 hr	1550	2 hr + 2 hr	1000	T	RT	177.0	146.3	WOLX	2.000	2.25	0.828			
		2 hr	1550	2 hr + 2 hr	1000	T	RT	177.0	102.3	WOLX	2.000	5.11	0.389			
		2 hr	1550	2 hr + 2 hr	1000	T	RT	177.0	95.7	WOLX	2.000	5.11	0.367			
		2 hr	1550	2 hr + 2 hr	1000	T	RT	177.0	107.0	WOLX	1.000	2.55	0.594			
		2 hr	1550	2 hr + 2 hr	1000	T	RT	177.0	114.4	WOLX	1.000	2.55	0.776			
		2 hr	1550	2 hr + 2 hr	1000	T	100	180.15	110.7	WOLX	1.000	2.55	0.616			
		2 hr	1550	2 hr + 2 hr	1000	T	100	180.15	104.0	WOLX	2.000	5.11	0.393			
		2 hr	1550	2 hr + 2 hr	1000	T	100	180.15	100.7	WOLX	2.000	5.11	0.378			
		2 hr	1550	2 hr + 2 hr	1000	T	150	174.63	110.7	WOLX	2.000	5.11	0.427			
		2 hr	1550	2 hr + 2 hr	1000	T	150	174.63	105.7	WOLX	2.000	5.11	0.406			
		2 hr	1550	2 hr + 2 hr	1000	T	150	174.63	119.2	WOLX	1.000	2.55	0.684			
		2 hr	1550	2 hr + 2 hr	1000	T	32	187.13	102.8	WOLX	1.000	5.11	0.371			
		2 hr	1550	2 hr + 2 hr	1000	T	32	187.13	104.5	WOLX	2.000	2.55	0.382			
		2 hr	1550	2 hr + 2 hr	1000	T	0	186.75	99.4	WOLX	2.000	5.11	0.371			
		2 hr	1550	2 hr + 2 hr	1000	T	0	186.75	103.0	WOLX	1.000	2.55	0.549			
		2 hr	1550	2 hr + 2 hr	1000	T	0	186.75	107.3	WOLX	2.000	5.11	0.387			
		2 hr	1550	2 hr + 2 hr	1000	T	0	186.75	105.2	WOLX	2.000	5.11	0.386			
		2 hr	1550	2 hr + 2 hr	1000	T	-40	187.9	117.6	WOLX	1.000	2.55	0.643			
		2 hr	1550	2 hr + 2 hr	1000	T	-40	187.9	109.8	WOLX	2.000	5.11	0.399			
		2 hr	1550	2 hr + 2 hr	1000	T	-75	186.7	112.2	WOLX	2.000	5.11	0.404			
		2 hr	1550	2 hr + 2 hr	1000	T	-75	186.7	105.8	WOLX	1.000	2.55	0.542			
		2 hr	1550	2 hr + 2 hr	1000	T	-75	186.7	107.0	WOLX	2.000	5.11	0.388			
		2 hr	1550	2 hr + 2 hr	1000	T	-75	186.7	123.0	WOLX	2.000	5.11	0.444			

TABLE I-F - TABULATION OF K_{Ic} DATA FERROUS ALLOYS - 12 Ni-5Cr-3Mo

Form	Composition (1)	Heat Treatment			Test Orientation (2)	Yield Strength 0.2% (ksi)	K_{Ic} (ksi \sqrt{in})	Specimen Type (3)	Specimen Size			σ_w/σ_{ys} (4)	Comments (5)	Ref. (6)
		Austenitizing Treatment		Temp. (°F)					Thick-ness B	Width w	Length L			
		Time	Temp. (°F)											
1.00"-Thick Plate	A	1500	900	3 hr	RT	194.0	133.0	NB3	1.000	1.500	9.00	1.15	PI	11
	A	1500	900	3 hr	RT	194.0	133.0	NB3	1.000	2.000	9.00	0.93	PI	11
	A	1500	900	3 hr	RT	194.0	142.0	NB3	1.000	2.000	9.00	0.98	PI	11
	A	1500	900	3 hr	RT	194.0	137.0	NB3	1.000	2.500	9.00	0.85	PI	11
	A	1500	900	3 hr	RT	194.0	142.0	NB3	1.000	3.000	9.00	0.81	PI	11
	A	1500	900	3 hr	RT	194.0	137.0	NB3	1.000	3.500	9.00	0.71	PI	11
	A	1500	900	3 hr	RT	194.0	135.0	NB3	1.000	4.000	9.00	0.66	PI	11
	A	1500	900	30 hr	RT	176.0	181.0	NB3	1.000	3.000	9.00	1.16	PI	11
	A	1500	900	30 hr	RT	176.0	176.0	NB3	1.000	3.000	9.00	1.05	PI	11
	A	1500	900	30 hr	RT	186.0	148.0	NB3	0.500	2.500	9.00	0.95	PI	11
	A	1500	900	30 hr	RT	186.0	150.0	NB3	0.980	2.500	9.00	0.97	PI	11
	1.50"-Thick Plate	A	1500	900	30 hr	RT	194.0	145.0	NB3	1.500	1.500	3.00	1.17	PI
A		1500	900	30 hr	RT	194.0	140.0	NB3	1.500	1.500	4.50	1.11	PI	11
A		1500	900	30 hr	RT	194.0	149.0	NB3	1.500	1.500	6.00	1.20	PI	11
2.00"-Thick Plate	A	1500	900	30 hr	RT	194.0	149.0	NB3	1.500	1.500	10.50	1.19	PI	11
	A	1500	900	30 hr	RT	186.0	145.0	NB3	1.500	1.500	12.00	1.19	PI	11
	A	1500	900	30 hr	RT	186.0	138.0	NB3	1.500	2.500	9.00	0.89	PI	11
2.00"-Thick Plate	A	1500	900	30 hr	RT	186.0	144.0	NB3	2.020	2.50	9.00	0.91	PI	11
	A	1500	900	30 hr	RT	186.0	151.0	NB3	2.000	2.000	9.00	1.07	PI	11

TABLE I-G - TABULATION OF K_{Ic} DATA FERROUS ALLOYS - AM 355

Form	Composition (1)	Heat Treatment			Test Orientation (2)	Yield Strength 0.2% (ksi)	K_{Ic} (ksi \sqrt{in})	Specimen Type (3)	Specimen Size			σ_w/σ_{ys} (4)	Comments (5)	Ref. (6)	
		Austenitizing Treatment		Temp. (°F)					Thick-ness B	Width w	Length L				
		Time	Temp. (°F)												
0.625"-Thick Plate	A	1710	850	10 min	RT	198.4	43.7	NB	0.625	1.000	3.50	0.53	PI	13	
	A	1710	850	10 min	RT	198.4	42.5	NB	0.625	1.000	3.50	0.52	PI	13	
	A	1710	850	10 min	RT	201.1	38.1	NB	0.625	1.000	3.50	0.47	PI	13	
	A	1710	925	10 min	RT	201.1	67.6	NB	0.625	1.000	3.50	0.80	PI	13	
	A	1710	925	10 min	RT	201.1	80.9	NB	0.625	1.000	3.50	0.95	PI	13	
	A	1710	925	10 min	RT	201.1	72.4	NB	0.625	1.000	3.50	0.86	PI	13	
	A	1710	950	3 hr	RT	206.8	46.5	NB	0.625	1.000	3.50	0.54	PI	13	
	A	1710	925	3 hr	RT	201.1	73.9	NB	0.625	1.000	3.50	0.88	PI	13	
	A	1710	925	3 hr	RT	201.1	77.3	NB	0.625	1.000	3.50	0.91	PI	13	
	A	1710	1025	3 hr	RT	171.7	25.4	NB	0.625	1.000	3.50	1.05	PI	13	
	9.00" x 9.00" Billet	B	1710	850	10 min	-110	203.2	25.4	CN	0.188	3.000	9.00	0.22	PI	12
		B	1710	850	10 min	-110	203.2	27.4	CN	0.375	6.000	24.00	0.108	PI	12
B		1710	850	10 min	-110	203.2	20.4	CN	1.000	9.000	24.00	0.101	PI	12	
B		1710	850	10 min	-110	166.7	67.2	CN	0.375	6.000	24.00	0.494	PI	12	
B		1710	850	10 min	-110	166.7	70.9	CN	1.000	9.000	24.00	0.499	PI	12	
B		1710	850	10 min	-110	166.7	55.1	CN	1.000	9.000	24.00	0.305	PI	12	
B		1710	850	10 min	-110	179.0	88.7	CN	0.181	3.000	9.00	0.496	PI	12	
B		1710	850	10 min	-110	161.1	67.2	CN	0.181	3.000	9.00	0.803	PI	12	
B		1710	850	10 min	-110	203.2	51.1	NR	D=1.120	d=0.820	3.00	0.56		12	
B		1710	850	10 min	-110	183.9	41.1	NR	D=1.120	d=0.820	3.00	0.48		12	
B		1710	850	10 min	-110	183.9	40.4	NR	D=1.120	d=0.820	3.00	0.49		12	
B		1710	850	10 min	-110	161.1	71.4	NR	D=1.120	d=0.820	3.00	0.96		12	
B	1710	850	10 min	-110	153.6	68.4	NR	D=1.120	d=0.820	3.00	0.96		12		
B	1710	850	10 min	-110	148.1	74.9	NR	D=1.120	d=0.820	3.00	1.09		12		
B	1710	850	10 min	-110	148.1	78.8	NR	D=1.120	d=0.820	3.00	1.07		12		
B	1710	850	10 min	-110	126.4	51.6	NR	D=1.120	d=0.820	3.00	0.79		12		
B	1710	850	10 min	-110	135.0	52.7	NR	D=1.120	d=0.820	3.00	0.85		12		
B	1710	850	10 min	-110	166.7	120.0	NR	D=2.750	d=1.900	12.00	0.98		12		
B	1710	850	10 min	-110	143.2	69.5	NR	D=2.750	d=1.900	9.00	0.69		12		
B	1710	850	10 min	-110	203.2	60.6	SC	D=0.190	d=3.000	12.00	0.71		12		
B	1710	850	10 min	-110	203.2	51.4	SC	D=0.190	d=3.000	12.00	0.48		12		

(1) Alloy compositions given in Tables IV-F and IV-G
 (2) L - longitudinal; T - transverse; ST - short transverse
 (3) NB3 - Notched Bend - 3-point loading; CN - Center-Notched Plate;
 NR - Notched Round; SC - Surface-Cracked Plate
 (4) σ_w/σ_{ys} = Nominal Stress/0.2% Yield Stress
 (5) PI - Pop-in load
 (6) References listed in Bibliography

TABLE I-H - TABULATION OF K_{Ic} DATA FERROUS ALLOYS - AISI 4335+V

Form	Composition (1)	Heat Treatment			Test Orientation (2)	Yield Strength 0.2% (ksi)	K_{Ic} ksi√in	Specimen Type (3)	Specimen Size			σ_N/σ_{YS} (4)	Comments (5)	Ref. (6)
		Austenitizing Treatment		Temp. °F					Thick-ness B	Width W	Length L			
		Time	Temp. °F											
0.095" -Thick Sheet	A	20 min	1550	Double Temper 1 hr + 1 hr 1 hr + 1 hr 1 hr + 1 hr 1 hr + 1 hr	L	194.2	CC	0.095	1.750	8.00	0.53	PI	13	
	A	20 min	1550		L	213.5	CC	0.095	1.750	8.00	0.29	PI	13	
	A	20 min	1550		L	202.0	CC	0.095	1.750	8.00	0.47	PI	13	
	A	20 min	1550		L	202.0	CC	0.095	1.750	8.00	0.45	PI	13	
	A	20 min	1550		L	202.0	CC	0.095	1.750	8.00	0.52	PI	13	

TABLE I-I - TABULATION OF K_{Ic} DATA FERROUS ALLOYS - 20% Ni Maraging

Form	Composition (1)	Heat Treatment	Test Orientation (2)	Yield Strength 0.2% (ksi)	K_{Ic} ksi√in	Specimen Type (3)	Thick-ness B	Width W	Length L	σ_N/σ_{YS} (4)	Comments (5)	Ref. (6)
0.041" -Thick Sheet Cold Rolled	A	Strip held at -100°F for 16 hrs, Aged 675°F 3 hrs	L	307.0	71.9	CC	0.041	3.000	12.00		PI	15
	A		L	307.0	70.4	CC	0.041	3.000	12.00		PI	15
	A		T	307.0	50.6	CC	0.041	3.000	12.00		PI	15
	A		T	307.0	37.4	CC	0.041	3.000	12.00		PI	15

TABLE I-J - TABULATION OF K_{Ic} DATA FERROUS ALLOYS - 300M

Form	Composition (1)	Heat Treatment	Test Orientation (2)	Yield Strength 0.2% (ksi)	K_{Ic} ksi√in	Specimen Type (3)	Thick-ness B	Width W	Length L	σ_N/σ_{YS} (4)	Comments (5)	Ref. (6)
0.080" -Thick Sheet	A	1600°F - 30 min, salt Q; 325°F, 5 min; Air cool to 125°F	L	232.0	88.0	CC	0.079	3.000	12.00		PI	15
	A		L	232.0	84.3	CC	0.079	3.000	12.00		PI	15
	A		T	232.0	82.8	CC	0.079	3.000	12.00		PI	15
	A		T	232.0	81.2	CC	0.079	3.000	12.00		PI	15
	A		L	232.0	89.3	CC	0.079	4.000	12.00		PI	15

TABLE I-K - TABULATION OF K_{Ic} DATA FERROUS ALLOYS - PH 13-8 Mo

Form	Composition (1)	Heat Treatment	Test Orientation (2)	Yield Strength 0.2% (ksi)	K_{Ic} ksi√in	Specimen Type (3)	Thick-ness B	Width W	Length L	σ_N/σ_{YS} (4)	Comments (5)	Ref. (6)
9.00" x 9.00" Forging	A	1700 min, salt Q; 325°F, 5 min; Air cool to 125°F	L	219.1	47.6	CN	0.183	3.000	9.00	0.25	PI	12
	A		L	219.1	39.3	CN	0.378	6.000	24.00	0.16	PI	12
	A		L	219.1	219.1	CN	1.000	8.500	24.00	0.12	PI	12
	A		L	205.0	92.0	CN	0.377	6.000	24.00	0.55	PI	12
	A		L	205.0	89.0	CN	0.377	6.000	24.00	0.49	PI	12
	A		L	205.0	97.5	CN	1.000	8.600	24.00	0.34	PI	12
	A		L	205.0	78.9	CN	1.000	8.600	24.00	0.28	PI	12
	A		T	218.0	58.2	CN	0.192	3.000	9.00	0.29	PI	12
	A		L	219.1	45.2	NR	D=1.122	d=0.781	3.00	0.47	PI	12
	A		L	219.1	51.4	NR	D=1.122	d=0.781	3.00	0.53	PI	12
	A		T	218.0	41.7	NR	D=1.122	d=0.781	3.00	0.43	PI	12
	A		T	218.0	45.0	NR	D=1.120	d=0.781	3.00	0.47	FR	12
	A		L	205.0	107.0	NR	D=1.120	d=0.781	3.00	1.10	FR	12
	A		L	205.0	98.2	NR	D=1.120	d=0.781	3.00	1.02	FR	12
	A		T	195.4	96.8	NR	D=1.120	d=0.781	3.00	1.06	FR	12
	A		T	195.4	57.4	NR	D=2.750	d=2.000	9.00	0.42	FR	12
	A		L	205.0	60.3	NR	D=2.750	d=2.000	12.00	0.43	FR	12
	A		T	179.1	126.2	NR	D=2.750	d=2.000	9.00	0.97	FR	12
	A		L	219.1	64.2	SC	0.250	3.000	12.00	0.74	PI	12
	A		L	219.1	62.4	SC	0.250	3.000	12.00	0.67	PI	12
	A		L	219.1	63.7	SC	0.250	3.000	12.00	0.56	PI	12

(1) Alloy compositions given in Tables IV-H to IV-K

(2) L - longitudinal; T - transverse

(3) CC - Center-Cracked Plate; CN - Center-Notched Plate;

NR - Notched Round; SC - Surface-Cracked Plate

(4) σ_N/σ_{YS} = Nominal Stress/0.2% Yield Stress

(5) PI - Pop-in load; FR - Ultimate load

(6) References listed in Bibliography

TABLE I-1 - TABULATION OF K_{Ic} DATA FERROUS ALLOYS - ASTM A302B

Form	Composition (1)	Heat Treatment	Test Orientation (2)	Test Temp. °F	Yield Strength 0.2% (ksi)	K_{Ic} ksi $\sqrt{\text{in}}$	Specimen Type (3)	Specimen Size			σ_N/σ_{YS} (4)	Comments (5)	Ref. (6)
								Thickness B	Width W	Length L			
7"-Thick Plate	A	Annealed 2 hrs at 2275°F, furnace cooled at 100°F/hr max. to 925°F, air cooled to R.T.	L	-320	117.0	26.2	WOLX	1.00	2.55	3.20	0.21	PI	28
	A		L	-320	117.0	26.3	WOLX	4.00	4.50	5.75	0.19	PI	28
	A		L	-320	117.0	25.9	WOLX	2.00	2.25	2.88	0.29	PI	28
	A		L	-320	117.0	25.5	WOLX	1.00	1.125	1.44	0.35	PI	28
	A		L	-200	77.0	35.8	WOLX	1.00	2.55	3.20	0.43	FR	28
	A		L	-200	77.0	36.1	WOLX	4.00	4.50	5.75	0.49	FR	28
	A		L	-200	77.0	36.8	WOLX	4.00	4.50	5.75	0.58	FR	28
	A		L	-200	77.0	30.2	WOLX	4.00	4.50	5.75	0.33	PI	28
	A		L	-200	77.0	31.4	WOLX	2.00	2.25	2.88	0.51	PI	28
	A		L	-200	77.0	25.3	WOLX	1.00	1.125	1.44	0.69	PI	28
	A		L	-200	77.0	34.7	WOLX	1.00	1.125	1.44	1.07	FR	28
	A		L	-200	77.0	28.2	WOLX	1.00	1.125	1.44	1.04	FR	28
	A		L	-100	58.0	37.2	WOLX	1.00	1.125	1.44	0.57	PI	28
	A		L	-100	58.0	40.1	WOLX	1.00	2.55	3.20	0.61	PI	28
	A		L	-100	58.0	30.2	WOLX	4.00	2.55	3.20	0.63	PI	28
	A		L	-100	58.0	42.1	WOLX	2.00	4.50	5.75	0.36	PI	28
	A		L	-100	58.0	45.4	WOLX	1.00	1.125	1.44	0.86	PI	28
	A		L	-100	58.0	30.6	WOLX	1.00	1.125	1.44	1.13	FR	28
	A		L	0	50.0	52.5	WOLX	4.00	4.50	5.75	1.07	PI	28
	7"-Thick Plate		A	Normalized 7 hrs at 1650°F, fan cooled to 200°F, air cooled. Stress relieved 7 hrs at 1200°F.	L	-320	133.0	26.3	WOLX	4.00	4.50	5.75	0.17
A		L	-320		133.0	25.4	WOLX	2.00	2.25	2.88	0.22	FR	28
A		L	-320		133.0	38.5	WOLX	2.00	2.25	2.88	0.42	FR	28
A		L	-320		133.0	30.0	WOLX	1.00	1.125	1.44	0.48	FR	28
A		L	-320		133.0	32.8	WOLX	1.00	1.125	1.44	0.61	FR	28
A		L	-320		133.0	24.1	WOLX	1.00	1.125	1.44	0.31	FR	28
A		L	-250		105.0	30.4	WOLX	1.00	1.125	1.44	0.52	FR	28
A		L	-200		85.0	34.9	WOLX	4.00	4.50	5.75	0.33	FR	28
A		L	-200		85.0	45.5	WOLX	1.69	2.25	2.88	0.84	FR	28
A		L	-200		85.0	30.1	WOLX	1.94	2.25	2.88	0.55	FR	28
A		L	-200		85.0	34.6	WOLX	2.00	2.25	2.88	0.47	FR	28
A		L	-200		85.0	35.3	WOLX	1.00	1.125	1.44	0.87	FR	28
A		L	-200		85.0	34.3	WOLX	1.00	1.125	1.44	0.85	FR	28
A		L	-200		85.0	32.1	WOLX	1.00	1.125	1.44	0.88	FR	28
A		L	-200		85.0	29.4	WOLX	1.00	1.125	1.44	0.81	FR	28
A		L	-200		85.0	30.4	WOLX	1.00	1.125	1.44	0.56	FR	28
A		L	-200		85.0	36.9	WOLX	1.00	1.125	1.44	0.74	FR	28
A		L	-200		85.0	28.3	WOLX	1.00	1.125	1.44	0.47	FR	28
A		L	-150		71.0	44.3	WOLX	1.69	2.25	2.88	0.69	FR	28
A		L	-150		71.0	36.9	WOLX	1.00	1.125	1.44	1.24	FR	28
A	L	-150	71.0	40.9	WOLX	1.00	1.125	1.44	1.37	FR	28		
A	L	-150	71.0	50.6	WOLX	0.93	1.125	1.44	1.07	FR	28		
A	L	-150	71.0	48.1	WOLX	1.00	1.125	1.44	1.06	FR	28		
A	L	-150	71.0	32.6	WOLX	1.00	1.125	1.44	0.72	FR	28		
A	L	-100	63.0	46.0	WOLX	4.00	4.50	5.75	0.59	FR	28		
A	L	-100	63.0	51.2	WOLX	1.99	2.25	2.88	0.77	FR	28		
A	L	-100	63.0	37.2	WOLX	2.00	2.25	2.88	1.26	FR	28		
A	L	-100	63.0	54.6	WOLX	1.00	1.125	1.44	1.26	FR	28		
A	L	-100	63.0	59.0	WOLX	1.00	1.125	1.44	1.38	FR	28		
A	L	-85	61.0	49.1	WOLX	2.00	2.25	2.88	0.88	FR	28		

(1) Alloy composition given in Table IV-L
 (2) L - longitudinal
 (3) WOLX - Wedge-Opening-Loading "m" Type
 WOLX - Wedge-Opening-Loading "X" Type

(4) σ_N/σ_{YS} = Nominal Stress/0.2% Yield Stress
 (5) PI - Pop-in load; FR - Ultimate load
 (6) References listed in Bibliography

TABLE I-M - TABULATION OF K_{Ic} DATA
FERROUS ALLOYS - Ni-Mo-V Forging Steel

Form	Composition (1)	Heat Treatment	Test Orientation (2)	Test Temp. Of	Yield Strength 0.2% (ksi)	K_{Ic} ksi \sqrt{in}	Specimen Type (3)	Specimen Size			σ_W/σ_{YS} (4)	Comments (5)	Ref. (6)
								Thickness B	Width W	Length L			
38" Dia. Rotor Forging	A	20 hours 1475°F, furnace cool to 600°F, hold at 600°F 30 hrs. 30 hours 1640°F, air cool to 530°F, hold 30 hrs. Temper 40 hrs 1130°F, furnace cool to 400°F, air cool to R.T.	T	-320	140.3	27.7	WOLT	1.00	2.55	3.20	0.20	FR	29
	A		T	-320	140.3	24.7	WOLT	2.00	5.11	6.20	0.12	FR	29
	A		T	-320	140.3	23.9	WOLX	1.00	1.125	1.44	0.29	FR	29
	A		T	-320	140.3	30.0	WOLX	2.00	2.25	2.88	0.26	FR	29
	A		T	-275	122.5	27.0	WOLX	1.00	1.125	1.44	0.36	FR	29
	A		T	-250	114.7	26.6	WOLX	1.00	1.125	1.44	0.41	FR	29
	A		T	-250	114.7	34.9	WOLX	2.00	2.25	2.88	0.37	FR	29
	A		T	-225	107.0	33.2	WOLX	1.00	1.125	1.44	0.51	PI	29
	A		T	-200	101.2	36.6	WOLX	1.00	1.125	1.44	0.61	PI	29
	A		T	-200	101.2	40.6	WOLX	2.00	2.25	2.88	0.47	FR	29
	A		T	-200	101.2	42.7	WOLX	1.00	1.125	1.44	0.41	FR	29
	A		T	-175	97.0	35.8	WOLX	1.00	1.125	1.44	0.65	PI	29
	A		T	-150	94.4	44.8	WOLX	1.00	1.125	1.44	0.77	PI	29
	A		T	-150	94.4	39.7	WOLX	2.00	2.25	2.88	0.49	FR	29
	A		T	-150	94.4	51.2	WOLX	2.00	2.25	2.88	0.63	PI	29
	A		T	-150	94.4	32.3	WOLX	1.00	1.125	1.44	0.33	PI	29
	A		T	-150	94.4	43.7	WOLX	2.00	2.25	2.88	0.32	FR	29
	A		T	-125	91.0	44.7	WOLX	1.00	1.125	1.44	0.85	PI	29
	A		T	-100	88.2	44.4	WOLX	1.00	1.125	1.44	0.82	PI	29
	A		T	-100	88.2	48.5	WOLX	1.00	1.125	1.44	1.22	FR	29
	A		T	-100	88.2	45.0	WOLX	2.00	2.25	2.88	0.58	PI	29
	A		T	-100	88.2	42.1	WOLX	2.00	2.25	2.88	0.33	FR	29
	A		T	-50	85.6	55.7	WOLX	1.00	1.125	1.44	1.05	FR	29
	A		T	-50	85.6	36.7	WOLX	1.00	1.125	1.44	0.70	FR	29
	A		T	-50	85.6	59.3	WOLX	2.00	2.25	2.88	0.80	FR	29
	A		T	-50	85.6	49.6	WOLX	2.00	2.25	2.88	0.70	PI	29
	A		T	-50	85.6	49.7	WOLX	1.00	1.125	1.44	0.57	PI	29
	A		T	-50	85.6	76.9	WOLX	3.00	7.67	9.20	0.48	FR	29
	A		T	-25	84.0	64.1	WOLX	1.00	1.125	1.44	1.30	FR	29
A	T	-25	84.0	78.2	WOLX	2.00	2.25	2.88	1.05	FR	29		
A	T	0	83.7	50.3	WOLX	2.00	2.25	2.88	0.41	FR	29		
A	T	0	83.7	60.2	WOLX	2.00	5.11	6.20	0.43	PI	29		
A	T	0	83.7	108.8	WOLX	3.00	7.67	9.20	0.71	FR	29		
A	T	25	82.0	69.0	WOLX	2.00	5.11	6.20	0.57	FR	29		

(1) Alloy composition given in Table IV-M
(2) T - Crack propagation in radial direction
(3) WOLT - Wedge-Opening-Loading "T" Type
WOLX - Wedge-Opening-Loading "X" Type
(4) σ_W/σ_{YS} = Nominal Stress/0.2% Yield Stress
(5) FR - Ultimate load; PI - Pop-in load
(6) References listed in Bibliography

TABLE II-A - TABULATION OF K_{Ic} DATA

TITANIUM ALLOYS - Ti-6Al-6V-2Sn

Form	Composition (1)	Heat Treatment		Test Orientation (2)	Test Temp. T_F	Yield Strength 0.2% (ksi)	K_{Ic} (3) ksi \sqrt{in}	Specimen Type (4)	Thickness B	Specimen Size		σ_W/σ_{YS} (5)	Comments (6)	Ref. (7)
		Solution Treatment Time	Aging Treatment Time							Width W	Length L			
0.100" Sheet	A	15 min	4 hr	L	RT	185.0	(10) 30.0	SC	0.100	1.000	8.00	0.80		9
	A	15 min	4 hr	T	RT	179.0	(8) 28.0	SC	0.100	3.000	8.00	0.15	PI	9
	A	30 min	2 hr		RT	197.0	(3) 25.0	SC	0.100	3.000	8.00	0.19		9
	A	30 min	4 hr		RT	188.0	(3) 30.0	SC	0.100	3.000	8.00	0.25		9
	A	30 min	4 hr		RT	179.0	(3) 36.0	SC	0.100	3.000	8.00	0.38		9
	A	30 min	2 hr		RT	172.0	(3) 44.0	SC	0.100	3.000	8.00	0.75		9
0.100" Sheet	B	Heat treated - Details not available			RT	184.9	29.4	SC	0.100	1.000	8.00	0.66		19
	B				RT	184.9	31.6	SC	0.100	1.000	8.00	0.61		19
	B				RT	184.9	30.4	SC	0.100	1.000	8.00	0.54		19
	B				RT	179.0	28.8	SC	0.100	1.000	8.00	0.57		19
	B				RT	179.0	31.2	SC	0.100	1.000	8.00	0.59		19
	B				RT	179.0	26.6	SC	0.100	1.000	8.00	0.46		19
1.00" Plate	C	1 hr	4 hr	L	79	179.0	(3) 32.4	NB3	0.250	0.500				20
	C	1 hr	4 hr	L	79	179.0	(3) 29.8	NB3	0.250	0.500				20
	C	1 hr	4 hr	L	79	170.0	(2) 38.1	NB3	0.250	0.500				20
	C	1 hr	4 hr	L	79	170.0	(2) 34.0	NB3	0.250	0.500				20
	C	1 hr	4 hr	L	-320	257.8	24.7	NB3	0.250	0.500				20
	C	1 hr	4 hr	L	-320	257.8	22.6	NB3	0.250	0.500				20
3.00" x 9.00" x 24.00" Forging	D	2 hr	4 hr	L	-110	171.8	52.4	CN	0.183	2.990	9.00	0.727	PI	12
	D	2 hr	4 hr	L	-110	171.8	27.8	CN	0.382	6.000	24.00	0.370	PI	12
	D	2 hr	4 hr	L	-110	171.8	27.4	CN	1.000	9.000	24.00	0.116	PI	12
	D	2 hr	4 hr	L	RT	142.1	71.6	CN	0.381	6.000	24.00	0.95	PI	12
	D	2 hr	4 hr	L	RT	142.1	54.0	CN	0.999	9.000	24.00	0.408	PI	12
	D	2 hr	4 hr	L	RT	142.1	60.4	CN	0.990	9.000	24.00	0.408	PI	12
	D	2 hr	4 hr	T	-110	169.5	32.8	CN	0.185	2.990	9.00	0.349	PI	12
	D	1 hr	4 hr	L	-110	190.0	43.8	CN	0.195	3.000	9.00	0.33	PI	12
	D	1 hr	4 hr	L	-110	190.0	37.8	CN	0.383	6.000	24.00	0.16	PI	12
	D	1 hr	4 hr	L	-110	190.0	26.6	CN	1.000	9.000	24.00	0.09	PI	12
	D	1 hr	4 hr	T	-110	190.0	38.0	CN	0.192	3.000	9.00	0.26	PI	12
	D	1 hr	4 hr	T	RT	168.5	70.5	CN	0.195	3.000	9.00	0.55	PI	12
D	1 hr	4 hr	T	RT	168.5	52.8	CN	0.181	3.000	9.00	0.42	PI	12	

(5) σ_W/σ_{YS} = Nominal Stress

(6) PI - Pop-in load

(7) References listed in Bibliography

(1) Alloy composition given in Table V-A

(2) L - longitudinal

T - transverse

ST - short transverse

(3) Average of number of tests indicated in ()

(4) SC - Surface-Cracked Plate

NB3 - Notched Bend - 3-point loading

CN - Center-Notched Plate

NR - Notched Round

TABLE II-A (Cont.)

Form	Composition	Heat Treatment			Test Orientation	Test Temp. of	Yield Strength 0.2% (ksi)	K _{IC} ksi√in	Specimen Type	Specimen Size			σ _N /σ _{YS}	Comments	Ref.
		Solution Treatment		Aging Treatment						Thick-ness B	Width W	Length L			
		Time	Temp. of	Time											
3.00" x 9.00" x 24.00" Forging	D	2 hr	1300			75	(4) 61.5	SC	0.189	3.000	12.00	0.95	PI	12	
	D	2 hr	1300		L	75	70.8	SC	0.188	3.000	12.00	0.86	PI	12	
	D	2 hr	1300		L	-110	171.8	NR	D=1.125	d=0.850		0.52	PI	12	
	D	2 hr	1300		L	-110	171.8	NR	D=1.125	d=0.845		0.39	PI	12	
	D	2 hr	1300		T	-110	169.5	NR	D=1.125	d=0.845		0.48	PI	12	
	D	2 hr	1300		T	-110	169.5	NR	D=1.125	d=0.845		0.56	PI	12	
	D	2 hr	1300		ST	-110	169.5	NR	D=1.125	d=0.845		0.50	PI	12	
	D	2 hr	1300		L	75	143.1	48.4	NR	D=1.125	d=0.850		0.74	PI	12
	D	2 hr	1300		L	75	143.1	43.6	NR	D=1.125	d=0.850		0.67	PI	12
	D	2 hr	1300		T	75	142.5	72.9	NR	D=1.125	d=0.850		1.08	PI	12
	D	2 hr	1300		T	75	142.5	57.3	NR	D=1.125	d=0.850		0.87	PI	12
	D	2 hr	1300		ST	75	138.6	56.3	NR	D=1.125	d=0.850		0.88	PI	12
	D	2 hr	1300		T	400	104.6	80.0	NR	D=2.750	d=2.050		1.04	PI	12
	D	2 hr	1300		L	75	105.7	33.8	NR	D=2.750	d=2.050		0.53	PI	12
	D	1 hr	1575	4 hr	1200	L	190.0	27.7	NR	D=			0.33	PI	12
	D	1 hr	1575	4 hr	1200	L	190.3	29.8	NR	D=1.125	d=0.853		0.35	PI	12
	D	1 hr	1575	4 hr	1200	ST	189.3	21.2	NR	D=1.122	d=0.854		0.25	PI	12
	D	1 hr	1575	4 hr	1200	L	160.3	(2) 29.4	NR	D=1.125	d=0.852		0.42	PI	12
	D	1 hr	1575	4 hr	1200	T	168.5	35.4	NR	D=1.122	d=0.854		0.47	PI	12
	D	1 hr	1575	4 hr	1200	T	129.9	78.3	NR	D=2.750	d=2.050		0.86	PI	12
D	1 hr	1575	4 hr	1200	L	126.4	68.8	NR	D=2.750	d=2.050		0.77	PI	12	
4.50"-Dia. Bar	E	1 hr	1650	4 hr	1050	79	(3) 31.9	NB3	0.250	0.501			PI	20	
	E	1 hr	1650	4 hr	1050	79	(3) 30.5	NB3	0.500	1.000			PI	20	
	E	1 hr	1650	4 hr	1050	-320	270.0	NB3	0.500	0.500			PI	20	
	E	1 hr	1650	4 hr	1050	-320	270.0	NB3	0.500	1.000			PI	20	

TABLE II-B - TABULATION OF K_{Ic} DATA

TITANIUM ALLOYS - Ti-6Al-4V

Form	Composition (1)	Heat Treatment			Test Orientation (2)	Yield Strength 0.2% (ksi)	K_{Ic} (3) ksi $\sqrt{\text{in}}$	Specimen Type (4)	Specimen Size			σ_N/σ_{YS} (5)	Comments (6)	Ref. (7)
		Solution Treatment		Aging Treatment					Thickness B	Width W	Length L			
		Time	Temp. C_F	Temp. C_F										
0.500" Plate	A	1 hr	1650		L	212.3	(3) 56.6	NR	D=0.500	d=0.354	4.00	0.86		4
	A	1 hr	1650		L	212.3	(3) 62.3	NR	D=0.500	d=0.354	4.00	0.90		4
	A	1 hr	1650		L	212.3	(2) 42.7	NR	D=0.500	d=0.354	4.00	0.65		4
	A	1 hr	1650		L	212.3	(2) 51.2	NR	D=0.500	d=0.354	4.00	0.77		4
	A	1 hr	1650		L	212.3	69.7	SC	0.257	6.000	27.00	0.60		4
	A	1 hr	1650		L	212.3	58.7	SC	0.255	6.000	27.00	0.44		4
	A	1 hr	1650		L	212.3	56.0	SC	0.266	6.000	27.00	0.35		4
	A	1 hr	1650		L	212.3	69.1	SC	0.252	6.000	27.00	0.71		4
	A	400					58.0							4
	A	200					76.0							4
3.00" x 9.00" x 24.00" Forging	B	1 hr	1100		L	176.4	61.4	CN	0.383	6.000	24.00	0.547		12
	B	1 hr	1100		L	176.4	47.3	CN	1.000	9.000	24.00	0.277		12
	B	1 hr	1100		L	176.4	34.8	NR	D=1.122	d=0.849		0.44		12
	B	1 hr	1100		L	176.4	37.7	NR	D=1.122	d=0.849		0.48		12
	B	1 hr	1100		T	176.4	(2) 35.5	NR	D=1.125	d=0.850		0.45		12
	B	1 hr	1100		ST	176.4	34.4	NR	D=1.125	d=0.848		0.43		12
	B	1 hr	1100		ST	176.4	40.3	NR	D=1.125	d=0.848		0.52		12
	B	1 hr	1100		L	176.4	37.8	NR	D=1.125	d=0.850		0.58		12
	B	1 hr	1100		T	176.4	(2) 36.0	NR	D=1.125	d=0.850		0.54		12
	B	1 hr	1100		ST	176.4	(2) 38.8	NR	D=1.125	d=0.850		0.57		12
3.00"-Thick Forged Plate	C	1 hr	1750	1000	L	140.4	80.6	WOLX	2.000		2.25	0.574		FR
	C	1 hr	1750	1000	L	140.4	84.6	WOLX	2.000		2.25	0.603		FR
	C	1 hr	1750	1000	L	140.4	77.5	WOLX	2.000		2.25	0.552		FR
	C	1 hr	1750	1000	T	140.4	140.4	WOLX	2.000		2.25	0.536		FR
	C	1 hr	1750	1000	T	140.4	77.9	WOLX	2.000		2.25	0.555		FR
	C	1 hr	1750	1000	T	140.4	79.7	WOLX	2.000		2.25	0.568		FR
	C	1 hr	1750	1000	T	140.4	58.4	WOLX	1.000		2.25	0.384		FR
	C	1 hr	1750	1000	T	140.4	60.9	WOLX	1.000		2.55	0.410		FR
	C	1 hr	1750	1000	T	140.4	76.6	WOLX	2.000		5.11	0.389		FR
	C	1 hr	1750	1000	T	140.4	76.3	WOLX	2.000		5.11	0.377		FR
	C	1 hr	1750	1000	T	140.4	84.9	WOLX	2.000		5.11	0.416		FR
	C	1 hr	1750	1000	T	140.4	63.2	WOLX	1.000		2.55	0.450		PI
	C	1 hr	1750	1000	T	140.4	132.7	WOLX	2.000		5.11	0.375		FR
	C	1 hr	1750	1000	T	140.4	132.7	WOLX	2.000		5.11	0.364		FR
	C	1 hr	1750	1000	T	140.4	72.9	WOLX	2.000		2.55	0.482		FR
	C	1 hr	1750	1000	T	140.4	63.4	WOLX	1.000		5.11	0.454		FR
	C	1 hr	1750	1000	T	140.4	82.0	WOLX	2.000		5.11	0.401		FR
	C	1 hr	1750	1000	T	140.4	74.0	WOLX	2.000		5.11	0.401		FR
	C	1 hr	1750	1000	T	140.4	68.3	WOLX	1.000		2.55	0.433		FR
	C	1 hr	1750	1000	T	140.4	64.4	WOLX	2.000		5.11	0.307		FR
C	1 hr	1750	1000	T	140.4	65.5	WOLX	2.000		5.11	0.309		FR	
C	1 hr	1750	1000	T	140.4	147.5	WOLX	2.000		5.11	0.417		FR	
C	1 hr	1750	1000	T	140.4	147.5	WOLX	2.000		5.11	0.351		FR	
C	1 hr	1750	1000	T	140.4	146.8	WOLX	2.000		5.11	0.312		FR	
C	1 hr	1750	1000	T	140.4	146.8	WOLX	2.000		5.11	0.312		FR	
C	1 hr	1750	1000	T	140.4	152.7	WOLX	2.000		2.55	0.401		FR	
C	1 hr	1750	1000	T	140.4	152.7	WOLX	2.000		2.55	0.357		FR	
C	1 hr	1750	1000	T	140.4	152.7	WOLX	2.000		5.11	0.304		FR	
C	1 hr	1750	1000	T	140.4	159.07	WOLX	2.000		2.55	0.371		PI	
C	1 hr	1750	1000	T	140.4	159.07	WOLX	2.000		5.11	0.314		PI	
C	1 hr	1750	1000	T	140.4	159.07	WOLX	2.000		5.11	0.289		FR	

(1) Alloy composition listed in Table V-B

(2) L - longitudinal; T - transverse; ST - short transverse

(3) Average of number of tests indicated in ()

(4) NR - Notched Round; SC - Surface-Cracked Plate;

CN - Center-Notched Plate; WOLX - Wedge-Opening-Loading "X" Type

WOLX - Wedge-Opening-Loading "W" Type

(5) σ_N/σ_{YS} = Nominal Stress

(6) FR - Ultimate load

PI - Pop-In load

(7) References listed in Bibliography

TABLE II-C - TABULATION OF K_{Ic} DATA
TITANIUM ALLOYS - Beta Titanium (B 120VCA-Ti)

Form	Composition (1)	Heat Treatment			Test Orientation (2)	Test Temp. °F	Yield Strength 0.2% (ksi)	K_{Ic} (3)	Specimen Type (4)	Specimen Size			σ_w/σ_{YS} (5)	Comments (6)	Ref. (7)	
		Solution Treatment		Aging Treatment						Thickness B.	Width W	Length L				
		Time	Temp. °F	Time												Temp. °F
0.042" Sheet	A	15 min	1425	72 hr	900	L	166	(3) 24.4	CC	0.042	1.750	8.00	0.23	PI	10	
	A	15 min	1425	72 hr	900	L	182	(3) 23.4	CC	0.042	1.750	8.00	0.22	PI	10	
	A	15 min	1425	72 hr	900	L	169.5	(3) 28.4	CC	0.042	1.750	8.00	0.28	PI	10	
	A	15 min	1425	72 hr	900	L	165.5	(3) 30.0	CC	0.042	1.750	8.00	0.36	PI	10	
	A	15 min	1425	72 hr	900	T	137.8	(3) 30.8	CC	0.042	1.750	8.00	0.39	PI	10	
	A	15 min	1425	72 hr	900	L	153.6	(3) 42.8	CC	0.042	1.750	8.00		Dev	10	
	A	15 min	1425	72 hr	900	L	146.0	(3) 40.2	CC	0.042	1.750	8.00	0.56	Dev	10	
	A	15 min	1425	72 hr	900	L		(3) 22.7	CC	0.042	1.750	8.00		PI	10	
	A	15 min	1425	72 hr	900	L	200.0	(3) 25.6	CC	0.042	1.750	8.00	0.20	PI	10	
	A	15 min	1425	72 hr	900	L	182.8	(3) 25.6	CC	0.042	1.750	8.00	0.24	PI	10	
	A	15 min	1425	72 hr	900	L	174.4	(3) 30.0	CC	0.042	1.750	8.00	0.30	PI	10	
	A	15 min	1425	72 hr	900	T	182.4	(2) 25.8	CC	0.042	1.750	8.00	0.23	PI	10	
	1.00" -Dia. Bar	A	30 min	1425	72 hr	900	L	200.0	(2) 27.7	NR	D=0.505	d=0.375	3.00	0.44		10
		A	30 min	1425	72 hr	900	L	182.0	(3) 33.3	NR	D=0.505	d=0.375	3.00	0.56		10
		A	30 min	1425	72 hr	900	L	181.0	(3) 31.9	NR	D=0.505	d=0.375	3.00	0.55		10
A		30 min	1425	72 hr	900	L	163.0	(3) 37.9	NR	D=0.505	d=0.375	3.00	0.72		10	
A		30 min	1425	72 hr	900	L	159.0	(3) 39.1	NR	D=0.505	d=0.375	3.00	0.71		10	

(1) Alloy composition listed in Table V-C

(2) L - longitudinal
T - transverse

(3) Average of number of tests indicated in ()

(4) CC - Center-Cracked Plate
NR - Notched Round

(5) $\sigma_w/\sigma_{YS} = \frac{\text{Nominal Stress}}{0.2\% \text{ Yield Stress}}$

(6) PI - Pop-in load

Dev - Load at deviation from linearity

(7) References listed in Bibliography

TABLE III-A - TABULATION OF K_{Ic} DATA
ALUMINUM ALLOYS - 7075-T6 and -T651

Form	Composition (1)	Heat Treatment			Test Orientation (2)	Yield Strength 0.2% (ksi)	K_{Ic} (3) ksi \sqrt{in}	Specimen Type (4)	Specimen Size			σ_W/σ_{YS} (5)	Comments (6)	Ref. (7)	
		Solution Treatment		Aging Treatment					Thickness B	Width W	Length L				
		Time	Temp. Of	Time											Temp. Of
0.200" Sheet Ext. 7075-T6	A	1 hr	870	24 hr	250	79.0	27.4	SEN	2.00	8.00	0.072	PI	27		
	A	1 hr	870	24 hr	250	79.0	(2) 27.8	CN	3.00	12.00	0.60	PI	27		
	B	1 hr	870	24 hr	250	71.5	(2) 22.2	CN	3.00	12.00	0.58	PI	27		
0.250" Sheet 7075-T6	C	10 min-4 hr	870	24-28 hr	250	75.0	(7) 29.0	SEN	0.250			PI	21		
	C	10 min-4 hr	870	24-28 hr	250	75.0	(8) 28.1	DEN	0.250			PI	21		
	C	10 min-4 hr	870	24-28 hr	250	75.0	(4) 30.7	CN	0.250			PI	21		
0.500" Plate 7075-T6	C	10 min-4 hr	870	24-28 hr	250	78.6	(5) 27.0	NB4	0.250	1.00		PI	22		
	C	10 min-4 hr	870	24-28 hr	250	74.6	(6) 26.0	NB4	0.500	1.00		PI	22		
	C	10 min-4 hr	870	24-28 hr	250	76.0	(8) 28.0	SEN	3.00			PI	22		
	C	10 min-4 hr	870	24-28 hr	250	79.3	(6) 27.2	SEN	0.500			PI	22		
	C	10 min-4 hr	870	24-28 hr	250	79.3	(8) 26.7	DEN	0.500			PI	22		
	C	10 min-4 hr	870	24-28 hr	250	79.3	(3) 29.1	CN	0.500			PI	22		
0.250" Sheet 7075-T651	C	1 hr	870	24-28 hr	250	75.0	(5) 24.1	CN	0.250			PI	23		
	C	1 hr	870	24-28 hr	250	75.0	(2) 25.1	SEN	0.250			PI	23		
	C	As-Received Material				75.0	(5) 24.1	CN	0.250	1.00		PI	24		
0.500" Sheet 7075-T651	C					74.5	(10) 26.0	SEN	0.500			PI	23		
	C					78.5	(10) 30.0	CN	0.500			PI	23		
	C						(10) 21.0	NR				PI	23		
1.00" Plate 7075-T651	C	1 hr	870	24-28 hr	250	79.5	(8) 22.8	WOLX	1.000			PI	25		
	C	1 hr	870	24-28 hr	250	82.8	(11) 25.9	WOLX	1.000			PI	25		
	C	1 hr	870	24-28 hr	250		(3) 20.0	WOLX	1.000			PI	25		
	C	1 hr	870	24-28 hr	250		32.8	CN	0.125			PI	23		
	C	1 hr	870	24-28 hr	250		30.0	CN	0.125			PI	23		
1.75"-Thick Forging 7075-T6	B	1 hr	870	24 hr	250	75.0	22.5	CN	0.180	3.00	0.665	PI	27		
	B	1 hr	870	24 hr	250	75.0	30.0	SEN	0.251	2.00		PI	27		
	B	1 hr	870	24 hr	250	71.5	24.0	SEN	0.251	2.00		PI	27		

(1) Alloy composition given in Table VI-A

(2) L - longitudinal

T - transverse

ST - short transverse

(3) Average of number of tests indicated in ()

(4) SEN - Single-Edge-Notched Plate

CN - Center-Notched Plate

DEN - Double-Edge-Notched Plate

NB4 - Notched Bend - 4-point loading

NR - Notched Round

WOLX -

(5) $\sigma_W/\sigma_{YS} = \frac{\text{Nominal Stress}}{0.2\% \text{ Yield Stress}}$

(6) PI - Pop-in load

(7) References listed in Bibliography

TABLE III-B - TABULATION OF K_{Ic} DATA ALUMINUM ALLOYS - 7079-T6

Form	Composition (1)	Solution Treatment		Aging Treatment		Test Orientation (2)	Test Temp. °F	Yield Strength 0.2% (ksi)	K_{Ic} (3) ksi $\sqrt{\text{in}}$	Specimen Type (4)	Specimen Size			σ_N/σ_{YS} (5)	Comments (6)	Ref. (7)
		Temp. °F		Temp. °F							Thickness B	Width W	Length L			
		Time	Temp. °F	Time	Temp. °F											
0.200" Thick Extrusion	A	1 hr	830	48 hr	240	T	RT	72.7	(2) 26.5	CN	0.176	3.00	12.00	0.74	PI	27
	A	1 hr	830	48 hr	240	L	RT	71.7	(2) 27.5	CN	0.179	3.00	12.00	0.835	PI	27
	A	1 hr	830	48 hr	240	L	RT	71.7	(2) 27.5	SEN	0.182	2.00	8.00		PI	27
	A	1 hr	830	48 hr	240	T	RT	72.7	(2) 29.0	SEN	0.182	2.00	8.00		PI	27
	B	1 hr	830	48 hr	240	T	RT	69.3	(2) 29.9	CN	0.176	3.00	12.00	0.86	PI	27
	B	1 hr	830	48 hr	240	L	RT	68.8	(2) 26.2	CN	0.184	3.00	12.00	0.77	PI	27
1.250" Thick Forging	B	1 hr	830	48 hr	240	L	RT	69.3	(3) 27.0	SEN	0.250	2.00	8.00		PI	27
	B	1 hr	830	48 hr	240	T	RT	68.8	(3) 30.5	SEN	0.250	2.00	8.00		PI	27
	C	4 hr	830	5 days RT+48 hr	240	T	75	63.5	(3) 30.5	WOLX	2.000	2.25	2.25	0.435	PI	27
	C	4 hr	830	5 days RT+48 hr	240	T	75	63.5	28.8	WOLX	2.000	2.25	2.25	0.474	PI	27
	C	4 hr	830	5 days RT+48 hr	240	T	75	63.5	29.5	WOLX	2.000	2.25	2.25	0.465	FR	27
	C	4 hr	830	5 days RT+48 hr	240	L	75	63.5	30.5	WOLX	2.000	2.25	2.25	0.480	PI	27
3" Thick Forged Plate	C	4 hr	830	5 days RT+48 hr	240	L	75	63.5	32.5	WOLX	2.000	2.25	2.25	0.512	PI	27
	C	4 hr	830	5 days RT+48 hr	240	L	75	63.5	28.2	WOLX	2.000	2.25	2.25	0.444	PI	27
	C	4 hr	830	5 days RT+48 hr	240	L	75	63.5	33.9	WOLX	2.000	2.25	2.25	0.534	PI	27
	C	4 hr	830	5 days RT+48 hr	240	L	75	63.5	33.3	WOLX	2.000	2.25	2.25	0.525	PI	27
	C	4 hr	830	5 days RT+48 hr	240	L	75	63.5	36.7	WOLX	2.000	2.25	2.25	0.578	PI	27
	C	4 hr	830	5 days RT+48 hr	240	L	75	63.5	29.5	WOLX	1.000	2.55	2.55	0.465	PI	27
	C	4 hr	830	5 days RT+48 hr	240	L	75	63.5	34.5	WOLX	1.000	2.55	2.55	0.544	PI	27
	C	4 hr	830	5 days RT+48 hr	240	L	75	63.5	38.5	WOLX	1.000	2.55	2.55	0.606	PI	27
	C	4 hr	830	5 days RT+48 hr	240	L	75	63.5	33.5	WOLX	1.000	2.55	2.55	0.528	FR	27
	C	4 hr	830	5 days RT+48 hr	240	L	75	63.5	30.4	WOLX	0.900	2.55	2.55	0.479	PI	27
	C	4 hr	830	5 days RT+48 hr	240	L	75	63.5	34.3	WOLX	0.900	2.55	2.55	0.540	FR	27
	C	4 hr	830	5 days RT+48 hr	240	L	75	63.5	30.7	WOLX	0.900	2.55	2.55	0.484	FR	27
	C	4 hr	830	5 days RT+48 hr	240	L	75	63.5	32.8	WOLX	0.900	2.55	2.55	0.517	PI	27
	C	4 hr	830	5 days RT+48 hr	240	L	75	63.0	35.6	WOLX	1.000	2.55	2.55	0.565	PI	27
	C	4 hr	830	5 days RT+48 hr	240	L	150	63.0	34.9	WOLX	2.000	2.55	2.25	0.534	PI	27
	C	4 hr	830	5 days RT+48 hr	240	L	150	63.0	36.0	WOLX	2.000	2.55	2.25	0.571	PI	27
	C	4 hr	830	5 days RT+48 hr	240	L	100	62.05	32.4	WOLX	2.000	2.25	2.25	0.523	PI	27
	C	4 hr	830	5 days RT+48 hr	240	L	100	62.05	37.1	WOLX	2.000	2.25	2.25	0.598	PI	27
	C	4 hr	830	5 days RT+48 hr	240	L	100	62.05	33.4	WOLX	1.000	2.55	2.55	0.539	PI	27
	C	4 hr	830	5 days RT+48 hr	240	L	32	65.65	32.2	WOLX	2.000	2.25	2.25	0.491	PI	27
	C	4 hr	830	5 days RT+48 hr	240	L	32	65.65	33.9	WOLX	2.000	2.25	2.25	0.517	PI	27
	C	4 hr	830	5 days RT+48 hr	240	L	0	69.2	33.7	WOLX	2.000	2.25	2.25	0.514	PI	27
	C	4 hr	830	5 days RT+48 hr	240	L	0	69.2	34.7	WOLX	2.000	2.25	2.25	0.502	PI	27
	C	4 hr	830	5 days RT+48 hr	240	L	0	69.2	30.7	WOLX	2.000	2.25	2.25	0.444	PI	27
C	4 hr	830	5 days RT+48 hr	240	L	0	69.2	35.0	WOLX	1.000	2.55	2.55	0.506	PI	27	
C	4 hr	830	5 days RT+48 hr	240	L	0	69.2	28.8	WOLX	1.000	2.55	2.55	0.421	PI	27	
C	4 hr	830	5 days RT+48 hr	240	L	0	69.2	34.5	WOLX	2.000	2.25	2.25	0.504	PI	27	
C	4 hr	830	5 days RT+48 hr	240	L	0	69.2	30.8	WOLX	2.000	2.25	2.25	0.450	PI	27	
C	4 hr	830	5 days RT+48 hr	240	L	0	69.2	28.4	WOLX	2.000	2.25	2.25	0.414	PI	27	
C	4 hr	830	5 days RT+48 hr	240	L	0	69.2	68.6	WOLX	2.000	2.25	2.25	0.576	PI	27	
C	4 hr	830	5 days RT+48 hr	240	L	0	69.2	68.6	WOLX	1.000	2.55	2.55	0.471	PI	27	

Data Generated During This Investigation

TABLE III-C - TABULATION OF K_{Ic} DATA ALUMINUM ALLOYS - 7001-T75

Form	Composition (1)	Solution Treatment	Aging Treatment	Test Orientation (2)	Test Temp. °F	Yield Strength 0.2% (ksi)	K_{Ic} (3) ksi $\sqrt{\text{in}}$	Specimen Type (4)	σ_N/σ_{YS} (5)	Comments (6)	Ref. (7)			
												Thickness B	Width W	Length L
0.2" Thick Extrusion	A	Not Disclosed	Not Disclosed	T	RT	78.1	(2) 17.5	CN	0.170	3.00	12.00	0.32	PI	27
	A	Not Disclosed	Not Disclosed	L	RT	77.0	(2) 18.0	CN	0.180	3.00	12.00	0.45	PI	27
	A	Not Disclosed	Not Disclosed	T	RT	77.0	(2) 20.0	SEN	0.180	2.00	8.00		PI	27
	A	Not Disclosed	Not Disclosed	L	RT	78.1	(3) 20.0	SEN	0.180	2.00	8.00		PI	27
	A	Not Disclosed	Not Disclosed	L	RT	70.4	(3) 20.0	CN	0.180	3.00	12.00	0.52	PI	27
	A	Not Disclosed	Not Disclosed	T	RT	70.6	(2) 16.0	CN	0.180	3.00	12.00	0.37	PI	27
A	Not Disclosed	Not Disclosed	L	RT	70.6	(2) 21.0	SEN	2.500	2.00	8.00		PI	27	

(5) $\sigma_N/\sigma_{YS} = 0.2\%$ Yield Stress

(6) PI - Pop-in load; FR - Ultimate load

(7) References listed in Bibliography

- (1) Alloy compositions given in Tables VI-B and VI-C
- (2) L - longitudinal; T - transverse
- (3) Average of number of tests indicated in ()
- (4) CN - Center-Notched Plate; SEN - Single-Edge-Notched Plate; WOLX - Wedge-Opening-Loading "X" Type; WOLT - Wedge-Opening-Loading "T" Type

TABLE IV - CHEMICAL COMPOSITIONS (Wt. %) - FERROUS ALLOYS

Table IV-A lists chemical compositions referred to in Table I-A;
 Table IV-B lists compositions referred to in Table I-B; etc.

IV-A - 18% Ni Maraging Steel

Composition Designation	C	Mn	P	S	Si	Ni	Al	Mo	Co	Ti	B	Zr	Ca	Cr
A	0.019	0.011	0.004	0.010	0.061	18.68	0.067	5.07	8.97	0.72				
B	0.030	0.04	0.004	0.007	0.040	18.91	0.110	5.00	8.79	0.61	0.0043	0.015	0.05	
C	0.013	Trace	0.004	0.004	0.045	18.63	0.070	4.66	9.00	0.660				
D	0.027		0.005	0.010	0.084	17.80	0.065	4.85	8.96	0.630				
E	0.270	0.050	0.006	0.009	0.010	18.8	0.050	4.95	8.98	0.630			0.10	
F	0.020	0.050	0.008	0.007	0.100	18.9	0.100	5.42	7.22	0.460				
G	0.020	0.070	0.004	0.006	0.090	18.39	0.070	4.82	7.83	0.350				
H	0.017	0.060	0.005	0.004	0.180	17.84	0.120	4.80	8.25	0.550				
I	0.020	0.040	0.004	0.009	0.080	17.83	0.110	4.70	7.41	0.460				
J	0.017	0.060	0.005	0.004	0.180	17.84	0.120	4.80	8.25	0.550				
K	0.026	0.110	0.006	0.006	0.070	18.46	0.080	4.80	8.82	0.620				
L	0.020	0.040	0.005	0.007	0.04	19.00	0.390	5.12	9.30	0.650				
M	0.030	0.060	0.005	0.010	0.100	18.37	0.130	4.70		0.420				
N						18.00			8.50					
O						18.00		5.00	7.00					
P	0.025	0.032	0.006	0.010	0.050	17.90	0.037	4.70	8.37	0.390	0.002			
Q	0.010	0.030	0.004	0.005	0.020	18.52	0.100	4.84	7.84	0.390	0.0035			

IV-B - 4340 Steel

Composition Designation	C	Mn	P	S	Si	Ni	Cr	Mo	H ₂	O ₂	N ₂
A	.38-.43	.60-.80	.040 max	.040 max	.20-.35	1.65-2.00	.70-.90	.20-.30			
B	0.43	0.065	0.010	0.005	0.30	1.85	0.82	0.26			
C	0.39	0.77	0.012	0.015	0.30	1.75	0.81	0.22			
D	0.42	0.67	0.007	0.010	0.25	1.83	0.90	0.20	2.7 ppm	15 ppm	17 ppm
E	0.43	0.65	0.010	0.006	0.30	1.87	0.82	0.20			

TABLE IV (Cont.)

IV-C - D6ac Steel

<u>Composition Designation</u>	<u>C</u>	<u>Mn</u>	<u>P</u>	<u>S</u>	<u>Si</u>	<u>Ni</u>	<u>Cr</u>	<u>Mo</u>	<u>V</u>	<u>Al</u>
A	0.47	0.85	0.007	0.005	0.20	0.57	1.07	1.01	0.08	0.06
B	0.45	0.69	0.008	0.006	0.26	0.55	1.08	1.01	0.08	0.07
C	0.47	0.84	0.006	0.006	0.24	0.56	1.10	1.00	0.08	
D	0.48	0.75	0.006	0.005	0.27	0.59	1.08	1.00	0.09	
E	0.45	0.75	0.006	0.005	0.27	0.59	1.08	1.00	0.09	

IV-D - H-11 Steel

<u>Composition Designation</u>	<u>C</u>	<u>Mn</u>	<u>P</u>	<u>S</u>	<u>Si</u>	<u>Cr</u>	<u>Mo</u>	<u>V</u>
A	0.40	0.25			0.10	5.00	1.30	0.50
B	0.40	0.35	0.021	0.008	0.87	4.90	1.27	0.51

IV-E - HP-9-4 Steel

<u>Composition Designation</u>	<u>C</u>	<u>Mn</u>	<u>P</u>	<u>S</u>	<u>Si</u>	<u>Ni</u>	<u>Cr</u>	<u>Mo</u>	<u>V</u>	<u>Co</u>
A	0.45	0.12	0.005	0.009	0.01	8.76	0.30	0.30	0.06	3.76
B	0.43	0.20			0.10	8.50	0.25	0.25	0.10	4.00
C	0.26	0.27	0.005	0.009	0.04	8.42	0.49	0.43	0.11	3.90
D	0.43	0.13	0.005	0.009	0.01	8.09	0.13	0.11	0.09	3.81
E	0.26	0.33	0.008	0.008	0.01	8.41	0.40	0.48	0.07	3.9

IV-F - 12Ni-5Cr-3Mo Steel

<u>Composition Designation</u>	<u>C</u>	<u>Mn</u>	<u>P</u>	<u>S</u>	<u>Si</u>	<u>Ni</u>	<u>Cr</u>	<u>Mo</u>	<u>Ti</u>	<u>Al</u>
A	0.024	0.044	0.007	0.013	0.042	11.72	5.38	3.18	0.30	0.47

TABLE IV (Cont.)

<u>IV-G - AM 355</u>										
<u>Composition Designation</u>	<u>C</u>	<u>Mn</u>	<u>P</u>	<u>S</u>	<u>Si</u>	<u>Ni</u>	<u>Cr</u>	<u>Mo</u>		
A	0.11	1.08	0.012	0.006	0.32	4.06	15.08	2.82		
B	0.12	1.21	0.015	0.009	0.44	4.49	15.02	2.76		

<u>IV-H - AISI 4335+V Steel (AMS 6434)</u>										
<u>Composition Designation</u>	<u>C</u>	<u>Mn</u>	<u>P</u>	<u>S</u>	<u>Si</u>	<u>Ni</u>	<u>Cr</u>	<u>Mo</u>	<u>V</u>	
A	0.37	0.79	0.005	0.005	0.400	1.770	0.820	0.33	0.21	

<u>IV-I - 20% Ni Maraging Steel</u>										
<u>Composition Designation</u>	<u>C</u>	<u>Mn</u>	<u>P</u>	<u>S</u>	<u>Si</u>	<u>Ni</u>	<u>Ti</u>	<u>Al</u>	<u>B</u>	<u>Zr</u>
A	0.008	0.008	0.004	0.005	0.019	19.97	1.85	0.47	0.001	0.018

<u>IV-J - 300M Steel</u>										
<u>Composition Designation</u>	<u>C</u>	<u>Mn</u>	<u>P</u>	<u>S</u>	<u>Si</u>	<u>Ni</u>	<u>Cr</u>	<u>Mo</u>	<u>V</u>	<u>Al</u>
A	0.42	0.87	0.007	0.008	1.61	1.68	0.87	0.43	0.056	0.054

<u>IV-K - PH-13Cr-8Mo Steel</u>										
<u>Composition Designation</u>	<u>C</u>	<u>Mn</u>	<u>P</u>	<u>S</u>	<u>Si</u>	<u>Ni</u>	<u>Cr</u>	<u>Mo</u>	<u>Al</u>	
A	0.043	0.10	0.003	0.004	0.32	8.40	12.72	2.14	0.96	

TABLE IV (Cont.)

IV-L - ASTM A302B

<u>Composition Designation</u>	<u>C</u>	<u>Mn</u>	<u>P</u>	<u>S</u>	<u>Si</u>	<u>Ni</u>	<u>Mo</u>
A	0.21	1.34	0.015	0.010	0.27	0.04	0.50

IV-M - Ni-Mo-V Forging Steel

<u>Composition Designation</u>	<u>C</u>	<u>Mn</u>	<u>P</u>	<u>S</u>	<u>Si</u>	<u>Ni</u>	<u>Cr</u>	<u>Mo</u>	<u>V</u>
A	0.23	0.50	0.009	0.010	0.21	3.4	0.08	0.30	0.07

TABLE V - CHEMICAL COMPOSITIONS (Wt. %) - TITANIUM ALLOYS

Table V-A lists chemical compositions referred to in Table II-A;

Table V-B lists those in Table II-B; and Table V-C those in Table II-C.

V-A - Ti-6Al-6V-2Sn

<u>Composition Designation</u>	<u>Al</u>	<u>V</u>	<u>Sn</u>	<u>Fe</u>	<u>Cu</u>	<u>C</u>	<u>N₂</u>	<u>H₂</u>	<u>O₂</u>
A	5.0-6.0	5.0-6.0	1.5-2.5	0.35-1.00	0.35-1.00	0.05 max	0.04 max	0.015 max	0.20 max
B	5.50	5.40	2.00	0.73	0.67	0.026	0.025	0.008	
C	5.33	5.34	1.96	0.59	0.65	0.015	0.018	0.006	0.081
D	5.70	5.30	2.20	0.69	0.79	0.08	43 ppm	59 ppm	1480 ppm
E	5.64	5.32	2.26	0.45	0.56	0.021	0.007	0.016	0.172

V-B - Ti-6Al-4V

<u>Composition Designation</u>	<u>V</u>	<u>Al</u>	<u>Ti</u>	<u>C</u>	<u>Fe</u>	<u>H₂</u>	<u>O₂</u>	<u>N₂</u>
A	4.10	6.10	Bal.	0.02	0.17			
B	4.10	6.50	Bal.	0.08	0.18	69 ppm	1210 ppm	33 ppm
C	4.10	6.30	Bal.	0.023	0.13	0.004	0.17	

V-C - Beta Titanium

<u>Composition Designation</u>	<u>Cr</u>	<u>V</u>	<u>Al</u>	<u>Ti</u>
A	11.0	13.00	3.00	Bal.

TABLE VI - CHEMICAL COMPOSITIONS (Wt. %) -- ALUMINUM ALLOYS

Table VI-A lists chemical compositions referred to in Table III-A;
 Table VI-B lists those in Table III-B; and Table VI-C those in Table III-C.

VI-A - 7075-T6 and T651 Aluminum

<u>Composition Designation</u>	<u>Cr</u>	<u>Cu</u>	<u>Fe</u>	<u>Mg</u>	<u>Mn</u>	<u>Si</u>	<u>Zn</u>	<u>Ti</u>	<u>Al</u>
A	0.19	1.50	0.18	2.59	0.03	0.11	5.78	0.02	Bal.
B	0.19	1.54	0.19	2.67	0.03	0.11	5.92	0.03	Bal.
C	0.30	1.60	0.20	2.50	0.12	0.18	5.60	0.01	Bal.

(Nominal Composition)

VI-B - 7079-T6 Aluminum

<u>Composition Designation</u>	<u>Cr</u>	<u>Cu</u>	<u>Fe</u>	<u>Mg</u>	<u>Mn</u>	<u>Si</u>	<u>Zn</u>	<u>Ti</u>	<u>Al</u>
A	0.16	0.66	0.20	3.29	0.18	0.10	4.73	0.02	Bal.
B	0.14	0.70	0.17	3.45	0.20	0.09	4.66	0.02	Bal.
C	0.10-0.25	0.40-0.80	0.4 max	2.9-3.7	0.10-0.30	0.30 max	3.8-4.8	0.10 max	Bal.

(Nominal Composition)

VI-C -

<u>Composition Designation</u>	<u>Cr</u>	<u>Cu</u>	<u>Fe</u>	<u>Mg</u>	<u>Mn</u>	<u>Si</u>	<u>Zn</u>	<u>Ti</u>	<u>Al</u>
A	0.21	2.26	0.16	3.03	0.04	0.12	7.61	0.02	Bal.

APPENDIX II

ULTRASONIC DETECTION OF FRACTURE INITIATION AND EXTENSION IN THE WOL TYPE FRACTURE TOUGHNESS SPECIMEN*

Introduction

The linear elastic fracture mechanics approach to the design against brittle failure of structural metals provides a technique whereby criteria are established for fracture instability. The essence of the approach is to relate the applied stress and material properties to the size of a defect which can result in failure at a given temperature.⁽¹⁾ The established criteria are related in terms of the fracture toughness parameter K (stress intensity) which describes the stress conditions at the tip of an existing crack.

Presently, several laboratory test specimens are available for the determination of fracture toughness characteristics.⁽²⁾ Although the specimen geometries vary considerably, compliance with several general criteria applicable to all specimen types is required to ensure valid test results. Among these criteria are the controlled extension of cracks from machined notches by low-stress fatigue cycling and instrumentation capable of distinguishing between slow crack growth and general yielding at the crack tip prior to rapid failure. Tests conducted under cyclic loading in order to establish crack growth characteristics require instrumentation capable of providing accurate measurement of the crack length during loading.⁽³⁾ As a result, the determination of fracture toughness parameters as well as slow crack growth characteristics requires a knowledge of the crack length under all conditions of loading.

*This investigation was not conducted as part of this contract however, due to it's relevance it has been included as Appendix II.

Available Instrumentation

Several crack initiation and extension measurement methods have been developed which yield satisfactory results in specific situations; however, each has associated limitations, more or less severe, depending upon the intended applications. Among these techniques are optical microscopy, displacement gauges, and electrical potential measurements.⁽²⁾

Although microscopy is an obvious technique offering a potential of extremely high sensitivity limited only by the maximum magnification available, it is severely limited by the fact that only accessible surface cracks can be examined, and the extent of the surface crack does not necessarily indicate the true extent of internal crack growth. In addition, the test procedure has to be interrupted in order to make measurements.

The primary objection to the use of displacement gauges for measuring crack growth is the inability of such instrumentation to differentiate between general yielding at the crack tip and actual crack extension. Bending deflection in the specimen will also appear as a variation in displacement similar to that caused by crack growth.

The electrical potential method of crack detection based upon the measurement of changes in electrical impedance induced by crack growth has been shown to yield a sensitivity capable of detecting 0.005-inch changes in crack depth.⁽⁴⁾ The limitations associated with this technique involve the insulation of the specimen from the grips, the difficulty of determining probe location, and the thermoelectric effects induced when testing at various temperatures.

Evaluation of the available crack growth measurement techniques has indicated that none of these procedures exhibit advantages over a more conventional nondestructive test - ultrasonic inspection. The ultrasonic method is not limited to the detection of surface cracks; it does not require frequent interruption of the test; it can be used successfully over a wide range of temperature (-200° to 450°F) without recalibrating; and the electrical or magnetic properties of the material do not affect the test. In addition, the test can be made sensitive to

changes in crack length as small as 0.0005 inch with commercially available equipment,⁽⁵⁾ and the results can readily be fed into an X-Y recorder for continuous monitoring.

Ultrasonic Detection of Crack Growth

In view of the potential advantages of an ultrasonic crack growth detection system, an investigation was undertaken to develop such a system for use with the Wedge-Opening-Loading (WOL) type fracture toughness specimen shown in Figure 1. The technique developed involves the use of a 3/8-inch-diameter, 10 MHz (megahertz, million cycles per second), ceramic ZR contact transducer operated by a high-resolution ultrasonic test instrument, the Sperry Type UM 715 Reflectoscope, equipped with a 10 MHz HFN pulser unit. (Both the HFN and 10 N pulser units produce satisfactory results.) The transducer is placed on the specimen at a predetermined location such that the high-frequency sound waves penetrate the specimen as shown in Figure 2. Much like sonar, the acoustic energy generated by the transducer travels through the specimen until it encounters a discontinuity - in this case, a machined notch, or, in the case of precracked specimens, a fatigue crack. A portion of the sound beam is reflected from that part of the discontinuity which is present within the scanning area of the transducer and the remaining energy is reflected from the bottom of the specimen (back reflection). The reflected incident energy returns to the transducer, is amplified, and presented on the oscilloscope screen as a signal. Under certain conditions, the amplitude of the resulting signal is directly related to the reflecting area of the discontinuity encountered by the sound beam.⁽⁶⁾

After fracture initiation or extension in the WOL specimen, the flaw area available for reflecting sound energy increases, causing an increase in the amplitude of the flaw signal and a corresponding decrease in the back reflection amplitude. Since the amplitude of the flaw signal can be made directly proportional to the reflecting area of the crack, one need only establish a calibration curve of crack length versus signal amplitude to provide an accurate measurement of crack growth.

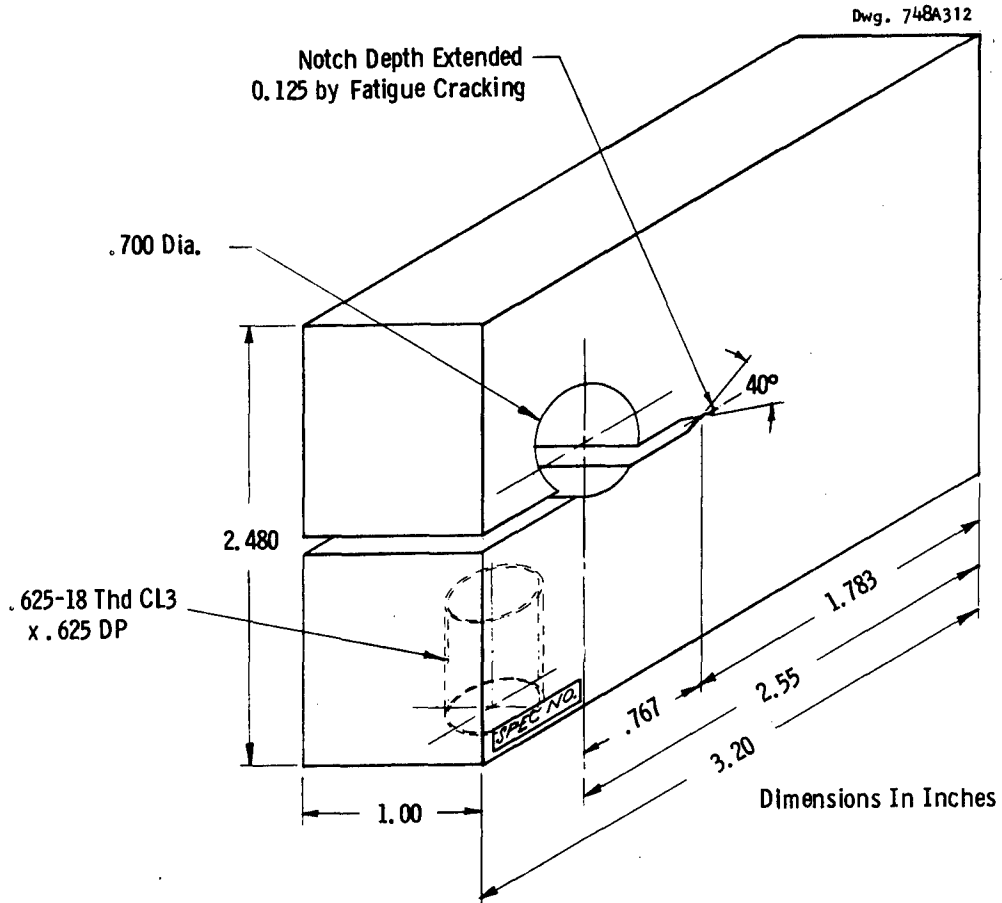


Fig. 1—Wedge opening loading type fracture toughness specimen ("IT" Geometry)

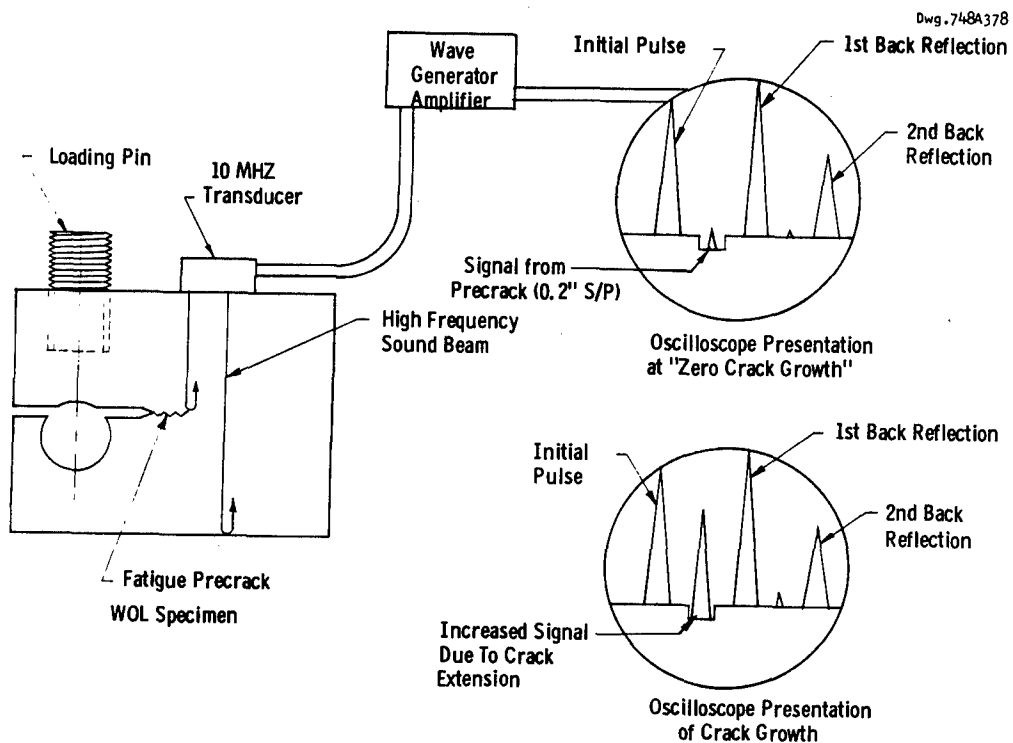
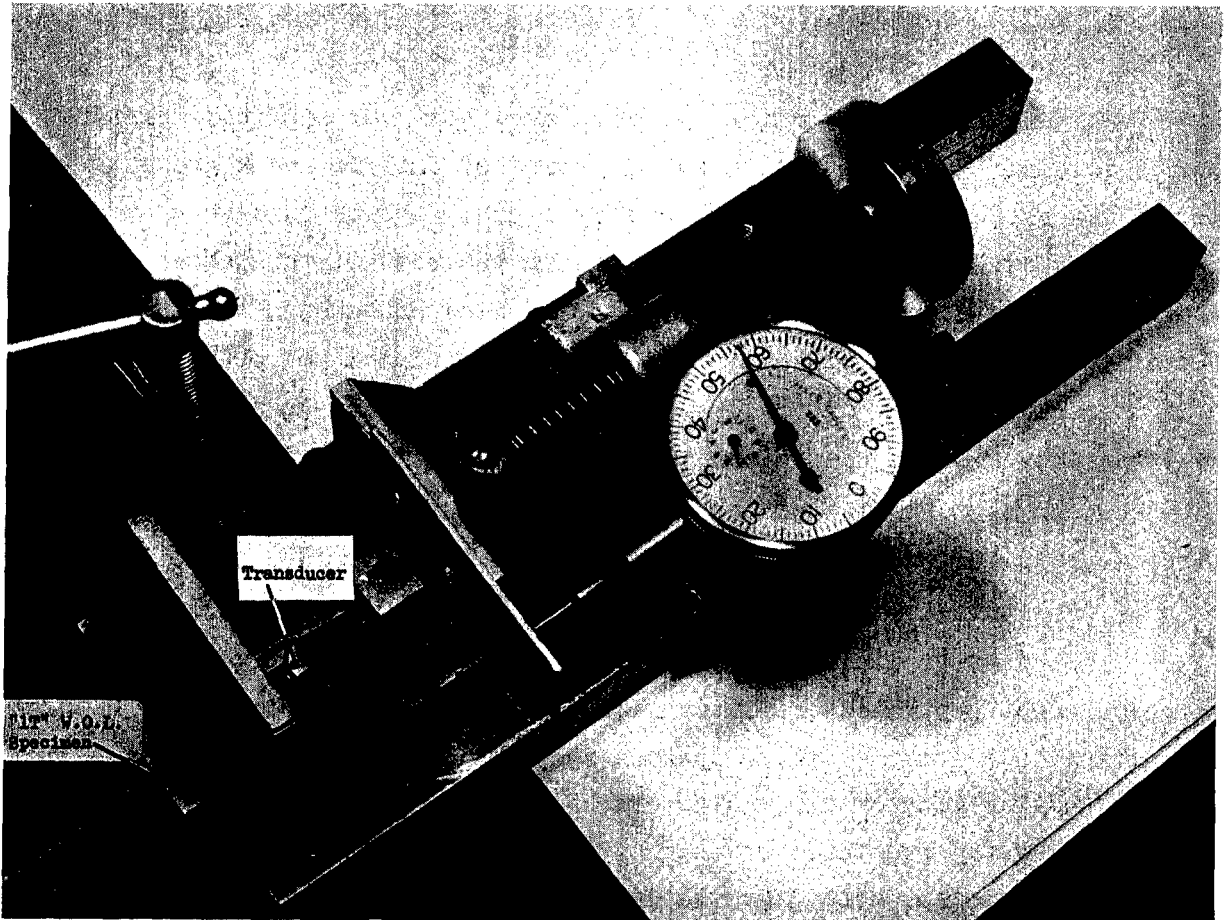


Fig. 2—Schematic illustration of the ultrasonic detection of fatigue crack growth in the WOL toughness specimen.

Figure 3 shows a typical crack growth-signal amplitude calibration curve developed for the ultrasonic detection of fatigue crack growth. This curve was established by simulating actual crack growth on several precracked "1T" WOL steel and aluminum specimens using the test fixture shown in Figure 4. The ultrasonic instrumentation was adjusted such that a two-inch sweep-to-peak (s/p) second back reflection signal was obtained through the uncracked portion of the test specimen. The spring-loaded transducer was then moved along the specimen surface towards the fatigue crack until a 0.20-inch s/p signal appeared on the oscilloscope screen. The transducer location, as indicated by the dial gauge, was then recorded along with the signal amplitude. The transducer was moved an additional increment (0.005 inch) in the same direction and the ultrasonic response recorded. This procedure was continued until the flaw signal reached 2.6 inches s/p, resulting in the data used to produce the calibration curve shown in Figure 3. The reliability of simulating crack growth by this means was established by comparing the predicted crack growth based upon the calibration curve (Figure 3) with the actual growth determined by visually examining many fractured WOL specimens. Table I illustrates the results of the correlation and the deviation encountered. A crack growth accuracy of at least ± 0.005 inch was observed.

Figure 5 shows the fracture surfaces of a steel "1T" WOL specimen which failed under cyclic loading. The beach marks were produced as the result of stopping the test at various intervals. Comparison of the amount of crack growth measured ultrasonically with that indicated by the distance between beach marks confirmed the reliability of the ultrasonic measurement technique and also indicated that the above technique for simulating crack growth produced test results comparable to those of a stationary transducer mounted on a specimen in which a crack is actually propagating.

A test frequency of 10 MHz was selected for the ultrasonic measurement of fatigue crack extension in order to provide adequate sensitivity. Investigation of test frequencies lower than 10 MHz indicated that the predicted crack length varied with the load applied to the specimen. This variation was caused by the opening of the fatigue crack upon



CONTACT TEST FIXTURE USED TO SIMULATE CRACK GROWTH

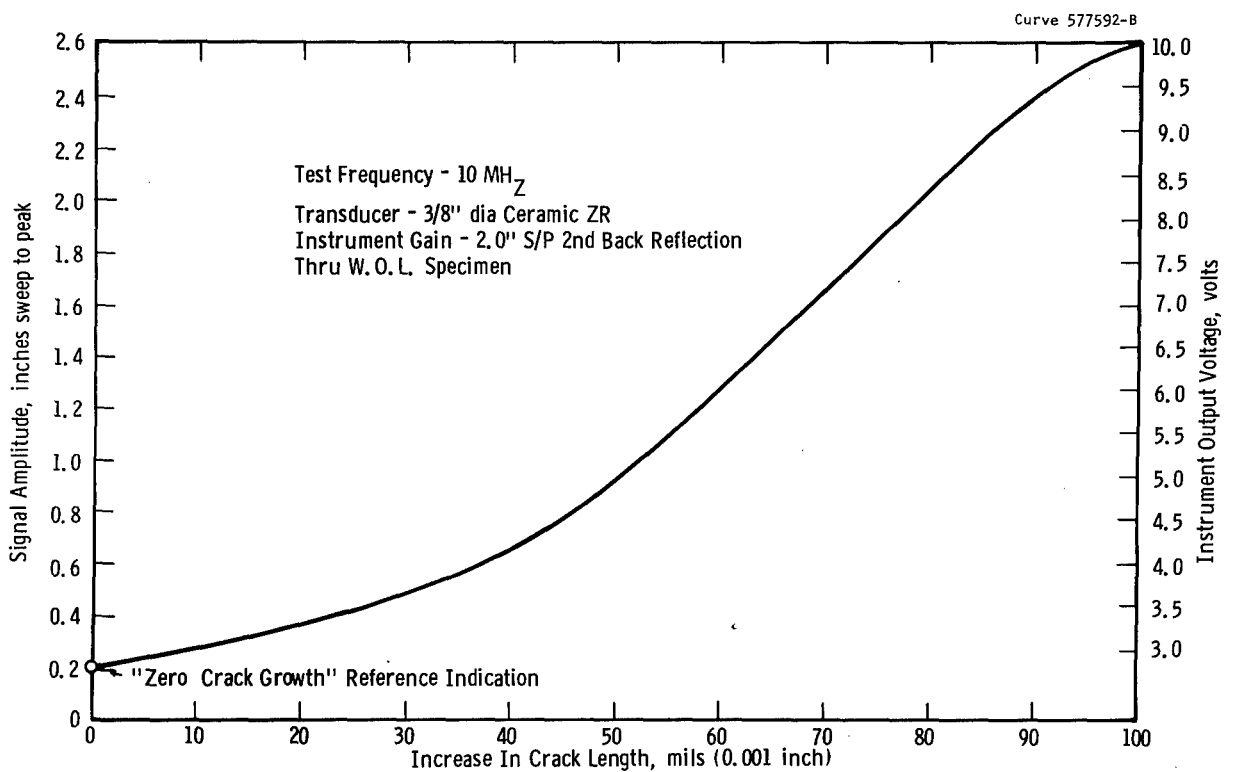
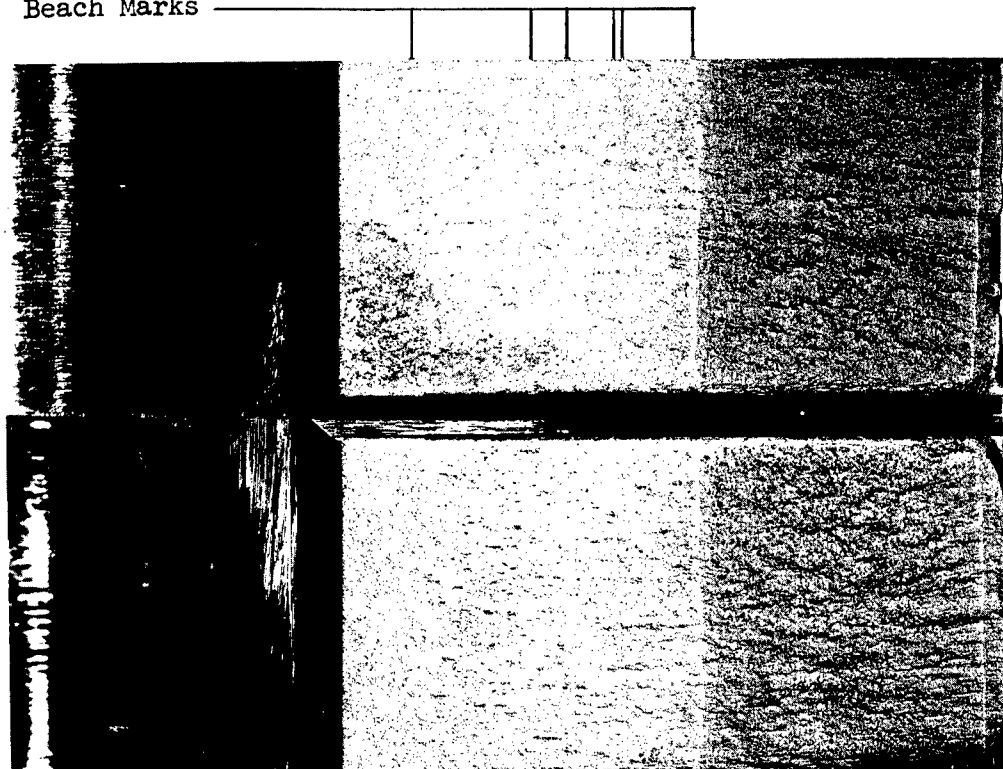


Fig. 3—Calibration curve for the ultrasonic detection of crack growth in the "1T" W.-O. L. fracture toughness specimen

Beach Marks



Mag. 2X

FIGURE 5 - FRACTURE SURFACES OF A STEEL (HP 9-4-25)
"1T" W.O.L. SPECIMEN WHICH FAILED UNDER
CYCLIC LOADING. NOTE THE PRESENCE OF THE
BEACH MARKS INDUCED BY TERMINATING THE TEST.

TABLE I

CORRELATION BETWEEN ULTRASONIC AND VISUAL MEASUREMENT OF CRACK GROWTH

<u>Specimen</u>	<u>Crack Growth Measured Ultrasonically (inches)</u>	<u>Crack Growth Measured Visually After Fracture (inches)</u>	<u>Deviation (inches)</u>
<u>HP 9-4-25 Steel</u>			
HP-3T-B13	0.254	0.250	+0.004
	0.517	0.520	-0.003
	0.627	0.630	-0.003
	0.732	0.737	-0.005
	0.979	0.980	-0.001
HP-3T-B16	0.215	0.215	0.000
	0.518	0.520	-0.002
	0.750	0.755	-0.005
	0.910	0.908	+0.002
	0.970	0.970	0.000
HP-3T-B25	0.052	0.050	+0.002
	0.153	0.150	+0.003
	0.239	0.240	-0.001
	0.321	0.320	+0.001
	0.504	0.500	+0.004
	0.586	0.590	-0.004
	0.885	0.890	-0.005
	0.991	0.990	+0.001
	1.111	1.110	+0.001
<u>7079-T6 Aluminum</u>			
All B17	0.153	0.155	-0.002
	0.221	0.225	-0.004
	0.308	0.310	-0.002
	0.642	0.642	0.000
	0.780	0.780	0.000
All B25	0.055	0.050	+0.005
	0.116	0.120	-0.004
	0.208	0.210	-0.002
	0.344	0.340	+0.004
	0.425	0.420	+0.005
	0.501	0.500	+0.001
	0.631	0.630	+0.001

loading. Tests conducted at 10 MHz indicated that the variation in measured crack length with increasing load were well within the ± 0.005 -inch crack length sensitivity. However, for improved accuracy, the calibration curve was established on specimens which were wedged open to eliminate any effect of crack opening.

The crack growth-signal amplitude curve shown in Figure 3 is valid only for the transducer used to develop the curve. Due to variations in transducer characteristics, especially ceramic transducers, a new calibration curve is required for each individual transducer involved. In addition, the curve can only be used with precracked specimens. As-notched specimens would require a calibration curve with the "zero crack growth" reference indication established on a signal from the tip of the machined notch rather than the tip of an existing fatigue crack.

The proper use of the calibration curve requires the fatigue crack to propagate perpendicular to the impinging sound beam. Therefore, the test specimens should be side notched in order to ensure crack propagation parallel to the ultrasonic test surface. To the best of my knowledge, shallow side-notching (<5% specimen thickness) has no adverse effect upon toughness testing other than to increase the specimen preparation cost.

Figure 6 illustrates the transducer arrangement used to monitor crack growth under loading conditions. A spring-loaded transducer holder is used in conjunction with an oil couplant to maintain uniform contact between the crystal and specimen surface.

Crack propagation in excess of that which can be accurately measured with the available instrumentation (0.100 inch) requires that the transducer be moved along the surface to a new "zero crack growth" reference point. The dial gauge shown in Figure 6 is used to accurately measure the new transducer location. The distance between transducer locations corresponds to the amount of crack growth encountered, thereby providing an additional check of the amount of crack propagation involved. This technique also provides a satisfactory method of measuring the extent of the fatigue crack in a precracked specimen since once a correlation between precrack length and transducer location has been established, transducer location can be converted directly to fatigue crack length.

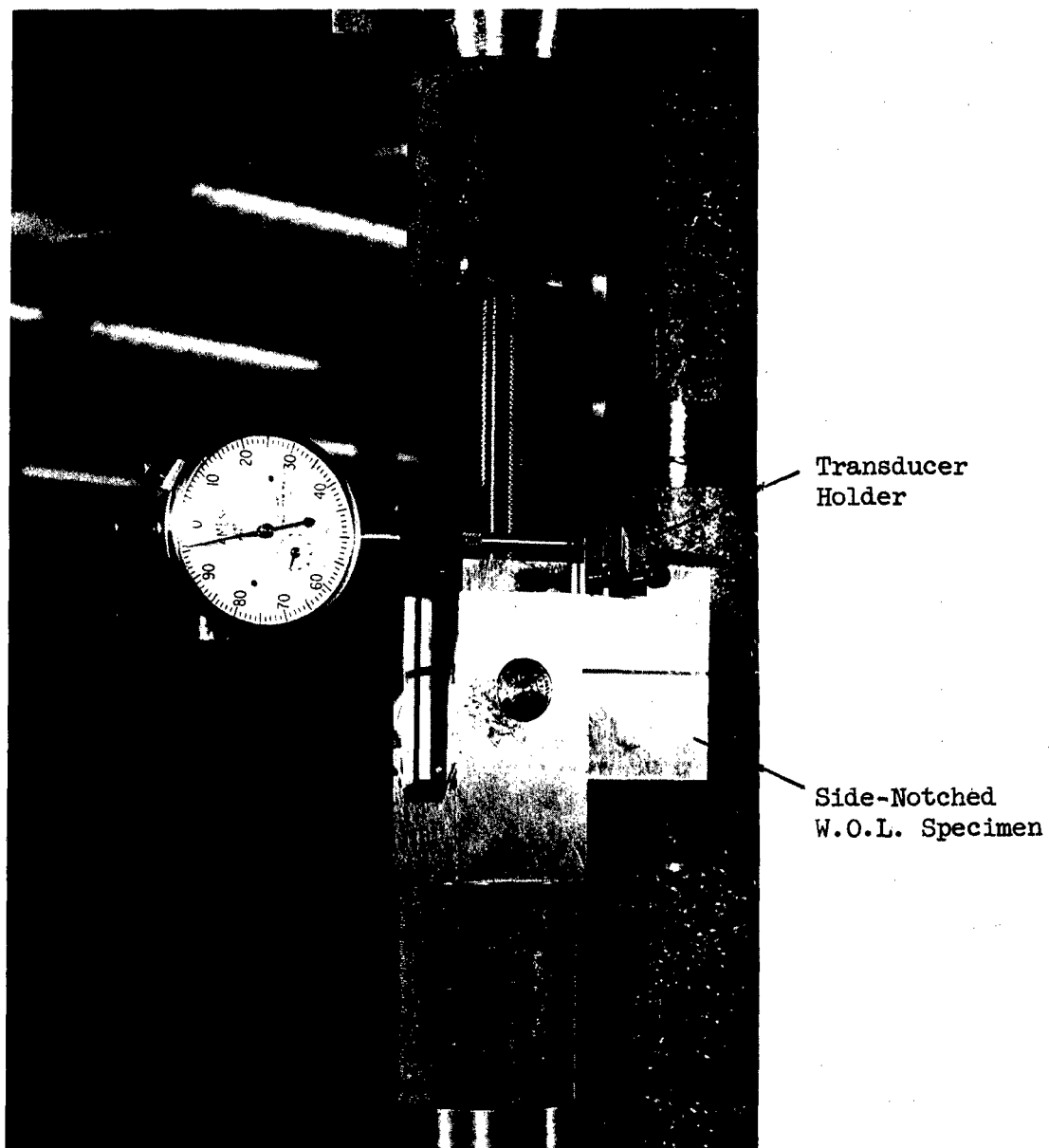
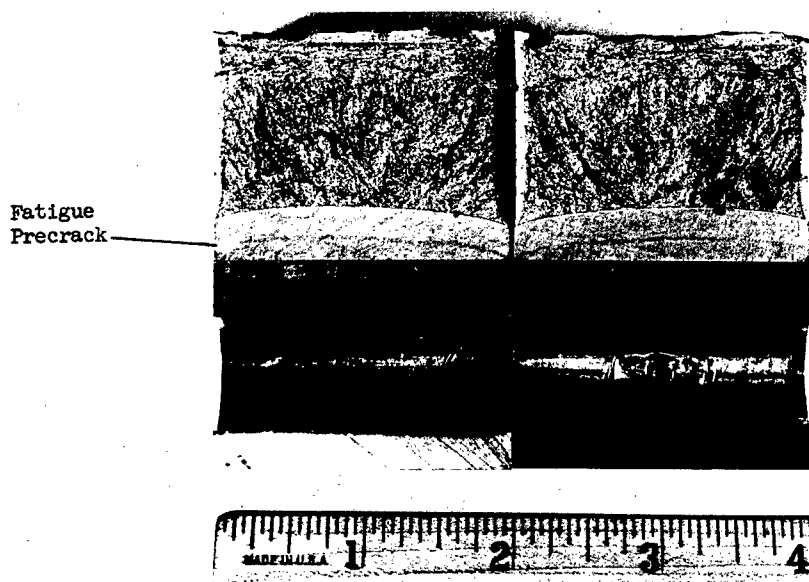


FIGURE 6 - ULTRASONIC DETECTION OF CRACK
GROWTH UNDER CYCLIC LOADING

Similar instrumentation was used to establish crack behavior under direct tension fracture toughness testing; however, the crack growth calibration curve established on precracked specimens could not be used to determine the extent of crack propagation. The surface roughness of a propagating crack depends upon the stress level involved as well as the test temperature and properties of the material. As the texture of a fracture surface varies from that of the smooth fatigue crack used to develop the ultrasonic crack growth calibration curve, the accuracy and reliability of the curve decreases. Figure 7 illustrates the fracture appearance of a Cr-Mo-V turbine rotor steel WOL ("X" series) toughness specimen which failed under direct tension loading.



Mag. 1X

FIGURE 7 - FRACTURE APPEARANCE OF A Cr-Mo-V TURBINE ROTOR STEEL "2X" W.O.L. TOUGHNESS SPECIMEN

Note the variation in fracture texture between the smooth fatigue crack and irregular cleavage fracture. The ultrasonic measurement of crack growth during cleavage fracture in a specimen such as this is virtually impossible since the rough surface of the crack induced under high stress levels (approaching the yield strength of the material) severely scatters the impinging high-frequency sound energy. On the other hand, those materials where the surface roughness of the precrack approximates that

of the crack induced by direct tension loading, the calibration curve is satisfactory and the extent of crack extension prior to rapid failure can accurately be determined. Furthermore, even in those cases where ultrasonic crack detection does not provide accurate measurement of crack length due to the irregular nature of the crack surface, the described technique does provide a method whereby crack extension can be distinguished from yielding at the crack tip, thus providing assurance that the test was conducted under desirable conditions.

Ultrasonic detection and measurement of crack propagation under cyclic loading has been adapted to an automatic monitoring system. The amplitude of the crack signal presented on the oscilloscope screen is monitored with a Sperry Transigate Type E550 gating system which permits conversion of signal amplitude to an output voltage (0-12 volts). The output voltage is amplified using a Kintel Model 111A amplifier and continuously recorded along with the number of elapsed cycles on an Esterline-Angus Model AW DC recorder. Figure 8 shows a typical instrumentation output and the corresponding reflectograms recorded for 0.090 inch (90 mils) of crack propagation in a steel WOL specimen under cyclic loading. The crack growth rate $\frac{\Delta a}{\Delta N}$ (mils per cycle) is readily determined by differentiating over a convenient interval of crack growth necessary to provide the required sensitivity. Figure 9 illustrates a typical crack growth rate curve established using the ultrasonic technique of measuring fatigue crack extension. The curve presents data established on seven HP 9-4-25 steel "1T" WOL specimens. The consistency of the data illustrates the reliability of the ultrasonic measurement of slow crack growth, as well as reproducibility of crack growth rates from sample to sample.

The automatic monitoring technique also provides a convenient method of controlling the precracking (fatiguing) operation to obtain a crack of desired length. The transducer is placed at a predetermined location on the specimen surface and the specimen subjected to cyclic loading. When the crack propagates to a sufficient length as indicated by a given ultrasonic presentation, the gating circuit can be adjusted

to trigger an alarm or a switch which in turn automatically terminates precracking. This technique eliminates the necessity of regularly interrupting the precracking operation in order to measure the crack propagation.

Discussion

Ultrasonic theory indicates that the amplitude of a flaw signal is directly proportional to the flaw size provided the major plane of the discontinuity is perpendicular to the sound beam and the area of the flaw is sufficiently smaller than that of the transducer.⁽⁷⁾ Side notching the WOL specimen ensures crack propagation perpendicular to the sound beam; the width of the fatigue crack is larger than the transducer diameter, and as a result a propagating crack rapidly approaches a reflecting area which saturates the transducer (further increases in crack length no longer produce measurable increases in the ultrasonic presentation).

Transducer saturation along with the vertical linearity of the flaw detection instrumentation (the signal amplitude range over which increases in input signal cause corresponding increases in signal amplitude) limit the length range over which crack growth can accurately be measured by means of an ultrasonic technique. Selection of a 0.2-inch s/p "zero crack growth" reference indication at the gain setting used (2-inch s/p second back reflection) permits the accurate measurement of crack growth to a flow signal amplitude of 2.6 inches s/p. This amplitude range corresponds to 0.100 inch of crack growth in the "1T" WOL specimen. A gain setting established on the first back reflection was found to be less satisfactory since the maximum measurement range was limited to amplitudes from 0.2 to 1.8 inches s/p (0.070 inch of crack extension).

The nonlinear nature of the signal amplitude-crack growth curve (Figure 3) is the result of a combination of two factors: (1) interpreting variations in reflecting area, measured with a circular transducer, as linear fatigue crack extension, and (2) variation in the transducer beam profile at the test distance involved. As the crack

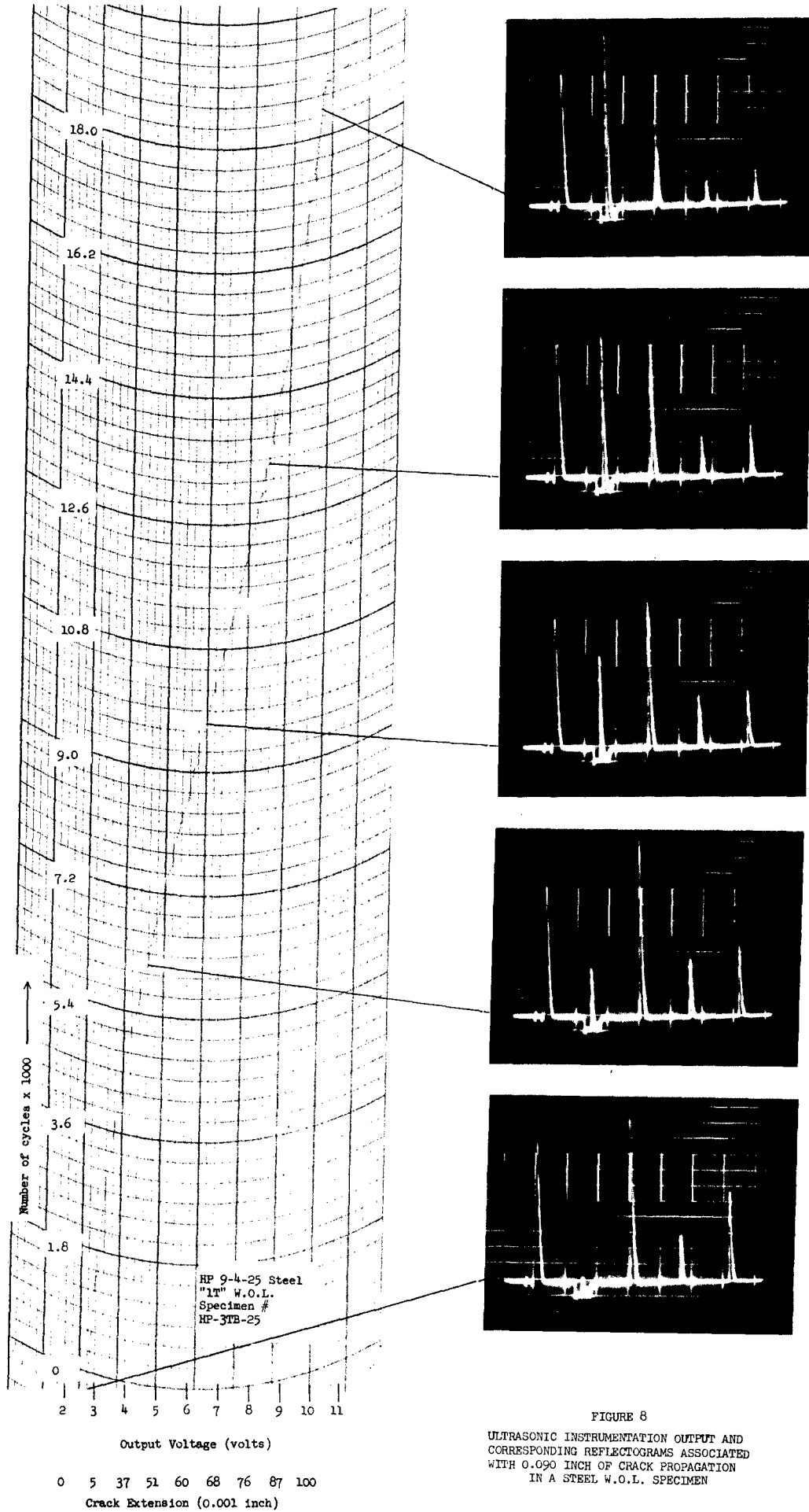


FIGURE 8
 ULTRASONIC INSTRUMENTATION OUTPUT AND
 CORRESPONDING REFLECTOGRAMS ASSOCIATED
 WITH 0.090 INCH OF CRACK PROPAGATION
 IN A STEEL W.O.L. SPECIMEN

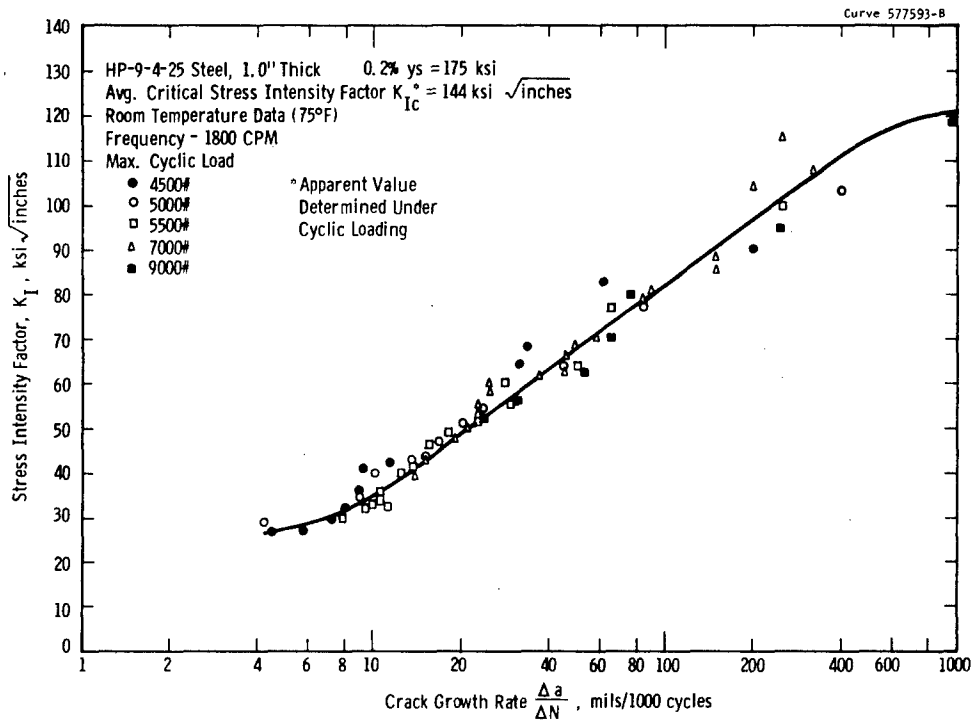


Fig. 9 - Crack growth rate as a function of stress intensity factor for HP-9-4-25 steel as determined on the "1T"WOL fracture toughness specimen

front propagates into the effective area of the transducer (a circular beam) the reflected energy increases with both the reflecting area and increase in incident energy resulting in a nonlinear relationship between crack length and signal amplitude. If a rectangular or square transducer were used, it is expected that a more nearly linear relationship would exist due to the elimination of the exponential increase in reflecting area.

The ultrasonic crack growth detection technique described herein has been modified slightly to enable the detection of fatigue crack extension in larger WOL specimens, and the preliminary results appear satisfactory. The geometric configuration of the WOL type fracture toughness specimen provides relatively ideal conditions for the ultrasonic detection of fatigue crack extension. As a result an ultrasonic technique can be utilized to its maximum potential. However, the development of such a technique for use with specimens of other geometry may be considerably more difficult since it may be necessary to use shear or surface waves rather than longitudinal waves to monitor crack behavior.

Summary

An ultrasonic inspection technique has been developed which is capable of continuously monitoring fatigue crack growth within the LT WOL type fracture toughness specimen. By means of commercially available equipment, the technique is capable of measuring crack extension to an accuracy of at least ± 0.005 inch under both tension and cyclic loading conditions. The procedure is of particular value for automatically controlling the precracking operation involved in specimen preparation and for the determination of slow crack growth characteristics. In addition, the technique can be used to distinguish between yielding and crack growth at the tip of an existing crack under load, thereby providing a better understanding of test conditions.

References

1. R. A. Davis and W. E. Quist, "Fracture Toughness," *Materials in Design Engineering*, November 1965, p. 93.
2. J. E. Srawley and W. F. Brown, "Fracture Toughness Testing Methods," *Fracture Toughness Testing and Its Applications*, ASTM ATP 381, June 1964, p. 133.
3. P. C. Paris, "The Fracture Mechanics Approach to Fatigue," *Proceedings of the 1963 Sagamore Conference*, Syracuse University Press, 1964.
4. J. O. Lyst and C. F. Babilon, "Detecting Fatigue Cracks in Notched Fatigue Specimens by Changes in Electrical Resistance," *Materials Research and Standards*, June 1962, p. 485.
5. S. J. Klima, D. J. Lesco and J. C. Freche, "Ultrasonic Technique for Detection and Measurement of Fatigue Cracks," *NASA Technical Note, TND-3007*, September 1965.
6. R. C. McMaster, *Nondestructive Testing Handbook*, Volume II, Society for Nondestructive Testing, 1959, Sec. 43, p. 46.
7. *Ibid*, Sec. 45, p. 19.

ACKNOWLEDGEMENTS

The authors are indebted to the sponsor of this program, the United States Army Tank-Automotive Center, for having made this work possible, and to the representatives of ATAC, Messrs. V. H. Pagano, E. Moritz and C. J. Kropf, who served as technical contacts during the course of the work.

Appreciation is also expressed to the authors' associates at the Westinghouse Research Laboratories who participated in this program. Particular acknowledgment is given to Messrs. W. H. Pryle, Metallurgy R&D, and R. B. Stouffer, Materials Testing and Evaluation R&D, for their contributions to the experimental phases of the program and to Dr. F. E. Werner, Manager, Metallurgy R&D, for his review and helpful comments concerning this final report.

DISTRIBUTION LIST

	<u>No. of Copies</u>
Commanding General U.S. Army Tank-Automotive Center Warren, Michigan 48090	
Attention: Director, Research & Engineering Directorate, SMOTA-R	1
Components Research & Development Labs, SMOTA-RC	3
Material Development & Engineering Div., SMOTA-RE	2
International Technical Programs Div., SMOTA-RI	1
Procurement Engineering Division, SMOTA-RS	2
Advanced Systems & Concepts Research Div., SMOTA-RR	2
Maintenance Directorate, SMOTA-M	2
Quality Assurance Directorate, SMOTA-Q	2
Plans and Commodity Office, SMOTA-W	2
Technical Data Coordination Branch, SMOTA-RTS	3
Combat Dev. Comd. Liaison Office, SMOTA-LCDC	2
Marine Corps Liaison Office, SMOTA-LMC	2
AF MIPR Liaison Office, SMOTA-USAF	2
Canadian Army Liaison Office, SMOTA-ICAN	2
USA EL Liaison Office, SMOTA-LEL	2
USA Weapons Comd. Liaison Office, SMOTA-LWC	2
Reliability Engineering Branch, SMOTA-RTT	1
Sheridan Project Managers Office, AMCPM-SH-D	1
General Purpose Vehicles Project Managers Ofc., AMCPM-GP	1
M60, M60A1, M48A3 Project Managers Office, AMCPM-M60	1
Combat Veh. Liaison Office, AMCPM-CV-D	1
US FRG MBT Detroit Office, AMCPM-MBT-D	1
XM651 Project Managers Office, AMCPM-GG	1
Commanding General U.S. Army Material Command Washington, D.C.	
Attention: AMCRD-DM-G	2
Commander Defense Documentation Center Cameron Station Alexandria, Virginia 22314	
Attention:	10
Harry Diamond Laboratories Washington, D.C.	
Attention: Technical Report Group	1

	No. of Copies
U. S. Naval Civil Engineer Res & Engr Lab Construction Battalion Center Port Hueneme, California	1
Commanding General U. S. Army Test and Evaluation Command Aberdeen Proving Ground, Maryland Attention: AMSTE-BB AMSTE-TA	1 1
Commanding General U. S. Army Mobility Command Warren, Michigan 48090 Attention: AMSMO-RR AMSMO-RDG AMSMO-RDO	1 1 1
Commanding General U. S. Army Supply and Maintenance Command Washington, D. C. 20310 Attention: AMSSM-MR	1
Commanding General 18th Airborne Corps Fort Bragg, North Carolina 28307	1
Commanding General U. S. Army Alaska APO 409 Seattle, Washington	1
Office, Chief of Research & Development Department of the Army Washington, D. C.	2
U. S. Army Deputy Chief of Staff for Logistics Washington, D. C.	2
U. S. Army Deputy Chief of Staff for Operations Washington, D. C.	2
Commander U. S. Marine Corps Washington, D. C. Attention: AO-4H	1
Commanding Officer U. S. Army Aviation Material Labs Fort Eustis, Virginia Attention: TCREC-SDL	1

	No. of Copies
Commanding General U. S. Army General Equipment Test Activity Fort Lee, Virginia 23801 Attention: Transportation Logistics Test Directorate	1
Commanding General U. S. Army Medical Services Combat Development Agency Fort Sam Houston, Texas 78234	2
Commanding Officer Signal Corps Fort Mommouth, New Jersey 07703 Attention: CSRDL	2
Commanding Officer Yuma Proving Ground Yuma, Arizona 85364 Attention: STEYP-TE	1
Corps of Engineers U. S. Army Engineer Research & Development Labs Fort Belvoir, Virginia 22060	1
President U. S. Army Maintenance Board Fort Knox, Kentucky 40121	1
President U. S. Army Armor Board Fort Knox, Kentucky 40121	1
President U. S. Army Artillery Board Fort Sill, Oklahoma 73503	1
President U. S. Army Infantry Board Fort Benning, Georgia 31905	1
President U. S. Army Airborne Electronic and Special Warfare Board Fort Bragg, North Carolina 28307	1
President U. S. Army Arctic Test Center APO Seattle, Washington 98733	1

	No. of Copies
Director, Marine Corps Landing Forces Development Center Quantico, Virginia 22134	1
Commanding Officer Aberdeen Proving Ground Aberdeen Proving Ground, Maryland 21005 Attention: STEAP-TL	1
Commanding Officer Air Force Materials Laboratory Wright-Patterson Air Base, Ohio Attention: Mr. S. O. Davis, MAAE Attention: Lt. R. Dunco, MAAE	1
Commanding Officer U. S. Army Arsenal, Frankford Philadelphia 37, Pennsylvania Attention: Mr. C. Carmen	1
Commanding Officer U. S. Army Arsenal, Watertown Watertown, Massachusetts 02172 Attention: Mr. R. Katz	1
David Taylor Model Basin United States Navy Attention: Mr. A. R. Wilner Carter Rock, Michigan	1
U. S. Naval Research Laboratories Attention: Dr. P. P. Pusak Washington, D. C.	1

DOCUMENT CONTROL DATA - R&D

(Security classification of title, body of abstract and indexing annotation must be entered when the overall report is classified)

ORIGINATING ACTIVITY (Corporate author) Westinghouse Research Laboratories Pittsburgh, Pennsylvania		2a. REPORT SECURITY CLASSIFICATION Unclassified	
		2b. GROUP	
1. REPORT TITLE ENGINEERING METHODS FOR THE DESIGN AND SELECTION OF MATERIALS AGAINST FRACTURE			
4. DESCRIPTIVE NOTES (Type of report and inclusive dates) Technical Report, Final June 1966			
5. AUTHOR(S) (Last name, first name, initial) Wessel, Edward T. Clark, William G., Jr. Wilson, William K.			
5. REPORT DATE June 24, 1966		7a. TOTAL NO. OF PAGES 400	7b. NO. OF REFS 313
8a. CONTRACT OR GRANT NO. DA-30-069-AMC-602 (T)		9a. ORIGINATOR'S REPORT NUMBER(S) Research Report 66-9B4-315-R1	
b. PROJECT NO. 1-DO-24401-A-105		9b. OTHER REPORT NO(S) (Any other numbers that may be assigned this report)	
c.			
d.			
10. AVAILABILITY/LIMITATION NOTICES			
11. SUPPLEMENTARY NOTES		12. SPONSORING MILITARY ACTIVITY Department of the Army United States Army Tank-Automotive Center Components Research and Development Labs Warren, Michigan 48090	
13. ABSTRACT Various approaches to the brittle fracture problem were reviewed and evaluated in terms of their applicability for satisfying ATAC's need for engineering procedures to be applied to materials selection and design criteria for the prevention of fracture in the future use of high-strength materials. Linear-elastic fracture mechanics technology was selected as the most applicable approach. A comprehensive review of the state of the art in fracture mechanics technology is presented. The fracture mechanics data available in the literature for high-strength steels, aluminum and titanium alloys were reviewed and evaluated with respect to their validity as fracture toughness parameters. All applicable fracture toughness data are tabulated. Additional fracture toughness (K_{Ic}) data were generated in the program for HP-9-4-25 steel, 7079-T6 aluminum and 6Al-4V titanium. Crack growth rates as a function of the stress intensity (K_I) were also determined for the steel and aluminum alloys. Engineering procedures and criteria for utilizing fracture mechanics technology were developed. Their application is illustrated by solutions to realistic hypothetical problems in the areas of design; evaluation and selection of materials; evaluations of nondestructive inspection capabilities; establishment of specifications, acceptance standards, and quality control procedures; and evaluating overall performance and life expectancy characteristics of the finished product. Detailed considerations are exemplified in all of these areas in the design and production of a hypothetical pressure vessel.			

14. KEY WORDS	LINK A		LINK B		LINK C	
	ROLE	WT	ROLE	WT	ROLE	WT
Fracture Toughness Crack Growth Defects Transition Temperature Stress Analysis Mechanics Stress Intensity Ferrous Alloys Aluminum Alloys Titanium Alloys Inspection Ultrasonics Proof Testing Design						
Life Expectancy Pressure Vessel Linear-Elastic Fracture-Mechanics						

INSTRUCTIONS

1. **ORIGINATING ACTIVITY:** Enter the name and address of the contractor, subcontractor, grantee, Department of Defense activity or other organization (*corporate author*) issuing the report.
- 2a. **REPORT SECURITY CLASSIFICATION:** Enter the overall security classification of the report. Indicate whether "Restricted Data" is included. Marking is to be in accordance with appropriate security regulations.
- 2b. **GROUP:** Automatic downgrading is specified in DoD Directive 5200.10 and Armed Forces Industrial Manual. Enter the group number. Also, when applicable, show that optional markings have been used for Group 3 and Group 4 as authorized.
3. **REPORT TITLE:** Enter the complete report title in all capital letters. Titles in all cases should be unclassified. If a meaningful title cannot be selected without classification, show title classification in all capitals in parenthesis immediately following the title.
4. **DESCRIPTIVE NOTES:** If appropriate, enter the type of report, e.g., interim, progress, summary, annual, or final. Give the inclusive dates when a specific reporting period is covered.
5. **AUTHOR(S):** Enter the name(s) of author(s) as shown on or in the report. Enter last name, first name, middle initial. If military, show rank and branch of service. The name of the principal author is an absolute minimum requirement.
6. **REPORT DATE:** Enter the date of the report as day, month, year; or month, year. If more than one date appears on the report, use date of publication.
- 7a. **TOTAL NUMBER OF PAGES:** The total page count should follow normal pagination procedures, i.e., enter the number of pages containing information.
- 7b. **NUMBER OF REFERENCES:** Enter the total number of references cited in the report.
- 8a. **CONTRACT OR GRANT NUMBER:** If appropriate, enter the applicable number of the contract or grant under which the report was written.
- 8b, 8c, & 8d. **PROJECT NUMBER:** Enter the appropriate military department identification, such as project number, subproject number, system numbers, task number, etc.
- 9a. **ORIGINATOR'S REPORT NUMBER(S):** Enter the official report number by which the document will be identified and controlled by the originating activity. This number must be unique to this report.
- 9b. **OTHER REPORT NUMBER(S):** If the report has been assigned any other report numbers (*either by the originator or by the sponsor*), also enter this number(s).
10. **AVAILABILITY/LIMITATION NOTICES:** Enter any limitations on further dissemination of the report, other than those

imposed by security classification, using standard statements such as:

- (1) "Qualified requesters may obtain copies of this report from DDC."
- (2) "Foreign announcement and dissemination of this report by DDC is not authorized."
- (3) "U. S. Government agencies may obtain copies of this report directly from DDC. Other qualified DDC users shall request through _____."
- (4) "U. S. military agencies may obtain copies of this report directly from DDC. Other qualified users shall request through _____."
- (5) "All distribution of this report is controlled. Qualified DDC users shall request through _____."

If the report has been furnished to the Office of Technical Services, Department of Commerce, for sale to the public, indicate this fact and enter the price, if known.

11. **SUPPLEMENTARY NOTES:** Use for additional explanatory notes.
12. **SPONSORING MILITARY ACTIVITY:** Enter the name of the departmental project office or laboratory sponsoring (*paying for*) the research and development. Include address.
13. **ABSTRACT:** Enter an abstract giving a brief and factual summary of the document indicative of the report, even though it may also appear elsewhere in the body of the technical report. If additional space is required, a continuation sheet shall be attached.

It is highly desirable that the abstract of classified reports be unclassified. Each paragraph of the abstract shall end with an indication of the military security classification of the information in the paragraph, represented as (TS), (S), (C), or (U).

There is no limitation on the length of the abstract. However, the suggested length is from 150 to 225 words.

14. **KEY WORDS:** Key words are technically meaningful terms or short phrases that characterize a report and may be used as index entries for cataloging the report. Key words must be selected so that no security classification is required. Identifiers, such as equipment model designation, trade name, military project code name, geographic location, may be used as key words but will be followed by an indication of technical context. The assignment of links, rules, and weights is optional.